UNIVERSITY OF CALIFORNIA,
IRVINE

Influences of Cyclopentadienyl and Arene Ligands on the Physical Properties and Reactivity of Rare Earth Metal Complexes in the +2 Oxidation State

DISSERTATION

submitted in partial satisfaction of the requirements
for the degree of

DOCTOR OF PHILOSOPHY

in Chemistry

by

Chad T. Palumbo

Dissertation Committee:
Professor William J. Evans, Chair
Professor Andrew S. Borovik
Professor Jenny Y. Yang

2017

DEDICATION

This dissertation is dedicated to Franco, Frankie, Margaret, Theresa, and Marianne.

Thank you all for your love and support.

“You’ve got to find a way of saying it without saying it.”

- Duke Ellington

TABLE OF CONTENTS

LIST OF FIGURES

LIST OF TABLES

LIST OF COMPLEXES

Molecular Formula	Number
[K(2.2.2-cryptand)][Cp″$_2$YCp]	**1-Y**
[K(2.2.2-cryptand)][Cp″$_2$GdCp]	**1-Gd**
[K(2.2.2-cryptand)][Cp″$_2$YCp^{Me}]	**2-Y**
[K(2.2.2-cryptand)][Cp″$_2$GdCp^{Me}]	**2-Gd**
Cp″$_2$YCp	**3-Y**
Cp″$_2$YCp	**3-Gd**
Cp″YCp$_2$	**4-Y**
Cp″GdCp$_2$	**4-Gd**
Cp″$_2$YCp^{Me}	**5-Y**
Cp″$_2$GdCp^{Me}	**5-Gd**
Cp″YCp$^{Me}_2$	**6-Y**
Cp″GdCp$^{Me}_2$	**6-Gd**
[K(2.2.2-cryptand)][Cp″$_3$La]	**7-La**
[K(2.2.2-cryptand)][Cp″$_3$Ce]	**7-Ce**
[K(2.2.2-cryptand)][Cp″$_3$Pr]	**7-Pr**
[K(2.2.2-cryptand)][Cp″$_3$Nd]	**7-Nd**
[K(2.2.2-cryptand)][Cp″$_3$U]	**7-U**
[Cp′$_2$La(μ-OMe)]$_2$	**8-La**
[Cp′$_2$Ce(μ-OMe)]$_2$	**8-Ce**
[K(2.2.2-cryptand)][(Cp″$_2$La)$_2$(μ-OH)(μ-O)]	**9-La**
[K(2.2.2-cryptand)][(Cp″$_2$Ce)$_2$(μ-OH)(μ-O)]	**9-Ce**

[K(2.2.2-cryptand)][Cp''_2K]	**10-K**
[K(2.2.2-cryptand)][$Cp'_2La(C_8H_8)$]	**11-La**
[K(2.2.2-cryptand)][$Cp'_2Ce(C_8H_8)$]	**11-Ce**
[K(2.2.2-cryptand)][$La(C_8H_8)_2$]	**12-La**
[K(2.2.2-cryptand)][$Ce(C_8H_8)_2$]	**12-Ce**
[K(2.2.2-cryptand)][$Pr(C_8H_8)_2$]	**12-Pr**
[K(2.2.2-cryptand)][$Nd(C_8H_8)_2$]	**12-Nd**
[K(2.2.2-cryptand)][Cp'_4Y]	**13-Y**
[K(2.2.2-cryptand)][Cp'_4La]	**13-La**
[K(2.2.2-cryptand)][Cp'_4Ce]	**13-Ce**
[K(2.2.2-cryptand)][Cp'_4Pr]	**13-Pr**
[K(2.2.2-cryptand)][Cp'_4Nd]	**13-Nd**
[K(2.2.2-cryptand)][Cp'_4Sm]	**13-Sm**
[K(2.2.2-cryptand)][Cp'_4Dy]	**13-Dy**
[K(2.2.2-cryptand)][Cp'_4Tm]	**13-Tm**
[K(2.2.2-cryptand)][$(Cp'_3Dy)_2H$],	**14-Dy**
[K(18-crown-6)$(THF)_2$][$(Cp''_2La)_2(\mu\text{-}\eta^6\text{:}\eta^6\text{-}C_6H_6)$]	**15-La**
$Cp''_2La(C_{14}H_{10})K$(18-crown-6)	**16-La**
[K(18-crown-6)$(THF)_2$][$Cp''_2La(C_{10}H_8)$]	**17-La**
[K(18-crown-6)][$(C_8H_8)LaCp''(C_8H_8)LaCp''_2$]	**18-La**
[K(2.2.2-cryptand)][$(Cp''_2La)_2(C_6H_6)$]	**19-La**
[$(K(18\text{-crown-6}))_2(THF)_3$]$_2$[$(Cp''_2Ce)_2(C_6H_6)$]	**20-Ce**
[K(2.2.2-cryptand)]$_2$[$(Cp'_2La)_2(C_6H_4(SiMe_3)_2)$]	**21-La**

[K(2.2.2-cryptand)][Cp′$_2$La(C$_7$H$_8$)]	**22-La**
[((^{Ad,Me}ArO)$_3$mes)Y]	**23-Y**
[((^{Ad,Me}ArO)$_3$mes)La]	**23-La**
[((^{Ad,Me}ArO)$_3$mes)Ce]	**23-Ce**
[((^{Ad,Me}ArO)$_3$mes)Pr]	**23-Pr**
[((^{Ad,Me}ArO)$_3$mes)Nd]	**23-Nd**
[((^{Ad,Me}ArO)$_3$mes)Sm]	**23-Sm**
[((^{Ad,Me}ArO)$_3$mes)Gd]	**23-Nd**
[((^{Ad,Me}ArO)$_3$mes)Dy]	**23-Nd**
[((^{Ad,Me}ArO)$_3$mes)Er]	**23-Er**
[((^{Ad,Me}ArO)$_3$mes)Yb]	**23-Yb**
[((^{Ad,Me}ArO)$_3$mes)U]	**23-U**
[K(2.2.2-cryptand)][((^{Ad,Me}ArO)$_3$mes)Y]	**24-Y**
[K(2.2.2-cryptand)][((^{Ad,Me}ArO)$_3$mes)La]	**24-La**
[K(2.2.2-cryptand)][((^{Ad,Me}ArO)$_3$mes)Ce]	**24-Ce**
[K(2.2.2-cryptand)][((^{Ad,Me}ArO)$_3$mes)Pr]	**24-Pr**
[K(2.2.2-cryptand)][((^{Ad,Me}ArO)$_3$mes)Nd]	**24-Nd**
[K(2.2.2-cryptand)][((^{Ad,Me}ArO)$_3$mes)Sm]	**24-Sm**
[K(2.2.2-cryptand)][((^{Ad,Me}ArO)$_3$mes)Gd]	**24-Gd**
[K(2.2.2-cryptand)][((^{Ad,Me}ArO)$_3$mes)Dy]	**24-Dy**
[K(2.2.2-cryptand)][((^{Ad,Me}ArO)$_3$mes)Er]	**24-Er**
[K(2.2.2-cryptand)][((^{Ad,Me}ArO)$_3$mes)Yb]	**24-Yb**
[K(2.2.2-cryptand)][((^{Ad,Me}ArO)$_3$mes)U]	**24-U**

[K(2.2.2-cryptand)][((^{Ad,Me}ArO)$_3$mes)YH]	**25-Y**
[K(2.2.2-cryptand)][((^{Ad,Me}ArO)$_3$mes)GdH]	**25-Gd**
[K(2.2.2-cryptand)][((^{Ad,Me}ArO)$_3$mes)DyH]	**25-Dy**
[K(2.2.2-cryptand)][((^{Ad,Me}ArO)$_3$mes)ErH]	**25-Er**
[K(2.2.2-cryptand)][((^{Ad,Me}ArO)$_3$mes)DyOH]	**26-Dy**
[K(18-crown-6)(THF)$_2$][((^{Ad,Me}ArO)$_3$mes)Dy]	**27-Dy**
[K(18-crown-6)(THF)$_2$][K(18-crown-6)(THF)$_2$][((^{Ad,Me}ArO)$_3$mes)DyH]	**28-Dy**
[K(2.2.2-cryptand)][((^{Ad,Me}ArO)$_3$(C$_6$Me$_3$(CH$_2$)$_2$CH)La(THF)]	**29-La**
Cp″$_2$Sm	**30-Sm**
Cp″$_2$Eu	**30-Eu**
Cp$^{tt}_2$Sm	**31-Sm**
Cp$^{tt}_2$Eu	**31-Eu**
Cp^{tt}Sm(μ-η^6:η^1-Ph)$_2$BPh$_2$	**32-Sm**
Cp^{tt}Eu(μ-η^6:η^1-Ph)$_2$BPh$_2$	**32-Eu**
[K(2.2.2-cryptand)][Cp′$_2$La(C$_4$Ph$_4$)]	**33-La**

ACKNOWLEDGEMENTS

I would like to acknowledge my advisor and committee chair, Professor William J. Evans. Working with you has been an invaluable experience and I have no doubt I will continue to integrate the lessons I have learned for many years to come. Thank you.

To my committee members, Professor Andy Borovik and Professor Jenny Yang, thank you for serving on my committee and for your advice and support throughout the years. I would also like to thank Professor Alan Heyduk for your advice and support following my oral exams.

Thank you to Dr. Joseph Ziller, along with Jordan Corbey, Jason Jones, and Mikey Wojnar, for your crystallographic assistance. To Professor Filipp Furche, along with Vamsee Voora, Guo Chen, and Alan Chan, thank you for the DFT work presented in this dissertation. I would like to thank Professor Andy Borovik, Sam Mann, Victoria Oswald, and Jason Jones for their spectroscopic assistance. Thank you to our collaborators, Professor Karsten Meyer, Professor Jeffery Long, Dr. Dominik Halter, Dr. Pete La Pierre, and Lucy Darago for your contributions and hard work. Thank you to Dr. Phillip Dennison for your NMR assistance. Thank you to the Evans lab, Megan Fieser, Jordan Corbey, Doug Kindra, Christopher Kotyk, Ryan Langeslay, Cory Windorff, David Woen, Monica Boshart, Megan Dumas, Daniel Huh, Austin Ryan, Samuel Moehring, and Tener Jenkins.

Lastly, I would like to thank my parents, Franco and Margaret, my brother Frank, and my sisters Theresa and Marianne. You all have been incredibly supportive and have always encouraged me to pursue my goals.

CURRICULUM VITAE

Chad T. Palumbo

2013 Bachelors of Science in Chemistry, Wayne State University

2013-2017 Research/Teaching Assistant, University of California, Irvine

2017 Ph.D. Chemistry, University of California, Irvine

Publications

"Ligand Effects in the Synthesis of Ln^{2+} Complexes by Reduction of Tris(cyclopentadienyl) Precursors Including C–H Bond Activation of an Indenyl" Jordan F. Corbey, David H. Woen, Chad T. Palumbo, Megan E. Fieser, Joseph W. Ziller, Filipp Furche, and William J. Evans, *Organometallics*, **2015**, *34*, 3909-3921.

"Isolation of +2 Rare Earth Ions with Three Anionic Carbocyclic Rings: Bimetallic Bis(cyclopentadienyl) Reduced Arene Complexes of La^{2+} and Ce^{2+} are Four Electron Reductants" Christopher M. Kotyk, Megan E. Fieser, Chad T. Palumbo, Joseph W. Ziller, Lucy E. Darago, Jeffery R. Long, Filipp Furche, and William J. Evans, *Chemical Science*, **2015**, *6*, 7267-7273.

"Comparisons of Lanthanide/Actinide +2 Ions in a Tris(aryloxide)arene Coordination Environment" Megan E. Fieser, Chad T. Palumbo, Henry S. La Pierre, Dominik P. Halter, Vamsee K. Voora, Joseph W. Ziller, Filipp Furche, Karsten Meyer, and William J. Evans, *Chemical Science*, **2017**, Advance Article.

"Reactivity of Complexes of $4f^n5d^1$ and $4f^{n+1}$ Ln^{2+} Ions with Cyclooctatetraene" Chad T. Palumbo, Megan E. Fieser, Joseph W. Ziller, and William J. Evans, *Organometallics*, **2017**, *36*, 3721-3728.

"Structural Characterization of the Bent Metallocenes, $[C_5H_3(SiMe_3)_2]Sm$ and $[C_5H_3(CMe_3)_2]Ln$ (Ln = Eu, Sm), and the Mono(cyclopentadienyl) Tetraphenylborate Complex, $[C_5H_3(CMe_3)_2]Eu(\mu\text{-}\eta^6\text{:}\eta^6\text{-}Ph)_2BPh_2$" Chad T. Palumbo, Joseph W. Ziller, William J. Evans, *Journal of Organometallic Chemistry*, **2017**, In Press.

"Trimethylsilyl- vs Bis(trimethylsilyl)-Substitution in Tris(cyclopentadienyl) Complexes of La, Ce, and Pr: Comparison of Structure, Magnetic Properties, and Reactivity" Chad T. Palumbo, Lucy E. Darago, Cory J. Windorff, Joseph W. Ziller, Jeffery R. Long, and William J. Evans, *Manuscript in preparation for submission to Inorganic Chemistry*.

"Metal Versus Ligand Reduction in Ln^{3+} Complexes of a Mesitylene-Anchored Tris(aryloxide) Ligand" Chad T. Palumbo, Dominik P. Halter, Guo P. Chen, Alan K. Chan, Vamsee K. Voora, Megan E. Fieser, Joseph W. Ziller, Wolfgang Hieringer, Filipp Furche, Karsten Meyer, and William J. Evans, *Manuscript in preparation for submission to the Journal of the American Chemical Society*.

"Electrocatalytic H_2O Reduction with *f*-Elements: Mechanistic Insight and Overpotential Tuning in a Series of Lanthanide Complexes" Dominik P. Halter, Chad T. Palumbo, Milan Gembicky, Arnold L. Rheingold, Joseph W. Ziller, William J. Evans, and Karsten Meyer, *Manuscript in preparation for submission to the Journal of the American Chemical Society*.

"Using Diamagnetic Yttrium and Lanthanum Complexes to Explore Ligand Reduction and C–H Bond Activation in the Tris(aryloxide)mesitylene Ligand System" Chad T. Palumbo, Dominik P. Halter, Vamsee K. Voora, Milan Gemicky, Arnold L. Rheingold, Joseph W. Ziller, Filipp Furche, Karsten Meyer, and William J. Evans, *Manuscript in preparation for submission to Chemistry - A European Journal.*

"Structure, Magnetism, and Multi-Electron Reduction Reactivity of the Reduced Arene La^{2+} Complex, $[(Cp''_2La)_2(\mu\text{-}\eta^6\text{:}\eta^6\text{-}C_6H_6)]^{1-}$" Chad T. Palumbo, Lucy E. Darago, Guo P. Chen, Joseph W. Ziller, Filipp Furche, Jeffery R. Long, and William J. Evans *Manuscript in preparation for submission to Chemistry - A European Journal.*

"Structural Variations in Reduced Arene Complexes of Lanthanum and Cerium" Chad T. Palumbo, Guo P. Chen, Joseph W. Ziller, Filipp Furche, and William J. Evans, *Manuscript in preparation for submission to Organometallics*.

"Reductive Coupling of Diphenylacetylene to a Benzyldiphenylindenyl Anion Via La^{2+}" Chad T. Palumbo, Joseph W. Ziller, and William J. Evans, *Manuscript in preparation for submission to Chemical Communications*.

Presentations

"Volatility and Thermal Stability of Mid-to-Late Transition Metal Complexes Containing α-Iminoalkoxide and α-Hydrazonoalkoxide Ligands as Precursors for Atomic Layer Deposition" Chad T. Palumbo, Christopher J. Snyder, Phillip D. Martin, Charles H. Winter, Poster Presentation at the 14th Annual Chemistry Graduate Research Symposium, Detroit, MI, Oct 19, 2012

"Volatility and Thermal Stability of Mid-to-Late Transition Metal Complexes Containing α-Iminoalkoxide and α-Hydrazonoalkoxide Ligands as Precursors for Atomic Layer Deposition"

Chad T. Palumbo, Christopher J. Snyder, Phillip D. Martin, Charles H. Winter, Poster Presentation at Ohio Inorganic Weekend, Detroit, MI, October 13th, 2012.

"Expanding the Chemistry of Lanthanides in the Divalent State" Chad T. Palumbo, William J. Evans, Oral Presentation at the Summer Research Program Research Symposium, Irvine, CA, August 14th, 2013.

"Reductive Chemistry in Heterleptic Coordination Environments: New Examples of Y and Gd ain the +2 State" Chad T. Palumbo, Joseph W. Ziller, William J. Evans, Poster Presentation at the 249th ACS National Meeting and Exposition, Denver, CO, March 2015.

"Synthesis of Low Valent Lanthanide Complexes using Cyclopentadienyl and Arene Ligands" Chad T. Palumbo, Dominik, P. Halter, Joseph W. Ziller, Karsten Meyer, and William J. Evans, Invited Oral Presentation at the Inorganic Chemistry Conference Erlangen (ICCE), Erlangen, Germany, September 7th, 2016.

"Lanthanide/Actinide Comparisons of Structure and Reactivity of Complexes with a Tris(aryloxide)mesitylene Ligand" Chad T. Palumbo, Megan E. Fieser, Dominik P. Halter, Vamsee K. Voora, Joseph W. Ziller, Filipp Furche, Karsten Meyer, and William J. Evans, Oral Presentation for the Chemistry Department at the University of California, Irvine, CA, February 9th, 2017.

"Exploration of Electronic Structure of Divalent Lanthanide Complexes using a Tris(aryloxide)mesitylene Ligand" Chad T. Palumbo, Megan E. Fieser, Dominik P. Halter, Henry S. La Pierre, Vamsee K. Voora, Joseph W. Ziller, Filipp Furche, Karsten Meyer, William J. Evans, Oral Presentation at the 253rd ACS National Meeting and Exposition, San Francisco, CA, June 8th, 2017.

"A New Class of Ln^{2+} Complexes, [K(2.2.2-cryptand)][Ln[$(OAr^{Ad,Me})_3$mes][: Synthesis, Structure, Spectroscopy, and Theoretical Characterization" Chad T. Palumbo, Dominik P. Halter, Megan E. Fieser, Vamsee K. Voora, Joseph W. Ziller, Filipp Furche, Karsten Meyer, William J. Evans, Poster Presentation at the 28th Rare Earth Research Conference, Ames, IA, June 20th, 2017.

Awards and Affiliations

2017	28th Rare Earth Research Conference Scholarship
2017	President's Dissertation Year (PDY) Fellowship Honorable Mention
2017	Ford Foundation Dissertation Fellowship Honorable Mention
2014	National Science Foundation Graduate Research Fellowship Program (NSF GRFP)

2013	Competitive Edge Summer Research Program
2012	ACS Division of Inorganic Chemistry Undergraduate Award
2012	George H. Wheatley Memorial Scholarship
2012	Howard and Mary Kehrl Endowed Scholarship
2011	Board of Governor's Academic Grant
2011	Howard and Mary Kehrl Endowed Scholarship
2011	Department of Chemistry Chair's Honor List
2010	Wayne State University Transfer Scholarship
2013-present	American Chemical Society, Division of Inorganic Chemistry, member

ABSTRACT OF THE DISSERTATION

Influences of Cyclopentadienyl and Arene Ligand on the Physical Properties and Reactivity of Rare Earth Metal Complexes in the +2 Oxidation State

Chad T. Palumbo

Doctor of Philosophy in Chemistry

University of California, Irvine, 2017

Professor William J. Evans, Chair

This dissertation describes the synthesis, physical characterization, and reactivity of new classes of rare earth metal complexes to explore the chemistry of the recently discovered +2 oxidation state. In each chapter, a new ligand arrangement that supports Ln^{2+} ions is presented with the goal of evaluating how physical properties, ground-state electron configuration, and reactivity are affected by the coordination environment. Chapters 1-3 describe Ln^{2+} complexes in tris(cyclopentadienyl) coordination environments. Specifically, Chapter 1 presents new heteroleptic complexes, $[K(2.2.2\text{-cryptand})][(C_5H_3(SiMe_3)_2)_2LnCp^R]$ (Ln = Y, Gd; $Cp^R = C_5H_5$, C_5H_4Me). Chapter 2 describes the homoleptic complexes, $[K(2.2.2\text{-cryptand})][(C_5H_3(SiMe_3)_2)_3Ln]$ (Ln = La, Ce, Pr, Nd). Chapter 3 consists of a reactivity survey of the three classes of Ln^{2+} ions, which are defined as the traditional Ln^{2+} ions (Ln = Eu, Yb, Sm, Tm), the new $4f^n5d^1$ ions (Ln = La, Ce, Pr, Gd, Tb, Ho, Er, Y, Lu) and the configurational crossover ions (Ln = Dy, Nd). Chapters 4 and 5 describe Ln^{2+} complexes supported by anionic arene ligands. Chapters 6-8 describe new Ln^{2+} complexes supported by a tris(aryloxide)mesitylene ligand; this work is a collaborative effort with the lab of Professor Karsten Meyer at the Friedrich-Alexander-Universität Erlangen-Nürnberg. Chapter 9 is a structural analysis of the base-free metallocenes $(C_5H_3R_2)_2Ln$ (Ln = Sm, Eu; R = CMe_3, $SiMe_3$) and the mono(cyclopentadienyl) tetraphenylborate

complex $[C_5H_3(CMe_3)_2]Eu(\mu\text{-}\eta^6\text{:}\eta^1\text{-}Ph)_2BPh_2$. The goal of Chapter 9 was to test whether the tris(carbocyclic) coordination environment of $(C_5H_3R_2)Ln(\mu\text{-}\eta^6\text{:}\eta^1\text{-}Ph)_2BPh_2$ would allow the observation of Ln^{1+}. Finally, Chapter 10 presents a reactivity study of the $5d^1$ La^{2+} complexes, $[K(2.2.2\text{-cryptand})][(C_5H_4SiMe_3)_3La]$ and $[K(2.2.2\text{-cryptand})]_2[((C_5H_4SiMe_3)_2La)_2(C_6H_6)]$, with diphenylacetylene.

INTRODUCTION

The purpose of this research is to investigate the physical properties and reactivity of rare earth containing molecules to expand our fundamental understanding of these elements and impact areas relevant to solving practical world problems, like those related to energy and the environment. These include, but are not limited to, catalysis pertaining to the hydrogen economy, molecular magnetism, and lanthanide/actinide chemistry related to advanced nuclear energy systems. The purpose of this Introduction is to provide some background information on the intrinsic properties of the rare earth elements that set them apart from the others on the periodic table. Also included in this Introduction is a section describing lanthanide redox chemistry and how that has evolved over the years. Finally, the last section is an outline of this dissertation chapter by chapter.

Properties of the Rare Earth Elements. The rare earth elements consist of the lanthanide series from lanthanum (57) to lutetium (71) along with lanthanum's lighter congeners, scandium (21) and yttrium (39), Figure 0.1. Contrary to their name, the rare earths are relatively abundant compared to other elements on the periodic table, as shown in Figure 0.2. Why are they called the rare earths? It has been suggested[1] that "rare" was used with its 15th century denotion, "strange, extraordinary, and astonishing", and "earth" meaning metal oxide. The rare earth elements find a wide range of technological applications due to their physical properties. In the early 2000s, the demand for yttrium, neodymium, europium, dysprosium, and terbium had increased substantially due to their use in clean energy technology, such that these five elements have been labeled as critical materials by the U.S. Department of Energy.[2]

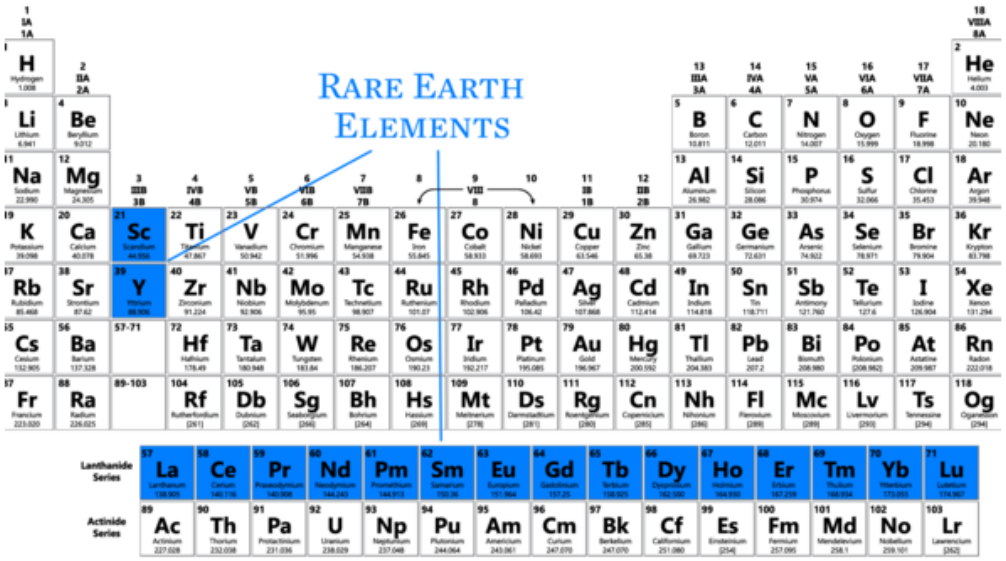

Figure 0.1. Periodic table of the elements displaying the rare earth elements in blue.

Iron	**43200**	Lead	**14.8**	**Europium**	**1.3**	Silver	**0.07**
Chromium	**126**	**Praseodymium**	**6.7**	Molybdenum	**1.1**	Mercury	**0.04**
Cerium	**60**	**Samarium**	**5.3**	Tungsten	**1**	Gold	**0.0025**
Nickel	**56**	**Gadolinium**	**4**	**Holmium**	**0.8**	Platinum	**0.0004**
Lanthanum	**30**	**Dysprosium**	**3.8**	**Terbium**	**0.65**	Rhodium	**0.00006**
Neodymium	**27**	**Erbium**	**2.1**	**Lutetium**	**0.35**		
Cobalt	**24**	**Ytterbium**	**2**	**Thulium**	**0.3**		

Figure 0.2. Abundance of the lanthanide elements (in bold) in the Earth's crust relative to other metallic elements (ppm).

The lanthanide elements are some of the largest elements of the periodic table, with 9-coordinate ionic radii ranging from 1.216 Å for the largest ion La^{3+} to 1.032 Å for Lu^{3+}.[3] Yttrium is intermediate at 1.075 Å for 9-coordinate Y^{3+} and scandium is the smallest rare earth with a 0.87 Å ionic radius for 8-coordinate Sc^{3+}.[3] The size of the lanthanides decrease regularly across the series due to influences of the lanthanide contraction, a phenomenon resulting in larger-than-

expected changes in ionic radii due to the poor shielding ability of the valence 4*f* electrons; *i.e.* the valence 6*s* electrons are more strongly affected by the charge of the nucleus than simple models would predict. The relative sizes of trivalent lanthanide ions are illustrated in Figure 0.3.

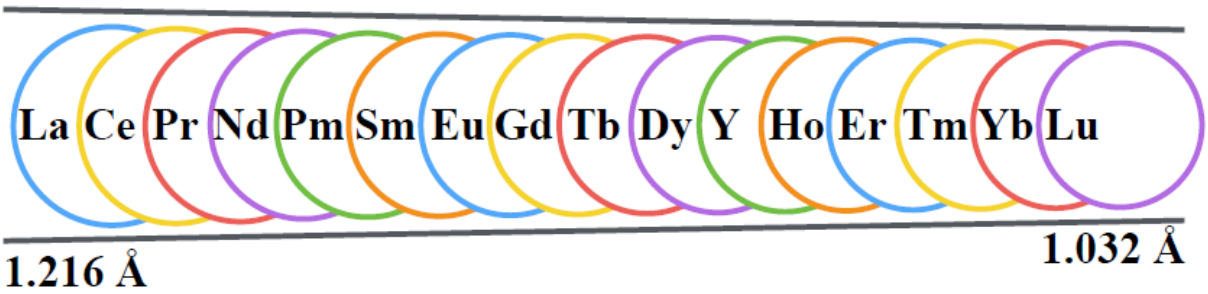

Figure 0.3. Illustration depicting the gradual decrease in size of 9-coordinate trivalent ions of the lanthanides and yttrium.

The bonding of the lanthanides can be described as primarily ionic with little valence orbital participation. Unlike transition metals with valence *d* orbitals that extend beyond the noble gas core and engage in bonding and reactivity, the valence 4*f* orbitals of the lanthanides do not.[4] This is illustrated in Figure 0.4a depicting the probability distribution of the electrons of $4f^3$ Nd^{3+} plotted as a function of distance from the nucleus. The situation with the actinides is slightly different; the actinides have accessible 5*f* electrons for bonding and reactivity,[4] but not to the degree that transition metals do with *d* electrons. Figure 0.4b shows the analogous probability distribution plot of $5f^3$ U^{3+}. The 5*d* electrons of the lanthanides are approximately 50,000 cm^{-1} above the 4*f* electrons[5] but traditionally they are not believed to be significant to their chemistry. Much of the work in this dissertation show that the 5*d* electrons are significant in the +2 oxidation state chemistry of the rare earth metals.

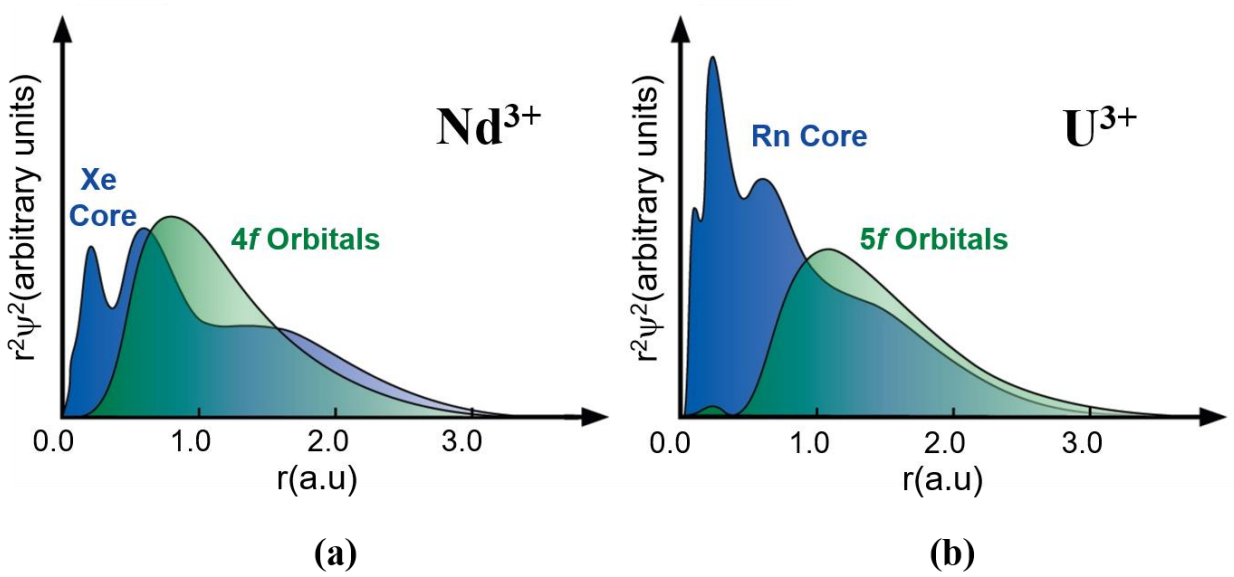

Figure 0.4. Electron probability distribution of two f^3 metal ions: (a) Nd^{3+} and (b) U^{3+}.[4]

Rare Earth Redox Chemistry. Redox reactions are one of two general types of chemical transformations (the other is acid/base). Hence, one of the most fundamental aspects of any element is its range of accessible oxidation states. Unlike transition metals, which can access a wide range of oxidation states, the lanthanides are most commonly found in the +3 state. Besides the +4 oxidation state of cerium and the fact that +2 ions of europium, ytterbium, and samarium[6-8] have been known for over a century, researchers believed the redox chemistry of the other lanthanides was limited to the +3 state. It was not until 1997-2001 when the first molecular examples of Tm^{2+}, Dy^{2+}, and Nd^{2+} were discovered.[9-11] This was thought to be the limit of isolable Ln^{2+} complexes on the basis of calculated reduction potentials,[12] which suggested that the other lanthanides would be too reactive to isolate from common solvents. In agreement with this, reductions done in benzene or 1,2-dimethoxyethane gave Ln^{3+} products with $(C_6H_6)^{2-}$ and $(OCH_3)^{1-}$ ligands.[13-15] Even the known Nd^{2+} was so unstable that compounds would undergo intramolecular transformations to give Nd^{3+} products.[16]

Nevertheless, researchers discovered novel ways of doing reduction chemistry with lanthanide complexes involving those without an accessible +2 oxidation state. For example, it was shown that the sterically crowded complexes $(C_5Me_5)_3Ln$[17-21] and the bridged hydrides $[(C_5Me_5)_2LnH]_2$[22] can act as a one- and two-electron reductants, respectively, Scheme 0.1. In the case of $(C_5Me_5)_3Ln$, one $(C_5Me_5)^{1-}$ ligand generates an electron and decamethyldicyclopentadiene. In $[(C_5Me_5)_2LnH]_2$, the hydrides couple to give dihydrogen.

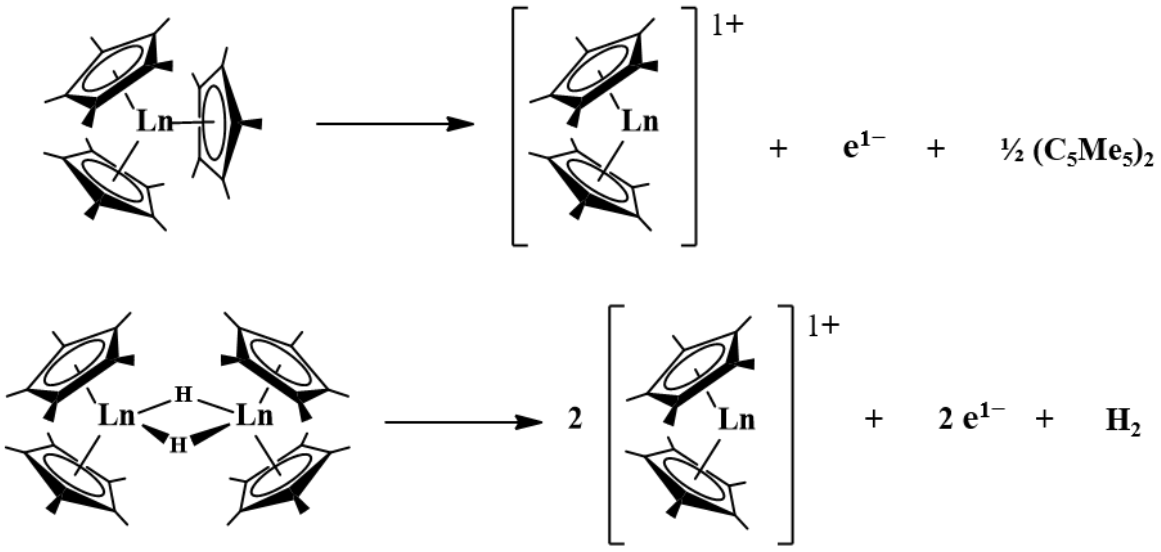

Scheme 0.1. Half-reactions displaying the reduction chemistry of trivalent lanthanide complexes $(C_5Me_5)_3Ln$ and $[(C_5Me_5)_2LnH]_2$.

Despite this reduction chemistry, complexes of the "traditional" six Ln^{2+} ions were still unique in that they did reactions that $(C_5Me_5)_3Ln$ and $[(C_5Me_5)_2LnH]_2$ could not. For example, it was discovered that Tm^{2+} under appropriate conditions can reduce dinitrogen to its dianion, $(N=N)^{2-}$, giving the side-on dinitrogen complex $[(C_5Me_5)_2Tm]_2N_2$,[23] eq 0.1, and that Dy^{2+} can do a similar transformation with the $[C_5H_3(SiMe_3)_2]^{1-}$ ligand.[24]

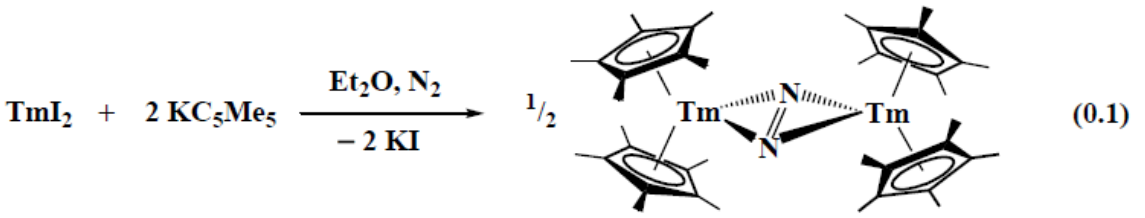

(0.1)

Over the years, activated dinitrogen complexes were obtained for all of the rare earth elements, but it was not necessary to use Ln^{2+} precursors. Most were obtained by reductions involving alkali metals in the presence of Ln^{3+} reagents,[16,25-34] eq 0.2, a reaction scheme generalized as the LnA_3/M reduction reaction where Ln = lanthanide, A = anionic ligand, and M = alkali metal. It seemed possible that transient "Ln^{2+}" intermediates were generated in these LnA_3/M reactions, but there was no evidence to support this.

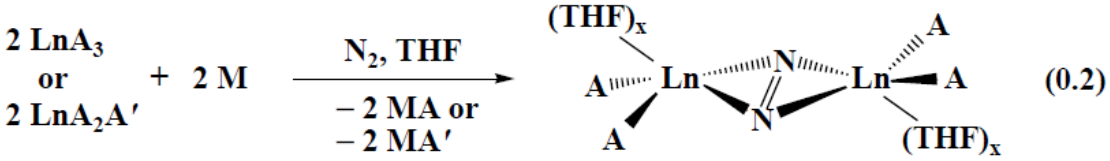

(0.2)

Ln = Sc, Y, La, Ce, Pr, Nd, Gd, Tb, Dy, Ho, Er, Tm, Lu
A = $N(SiMe_3)_2$, $OC_6H_3{}^tBu_2$-2,6, C_5Me_5, C_5Me_4H, $C_5H_4SiMe_3$, $C_5H_2{}^tBu_3$
A′ = BPh_4, I, H; M = K, KC_8, Na; x = 0-2

Spectroscopic confirmation of La^{2+} was first presented by Lappert and coworkers who found that the reduction of $[C_5H_3(SiMe_3)_2]_3La$ in 1,2-dimethoxyethane generates a dark solution with an EPR spectrum with an eight-line hyperfine pattern consistent with the $I = {}^7/_2$ nucleus of ^{139}La (99.9% natural abundance).[15] Subsequently, the first example of La^{2+} was obtained in crystalline form.[35] Similarly, Evans and coworkers obtained the first EPR evidence of Y^{2+} while studying the LnA_3/M reductions[34] and shortly thereafter crystallized the first example of Y^{2+} in the anion $[(C_5H_4SiMe_3)_3Y]^{1-}$.[36] The $[(C_5H_4SiMe_3)_3]^{3-}$ coordination environment proved to be

optimal; subsequent reductions with this ligand set gave the entire series of lanthanides with metals in the +2 oxidation state as the isolable molecular complexes [K(2.2.2-cryptand)][$(C_5H_4SiMe_3)_3$Ln] (Ln = Y, lanthanides except Pm which was not studied due to its radioactivity).[37-41] These reactions, in addition to the extension of this chemistry to Th, U, and Pu, are summarized in eq 0.3.[35-39,42-45]

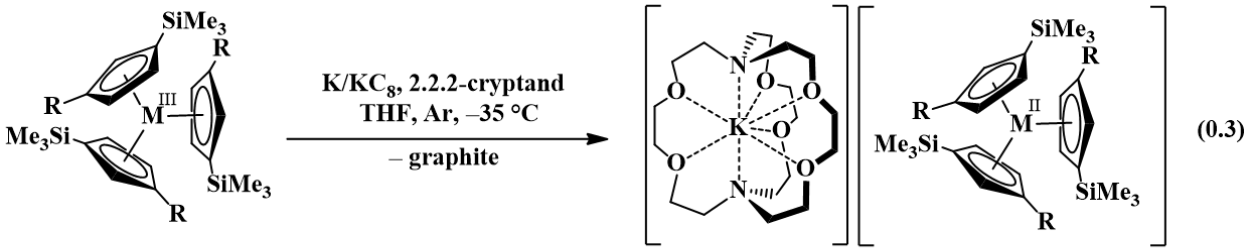

(0.3)

R = $SiMe_3$; M = La, Th, U, Pu
R = H; M = Y, La, Ce, Pr, Nd, Sm, Gd, Tb, Dy, Ho, Er, Tm, Lu, U

This dissertation describes attempts to move beyond the $[(C_5H_4SiMe_3)_3]^{3-}$ coordination environment with the goal of evaluating how changes to the primary coordination sphere affect the chemical and physical properties of Ln^{2+} and the overall complex.

Dissertation Outline. The research presented in this dissertation spans several themes. Chapter 1 describes the synthesis, structural, and spectroscopic characterization of the heteroleptic Ln^{2+} complexes [K(2.2.2-cryptand)][$(C_5H_3(SiMe_3)_2)_2LnCp^R$] (Ln = Y, Gd; $Cp^R = C_5H_5$, C_5H_4Me). These complexes were found to have similar structures and spectroscopic properties as [K(2.2.2-cryptand)][$(C_5H_4SiMe_3)_3$Ln], but the observed hyperfine coupling of Y^{2+} varied depending on the substituents of the cyclopentadienyl ligand. Density functional theory calculations correlated the hyperfine coupling constants to the *s* orbital spin density on the Y center of the complexes. These [K(2.2.2-cryptand)][$(C_5H_3(SiMe_3)_2)_2LnCp^R$] complexes were less stable than their [K(2.2.2-cryptand)][$(C_5H_4SiMe_3)_3$Ln] analogues.

In Chapter 2, the synthesis and characterization of the homoleptic [K(2.2.2-cryptand)][$(C_5H_3(SiMe_3)_2)_3Ln$] (Ln = La, Ce, Pr, and Nd) is described. These [K(2.2.2-cryptand)][$(C_5H_3(SiMe_3)_2)_3Ln$] complexes also have properties similar to their monosilyl analogues, [K(2.2.2-cryptand)][$(C_5H_4SiMe_3)_3Ln$], and they are slightly less stable. This is in contrast to the result with the actinides, where the [K(2.2.2-cryptand)][$(C_5H_3(SiMe_3)_2)_3An$] complexes were significantly more stable than their [K(2.2.2-cryptand)][$(C_5H_4SiMe_3)_3An$] analogues.[43-45] In addition, the reactivity of [K(2.2.2-cryptand)][$(C_5H_3(SiMe_3)_2)_3Ln$] with 1,2-dimethoxyethane was studied to compare with the early results presented by Lappert and coworkers.[14,15] Lappert found that LnA_3/M reductions of $[C_5H_3(SiMe_3)_2]_3Ln$ in 1,2-dimethoxyethane gave methoxide products. In contrast, the reactions starting from the *bona fide* Ln^{2+} precursors, [K(2.2.2-cryptand)][$(C_5H_3(SiMe_3)_2)_3Ln$], did not give the analogous methoxide products. This indicates that the LnA_3/M and Ln^{2+} reductions are different.

Chapter 3 presents a survey of the reactivity with cyclooctatetraene of the three classes of Ln^{2+} ions obtained in the [K(2.2.2-cryptand)][$(C_5H_4SiMe_3)_3Ln$] series, *i.e.* the traditional $4f^{n+1}$ ions, the new $4f^n5d^1$ Ln^{2+} ions, and the configurational crossover Ln^{2+} ions. Three types of products formed, *i.e.* [K(2.2.2-cryptand)][$(C_5H_4SiMe_3)_2Ln(C_8H_8)$], [K(2.2.2-cryptand)][$Ln(C_8H_8)_2$], and [K(2.2.2-cryptand)][$(C_5H_4SiMe_3)_4Ln$]. It was concluded that the product distribution does not depend on the electron configuration of the Ln^{2+} reductant. Instead, the distribution appears to be more influenced by the size of the Ln^{3+} ion in the product.

Chapter 4 presents a study of an unusually stable bimetallic La^{2+} complex, [K(18-crown-6)$(THF)_2$][$((C_5H_3(SiMe_3)_2)_2La)_2(C_6H_6)$], bridged by a benzenide monoanion ligand $(C_6H_6)^{1-}$. Magnetometry measurements demonstrate that the $(C_6H_6)^{1-}$ ligand mediates magnetic exchange coupling between the two $5d^1$ La^{2+} ions. The reactivity of this three-electron-reductant was

analyzed with the substrates anthracene, naphthalene, and cyclooctatetraene to compare with the four-electron reduction chemistry of $[K(2.2.2\text{-cryptand})]_2[((C_5H_4SiMe_3)_2La)_2(C_6H_6)]$. It was concluded that although similar Ln^{3+} products $[K(chelate)][(cyclopentadienyl)_2Ln(substrate)]$ are obtained, the reactions with $[K(18\text{-crown-6})(THF)_2][((C_5H_3(SiMe_3)_2)_2La)_2(C_6H_6)]$ appear to be more complicated.

Chapter 5 describes the preparation and the structural characterization of new Ln^{2+} complexes with anionic arene ligands. These results demonstrate the structural variety of these complexes and suggest it is difficult to draw correlations between the oxidation states of the metal/arene and the planarity of the arene. The planarity appears to be more affected by the arrangement of the cyclopentadienyl ligands in the overall structure, which may be due to the crystal packing. Attempts to generate analogous complexes with the smaller lanthanides are also described.

In Chapter 6, a comparison of analogous $[K(2.2.2\text{-cryptand})][(({}^{Ad,Me}ArO)_3mes)M]$ complexes of Nd^{2+} and its congener U^{2+} is presented. Both Nd^{2+} and U^{2+} adopt nf^4 configurations with this ligand as opposed to their tris(cyclopentadenyl) complexes, which adopt nf^3d^1 configurations. Complexes of Gd, Dy, and Er are also described but their reduction products $[K(2.2.2\text{-cryptand})][(({}^{Ad,Me}ArO)_3mes)Ln]$ were found to co-crystallize with an unanticipated Ln^{3+}–H hydride product, $[K(2.2.2\text{-cryptand})][(({}^{Ad,Me}ArO)_3mes)LnH]$. It was concluded that Gd^{2+} in $[K(2.2.2\text{-cryptand})][(({}^{Ad,Me}ArO)_3mes)Gd]$ adopts the $4f^75d^1$ configuration as in $[K(2.2.2\text{-cryptand})][(C_5H_4SiMe_3)_3Gd]$.

Chapter 7 describes the extension of the tris(aryloxide)mesitylene chemistry to the early metals La, Ce, and Pr, and also to Sm and Yb. It was found that La, Ce, and Pr do not give Ln^{2+} products, but instead Ln^{3+} products bound to the reduced ligand radical, $[({}^{Ad,Me}ArO)_3mes]^{4-}$. The

Sm and Yb complexes adopt the $4f^{n+1}$ configurations expected for these "traditional" Ln^{2+} ions and display unique structural changes. The reduction products of these five metals, [K(2.2.2-cryptand)][((^{Ad,Me}ArO)$_3$mes)Ln] were obtained in pure form without any hydride contamination.

Chapter 8 presents a study that focuses on the tris(aryloxide)mesitylene chemistry of Y and La. The diamagnetic properties of these metals were exploited to provide more definitive characterization of the [K(2.2.2-cryptand)][((^{Ad,Me}ArO)$_3$mes)LnH] product that has contaminated the crystals of [K(2.2.2-cryptand)][((^{Ad,Me}ArO)$_3$mes)Ln] for Ln = Gd, Dy, and Er. The complex [K(2.2.2-cryptand)][((^{Ad,Me}ArO)$_3$mes)Y], like La, Ce, and Pr, was identified as a trivalent Y^{3+} complex bound to the ligand radical [(^{Ad,Me}ArO)$_3$mes]$^{4-}$. Like Gd, Dy and Er, [K(2.2.2-cryptand)][((^{Ad,Me}ArO)$_3$mes)Y] co-crystallizes with the hydride, [K(2.2.2-cryptand)][((^{Ad,Me}ArO)$_3$mes)YH], which could be definitively identified by its characteristic Y–H coupling. Additionally, a new La complex [K(2.2.2-cryptand)][((^{Ad,Me}ArO)$_3$($C_6Me_3(CH_2)_2CH$)La] was structurally characterized. This complex shows that the benzylic C–H bonds of the tris(aryloxide)mesitylene ligand can be activated.

Chapter 9 presents a structural study of $[C_5H_3(SiMe_3)_2]_2Sm$, $[C_5H_3(CMe_3)_2]_2Ln$ (Ln = Eu, Sm), and the mono(cyclopentadienyl) tetraphenylborate complex, $[C_5H_3(CMe_3)_2]_2Eu(\mu\text{-}\eta^6\text{:}\eta^1\text{-}Ph)_2BPh_2$. These $[C_5H_3(CMe_3)_2]_2Ln(\mu\text{-}\eta^6\text{:}\eta^1\text{-}Ph)_2BPh_2$ (Ln = Sm, Eu) compounds were prepared and investigated as synthons for Ln^{1+}. Treatment of $[C_5H_3(CMe_3)_2]_2Ln(\mu\text{-}\eta^6\text{:}\eta^1\text{-}Ph)_2BPh_2$ with potassium or potassium graphite, however, did not give observable Ln^{1+} products.

Chapter 10 presents a reactivity study of two $5d^1$ La^{2+} complexes, [K(2.2.2-cryptand)][$(C_5H_4SiMe_3)_3$La] and [K(2.2.2-cryptand)]$_2$[$(Cp'_2La)_2(C_6H_6)$], with diphenylacetylene. It was discovered that these $5d^1$ La^{2+} complexes reductively couple phenylacetylene to give a benzyldiphenyl-substituted indenyl anion. This type of chemistry is known with complexes that

deliver the equivalent of zirconocene, $(C_5H_5)_2Zr$, but reactions with Sm^{2+} and Dy^{2+} give trans- and cis-stilbene, respectively. This is the first example of transition metal-like reactivity from $5d^1$ La^{2+}.

Finally, additional results are reported in Appendix A. The results span many topics. Included are the titles: (1) Synthesis, Structure, and Reactivity of Tris(aryloxide)mesitylene Complexes Related to their Electrocatalytic Generation of H_2 from H_2O; (2) Synthesis and Structure of Solvated and Base-free Tris(amide) Complexes $Ln(NPh_2)_3(THF)_2$ (Ln = Y, Er) and $[(NPh_2)_2Ln(\mu\text{-}\eta^6\text{:}\eta^1\text{-Ph-}\kappa^1N\text{-NPh})]_2$ (Ln = Y, Dy); (3) Ligand Exchange Reactions of a Bimetallic La^{2+} Complex $[K(2.2.2\text{-cryptand})]_2[(Cp'La)_2(C_6H_6)]$ with $[N(SiMe_3)_2]^{1-}$ and $(C_5Me_5)^{1-}$; (4) Reactivity of $[K(2.2.2\text{-cryptand})][Cp'_3Ln]$ Complexes with Alkyl and Aryl

REFERENCES

(1) Reiners, C. S. *Chemie in unserer Zeit.* **2001**, *35*, 110-115.
(2) U.S. Department of Energy *Critical Materials Strategy* **2011**.
(3) Shannon, R. D. *Acta Crystallogr A* **1976**, *32*, 751-767.
(4) Crosswhite, H. M.; Crosswhite, H.; Carnall, W. T.; Paszek, A. P. *J. Chem. Phys.* **1980**, *72*, 5103-5117.
(5) Dieke, G. H.; Crosswhite, H. M.; Crosswhite, H. *Spectra and Energy Levels of Rare Earth Ions in Crystals*; Interscience Publishers, 1968.
(6) Klemm, W.; Schuth, W. *Z. Anorg. Allg. Chem.* **1929**, *184*, 352-358.
(7) Jantsch, G.; Grubitsch, H.; Hoffmann, F. *Z. Anorg. Allg. Chem.* **1929**, *185*, 49-64.
(8) Matignon, C. A.; Cazes, E. *C. R. Hebd. Seances Acad. Sci. Paris* **1906**, *142*, 83-85.
(9) Bochkarev, M. N.; Fedushkin, I. L.; Fagin, A. A.; Petrovskaya, T. V.; Ziller, J. W.; Broomhall-Dillard, R. N. R.; J., E. W. *Angew. Chem. Int. Ed.* **1997**, *36*, 133-135.
(10) Bochkarev, M. N.; Fedushkin, I. L.; Dechert, S.; Fagin, A. A.; Schumann, H. *Angew. Chem. Int. Ed.* **2001**, *40*, 3176-3178.
(11) Bochkarev, M. N.; Fagin, A. A. *Chem. Eur. J.* **1999**, *5*, 2990-2992.
(12) Morss, L. R. *Chem. Rev.* **1976**, *76*, 827-841.
(13) Cassani, M. C.; Gun'ko, Y. K.; Hitchcock, P. B.; Lappert, M. F. *Chem. Commun. (Cambridge, U.K.)* **1996**, *1996*, 1987-1988.
(14) Gun'ko, Y. K.; Hitchcock, P. B.; Lappert, M. F. *J. Organomet. Chem.* **1995**, *499*, 213-219.
(15) Cassani, M. C.; Lappert, M. F.; Laschi, F. *Chem. Commun.* **1997**, 1563-1564.
(16) Jaroschik, F.; Momin, A.; Nief, F.; Le Goff, X. F.; Deacon, G. B.; Junk, P. C. *Angew. Chem. Int. Ed.* **2009**, *48*, 1117-1121.

(17) Evans, W. J.; Davis, B. L.; Champagne, T. M.; Ziller, J. W. *Proc. Natl. Acad. Sci. U.S.A.* **2006**, *103*, 12678-12683.
(18) Evans, W. J.; Seibel, C. A.; Ziller, J. W. *J. Am. Chem. Soc.* **1998**, *120*, 6745-6752.
(19) Evans, W. J.; Forrestal, K. J.; Ziller, J. W. *J. Am. Chem. Soc.* **1998**, *120*, 9273-9282.
(20) Evans, W. J.; Davis, B. L.; Ziller, J. W. *Inorg. Chem.* **2001**, *40*, 6341-6348.
(21) Evans, W. J.; Perotti, J. M.; Kozimor, S. A.; Champagne, T. M.; Davis, B. L.; Nyce, G. W.; Fujimoto, C. H.; Clark, R. D.; Johnston, M. A.; Ziller, J. W. *Organometallics* **2005**, *24*, 3916-3931.
(22) Evans, W. J.; Schmiege, B. M.; Lorenz, S. E.; Miller, K. A.; Champagne, T. M.; Ziller, J. W.; DiPasquale, A. G.; Rheingold, A. L. *J. Am. Chem. Soc.* **2008**, *130*, 8555-8563.
(23) Evans, W. J.; Allen, N. T.; Ziller, J. W. *J. Am. Chem. Soc.* **2001**, *123*, 7927-7928.
(24) Evans, W. J.; Allen, N. T.; Ziller, J. W. *Angew. Chem.* **2002**, *41*, 359-361.
(25) Evans, W. J.; Lee, D. S.; Lie, C.; Ziller, J. W. *Angew. Chem. Int. Ed.* **2004**, *43*, 5517.
(26) Evans, W. J.; Lee, D. S.; Rego, D. B.; Perotti, J. M.; Kozimor, S. A.; Moore, E. K.; Ziller, J. W. *J. Am. Chem. Soc.* **2004**, *126*, 14574-14582.
(27) Evans, W. J.; Lee, D. S. *Can. J. Chem.* **2005**, *83*, 375-384.
(28) Evans, W. J.; Rego, D. B.; Ziller, J. W. *Inorg. Chem.* **2006**, *45*, 10790-10798.
(29) Evans, W. J. *Inorg. Chem.* **2007**, *46*, 3435-3449.
(30) Evans, W. J.; Fang, M.; Zucchi, G.; Furche, F.; Ziller, J. W.; Hoekstra, R. M.; Zink, J. I. *J. Am. Chem. Soc.* **2009**, *131*, 11195-11202.
(31) Schmiege, B. M.; Ziller, J. W.; Evans, W. J. *Inorg. Chem.* **2010**, *49*, 10506-10511.
(32) Demir, S.; Lorenz, S. E.; Fang, M.; Furche, F.; Meyer, G.; Ziller, J. W.; Evans, W. J. *J. Am. Chem. Soc.* **2010**, *132*, 11151-11158.
(33) Fang, M.; Bates, J. E.; Lorenz, S. E.; Lee, D. S.; Rego, D. B.; Ziller, J. W.; Furche, F.; Evans, W. J. *Inorg. Chem.* **2011**, *50*, 1459-1469.
(34) Fang, M.; Lee, D. S.; Ziller, J. W.; Doedens, R. J.; Bates, J. E.; Furche, F.; Evans, W. J. *J. Am. Chem. Soc.* **2011**, *133*, 3784-3787.
(35) Hitchcock, P. B.; Lappert, M. F.; Maron, L.; Protchenko, A. V. *Angew. Chem. Int. Ed.* **2008**, *47*, 1488-1491.
(36) MacDonald, M. R.; Ziller, J. W.; Evans, W. J. *J. Am. Chem. Soc.* **2011**, *133*, 15914-159147.
(37) MacDonald, M. R.; Bates, J. E.; Fieser, M. E.; Ziller, J. W.; Furche, F.; Evans, W. J. *J. Am. Chem. Soc.* **2012**, *134*, 8420-8423.
(38) MacDonald, M. R.; Bates, J. E.; Ziller, J. W.; Furche, F.; Evans, W. J. *J. Am. Chem. Soc.* **2013**, *135*, 9857-9868.
(39) Fieser, M. E.; MacDonald, M. R.; Krull, B. T.; Bates, J. E.; Ziller, J. W.; Furche, F.; Evans, W. J. *J. Am. Chem. Soc.* **2015**, *137*, 369-382.
(40) Woen, D. H.; Evans, W. J. In *Handbook on the Physics and Chemistry of Rare Earths*; 1st ed.; Elsevier: Amsterdam, 2016; Vol. 50, p 337-394.
(41) Evans, W. J. *Organometallics* **2016**, *35*, 3088-3100.
(42) MacDonald, M. R.; Fieser, M. E.; Bates, J. E.; Ziller, J. W.; Furche, F.; Evans, W. J. *J. Am. Chem. Soc.* **2013**, *135*, 13310-13313.

(43) Windorff, C. J.; MacDonald, M. R.; Meihaus, M. R.; Ziller, J. W.; Long, J. R.; Evans, W. J. *Chem. Eur. J.* **2016**, *22*, 772-782.
(44) Langeslay, R. R.; Fieser, M. E.; Ziller, J. W.; Furche, F.; Evans, W. J. *Chem. Sci.* **2015**, *6*, 517-521.
(45) Windorff, C. J.; Chen, G. P.; Cross, J. N.; Evans, W. J.; Furche, F.; Gaunt, A. J.; Janicke, M. T.; Kozimor, S. A.; Scott, B. L. *J. Am. Chem. Soc.* **2017**, *139*, 3970-3973.

CHAPTER 1

Ligand Effects in the Synthesis of Ln^{2+} Complexes by Reduction of Heteroleptic Tris(cyclopentadienyl) Precursors

INTRODUCTION†

The reduction chemistry of yttrium and the *f* elements has shown that +2 ions are available for yttrium,[1] all the lanthanides[2-5] (except promethium, which was not studied due to its radioactivity), thorium,[6] uranium,[7,8] and plutonium.[9] These new oxidation states have been obtained by reduction of the tris(cyclopentadienyl) complexes, Cp'_3M and Cp''_3M [Cp' = $C_5H_4SiMe_3$, M = Y, lanthanide, U; Cp'' = $C_5H_3(SiMe_3)_2$, M = La, Ce, Th, U, Pu] to form $(Cp'_3M)^{1-}$ and $(Cp''_3M)^{1-}$ complexes, eq 1.1.

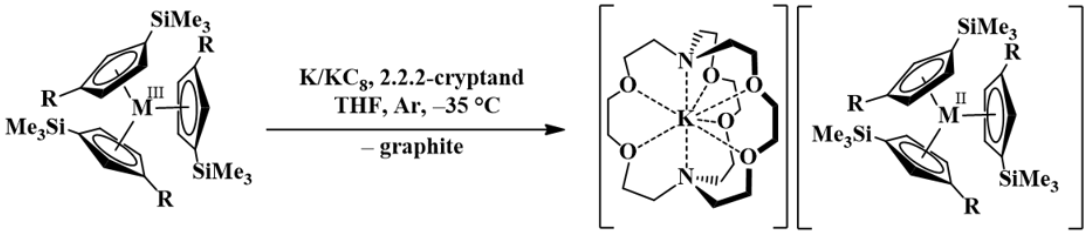

(1.1)

R = $SiMe_3$; M = La, Th, U, Pu
R = H; M = Y, La, Ce, Pr, Nd, Sm, Gd, Tb, Dy, Ho, Er, Tm, Lu, U

Structural, spectroscopic, and density functional theory analyses suggest that these new ions could be accessed for the first time because the $(Cp'_3)^{3-}$ and $(Cp''_3)^{3-}$ ligand sets allow the d_z^2 orbital to be populated such that the new ions have $4f^n5d^1$ electron configurations for the lanthanides, $5f^36d^1$ for uranium, $6d^2$ for thorium, and $4d^1$ for yttrium. This is consistent with numerous theoretical analyses of the f elements in trigonal tris(cyclopentadienyl) coordination environments.[10-15] Whereas reduction of a $4f^n$ Ln^{3+} ion to a $4f^{n+1}$ Ln^{2+} product would be difficult

† Portions of this chapter have been published: Corbey, J. F.; Woen, D. H.; Palumbo, C. T.; Fieser, M. E.; Ziller, J. W.; Furche, F.; Evans, W. J. *Organometallics*,. **2015**, *34*, 3909-3921.

due to the highly negative calculated generic reduction potentials for such a process (−2.7 to −3.9 V vs NHE[16,17]), reduction to $4f^n5d^1$ ions appears to be achievable.

Although these new ions are now isolable in molecules, the complexes are highly reactive. They must be synthesized at low temperature or with very short reactions times and should be stored at low temperature. Physical characterization of the complexes of the new ions is challenging, since decomposition can occur in the course of preparing the samples and making the measurements. This Chapter describes attempts to prepare more stable variants of these complexes for physical characterization studies. Specifically, mixed ligand tris(cyclopentadienyl) complexes, [K(2.2.2-cryptand)][Cp''_2LnCp^R] (Ln = Gd, Y; Cp^R = C_5H_5, **1-Ln**; C_5H_4Me, **2-Ln**), have been prepared since a combination of these ligands could give enhanced stability. Also included is an analysis of their thermal stability.

Yttrium was chosen as the primary metal for this investigation, since EPR spectroscopy can provide good evidence for the presence of Y^{2+} due to the 100% naturally abundant ^{89}Y nucleus that gives a doublet signal for this ion.[1,18] Reductions with the larger rare earth, gadolinium, were also investigated since the EPR spectrum of [K(2.2.2-cryptand)][Cp'_3Gd] is a relatively sharp singlet at room temperature.[3] Earlier studies by Lappert and co-workers comparing Cp''_3Ln with Cp^{tt}_3Ln [Cp^{tt} = $C_5H_3(CMe_3)_2$] suggest that trimethylsilyl-substituted complexes are less difficult to reduce than their alkyl analogs,[19] but steric effects, particularly for the smaller rare earth metals, could also affect stability. The effects of silyl substitution on complexes of cyclopentadienyl ligands have been examined in a number of systems,[19-21] but it appears that the specific effect is system dependent.[22]

EXPERIMENTAL

All manipulations and syntheses described below were conducted with rigorous exclusion of air and water using standard Schlenk line and glovebox techniques under an argon or dinitrogen atmosphere. Solvents were sparged with UHP argon and dried by passage through columns containing Q-5 and molecular sieves prior to use. Deuterated NMR solvents were dried over NaK alloy, degassed by three freeze-pump-thaw cycles, and vacuum transferred before use. Indene, dicyclopentadiene, and methylcyclopentadiene were dried over molecular sieves and degassed by three freeze-pump-thaw cycles. KC_5H_5 and NaC_5H_4Me were synthesized via an adaptation of a literature procedure[23] in which the organic dimer is cracked and distilled onto a toluene solution of $KN(SiMe_3)_2$ or $NaN(SiMe_3)_2$, respectively. The resulting white precipitate was then washed with hexane and dried. KC_8,[24] anhydrous $LnCl_3$[25] (Ln = Y, Gd), $GdI_3(THF)_{3.5}$,[26] Cp''_3Ln (Ln = Y, Gd),[27] Cp''_2YI,[28] and $(Cp''_2GdCl)_2$[27] were prepared according to the literature. ^1H NMR spectra were recorded on Bruker GN500 or CRYO500 MHz spectrometers (^{13}C NMR at 125 MHz) at 298 K unless otherwise stated and referenced internally to residual protio-solvent resonances. Electron paramagnetic resonance spectra were collected using a Bruker EMX spectrometer equipped with an ER041XG microwave bridge in THF at 298 K and 77 K unless otherwise specified. EPR simulations were performed using P.E.S.T. WinSim developed by the National Institutes of Environmental Health Sciences or EasySpin.[29] Electronic absorption spectra were collected using a Varian Cary 50 Scan UV-vis spectrophotometer in THF at 298 K. IR samples were prepared as KBr pellets on a Varian 1000 FT-IR system. Elemental analyses were conducted on a Perkin-Elmer 2400 Series II CHNS elemental analyzer.

$Cp''_2YCp/Cp''YCp_2$, 3-Y/4-Y. In a glovebox free of coordinating solvents, a white slurry of KCp (30 mg, 0.29 mmol) in toluene (5 mL) was added to a gray slurry of Cp''_2YI (160 mg,

0.252 mmol) in toluene (5 mL). After stirring overnight, the resulting pale yellow slurry was centrifuged to remove white insoluble material. The yellow supernatant was filtered, solvent was removed under reduced pressure, and the product was extracted using hexane. The extract was filtered and solvent was removed under reduced pressure to yield a waxy yellow solid (121 mg). The NMR spectrum was consistent with a mixture of **3-Y** and **4-Y** in an approximate ratio of 3:1. ^{1}H NMR of the major product **3-Y** (C_6D_6): δ 6.91 (td, $^{4}J_{HH}$ = 1.98, J_{HY} = 0.59 Hz, $C_5H_3(SiMe_3)_2$, 2H), 6.70 (dd, $^{4}J_{HH}$ = 1.98, J_{HY} = 0.65 Hz, $C_5H_3(SiMe_3)_2$, 4H), 6.36 (s, C_5H_5, 5H), 0.25 (s, SiMe_3, 36H). ^{13}C NMR (C_6D_6): δ 134.87, 125.27, 114.50, 113.89. Re-crystallization from hexane of the 3:1 mixture gave solids with the ratio reversed to approximately 1:3 of **3-Y** to **4-Y**. ^{1}H NMR of the major product **4-Y** (C_6D_6): δ 6.83 [s, $C_5H_3(SiMe_3)_2$, 1H], 6.53 [br m, $C_5H_3(SiMe_3)_2$, 2H], 6.10 (s, C_5H_5, 10H), 0.14 (s, SiMe_3, 18H).

Cp″$_2$GdCp/Cp″GdCp$_2$, 3-Gd/4-Gd. Following the procedure for **3-Y/4-Y**, KCp (17 mg, 0.165 mmol) was added to (Cp″$_2$GdCl)$_2$ (100 mg, 0.0820 mmol) to yield a waxy green-yellow solid (75 mg) after work up. The paramagnetism of Gd^{3+} precluded NMR analysis, and the mixture was used as formed.

Cp″$_2$YCp^{Me}/Cp″YCp$^{Me}_2$, 5-Y/6-Y. Similar to the procedure for **3-Y/4-Y**, NaCp^{Me} (30 mg, 0.29 mmol) was added to Cp″$_2$YI (158 mg, 0.249 mmol) to yield a yellow waxy solid (131 mg). NMR spectroscopy was consistent with a 3:1 mixture of **5-Y** and **6-Y**. ^{1}H NMR of the major product **5-Y** (C_6D_6): δ 6.95 [td, $^{4}J_{HH}$ = 1.99, J_{HY} = 0.59 Hz, $C_5H_3(SiMe_3)_2$, 2H], 6.75 [dd,$^{4}J_{HH}$ = 1.98, J_{HY} = 0.65 Hz, $C_5H_3(SiMe_3)_2$, 4H], 6.21 (m, C_5H_4Me, 4H), 2.15 (s, C_5H_4Me, 3H), 0.27 (s, 36 H, SiMe_3). ^{13}C NMR (C_6D_6): δ 134.72, 125.36, 124.79, 116.45, 113.11, 112.30, 16.07.

Cp″$_2$GdCp^{Me}/Cp″GdCp$^{Me}_2$, 5-Gd/6-Gd. Similar to the procedure for **3-Y/4-Y**, NaCp^{Me} (17 mg, 0.17 mmol) was added to Cp″$_2$GdI [100 mg, 0.142 mmol, prepared from $GdI_3(THF)_{3.5}$

(1.53 g, 1.93 mmol) and KCp″ (1.00 g, 4.03 mmol) as an off-white solid (1.11 g, 82%) to yield a waxy green-yellow solid (75 mg), which was used as formed.

Generic Reduction Method. An empty scintillation vial, a flash reduction column[2,3] packed with excess KC_8, a pipette for solution transfer, a glass beaker, and a vial containing hexane were pre-chilled to −35 °C in a glovebox freezer. In the glovebox, the empty vial was placed in the beaker containing cold hexane. A pre-chilled solution in THF or Et_2O containing the tris(cyclopentadienyl)lanthanide precursor and 2.2.2-cryptand was then passed through the flash reduction column of KC_8 in less than a minute into the empty vial. The column containing black graphite and residual bronze KC_8 was removed from the vial and the resultant dark purple and red solutions for Y^{2+} and Gd^{2+}, respectively, pipetted into another vial under a layer of hexane. This mixture was stored in the freezer for crystallization.

EPR Characterization. For the reduction products of Cp''_3Ln, Cp''_2LnCp, Cp''_2LnCp^{Me} (Ln = Gd, Y), Cp_3Y, and Cp^{Me}_3Y, ~10 mM solutions containing these precursors with 2.2.2-cryptand in THF were pre-chilled to −35 °C in a glovebox freezer before they were passed through a flash reduction column of KC_8 into a cold EPR tube chilled in cold hexane. The solutions were dark purple for Y^{2+} and dark red for Gd^{2+}. The EPR tube was taken out of the glovebox and immediately cooled in liquid nitrogen. EPR characterization was performed at 77 K and room temperature.

[K(2.2.2-cryptand)][Cp″$_2$YCp], 1-Y. In an argon-filled glovebox, 88 mg of the 3:1 mixture of **3-Y** and **4-Y** (approx 70 mg, 0.12 mmol of **3-Y**) and 2.2.2-cryptand (58 mg, 0.15 mmol) were combined, dissolved in Et_2O (4 mL) and cooled to −35 °C. This solution was passed through a pre-chilled flash reduction column packed with excess KC_8. The dark-violet filtrate was collected in a pre-chilled vial and was kept cool using a cold hexane bath. Layering the solution

with cold hexane (14 mL, −35 °C) and storing at −35 °C for 24 h produced **1-Y** as a black microcrystalline solid (80 mg). Black crystals of **1-Y** suitable for X-ray diffraction were grown from a solution in THF (4 mL) layered with hexane (14 mL). Anal. Calcd for $C_{45}H_{83}KN_2O_6Si_4Y$: C, 54.68; H, 8.46; N, 2.83. Found: C, 54.78; H, 8.44; N, 2.59. IR: 3058w, 2950s, 2888s, 2817s, 1479m, 1446m, 1399w, 1360s, 1299m, 1242s, 1208m, 1174w, 1134s, 1105s, 1077s, 1012w, 951s, 924s, 832s, 746s, 676w, 631m cm^{-1}. UV-vis λ_{max}, nm (ε, M^{-1} cm^{-1}): 290 (4800 shoulder), 400 (1400 shoulder), 550 (2100), 708 (600 shoulder).

[K(2.2.2-cryptand)][Cp″$_2$GdCp], 1-Gd. Following the procedure for **1-Y**, 75 mg of the mixture of **3-Gd** and **4-Gd** and 2.2.2-cryptand (40 mg, 0.11 mmol) were passed through a pre-chilled flash reduction column packed with excess KC_8 at −35 °C producing **1-Gd** as a black microcrystalline solid (79 mg). Black crystals of **1-Gd** suitable for X-ray diffraction were grown from a solution in THF (4 mL) layered with hexane (14 mL). Anal. Calcd for $C_{45}H_{83}KN_2O_6Si_4Gd$: C, 51.14; H, 7.97; N, 2.65. Found: C, 50.88; H, 7.60; N, 2.33IR: 3072w, 2949s, 2888s, 2816s, 1479m, 1446m, 1356s, 1299m, 1242s, 1210m, 1132s, 1105s, 1077s, 1009w, 951m, 924m, 831s, 743s, 678w, 635m cm^{-1}. UV-vis λ_{max}, nm (ε, M^{-1} cm^{-1}): 285 (12600), 390 (7300 shoulder), 505 (8800), 650 (2100 shoulder).

[K(2.2.2-cryptand)][Cp″$_2$YCp^{Me}], 2-Y. Similar to the procedure for **1-Y**, in an argon-filled glovebox, 63 mg of the 3:1 mixture of **5-Y** and **6-Y** (approx. 50 mg, 0.085 mmol of **5-Y**) and 2.2.2-cryptand (40 mg, 0.11 mmol) were passed through a pre-chilled flash reduction column packed with excess KC_8 at −35 °C to produce **5-Y** as a black microcrystalline solid (84 mg). Anal. Calcd for $C_{46}H_{85}KN_2O_6Si_4Y$: C, 55.11; H, 8.55; N, 2.79. Found: C, 54.70; H, 8.60; N, 2.53. IR: 3078w, 2950s, 2888s, 2817s, 1479m, 1447m, 1397w, 1360s, 1298m, 1243s, 1205m, 1175w,

1139s, 1104s, 1076s, 951s, 924s, 836s, 749m, 679w, 627m cm^{-1}. UV-vis (THF) λ_{max}, nm (ε, M^{-1} cm^{-1}): 300 (3800 shoulder), 400 (1100 shoulder), 551 (1600), 710 (500).

[K(2.2.2-cryptand)][Cp″$_2$GdCp^{Me}], 2-Gd. Similar to the procedure for **1-Y**, 69 mg of the mixture of **5-Gd** and **6-Gd** and 2.2.2-cryptand (40 mg, 0.11 mmol) were passed through a pre-chilled flash reduction column packed with excess KC_8 at −35 °C to produce **2-Gd** as a black microcrystalline solid (56 mg). Anal. Calcd for $C_{46}H_{85}KN_2O_6Si_4Gd$: C, 51.59; H, 8.00; N, 2.62. Found: C, 51.03; H, 7.91; N, 2.39. IR: 3075w, 2951s, 2889s, 2819m, 1598w, 1562w, 1478m, 1449m, 1355s, 1300m, 1243s, 1208m, 1174w, 1133m, 1103s, 1076s, 951s, 924s, 833s, 754m, 677w, 627m cm^{-1}. UV-vis (THF) λ_{max}, nm (ε, M^{-1} cm^{-1}): 232 (14800), 410 (3400), 505 (4000), 640 (1100).

X-ray Data Collection, Structure Solution and Refinement for [(2.2.2-cryptand)][Cp″$_2$YCp], 2-Y. A black crystal of approximate dimensions 0.280 x 0.232 x 0.096 mm was mounted on a glass fiber and transferred to a Bruker SMART APEX II diffractometer. The APEX2[30] program package was used to determine the unit-cell parameters and for data collection (30 sec/frame scan time for a sphere of diffraction data). The raw frame data was processed using SAINT[31] and SADABS[32] to yield the reflection data file. Subsequent calculations were carried out using the SHELXTL[33] program. There were no systematic absences nor any diffraction symmetry other than the Friedel condition. The centrosymmetric triclinic space group $P\bar{1}$ was assigned and later determined to be correct. The structure was solved by direct methods and refined on F^2 by full-matrix least-squares techniques. The analytical scattering factors[34] for neutral atoms were used throughout the analysis. There were three molecules of the formula-unit and four molecules of tetrahydrofuran solvent present, (Z = 6). Atoms O(2), O(7), O(8), C(30), C(31), C(50), C(51), and C(53) were disordered and included using multiple components with

partial site-occupancy-factors. Hydrogen atoms were included using a riding model. Least-squares analysis yielded wR2 = 0.1672 and Goof = 1.001 for 1797 variables refined against 42773 data (0.75 Å), R1 = 0.0625 for those 27921 data with I > 2.0σ(I). Details are given in Table 1.1.

X-ray Data Collection, Structure Solution and Refinement for [(2.2.2-cryptand)][Cp″$_2$GdCp], 2-Gd. A red crystal of approximate dimensions 0.284 x 0.113 x 0.042 mm was mounted on a glass fiber and transferred to a Bruker SMART APEX II diffractometer. The APEX2[30] program package was used to determine the unit-cell parameters and for data collection (60 sec/frame scan time for a sphere of diffraction data). The raw frame data was processed using SAINT[31] and SADABS[32] to yield the reflection data file. Subsequent calculations were carried out using the SHELXTL[33] program. There were no systematic absences nor any diffraction symmetry other than the Friedel condition. The centrosymmetric triclinic space group $P\bar{1}$ was assigned and later determined to be correct. The structure was solved using the coordinates from **3-Y**. The analytical scattering factors[34] for neutral atoms were used throughout the analysis. There were three molecules of the formula-unit and four molecules of tetrahyrofuran solvent molecules present, (Z = 6). Atoms O(2), O(8), C(30), C(31), C(47), C(50), C(51), and C(53) were disordered and included using multiple components with partial site-occupancy-factors. Hydrogen atoms were included using a riding model. At convergence, wR2 = 0.1112 and Goof = 0.994 for 1777 variables refined against 42965 data (0.75 Å), R1 = 0.0534 for those 27338 data with I > 2.0σ(I). Details are given in Table 1.1.

RESULTS

Synthesis of Heteroleptic Ln^{3+} Precursors. The complexes, $(C_5Me_5)_2Ln(\mu\text{-}Ph_2)BPh_2$ and $(C_5Me_5)_2MCl$**(**THF), have been shown to be good precursors for heteroleptic Ln^{3+} compounds.[35-37]

Another complex that was thought to be an appropriate precursor for the desired complexes is the known iodide, Cp''_2YI.[28] The precursor $(Cp''_2GdCl)_2$ was also used.[27]

Reactions with Cp''_2YI were complicated by the formation of mixtures of products. When Cp''_2YI was stirred with KCp or $NaCp^{Me}$ for 4 h, ^1H NMR spectroscopy indicated 3:1 mixtures of $Cp''_2YCp/Cp''YCp_2$, **3-Y/4-Y** and $Cp''_2YCp^{Me}/Cp''YCp^{Me}_2$, **5-Y/6-Y**, eq 1.2. The distribution did not change upon stirring overnight. Crystals isolated from a concentrated pentane solution of the **3-Y**/**4-Y** mixture gave solids with the ratio reversed to 1:3. Heating up the NMR sample of the 3:1 mixture in a J-Young tube produced no change in the spectrum.

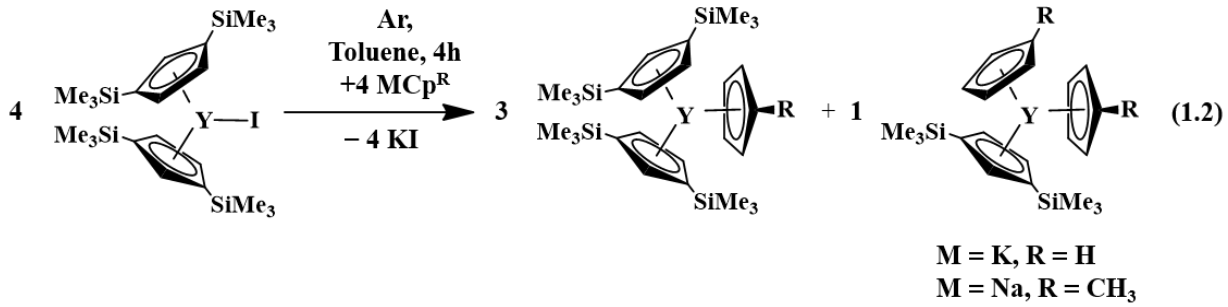

The syntheses of heteroleptic gadolinium compounds were attempted via reactions of $(Cp''_2GdCl)_2$ with the appropriate alkali cyclopentadienyl salt in toluene. Bright green slurries resulted and the removal of the KCl yielded green waxy solids that were presumed to be mixtures of Cp''_2GdCp/Cp''_2GdCp_2, **3-Gd/4-Gd**, and $Cp''_2GdCp^{Me}/Cp''GdCp^{Me}_2$, **5-Gd/6-Gd**. The paramagnetism of Gd^{3+} precluded NMR analysis and a concentrated pentane solution only produced opaque green solids that were not suitable for X-ray diffraction. Hence, the purity of the product mixtures were unclear and they were used as formed assuming that the Cp''_2GdCp^R products were the major products as in the yttrium analogs.

Yttrium Reduction Reactions. Reduction reactions were conducted with Cp''_3Y, with the **3-Y/4-Y** mixture, and with the **5-Y**/**6-6** mixture. In each of these three cases, reduction with potassium graphite in the presence of 2.2.2-cryptand generates dark EPR active solutions like the

reduction of Cp'_3Y to make $[K(2.2.2\text{-cryptand}][Cp'_3Y]^3$ **(**$Cp' = C_5H_4SiMe_3$). EPR spectra of these compounds were obtained by transferring the freshly-made cold solution to an EPR tube and freezing it in liquid nitrogen until it was inserted into the spectrometer. The EPR spectra of the reduction products obtained at room temperature are shown in Figure 1.1 along with simulated spectra. The *g* values and hyperfine coupling constants are given in Table 1.2.

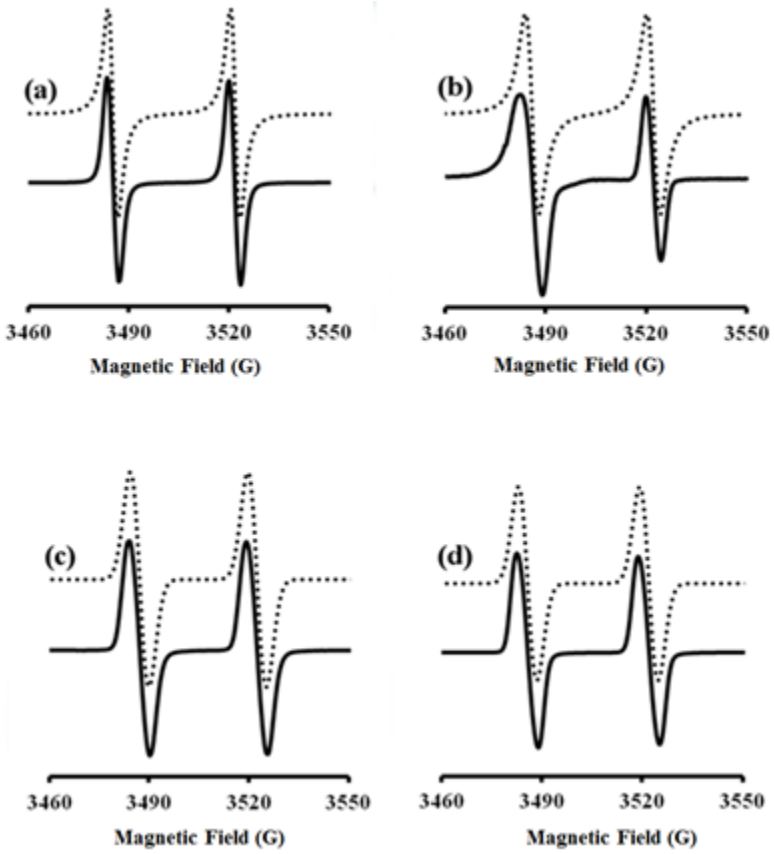

Figure 1.1. Experimental (solid) and simulated (dotted) X-band EPR spectra of solutions after reduction of (a) Cp'_3Y,[1,3] (b) Cp''_3Y, (c) 3:1 **3-Y/4-Y**, and (d) 3:1 **5-Y/6-Y** using KC_8 in the presence of 2.2.2-cryptand at 298 K.

Although EPR spectra indicating the presence of Y^{2+} were obtained from each reaction, the only system that gave crystals of the reduction product that were isolable and characterizable

by X-ray diffraction was the reduction of a 3:1 mixture of $Cp''_2YCp/Cp''YCp_2$, eq 1.3. This reaction produced crystals of [K(2.2.2-cryptand)][Cp''_2YCp], **1-Y**, Figure 1.2, upon layering a dark THF solution with cold hexane and storing the layered mixture at −35 °C. No evidence for the other possible product, $[Cp''YCp_2]^{1-}$, was observed by crystallography or EPR spectroscopy.

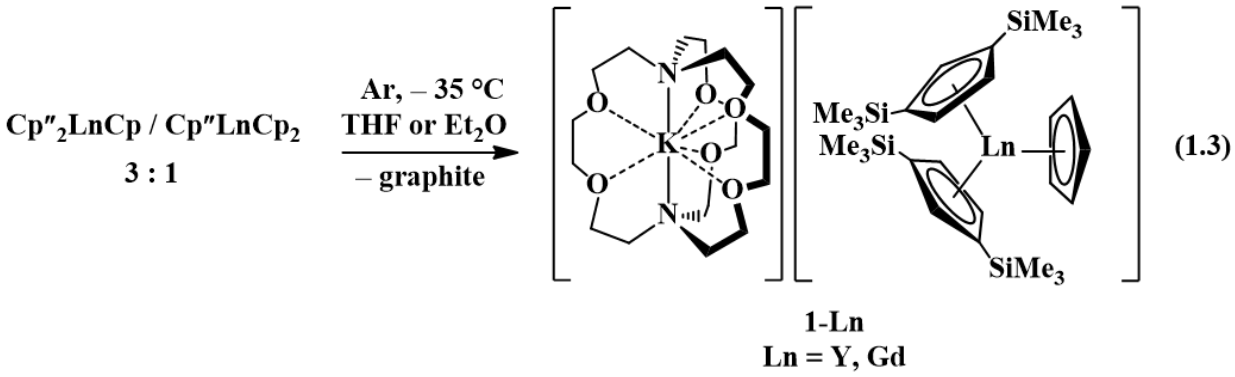

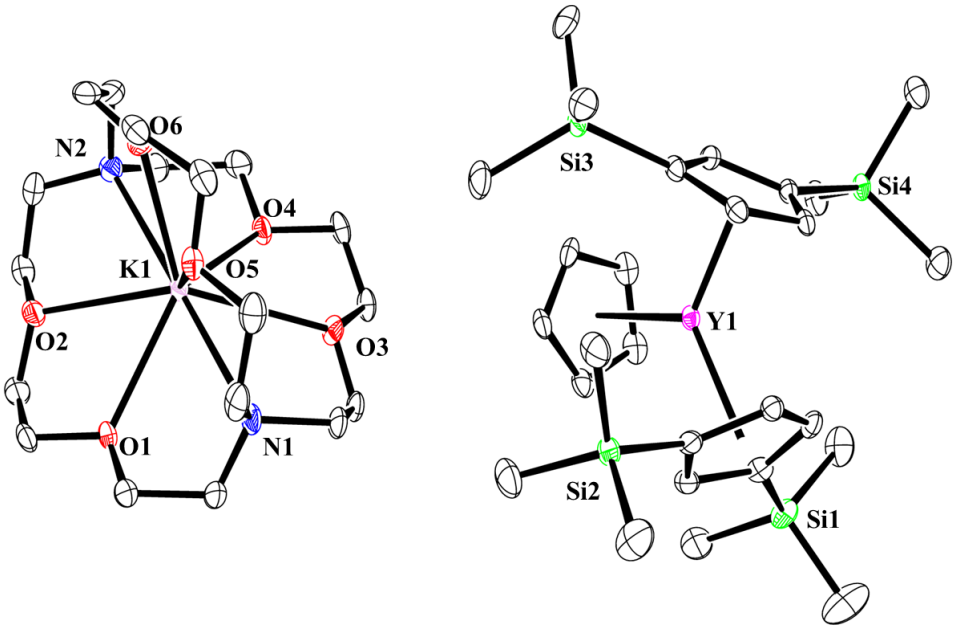

Figure 1.2. Thermal ellipsoid plot of [K(2.2.2-cryptand)][Cp''_2YCp], **1-Y**, drawn at the 50% probability level. Hydrogen atoms and co-crystallized solvent molecules are omitted for clarity. [K(2.2.2-cryptand)][Cp''_2GdCp], **1-Gd**, is isomorphous.

The metrical parameters of **1-Y** and [K(2.2.2-cryptand)][Cp'_3Y][3] are shown in Table 1.3. The ranges of distances for the three independent molecules in the asymmetric unit of **1-Y** are presented. The Y–Cp distances and angles in [K(2.2.2-cryptand)][Cp'_3Y] are very similar to those in **1-Y**, suggesting that this heteroleptic $(Cp''_2Cp)^{3-}$ ligand environment is similar to the homoleptic $(Cp'_3)^{3-}$. Crystals of [K(2.2.2-cryptand)][Cp''_2YCp^{Me}], **2-Y**, were obtained but were not characterizable by X-ray diffraction.

Gadolinium Reduction Reactions. Reduction reactions using the best of the ligand combinations determined for yttrium were examined with the larger metal gadolinium since Gd^{2+} can be observed by EPR spectroscopy.[3] Treatment of Cp''_3Gd, the **3-Gd/4-Gd** mixture, and the **5-Gd/6-Gd** mixture with potassium graphite in each case also gave dark EPR active solutions. The experimental and simulated EPR spectra and their respective *g* values, shown in Figure 1.3 and Table 1.4, respectively, are similar to those of [K(2.2.2-cryptand][Cp'_3Gd][3] and

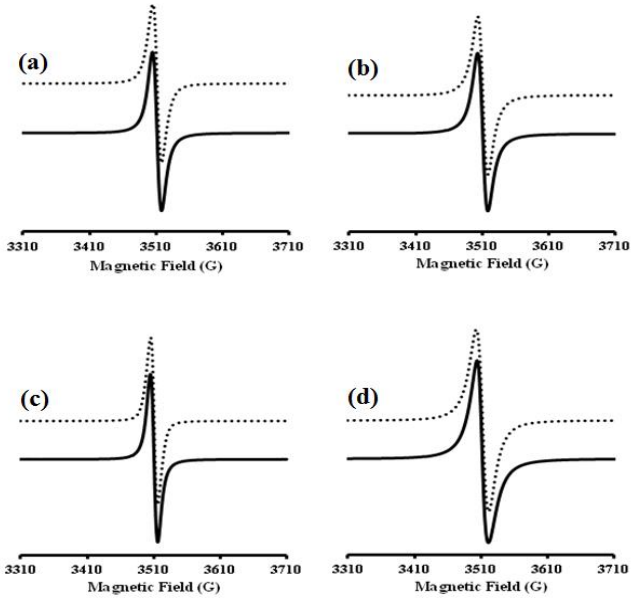

Figure 1.3. Experimental (solid) and simulated (dotted) X-band EPR spectra of solutions after the reduction of (a) Cp'_3Gd,[3] (b) Cp''_3Gd, (c) **3-Gd/4-Gd**, and (d) **5-Gd/6-Gd** in the presence of 2.2.2-cryptand at 298 K.

are therefore consistent with the presence of Gd^{2+}. As in the yttrium series, the only crystallographically characterizable reduction product was a mixed ligand complex, [K(2.2.2-cryptand)][Cp″$_2$GdCp], **1-Gd**, which is isomorphous with **1-Y**. A comparison of bond distances and angles with [K(2.2.2-cryptand][Cp′$_3$Gd][3] is given in Table 1.3. These data parallel those of [K(2.2.2-cryptand][Cp′$_3$Y] and **1-Y** when considering the larger size of gadolinium with respect to yttrium.

Thermal Stability. The thermal stability of [K(2.2.2-cryptand)][Cp″$_2$LnCp], **1-Y**, and **1-Gd**, and [K(2.2.2-cryptand)][Cp″$_2$LnCp^{Me}], **2-Y** and **2-Gd**, in THF was evaluated by monitoring the disappearance of the most intense absorption at λ_{max} near 550 nm for **1-Y** and **2-Y** and λ_{max} near 510 nm for **1-Gd** and **2-Gd**. The UV-vis absorption spectra of **1-Y** and **2-Y** are shown below in Figure 1.4. Compounds **1-Gd** and **2-Gd** are shown in Figure 1.5. Similarly, the kinetic plots of **1-Y** and **2-Y** are shown in Figure 1.6 and the kinetic plots of **1-Gd** and **2-Gd** are shown in Figure 1.7. Compounds [K(2.2.2-cryptand][Cp′$_3$Ln][3] (Ln = Y, Gd) have been added to Figures 1.4 - 1.7 for comparison.

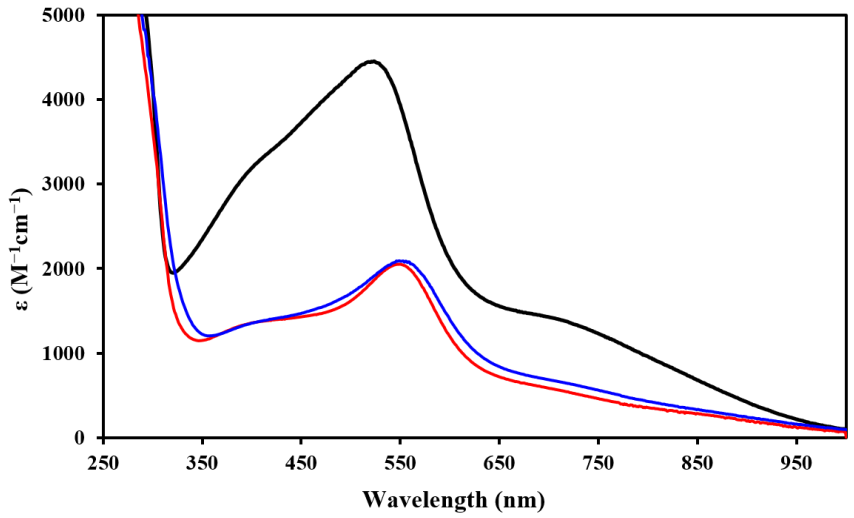

Figure 1.4. Experimental UV-Vis spectra of [K(2.2.2-cryptand)][Cp′$_3$Y][3] (black, top), [K(2.2.2-cryptand)][Cp″$_2$YCp], **1-Y** (red, bottom), and [K(2.2.2-cryptand)][Cp″$_2$YCp^{Me}], **2-Y** (blue, middle), in THF at 298 K.

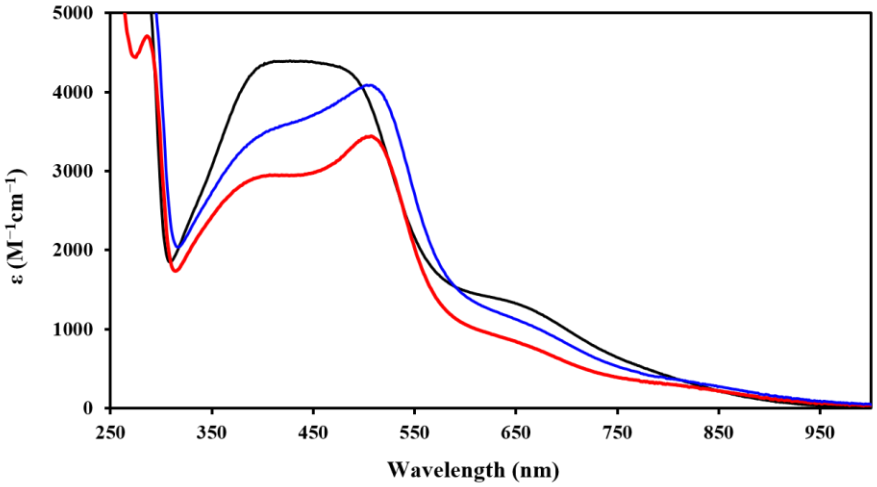

Figure 1.5. Experimental UV-Vis spectra of [K(2.2.2-cryptand)][Cp′$_3$Gd][3] (black, top at 450 nm), [K(2.2.2-cryptand)][Cp″$_2$GdCp], **1-Gd** (red, bottom at 450 nm), and [K(2.2.2-cryptand)][Cp″$_2$GdCp^{Me}], **2-Gd** (blue, middle at 450 nm), in THF at 298 K.

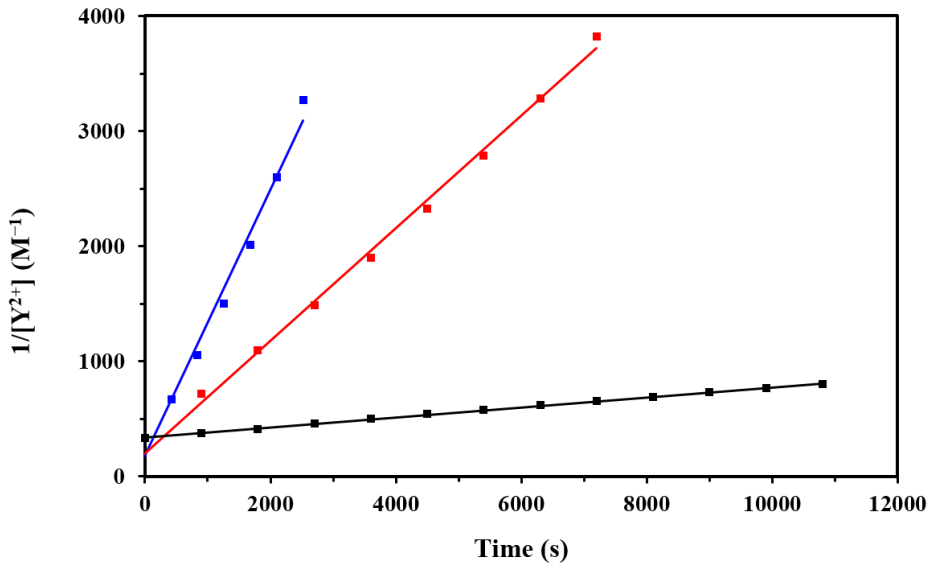

Figure 1.6. Kinetic data for the decomposition of 3 mM solutions of [K(2.2.2-cryptand)][Cp′$_3$Y][3] (black, bottom), [K(2.2.2-cryptand)][Cp″$_2$YCp], **1-Y** (red, middle), and [K(2.2.2-cryptand)][Cp″$_2$YCp^{Me}], **2-Y** (blue, top), in THF under argon at 298 K.

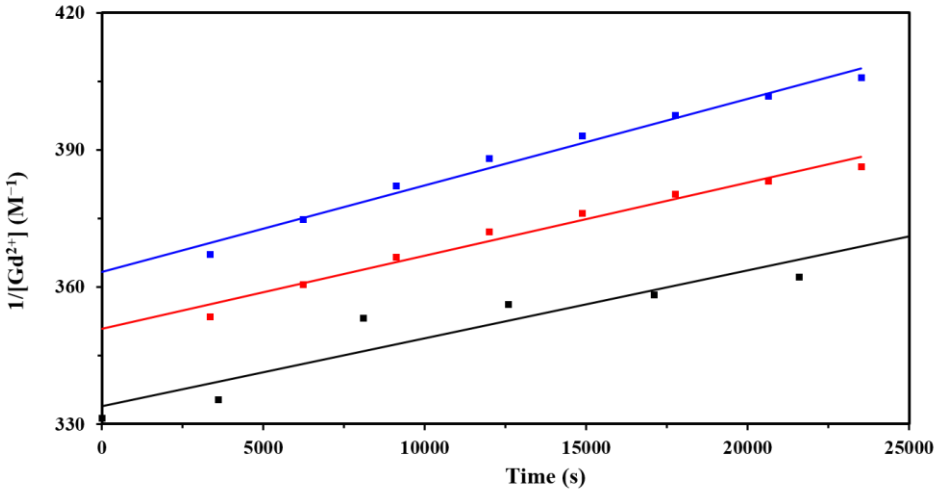

Figure 1.7. Kinetic data for the decomposition of 3 mM solutions of [K(2.2.2-cryptand)][Cp′$_3$Gd][3] (black, bottom), [K(2.2.2-cryptand)][Cp″$_2$GdCp], **1-Gd** (red, middle), and [K(2.2.2-cryptand)][Cp″$_2$GdCp^{Me}], **2-Gd** (blue, top), in THF under argon at 298 K.

The kinetics plots of $1/[Ln^{2+}]$ vs time are linear and consistent with a rate-determining step that is second order with respect to **1-Y**, **2-Y**, **1-Gd**, and **2-Gd**. The observed rate constants k_{obs} = 4.9 x 10^{-1} M^{-1} s^{-1} for **2-Y** and 1.2 M^{-1} s^{-1} for **3-Y** gave calculated initial half-lives for 3 mM solutions in THF of $t_{1/2}$ = 13 min and 6 min, respectively. These values are much shorter than the $t_{1/2}$ = 2.3 h initial half-life a 3 mM solution of [K(2.2.2-cryptand)][Cp'_3Y] in THF [k_{obs} = 3.97(4) x 10^{-2} M^{-1} s^{-1}]. Similarly, the k_{obs} = 1.6 x 10^{-1} M^{-1} s^{-1} for **1-Gd** and 1.9 x 10^{-1} M^{-1} s^{-1} for **2-Gd** gave calculated initial half-lives for 3 mM solutions in THF of $t_{1/2}$ = 27 h and 18 h, respectively, which are also shorter than the $t_{1/2}$ = 3.7 days for [K(2.2.2-cryptand)][Cp'_3Gd] in THF [k_{obs} = 1.04(2) x 10^{-3} M^{-1} s^{-1}]. These data are summarized in Table 1.5. Interestingly, in all three ligand sets, the gadolinium complexes are more stable than the yttrium complexes.

Density Functional Theory Analysis. Cp^x_3Y Complexes. DFT calculations were performed by Dr. Megan Fieser in collaboration with the group of Professor Filipp Furche. Calculations were done on the following Cp^x_3Y complexes, Cp''_3Y, Cp''_2YCp, and Cp''_2YCp^{Me}, as well as their anionic reduced forms $(Cp^x_3Y)^{1-}$ for comparison with the previously published results on Cp'_3Y and $(Cp'_3Y)^{1-}$.[2] In each case, the results are similar to those found for the $(Cp'_3)^{3-}$ ligand set, namely the LUMOs of the Y^{3+} species, Cp^x_3Y, and the HOMOs of the Y^{2+} species, $(Cp^x_3Y)^{1-}$, have mainly d_{z^2} character, Figure 1.8. Mulliken population analysis (MPA) of each Y^{2+} HOMO predicts the molecular orbitals to be primarily metal-based, with the d character being the most prominent, Table 1.6.[38] As shown in Table 1.7, the predicted change in Y–(Cp centroid) distances between the Y^{3+} and Y^{2+} complexes is approximately 0.03 Å in each case. This is consistent with the experimental findings for both the Cp''_3Ln[5] and Cp'_3Ln[1-3,7] systems and suggests that the reduction products of these five Cp^x_3Y complexes have similar properties to $(Cp'_3Y)^{1-}$ and $4d^1$ electron configurations. The DFT results and the reducibility observed are consistent with the

importance of the tris(cyclopentadienyl) coordination environment in providing access to the new +2 ions.

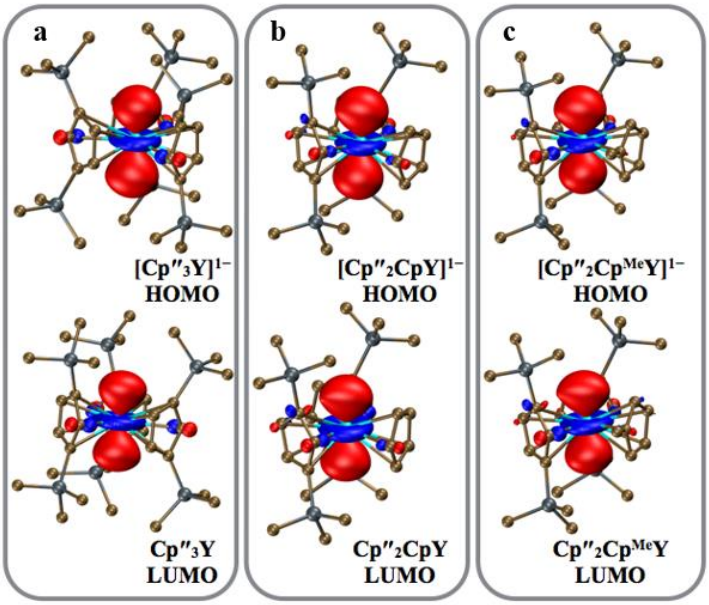

Figure 1.8. Molecular orbital plots of the HOMOs of $(Cp^{x}_{3}Y)^{1-}$ (top) and the LUMOs of $Cp^{x}_{3}Y$ (bottom) for (a) $Cp''_{3}Y$, (b) $Cp''_{2}YCp$, and (c) $Cp''_{2}YCp^{Me}$, using a contour value of 0.05.

Hyperfine Coupling Constants in $(Cp^{x}_{3}Y)^{1-}$. The hyperfine coupling constants of $(Cp^{x}_{3}Y)^{1-}$ complexes are shown in Table 1.6.[39] They display a progression of increasing A values for the $Cp^{x}_{3}Y$ reduction products ligated with $C_5H_3(SiMe_3)_2$ (Cp″), $C_5H_4SiMe_3$ (Cp′), C_5H_5 (Cp), and C_5H_4Me (Cp^{Me}), respectively. Hence, an increase in A is correlated with increasing donating ability of the ligands, if it is assumed that Me_3Si is less electron donating than H. As mentioned in the introduction, the relative effect of silyl groups appears to be system dependent.[22] If the more electron donating ligands lead to more unpaired electron density on the metal, this would be expected to increase A.

The DFT calculations also show a correlation of the hyperfine coupling constants with the percent metal character and the percent s character of the HOMOs in the $(Cp^{x}_{3}Y)^{1-}$ complexes, Table 1.6. Calculations on $\{[(Me_3Si)_2N]_3Y\}^{1-}$ previously done by Dr. Megan Fieser[40] also follow

this trend in that this species has the highest amount of metal and s character and a much higher A value, 110 G, Table 1.6. This general trend is also observed when looking at the s orbital spin density at the yttrium metal center, using natural population analysis,[41] Table 1.6. The s orbital spin density is very similar in the $(Cp^{x}_{3}Y)^{1-}$ complexes, but is much larger for $\{Y[N(SiMe_3)_2]_3\}^{1-}$. While analyzing these values for both MPA and NPA, it should be emphasized that we are only looking at trends between complexes, not the specific values for each complex.

The A value for the mixed ligand complex, [K(2.2.2-cryptand)][Cp″$_2$YCp], **1-Y**, does not follow this trend since it is the lowest of all, and the A value for the reduction product of the other mixed ligand system Cp″$_2$YCp^{Me} is intermediate compared to the other values in Table 1.6. However, if the mixed ligand complexes are on a different scale from the homoleptic complexes, then the two mixed ligand complexes also have values that parallel an increase in A with donor power of the ligand set. The larger A value is found for the Cp^{Me} vs the Cp mixed ligand complex.

DISCUSSION

This study shows that the reduction chemistry of the tris(cyclopentadienyl) rare earth complexes Cp′$_3$Ln and Cp″$_3$Ln, shown in eq 1.1, can be generalized to other tris(cyclopentadienyl) ligand sets. This is consistent with the expectation that the d_{z^2} orbital is energetically accessible in tris(cyclopentadienyl) environments and reduction occurs to form a d^1 product in these reactions. Although the color changes observed and the EPR spectra of reduction reactions of solutions of Cp″$_3$Y, Cp″$_2$YCp/Cp″YCp$_2$ (**3-Y**/**4-Y**), and Cp″$_2$YCp^{Me}/Cp″YCp$^{Me}_2$ (**5-Y**/**6-Y**) are clearly indicative of formation of Y^{2+}, crystallographic characterization of these reduced products has been elusive except in the case of the mixed ligand complex, [K(2.2.2-cryptand)][Cp″$_2$YCp], **1-Y**. Difficulty in obtaining crystallographic information for the new Y^{2+} complexes is related to their

relative instability compared to that of [K(18-crown-6)][Cp'_3Y][1] and [K(2.2.2-cryptand)][Cp'_3Y].[3] The isolation of these Cp′ complexes and their apparent greater stability compared to the other ligand sets described here may be another example of the principle of initial optimization.[42]

Attempts to determine if the optimum ligand environment would be different for the larger metal gadolinium gave results similar to the yttrium chemistry. Hence, dark solutions and EPR spectra consistent with the formation of new Gd^{2+} complexes were observed, but only in the case of the mixed ligand complex [K(2.2.2-cryptand)][Cp''_2GdCp], **1-Gd**, were crystals obtained. None of these reduced products were more stable than their Cp′ analogs. However, the mixed ligand **1-Gd** was more stable than the mixed ligand **1-Y**, and [K(2.2.2-cryptand)][Cp''_2GdCp^{Me}], **2-Gd**, was more stable than [K(2.2.2-cryptand)][Cp''_2YCp^{Me}], **2-Y**, which parallels the stability of [K(2.2.2-cryptand)][Cp'_3Gd] and [K(2.2.2-cryptand)][Cp'_3Y]. Hence, regardless of the ligand set, the larger metal forms more stable complexes. However, attempts to get enhanced stability by putting smaller ligands on the smaller metal, yttrium, were not successful.

Calculations performed on the Cp^x_3Y precursors and their predicted reduction products, $(Cp^x_3Y)^{1-}$, are consistent with the experimental results and suggest that altering the substituents does not change the Y^{3+} LUMOs or the Y^{2+} HOMOs from those that were found in the calculations on Cp'_3Y and $(Cp'_3Y)^{1-}$.[2] The expected structural changes between Y^{3+} and Y^{2+} complexes are well reproduced by the calculations. In addition, MPA analysis of the Y^{2+} HOMOs was successful in correlating the percent metal and percent s character in the reduced molecules with their experimentally observed EPR hyperfine coupling constants, Table 1.6. NPA analysis of the s orbital spin density at the yttrium metal center also was successful in matching the experimentally observed EPR hyperfine coupling constants.

CONCLUSION

Attempts to make more stable derivatives of [K(2.2.2-cryptand)][Cp′$_3$Y], via reduction of Cp″$_3$Y, and mixtures of Cp″$_2$YCp/Cp″YCp$_2$, **3-Y/4-Y**, and Cp″$_2$YCp^{Me}/Cp″YCp$^{Me}_2$, **5-Y/6-Y**, collectively called Cp$^x_3$Y, with potassium graphite revealed that the characteristic EPR doublet of a Y^{2+} ion can be generated in a variety of tris(cyclopentadienyl) coordination environments. However, none of these ligand sets gave Y^{2+} complexes more stable than [K(2.2.2-cryptand)][Cp′$_3$Y]. Moreover, [K(2.2.2-cryptand)][Cp″$_2$YCp], **1-Y**, was the only case in which crystallographic confirmation of the Y^{2+} species was possible. Similar results were observed with the larger metal gadolinium to produce [K(2.2.2-cryptand)][Cp″$_2$GdCp], **1-Gd**. DFT analysis of these reductions revealed that differences in the LUMOs of the Ln^{3+} precursors correlate with the observed reduction chemistry, since the LUMOs of the Cp$^x_3$Ln complexes are primarily d_z^2.

The fact that only two crystallographically characterized examples of Gd^{2+} complexes have been isolated, [K(2.2.2-cryptand)][Cp′$_3$Gd] and **1-Gd**, and only three for Y^{2+}, namely [K(2.2.2-cryptand)][Cp′$_3$Y], its 18-crown-6 analog, and **1-Y**, attests to the high reactivity of these new oxidation states. In retrospect, the choice of the optimum $(C_5H_4SiMe_3)^{1-}$ ligand was crucial in discovering these new ions.

Table 1.1. Crystal Data and Structure Refinement Parameters for [K(2.2.2-cryptand)][Cp″$_2$LnCp] (Ln = Y, **2-Y**; Gd, **2-Gd**).

	2-Y	**2-Gd**
Empirical formula	$C_{45}H_{83}KN_2O_6Si_4Y$ • 1⅓(C_4H_8O)	$C_{45}H_{83}GdKN_2O_6Si_4$ • 1⅓(C_4H_8O)
Formula weight	1084.64	1152.98
Temperature (K)	88(2) K	88(2) K
Space group	$P\bar{1}$	$P\bar{1}$
a (Å)	11.7555(10)	11.7545(11)
b (Å)	27.604(2)	27.696(3)
c (Å)	30.637(3)	30.708(3)
α (°)	116.1434(11)	116.0433(11)
β (°)	91.3921(12)	91.3051(12)
γ (°)	94.2639(12)	94.4470(12)
Volume (Å^3)	8881.8(13)	8936.7(14)
Z	6	6
ρ_{calcd} (Mg/m^3)	1.217	1.285
μ (mm^{-1})	1.183	1.310
$R1^a$	0.1094	0.1076
$wR2^b$	0.1672	0.1112

$^aR1 = \Sigma||F_o|-|F_c|| / \Sigma|F_o|$. $^bwR2 = [\Sigma[w(F_o^2-F_c^2)^2] / \Sigma[w(F_o^2)^2]]^{1/2}$

Table 1.2. EPR spectroscopic parameters for the spectra in Figure 1.1.

Spectrum	**g_{iso}**	**A (G)**
a) [Cp′$_3$Y]$^{1-}$ [1,3]	1.991	36.6
b) [Cp″$_3$Y]$^{1-}$	1.9908	36.1
c) [Cp″$_2$YCp]$^{1-}$	1.9904	34.6
d) [Cp″$_2$YCp^{Me}]$^{1-}$	1.9904	36.4

Table 1.3. Selected ranges of distances (Å) and angles (°) for [K(2.2.2-cryptand)][Cp′$_3$Ln][3] and **1-Ln** (Ln = Y, Gd).

Compound	Ln–(Cp-centroid)	Ln–C	(Cp-centroid)–Ln–(Cp-centroid)
[K(2.2.2-cryptand)][Cp′$_3$Y]	2.428-2.443	2.680(2) - 2.750(2)	118.2-123.3
2-Y	2.421-2.468	2.671(3) - 2.795(3)	118.4-122.6
[K(2.2.2-cryptand)][Cp′$_3$Gd]	2.463-2.475	2.711(2) - 2.778(2)	118.2-123.2
2-Gd	2.461-2.504	2.704(5) - 2.844(4)	118.2-123.1

Table 1.4. EPR spectroscopic parameters for the spectra in Figure 1.3.

Spectrum	g_{iso}
a) [Cp′$_3$Gd]$^{1-}$ [3]	1.991
b) [Cp″$_3$Gd]$^{1-}$	1.987
c) [Cp″$_2$GdCp]$^{1-}$	1.986
d) [Cp″$_2$GdCp^{Me}]$^{1-}$	1.987

Table 1.5. Summary of kinetic data of the decomposition of 3 mM solutions of [K(2.2.2-cryptand)][Cp′$_3$Ln], [K(2.2.2-cryptand)][Cp″$_2$LnCp], **1-Ln**, and [K(2.2.2-cryptand)][Cp″$_2$LnCp^{Me}], **2-Ln**, in THF at 298K (Ln = Y, Gd).

Complex	λ_{max} (nm)	Reaction Order	k_{obs}
[K(2.2.2-cryptand)][Cp′$_3$Y]	530	2	6.2(8) x 10^{-4} M^{-1} s^{-1}
1-Y	550	2	1.2(3) x 10^{-3} M^{-1} s^{-1}
2-Y	550	2	1.9(8) x 10^{-4} M^{-1} s^{-1}
[K(2.2.2-cryptand)][Cp′$_3$Gd]	517	2	1.8(4) x 10^{-3} M^{-1} s^{-1}
1-Gd	417	2	7.2(5) x 10^{-4} M^{-1} s^{-1}
2-Gd	457	2	1.5(1) x 10^{-3} M^{-1} s^{-1}

Table 1.6. Mulliken population analysis (MPA) summary for the HOMOs of $(Cp^{x}_{3}Y)^{1-}$ computed using TPSSh and TZVP basis sets. The % metal column indicates the total metal contribution to the molecular orbital and the % s and % d columns indicate how much of the total orbital comes directly from the metal s and d orbitals, respectively. Also included are natural population analyses of the s orbital spin density (# electrons) for each compound.

Compound	HOMO Metal Contribution			NPA s orbital spin density	Experimental Hyperfine Coupling
	% metal	% s	% d		
$(Cp''_2YCp)^{1-}$	73	17	56	0.11	34.6
$(Cp''_3Y)^{1-}$	73	16	57	0.11	36.1
$(Cp''_2YCp^{Me})^{1-}$	74	17	57	0.11	36.4
$(Cp'_3Y)^{1-}$	74	17	57	0.12	36.6
$(Cp_3Y)^{1-}$	84	20	64	0.15	42.8[39]
$(Cp^{Me}_3Y)^{1-}$	86[a]	25	59	0.14	46.9[39]
$\{Y[N(SiMe_3)_2]_3\}^{1-}$	107[b]	51	56	0.27	110[18]

[a]A small amount of p orbital population is found in this case. [b]MPA is known to overestimate populations and this is reflected in this value over 100%. The MPA numbers should only be used in a comparative not absolute sense.

Table 1.7. Calculated average Y–(Cp centroid) Distances (Å) in $Cp^{x}_{3}Y$ and $(Cp^{x}_{3}Y)^{1-}$ using TPSSh and TZVP basis sets.

Y^{3+}	M–(Cp Cnt) (Å)	Y^{2+}	M–(Cp Cnt) (Å)	Difference (Å)
Cp''_2YCp	2.427	**$(Cp''_2CpY)^{1-}$**	2.457	0.030
Cp''_3Y	2.444	**$(Cp''_3Y)^{1-}$**	2.475	0.031
Cp''_2YCp^{Me}	2.438	**$(Cp''_2Cp^{Me}Y)^{1-}$**	2.470	0.032
Cp'_3Y[2]	2.421	**$(Cp'_3Y)^{1-}$**[2]	2.453	0.032

REFERENCES

(1) MacDonald, M. R.; Ziller, J. W.; Evans, W. J. *J. Am. Chem. Soc.* **2011**, *133*, 15914-159147.

(2) MacDonald, M. R.; Bates, J. E.; Fieser, M. E.; Ziller, J. W.; Furche, F.; Evans, W. J. *J. Am. Chem. Soc.* **2012**, *134*, 8420-8423.

(3) MacDonald, M. R.; Bates, J. E.; Ziller, J. W.; Furche, F.; Evans, W. J. *J. Am. Chem. Soc.* **2013**, *135*, 9857-9868.

(4) Fieser, M. E.; MacDonald, M. R.; Krull, B. T.; Bates, J. E.; Ziller, J. W.; Furche, F.; Evans, W. J. *J. Am. Chem. Soc.* **2015**, *137*, 369-382.

(5) Hitchcock, P. B.; Lappert, M. F.; Maron, L.; Protchenko, A. V. *Angew. Chem., Int. Ed.* **2008**, *47*, 1488-1491.

(6) Langeslay, R. R.; Fieser, M. E.; Ziller, J. W.; Furche, F.; Evans, W. J. *Chem. Sci.* **2015**, *6*, 517-521.

(7) MacDonald, M. R.; Fieser, M. E.; Bates, J. E.; Ziller, J. W.; Furche, F.; Evans, W. J. *J. Am. Chem. Soc.* **2013**, *135*, 13310-13313.

(8) Windorff, C. J.; MacDonald, M. R.; Meihaus, M. R.; Ziller, J. W.; Long, J. R.; Evans, W. J. *Chem. Eur. J.* **2016**, *22*, 772-782.

(9) Windorff, C. J.; Chen, G. P.; Cross, J. N.; Evans, W. J.; Furche, F.; Gaunt, A. J.; Janicke, M. T.; Kozimor, S. A.; Scott, B. L. *J. Am. Chem. Soc.* **2017**, *139*, 3970-3973.

(10) Bursten, B. E.; Rhodes, L. F.; Strittmatter, R. J. *J. Am. Chem. Soc.* **1989**, *111*, 2756-2758.

(11) Bursten, B. E.; Rhodes, L. F.; Strittmatter, R. J. *J. Am. Chem. Soc.* **1989**, *111*, 2758-2766.

(12) Strittmatter, R. J.; Bursten, B. E. *J. Am. Chem. Soc.* **1991**, *113*, 552-559.

(13) Lauher, J. W.; Hoffmann, R. *J. Am. Chem. Soc.* **1976**, *113*, 1729-1742.

(14) Lukens, J., W. W.; Andersen, R. A. *Organometallics* **1995**, *14*, 3435-3439.

(15) Denning, R. G.; Harmer, J.; Green, J. C.; Irwin, M. *J. Am. Chem. Soc.* **2011**, *133*, 20644-20660.

(16) Morss, L. R. *Chem. Rev.* **1976**, *76*, 827-841.

(17) Mikheev, N. B.; Auerman, L. N.; Rumer, I. A.; Kamenskaya, A. N.; Kazakevich, M. Z. *Russ. Chem. Rev.* **1992**, *61*, 990-998.

(18) Fang, M.; Lee, D. S.; Ziller, J. W.; Doedens, R. J.; Bates, J. E.; Furche, F.; Evans, W. J. *J. Am. Chem. Soc.* **2011**, *133*, 3784-3787.

(19) Cassani, M. C.; Duncalf, D. J.; Lappert, M. F. *J. Am. Chem. Soc.* **1998**, *120*, 12958-12959.

(20) Gun'ko, Y. K.; Hitchcock, P. B.; Lappert, M. F. *Organometallics* **2000**, *19*, 2832-2834.

(21) Hanusa, T. P. *Chem. Rev.* **1993**, *93*, 1023-1036.

(22) Zachmanoglou, C. E.; Docrat, A.; Bridgewater, B. M.; Parkin, G.; Brandow, C. G.; Bercaw, J. E.; Jardine, C. N.; Lyall, M.; Green, J. C.; Keister, J. B. *J. Am. Chem. Soc.* **2002**, *124*, 9525-9546.

(23) Reynolds, L. T.; Wilkinson, G. *J. Inorg. Nucl. Chem.* **1959**, *9*, 86-92.

(24) Bergbreiter, D. E.; Killough, J. M. *J. Am. Chem. Soc.* **1978**, *100*, 2126-2134.

(25) Meyer, G.; Ax, P. *Mater. Res. Bull.* **1982**, *17*, 1447-1455.

(26) Izod, K.; Liddle, S. T.; Clegg, W. *Inorg. Chem.* **2004**, *43*, 214-218.

(27) Xie, Z.; Chui, K.; Liu, Z.; Xue, F.; Zhang, Z.; W., M. T. C.; Sun, J. *J. Organomet. Chem.* **1997**, *549*, 239-244.
(28) Coles, M. P.; Hitchcock, P. B.; Lappert, M. F.; Protchenko, A. V. *Organometallics* **2012**, *31*, 2682-2690.
(29) Stoll, S.; Schweiger, A. J. *J. Magn. Reson.* **2006**, *178*, 42-55.
(30) APEX2 Version 2014.1-1, Bruker AXS, Inc.; Madison, WI 2014.
(31) SAINT Version 8.34a, Bruker AXS, Inc.; Madison, WI 2013.
(32) Sheldrick, G. M., SADABS, Version 2014/4, Bruker AXS, Inc.; Madison, WI 2014.
(33) Sheldrick, G. M., SHELXTL, Version 2014/6, Bruker AXS, Inc.; Madison, WI 2014.
(34) International Tables for X-Ray Crystallography, 1992, Vol. C., Dordrecht: Kluwer Academic Publishers.
(35) Demir, S.; Mueller, T. J.; Ziller, J. W.; Evans, W. J. *Angew. Chem. Int. Ed.* **2011**, *50*, 515-518.
(36) Haan, K. H.; Boer, J. L.; Teuben, J. H. *Organometallics* **1986**, *5*, 1726-1733.
(37) Heeres, H. J.; Renkema, J.; Booij, M.; Meetsma, A.; Teuben, J. H. *Organometallics* **1988**, *7*, 2495-2502.
(38) Mulliken, R. S. *J. Phys. Chem.* **1955**, *23*, 1833-1840.
(39) Corbey, J. F.; Woen, D. H.; Palumbo, C. T.; Fieser, M. E.; Ziller, J. W.; Furche, F.; Evans, W. J. *Organometallics* **2015**, *34*, 3909-3921.
(40) Fieser, M. E., University of California, Irvine, 2015.
(41) Reed, A. E.; Weinstock, R. B.; Weinhold, F. *J. Phys. Chem.* **1985**, *83*, 735-746.
(42) Bercaw, J. E. Personal Communication. As cited by William B. Tolman in *Activation of Small Molecules: Organometallic and Bioinorganic Perspectives*; Wiley-VCH; Weinheim, Germany, **2006**, p 82.

CHAPTER 2

Trimethylsilyl- vs Bis(trimethylsilyl)-Substitution in Tris(cyclopentadienyl) Complexes of La, Ce, Pr, and Nd: Comparison of Structure, Magnetic Properties, and Reactivity

INTRODUCTION

For many years, only six of the lanthanide metals were thought to be able to form complexes with the metal in the +2 oxidation state: Eu, Yb, Sm, Tm, Dy, and Nd.[1-3] This belief was supported by extensive solid state and solution studies,[1-5] as well as calculations of the reduction potentials.[6-10] However, further studies of rare earth reduction chemistry have shown that +2 ions are available for all the lanthanides (except the radioactive promethium) by reduction of tris(cyclopentadienyl) metal complexes with potassium or potassium graphite in the presence of a chelate.[11-15] This was originally shown with La and Ce by reduction of Cp''_3Ln precursors [$Cp'' = C_5H_3(SiMe_3)_2$][11] and subsequently for all the lanthanides with Cp'_3Ln complexes, ($Cp' = C_5H_4SiMe_3$).[4,5,12-14] These reactions as well as results with Th,[16] U,[17,18] and Pu,[19] are summarized in eq 2.1.

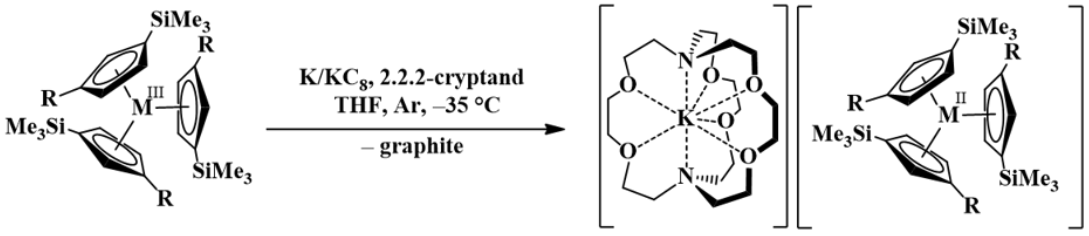

(2.1)

R = $SiMe_3$; M = La, Th, U, Pu
R = H; M = Y, La, Ce, Pr, Nd, Sm, Gd, Tb, Dy, Ho, Er, Tm, Lu, U

The complexes of the new Ln^{2+} ions of Y, La, Ce, Pr, Gd, Tb, Ho, Er, Lu differ from those traditionally known for Nd, Sm, Eu, Dy, Tm, and Yb in several ways. They display only small increases in their M–(Cp′ ring centroid) bond distances compared to their +3 analogs and show

much more intense absorptions in the visible region of their electronic absorption spectra compared to complexes of the traditional ions. These results have been rationalized by density functional theory (DFT) calculations that indicate that reductions of $4f^n$ Ln^{3+} ions make $4f^n5d^1$, not $4f^{n+1}$, ions for these new +2 complexes. This is consistent with the crystal field splitting diagram of the tris(cyclopentadienyl) coordination environment which has a single orbital, d_z^2, as the lowest in energy. It was found that Nd^{2+} and Dy^{2+} also adopted $4f^n5d^1$ configurations in this tris(cyclopentadienyl) environment.

Although the entire series of $(Cp'_3Ln)^{1-}$ has been synthesized and isolated (except Pm), for the Cp″ ligand, the only [K(2.2.2-cryptand)][Cp''_3Ln], **7-Ln**, complex that has been isolated in pure form is **7-La**. The cerium analog was isolated as a component in a crystal of [K(18-crown-6)$(OEt_2)_2$][Cp''_3Ce]·[Cp''_3Ce] in which one of the cerium positions was assigned as Ce^{2+} and the other as Ce^{3+}.[11] Attempts to make $(Cp''_3Y)^{1-}$ with the smaller metal yttrium were unsuccessful.[20]

The $(Cp''_3)^{3-}$ coordination environment also allowed the isolation of the first molecular examples of Th^{2+}[16] and Pu^{2+},[19] eq 1. In these actinide complexes, along with the U^{2+} analogs,[17] it appears that the $(Cp''_3)^{3-}$ coordination environment provides more stable complexes than the $(Cp'_3)^{3-}$ ligand set.

The research in this chapter was initiated to compare these two coordination geometries with the large early lanthanides most likely to accommodate three Cp″ ligands. Reported in this Chapter is the synthesis of pure samples of [K(2.2.2-cryptand)][Cp''_3Ln] (Ln = Ce, Pr, Nd), **7-Ln**, for the first time along with the previously known **7-La**[11] for comparison with the [K(2.2.2-cryptand)][Cp'_3Ln] analogs. In terms of reactivity, the relative thermal stability of [K(2.2.2-cryptand)][Cp'_3Ln] vs **7-Ln** is reported as well as reactivity with dimethoxyethane (DME).

The initial attempts by Lappert *et al*. to make Ln^{2+} complexes according to eq 2.1 were conducted in 1,2-dimethoxyethane (DME). However, these DME reactions only yielded mixtures of methoxide products, such as $[Cp''_2Ln(\mu\text{-}OMe)]_2$ (Ln = La,[21] Ce,[22] Nd[22]), eq 2.2, and $[Cp''_2Nd(\mu\text{-}OMe)_2Li(DME)]$,[22] along with KCp″ and unidentified polymetallic methoxide products.

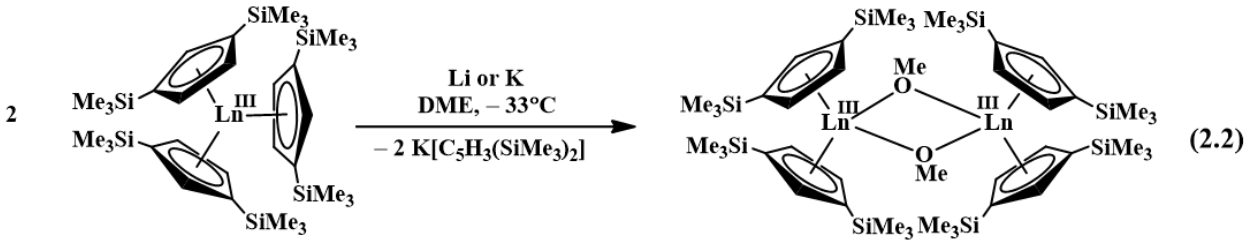

Since eq 2.1 is successful in THF and Et_2O and not in DME, it is presumed that the Ln^{2+} complexes react with DME. However, this had not been directly tested until this study.

In terms of physical properties, it was of great interest to obtain data on additional examples of Ce^{2+} and Pr^{2+} since the measured magnetic susceptibilities of [K(2.2.2-cryptand)][Cp′$_3$Ce] and [K(2.2.2-cryptand)][Cp′$_3$Pr] did not match exactly the two most likely models for $4f^15d^1$ and $4f^25d^1$ complexes.[23] The uncoupled $4f^n5d^1$ model has the LS component of the $4f^n$ core contributing to the moment along with the spin of the 5d electron. In the coupled $4f^n5d^1$ model, the spin of the $4f^n$ core couples with the spin of 5d electron and this total spin along with the orbital angular momentum of the $4f^n$ core contributes to the moment. For [K(2.2.2-cryptand)][Cp′$_3$Ce] the measured μ_{eff} = 2.62 μ_B did not match the 3.58 μ_B value predicted for $4f^2$, but it was in between the values of 3.07 μ_B and 1.62 μ_B for the uncoupled and coupled models of a $4f^15d^1$ configuration.[23] For [K(2.2.2-cryptand)][Cp′$_3$Pr], the measured 2.93 μ_B also does not match that calculated for $4f^3$, 3.62 μ_B, and it is closer to the 2.65 μ_B for the coupled $4f^25d^1$ model than the 3.98 μ_B for the uncoupled model. Hence, data on additional samples was sought.

EXPERIMENTAL

The syntheses and manipulations described below were conducted under argon with rigorous exclusion of air and water using glovebox, vacuum line, and Schlenk techniques. Solvents were sparged with UHP grade argon (Praxair) and passed through columns containing Q-5 and molecular sieves before use. NMR solvents (Cambridge Isotope Laboratories) were dried over NaK, degassed by three freeze–pump–thaw cycles, and vacuum-transferred before use. Methanol and 1,2-dimethoxyethane were dried with molecular sieves, degassed by three freeze-pump-thaw cycles, and vacuum-transferred before use. KC_8,[24] Cp''_3Ln (Ln = La,[25] Ce,[22] Pr[25], Nd[22]), and [K(2.2.2-cryptand)][Cp''_3La], **7-La**,[11] were prepared according to the literature. 2.2.2-Cryptand (4,7,13,16,21,24-hexaoxa-1,10-diazabicyclo[8,8,8]hexacosane, VWR), was placed under vacuum (10^{-3} Torr) for 12 h before use. 18-Crown-6 (1,4,7,10,13,16-hexaoxacyclooctadecane, Aldrich) was sublimed before use. Cyclooctatetraene (Aldrich) was placed over molecular sieves and degassed by three freeze-pump-thaw cycles before use. ^{1}H (500 MHz) and ^{13}C (125 MHz) NMR spectra were obtained on a Bruker GN500 or CRYO500 MHz spectrometer at 298 K. IR samples were prepared as KBr pellets and the spectra were obtained on a Jasco FT/IR-4700 spectrometer. Elemental analyses were performed on a Perkin-Elmer 2400 Series II CHNS elemental analyzer. UV-vis spectra were collected in THF at 298 K using a Varian Cary 50 Scan UV-vis spectrophotometer. Kinetics experiments were conducted by quickly dissolving 14-20 mg of the analyte in 5.00 mL of THF (~3 mM), transferring the solution into a quartz cuvette (1 mm path length) equipped with a greaseless stopcock, and immediately cooling the sample to 0 °C until measurement. The sample was quickly warmed to room temperature in a water bath and the spectra were collected at 298 K at intervals of 30 min for complexes [K(2.2.2-cryptand)][Cp'_3Ln] (Ln = La, Ce, Nd) and [K(2.2.2-cryptand)][Cp''_3Ln], **7-Ln** (Ln = La, Ce, Pr,

Nd). The absorbance at λ_{max} was used to monitor changes in concentrations over time and the experiments were performed in duplicate.

Magnetic Measurements. Magnetic samples were prepared by Lucy E. Darago in the group of Professor Jeffrey R. Long at the University of California, Berkeley, by adding the powdered crystalline compound to a 5 mm inner diameter quartz tube with a quartz platform ¾ down the length of the tube. For all samples, solid eicosane was added to prevent crystallite torqueing and provide good thermal contact between the sample and the bath. The tubes were fitted with Teflon sealable adapters, evacutated using a glovebox vacuum pump, and flame-sealed under static vacuum. Following flame sealing, the solid eicosane was melted in a water bath held at 40 °C. Magnetic susceptibility measurements were performed using a Quantum Design MPMS2 SQUID magnetometer. Dc susceptibility data measurements were performed at temperatures ranging from 1.8 to 300 K, using applied fields of 1, 0.5, and 0.1 T (variable temperature) and fields ranging from 0 to 7 T (magnetization measurements were performed using a 4 Oe switching field. All data were corrected for diamagnetic contributions from the core diamagnetism estimated using Pascal's constants.[26]

[K(2.2.2-cryptand)][Cp″$_3$Ce], 7-Ce. In an argon-filled glovebox, Cp″$_3$Ce (107 mg, 0.139 mmol) and 2.2.2-cryptand (52 mg, 0.14 mmol) were combined, dissolved in THF (2 mL), and the resultant blue solution was chilled to −35 °C in the glovebox freezer. KC_8 (28 mg, 0.21 mmol) was quickly added to the stirred blue solution and the reaction mixture immediately turned purple. After 2 min of stirring, the mixture was centrifuged using a prechilled centrifuge tube (−35 °C) to remove the graphite. The supernatant was collected and Et_2O (2 mL) was added. The resultant dark-purple solution was layered with hexanes (15 mL) and stored at −35 °C for 3 days to yield **7-Ce** as black/purple single-crystals suitable for X-ray diffraction (110 mg, 67%). IR: 3033w,

2949s, 2884s, 2811m, 1477m, 1456w, 1443m, 1434m, 1396w, 1384w, 1361s, 1355s, 1313w, 1299m, 1258s, 1243s, 1204m, 1134m, 1107s, 1077s, 992w, 951m, 934w, 921m, 828s, 799m, 746s, 679w, 638w, 620w cm^{-1}. UV-vis (THF) λ_{max} nm (ε, $M^{-1}cm^{-1}$): 250 (8200), 314 (5100), 400 (3200 shoulder), 565 (4300), 668 (3900). Anal. Calcd for $C_{51}H_{99}CeKN_2O_6Si_6$: C, 51.73; H, 8.43; N, 2.37. Found: C, 51.77; H, 8.86; N, 2.76.

[K(2.2.2-cryptand)][Cp″$_3$Pr], 7-Pr. As described for **7-Ce**, a yellow-green solution of Cp″$_3$Pr (200 mg, 0.260 mmol) and 2.2.2-cryptand (98 mg, 0.26 mmol) in THF (2 mL) was combined with KC_8 (53 mg, 0.39 mmol) to produce **7-Pr** as black/maroon single crystals suitable for X-ray diffraction (175 mg, 57%). IR: 3043w, 2963s, 2949s, 2888s, 2813m, 1477m, 1457w, 1445m, 1436m, 1395w, 1383w, 1361s, 1354s, 1314w, 1294m, 1260s, 1240s, 1205m, 1136s, 1108s, 1077s, 994w, 952m, 933w, 921m, 833s, 801m, 795m, 744s, 678w, 634w, 622w cm^{-1}. UV–vis (THF) λ_{max} nm (ε, $M^{-1}cm^{-1}$): 248 (12100), 310 (4700), 450 (3400 shoulder), 517 (3600), 715 (1100). Anal. Calcd for $C_{51}H_{99}PrKN_2O_6Si_6$: C, 51.69; H, 8.44; N, 2.36. Found: C, 51.56; H, 8.57; N, 2.42.

[K(2.2.2-cryptand)][Cp″$_3$Nd], 7-Nd. As described for **7-Ce**, a green colored solution of Cp″$_3$Nd (239 mg, 0.309 mmol) and 2.2.2-cryptand (116 mg, 0.309 mmol) in THF (2 mL) was combined with KC_8 (63 mg, 0.46 mmol) to produce **7-Nd** as black/maroon single crystals suitable for X-ray diffraction (325 mg, 89%). IR: 3057w, 3034w, 2949s, 2886s, 2812m, 2760w, 2729w, 1478m, 1456m, 1445m, 1435m, 1397w, 1383w, 1361s, 1356s, 1314w, 1300m, 1260s, 1244s, 1206s, 1175w, 1136s, 1107s, 1078s, 1032w, 994w, 951s, 935m, 922s, 831s, 802s, 746s, 677m, 637m, 621m, 569w, 525w, 480w cm^{-1}. UV–vis (THF) λ_{max} nm (ε, $M^{-1}cm^{-1}$): 246 (13000), 308 (5800), 420 (4400 shoulder), 525 (4300 shoulder), 650 (1700 shoulder). Anal. Calcd for $C_{51}H_{99}NdKN_2O_6Si_6$: C,51.55; H, 8.40; N, 2.36. Found: C, 51.61; H, 8.62; N, 2.43.

[(Cp′$_2$La(μ-OMe)]$_2$, 8-La. In an argon-filled glovebox, methanol (12.8 μL, 0.360 mmol) was added to 10 mL of Et_2O and stirred. The methanol solution was then added dropwise to a colorless solution of Cp′$_3$La(THF) (200 mg, 0.360 mmol) in Et_2O (10 mL); no color change was observed. The mixture was stirred for 2 h before the volatiles were removed under reduced pressure. The resultant colorless solids were characterized as analytically pure **8-La** (129 mg, 91%). Clear colorless single crystals of **8-La** characterizable by X-ray diffraction were obtained by cooling a concentrated hexane solution to −35 °C. ^{1}H NMR (C_6D_6): δ 6.67 (t, J_{HH} = 2.4 Hz, C_5H_4, 8H), 6.43 (t, J_{HH} = 2.4 Hz, C_5H_4, 8H), 3.22 (s, OCH_3, 6H), 0.36 (s, SiMe_3, 36H). ^{13}C NMR (C_6D_6): δ 124.9 ($C_5H_4SiMe_3$), 121.3 ($C_5H_4SiMe_3$), 118.2 ($C_5H_4SiMe_3$), 52.7 (OCH_3), 0.62 ($C_5H_4SiMe_3$). IR: 3084m, 3071m, 3057m, 2951s, 2926m, 2893m, 2855m, 2814m, 2708w, 2664w, 2616w, 2081w, 1932w, 1871w, 1707w, 1638w, 1599w, 1541w, 1441m, 1402m, 1360m, 1310w, 1244s, 1179s, 1042s, 905s, 831s, 772s, 754s, 689m, 637m, 629m, 419m cm^{-1}. Anal. Calcd for $C_{34}H_{58}LaO_2Si_4$: C, 45.94; H, 6.58. Found: C, 46.22; H, 6.42.

[(Cp′$_2$Ce(μ-OMe)]$_2$, 8-Ce. As described for **8-La**, methanol (3.7 μL, 0.091 mmol) in 5 mL of Et_2O was added dropwise to a royal blue solution of Cp′$_3$Ce (50 mg, 0.091 mmol) in Et_2O (5 mL) which caused an immediate color change to bright yellow. Removal of the solvent and crystallization of the resultant yellow solids from hexane yielded single crystals of **8-Ce** characterizable by X-ray diffraction (16 mg, 40%). ^{1}H NMR (C_6D_6): δ 24.7 (br, C_5H_4, 8H), 3.47 (br, C_5H_4, 8H), −2.72 (s, SiMe_3, 36H), −36.7 (br, μ-CH_3, 6H). IR: 3086m, 3073m, 3059m, 2951s, 2914m, 2893m, 2860m, 2760w, 2710w, 2139w, 2083w, 1935w, 1707w, 1641w, 1599w, 1543w, 1441m, 1402m, 1360m, 1310w, 1244s, 1177s, 1042s, 905s, 833s, 773s, 754s, 689m, 637m, 629m cm^{-1}. UV–vis (toluene) λ_{max} nm (ε, M^{-1}cm^{-1}): 290 (5900), 330 (330 shoulder), 402 (100

shoulder), 475 (610). Anal. Calcd for $C_{34}H_{58}CeO_2Si_4$: C, 45.81; H, 6.56. Found: C, 45.58; H, 6.26.

General 1,2-Dimethoxyethane Reaction Method. A scintillation vial was charged with 50 mg of Ln^{2+} reagent, either [K(2.2.2-cryptand)][Cp′$_3$Ln] or [K(2.2.2-cryptand)][Cp″$_3$Ln], **7-Ln**. 1,2-Dimethoxyethane (8-10 mL) was subsequently added and the dark mixtures were left to stir vigorously for up to 4 days after which the solutions were pale and did not appear to be changing color. For diamagnetic La^{3+}, the product mixtures were analyzed by ^{1}H and ^{13}C NMR spectroscopy to check whether [Cp″$_2$La(μ-OMe)]$_2$[21] or [(Cp′$_2$La(μ-OMe)]$_2$, **8-La**, products had formed. Attempts to crystallize the products from these reactions gave various oxide and hydroxide products that were characterized by X-ray crystallography but were not fully refined: [K(2.2.2-cryptand)][(Cp″$_2$La)$_2$(μ-OH)(μ-O)], **9-La**, crystallizes in the space group *C*2/*c* with a = 31.991(3) Å, b = 14.534(1) Å, c = 22.429(3) Å, β = 126.603(4)°, V = 8110.1(16) Å^3; [K(2.2.2-cryptand)][(Cp″$_2$Ce)$_2$(μ-OH)(μ-O)], **9-Ce**, crystallizes in the space group *C*2/*c* with a = 31.046(10) Å, b = 14.400(5) Å, c = 22.330(7) Å, β = 126.402(4)°, V = 8036(5) Å^3; A trimetallic La^{3+} hydroxo-oxo- cluster [K(2.2.2-cryptand)][(Cp′$_2$La)$_3$(μ-OH)$_x$(μ-O)$_y$] crystallizes in the space group *C*2/*c* with a = 26.6124(7) Å, b = 15.2032(4) Å, c = 26.7389(7) Å, β = 95.465(1)°, V = 10769.2(5) Å^3; [K(2.2.2-cryptand)][K$_2$O$_2$] crystallizes in the *C*2/*c* space group with a = 23.870(3) Å, b = 10.182(1) Å, c = 21.162(4) Å, β = 110.449(2)°, V = 4819(1) Å^3; a bimetallic La^{3+} / Cp″ complex with an unknown bridge crystallizes in the space group *C*2/*c* with a = 32.3398(8) Å, b = 14.4565(3) Å, c = 23.4154(6) Å, β = 128.919(1)°; a potassium metallocene [K(2.2.2-cryptand)][Cp″$_2$K], **10-K**, was fully refined and found to crystallize in the space group $P\bar{1}$ with a = 10.1528(14) Å, b = 16.177(2) Å, c = 16.484(2) Å, α = 73.9304(17), β = 88.2931(17), γ = 86.2250(18), V = 2595.9(6) Å^3.

X-ray Data Collection, Structure Solution and Refinement for [K(2.2.2-cryptand)][Cp″$_3$Ce], 7-Ce. A red crystal of approximate dimensions 0.133 x 0.222 x 0.246 mm was mounted on a glass fiber and transferred to a Bruker SMART APEX II diffractometer. The APEX2[27] program package was used to determine the unit-cell parameters and for data collection (20 sec/frame scan time for a sphere of diffraction data). The raw frame data was processed using SAINT[28] and SADABS[29] to yield the reflection data file. Subsequent calculations were carried out using the SHELXTL[30] program. There were no systematic absences nor any diffraction symmetry other than the Friedel condition. The centrosymmetric triclinic space group $P\bar{1}$ was assigned and later determined to be correct. The structure was solved by direct methods and refined on F^2 by full-matrix least-squares techniques. The analytical scattering factors[31] for neutral atoms were used throughout the analysis. Hydrogen atoms were included using a riding model. At convergence, wR2 = 0.0697 and Goof = 1.029 for 622 variables refined against 16158 data (0.73Å), R1 = 0.0283 for those 14301 data with I > 2.0σ(I). Details are given in Table 2.1.

X-ray Data Collection, Structure Solution and Refinement for [K(2.2.2-cryptand)][Cp″$_3$Pr], 7-Pr. A black crystal of approximate dimensions 0.292 x 0.294 x 0.416 mm was mounted on a glass fiber and transferred to a Bruker SMART APEX II diffractometer. The APEX2[27] program package was used to determine the unit-cell parameters and for data collection (30 sec/frame scan time for a sphere of diffraction data). The raw frame data was processed using SAINT[28] and SADABS[29] to yield the reflection data file. Subsequent calculations were carried out using the SHELXTL[30] program. There were no systematic absences nor any diffraction symmetry other than the Friedel condition. The centrosymmetric triclinic space group $P\bar{1}$ was assigned and later determined to be correct. The structure was solved using the coordinates of the Lanthanum analogue[11] and refined on F^2 by full-matrix least-squares techniques. The analytical

scattering factors[31] for neutral atoms were used throughout the analysis. Hydrogen atoms were included using a riding model. At convergence, wR2 = 0.0688 and Goof = 1.069 for 622 variables refined against 15334 data (0.74Å), R1 = 0.0266 for those 14214 data with I > 2.0σ(I). Details are given in Table 2.1.

X-ray Data Collection, Structure Solution and Refinement for [K(2.2.2-cryptand)][Cp″$_3$Nd], 7-Nd. A purple crystal of approximate dimensions 0.484 x 0.398 x 0.306 mm was mounted on a glass fiber and transferred to a Bruker SMART APEX II diffractometer. The APEX2[27] program package was used to determine the unit-cell parameters and for data collection (20 sec/frame scan time for a sphere of diffraction data). The raw frame data was processed using SAINT[28] and SADABS[29] to yield the reflection data file. Subsequent calculations were carried out using the SHELXTL[30] program. There were no systematic absences nor any diffraction symmetry other than the Friedel condition. The centrosymmetric triclinic space group $P\bar{1}$ was assigned and later determined to be correct. The structure was solved by direct methods and refined on F^2 by full-matrix least-squares techniques. The analytical scattering factors[31] for neutral atoms were used throughout the analysis. Hydrogen atoms were included using a riding model. At convergence, wR2 = 0.0600 and Goof = 1.061 for 622 variables refined against 15275 data (0.74 Å), R1 = 0.0239 for those 14376 data with I > 2.0σ(I). Details are given in Table 2.1.

X-ray Data Collection, Structure Solution and Refinement for [Cp′$_2$La(μ-OMe)]$_2$, 8-La. A colorless crystal of approximate dimensions 0.175 x 0.178 x 0.374 mm was mounted in a cryoloop and transferred to a Bruker SMART APEX II diffractometer. The APEX2[27] program package was used to determine the unit-cell parameters and for data collection (10 sec/frame scan time for a sphere of diffraction data). The raw frame data was processed using SAINT[28] and SADABS[29] to yield the reflection data file. Subsequent calculations were carried out using the

SHELXTL[30] program. There were no systematic absences nor any diffraction symmetry other than the Friedel condition. The centrosymmetric triclinic space group $P\bar{1}$ was assigned and later determined to be correct. The structure was solved by dual space methods and refined on F^2 by full-matrix least-squares techniques. The analytical scattering factors[31] for neutral atoms were used throughout the analysis. Hydrogen atoms were located from a difference-Fourier map and refined (x,y,z and U_{iso}). The molecule was located about an inversion center. At convergence, wR2 = 0.0358 and Goof = 1.044 for 306 variables refined against 4827 data (0.73Å), R1 = 0.0155 for those 4596 data with I > 2.0σ(I). Details are given in Table 2.2.

X-ray Data Collection, Structure Solution and Refinement for [Cp′$_2$Ce(μ-OMe)]$_2$, 8-Ce. A yellow crystal of approximate dimensions 0.094 x 0.164 x 0.242 mm was mounted in a cryoloop and transferred to a Bruker SMART APEX II diffractometer. The APEX2[27] program package and the CELL_NOW[32] were used to determine the unit-cell parameters. Data was collected using a 90 sec/frame scan time for a sphere of diffraction data. The raw frame data was processed using SAINT[28] and TWINABS[33] to yield the reflection data file (HKLF5 format).[33] Subsequent calculations were carried out using the SHELXTL[30] program. There were no systematic absences nor any diffraction symmetry other than the Friedel condition. The centrosymmetric triclinic space group $P\bar{1}$ was assigned and later determined to be correct. The structure was solved by dual space methods and refined on F^2 by full-matrix least-squares techniques. The analytical scattering factors[31] for neutral atoms were used throughout the analysis. Hydrogen atoms were included using a riding model. The molecule was located about an inversion center. At convergence, wR2 = 0.0650 and Goof = 1.060 for 199 variables refined against 5322 data (0.73 Å), R1 = 0.0247 for those 5020 with I > 2.0σ(I). The structure was refined as a three-component twin. Details are given in Table 2.2.

X-ray Data Collection, Structure Solution and Refinement for [K(2.2.2-cryptand)][Cp″$_2$K], 10-K. A colorless crystal of approximate dimensions 0.168 x 0.195 x 0.233 mm was mounted in a cryoloop and transferred to a Bruker SMART APEX II diffractometer. The APEX2[27] program package was used to determine the unit-cell parameters and for data collection (60 sec/frame scan time for a sphere of diffraction data). The raw frame data was processed using SAINT[28] and SADABS[29] to yield the reflection data file. Subsequent calculations were carried out using the SHELXTL[30] program. There were no systematic absences nor any diffraction symmetry other than the Friedel condition. The centrosymmetric triclinic space group $P\bar{1}$ was assigned and later determined to be correct. The structure was solved by direct methods and refined on F^2 by full-matrix least-squares techniques. The analytical scattering factors[31] for neutral atoms were used throughout the analysis. Hydrogen atoms were included using a riding model. Atoms Si(4), C(20) and C(21) were disordered and included using multiple components with partial site-occupancy-factors. Least-squares analysis yielded wR2 = 0.1579 and Goof = 1.018 for 508 variables refined against 9857 data (0.82Å), R1 = 0.0597 for those 7659 data with I > 2.0σ(I). Details are given in Table 2.3.

RESULTS AND DISCUSSION

Synthesis, Structural, and Spectroscopic Characterization of [K(2.2.2-cryptand)][Cp″$_3$Ln], 7-Ln. The Ln^{2+} complexes [K(2.2.2-cryptand)][Cp″$_3$Ln], **7-Ln** (Ln = Ce, Pr, Nd), were prepared by the same method used to synthesize the [K(2.2.2-cryptand)][Cp′$_3$Ln] complexes in eq 2.1. Potassium graphite was added to pre-chilled THF solutions (−35 °C) containing Cp″$_3$Ln and 2.2.2-cryptand. Dark crystals of **7-Ln** characterizable by X-ray diffraction

were grown upon diffusion of hexane into dark THF/Et_2O solutions containing **7-Ln** at −35 °C in the glovebox freezer, Figure 2.1, Table 2.4.

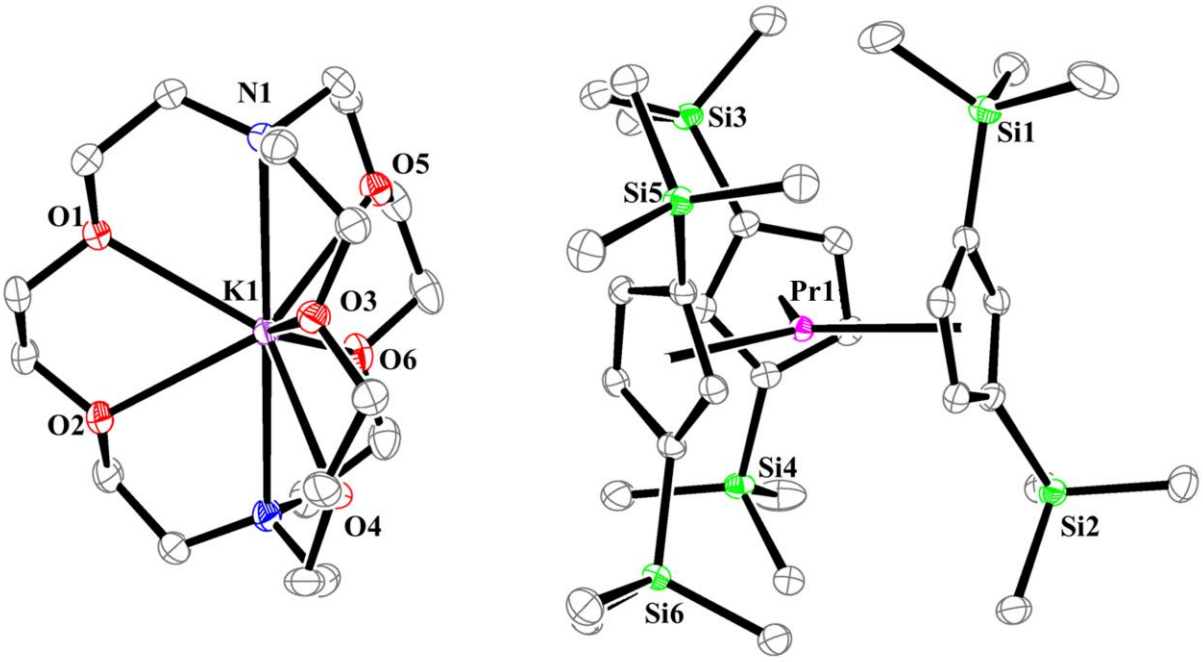

Figure 2.1. Thermal ellipsoid plot of [K(2.2.2-cryptand)][Cp''_3Pr], **7-Pr**, drawn at the 50% probability level. Hydrogen atoms are omitted for clarity. **7-Ce** and **7-Nd** are isomorphous.

7-Ce and **7-Pr** crystallize in the $P\bar{1}$ space group and are isomorphous with **7-La**, previously reported by Lappert *et al.*[11] **7-Nd** is not isomorphous, but has a similar coordination geometry and space group. **7-Nd** is isomorphous with the actinide analogs, [K(2.2.2-cryptand)][Cp''_3An] (An = Th, Pu). The anions of **7-Ln** contain formally 9-coordinate Ln^{2+} ions with three cyclopentadienyl ligands coordinated in a trigonal planar fashion. The average Ln–(Cp″ ring centroid) distances for **7-Ln** decrease from La to Ce to Pr to Nd by the amount of change of the ionic radii of the Ln^{3+} ions of these metals.[34] The Ln–C(Cp″) average distances in both **7-Ce** and **7-Nd** are 0.03 Å larger than those in their Cp''_3Ln precursors. These match the 0.032 Å difference of **7-La** and Cp''_3La,

reported by Lappert.[11] Although Cp''_3Pr was crystallized to get metrical data to compare with **7-Pr**, the data were too disordered to obtain bond distances. However, by interpolation in the Cp''_3Ln series, the Pr–C(Cp") average distance is about 0.03 Å larger as with the other compounds. This is consistent with the differences found between [K(2.2.2-cryptand)][Cp'_3Ln] and Cp'_3Ln.

The UV-visible spectra of **7-Ln** are similar to their [K(2.2.2-cryptand)][Cp'_3Ln] analogs, Figures 2.2, 2.3, and 2.4, for Ln = Ce, Pr, and Nd, respectively. The molar extinction coefficients ε = 2,000-6,000 M^{-1} cm^{-1} of the **7-Ln** series are consistent with those of the $4f^n5d^1$ Ln^{2+} ions found in [K(2.2.2-cryptand)][Cp'_3Ln].[4,5,14,15] Interestingly the absorptions of **7-Ln** are red shifted with respect to [K(2.2.2-cryptand)][Cp'_3Ln] by ca. 700 cm^{-1} in the high energy region and 800 cm^{-1} in the low energy region. The data on **2-Nd** constitute another example of Nd^{2+} being a configurational crossover ion.[4,5,15]

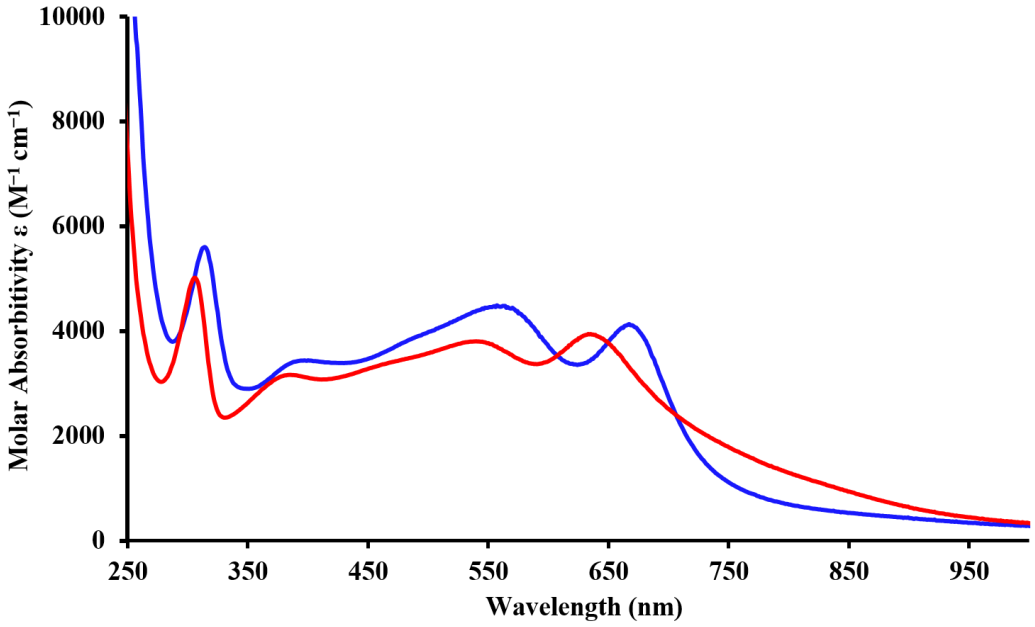

Figure 2.2. Experimental UV−vis spectra of 3 mM solutions of [K(2.2.2-cryptand)][Cp'_3Ce] (red) and [K(2.2.2-cryptand)][Cp''_3Ce] (blue), **7-Ce**, in THF at 298 K.

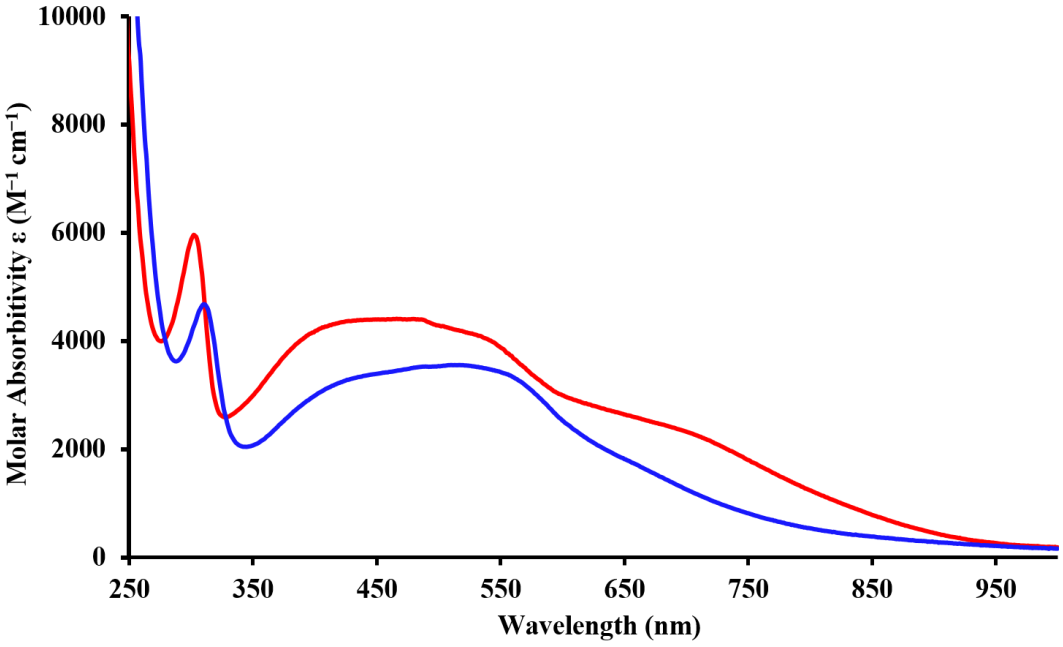

Figure 2.3. Experimental UV−vis spectra of 3 mM solutions of [K(2.2.2-cryptand)][Cp′$_3$Pr] (red) and [K(2.2.2-cryptand)][Cp″$_3$Pr] (blue), **7-Pr** in THF at 298 K.

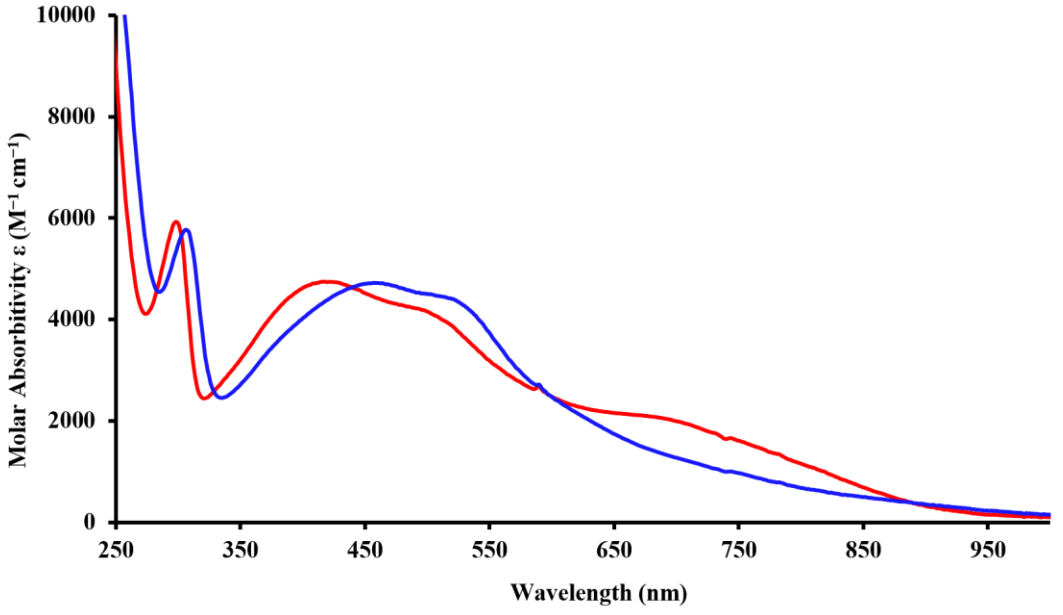

Figure 2.4. Experimental UV−vis spectra of 3 mM solutions of [K(2.2.2-cryptand)][Cp′$_3$Nd] (red) and [K(2.2.2-cryptand)][Cp″$_3$Nd] (blue), **7-Nd** in THF at 298 K.

Magnetic Susceptibility. Magnetic susceptibility measurements on **7-Ce** and **7-Pr**, Figure 2.5, were performed by Lucy E. Durago of the Long group at UC Berkeley. The data of **7-Ln** were found to be similar to [K(2.2.2-cryptand)][Cp′$_3$Ln], Table 2.5. The X_MT value of 0.78 emu·K/mol (μ_{eff} = 2.50 μ_B) for **7-Ce** at 300 K is close to the X_MT = 0.86 (μ_{eff} = 2.62 μ_B) emu·K/mol found for [K(2.2.2-cryptand)][Cp′$_3$Ln].[23] Similarly, for **7-Pr**, the room temperature X_MT = 1.04 (μ_{eff} = 2.88 μ_B) is close to the X_MT = 1.07 emu·K/mol (μ_{eff} = 2.93 μ_B) measured for [K(2.2.2-cryptand)][Cp′$_3$Ln].[23] As shown in the table, these values do not match the calculated values for $4f^2$ and $4f^3$ configurations. The experimental values fall in between the values for the coupled and uncoupled $4f^n5d^1$ configuration models, but are not close to either. Hence, the new data on these Cp″ complexes reaffirms the notion that the magnetism of Ce^{2+} and Pr^{2+} is not readily approximated by these simple models.

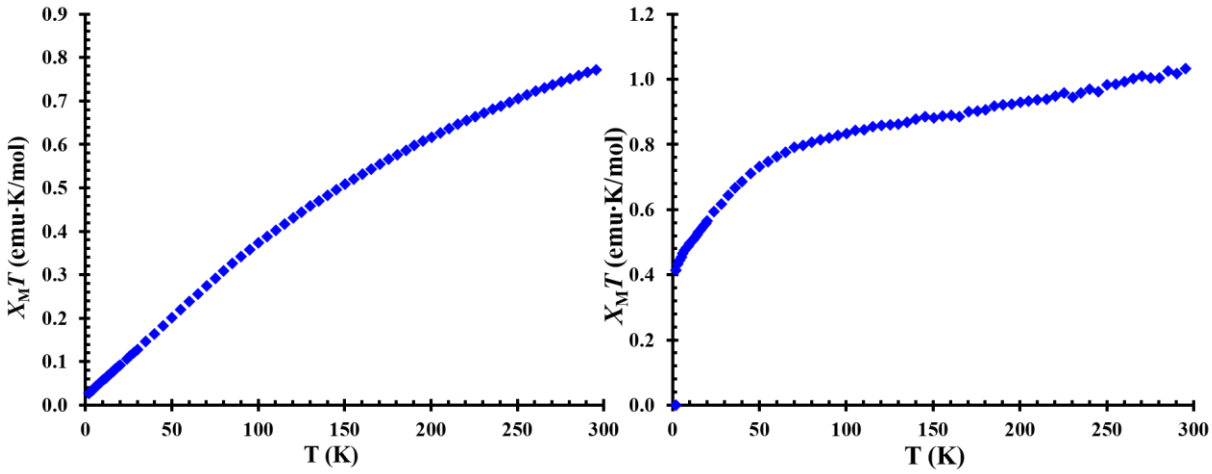

Figure 2.5. X_MT vs T plots for [K(2.2.2-cryptand)][Cp″$_3$Ln], **7-Ce** (left) and **7-Pr** (right) under an applied field of 1 T (0.1 T for **7-Ce**).

Reactivity. The thermal stability of the **7-Ln** series was evaluated following the protocols used for [K(2.2.2-cryptand)][Cp′$_3$Ln]. The concentration of Ln^{2+} was monitored at λ_{max} = 540 nm

for [K(2.2.2-cryptand)][Cp′$_3$Ce], 561 nm for **7-Ce**, 517 nm for **7-Pr**, 417 nm for [K(2.2.2-cryptand)][Cp′$_3$Nd], and 457 nm for **7-Nd**. The decomposition of the **7-Ln** series was found to follow second-order kinetics like the [K(2.2.2-cryptand)][Cp′$_3$Ln] complexes of these metals.[14] Table 2.6 summarizes kinetic data for [K(2.2.2-cryptand)][Cp′$_3$Ln] and **7-Ln** as well as for the corresponding uranium complexes, [K(2.2.2-cryptand)][Cp′$_3$U] and **7-U**. In contrast to the situation with the uranium complexes, where **7-U** is significantly more stable than [K(2.2.2-cryptand)][Cp′$_3$Ln], all of the **7-Ln** complexes decompose slightly faster than their [K(2.2.2-cryptand)][Cp′$_3$Ln] analogs. Hence, the $(Cp''_3)^{3-}$ coordination environment appears to have more of an effect on the stability of +2 complexes of the actinides than the lanthanides. This is reinforced by the fact that the Th^{2+} complex [K(18-crown-6)(THF)$_2$][Cp″$_3$Th],[16] shows only 8% decomposition after 8 days at room temperature and a Pu^{2+} complex, [K(2.2.2-cryptand)][Cp″$_3$Pu], could be isolated with this ligand set,[19] whereas attempts to isolate a crystalline Np^{2+} complex with Cp′ were unsuccessful.[35]

Reactions of [K(2.2.2-cryptand)][Cp′$_3$Ln] and **7-Ln** with dimethoxyethane (DME) were examined to determine if the isolated Ln^{2+} complexes would react to form the methoxides [Cp″$_2$Ln(μ-OMe)]$_2$ (Ln = La,[21] Ce,[22] Nd[22]), as observed by Lappert in reductions of Cp″$_3$Ln and $(C_5H_3{}^tBu_2)_3$Ln with Li or K in DME, e.g. eq 2.2. To insure that the Cp′ methoxides could be identified in these reactions, the [Cp′$_2$Ln(μ-OMe)]$_2$ complexes (Ln = La, Ce), **8-Ln**, were independently prepared and crystallographically characterized. The reaction of Cp′$_3$Ln with methanol yields colorless and yellow solutions for La and Ce (see Figure 2.6 for the UV-visible spectrum of **3-Ce**), respectively, from which single crystals of **8-Ln** were isolated, eq 2.3, Figure 2.7. The metrical parameters of **8-La** and **8-Ce** are consistent with those of the previously characterized **3-Y**[36] and [$(C_5H_3{}^tBu_2)_2$Ce(μ-OMe)]$_2$,[22] Table 2.7.

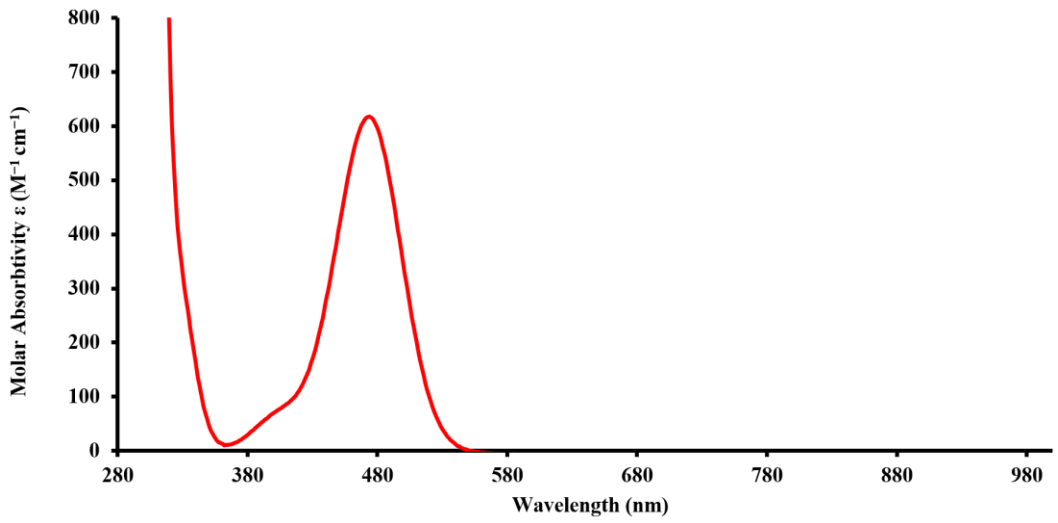

Figure 2.6. Experimental UV−vis spectrum of a 5 mM solution of [Cp′$_2$Ce(μ-OMe)], **8-Ce**, in toluene at 298 K.

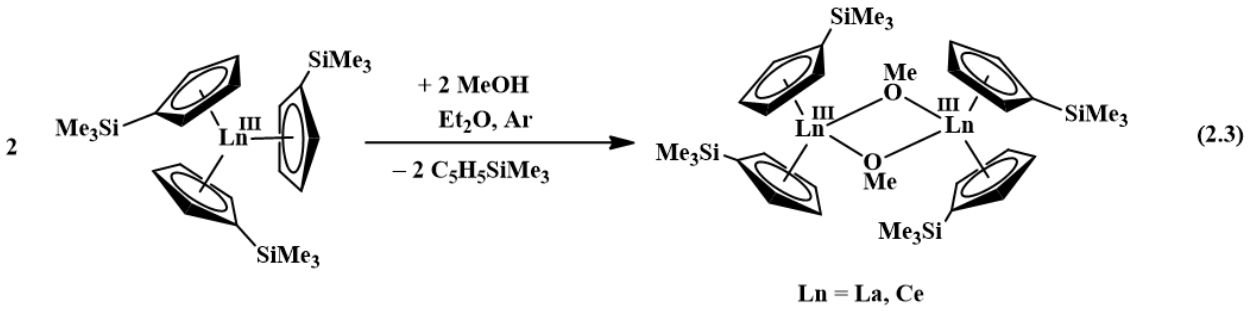

(2.3)

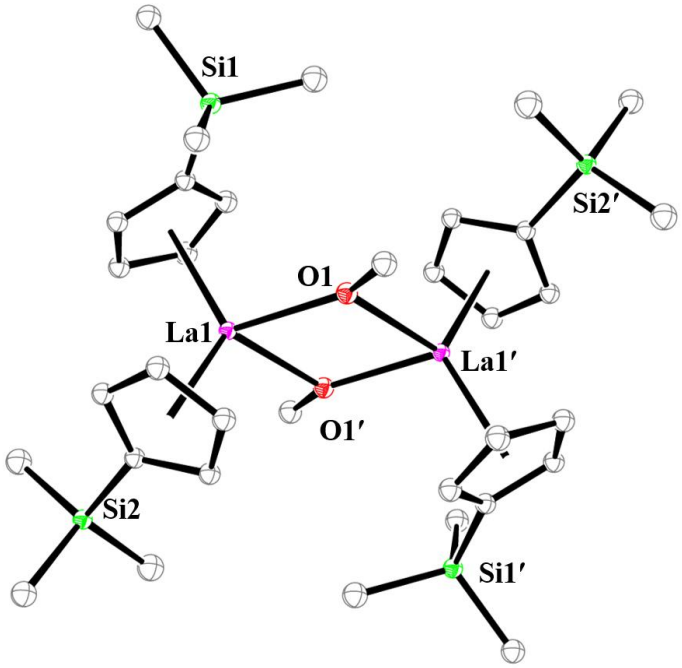

Figure 2.7. Thermal ellipsoid plot of $[Cp'_2La(\mu\text{-}OMe)]_2$, **3-La**, drawn at the 50% probability level. Hydrogen atoms are omitted for clarity. **3-Ce** is isomorphous. Selected bond lengths in **2-La**: La1–Cnt(Cp′), 2.562, 2.572 Å; La1–$C(Cp')_{avg}$, 2.84(2) Å; La1–O1, 2.375(1) Å; La1–O1′, 2.413(1) Å; O1–La1–O1′, 72.69(4)°; La1–O1–La1′, 107.31(4)°. Selected bond lengths in **2-Ce**: Ce1–Cnt(Cp′), 2.531, 2.539 Å; Ce1–$C(Cp')_{avg}$, 2.81(2) Å; Ce1–O, 2.350(2) Å; Ce1′–O, 2.387(2) Å; O1–Ce1–O1′, 72.16(8)°; Ce1–O1–Ce1′, 107.84(8)°.

Over 3-4 days, the dark purple DME solutions of **7-La**, **7-Ce**, and **7-Pr** and the dark red/brown DME solution of **7-Nd** slowly turned colorless for La, yellow for Ce, pale yellow for Pr, and blue for Nd. The colors of the [K(2.2.2-cryptand)][Cp'_3Ln] reactions were similar except Ce gave an almost colorless solution and the Nd reaction turned yellow. Unfortunately, only intractable oils were recovered from these reactions. The ^{1}H NMR spectrum of the diamagnetic product mixture from the **7-La** reaction was complicated, although Cp''_3La was observed as the major component. The reaction with [K(2.2.2-cryptand)][Cp'_3La] similarly gave a complicated

spectrum except there were no identifiable resonances. Neither the previously characterized $[Cp''_2La(\mu\text{-}OMe)]_2$[21] nor the $[Cp'_2Ln(\mu\text{-}OMe)]_2$, **8-Ln**, complexes synthesized for this study were observed despite multiple reactions. The only crystalline product definitively identified was the potassium metallocene [K(2.2.2-cryptand)][Cp''_2K], **10-K**, which was characterized by X-ray crystallography, Figure 2.8.

These DME reactions represent another example of the difference in reactivity observed between isolated Ln^{2+} complexes with the alkali metal sequestered in 2.2.2-cryptand vs LnA_3/M reactions that should generate the same species in solution.[12] Apparently, the cryptand stabilized salts, [K(2.2.2-cryptand)][Cp'_3Ln] and **7-Ln**, have different reaction patterns that the Ln^{2+} intermediates generated *in situ* from reduction of Cp'_3Ln and Cp''_3Ln with Li or K and no chelate.

In one attempt, the 18-crown-6 analog [K(18-crown-6)][Cp''_3La] was reacted with DME and the ^1H NMR spectrum generated from the product mixture indicated a clean reaction with $[Cp''_2La(\mu\text{-}OMe)]_2$ along with Cp''_3La and [K(18-crown-6)][Cp''] as the only NMR observable products. This further confirms that the cation $[M(chelate)]^{1+}$ effects the products of Ln^{2+} reactivity.

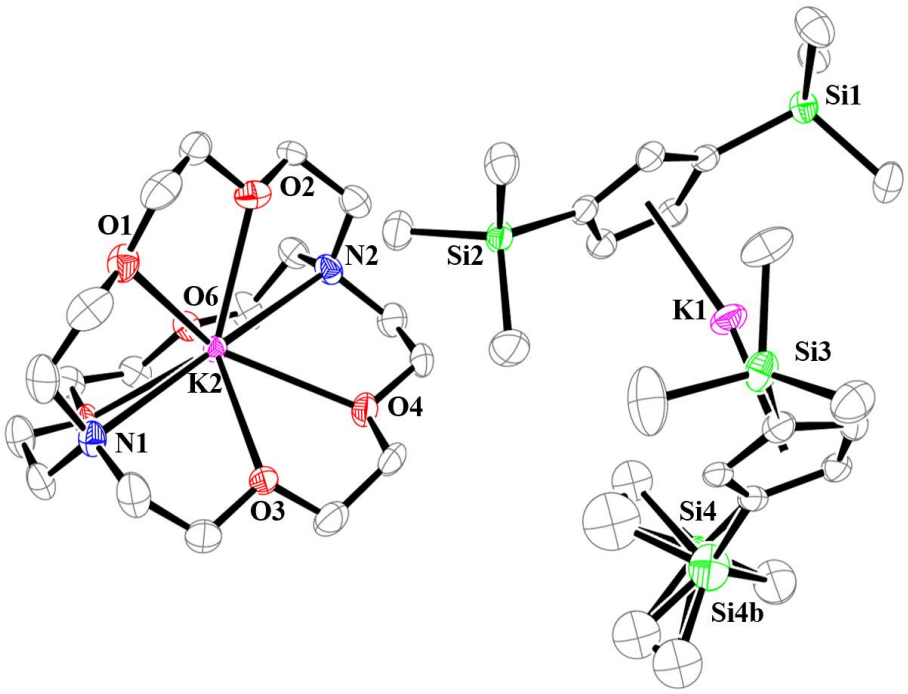

Figure 2.8. Molecular structure of [K(2.2.2-cryptand)][Cp″$_2$K], **10-K**, with thermal ellipsoids drawn at the 50% probability level and hydrogen atoms omitted for clarity.

CONCLUSION

Crystallographic characterization of the [K(2.2.2-cryptand)][Cp″$_3$Ln], **7-Ln**, complexes for Ce, Pr, and Nd shows that additional members of this series can be synthesized in pure form in addition to **7-La**.[11] The results show that this $(Cp''_3)^{3-}$ ligand environment gives Ln^{2+} complexes for these early lanthanides that are analogous to those found for the $(Cp'_3)^{3-}$ ligand set.[4,5,12-14] The crystal structures and UV-vis spectra of all three new Ln^{2+} complexes are consistent with the presence of $4f^n5d^1$ ions as found for [K(2.2.2-cryptand)][Cp′$_3$Ln]. The magnetic susceptibility data on **7-Ce** and **7-Pr** are similar to those of [K(2.2.2-cryptand)][Cp′$_3$Ce] and [K(2.2.2-cryptand)][Cp′$_3$Pr] in that the data do not match that expected for $4f^n$ ions, but also do not fit simple models for the magnetism of $4f^n5d^1$ ions.

The thermal stability of the [K(2.2.2-cryptand)][Cp''_3Ln], **7-Ln** (Ln = Ce, Pr, Nd), complexes was found to be slightly less than that of their [K(crypt)][Cp'_3Ln] analogs. This contrasts with the greater stability of $(Cp''_3U)^{1-}$ vs $(Cp'_3U)^{1-}$ and the successful isolation of $(Cp''_3Th)^{1-}$ and $(Cp''_3Pu)^{1-}$ using the bis(silyl)cyclopentadienyl ligand set. Reactions between DME and the isolated Ln^{2+} complexes, [K(2.2.2-cryptand)][Cp'_3Ln] and **7-Ln**, did not readily form the methoxide complexes previously observed in Cp''_3Ln/M reductions in DME. This provides additional examples of the differences between the reactivity of isolated complexes of Ln^{2+} and the dark solutions formed by reducing analogous Ln^{3+} complexes. Hence, although Cp″ is as viable as Cp′ for supporting Ln^{2+} complexes of the larger early metals, no particular advantages were observable from this study.

Table 2.1. Crystal Data and Structure Refinement Parameters for [K(2.2.2-cryptand)][Cp″$_3$Ln] (Ln = Ce, Pr, Nd), **7-Ln**.

	7-Ce	**7-Pr**	**7-Nd**
Empirical formula	$C_{51}H_{99}KN_2O_6Si_6Ce$	$C_{51}H_{99}KN_2O_6Si_6Pr$	$C_{51}H_{99}KN_2NdO_6Si_6$
Formula weight	1184.08	1184.87	1188.20
Temperature (K)	88(2) K	133(2)	133(2)
Space group	$P\bar{1}$	$P\bar{1}$	$P\bar{1}$
a (Å)	11.9540(7)	11.9579(8)	12.2217(8)
b (Å)	12.8185(7)	12.8133(9)	12.7389(8)
c (Å)	21.3254(12)	21.3331(15)	22.2835(14)
α (°)	83.8061(7)	83.8776(8)	100.9620(10)
β (°)	89.2175(7)	89.1207(8)	104.5290(10)
γ (°)	87.7638(7)	87.6759(8)	95.4640(10)
Volume (Å^3)	3246.0(3)	3247.1(4)	3259.6(4)
Z	2	2	2
ρ_{calcd} (Mg/m^3)	1.211	1.212	1.211
μ (mm^{-1})	0.918	0.967	1.012
$R1^a$	0.0283	0.0866	0.0239
$wR2^b$	0.0697	0.0688	0.0600

$^aR1 = \Sigma||F_o|-|F_c|| / \Sigma|F_o|$. $^bwR2 = [\Sigma[w(F_o^2-F_c^2)^2] / \Sigma[w(F_o^2)^2]]^{1/2}$

Table 2.2. Crystal Data and Structure Refinement Parameters for $[Cp'_2Ln(\mu\text{-}OMe)]_2$ (Ln = La, Ce), **8-Ln**.

	8-La	**8-Ce**
Empirical formula	$C_{34}H_{58}La_2O_2Si_4$	$C_{34}H_{58}Ce_2O_2Si_4$
Formula weight	888.98	891.40
Temperature (K)	88(2)	88(2)
Space group	$P\bar{1}$	$P\bar{1}$
a (Å)	8.6987(6)	8.6891(13)
b (Å)	9.8934(7)	9.8629(14)
c (Å)	12.6865(8)	12.6428(19)
α (°)	68.5117(7)	68.7401(17)
β (°)	76.5109(7)	76.5896(19)
γ (°)	88.5816(7)	88.5057(18)
Volume (Å^3)	985.66(12)	980.2(3)
Z	1	1
ρ_{calcd} (Mg/m^3)	1.498	1.510
μ (mm^{-1})	2.286	2.442
$R1^a$	0.0155	0.0247
$wR2^b$	0.0358	0.0650

$^aR1 = \Sigma||F_o|-|F_c|| / \Sigma|F_o|$. $^bwR2 = [\Sigma[w(F_o^2-F_c^2)^2] / \Sigma[w(F_o^2)^2]]^{1/2}$

Table 2.3. Crystal Data and Structure Refinement Parameters for [K(2.2.2-cryptand)][Cp″$_2$K], **10-K**.

	2-K
Empirical formula	$C_{40}H_{78}K_2N_2O_6Si_4$
Formula weight	873.60
Temperature (K)	88(2)
Space group	$P\bar{1}$
a (Å)	10.1528(14)
b (Å)	16.177(2)
c (Å)	16.484(2)
α (°)	73.9304(17)
β (°)	88.2931(17)
γ (°)	86.2250(18)
Volume (Å^3)	2595.9(6)
Z	2
ρ_{calcd} (Mg/m^3)	1.118
μ (mm^{-1})	0.315
$R1^a$	0.0597
$wR2^b$	0.1579

$^aR1 = \Sigma||F_o|-|F_c|| / \Sigma|F_o|$. $^bwR2 = [\Sigma[w(F_o^2-F_c^2)^2] / \Sigma[w(F_o^2)^2]]^{1/2}$

Table 2.4. Selected bond lengths (Å) and angles (°) for **7-Ln** compounds and Cp″$_3$Ln precursors.

Parameter	**LaCp″$_3$**[37]	**7-La**[11]	**CeCp″$_3$**[38]	**7-Ce**	**7-Pr**	**NdCp″$_3$**[37]	**7-Nd**
Ln–(Cp″ ring	2.615	2.606(3)	2.542	2.579	2.558	2.468	2.530
centroid)	2.586	2.612(3)	2.579	2.574	2.552	2.558	2.559
	2.605	2.642(3)	2.575	2.609	2.588	2.548	2.543
Ln–(Cp″ ring	2.60(1)	2.62(1)	2.58(3)	2.59(2)	2.57(2)	2.52(4)	2.54(1)
centroid)$_{avg}$							
Ln–C(Cp″)$_{avg}$	2.852(8)	2.89(2)	2.83(4)	2.86(4)	2.84(3)	2.789(2)	2.82(3)

Table 2.5. Experimental and predicted X_MT values for [K(2.2.2-cryptand)][Cp′$_3$Ln] and [K(2.2.2-cryptand)][Cp″$_3$Ln], **7-Ln**, collected under a field of 1 T (0.1 T for **7-Ce**).

Complex	*n* (*f* electrons)	exp. X_MT[a]	X_MT ($4f^n5d^1$) coupled[a]	X_MT ($4f^n5d^1$) uncoupled[a]	X_MT ($4f^{n+1}$) [a]
1-Ce	1	0.86	0.33	1.18	1.6
2-Ce	1	0.78	0.33	1.18	1.6
1-Pr	2	1.07	0.875	1.98	1.64
2-Pr	2	1.04	0.875	1.98	1.64

[a]All X_MT are reported in units of emu·K/mol.

Table 2.6. Summary of kinetic data of the decomposition of 3 mM solutions of [K(2.2.2-cryptand)][Cp′$_3$Ln] and [K(2.2.2-cryptand)][Cp″$_3$Ln], **7-Ln**, in THF at 298K. [K(2.2.2-cryptand)][Cp′$_3$U] and **7-U** have been added for comparison.

Complex	λ_{max} (nm)	Reaction Order	k_{obs}
1-Ce	540	2	6.2(8) x 10^{-4} M^{-1} s^{-1}
2-Ce	561	2	1.2(3) x 10^{-3} M^{-1} s^{-1}
1-Pr[a]	465	2	1.9(8) x 10^{-4} M^{-1} s^{-1}
2-Pr	517	2	1.8(4) x 10^{-3} M^{-1} s^{-1}
1-Nd	417	2	7.2(5) x 10^{-4} M^{-1} s^{-1}
2-Nd	457	2	1.5(1) x 10^{-3} M^{-1} s^{-1}
1-U[b]	412	1	1.3(9) x 10^{-4} s^{-1}
2-U[c]	470	1	9.8(3) x 10^{-6} s^{-1}

[a] Ref 4. [b] Ref 8. [c] Ref 7.

Table 2.7. Selected bond lengths (Å) and angles (°) for $[Cp'_2Ln(\mu\text{-}OCH_3)]_2$, **8-Ln** (Ln = La, Ce, Y[36]), and $[(C_5H_3{}^tBu_2)_2Ce(\mu\text{-}OCH_3)]_2$.

Parameter	**8-La**	**8-Ce**	**8-Y**[36]	**$[(C_5H_3{}^tBu_2)_2Ce(\mu\text{-}OMe)]_2$**[22]
Ln–(Cp ring centroid)	2.562, 2.572	2.531, 2.539	2.279, 2.384	2.596, 2.564
$Ln–C(Cp)_{avg}$	2.84(2)	2.81(2)	2.67(1)	2.84(5)
Ln–O	2.375(1), 2.413(1)	2.350(2), 2.387(2)	2.217(3), 2.233(3)	2.366(4), 2.386(4)
Ln…Ln	3.8567(3)	3.8285(6)	3.562(1)	3.887
Cp–Ln–Cp	128.2	127.7	131.3	126.2
Ln–O–Ln	107.31(4)	107.84(8)	106.4	109.8

REFERENCES

(1) Bochkarev, M. N. *Coord. Chem. Rev.* **2004**, *248*, 835-851.

(2) Nief, F. In *Handbook on the Physics and Chemistry of Rare Earths*; Gschneidner, K. A., Bünzli, J.-C. G., Pecharsky, V. K., Eds.; Elsevier: Amsterdam, 2010; Vol. 40, p 241-300.

(3) Meyer, G. *The Divalent State in Solid Rare Earth Metal Halides*, 2012.

(4) Evans, W. J. *Organometallics* **2016**, *35*, 3088-3100.

(5) Woen, D. H.; Evans, W. J. In *Handbook on the Physics and Chemistry of Rare Earths*; 1st ed.; Elsevier: Amsterdam, 2016; Vol. 50, p 337-394.

(6) Morss, L. R. *Chem. Rev.* **1976**, *76*, 827-841.

(7) Morss, L. R. In *Handbook on the Physics and Chemistry of Rare Earths*; Gschneidner, K. A., Eyring, L., Choppin, G. R., Lander, G. H., Eds.; Elsevier: Amsterdam, 1994; Vol. 18, p 239-291.

(8) Kamenskaya, A. N. *Russ. J. Inorg. Chem.* **1984**, *29*, 251-258.

(9) Mikheev, N. B. *Inorg. Chim. Acta.* **1984**, *94*, 241-248.

(10) Mikheev, N. B.; Kamenskaya, A. N. *Coord. Chem. Rev.* **1991**, *109*, 1-59.

(11) Hitchcock, P. B.; Lappert, M. F.; Maron, L.; Protchenko, A. V. *Angew. Chem. Int. Ed.* **2008**, *47*, 1488-1491.

(12) MacDonald, M. R.; Ziller, J. W.; Evans, W. J. *J. Am. Chem. Soc.* **2011**, *133*, 15914-159147.

(13) MacDonald, M. R.; Bates, J. E.; Fieser, M. E.; Ziller, J. W.; Furche, F.; Evans, W. J. *J. Am. Chem. Soc.* **2012**, *134*, 8420-8423.

(14) MacDonald, M. R.; Bates, J. E.; Ziller, J. W.; Furche, F.; Evans, W. J. *J. Am. Chem. Soc.* **2013**, *135*, 9857-9868.

(15) Fieser, M. E.; MacDonald, M. R.; Krull, B. T.; Bates, J. E.; Ziller, J. W.; Furche, F.; Evans, W. J. *J. Am. Chem. Soc.* **2015**, *137*, 369-382.

(16) Langeslay, R. R.; Fieser, M. E.; Ziller, J. W.; Furche, F.; Evans, W. J. *Chem. Sci.* **2015**, *6*, 517-521.

(17) Windorff, C. J.; MacDonald, M. R.; Meihaus, M. R.; Ziller, J. W.; Long, J. R.; Evans, W. J. *Chem. Eur. J.* **2016**, *22*, 772-782.

(18) MacDonald, M. R.; Fieser, M. E.; Bates, J. E.; Ziller, J. W.; Furche, F.; Evans, W. J. *J. Am. Chem. Soc.* **2013**, *135*, 13310-13313.

(19) Windorff, C. J.; Chen, G. P.; Cross, J. N.; Evans, W. J.; Furche, F.; Gaunt, A. J.; Janicke, M. T.; Kozimor, S. A.; Scott, B. L. *J. Am. Chem. Soc.* **2017**, *139*, 3970-3973.

(20) Coles, M. P.; Hitchcock, P. B.; Lappert, M. F.; Protchenko, A. V. *Organometallics* **2012**, *31*, 2682-2690.

(21) Cassani, M. C.; Lappert, M. F.; Laschi, F. *Chem. Commun.* **1997**, 1563-1564.

(22) Gun'ko, Y. K.; Hitchcock, P. B.; Lappert, M. F. *J. Organomet. Chem.* **1995**, *499*, 213-219.

(23) Meihaus, M. R.; Fieser, M. E.; Corbey, J. F.; Evans, W. J.; Long, J. R. *J. Am. Chem. Soc.* **2015**, *137*, 9855-9860.

(24) Bergbreiter, D. E.; Killough, J. M. *J. Am. Chem. Soc.* **1978**, *100*, 2126-2134.

(25) Cassani, M. C.; Gun'ko, Y. K.; Hitchcock, P. B.; Lappert, M. F.; Laschi, F. *Organometallics* **1999**, *18*, 5539-5547.

(26) Bain, G. A.; Berry, J. F. *J. Chem. Educ.* **2008**, *85*, 532-536.

(27) APEX2 Version 2014.1-1, Bruker AXS, Inc.; Madison, WI, 2014.

(28) SAINT Version 8.34a., Bruker AXS, Inc.; Madison, WI, 2013.
(29) Sheldrick, G. M.; SADABS, Version 2014/4, Bruker AXS, Inc.; Madison, WI, 2014.
(30) Sheldrick, G. M.; SHELXTL, Version 2014/6, Bruker AXS, Inc.; Madison, WI, 2014.
(31) International Tables for X-Ray Crystallography, 1992, Vol. C. ed.; Dordrecht: Kluwer Academic Publishers.
(32) Sheldrick, G. M.; Version 2008/4, Bruker AXS, Inc.; Madison, WI, 2008.
(33) Sheldrick, G. M.; Version 2012/1, Bruker AXS, Inc.; Madison, WI, 2012.
(34) Shannon, R. D. *Acta Crystallogr A* **1976**, *32*, 751-767.
(35) Dutkiewicz, M. S.; Apostolidis, C.; Walter, O.; Arnold, P. L. *Chem. Sci.* **2017**, *8*, 2553-2561.
(36) Evans, W. J.; Sollberger, M. S.; Shreeve, J. L.; Olofson, J. M.; Hain, J. H., Jr.; Ziller, J. W. *Inorg. Chem.* **1992**, *31*, 2492-2501.
(37) Xie, Z.; Chui, K.; Liu, Z.; Xue, F.; Zhang, Z.; W., M. T. C.; Sun, J. *J. Organomet. Chem.* **1997**, *549*, 239-244.
(38) Stults, S. D.; Andemen, R. A.; Zalkin, A. *Organometallics* **1990**, *9*, 115-122.

CHAPTER 3

Reactivity of Complexes of $4f^n5d^1$ and $4f^{n+1}$ Ln^{2+} Ions with Cyclooctatetraene

INTRODUCTION[†]

As described in Chapters 1 and 2, it was found that complexes of Ln^{2+} ions can be isolated for all the lanthanides except promethium.[1-7] Crystallographic,[2-5] spectroscopic,[2-5] and magnetic characterization[8] along with density functional theory (DFT) analysis[2-5] for the homologous series of Ln^{2+} complexes, [K(2.2.2-cryptand)][Cp′$_3$Ln] (Cp′ = $C_5H_4SiMe_3$), suggested that the +2 ions can be classified into three categories based on their physical properties which have been related to electron configurations.[6,7] In the tris(cyclopentadienyl) coordination environment of complex [K(2.2.2-cryptand)][Cp′$_3$Ln], Eu^{2+}, Yb^{2+}, Sm^{2+}, and Tm^{2+} have the traditional $4f^{n+1}$ ground state electron configuration expected from reduction of $4f^n$ Ln^{3+} precursors, Cp′$_3$Ln.[5] In contrast, La^{2+}, Ce^{2+}, Pr^{2+}, Gd^{2+}, Tb^{2+}, Ho^{2+}, Er^{2+}, and Lu^{2+} have non-traditional $4f^n5d^1$ electron configurations arising from a low lying d_z^2 orbital in the trigonal planar geometry.[2-7] Y^{2+} also has a d^1 configuration, which for this second row transition metal is $4d^1$.[2,4] Nd^{2+} and Dy^{2+} comprise a third category of configurational crossover ions since they have $4f^n5d^1$ ground states in [K(2.2.2-cryptand)][Cp′$_3$Ln],[5] but have $4f^{n+1}$ configurations in other ligand environments.[9-11]

Reactivity studies of the [K(2.2.2-cryptand)][Cp′$_3$Ln] complexes of Ln = La, Ce, Dy, and Y have demonstrated that these new Ln^{2+} complexes can reduce substrates such as naphthalene (−2.36 V vs SHE) to generate Ln^{3+} complexes of the $(C_{10}H_8)^{2-}$ ligand, [K(2.2.2-cryptand)][Cp′$_2$Ln(η^4-$C_{10}H_8$)], eq 1.[12] In the case of Y and La, the Ln^{3+} co-product of the two electron naphthalene reduction was also identified, [K(2.2.2-cryptand)][Cp′$_4$Ln]. These new

[†] Portions of this chapter have been published: Palumbo, C. T.; Fieser, M. E.; Ziller, J. W.; Evans, W. J. *Organometallics*, **2017**, *36*, 3721-3728.

$4f^n5d^1$ Ln^{2+} ions ($4d^1$ for Y^{2+}) are thus more powerful reductants than $4f^6$ $(C_5Me_5)_2Sm$,[13] which is capable of reducing stilbene (−1.96 V vs SHE)[14] but not naphthalene,[15] and are at least as reducing as the $4f^{n+1}$ compounds DyI_2[16] and NdI_2,[16] which reduce naphthalene.[9]

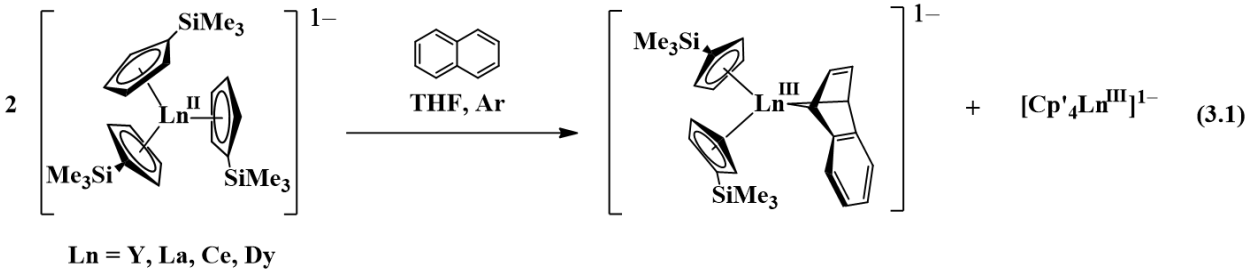

This Chapter examines consists of a reactivity study of the three categories of the [K(2.2.2-cryptand)][Cp′$_3$Ln] series to see whether differences in reactivity could be correlated to their electron configurations. The reactivity of Ln^{3+} complexes typically does not depend on the electron configuration, since the 4*f* orbitals have a limited radial extension away from the nucleus. Instead, reactivity is more often correlated with the size of the metal. Such correlations were not established for Ln^{2+} complexes, however, since the full series had not previously been available. To examine this question, a substrate reducible by all three types of Ln^{2+} complexes was necessary.

Cyclooctatetraene (−1.59 V vs SHE),[17] C_8H_8, was chosen as a substrate since it should be reduced by most of the variants of [K(2.2.2-cryptand)][Cp′$_3$Ln] and it also was successful in differentiating the chemistry of Th^{2+} vs U^{2+}.[18,19] A comparison of reactivity of the first molecular example of Th^{2+}, [K(18-crown-6)(THF)$_2$][Cp″$_3$Th] [Cp″ = $C_5H_3(SiMe_3)_2$],[19] and the analogous U^{2+} complex, [K(18-crown-6)(THF)$_2$][Cp″$_3$U],[18] with C_8H_8 gave Cp″$_2$Th(C_8H_8) and U(C_8H_8)$_2$ products, respectively, as shown in eqs 3.2 and 3.3.

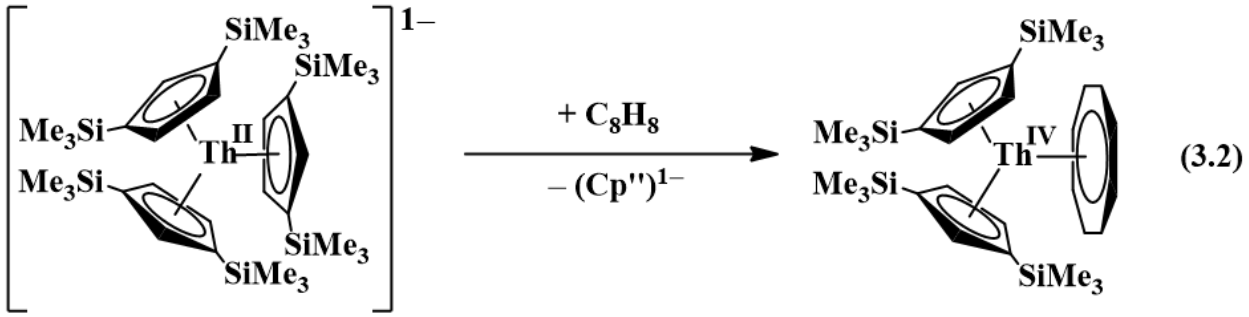

(3.2)

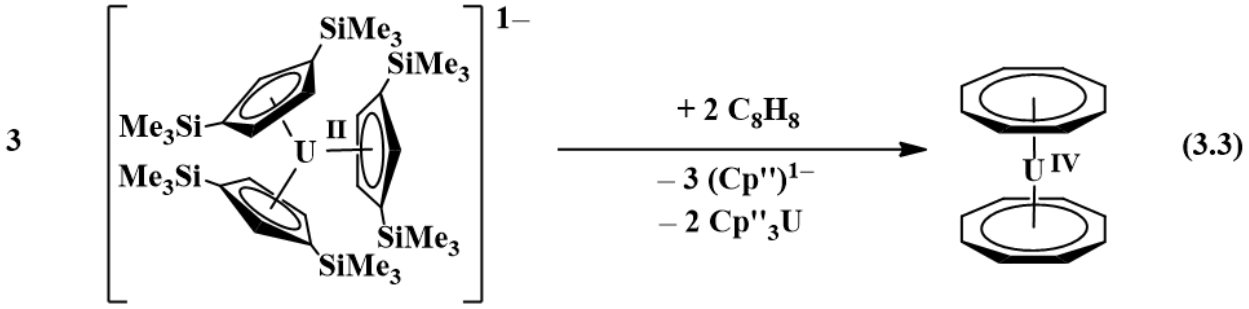

(3.3)

While there are numerous reduced C_8H_8 lanthanide complexes in the literature, most have been formed by salt metathesis with an already reduced $(C_8H_8)^{2-}$ starting material such as $K_2(C_8H_8)$.[20-25] However, reactions of C_8H_8 with Ln^0 metals (either by themselves or in the presence of I_2) are known, as well as reactions of Sm^{2+} and Tm^{2+} complexes with C_8H_8.[24,26-31] Additionally, $(C_5Me_5)Ln(C_8H_8)$ complexes have been formed from the reduction of C_8H_8 by Ln^{2+} complexes, such as $(C_5Me_5)_2Sm$,[17] and by Ln^{3+} complexes, such as the sterically crowded $(C_5Me_5)_3Ln$ complexes[17,32] and the metal hydrides $[(C_5Me_5)_2LnH]_2$ (Ln = Y, La, Sm).[33,34] Some of the resulting $(C_8H_8)^{2-}$ complexes, e.g. $(C_8H_8)Er(C_5Me_5)$,[35] are of interest as single-molecule magnets.[25,36-41] Reported here is a study of the reactivity of cyclooctatetraene with eight members of the [K(2.2.2-cryptand)][Cp′$_3$Ln] series.

EXPERIMENTAL

The syntheses and manipulations described below were conducted under argon with rigorous exclusion of air and water using glovebox, vacuum line, and Schlenk techniques. Solvents were sparged with UHP grade argon (Airgas) and passed through columns containing Q-5 and molecular sieves before use. NMR solvents (Cambridge Isotope Laboratories) were dried over NaK, degassed by three freeze–pump–thaw cycles, and vacuum-transferred before use. KC_8,[42] Cp'_3Ln (Ln = La, Sm, Dy, Nd,) and [K(2.2.2-cryptand)][Cp'_3Ln] (Ln = Ce, Pr, Sm, Eu, Dy, Tm, Yb),[4,43] were prepared according to the literature. 2.2.2-Cryptand (4,7,13,16,21,24-hexaoxa-1,10-diazabicyclo[8,8,8]hexacosane) (VWR), was placed under vacuum (10^{-3} Torr) for 12 h before use. Cyclooctatetraene (Aldrich) was placed over molecular sieves, degassed by three freeze–pump–thaw cycles, and vacuum-transferred before use. ^1H (500 MHz) and ^{13}C (125 MHz) NMR spectra were obtained on a Bruker GN500, CRYO500, or a AVANCE600 MHz spectrometer at 298 K.

[K(2.2.2-cryptand)][$Cp'_2La(C_8H_8)$], 11-La. In an argon-filled glovebox, [K(2.2.2-cryptand)][Cp'_3Ln] (50 mg, 0.048 mmol) was dissolved in in THF (10 mL) and the black/purple solution was stirred. C_8H_8 (1 drop, excess) was added and the reaction mixture immediately turned yellow. After allowing the reaction to stir for 20 min, the volatiles were removed under vacuum to yield pale green solids. The solids were extracted with Et_2O, the mixture was filtered to remove the solids, and the pale yellow solution was concentrated under vacuum. Storage of the solution at −35 °C in the glovebox freezer yielded colorless crystals of the previously characterized [K(2.2.2-cryptand)][Cp'_4La] (6 mg, 11%).[12] The left-over green solids were dissolved in THF (2 mL) and layered with a 1:1 mixture of Et_2O/hexane (15 mL). Storage of this mixture at −35 °C

overnight yielded pale green single crystals of **11-La**, suitable for X-ray diffraction (13 mg, 28%). IR: 3082m, 3044m, 3021m, 2953s, 2886s, 2816s, 2762m, 2731m, 1479s, 1458m, 1447s, 1416w, 1360s, 1356s, 1300s, 1260s, 1242s, 1186m, 1175w, 1134s, 1105s, 1080s, 1059m, 1040m, 1011s, 986s, 951s, 932s, 907m, 831s, 748s, 739s, 700m, 679m, 636w, 629w cm^{-1}. ^{1}H NMR (THF-d_8): δ 5.93 (t, $^{3}J_{HH}$ = 2.3 Hz, $C_5H_4SiMe_3$, 4H), 5.74 (s, C_8H_8, 8H) 5.41 (t, $^{3}J_{HH}$ = 2.2 Hz, $C_5H_4SiMe_3$, 4H), 3.42 (s, OCH_2CH_2O, 12H), 3.37 (t, $^{3}J_{HH}$ = 4.7 Hz, NCH_2CH_2O, 12H), 2.40 (t, $^{3}J_{HH}$ = 4.7 Hz, NCH_2CH_2O, 12H), 0.22 (s, $C_5H_4SiMe_3$, 18H). ^{13}C NMR (THF-d_8): 119.0 ($C_5H_4SiMe_3$), 113.5 ($C_5H_4SiMe_3$), 112.7 ($C_5H_4SiMe_3$), 95.3 (C_8H_8), 71.0 (OCH_2CH_2O), 68.2 (NCH_2CH_2O), 54.1 (NCH_2CH_2O), 1.5 ($C_5H_4SiMe_3$). Anal. Calcd for $C_{42}H_{70}N_2O_6Si_2KLa$: C, 54.06; H, 7.56; N, 3.00. Found: C, 53.79; H, 7.73; N, 2.56. The previously identified [K(2.2.2-cryptand)][La(C_8H_8)$_2$], **12-La**,[44] was also observed as a minor product by ^{1}H NMR spectroscopy. ^{1}H NMR (THF-d_8): δ 5.78 (s, C_8H_8, 16H), 3.49 (s, OCH_2CH_2O, 12H), 3.45 (t, $^{3}J_{HH}$ = 4.6 Hz, NCH_2CH_2O, 12H), 2.47 (t, $^{3}J_{HH}$ = 4.6 Hz, NCH_2CH_2O, 12H). ^{13}C NMR (THF-d_8): 97.9 (C_8H_8), 71.0 (OCH_2CH_2O), 68.2 (NCH_2CH_2O), 54.5 (NCH_2CH_2O).

[K(2.2.2-cryptand)][Cp′$_2$Ce(C_8H_8)], 11-Ce, [K(2.2.2-cryptand)][Ce(C_8H_8)$_2$], 12-Ce, and [K(2.2.2-cryptand)][Cp′$_4$Ce], 13-Ce. In an argon-filled glovebox, [K(2.2.2-cryptand)][Cp′$_3$Ce] (50 mg, 0.048 mmol) was dissolved in THF to yield a black/purple solution. C_8H_8 (1 drop, excess) was added and the color of the solution immediately changed to orange. After allowing the reaction to stir for 20 min, the volatiles were removed under vacuum. The resultant light orange solids were extracted with Et_2O and the mixture was centrifuged. The orange supernatant was filtered and left to stand at room temperature and in one attempt, red rectangular single crystals of **12-Ce** were obtained and characterized by X-ray diffraction (5 mg, 15%). Since these crystals were only isolated in one reaction, full characterization is not reported. Cooling the

resultant yellow mother liquor to −35 °C in the glovebox freezer gave pale yellow single crystals of [K(2.2.2-cryptand)][Cp′$_4$Ce]·Et$_2$O, **13-Ce·Et$_2$O**, as determined by X-ray crystallography (8 mg, 15%). ^{1}H NMR (THF-d_8): 5.5 (b, FWHH = 234 Hz, C$_5$*H*$_4$SiMe$_3$), 3.33 (s, OC*H*$_2$C*H*$_2$O, 12H), 3.30 (t, $^3J_{HH}$ = 4.7 Hz, NCH$_2$C*H*$_2$O, 12H), 2.32 (t, $^3J_{HH}$ = 4.7 Hz, NC*H*$_2$CH$_2$O, 12H), 0.25 (b, FWHH = 120 Hz, C$_5$*H*$_4$SiMe$_3$), −0.78 (b, FWHH = 64 Hz, C$_5$H$_4$Si*Me*$_3$). IR: 3081m, 3068m, 3034w, 2952s, 2889s, 2815s, 2762w, 2729w, 1476s, 1457m, 1443s, 1416w, 1398w, 1380w, 1361s, 1354s, 1299s, 1260s, 1243s, 1180s, 1134s, 1106s, 1080s, 1058m, 1039s, 1029m, 971w, 950s, 932m, 904s, 832s, 778m, 769m, 751s, 734m, 715w, 696w, 682w, 663w, 640m, 626m, 606m cm^{-1}. Anal. Calcd for C$_{50}$H$_{88}$N$_2$O$_6$Si$_4$KCe: C, 54.36; H, 8.03; N, 2.54. Found: C, 54.15; H, 8.06; N, 2.36. The Et$_2$O insoluble fraction was dissolved in THF (2 mL) and layered with a 1:1 Et$_2$O/hexane solution (15 mL). The mixture was left at room temperature for several hours which gave orange needles that were identified as **11-Ce** by X-ray crystallography (7 mg, 15%). IR: 3081m, 3023m, 2962s, 2943s, 2881s, 2815s, 2757w, 2731w, 1479s, 1457m, 1445s, 1415w, 1396w, 1360s, 1354s, 1301s, 1259s, 1242s, 1186s, 1174w, 1115s, 1099s, 1080s, 1055m, 1039s, 949s, 932s, 907m, 896m, 889w, 855m, 833, 814m, 794w, 785w, 763m, 751s, 748s, 740s, 701s, 689m, 679m, 674m, 669m, 664m, 655w, 634w, 629 cm^{-1}. ^{1}H NMR (THF-d_8): δ 24.4 (b, FWHH = 465 Hz, C$_5$*H*$_4$SiMe$_3$, 4H), 10.7 (b, FWHH = 232 Hz, C$_5$*H*$_4$SiMe$_3$, 4H), 3.22 (s, OC*H*$_2$C*H*$_2$O, 12H), 3.15 (t, $^3J_{HH}$ = 4.0 Hz, NCH$_2$C*H*$_2$O, 12H), 2.18 (t, $^3J_{HH}$ = 3.9 Hz, NC*H*$_2$CH$_2$O, 12H), −1.42 (b, FWHH = 100 Hz, C$_8$*H*$_8$, 8H), −6.28 (b, FWHH = 60 Hz, C$_5$H$_4$Si*Me*$_3$, 18H). ^{13}C NMR (THF-d_8): 98.2 (*C*$_8$H$_8$), 70.8 (O*C*H$_2$*C*H$_2$O), 68.0 (NCH$_2$*C*H$_2$O), 54.3 (N*C*H$_2$CH$_2$O), −8.8 (C$_5$H$_4$Si*Me*$_3$). The *C*$_5$H$_4$SiMe$_3$ ^{13}C NMR ring resonances were not definitively identifiable even on the 600 MHz spectrometer. Anal. Calcd for C$_{42}$H$_{70}$N$_2$O$_6$Si$_2$KCe: C, 53.99; H, 7.55; N, 3.00. Found: C, 53.39; H, 7.40; N, 2.74.

[K(2.2.2-cryptand)][Pr(C_8H_8)$_2$], 12-Pr, and [K(2.2.2-cryptand)][Cp′$_4$Pr], 13-Pr. In an argon-filled glovebox, [K(2.2.2-cryptand)][Cp′$_3$Pr] (40 mg, 0.038 mmol) was dissolved in THF (5 mL) to give a maroon/black solution. C_8H_8 (1 drop, excess) was added and the mixture immediately turned yellow. After 20 min, the volatiles were evaporated under reduced pressure and the resultant yellow solids were extracted with Et_2O (10 mL). The mixture was centrifuged and the supernatant concentrated and stored in the freezer to give **13-Pr·Et$_2$O** as characterized by X-ray crystallography (13 mg, 27%). ^{1}H NMR (THF-d_8): −3.4 (b, FWHH = 440 Hz, SiMe_3). IR: 3083m, 3068m, 3035w, 2968s, 2951s, 2887s, 2812s, 2763w, 2730w, 1476s, 1458m, 1443s, 1415w, 1398w, 1380w, 1360s, 1354s, 1297s, 1260s, 1242s, 1181s, 1134s, 1106s, 1079s, 1058m, 1039s, 1028m, 975w, 950s, 932m, 904s, 831s, 771m 751s, 733s, 715w, 701w, 696w, 684w, 663w, 641m, 627m, 605w cm^{-1}. Anal. Calcd for $C_{50}H_{88}N_2O_6Si_4KPr$: C, 54.32; H, 8.02; N, 2.53. Found: C, 54.17; H, 8.07; N, 2.40. The Et_2O insoluble fraction was dissolved in THF (5 mL), filtered, and layered with a 1:1 mixture of Et_2O/hexane (15 mL). The layered mixture was left at ambient temperature for 12 h to yield pale yellow single crystals of **12-Pr** suitable for X-ray diffraction (6 mg, 21%). ^{1}H NMR (THF-d_8): δ 5.90 (b, FWHH = 26 Hz, NCH$_2$CH_2O, 12H), 5.86 (b, FWHH = 26 Hz, OCH_2CH_2O, 12H), 4.86 (b, FWHH = 26 Hz, NCH_2CH$_2$O, 12H), −7.64 (b, FWHH = 250 Hz, C$_8H_8$, 8H), −6.28 (b, FWHH = 60 Hz, C$_5$H$_4$SiMe_3, 16H) . ^{13}C NMR (THF-d_8): δ 208.0 (C_8H_8) 74.1 (crypt), 71.4 (crypt), 57.6 (crypt). IR: 3031m, 3011m, 2960m, 2882s, 2842m, 2823m, 1478m, 1458m, 1446m, 1412w, 1389w, 1356s, 1351s, 1305m, 1292m, 1255m, 1235w, 1171w, 1132s, 1115s, 1097s, 1078s, 1053m, 1040w, 1032w, 951s, 931m, 895s, 830m, 819w, 797w, 752w, 742m, 670s cm^{-1}. Anal. Calcd for $C_{34}H_{52}N_2O_6KPr$: C, 53.40; H, 6.85; N, 3.66. Found: C, 52.53; H, 6.32; N, 3.31.

[K(2.2.2-cryptand)][(C_8H_8)$_2$Sm], 12-Sm and [K(2.2.2-cryptand)][Cp′$_4$Sm], 13-Sm. In an argon-filled glovebox, [K(2.2.2-cryptand)][Cp′$_3$Sm] (50 mg, 0.048 mmol) was dissolved in THF to produce a dark purple solution. C_8H_8 (1 drop, excess) was added and the solution immediately turned dark orange. After allowing the reaction to stir for 30 min, the volatiles were removed under reduced pressure. The solids were stirred in Et_2O, centrifuged, and filtered. Cooling of the concentrated Et_2O supernatant gave single-crystals of **13-Sm·Et$_2$O** characterizable by X-ray crystallography (5 mg, 9%). ^{1}H NMR (THF-d_8): −0.24 (b, FWHH = 75 Hz, SiMe_3). Red single crystals of **12-Sm** (5 mg, 13%) suitable for X-ray diffraction were grown from a concentrated THF solution at −35 °C. ^{1}H NMR (THF-d_8): 13.3 (s, C_8H_8, 16H), 2.50 (s, OCH_2CH_2O, 12H), 2.42 (t, $^3J_{HH}$ = 4.6 Hz, NCH_2CH_2O, 12H), 1.47 (t, $^3J_{HH}$ = 4.6 Hz, NCH_2CH_2O, 12H). IR: 3030m, 3009m, 2959m, 2881s, 2843m, 2820m, 1478m, 1458m, 1447m, 1410w, 1385w, 1352s, 1304m, 1294m, 1256m, 1234w, 1215w, 1165w, 1134s, 1115s, 1098s, 1080s, 1055m, 1040w, 1032w, 951s, 932m, 895s, 831m, 820m, 797w, 760w, 750w, 741m, 671s cm^{-1}.

[K(2.2.2-cryptand)][Cp′$_4$Tm], 13-Tm. In an argon-filled glovebox, [K(2.2.2-cryptand)][Cp′$_3$Tm] (40 mg, 0.037 mmol) was dissolved in THF (10 mL) to give a dark red solution. C_8H_8 (one drop, excess) was added and the solution immediately turned peach in color. The volatiles were removed under reduced pressure to give peach solids, which were extracted with Et_2O. The extract was centrifuged and filtered. The supernatant was concentrated under reduced pressure until saturation and stored at −35 °C which gave colorless single-crystalline **13-Tm**, suitable for X-ray diffraction (15 mg, 35%). To fully characterize this complex, an independent sample was prepared by adding KCp′ (61 mg, 0.34 mmol) to a stirred solution of Cp′$_3$Tm (200 mg, 0.344 mmol) and 2.2.2-cryptand (130 mg, 0.344 mmol) in THF (10 mL). The solvent was removed and the solids were dissolved in Et_2O (20 mL). Concentration of the Et_2O

solution and storage at −35 °C gave analytically pure crystals of **13-Tm** (336 mg, 86%). IR: 3073m, 3054m, 3046m, 3033m, 2952s, 2889s, 2875s, 2812s, 2761w, 2757w, 2729w, 1474s, 1455m, 1444s, 1414w, 1398w, 1360s, 1354s, 1298s, 1259s, 1242s, 1181s, 1133s, 1105s, 1079s, 1058m, 1041s, 1026s, 950s, 932s, 908s, 903s, 856m, 831s, 800m, 779s, 749s, 732s, 702m, 682m, 641m, 634m, 627m, 605m. Anal. Calcd for $C_{50}H_{88}N_2O_6KTm$: C, 52.97; H, 7.82; N, 2.47. Found: C, 52.47; H, 7.57; N, 2.34.

[K(2.2.2-cryptand)][Cp′$_4$Dy], 13-Dy. In an argon-filled glovebox, a pale-yellow solution of Cp′$_3$Dy (25 mg, 0.043 mmol) and 2.2.2-cryptand (16 mg, 0.043 mmol) in THF (3 mL) were combined with KC_8 (7 mg, 0.05 mmol) to produce a dark red/brown solution. The mixture was centrifuged and filtered. C_8H_8 (1 drop, excess) was added to the supernatant, which resulted in the immediate color change to pale yellow. The volatiles were removed under reduced pressure and the resultant solids were extracted with Et_2O (5 mL), centrifuged, and filtered. The supernatant was concentrated under reduced pressure and stored at −35 °C which gave single-crystalline blocks of **13-Dy·Et$_2$O** suitable for X-ray diffraction (8 mg, 15%). IR: 3088m, 3070m, 3034w, 2968s, 2950s, 2889s, 2820s, 2762w, 2732w, 1479s, 1452m, 1444s, 1412w, 1400w, 1380w, 1360s, 1300s, 1260s, 1246s, 1182s, 1134s, 1105s, 1082s, 1051m, 1039s, 1029m, 948s, 932m, 903s, 831s, 791m 774s, 765m, 751s, 731s, 715w, 701w, 683w, 667w, 641m, 629m, 605w cm^{-1}.

[K(2.2.2-cryptand)][Nd(C$_8$H$_8$)$_2$], 12-Nd and [K(2.2.2-cryptand)][Cp′$_4$Nd], 13-Nd. In an argon-filled glovebox, [K(2.2.2-cryptand)][Cp′$_3$Nd] (40 mg, 0.038 mmol) was dissolved in THF (3 mL) and stirred to produce a dark red/brown solution. C_8H_8 (1 drop, excess) was added, which resulted in the immediate color change to pale green. The volatiles were removed under reduced pressure and the resultant solids were extracted with Et_2O (5 mL) centrifuged, and filtered. The supernatant was concentrated under reduced pressure and stored at −35 °C which gave light-blue

single-crystalline blocks of **13-Nd·Et$_2$O** suitable for X-ray diffraction (11 mg, 24%). ^{1}H NMR (THF-d_8): −2.1 (b, FWHH = 310 Hz, SiMe_3). IR: 3084m, 3069m, 3034w, 2953s, 2893s, 2816s, 2762w, 2729w, 1478s, 1454m, 1445s, 1416w, 1400w, 1383w, 1360s, 1298s, 1260s, 1244s, 1180s, 1134s, 1105s, 1080s, 1059m, 1040s, 1028m, 951s, 934m, 905s, 829s, 781m 772s, 752s, 733s, 698w, 683w, 664w, 640w, 629w, 606w cm^{-1}. Anal. Calcd for $C_{54}H_{98}N_2O_7KNd$: C, 54.82; H, 8.35; N, 2.37. Found: C, 53.28; H, 7.42; N, 2.15 and C, 53.98; H, 7.16; N, 2.04. The left-over green solids from the centrifugation were dissolved in THF (2 mL) and layered with a 1:1 Et$_2$O/hexane solution (15 mL) to yield yellow single crystals of **12-Nd** suitable for X-ray diffraction (9 mg, 31%). ^{1}H NMR (THF-d_8): δ 3.64 (b, FWHH = 12 Hz, NCH$_2$CH_2O, 12H), 3.60 (b, FWHH = 15 Hz, OCH_2CH_2O, 12H), 2.63 (b, FWHH = 12 Hz, NCH_2CH$_2$O, 12H), −8.87 (b, FWHH = 175 Hz, C$_8H_8$, 16H). ^{13}C NMR (THF-d_8): δ 125.3 (C_8H$_8$) 71.8 (crypt), 69.0 (crypt), 55.2 (crypt). IR: 3031m, 3011m, 2958m, 2882s, 2842m, 2824m, 1478m, 1459m, 1446m, 1413w, 1388w, 1357s, 1351s, 1304m, 1292m, 1255m, 1236m, 1171w, 1134s, 1116s, 1098s, 1078s, 1053m, 1040w, 1032w, 951s, 932m, 895s, 830m, 818w, 792w, 752w, 741m, 671s cm^{-1}.

[K(2.2.2-cryptand)][(Cp′$_3$Dy)$_2$H], 14-Dy. In an argon-filled glovebox, C$_8$H$_8$ (11 mg, 0.10 mmol) was added to a dark red/brown stirred solution of [K(2.2.2-cryptand)][Cp′$_3$Dy] (100 mg, 0.105 mmol) in THF (10 mL). The dark mixture immediately turned bright green and after stirring for 30 min, the volatiles were removed from the resultant pale green solution. The resultant solids were extracted with Et$_2$O (10 mL) and the mixture was centrifuged. The supernatant was concentrated under reduced pressure until saturation and stored at −30 °C which gave single-crystalline blocks of **13-Dy·Et$_2$O** identified by X-ray diffraction. The leftover green solids were dissolved in a 1:1 THF/Et2O mixture (5 mL), filtered, and the resultant solution was layered with

hexane (15 mL) and stored at −30 °C for two days to yield hexagonal shaped single-crystals characterized as **14-Dy** by X-ray diffraction.

X-ray Data Collection, Structure Solution and Refinement for [K(2.2.2-cryptand)][Cp′$_2$La(C$_8$H$_8$)], 11-La. A colorless crystal of approximate dimensions 0.132 x 0.183 x 0.260 mm was mounted on a glass fiber and transferred to a Bruker SMART APEX II diffractometer. The APEX2[45] program package was used to determine the unit-cell parameters and for data collection (10 sec/frame scan time for a sphere of diffraction data). The raw frame data was processed using SAINT[46] and SADABS[47] to yield the reflection data file. Subsequent calculations were carried out using the SHELXTL[48] program. There were no systematic absences nor any diffraction symmetry other than the Friedel condition. The centrosymmetric triclinic space group P was assigned and later determined to be correct. The structure was solved by direct methods and refined on F2 by full-matrix least-squares techniques. The analytical scattering factors[49] for neutral atoms were used throughout the analysis. Hydrogen atoms were included using a riding model. At convergence, wR2 = 0.0591 and Goof = 1.037 for 493 variables refined against 12127 data (0.73Å), R1 = 0.0274 for those 10674 data with I > 2.0 σ(I). There were several high residuals present in the final difference-Fourier map. It was not possible to determine the nature of the residuals although it was probable that tetrahydrofuran and/or diethylether solvent was present. The SQUEEZE routine in the PLATON[50,51] program package was used to account for the electrons in the solvent accessible voids. Details are given in Table 3.1.

X-ray Data Collection, Structure Solution and Refinement for [K(2.2.2-cryptand)][Cp′$_2$Ce(C$_8$H$_8$)], 11-Ce. An orange crystal of approximate dimensions 0.148 x 0.205 x 0.286 mm was mounted in a cryoloop and transferred to a Bruker SMART APEX II diffractometer. The APEX2[45] program package was used to determine the unit-cell parameters

and for data collection (20 sec/frame scan time for a sphere of diffraction data). The raw frame data was processed using SAINT[46] and SADABS[47] to yield the reflection data file. Subsequent calculations were carried out using the SHELXTL[48] program. There were no systematic absences nor any diffraction symmetry other than the Friedel condition. The centrosymmetric triclinic space group $P\bar{1}$ was assigned and later determined to be correct. The structure was solved using the coordinates of the lanthanum analogue direct methods and refined on F^2 by full-matrix least-squares techniques. The analytical scattering factors[49] for neutral atoms were used throughout the analysis. Hydrogen atoms were included using a riding model. At convergence, wR2 = 0.0658 and Goof = 1.050 for 493 variables refined against 11562 data (0.74Å), R1 = 0.0260 for those 10706 data with $I > 2.0\sigma(I)$. There were several high residuals present in the final difference-Fourier map. It was not possible to determine the nature of the residuals although it was probable that diethylether solvent was present. The SQUEEZE routine in the PLATON[50,51] program package was used to account for the electrons in the solvent accessible voids. Details are given in Table 3.1.

X-ray Data Collection, Structure Solution and Refinement for [K(2.2.2-cryptand)][Ce(C_8H_8)$_2$], 12-Ce. A green crystal of approximate dimensions 0.122 x 0.184 x 0.304 mm was mounted in a cryoloop and transferred to a Bruker SMART APEX II diffractometer. The APEX2[45] program package was used to determine the unit-cell parameters and for data collection (20 sec/frame scan time for a sphere of diffraction data). The raw frame data was processed using SAINT[46] and SADABS[47] to yield the reflection data file. Subsequent calculations were carried out using the SHELXTL[48] program. The diffraction symmetry was 2/m and the systematic absences were consistent with the monoclinic space groups Cc and C2/c. It was later determined that space group Cc was correct. The structure was solved using the coordinates of the samarium

analogue and refined on F2 by full-matrix least-squares techniques. The analytical scattering factors[49] for neutral atoms were used throughout the analysis. Hydrogen atoms were included using a riding model. At convergence, wR2 = 0.0427 and Goof = 0.895 for 398 variables refined against 8806 data (0.73Å), R1 = 0.0232 for those 8172 data with I > 2.0σ(I). The structure was refined as a two-component inversion twin. Details are given in Table 3.2.

X-ray Data Collection, Structure Solution and Refinement for [K(2.2.2-cryptand)][Pr(C_8H_8)$_2$], 12-Pr. A yellow crystal of approximate dimensions 0.136 x 0.193 x 0.287 mm was mounted in a cryoloop and transferred to a Bruker SMART APEX II diffractometer. The APEX2[45] program package was used to determine the unit-cell parameters and for data collection (30 sec/frame scan time for a sphere of diffraction data). The raw frame data was processed using SAINT[46] and SADABS[47] to yield the reflection data file. Subsequent calculations were carried out using the SHELXTL[48] program. The diffraction symmetry was 2/*m* and the systematic absences were consistent with the monoclinic space groups *Cc and C*2/*c*. It was later determined that space group *Cc* was correct. The structure was solved using the coordinates of the samarium analogue and refined on F^2 by full-matrix least-squares techniques. The analytical scattering factors[49] for neutral atoms were used throughout the analysis. Hydrogen atoms were included using a riding model. At convergence, wR2 = 0.0468 and Goof = 0.992 for 398 variables refined against 8330 data (0.74Å), R1 = 0.0223 for those 8614 data with I > 2.0σ(I). The structure was refined as a two-component inversion twin. Details are given in Table 3.2.

X-ray Data Collection, Structure Solution and Refinement for [K(2.2.2-cryptand)][Nd(C_8H_8)$_2$], 12-Nd. A yellow crystal of approximate dimensions 0.114 x 0.264 x 0.305 mm was mounted on a glass fiber and transferred to a Bruker SMART APEX II diffractometer. The APEX2[45] program package was used to determine the unit-cell parameters

and for data collection (15 sec/frame scan time for a sphere of diffraction data). The raw frame data was processed using SAINT[46] and SADABS[47] to yield the reflection data file. Subsequent calculations were carried out using the SHELXTL[48] program. The diffraction symmetry was 2/*m* and the systematic absences were consistent with the monoclinic space groups *Cc and C*2/*c*. It was later determined that space group *Cc* was correct. The structure was solved using the coordinates of the samarium analogue and refined on F^2 by full-matrix least-squares techniques. The analytical scattering factors[49] for neutral atoms were used throughout the analysis. Hydrogen atoms were included using a riding model. At convergence, wR2 = 0.0404 and Goof = 1.027 for 398 variables refined against 8793 data (0.73Å), R1 = 0.0171 for those 8614 data with $I > 2.0\sigma(I)$. The structure was refined as a two-component inversion twin. Details are given in Table 3.2.

X-ray Data Collection, Structure Solution and Refinement for [K(2.2.2-cryptand)][Sm(C_8H_8)$_2$], 12-Sm. A red crystal of approximate dimensions 0.146 x 0.306 x 0.535 mm was mounted on a glass fiber and transferred to a Bruker SMART APEX II diffractometer. The APEX2[45] program package was used to determine the unit-cell parameters and for data collection (10 sec/frame scan time for a sphere of diffraction data). The raw frame data was processed using SAINT[46] and SADABS[47] to yield the reflection data file. Subsequent calculations were carried out using the SHELXTL[48] program. The diffraction symmetry was 2/*m* and the systematic absences were consistent with the monoclinic space groups *Cc and C*2/*c*. It was later determined that space group *Cc* was correct. The structure was solved by direct methods and refined on F^2 by full-matrix least-squares techniques. The analytical scattering factors[49] for neutral atoms were used throughout the analysis. Hydrogen atoms were included using a riding model. At convergence, wR2 = 0.0329 and Goof = 1.046 for 398 variables refined against 8683 data

(0.73Å), R1 = 0.0128 for those 8652 data with I > 2.0σ(I). The structure was refined as a two-component inversion twin. Details are given in Table 3.2.

X-ray Data Collection, Structure Solution and Refinement for [K(2.2.2-cryptand)][Cp′$_4$Ce], 13-Ce. A yellow crystal of approximate dimensions 0.464 x 0.341 x 0.240 mm was mounted on a glass fiber and transferred to a Bruker SMART APEX II diffractometer. The APEX2[45] program package was used to determine the unit-cell parameters and for data collection (20 sec/frame scan time for a sphere of diffraction data). The raw frame data was processed using SAINT[46] and SADABS[47] to yield the reflection data file. Subsequent calculations were carried out using the SHELXTL[48] program. There were no systematic absences nor any diffraction symmetry other than the Friedel condition. The centrosymmetric triclinic space group $P\bar{1}$ was assigned and later determined to be correct. The structure was solved by direct methods and refined on F^2 by full-matrix least-squares techniques. The analytical scattering factors[49] for neutral atoms were used throughout the analysis. H(26A) was located from a difference-Fourier map and refined (x,y,z and U_{iso}). There was one half molecule of diethylether solvent present per formula unit which was disordered about an inversion center and included using multiple components with partial site-occupancy-factors. Hydrogen atoms associated with the disordered solvent were not included in the refinement. All remaining hydrogen atoms were included using a riding model. At convergence, wR2 = 0.0735 and Goof = 1.048 for 613 variables refined against 14394 data (0.74 Å), R1 = 0.0282 for those 12979 data with I > 2.0σ(I). Details are given in Table 3.3.

X-ray Data Collection, Structure Solution and Refinement for [K(2.2.2-cryptand)][Cp′$_4$Pr], 13-Pr. A pale green crystal of approximate dimensions 0.216 x 0.230 x 0.444 mm was mounted in a cryoloop and transferred to a Bruker SMART APEX II diffractometer.

The APEX2[45] program package was used to determine the unit-cell parameters and for data collection (20 sec/frame scan time for a sphere of diffraction data). The raw frame data was processed using SAINT[46] and SADABS[47] to yield the reflection data file. Subsequent calculations were carried out using the SHELXTL[48] program. There were no systematic absences nor any diffraction symmetry other than the Friedel condition. The centrosymmetric triclinic space group $P\bar{1}$ was assigned and later determined to be correct. The structure was solved using the coordinates of the cerium analogue and refined on F^2 by full-matrix least-squares techniques. The analytical scattering factors[49] for neutral atoms were used throughout the analysis. H(26A) was located from a difference-Fourier map and refined (x,y,z and U_{iso}). All remaining hydrogen atoms were included using a riding model. There was one half molecule of diethylether solvent present per formula unit which was disordered about an inversion center and included using multiple components with partial site-occupancy-factors. At convergence, wR2 = 0.0868 and Goof = 1.042 for 615 variables refined against 14960 data (0.73 Å), R1 = 0.0327 for those 13226 data with I > 2.0σ(I). Details are given in Table 3.3.

X-ray Data Collection, Structure Solution and Refinement for [K(2.2.2-cryptand)][Cp′$_4$Nd], 13-Nd. A blue crystal of approximate dimensions 0.273 x 0.305 x 0.408 mm was mounted in a cryoloop and transferred to a Bruker SMART APEX II diffractometer. The APEX2[45] program package was used to determine the unit-cell parameters and for data collection (10 sec/frame scan time for a sphere of diffraction data). The raw frame data was processed using SAINT[46] and SADABS[47] to yield the reflection data file. Subsequent calculations were carried out using the SHELXTL[48] program. There were no systematic absences nor any diffraction symmetry other than the Friedel condition. The centrosymmetric triclinic space group $P\bar{1}$ was assigned and later determined to be correct. The structure was solved using the coordinates of the

cerium analogue and refined on F^2 by full-matrix least-squares techniques. The analytical scattering factors[49] for neutral atoms were used throughout the analysis. H(26A) was located from a difference-Fourier map and refined (x,y,z and U_{iso}). All remaining hydrogen atoms were included using a riding model. There was one half molecule of diethylether solvent present per formula unit which was disordered about an inversion center and included using multiple components with partial site-occupancy-factors. At convergence, wR2 = 0.0734 and Goof = 1.033 for 615 variables refined against 15162 data (0.73 Å), R1 = 0.0291 for those 13478 data with I > 2.0σ(I). Details are given in Table 3.3.

X-ray Data Collection, Structure Solution and Refinement for [K(2.2.2-cryptand)][Cp′$_4$Sm], 13-Sm. A yellow crystal of approximate dimensions 0.183 x 0.323 x 0.386 mm was mounted in a cryoloop and transferred to a Bruker SMART APEX II diffractometer. The APEX2[45] program package was used to determine the unit-cell parameters and for data collection (10 sec/frame scan time for a sphere of diffraction data). The raw frame data was processed using SAINT[46] and SADABS[47] to yield the reflection data file. Subsequent calculations were carried out using the SHELXTL[48] program. There were no systematic absences nor any diffraction symmetry other than the Friedel condition. The centrosymmetric triclinic space group $P\bar{1}$ was assigned and later determined to be correct. The structure was solved using the coordinates of the neodymium analogue and refined on F^2 by full-matrix least-squares techniques. The analytical scattering factors[49] for neutral atoms were used throughout the analysis. H(26A) was located from a difference-Fourier map and refined (x,y,z and U_{iso}). All remaining hydrogen atoms were included using a riding model. Carbon atoms C(6), C(7) and C(8) were disordered and were included using multiple components with partial site-occupancy-factors. There was one half molecule of diethylether solvent present per formula unit which was disordered about an inversion

center and included as above. At convergence, wR2 = 0.0660 and Goof = 1.060 for 670 variables refined against 13265 data (0.78 Å), R1 = 0.0291 for those 12024 data with I > 2.0σ(I). Details are given in Table 3.3.

X-ray Data Collection, Structure Solution and Refinement for [K(2.2.2-cryptand)][Cp′$_4$Dy], 13-Dy. A yellow crystal of approximate dimensions 0.210 x 0.284 x 0.431 mm was mounted in a cryoloop and transferred to a Bruker SMART APEX II diffractometer. The APEX2[45] program package was used to determine the unit-cell parameters and for data collection (10 sec/frame scan time for a sphere of diffraction data). The raw frame data was processed using SAINT[46] and SADABS[47] to yield the reflection data file. Subsequent calculations were carried out using the SHELXTL[48] program. There were no systematic absences nor any diffraction symmetry other than the Friedel condition. The centrosymmetric triclinic space group $P\bar{1}$ was assigned and later determined to be correct. The structure was solved by direct methods and refined on F^2 by full-matrix least-squares techniques. The analytical scattering factors[49] for neutral atoms were used throughout the analysis. H(26A) was located from a difference-Fourier map and refined (x,y,z and U_{iso}). The remaining hydrogen atoms were included using a riding model. At convergence, wR2 = 0.0510 and Goof = 1.042 for 593 variables refined against 13458 data (0.74 Å), R1 = 0.0204 for those 12760 data with I > 2.0σ(I). Details are given in Table 3.3.

X-ray Data Collection, Structure Solution and Refinement for [K(2.2.2-cryptand)][Cp′$_4$Tm], 13-Tm. A colorless crystal of approximate dimensions 0.208 x 0.238 x 0.315 mm was mounted on a glass fiber and transferred to a Bruker SMART APEX II diffractometer. The APEX2[45] program package was used to determine the unit-cell parameters and for data collection (15 sec/frame scan time for a sphere of diffraction data). The raw frame data was processed using SAINT[46] and SADABS[47] to yield the reflection data file. Subsequent

calculations were carried out using the SHELXTL[48] program. There were no systematic absences nor any diffraction symmetry other than the Friedel condition. The centrosymmetric triclinic space group $P\bar{1}$ was assigned and later determined to be correct. The structure was solved by direct methods and refined on F^2 by full-matrix least-squares techniques. The analytical scattering factors[49] for neutral atoms were used throughout the analysis. Hydrogen atoms H(18A), H(19A) and H(26A) were located from a difference-Fourier map and refined (x,y,z and riding U_{iso}). The remaining hydrogen atoms were included using a riding model. At convergence, wR2 = 0.0656 and Goof = 1.058 for 599 variables refined against 14284 data (0.73Å), R1 = 0.0270 for those 13424 data with $I > 2.0\sigma(I)$. Details are given in Table 3.3.

X-ray Data Collection, Structure Solution and Refinement for [K(2.2.2-cryptand)][(Cp′$_3$Dy)$_2$H], 14-Dy. A crystal was mounted on a Bruker SMART APEX II diffractometer. The APEX2[45] program package was used to determine the unit-cell parameters and for data collection (5 sec/frame scan time for a sphere of diffraction data). The raw frame data was processed using SAINT[46] and SADABS[47] to yield the reflection data file. Subsequent calculations were carried out using the SHELXTL[48] program. The diffraction symmetry was 2/*m* and the systematic absences were consistent with the monoclinic space groups *Cc* and *C*2/*c*. It was later determined that space group *C*2/*c* was correct. The structure was solved by dual space methods and refined on F^2 by full-matrix least-squares techniques. The analytical scattering factors[49] for neutral atoms were used throughout the analysis. Hydrogen atom H1) was located from a difference-Fourier map and refined (x,y,z and U_{iso}). The remaining hydrogen atoms were included using a riding model. Refinement yielded wR2 = 0.1967 and Goof = 1.028 for 397 variables refined against 7630 data (0.83Å), R1 = 0.0717 for those 5345 data with $I > 2.0\sigma(I)$. Details are given in Table 3.4.

RESULTS

Reactivity of Non-Traditional $4f^n5d^1$ Ln^{2+} Ions. Lanthanum, Cerium and Praseodymium. Treatment of THF solutions of [K(2.2.2-cryptand)][Cp′$_3$Ln] (Ln = La, Ce, Pr), **1-Ln**, with C_8H_8 caused immediate color changes of the highly absorbing purple (La, Ce) and maroon (Pr) solutions to yellow, orange, and pale yellow, respectively. The reactions of **1-La** and **1-Ce** with C_8H_8 are similar in that both produced [K(2.2.2-cryptand)][Cp′$_2$Ln(C_8H_8)], **2-Ln**, Figure 1, the product of reduction of C_8H_8 by two equiv of the Ln^{2+} complex, as well as the expected[10] tetra(cyclopentadienyl) co-product,

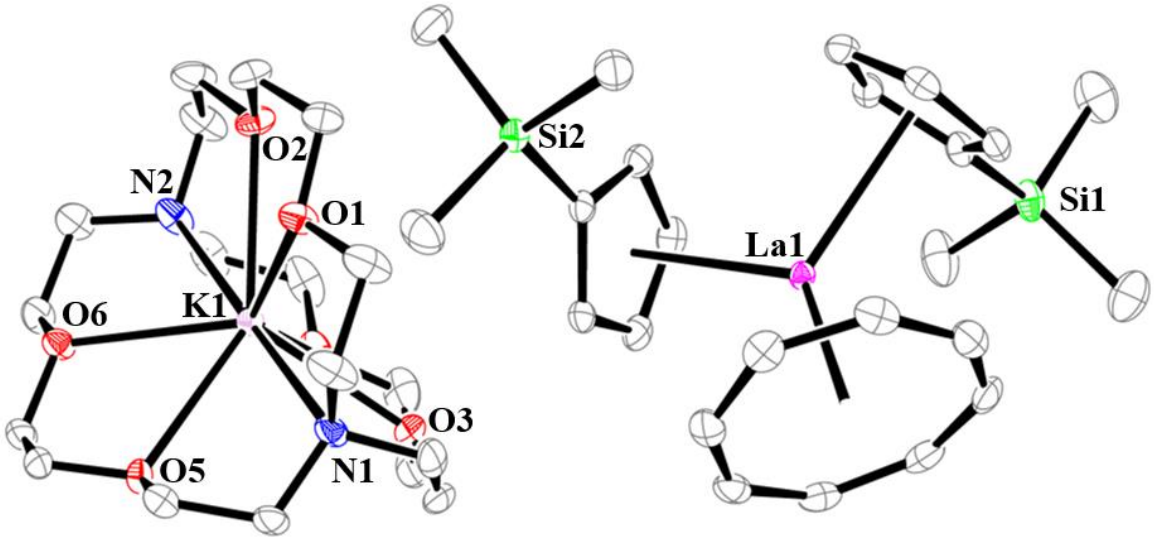

Figure 3.1. Thermal ellipsoid plot of [K(2.2.2-cryptand)][Cp′$_2$La(C_8H_8)], **11-La**, with thermal ellipsoids drawn at the 50% probability level. Hydrogen atoms are omitted for clarity. **11-Ce** is isomorphous.

[K(2.2.2-cryptand)][Cp′$_4$Ln], **13-Ln**. The **13-Ln** products are analogous to [K(2.2.2-cryptand)][Cp′$_2$Ln($C_{10}H_8$)] previously obtained from the two-electron reduction of naphthalene by

[K(2.2.2-cryptand)][Cp′$_3$Ln], which forms **13-Ln** as a co-product, eq 3.1. The **11-Ln** products are also the Ln^{3+} analogs of the Th^{4+} complex, Cp″$_2$Th(C_8H_8), in eq 3.2.

The ^{1}H NMR spectrum of the lanthanum product mixture shows resonances for **11-La** and **13-La** in an approximate 1:1 molar ratio. However, complex **13-La** was isolated in only about half the yield (11%) of that of isolated **11-La** (28%), since the crystalline yield depends on the relative solubilities of the compounds and their capacity to crystallize. The known bis(cyclooctatetraenyl) complex [K(2.2.2-cryptand)][La(C_8H_8)$_2$], **12-La**,[44] the Ln^{3+} analog of uranocene, U(C_8H_8)$_2$, in eq 3, was also observed by ^{1}H NMR spectroscopy, but only as a minor product (ca. 1:16 molar ratio of **12-La/11-La** by ^{1}H NMR spectroscopy). Since this reaction forms a mixture of three products separable only by fractional crystallization, it is not suitable as a synthetic route to these complexes. However, it does allow discrimination of Ln^{2+} reactivity when compared to the other metals described below and this is the point of the study. Complete characterization of all the products in these reactions has not been achievable due to the complexity of the reactions and the low yield of some of the minor products. However, the anion in **12-Ln**, *i.e.* [Ln(C_8H_8)$_2$]$^{1-}$,[21,22,25,41,52-54] and **13-Ln**[12] are known classes of complexes.

In the cerium reaction, both the mono(cyclooctatetraenyl) reduction product, **11-Ce**, and the bis(cyclooctatetraenyl) reduction product, **12-Ce**, could be isolated and crystallographically characterized, as well as the tetra(cyclopentadienyl) co-product, **13-Ce**, eq 3.4. Red single-crystals

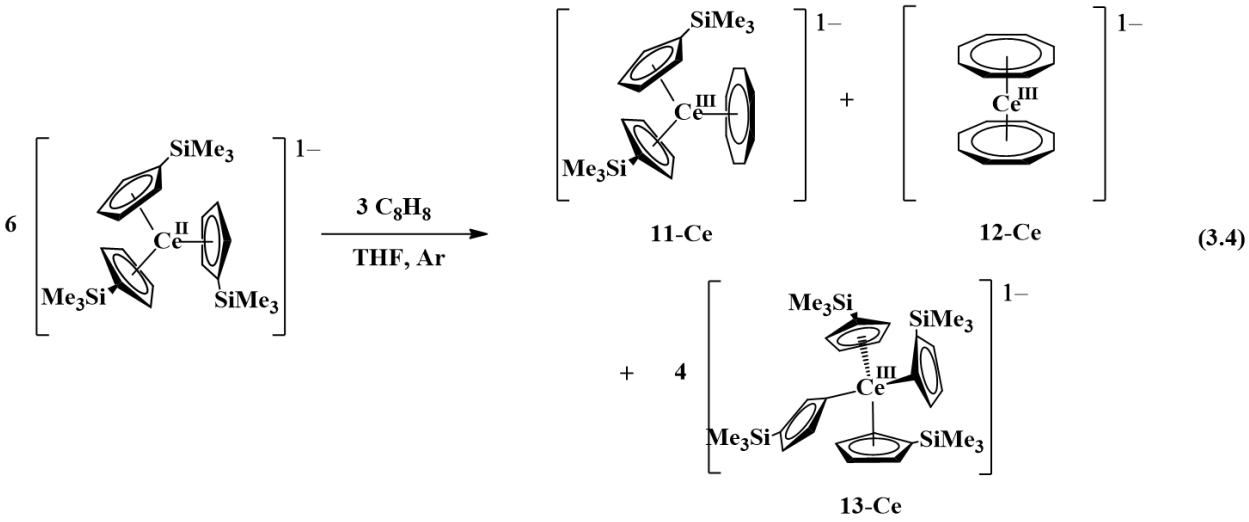

of the bis(cyclooctatetraenyl) complex [K(2.2.2-cryptand)][Ce(C_8H_8)$_2$], **12-Ce**, Figure 3.2, crystallized out of an Et_2O extract at room temperature. Cooling the concentrated mother liquor to −35 °C gave pale yellow crystals of the tetra(cyclopentadienyl) byproduct [K(2.2.2-cryptand)][Cp′$_4$Ce], **13-Ce**, Figure 3.3. Crystallization of the Et_2O insoluble product from THF yielded single crystals of **11-Ce**.

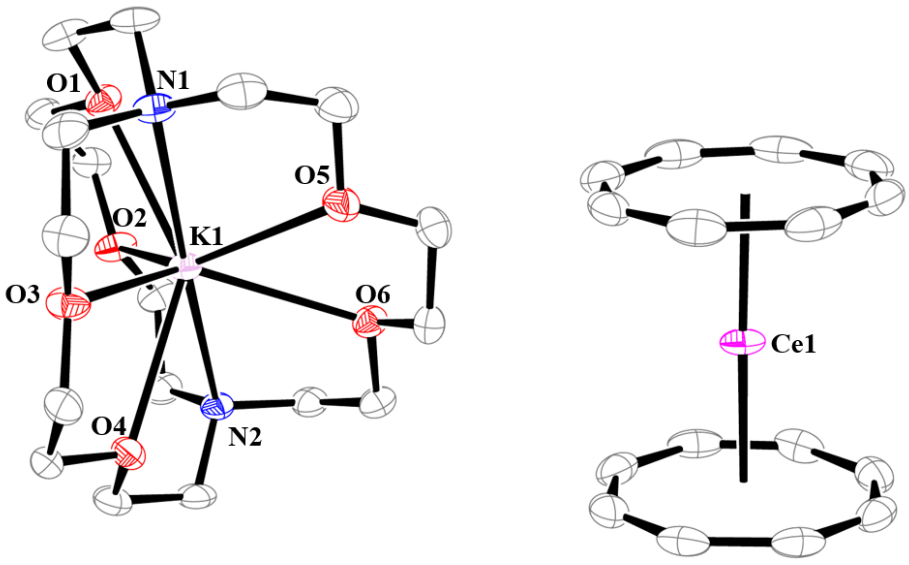

Figure 3.2. Thermal ellipsoid plot of [K(2.2.2-cryptand)][Ce(C_8H_8)], **12-Ce**, with thermal ellipsoids drawn at the 50% probability level. Hydrogen atoms are omitted for clarity. **12-Pr**, **12-Nd,** and **12-Sm** are isomorphous.

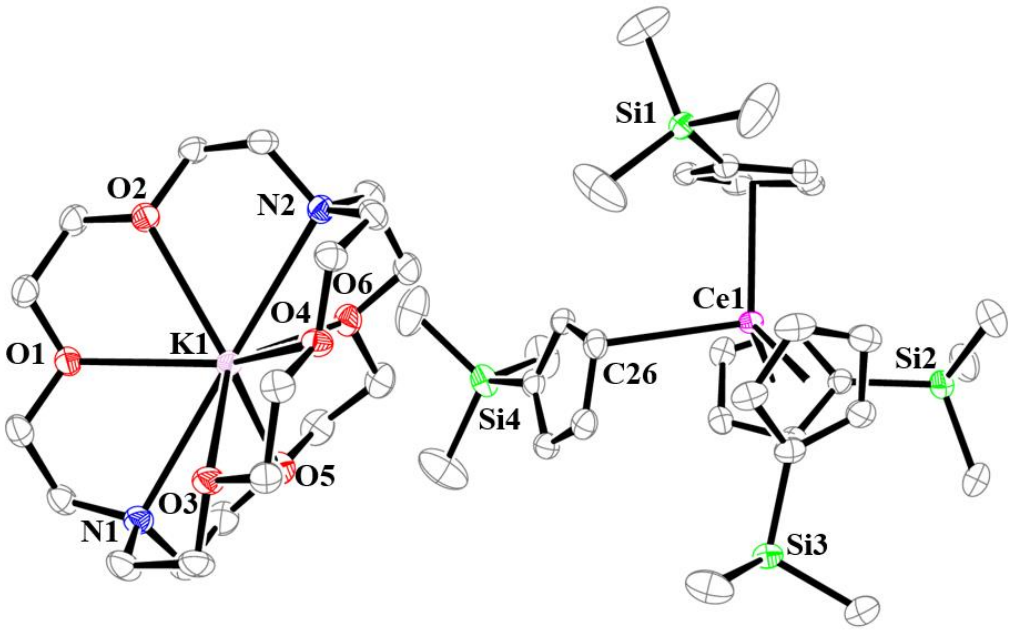

Figure 3.3. Thermal ellipsoid plot of [K(2.2.2-cryptand)][Cp′$_4$Ce], **13-Ce**, with thermal ellipsoids drawn at the 50% probability level. Hydrogen atoms and a co-crystallized Et_2O molecule have been omitted for clarity. **13-Ln** (Ln = Pr, Nd, Dy) are isomorphous.

The reaction between [K(2.2.2-cryptand)][Cp′$_3$Pr] and C_8H_8 differed from those of [K(2.2.2-cryptand)][Cp′$_3$La] and [K(2.2.2-cryptand)][Cp′$_3$Ce] in that the **11-Ln** product was not isolated: only the bis(cyclooctatetraenyl) complex, **12-Pr**, and the **13-Pr** co-product were obtained. Both praseodymium products could be characterized by X-ray crystallography, but were not isolated in synthetically useful amounts.

Reactivity of Traditional 4f^{n+1} Ions. Europium, Samarium, Thulium, and Ytterbium. Treatment of the dark purple solution of **1-Sm** with C_8H_8 gave an orange solution from which orange crystals of [K(2.2.2-cryptand)][Sm(C_8H_8)$_2$], **12-Sm**, were obtained. The crystals are isomorphous with **13-Ce**, Figure 2. The [Sm(C_8H_8)$_2$]$^{1-}$ anion has previously been isolated as the [Li(THF)$_4$]$^{1+}$ salt.[54] Crystals of the tetra(cyclopentadienyl) co-product, **13-Sm**, were also obtained from this reaction and structurally characterized, but no evidence of **11-Sm** was observed.

In contrast, addition of C_8H_8 to [K(2.2.2-cryptand)][Cp′$_3$Yb] caused no color change and the ^{1}H NMR spectrum of the mixture showed only unreacted starting materials. Similarly, addition of C_8H_8 to [K(2.2.2-cryptand)][Cp′$_3$Eu] caused no change. These results are consistent with the standard reduction potentials of Eu^{2+} and Yb^{2+} (Eu, −0.35; Yb, −1.15 V vs SHE)[55,56] in comparison with the −1.59 V vs SHE reduction potential of C_8H_8 to $(C_8H_8)^{2-}$.[17]

When the dark red THF solution of [K(2.2.2-cryptand)][Cp′$_3$Tm] was treated with C_8H_8, an immediate color change to peach was observed. Multiple crystallization attempts failed to yield cyclooctatetraenyl thulium products. However, the tetra(cyclopentadienyl) co-product, **13-Tm**, was obtained and structurally characterized to reveal a bis(η^5-Cp) bis(η^1-Cp′) coordination geometry, Figure 3.4.

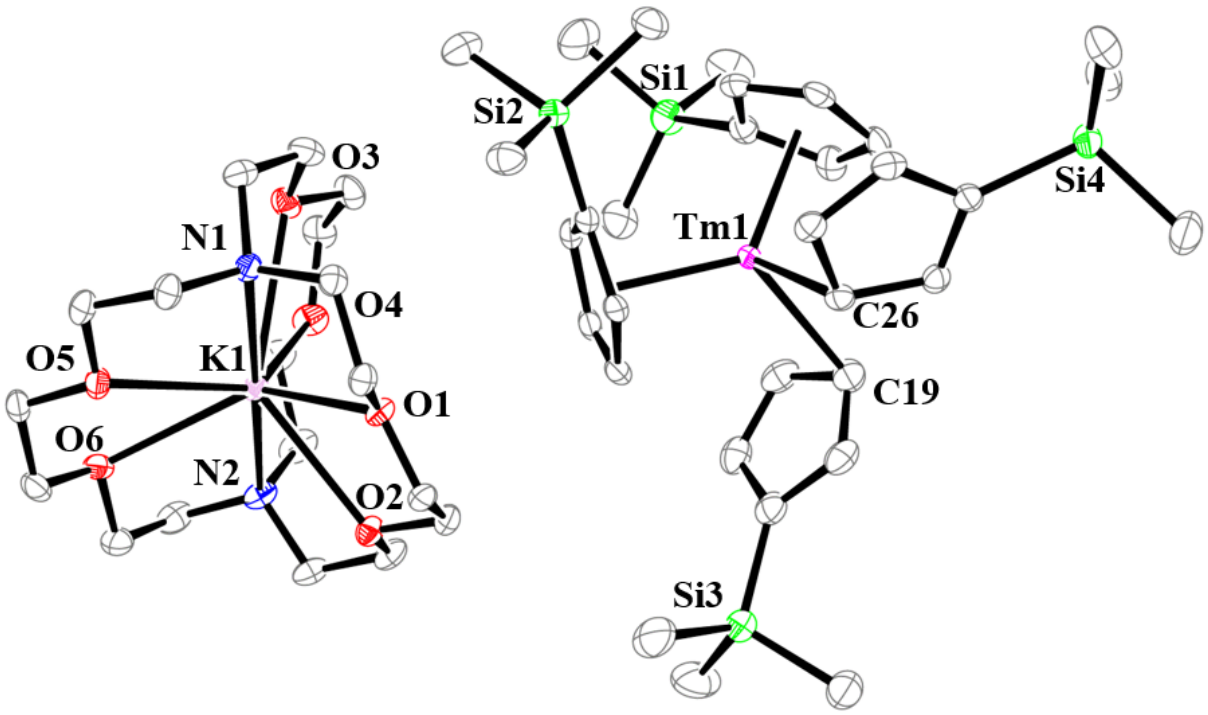

Figure 3.4. Thermal ellipsoid plot of [K(2.2.2-cryptand)][Cp′$_4$Tm], **13-Tm**, with thermal ellipsoids drawn at the 50% probability level. Hydrogen atoms have been omitted for clarity.

Reactivity of Configurational Crossover Ions. Neodymium, and Dysprosium. Dark red/brown THF solutions of [K(2.2.2-cryptand)][Cp′$_3$Nd] and [K(2.2.2-cryptand)][Cp′$_3$Dy] reacted with C_8H_8 to give pale green and pale yellow solutions, respectively. Workup of the Nd reaction gave single-crystals of **12-Nd** and **13-Nd** that were characterized by X-ray diffraction. For the small metal, Dy, only crystals of **13-Dy** were obtained despite multiple crystallization attempts. This is similar to the results with thulium, which is also one of the smaller lanthanides. In one attempt, [K(2.2.2-cryptand)][Cp′$_3$Dy] was treated with one equiv of C_8H_8, a crystal of the bimetallic bridged hydride complex, [K(2.2.2-cryptand)[(Cp′$_3$Dy)$_2$(μ-H)], **14-Dy**, was obtained from the product mixture and characterized by X-ray crystallography, Figure 3.5. Reactions of

[K(2.2.2-cryptand)][Cp′$_3$Ln] (Ln = Ce, Nd, Tm) were also conducted with one equivalent of C_8H_8, but no products beyond those mentioned above from excess C_8H_8 reactions were characterizable.

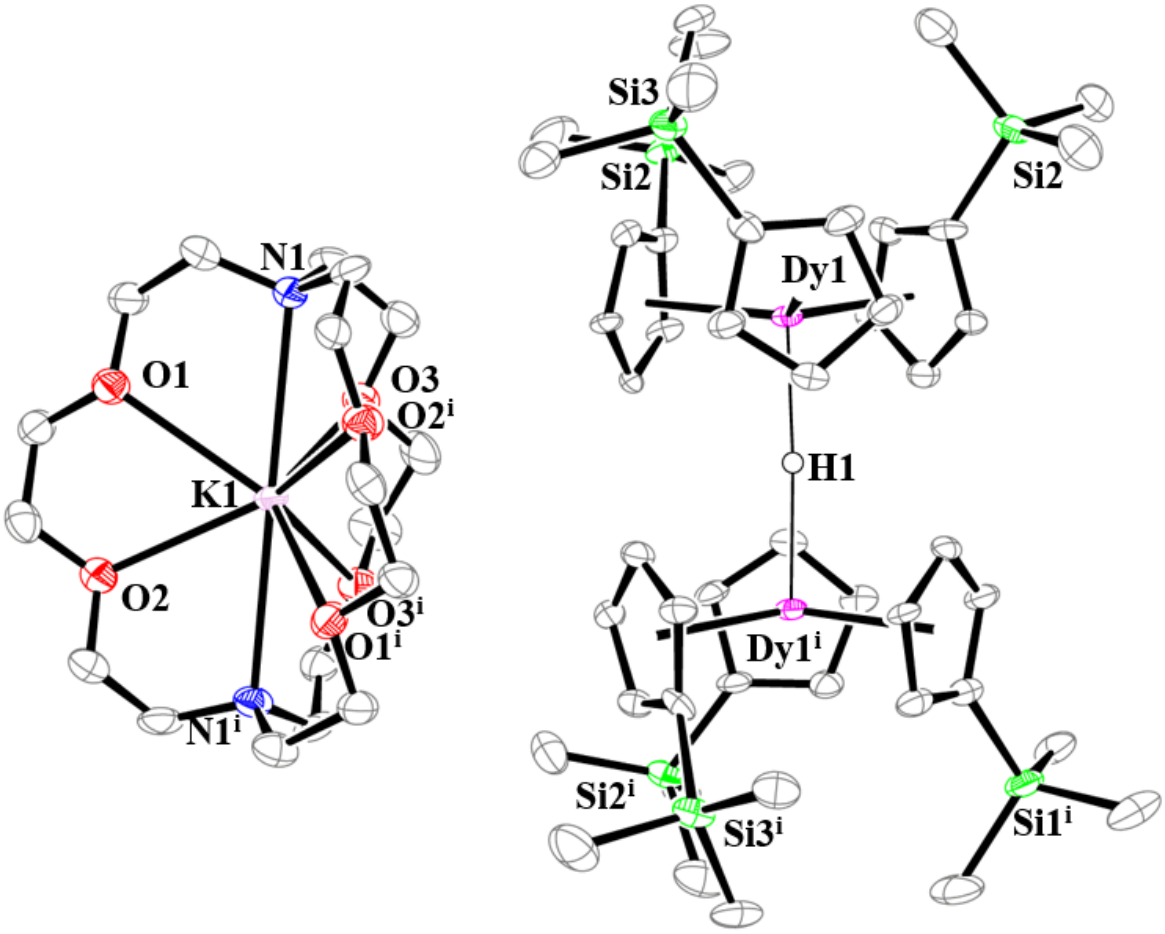

Figure 3.5. Thermal ellipsoid plot of [K(2.2.2-cryptand)][(Cp′$_3$Dy)$_2$H], **14-Dy**, with thermal ellipsoids drawn at the 50% probability level. Hydrogen atoms except H1 and a co-crystallized Et_2O molecule have been omitted for clarity. Selected bond lengths (Å) and angles (°): Dy1–(Cp′ Cnt)$_{avg}$, 2.486(5); Dy1–C(Cp′)$_{avg}$, 2.76(6); Dy1–H1, 2.170(7); Dy1…Dy1^i, 4.333 Dy1–H1–Dy1^i, 173.4.

Structural Analysis. [K(2.2.2-cryptand)][Cp′$_2$Ln(C$_8$H$_8$)], 11-Ln. The structures of the anions in **11-Ln** are analogous to the neutral Th^{4+} complex obtained previously when Th^{2+} was

treated with C_8H_8, eq 2,[19] but represent the first structurally characterized examples of a Ln^{3+} cyclooctatetraenyl complex with two cyclopentadienyl ligands. **11-La** and **11-Ce** are isomorphous and crystallize in the $P\bar{1}$ space group. The metrical parameters, Table 3.5, change as expected based on the fact that the Shannon ionic radius for Ce^{3+} is approximately 0.02 Å smaller than that of La^{3+}.[57] The metal–(ring centroid) distances for the neutral Th^{4+} analog, $Cp'_2Th(C_8H_8)$,[19] are only 0.02 to 0.06 Å less than those of the Ce^{3+} complex, **11-Ce**, even though the ionic radius of Th^{4+} is about 0.12 Å smaller than that of Ce^{3+}.[57]

The $Ln–Cnt(Cp')_{avg}$ distances, 2.690(3) and 2.666(6) Å, for **11-La** and **11-Ce**, respectively, are longer than their analogs in $[K(2.2.2\text{-cryptand})][Cp'_2Ln(C_{10}H_8)]$, eq 3.1,[12] 2.601(9) and 2.569(3) Å, respectively. In addition, the Cnt2(Cp′)–Ln–Cnt3(Cp′) angles, 107.1° and 107.0°, in the metallocene units in **11-Ln** are smaller than the 117.3 and 117.5° analogs in the $[K(2.2.2\text{-cryptand})][Cp'_2Ln(C_{10}H_8)]$ complexes, respectively. This appears to be a consequence of the fact that the 2.159 and 2.132 Å $Ln–Cnt1(C_8H_8)$ distances in **11-La** and **11-Ce** are shorter than the distances from the metal to the midpoint of the C1-C4 vector of the bound bent C_6 ring in the $(naphthalenide)^{2-}$ complexes, 2.230 and 2.225 Å, respectively. Hence, the $(C_8H_8)^{2-}$ ligand has a larger steric effect on the metallocene units than the $(C_{10}H_8)^{2-}$ ligand.

$[K(2.2.2\text{-cryptand})][Ln(C_8H_8)_2]$, 12-Ln. The metrical parameters of the **12-Ln** complexes are shown in Table 3.6. This structural class has been crystallographically defined with a variety of rare earth metals with other countercations. Examples include $[(glyme)_3K(\mu\text{-}\eta^8\text{:}\eta^8\text{-}C_8H_8)]_2Yb$,[52] $[K(glyme)][Yb(C_8H_8)_2]$,[52] $[K(THF)_2][Er(C_8H_8)_2]$,[25] $(C_8H_8)Ln(\mu\text{-}\eta^2\text{:}\eta^8\text{-}C_8H_8)Li(THF)_3$ (Ln = La, Nd, Tm),[31,58] $[K(diglyme)][Ln(C_8H_8)_2]$ (Ln = Ce, Yb),[21,53] $[Li(THF)_4][Ln(C_8H_8)_2]$ (Ln = Ce, Sm),[22,54] $[Na(THF)_3][Ce(C_8H_8)_2]$,[22] $[(THF)_3K(\mu\text{-}\eta^8\text{:}\eta^8\text{-}C_8H_8)]_2Eu$,[59] and $[K(18\text{-crown-}6)][Ln(C_8H_8)_2]$ (Ln = Sm, Dy, Er).[25,41]

The **12-Ln** complexes crystallize in the monoclinic *Cc* space group and are isomorphous. The **12-Ln** Ln1–Cnt(C_8H_8)$_{avg}$ distances are consistent with the lanthanide contraction and decrease regularly from 2.060(1) Å for Ln = Ce to 1.978(2) Å for Ln = Sm. The 179.2-179.5° range of Cnt1(C_8H_8)–Ln1–Cnt2(C_8H_8) angles reflect the near axial coordination of the two $(C_8H_8)^{2-}$ ligands. These parameters are consistent with previously published compounds with the $[Ln(C_8H_8)_2]^{1-}$ anion listed above.[21,22,25,31,41,52,53,58,59]

[K(2.2.2-cryptand)][Cp′$_4$Ln], 13-Ln. The structures of [K(2.2.2-cryptand)][Cp′$_4$Ln], **13-Ln**, (Ln = Ce, Pr, Nd, Sm, Dy, and Tm) provide a chance to compare this tetracyclopentadienyl ligand set across the lanthanide series, since previously only the structures of **13-La** and **13-Y**[12] were known. [K(2.2.2-cryptand)][Cp′$_4$U], **13-U**,[18] is also included in this comparison to provide data on the use of lanthanide structures as models for actinide complexes.[60,61] The metrical parameters of the **13-Ln**, **13-Y**, and **13-U** are shown in Table 3.7.

The complex of the largest metal, **13-La**, has four η^5-cyclopentadienyl ligands and the complex of the smallest metal, **13-Tm**, is bound to only two η^5-cyclopentadienyl ligands with two η^1-ligands bound at C26 and C19. The **13-Ln** complexes of metals with intermediate size, Ln = Ce, Pr, Nd, Sm, Dy, are similar to **13-Y** in that they crystallize in the $P\bar{1}$ space group and feature three η^5-cyclopentadienyl ligands with one η^1-ligand bound via C26. The complexes **13-Ce**, **13-Pr**, **13-Nd**, and **13-Sm** constitute one isomorphous set and **13-Dy** is isomorphous with **13-Y**. The actinide analog, [K(2.2.2-cryptand)][Cp′$_4$U], **13-U** is isomorphous with **13-Ce**, **13-Pr**, **13-Nd**, and **13-Sm**.[18]

The metrical parameters of **13-Ln** for the structurally analogous examples of Ln = Ce, Pr, Nd, Sm, Dy, and Y are consistent with the decrease in ionic radius of these metals. Each complex has two similar Ln–η^5-Cp′ centroid distances and one that is about 0.05 Å shorter. The Ln–C(η^1-

Cp′) distances are about 0.03 Å shorter than the average Ln–C(η^5-Cp′) distances. These parameters are similar in **13-U**, *i.e.* the lanthanide complexes of similar radial size are good models for this actinide. The metrical parameters for La are larger due to the higher coordination number in **13-La**; similarly, the distances are shorter for Tm due to the lower coordination number of **13-Tm**.

[K(2.2.2-cryptand)][(Cp′$_3$Dy)$_2$H], 14-Dy. Compound **14-Ln** crystallizes in the *C*2/*c* space group and features two formally 10-coordinate Cp′$_3$Dy units bridged by a hydride ligand in its anion. This type of structural motif has been observed previously in [K(18-crown-6)(η^2-C_7H_8)$_2$]{[($C_5H_4SiMe_2{}^tBu_3$)$_3$Ln]$_2$H} for La and Ce,[62] [K(THF)$_2$][(Cp$_3$Ln)$_2$H] and [Li(DME)$_3$][(Cp$_3$Nd)$_2$H],[63,64] and [K(THF)$_6$][(Cp$_3$Lu)$_2$H],[65] but the hydrides were not crystallographically located in the Ce and Lu cases. Instead, the Ln–H distances of 2.256 and 2.09 Å were estimated assuming the hydride was in the middle of the Ln…Ln vector. In the Nd structures, the hydride was positioned in the refinement at the midpoint of the Nd…Nd vectors with Nd–H distances of 2.173 and 2.19 Å. In **14-Dy**, the model for the X-ray data indicates the hydride is not exactly in the middle of the Dy…Dy vector since the Dy–H–Dy angle refined to 173.3°. The 2.170(7) Å Dy–H distance is longer than expected based on the estimates from the other structures considering the difference in ionic radii, but it is difficult to evaluate Ln–H distances due to the great difference in electron density between the metals and hydrogen.

DISCUSSION

The [K(2.2.2-cryptand)][Cp′$_3$Ln] complexes of the +2 ions of La, Ce, Pr, Nd, Sm, Dy, and Tm, all react rapidly with C_8H_8, as indicated by the immediate color changes of the dark [K(2.2.2-cryptand)][Cp′$_3$Ln] solutions in THF to give pale colored products. Only for the Eu and Yb analogs was no reactivity observed which is consistent with their established redox potentials.[55,56]

The goal of this investigation was to determine if reactivity varied based on the classifications of Ln^{2+} ions, *i.e.* traditional $4f^{n+1}$, non-traditional $4f^n5d^1$, or configurational crossover. Since $5d^1$ [K(2.2.2-cryptand)][Cp′$_3$La] reacted to form [K(2.2.2-cryptand)][Cp′$_2$La(C_8H_8)], **11-La**, and $4f^6$ [K(2.2.2-cryptand)][Cp′$_3$Sm] reacted to form [K(2.2.2-cryptand)][Sm(C_8H_8)$_2$], **12-Sm**, the initial results suggested there might be a dichotomy of cyclooctatraenyl products based on $4f^n5d^1$ vs $4f^{n+1}$ configurations. However, the $4f^15d^1$ [K(2.2.2-cryptand)][Cp′$_3$Ce] forms *both* types of cyclooctatetraenyl complexes isolated from these reactions, [K(2.2.2-cryptand)][Cp′$_2$Ce(C_8H_8)], **11-Ce**, and [K(2.2.2-cryptand)][Ce(C_8H_8)$_2$], **12-Ce**, and **13-La** is a minor co-product in the lanthanum reaction. Hence, isolation of **11-Ln** vs **12-Ln** is not definitive for an electron configuration.

The cerium reaction proved to be optimal in terms of obtaining X-ray structural data since both **11-Ce** and **12-Ce** as well as the expected reduction co-product [K(2.2.2-cryptand)][Cp′$_4$Ce], **13-Ce**, could be crystallographically characterized. Cerium is the only metal for which all three products could be crystallized. In the case of the smaller metals, Dy and Tm, only the **13-Ln** co-product was isolable. Since the paramagnetism of these latter metals precludes NMR analysis and the cyclooctatetraenyl products did not crystallize, details of these reactions are not known. The color changes and isolation of **13-Ln** are consistent with cyclooctatetrene reduction, but more cannot be said in the absence of crystal data. A bridged hydride complex [K(2.2.2-

cryptand)][(Cp′$_3$Dy)$_2$H], **14-Dy**, was also structurally characterized from one reaction of [K(2.2.2-cryptand)][Cp′$_3$Dy] with C_8H_8. Formation of hydride byproducts in reactions of Ln^{2+} ions has previously been observed in several cases.[11,66] With the largest metal, La, only **11-La** was crystallizable from the C_8H_8 reaction although the known **13-La**[12] was identified by NMR spectroscopy as a 1:1 co-product with respect to **11-La**. **12-La** is also present, but only as a minor product.

The results reiterate the fact that a key factor in defining reactivity of the paramagnetic lanthanides is the ability to crystallize the products, and this can depend crucially on the relative size of the ligand set vs the metal ionic radius. These results show that the products isolated from the C_8H_8 reduction by [K(2.2.2-cryptand)][Cp′$_3$Ln] depend more on the size of the metal and its suitability to form crystals than the electron configuration or the category of Ln^{2+} ion. It is interesting to note that in the actinide series with the $[C_5H_3(SiMe_3)_2]^{1-}$ $(Cp'')^{1-}$ ligand, the $6d^2$ complex $(Cp''_3Th)^{1-}$ forms a neutral analog of **11-Ln**, *i.e.* Cp″$_2$Th(C_8H_8), while the $5f^36d^1$ complex $(Cp''_3U)^{1-}$ forms the neutral analog of **12-Ln**, *i.e.* uranocene, U(C_8H_8)$_2$. It is possible that in the more ionic lanthanides series there is no strong preference for **11-Ln** over **12-Ln** since both are stable sterically-saturated complexes with favorable ligand arrangements.

CONCLUSION

The reactions of the divalent complexes [K(2.2.2-cryptand)][Cp′$_3$Ln] with C_8H_8 were examined to determine if complexes of Ln^{2+} ions with $4f^n5d^1$ electron configurations would differ from those with $4f^{n+1}$ electron configurations. Two types of cyclooctatetraenyl products, [K(2.2.2-cryptand)][Cp′$_2$Ln(C_8H_8), **11-Ln** and [K(2.2.2-cryptand)][Ln(C_8H_8)$_2$], **12-Ln**, are formed in these reactions, but since cerium forms both types, these products do not allow the discrimination of

reactivity based on electron configurations. With cyclooctatetraene as a substrate for reactions of new Ln^{2+} complexes, isolation of reaction products and their structures are more dependent on the size of the Ln^{3+} ion in the product than the electron configuration of the Ln^{2+} ion in the reactant. Inherent in the two-electron reduction of C_8H_8 with two equiv of [K(2.2.2-cryptand)][Cp′$_3$Ln] is the formation of the tetra(cyclopentadienyl) complexes, [K(2.2.2-cryptand)][Cp′$_4$Ln], **13-Ln**. These have been isolated for Ce, Pr, Nd, Sm, Dy, and Tm. The crystallographic data on these compounds, along with that known for the La and Y analogs, comprises another rare-earth metal series of complexes with structural features consistent with the size of the ions. The La complex has four η^5-Cp rings, the Tm complex has two, and the metals of intermediate size have three.

Table 3.1. Crystal data and structure refinement for [K(2.2.2-cryptand)][Cp′$_2$Ln(C$_8$H$_8$)] **11-Ln** (Ln = La, Ce).

	La	**Ce**
Empirical formula	$C_{42}H_{70}KLaN_2O_6Si_2$	$C_{42}H_{70}KLaN_2O_6Si_2$
Formula weight	933.19	934.40
Temperature (K)	88(2)	133(2)
Space group	$P\bar{1}$	$P\bar{1}$
a (Å)	12.7159(5)	12.7480(13)
b (Å)	13.3585(5)	13.3467(14)
c (Å)	16.1532(6)	16.1234(16)
α (°)	114.1946(4)	114.1205(11)
β (°)	101.0392(5)	101.0787(12)
γ (°)	91.1941(5)	90.9625(12)
Volume (Å^3)	2441.37(16)	2443.2(4)
Z	2	2
ρ_{calcd} (g/cm^3)	1.269	1.270
μ (mm^{-1})	1.051	1.108
$R1^a$	0.0274	0.0260
$wR2^b$	0.0591	0.0658

Definitions: $^aR1 = \Sigma||F_o|-|F_c|| / \Sigma|F_o|$. $^bwR2 = [\Sigma[w(F_o^2-F_c^2)^2] / \Sigma[w(F_o^2)^2]]^{1/2}$.

Table 3.2. Crystal data and structure refinement for [K(2.2.2-cryptand)][Ln(C_8H_8)$_2$], **12-Ln** (Ln = Ce, Pr, Nd, Sm).

	Ce	**Pr**	**Nd**	**Sm**
Empirical formula	$C_{34}H_{52}CeKN_2O_6$	$C_{34}H_{52}PrKN_2O_6$	$C_{34}H_{52}NdKN_2O_6$	$C_{34}H_{52}NdKN_2O_6$
Formula weight	763.99	764.78	768.11	774.22
Temperature (K)	163(2)	133(2)	88(2)	88(2)
Space group	*Cc*	*Cc*	*Cc*	*Cc*
a (Å)	20.471(2)	20.361(2)	20.3176(8)	20.2352(8)
b (Å)	14.5866(18)	14.5274(14)	14.5288(5)	14.5604(6)
c (Å)	14.1304(17)	14.0800(14)	14.0816(5)	14.0834(6)
α (°)	90	90	90	90
β (°)	121.9832(12)	121.8367(10)	121.7919(4)	121.7866(4)
γ (°)	90	90	90	90
Volume (Å^3)	3578.9(7)	3538.2(6)	3533.1(2)	3527.1(3)
Z	4	4	4	4
ρ_{calcd} (g/cm^3)	1.418	1.436	1.444	1.458
μ (mm^{-1})	1.431	1.538	1.631	1.827
*R*1[a]	0.0232	0.0223	0.0171	0.0128
*wR*2[b]	0.0427	0.0468	0.0404	0.0329

Definitions: [a]R1 = $\sum||Fo| - |Fc||/\sum|Fo|$; [b]wR2 = $[\sum[w(Fo^2 - Fc^2)^2]/\sum[w(Fo^2)^2]\ ]^{1/2}$.

Table 3.3. Crystal data and structure refinement for [K(2.2.2-cryptand)][Cp′$_4$Ln], **13-Ln** (Ln = Ce, Pr, Nd, Dy, Tm).

	Ce	**Pr**	**Nd**	**Sm**	**Dy**	**Tm**
Empirical formula	$C_{50}H_{88}KN_2O_6Si_4Ce$•½($OC_4H_{10}$)	$C_{50}H_{88}KN_2O_6Si_4Pr$•½($C_4H_{10}O$)	$C_{50}H_{88}KN_2O_6Si_4Nd$•½($C_4H_{10}O$)	$C_{50}H_{88}KN_2O_6Si_4Sm$•½($C_4H_{10}O$)	$C_{50}H_{88}KN_2O_6Si_4Sm$	$C_{50}H_{88}KN_2O_6Si_4Tm$
Formula weight	1141.86	1142.65	1145.98	1152.09	1127.18	1133.61
Temperature (K)	133(2)	88(2)	153(2)	88(2)	133(2)	88(2)
Space group	*P*-1	*P*-1	*P*-1	$P\bar{1}$	*P*-1	*P*-1
a (Å)	13.9859(9)	13.9773(14)	13.9733(13)	13.958(2)	14.0666(8)	14.1976(5)
b (Å)	14.8246(9)	14.7948(15)	14.8573(14)	14.817(3)	14.0707(8)	14.3176(5)
c (Å)	17.2516(11)	17.2247(17)	17.2753(17)	17.226(3)	17.1651(10)	16.5300(6)
α (°)	73.4355(7)	73.4301(12)	73.3105(12)	73.258(2)	104.7308(7)	77.0860(5)
β (°)	77.6893(7)	77.6197(12)	77.6949(12)	77.474(2)	110.1151(6)	80.7379(5)
γ (°)	63.1783(7)	63.2161(12)	63.2217(11)	63.0717(19)	105.2332(7)	61.6812(4)
Volume (Å^3)	3044.6(3)	3032.3(5)	3052.2(5)	3025.9(9)	2846.7(3)	2877.28(18)
Z	2	2	2	2	2	2
ρ_{calcd} (g/cm^3)	1.246	1.251	1.247	1.302	1.315	1.308
μ (mm^{-1})	0.939	0.996	1.042	1.264	1.514	1.742
$R1^a$	0.0282	0.0327	0.0291	0.0291	0.0204	0.0270
$wR2^b$	0.0735	0.0868	0.0734	0.0660	0.0510	0.0656

Definitions: ^{a}R1 = $\sum||Fo| - |Fc||/\sum|Fo|$; ^{b}wR2 = $[\sum[w(Fo^2 - Fc^2)^2]/\sum[w(Fo^2)^2]\ ]^{1/2}$.

Table 3.4. Crystal data and structure refinement for [K(2.2.2-cryptand)][(Cp′$_2$Ln)$_2$H], **14-Dy**.

	Dy
Empirical formula	$C_{70}H_{125}Dy_2KN_2O_7Si_6$
Formula weight	1639.35
Temperature (K)	88(2)
Space group	*C*2/*c*
a (Å)	13.694(3)
b (Å)	22.140(5)
c (Å)	27.445(6)
α (°)	90
β (°)	90.991(3)
γ (°)	90
Volume (Å^3)	8319(3)
Z	4
ρ_{calcd} (g/cm^3)	1.309
μ (mm^{-1})	1.965
*R*1[a]	0.0717
*wR*2[b]	0.1967

Definitions: [a]R1 = $\sum||Fo| - |Fc||/\sum|Fo|$; [b]wR2 = $[\sum[w(Fo^2 - Fc^2)^2]/\sum[w(Fo^2)^2]\ ]^{1/2}$.

Table 3.5. Selected Bond Distances (Å) and Angles (°) for [K(2.2.2-cryptand)][Cp′$_2$Ln(C$_8$H$_8$)], **11-Ln** (Ln = La, Ce) (Cnt = ring centroid) and Cp″$_2$Th(C$_8$H$_8$)[19]

Parameter	**La**	**Ce**	**Cp″$_2$Th(C$_8$H$_8$)[a]**
Ln1–Cnt1(C$_8$H$_8$)	2.159	2.132	2.106
Ln1–Cnt2(Cp)	2.693	2.671	2.611
Ln1–Cnt3(Cp)	2.687	2.660	2.611
Ln1–Cnt(Cp′)$_{avg}$	2.690(3)	2.666(6)	2.611
Ln1–C(Cp′)$_{avg}$	2.95(2)	2.92(3)	2.88(2)
Ln1–C(C$_8$H$_8$)$_{avg}$	2.83(3)	2.81(3)	2.79(4)
Cnt1(C$_8$H$_8$)–Ln1–Cnt2(Cp′)	126.4	126.5	126.0
Cnt1(C$_8$H$_8$)–Ln1–Cnt3(Cp′)	126.4	126.4	126.0
Cnt2(Cp′)–Ln1–Cnt3(Cp′)	107.1	107.0	107.9

[a] Cnt2 and Cnt3 of Cp′$_2$Th(C$_8$H$_8$) are equivalent by symmetry.

Table 3.6. Selected Bond Distances (Å) and Angles (°) for [K(2.2.2-cryptand)][Ln(C$_8$H$_8$)$_2$], **12-Ln** (Ln = Ce, Pr, Nd, Sm)

Parameter	**Ce**	**Pr**	**Nd**	**Sm**
10-coordinate ionic radius	1.25	1.23[a]	1.22[a]	1.19[a]
Ln1–Cnt1(C$_8$H$_8$)	2.061	2.035	2.015	1.980
Ln1–Cnt2(C$_8$H$_8$)	2.059	2.031	2.014	1.976
Ln1–C(C$_8$H$_8$)$_{avg}$	2.759(6)	2.741(6)	2.730(7)	2.705(7)
Cnt1(C$_8$H$_8$)–Ln1–Cnt2(C$_8$H$_8$)	179.5	179.3	179.3	179.2

[a] Estimated by extrapolation of reported Shannon radii.[57]

Table 3.7. Selected Bond Distances (Å) and Angles (°) for [K(2.2.2-cryptand)][Cp′$_4$Ln], **13-Ln** (Ln = Y, La, Ce, Pr, Nd, Sm, Dy, Tm) and [K(2.2.2-cryptand)][Cp′$_4$U], **13-U**[18]

Parameter	**La**	**Ce**	**Pr**	**Nd**	**Sm**	**Dy**	**Y**[12]	**Tm**	**U**[18]
9-coordinate ionic radius[45]	1.216	1.196	1.179	1.163	1.132	1.083	1.075	1.052	1.18[a]
Ln–(η^5-Cp′)	2.710 2.715 2.728 2.741	2.553 2.604 2.605	2.535 2.586 2.588	2.519 2.574 2.575	2.491 2.544 2.551	2.439 2.492 2.513	2.437 2.491 2.509	2.345 2.366	2.531 2.571 2.574
Ln–Cnt(η^5-Cp′)$_{avg}$	2.724(4)	2.59(2)	2.57(3)	2.56(3)	2.53(3)	2.48(3)	2.48(1)	2.35(1)	2.56(2)
Ln–C(η^5-Cp′)$_{avg}$	2.95(6)	2.85(6)	2.84(6)	2.82(6)	2.80(6)	2.76(6)	2.75(7)	2.65(4)	2.82(5)
Ln–C26(η^1-Cp′)	-	2.824(2)	2.811(2)	2.795(2)	2.784(2)	2.693(2)	2.680(2)	2.601(2)	2.776(2)
Ln–C19(η^1-Cp′)	-	-	-	-	-	-	-	2.567(2)	-

[a] Estimated by extrapolation from the six coordinate ionic radius and the radii of U^{4+}.[45]

REFERENCES

(1) Hitchcock, P. B.; Lappert, M. F.; Maron, L.; Protchenko, A. V. *Angew. Chem. Int. Ed.* **2008**, *47*, 1488-1491.

(2) MacDonald, M. R.; Ziller, J. W.; Evans, W. J. *J. Am. Chem. Soc.* **2011**, *133*, 15914-159147.

(3) MacDonald, M. R.; Bates, J. E.; Fieser, M. E.; Ziller, J. W.; Furche, F.; Evans, W. J. *J. Am. Chem. Soc.* **2012**, *134*, 8420-8423.

(4) MacDonald, M. R.; Bates, J. E.; Ziller, J. W.; Furche, F.; Evans, W. J. *J. Am. Chem. Soc.* **2013**, *135*, 9857-9868.

(5) Fieser, M. E.; MacDonald, M. R.; Krull, B. T.; Bates, J. E.; Ziller, J. W.; Furche, F.; Evans, W. J. *J. Am. Chem. Soc.* **2015**, *137*, 369-382.

(6) Evans, W. J. *Organometallics* **2016**, *35*, 3088-3100.

(7) Woen, D. H.; Evans, W. J. In *Handbook on the Physics and Chemistry of Rare Earths*; 1st ed.; Elsevier: Amsterdam, 2016; Vol. 50, p 337-394.

(8) Meihaus, M. R.; Fieser, M. E.; Corbey, J. F.; Evans, W. J.; Long, J. R. *J. Am. Chem. Soc.* **2015**, *137*, 9855-9860.

(9) Evans, W. J.; Allen, N. T.; Ziller, J. W. *J. Am. Chem. Soc.* **2000**, *122*, 11749-11750.

(10) Bochkarev, M. N.; Fedushkin, I. L.; Dechert, S.; Fagin, A. A.; Schumann, H. *Angew. Chem. Int. Ed.* **2001**, *40*, 3176-3178.

(11) Jaroschik, F.; Momin, A.; Nief, F.; Le Goff, X. F.; Deacon, G. B.; Junk, P. C. *Angew. Chem. Int. Ed.* **2009**, *48*, 1117-1121.

(12) Kotyk, C. M.; MacdDonald, M. R.; Ziller, J. W.; Evans, W. J. *Organometallics* **2015**, *34*, 2287-2295.

(13) Evans, W. J.; Hughes, L. A.; Hanusa, T. P. *J. Am. Chem. Soc.* **1984**, *106*, 4270-4272.

(14) de Boer, E. *Adv. Organomet. Chem.* **1964**, *2*, 115-155.

(15) Evans, W. J.; Gonzales, S. L.; Ziller, J. W. *J. Am. Chem. Soc.* **1994**, *116*, 2600-2608.

(16) Bochkarev, M. N.; Fagin, A. A. *Chem. Eur. J.* **1999**, *5*, 2990-2992.

(17) Evans, W. J.; Gonzales, S. L.; Ziller, J. W. *J. Am. Chem. Soc.* **1991**, *113*, 7423-7424.

(18) Windorff, C. J.; MacDonald, M. R.; Meihaus, M. R.; Ziller, J. W.; Long, J. R.; Evans, W. J. *Chem. Eur. J.* **2016**, *22*, 772-782.

(19) Langeslay, R. R.; Fieser, M. E.; Ziller, J. W.; Furche, F.; Evans, W. J. *Chem. Sci.* **2015**, *6*, 517-521.

(20) Mares, F.; Hodgson, K.; Streitwieser Jr., A. *J. Organomet. Chem.* **1970**, *469*, C68-C70.

(21) Hodgson, K. O.; Raymond, K. N. *Inorg. Chem.* **1972**, *11*, 3030-3035.

(22) Kilimann, U.; Schafer, M.; HerbstIrmer, R.; Edelmann, F. T. *J. Organomet. Chem.* **1994**, *469*, C15-C18.

(23) Cendrowski-Guillaume, S. M.; Nierlich, M.; Lance, M.; Ephritikhine, M. *Organometallics* **1998**, *17*, 786-788.

(24) Evans, W. J.; Clark, R. D.; Ansari, M. A.; Ziller, J. W. *J. Am. Chem. Soc.* **1998**, *120*, 9555-9563.

(25) Meihaus, M. R.; Long, J. R. *J. Am. Chem. Soc.* **2013**, *135*, 17952-17957.
(26) Hayes, R. G.; Thomas, J. L. *J. Am. Chem. Soc.* **1969**, *91*, 6876-6876.
(27) DeKock, C. W.; Ely, S. R.; Hopkins, T. E.; Brault, M. A. *Inorg. Chem.* **1978**, *17*, 625-631.
(28) Mashima, K.; Takaya, H. *Tetrahedron Lett.* **1989**, *30*, 3697-3700.
(29) Evans, W. J.; Johnston, M. A.; Greci, M. A.; Ziller, J. W. *Organometallics* **1999**, *18*, 1460-1464.
(30) Fedushkin, I. L.; Bochkarev, M. N.; Dechert, S.; Schumann, H. *Chem. -Eur. J.* **2001**, *7*, 3558-3563.
(31) Meermann, C.; Ohno, K.; Törnroos, K. W.; Mashima, K.; Anwander, R. *Eur. J. Inorg. Chem.* **2009**, 76-85.
(32) Evans, W. J.; Perotti, J. M.; Kozimor, S. A.; Champagne, T. M.; Davis, B. L.; Nyce, G. W.; Fujimoto, C. H.; Clark, R. D.; Johnston, M. A.; Ziller, J. W. *Organometallics* **2005**, *24*, 3916-3931.
(33) Evans, W. J.; Mueller, T. J.; Ziller, J. W. *J. Am. Chem. Soc.* **2009**, *131*, 2678.
(34) Evans, W. J.; Schmiege, B. M.; Lorenz, S. E.; Miller, K. A.; Champagne, T. M.; Ziller, J. W.; DiPasquale, A. G.; Rheingold, A. L. *J. Am. Chem. Soc.* **2008**, *130*, 8555-8563.
(35) Evans, W. J.; Johnston, M. A.; Clark, R. D.; Ziller, J. W. *J. Chem. Soc., Dalton Trans.* **2000**, 1609-1612.
(36) Jeletic, M.; Lin, P.-H.; Le Roy, J. J.; Korobkov, I.; Gorelsky, S. I.; Murugesu, M. *J. Am. Chem. Soc.* **2011**, *133*, 19286-19289.
(37) Jiang, S.-D.; Wang, B.-W.; Sun, H.-L.; Wang, Z.-M.; Gao, S. *J. Am. Chem. Soc.* **2011**, *133*, 4730-4733.
(38) Le Roy, J. J.; Jeletic, M.; Gorelsky, S. I.; Korobkov, I.; Ungur, L.; Chibotaru, L. F.; Murugesu, M. *J. Am. Chem. Soc.* **2013**, *135*, 3502-3510.
(39) Le Roy, J. J.; Korobkov, I.; Kim, J. E.; Schelter, E. J.; Murugesu, M. *J. Chem. Soc., Dalton Trans.* **2014**, *43*, 2737-2740.
(40) Le Roy, J. J.; Korobkov, I.; Murugesu, M. *J. Chem. Soc., Chem. Commun.* **2014**, *50*, 1602-1604.
(41) Ungur, L.; Le Roy, J. J.; Korobkov, I.; Murugesu, M.; Chibotaru, L. F. *Angew. Chem. Int. Ed.* **2014**, *53*, 4413-4417.
(42) Bergbreiter, D. E.; Killough, J. M. *J. Am. Chem. Soc.* **1978**, *100*, 2126-2134.
(43) Fieser, M. E.; MacDonald, M. R.; Krull, B. T.; Bates, J. E.; Ziller, J. W.; Furche, F.; Evans, W. J. *J. Am. Chem. Soc.* **2015**, *137*, 369-382.
(44) Kotyk, C. M.; Fieser, M. E.; Palumbo, C. T.; Ziller, J. W.; Darago, L. E.; Long, J. R.; Furche, F.; Evans, W. J. *Chem. Sci.* **2015**, *6*, 7267-7273.
(45) APEX2 Version 2014.1-1, Bruker AXS, Inc.; Madison, WI, 2014.
(46) SAINT Version 8.34a, Bruker AXS, Inc.; Madison, WI, 2013.
(47) Sheldrick, G. M., SADABS, Version 2014/4, Bruker AXS, Inc.; Madison, WI, 2014.
(48) Sheldrick, G. M., SHELXTL, Version 2014/7, Bruker AXS, Inc.; Madison, WI, 2014.
(49) International Tables for X-Ray Crystallography, 1992, Vol. C. ed.; Dordrecht: Kluwer Academic Publishers.
(50) Spek, A. L., SQUEEZE, Acta Cryst. 2015, C71, 9-19.
(51) Spek, A. L., PLATON, Acta. Crys. 2009, D65, 148-155.

(52) Kinsley, S. A.; Streitwieser, J. A.; Zalkin, A. *Organometallics* **1985**, *4*, 52-57.
(53) Boussie, T. R.; Eisenberg, D. C.; Rigsbee, J.; Streitwieser, A.; Zalkin, A. *Organometallics* **1991**, *10*, 1922-1928.
(54) Anfang, S.; Seybert, G.; Harms, K.; Geiseler, G.; Massa, W.; Dehnicke, K. *Z. Anorg. Allg. Chem.* **1998**, *624*, 1187-1192.
(55) Morss, L. R. *Chem. Rev.* **1976**, *76*, 827-841.
(56) Mikheev, N. B.; Auerman, L. N.; Rumer, I. A.; Kamenskaya, A. N.; Kazakevich, M. Z. *Russ. Chem. Rev.* **1992**, *61*, 990-998.
(57) Shannon, R. D. *Acta Crystallogr A* **1976**, *32*, 751-767.
(58) Rabe, G. W.; Zhang-Preße, M.; Golen, J. A.; Rheingold, A. L. *Acta Cryst.* **2003**, *E59*, m255-m256.
(59) Evans, W. J.; Shreeve, J. L.; Ziller, J. W. *Polyhedron* **1995**, *14*, 2945-2951.
(60) Gaunt, A. J.; Reilly, S. D.; Enriquex, A. E.; Hayton, T. W.; Boncella, J. M.; Scott, B. L.; Neu, M. P. *Inorg. Chem.* **2008**, *47*, 8412-8419.
(61) Windorff, C. J.; Chen, G. P.; Cross, J. N.; Evans, W. J.; Furche, F.; Gaunt, A. J.; Janicke, M. T.; Kozimor, S. A.; Scott, B. L. *J. Am. Chem. Soc.* **2017**, *139*, 3970-3973.
(62) Gun'ko, Y. K.; Hitchcock, P. B.; Lappert, M. F. *Organometallics* **2000**, *19*, 2832-2834.
(63) Burin, M. E.; Logunov, A. A.; Fukin, G. K.; Bochkarev, M. N. *J. Coord. Chem.* **2009**, *62*, 3134-3141.
(64) Shen, Q.; Chen, W.; Jin, Y.; Shan, C. *Pure Appl. Chem.* **1988**, *60*, 1251-1256.
(65) Shumann, H.; Genthe, W.; Hahn, E.; Hossain, M.-B.; van der Helm, D. *J. Organomet. Chem.* **1986**, *299*, 67-84.
(66) Corbey, J. F.; Woen, D. H.; Palumbo, C. T.; Fieser, M. E.; Ziller, J. W.; Furche, F.; Evans, W. J. *Organometallics* **2015**, *34*, 3909-3921.

CHAPTER 4

Synthesis, Magnetic Characterization, and Reactivity of a Bimetallic La^{2+} Complex with a Benzenide Monoanion Bridge

INTRODUCTION

Studies in reductive rare-earth metal chemistry in the presence of arenes by Lappert and co-workers revealed a series of $(C_5R_5)_3Ln/K$ reduction reactions that gave products formulated to contain $(arene)^{1-}$ and $(arene)^{2-}$ anions on the basis of X-ray crystallography.[1-3] Eq 4.1 shows the formation of a La^{3+} complex of a bent $(C_6H_6)^{2-}$ dianion by reduction of the tris(cyclopentadienyl) complex, Cp''_3Ln ($Cp'' = C_5H_3(SiMe_3)_2$), with excess K in the presence of 18-crown-6.[1] Eq 4.2 shows a variation of this reaction using 1.5 equiv of K per La and the all carbon analog of the Cp″ ligand, namely $Cp^{tt} = C_5H_3{}^tBu_2$. In this case,

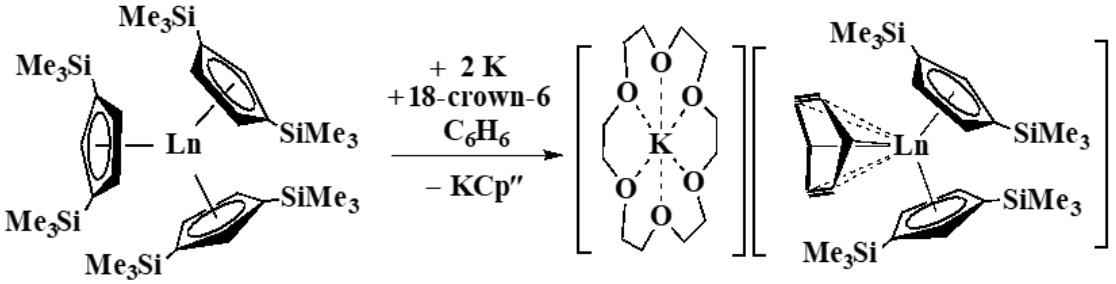

(4.1)

Ln = La, Ce, Pr, Nd

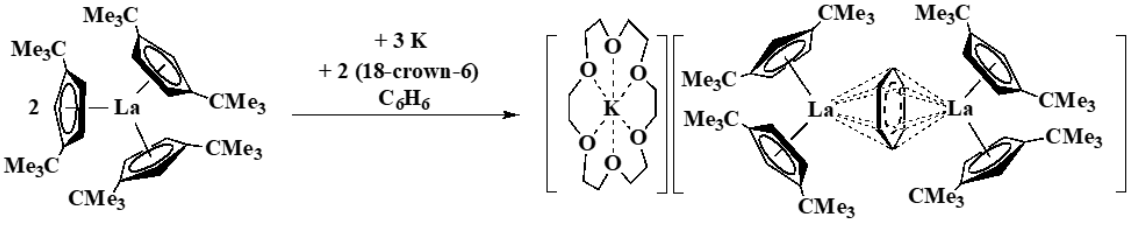

(4.2)

the reduction gave a compound that was postulated to be a La^{2+} complex of a planar $(C_6H_6)^{1-}$ monoanion rather than a Ln^{3+} complex of $(C_6H_6)^{3-}$. An analogous reaction with Cp″ was reported, but crystals suitable for X-ray diffraction were not obtained. Reactions with the stoichiometry of eq 4.2 with the silyl analogs, Cp''_3Ln (Ln = La, Ce) but with toluene were also described, eq 4.3.[2,3] Although there was disorder in the crystal structure that limited the quality of the data, these complexes were reported as Ln^{2+} complexes of planar monoanions derived from toluene, $(C_6H_5CH_3)^{1-}$.

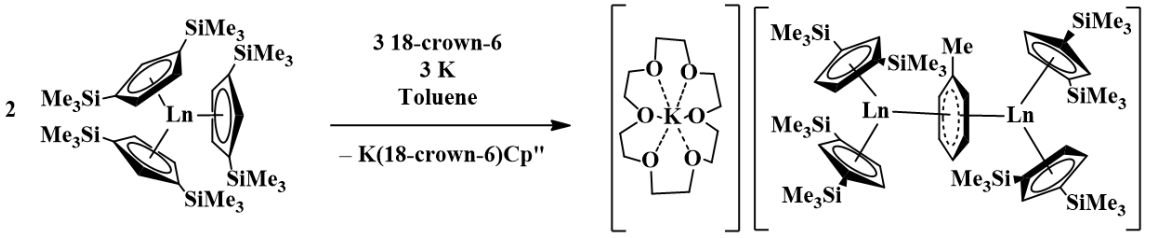

(4.3)

The known difficulty in assigning oxidation states in bridging arene systems[4-12] and the disorder in the crystal structure complicated the oxidation state assignments until unambiguous examples of complexes of La^{2+} were found as shown in eq 4.4. Subsequently, Ln^{2+} complexes of all the lanthanides except radioactive promethium were isolated from Cp'_3Ln precursors, eq 4.4.

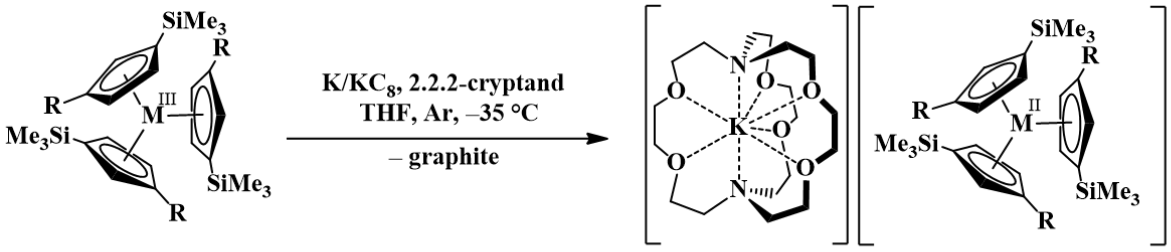

(4.4)

R = $SiMe_3$; M = La, Th
R = H; M = Y, La, Ce, Pr, Nd, Sm, Gd, Tb, Dy, Ho, Er, Tm, Lu, U

Further studies of reductions analogous to eq 4.1 and 4.2 but with tris(monosilylcyclopentadienyl) lanthanide precursors gave Ln^{2+} complexes of the benzene dianion, $(C_6H_6)^{2-}$, eq 4.5.[13]

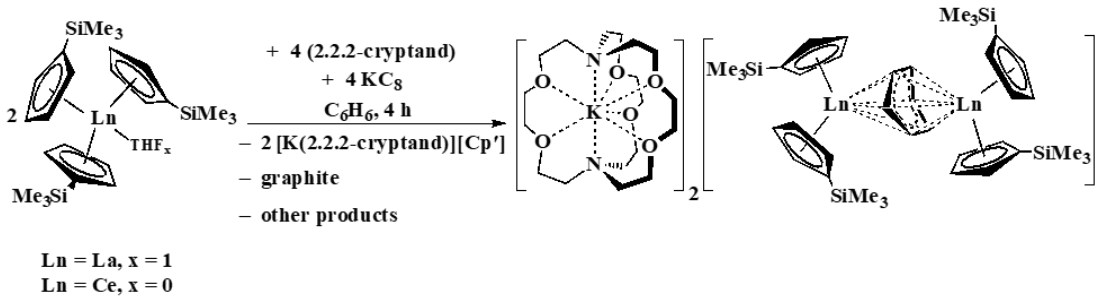

(4.5)

These complexes were found to act as four electron reductants, eq 4.6.

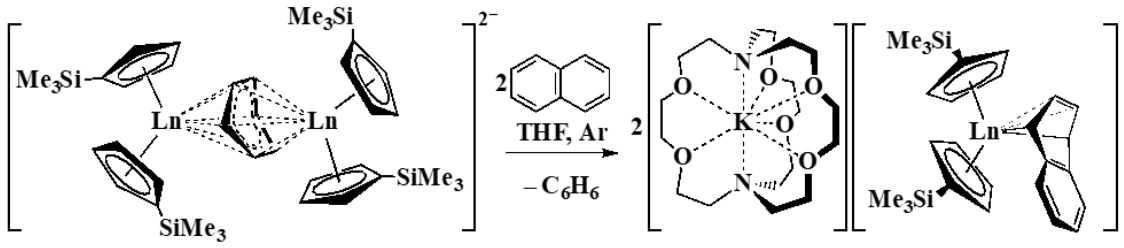

(4.6)

Ln = La, Ce

$$[(Cp'_2Ln)_2(\mu\text{-}\eta^6\text{:}\,\eta^6\text{-}C_6H_6)]^{2-} \longrightarrow 4\ e^- + C_6H_6 + 2[Cp'_2Ln]^{1+}$$

$$2\ C_{10}H_8 + 4\ e^- \longrightarrow 2\ (C_{10}H_8)^{2-}$$

It was of interest in terms of multi-electron reduction chemistry to ask if $(arene)^{1-}$ monoanion complexes of Ln^{2+} postulated in eq 4.2 and 4.3 could also act as multi-electron reductants. These complexes could exhibit different reactivity from that in eq 4.6 since they are potentially three-electron reductants. This study focused on lanthanum as the metal, since La^{3+} is diamagnetic, and on Cp″ as the ligand in order to make a Cp″ vs Cp′ comparison with eq 4.6. In

this Chapter, the successful crystallization of the Cp″ analog of eq 4.2, namely [K(18-crown-6)(THF)$_2$][(Cp"$_2$La)$_2$(μ-η^6:η^6-C_6H_6)], **15-La**, and its multi-electron reactivity with anthracene, naphthalene, and cyclooctatetraene are described. The magnetic susceptibility of **15-La** was also studied since it formally contains two $5d^1$ La^{2+} ions bridged by a radical anion. This was of interest in terms for understanding the single-molecule magnet behavior of bimetallic rare-earth metal complexes bridged by radicals. Complex **15-La** was of particular interest because of its apparent thermal stability: Lappert and co-workers reported that it could be made from the [K(crown)][Cp″$_2$La(C_6H_6)] product of eq 4.1 by heating this compound at 70 °C for over 7 d.

EXPERIMENTAL

The syntheses and manipulations described below were conducted under argon with rigorous exclusion of air and water using glovebox, vacuum line, and Schlenk techniques. Solvents were sparged with UHP grade argon (Praxair) and passed through columns containing Q-5 and molecular sieves before use. NMR solvents (Cambridge Isotope Laboratories) were dried over NaK/benzophenone, degassed by three freeze−pump−thaw cycles, and vacuum transferred prior to use. Anhydrous Cp″$_3$La[14] was prepared according to the literature. 18-crown-6 (1,4,7,10,13,16-hexaoxacyclooctadecane, Aldrich) was sublimed before use. ^{1}H NMR (500 MHz) and ^{13}C NMR (125 MHz) were obtained on a Bruker GN500 or CRYO500 MHz spectrometer at 298 K. IR samples were prepared as KBr pellets and the spectra were obtained on a Jasco FT/IR-4700 spectrometer. Elemental analyses were performed on a Perkin-Elmer 2400 Series II CHNS elemental analyzer. UV–vis spectra were collected in THF at 298 K using a Varian Cary 50 Scan UV–vis spectrophotometer.

[K(18-crown-6)(THF)$_2$][(Cp″$_2$La)$_2$(μ-η^6:η^6-C$_6$H$_6$)]•THF, 15-La. Compound **15-La** was prepared as an adaptation to the previously reported literature.[2] In a glovebox free of coordinating solvents, Cp″$_3$La (373 mg, 0.486 mmol) and 18-crown-6 (193 mg, 0.729 mmol) were dissolved in C_6H_6 and then transferred to a vial containing potassium (29 mg, 0.729 mmol) and a slow color change to dark purple was observed. Over the course of 4 days, the solution turned to a dark slurry. Dark green solids were separated from the dark red supernatant and subsequently washed with benzene (2 x 5 mL). The resultant dark green solids were transferred to another glovebox and dissolved in THF (5 mL), which gave an intense blue solution. The dark blue THF solution was layered with Et_2O (15 mL) and stored at −35 °C in the glovebox freezer for 4 d to yield dark green single crystals characterized by X-ray diffraction as **15-La** (246 mg, 61%). The ^{1}H NMR spectrum of **15-La** in THF-d_8 matched that previously reported. IR: 3066w, 3053w, 2948s, 2890m, 1471w, 1453w, 1432w, 1398w, 1351m, 1314w, 1283w, 1246s, 1213w, 1107s, 1077s, 1056m, 961m, 923m, 828s, 770m, 749s, 683m, 638m, 625w, 601w cm^{-1}. UV–vis (THF) λ_{max} nm (ε, M^{-1}cm^{-1}): 268 (17200), 340 (1440), 410 (8300 shoulder), 583 (11900), 710 (6700). Anal. Calcd for $C_{74}H_{138}KLa_2O_9Si_8$: C, 51.87; H, 8.12. Numerous samples were analyzed and representative data follow: C, 47.10; H, 7.41; C, 44.82; H, 7.06; C, 41.16; H, 6.57. The low values in each case suggest incomplete analysis and the found CH ratios of $C_{74}H_{138.7}$, $C_{74}H_{138.9}$, and $C_{74}H_{140.8}$, respectively, are consistent with the calculated $C_{74}H_{138}$ formula.

Cp″$_2$La(C$_{14}$H$_{10}$)K(18-crown-6), 16-La. In a glovebox, a scintillation vial was charged with compound **15-La** (40 mg, 28 μmol) and THF (5 mL) to give an intensely colored ink-blue solution. The solution was stirred until compound **15-La** was fully dissolved and then anthracene (5 mg, 28 μmol) in THF (5 mL) was added and the mixture was left to stir for 1 h. After 1 h, the

reaction mixture was heated with a hot plate set to 75 °C and left to stir again for 1 h and the solution turned from dark blue to dark violet. The volatiles were removed *in vacuo* and the resultant dark solids were extracted into toluene (10 mL). The green insolubles (presumably unreacted **15-La**) were removed via centrifugation and the toluene of the supernatant was removed *in vacuo*. The resultant solids were dissolved in Et_2O (8 mL), filtered, and concentrated before 5-8 drops of toluene was added. The solution was stored overnight at −35 °C in the glovebox freezer to yield violet single crystals of $Cp''_2La(C_{14}H_{10})K$(18-crown-6), **16-La**, characterized by X-ray crystallography (11 mg, 38%). IR: 3075w, 3051w, 2953s, 2895m, 1451m, 1435m, 1425m, 1402m, 1385w, 1352m, 1315m, 1246s, 1211m, 1113m, 1078s, 1059m, 962m, 920s, 831s, 775s, 750s, 716w, 691m, 640m, 621m cm^{-1}. Anal. Calcd for $C_{48}H_{76}KLaO_6Si_4$: C, 55.46; H, 7.37. As for 1, numerous samples were examined that had low values suggesting incomplete analysis: C, 53.86; H, 6.92; C, 53.60; H, 7.04; C, 49.53; H, 6.62. The found CH ratios of $C_{48}H_{73.5}$, $C_{48}H_{75.1}$, and $C_{48}H_{76.4}$, are close with the calculated $C_{48}H_{76}$ formula

[K(18-crown-6)(THF)$_2$][Cp″$_2$La(C$_{10}$H$_8$)], 17-La. In a glovebox, a scintillation vial was charged with compound **15-La** (25 mg, 18 μmol) and THF (4 mL) to give an intensely colored ink-blue solution. The solution was stirred until compound **15-La** was fully dissolved and then naphthalene (2 mg, 18 μmol) in THF (4 mL) was added and the mixture was left to stir for 1 h. After 1 h, the reaction mixture was heated with a hot plate set to 75 °C and left to stir again for 1 h and the solution turned from dark blue to dark green. The volatiles were removed *in vacuo* and the resultant dark solids were extracted into toluene (10 mL). The green insolubles (presumably unreacted **15-La**, dissolution in THF gave a dark blue solution) were removed via centrifugation and the toluene of the supernatant was removed *in vacuo*. The resultant solids were dissolved in a 4:1:1 Et_2O/THF/toluene solution (2 mL) and filtered. Dark green single crystals characterized

by X-ray crystallography as [K(18-crown-6)(THF)$_2$][Cp″$_2$La(C$_{10}$H$_8$)], **17-La**, were obtained by vapor diffusion of pentane into the dark green solution at −35 °C (7 mg, 35%). IR: 3069w, 3038w, 2951s, 2897s, 1476m, 1452m, 1437m, 1400m, 1385m, 1352s, 1315w, 1285w, 1265m, 1248s, 1215w, 1184w, 1111s, 1078s, 1057w, 1005w, 999w, 962m, 924m, 833s, 787w, 773w, 750m, 731w, 692w, 685w, 640w cm^{-1}. Anal. Calcd for C$_{52}$H$_{90}$KLaO$_8$Si$_4$: C, 55.09; H, 8.00. Found: C, 50.51; H, 7.14. The found CH ratio of C$_{48}$H$_{86.4}$ is consistent with the formula and suggests incomplete combustion.

[K(18-crown-6)][(C$_8$H$_8$)LaCp″(C$_8$H$_8$)LaCp″$_2$], 18-La. In a glovebox, a scintillation vial was charged with **15-La** (100 mg, 58 μmol) and THF (10 mL) to give an intensely colored ink-blue solution. To the stirred solution was added C$_8$H$_8$ (9 mg, 88 μmol) dissolved in THF (2 mL) and the reaction mixture immediately turned bright yellow. After 1 h, the volatiles were removed to yield yellow solids. Et$_2$O was added (10 mL) and the yellow slurry was filtered and concentrated to ca. 3 mL). The yellow solution was then layered with hexane (15 mL) and stored at −35 °C in the glovebox freezer to yield yellow single crystals characterized by X-ray crystallography as [K(18-crown-6)][(C$_8$H$_8$)LaCp″(C$_8$H$_8$)LaCp″$_2$], **18-La**.

Magnetic Measurements. Magnetic samples were prepared by Lucy E. Darago in the group of Professor Jeffrey R. Long at the University of California, Berkeley, by adding the powdered crystalline compound to a 5 mm inner diameter quartz tube with a quartz platform ¾ down the length of the tube. For all samples, solid eicosane was added to prevent crystallite torqueing and provide good thermal contact between the sample and the bath. The tubes were fitted with Teflon sealable adapters, evacutated using a glovebox vacuum pump, and flame-sealed under static vacuum. Following flame sealing, the solid eicosane was melted in a water bath held at 40 °C. Magnetic susceptibility measurements were performed using a Quantum Design MPMS2

SQUID magnetometer. Dc susceptibility data measurements were performed at temperatures ranging from 1.8 to 300 K, using applied fields of 1, 0.5, and 0.1 T (variable temperature) and fields ranging from 0 to 7 T (magnetization measurements were performed using a 4 Oe switching field. All data were corrected for diamagnetic contributions from the core diamagnetism estimated using Pascal's constants.[15]

X-ray Data Collection, Structure Solution and Refinement for Cp″$_2$La(C$_{14}$H$_{10}$)K(18-crown-6), 16-La. A black crystal of approximate dimensions 0.114 x 0.220 x 0.371 mm was mounted on a glass fiber and transferred to a Bruker SMART APEX II diffractometer. The APEX2[16] program package was used to determine the unit-cell parameters and for data collection (25 sec/frame scan time for a sphere of diffraction data). The raw frame data was processed using SAINT[17] and SADABS[18] to yield the reflection data file. Subsequent calculations were carried out using the SHELXTL[19] program. The diffraction symmetry was 2/*m* and the systematic absences were consistent with the monoclinic space group $P2_1/n$ that was later determined to be correct. The structure was solved by direct methods and refined on F^2 by full-matrix least-squares techniques. The analytical scattering factors[20] for neutral atoms were used throughout the analysis. Hydrogen atoms were included using a riding model. There were several disordered atoms which were included using multiple components with partial site-occupancy-factors. Least-squares analysis did not converge, yielding wR2 = 0.3124 and Goof = 1.091 for 404 variables refined against 9278 data (0.75Å), R1 = 0.1245 for those 7998 data with $I > 2.0\sigma(I)$. There were several high peaks in the final difference-map and indications of twinning, however, attempts to resolve those issues were not successful. Details are given in Table 4.1

X-ray Data Collection, Structure Solution and Refinement for [K(18-crown-6)(THF)$_2$][Cp″$_2$La(C$_{10}$H$_8$)], 17-La. A green crystal of approximate dimensions 0.150 x 0.348 x

0.397 mm was mounted in a cryoloop and transferred to a Bruker SMART APEX II diffractometer. The APEX2[21] program package was used to determine the unit-cell parameters and for data collection (60 sec/frame scan time for a sphere of diffraction data). The raw frame data was processed using SAINT[17] and SADABS[18] to yield the reflection data file. Subsequent calculations were carried out using the SHELXTL[19] program. The diffraction symmetry was *mmm* and the systematic absences were consistent with the orthorhombic space group *Pbcn* that was later determined to be correct. The structure was solved by dual space methods and refined on F^2 by full-matrix least-squares techniques. The analytical scattering factors[20] for neutral atoms were used throughout the analysis. Hydrogen atoms were included using a riding model. There are two half-molecules of K 18-crown-6 present. One molecule was located on a two-fold rotation axis and one was located on an inversion center. Several atoms were disordered and included using multiple components with partial site-occupancy-factors. Least squares analysis yielded wR2 = 0.1247 and Goof = 1.032 for 666 variables refined against 12608 data (0.80 Å), R1 = 0.0455 for those 10978 data with $I > 2.0\sigma(I)$.

X-ray Data Collection, Structure Solution and Refinement for [K(18-crown-6)][(C_8H_8)LaCp″(C_8H_8)LaCp″$_2$], 18-La. A yellow crystal of approximate dimensions 0.066 x 0.426 x 0.456 mm was mounted in a cryoloop and transferred to a Bruker SMART APEX II diffractometer. The APEX2[21] program package was used to determine the unit-cell parameters and for data collection (60 sec/frame scan time for a sphere of diffraction data). The raw frame data was processed using SAINT[17] and SADABS[18] to yield the reflection data file. Subsequent calculations were carried out using the SHELXTL[19] program. The diffraction symmetry was *mmm* and the systematic absences were consistent with the orthorhombic space groups *Pnma* and $Pna2_1$. It was later determined that space group $Pna2_1$ was correct. The structure was solved by dual

space methods and refined on F^2 by full-matrix least-squares techniques. The analytical scattering factors[20] for neutral atoms were used throughout the analysis. Hydrogen atoms were included using a riding model. Several atoms were disordered and included using multiple components with partial site-occupancy-factors. The cyclooctatetraene ring defined by atoms C(42)-C(48) was included using components each with site-occupancy of 0.57143 to account for the eight atoms disordered over fourteen sites. Least-squares analysis yielded wR2 = 0.1050 and Goof = 1.015 for 673 variables refined against 18324 data (0.80Å), R1 = 0.0447 for those 14817 data with $I > 2.0\sigma(I)$. The structure was refined as a two-component inversion twin, BASF[20] = 0.2455. There were high residuals present in the final difference-Fourier map. It was not possible to determine the nature of the residuals although it was probable that THF, ether, hexane or benzene solvent was present. The SQUEEZE[22] routine in the PLATON[23] program package was used to account for the electrons in the solvent accessible voids.

RESULTS

Synthesis and Crystallographic Characterization of [K(18-crown-6)(THF)$_2$][(Cp″$_2$La)$_2$(μ-η^6:η^6-C$_6$H$_6$)]•THF, 15-La. The reduction of Cp″$_3$La with 1.5 equiv of K with equimolar amounts of 18-crown-6 in benzene was repeated as originally reported by Lappert et al.[2] in the paper that reported the structure of the Cp^{tt} complex in eq 2. A dark green powder with broad ^{1}H NMR resonances and a highly absorbing UV-visible spectrum was obtained as they reported. Dark green crystals of **15-La** could be obtained upon diffusion of Et_2O into an intense ink-blue colored THF solution generated after dissolution of the green solids. The UV-visible spectrum of the ink-blue solution is shown in Figure 4.1. X-ray crystallography showed

that this was the Cp″ analog of the complex in eq 4.2, as previously postulated, eq 4.7, Figure 4.2.

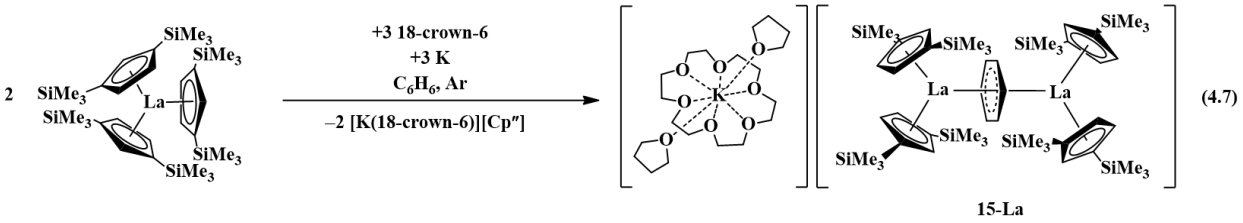

(4.7)

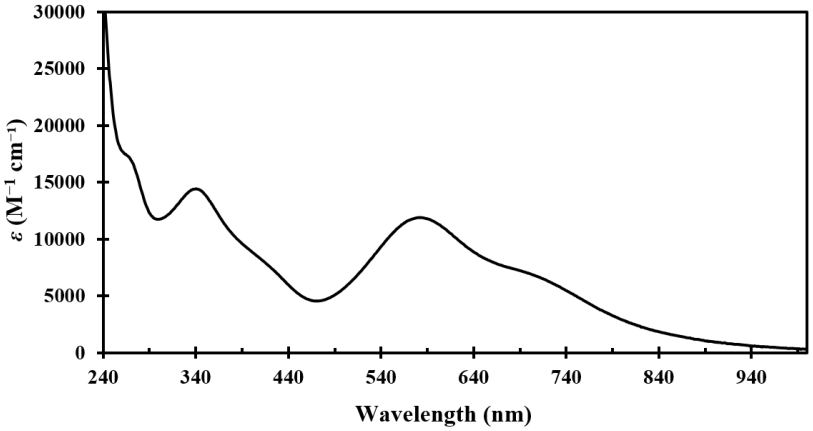

Figure 4.1. UV-visible spectrum of a 0.75 mM solution of [K(18-crown-6)(THF)$_2$][(Cp″$_2$La)$_2$(μ-η^6:η^6-C_6H_6)]•THF, **15-La**, in THF at 298 K.

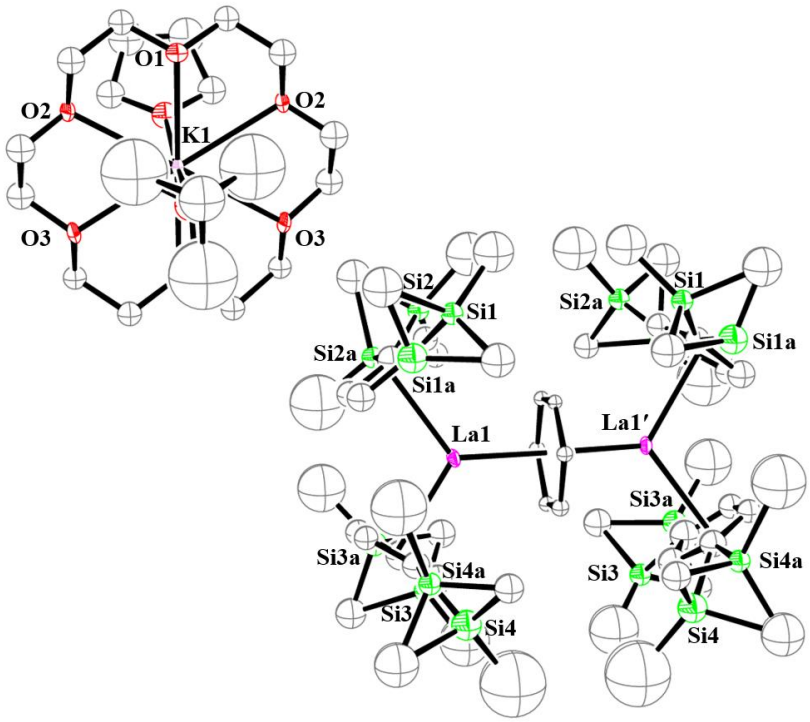

Figure 4.2. Molecular structure of [K(18-crown-6)(THF)$_2$][(Cp″$_2$La)$_2$(μ-η^6:η^6-C$_6$H$_6$)], **15-La**, with thermal ellipsoids drawn at the 30% probability level. Hydrogen atoms are omitted for clarity. All silicon atoms are disordered with 50% occupancy between two positions.

Compound **15-La** crystallizes in the *Pnma* space group and the centrosymmetric anion can be described as two Cp″$_2$La(II) metallocene units bridged by a monoanionic arene ligand. There was disorder in the cyclopentadienyl rings in this compound such that this is a "connectivity only" structure. The overall structure had a square planar array of Cp″ ring centroids and a planar bridging arene anion.

Magnetic Susceptibility. Magnetic studies were done by Lucy E. Darago in the group of Professor Jeffrey R. Long at the University of California, Berkeley. The magnetism of **15-La** at low temperature is consistent with a coupled S = ½ system. Compound **15-La** displays a waist-

restricted "butterfly" hysteresis at 2 K, Figure 4.3a. The saturation magnetization at 2 K also agrees with a ground state coupled S = ½ system, but the M vs. H plots show curvature indicative of magnetic anisotropy, Figure 4.3b. This magnetic anisotropy could stem from either: (a) low lying J excited states – if the La^{2+} centers have ground states of d^1, they could have low lying excited f^1 states that are being populated with increasing temperature, or (b) an intrinsically mixed ground state with contributions of *d* and *f* character on each La^{2+} center. The low temperature data is consistent with this electron being primarily *d* in character, since the low temperature moment matches that of a coupled S = ½ system, but the magnetic anisotropy could still originate from small mixing (possibly magnetic field-induced) with a f^1 state. Both of these explanations are consistent with the higher temperature X_T data, which shows a linear increase in X_T with temperature, Figure 4.4, leading to X_T values that at room temperature better reflect f^1 J states for the La^{2+} ions; *i.e.*, at 300 K the La^{2+} ions show magnetic behavior closer to that of Ce^{3+}, rather than that of the coupled S = ½ molecule observed at low temperature.

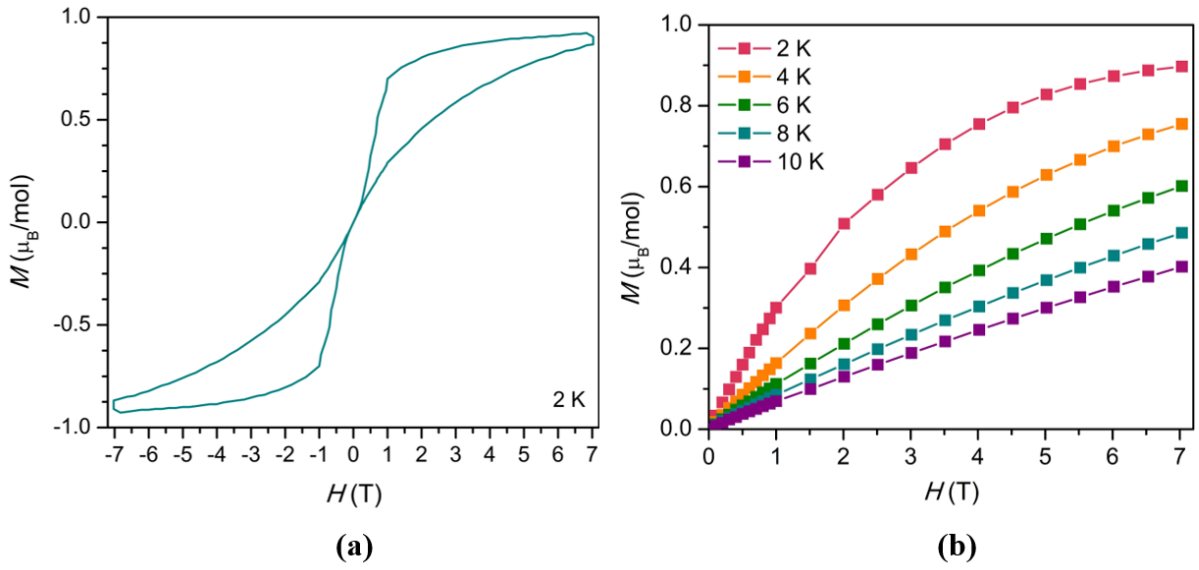

Figure 4.3. (a) Magnetization (M) versus d.c. magnetic field (H) for **15-La** at 2 K, and (b) Magnetization (M) versus d.c. magnetic field (H) for **15-La** at 2-10 K.

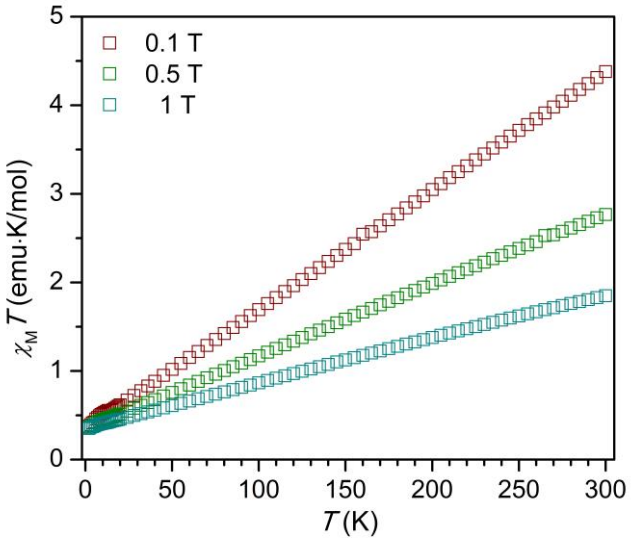

Figure 4.4. Plot of X_T versus temperature (K) of **15-La** using applied fields of 0.1 T (red), 0.5 T (green), and 1 T (blue).

Reactivity Studies. Anthracene. Addition of anthracene (−1.74 V vs SHE)[24] to a dark blue solution of **15-La** in THF caused no color change. After the reaction was heated to 75 °C for one, the color changed to dark violet and the anthracenide complex, $Cp''_2La(C_{14}H_{10})K(18\text{-crown-}6)$, **16-La**, was isolated and identified by X-ray crystallography, eq 4.8, Figure 4.5.

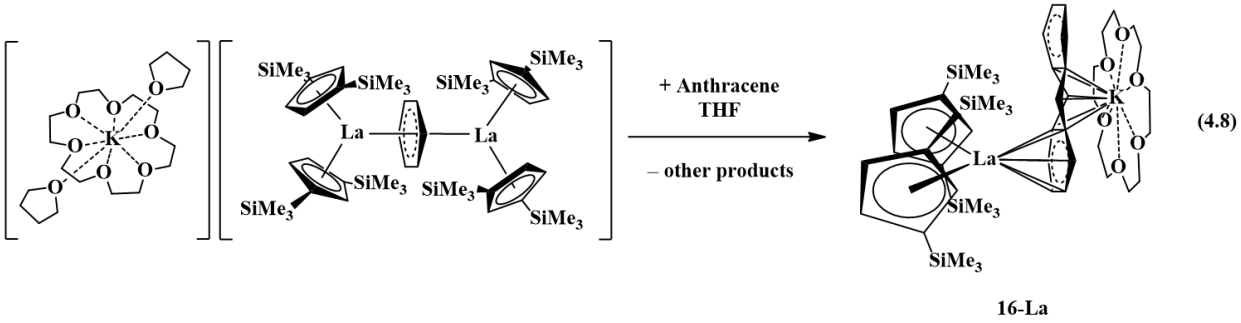

(4.8)

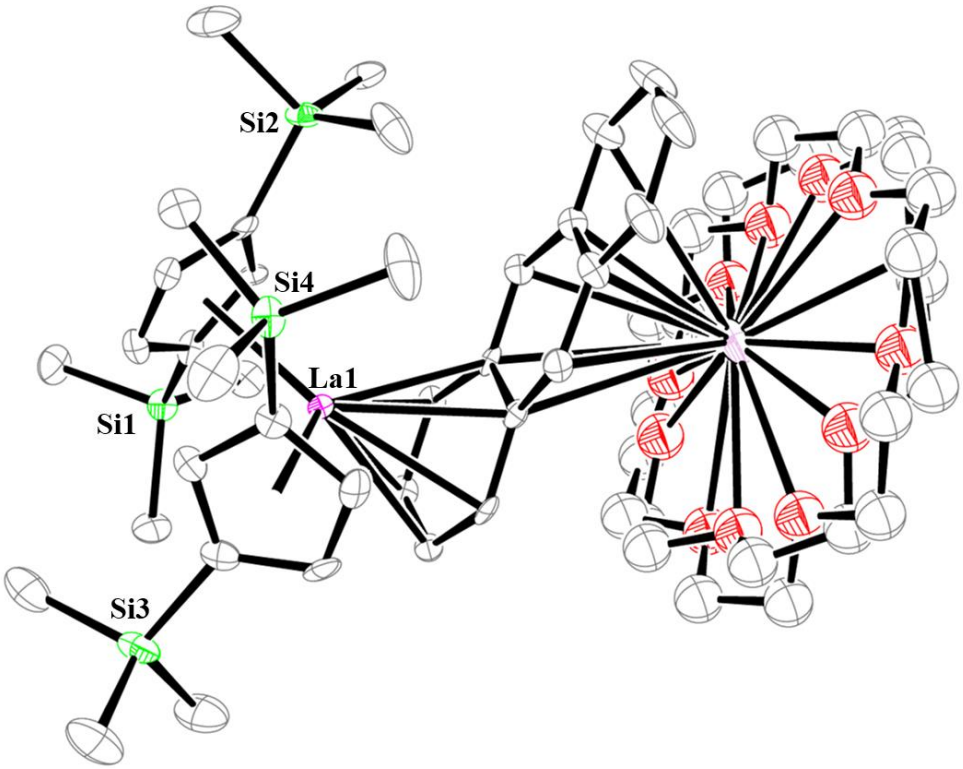

Figure 4.5. Thermal ellipsoid plot of $Cp''_2La(\mu\text{-}\eta^6\text{:}\ \eta^6\text{-}C_{14}H_{10})K(18\text{-crown-6})$, **16-La**, with thermal ellipsoids drawn at the 50% probability level. Hydrogen atoms are omitted for clarity. The 18-crown-6 was disordered at 50% occupancy between two positions.

In **16-La**, a $(Cp''_2La)^{1+}$ unit is bound to an end ring of anthracene and the $[K(18\text{-crown-6}]^{1+}$ component to the middle ring. The 18-crown-6 ring is disordered over at least two positions and the data are not of sufficient quality to discuss bond distances. Previous studies of anthracenide dianions with rare-earth metals include: the ferrocene diamide complexes, $[Fe(C_5H_4{}^{TBS}N)_2Ln(THF)]_2(C_{14}H_{10})$ (Ln = Sc,[25] Y[26]; ^{TBS}N = $N(SiMe_2{}^tBu)$), and $[K(18\text{-crown-6})][Fe(C_5H_4{}^{TBS}N)_2Y(C_{14}H_{10})]$[7], and the bimetallic Y^{3+} amido phosphine, $[(P_2N_2)Y]_2(C_{14}H_{10})$ (P_2N_2 = $PhP(CH_2SiMe_2NSiMe_2CH_2)_2PPh$).[27]

Naphthalene. Similarly, addition of naphthalene (−2.36 V vs SHE)[24] to a dark blue solution of **15-La** in THF did not cause a color change. However, heating the mixture to 75 °C for one hour generated a green solution from which crystals of [K(18-crown-6)(THF)$_2$][Cp″$_2$La(C$_{10}$H$_8$)], **17-La**, could be isolated, eq 4.9, Figure 4.6.

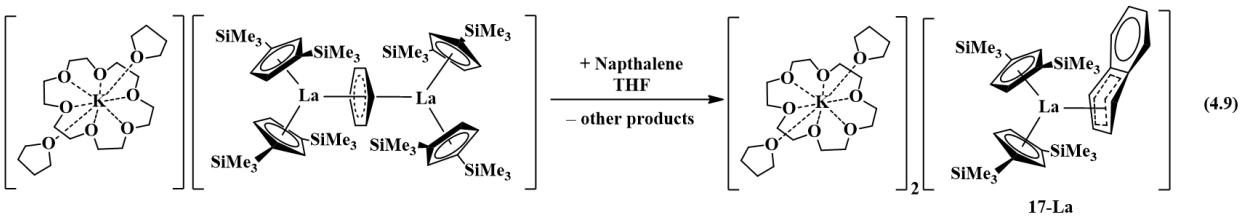

(4.9)

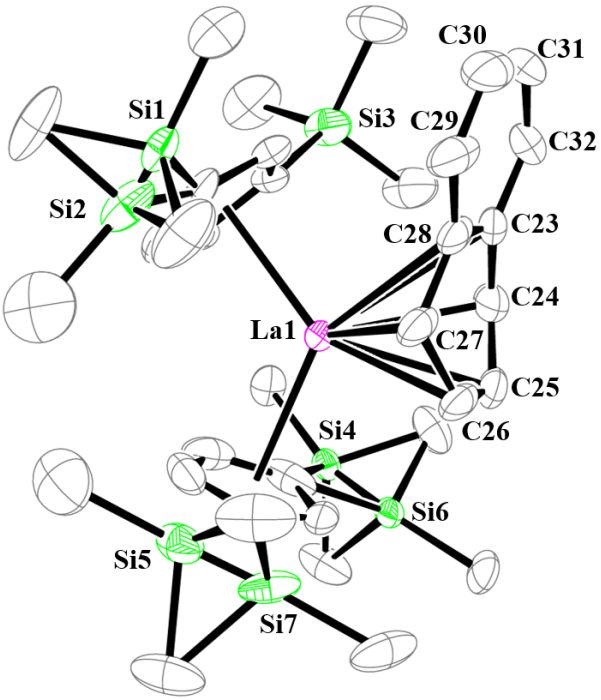

Figure 4.6. Thermal ellipsoid plot of [K(18-crown-6)(THF)$_2$][Cp″$_2$La(C$_{10}$H$_8$)], **17-La**, with thermal ellipsoids drawn at the 50% probability level. Hydrogen atoms and a [K(18-crown-6)(THF)$_2$]$^{1+}$ cation are omitted for clarity. Si1 and Si2 are disordered with a 72:28 occupancy. Si4 and Si6 are disordered 33:67. Si5 and Si7 are disordered 34:66.

The **17-La** complex is the Cp″ 18-crown-6 analogue of the previously reported [K(2.2.2-cryptand)][Cp′$_2$La(C$_{10}$H$_8$)][28] shown in eq 4.6.

The bond distances and angles of **17-La** are presented with [K(2.2.2-cryptand)][Cp′$_2$La(C$_{10}$H$_8$)][28] in Table 4.2. Both complexes feature a (Cp$_2$Ln)$^{1+}$ metallocene unit oriented towards four carbon atoms of one ring of the (C$_{10}$H$_8$)$^{2-}$ ligand. The four carbon atoms are not coplanar with the remaining six carbon atoms. The angle between the two planes generated from (C24-C27) and (C23, C24, C27, C28) in **17-La** is 152.6°, which is similar to the 155.5 angle in [K(2.2.2-cryptand)][Cp′$_2$La(C$_{10}$H$_8$)]. The 2.263 Å La–Mid1 distance defined by the midpoint of the vector between C24 and C27 in **17-La** is slightly longer than the analogous 2.230 Å distance in [K(2.2.2-cryptand)][Cp′$_2$La(C$_{10}$H$_8$)]. The La–Cnt(Cp) distances of **17-La** are also slightly larger; in **17-La** they are 2.619 and 2.646 Å and in [K(2.2.2-cryptand)][Cp′$_2$La(C$_{10}$H$_8$)] they are 2.610 and 2.592 Å. The 152.6° and 155.5° Cnt(Cp)–La–Cnt(Cp) angles are similar. These data suggest that the Cp″ coordination environment is comparable to Cp′ in the [K(chelate)][(Cp)$_2$Ln(C$_{10}$H$_8$)] complexes.

Unlike [K(2.2.2-cryptand)][Cp′$_2$La(C$_{10}$H$_8$)], whose structure was disordered, preventing a discussion of the metrical parameters of (C$_{10}$H$_8$)$^{2-}$, in **17-La** the (C$_{10}$H$_8$)$^{2-}$ ligand is not disordered. Examination of the C–C bonds of (C$_{10}$H$_8$)$^{2-}$ in **17-La** reveal that the 1.363(7) Å C25–C26 bond distance is the shortest distance C–C of the ring. This suggests localization of charge on the nonplanar C$_6$ ring with more double bond character between C25 and C26 and charge on C24 and C27. This has been observed in [K(2.2.2-cryptand)][Cp′$_2$Ln(C$_{10}$H$_8$)] (Ln = Y, Ce, Dy)[28] as well as other rare earth napththalenide complexes such as (C$_5$H$_5$)Lu(C$_{10}$H$_8$)(DME),[29] (C$_{10}$H$_8$)DyI(DME)$_2$,[30] and [Tm(DME)]$_2$(η^2-C$_{10}$H$_8$)$_2$(μ-η^4:η^4-C$_{10}$H$_8$).[31]

Cyclooctatetraene Reduction. The reaction of **15-La** with 1,3,5,7-cyclooctatetraene (reduction potential −1.59 V vs SHE)[24] was also examined. In contrast to the above reactions, addition of 1,3,5,7-cyclooctatetraene to **15-La** in THF caused an immediate color change to bright yellow without heating. Upon work-up, yellow crystals of [K(18-crown-6)][(C_8H_8)LaCp″(C_8H_8)LaCp″$_2$], **18-La**, were isolated, eq 4.10, Figure 4.7.

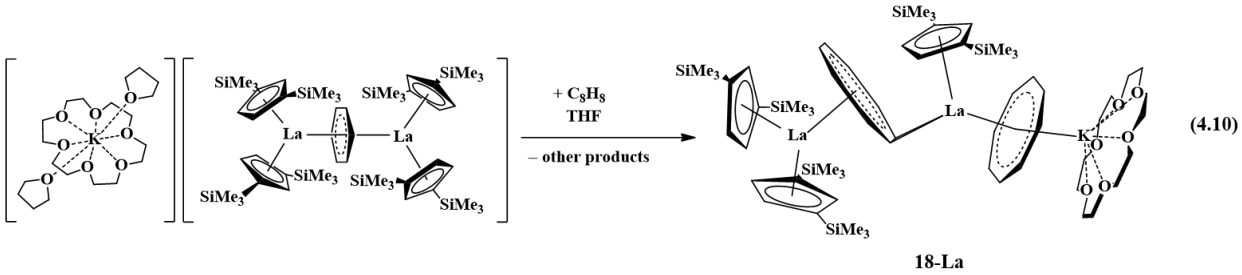

(4.10)

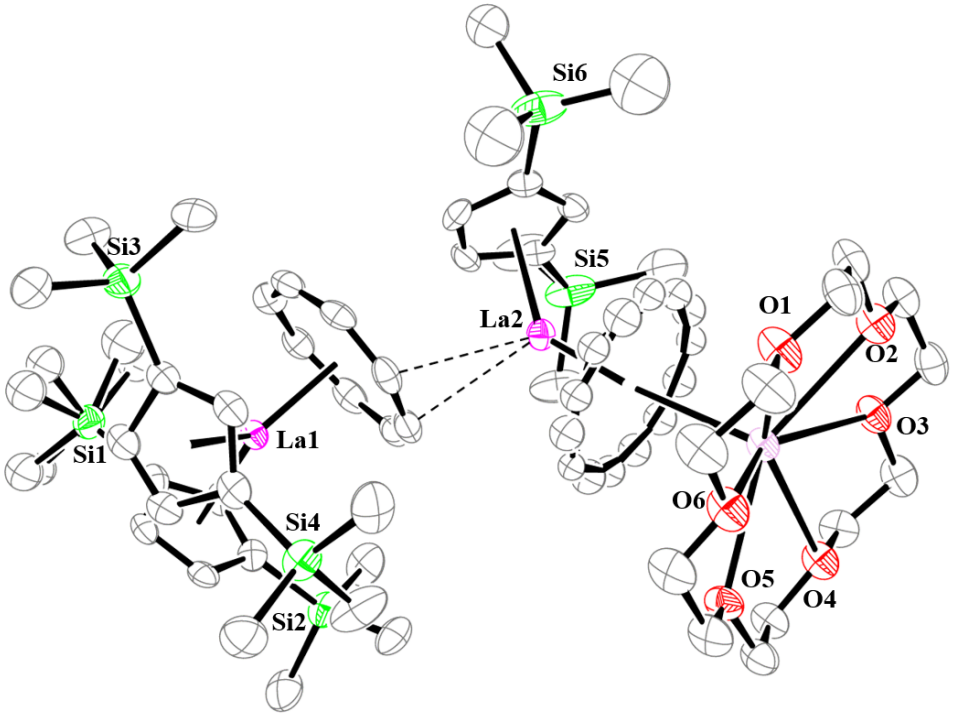

Figure 4.7. Thermal ellipsoid plot of [K(18-crown-6)][(C_8H_8)LaCp″(C_8H_8)LaCp″$_2$], **18-La**, with thermal ellipsoids drawn at the 50% probability level. Hydrogen atoms are omitted for clarity. The methyl groups on Si1 are disordered 55:45. The carbons of the $(C_8H_8)^{2-}$ bound to La2 were best refined with 57% occupancy.

18-La crystallizes in the *Pna*2$_1$ space group and appears to consist of an anionic component, $[Cp''_2La(C_8H_8)]^{1-}$, similar to the $[Cp'_2La(C_8H_8)]^{1-}$ anion of [K(2.2.2-cryptand)][$Cp'_2La(C_8H_8)$], **11-La**, introduced in Chapter 3, but with a $[Cp''La(C_8H_8)K(18\text{-crown-}6)]^{1+}$ cation instead of $[K(2.2.2\text{-cryptand})]^{1+}$. This is the first example of a cation of the general formula $[CpLn(C_8H_8)M(chelate)]^{1+}$, where M = alkali metal. The metrical data on **18-La** are compared with that of **11-La** in Table 4.3. The $[Cp''_2La(C_8H_8)]^{1-}$ anion in **18-La** appears to be interacting with the $[Cp''La(C_8H_8)K(18\text{-crown-}6)]^{1+}$ cation via an η^2 interaction of La2 with the $(C_8H_8)^{2-}$ ring bound η^8 to La1. This does not appear to have a substantial effect on the $[Cp''_2La(C_8H_8)]^{1-}$ unit, however. The 2.687 and 2.704 Å La1–Cnt(Cp″) distances in **18-La** are similar to the 2.693 and 2.687 Å La1–Cnt(Cp′) bond distances in **11-La**, despite the larger Cp″ ligand in **18-La**. The La–Cnt(C_8H_8) distances are also similar; the 2.190 Å La1–Cnt(C_8H_8) distance in **18-La** is only 0.031 Å longer than the 2.159 Å distance in **11-La**. The 109.3° Cnt(Cp″)–La1–Cnt(Cp″) angle of **18-La** is only slightly larger than the analogous 107.1° angle in **11-La**, both of which are significantly smaller than the 123.8° angle of the cationic $[Cp''_2La(DME)(NC^tBu)][BPh_4]$,[32] the 133.2° of $(C_5Me_5)_2La[N(SiMe_3)_2]$,[33] and the 131.6° angle in $(C_5Me_5)_2La(BPh_4)$.[34] The $[Cp''La(C_8H_8)K(18\text{-crown-}6)]^{1+}$ cation in **18-La** consists of an inverse sandwich of a disordered $(C_8H_8)^{2-}$ ligand between $[Cp''La]^{2+}$ and $[K(18\text{-crown-}6)]^{1+}$ moieties. The 2.547 Å La2–Cnt(Cp) distance in the cation is significantly shorter than the 2.687 and 2.704 Å La1–Cnt(Cp) distances of the anion. The disorder in the $(C_8H_8)^{2-}$ prevents further discussion of the metrical parameters.

DISCUSSION

The crystallographic characterization of [K(18-crown-6)(THF)$_2$][(Cp″$_2$La)$_2$(μ-η^6:η^6-C_6H_6)], **15-La**, confirms the identity of the dark green powder first described by Lappert[2] as the bimetallic La^{2+} complex bridged by a benzenide monoanion ligand, $(C_6H_6)^{1-}$. The structure of **15-La** is similar to the Cp^{tt} analog shown in eq 4.2 in that the cyclopentadienyl ligands are oriented planar and the $(C_6H_6)^{1-}$ ligand is also planar. Also like the Cp^{tt} analog, the structure is highly disordered, limiting an analysis of the metrical parameters.

Magnetic studies on **15-La** are consistent with an S = ½ system and are indicative of magnetic exchange coupling between the two La^{2+} ions. **15-La** is another example of a complex with an anionic radical ligand bridge mediating magnetic exchange coupling between the rare earth ions. Previously, the complexes {[(Me$_3$Si)$_2$N)$_2$(THF)Ln]$_2$(μ-η^2:η^2-N_2)}[K(L)] [Ln = Y, Gd, Tb, Ho, Er, Lu; L = 18-crown-6 or (THF)$_6$] with a radical $(N_2)^{3-}$ bridge were obtained as products from LnA_3/M reductions[35-37] and magnetometry measurements revealed that the $(N_2)^{3-}$ ligand couples the moments of the Ln^{3+} ions resulting in high magnetic moments and single-molecule magnet behavior.[38,39] Complex **15-La** was of interest because it contains two Ln^{2+} ions, which have been shown previously to have higher magnetic moments than Ln^{3+} ions.[40] Attempts to synthesize compounds like **15-La** with the smaller lanthanides, however, were unsuccessful, yielding only intractable brown oils.

The thermal stability of **15-La** is apparent in its reactivity with anthracene (−1.74 V vs SHE)[24] and naphthalene (−2.36 V vs SHE)[24] in that **15-La** does not immediately react with these polycyclic arenes at room temperature. The unusual stability of **15-La** is also apparent by the fact that **15-La** is formed after heating the La^{3+} complex [K(18-crown-6)][Cp″La(C_6H_6)] to 70°C for over 7 days.[2] However, **15-La** reacts with cyclooctatetraene (−1.59 V vs SHE)[24] without heat,

suggesting that the reduction potential of the first redox event of **15-La** is more negative than −1.59 V. Evidently, this three-electon-reductant is less reducing than the four-electron- and the one-electron reductants, [K(2.2.2-cryptand)]$_2$[(Cp′$_2$La)$_2$(C$_6$H$_6$)], and [K(2.2.2-cryptand)][Cp′$_3$La], which do reduce naphthalene at room temperature.[13,28] The stoichiometry of the reactions with **15-La** are unknown and appear complicated. For example, **15-La** does not give an observable EPR signal as a 10 mM solution in THF at room temperature; after treatment with anthracene, an eight-line pattern with hyperfine coupling identical to [Cp″$_3$La]$^{1-}$ is observed.

The crystallographic characterization of [K(18-crown-6)(THF)$_2$][Cp″$_2$La(C$_{10}$H$_8$)], **17-La**, and [K(18-crown-6)][(C$_8$H$_8$)LaCp″(C$_8$H$_8$)LaCp″$_2$], **18-La**, has provided additional information of the Cp″ ligand in complexes of the [Cp$_2$Ln(substrate)]$^{1-}$ anion. The metrical parameters of **17-La** with the Cp″ ligand are comparable to Cp′ suggesting that the coordination environments with these two ligands are very similar. In addition, the **17-La** product with the Cp″ ligand, in contrast to [Cp′$_2$La(C$_{10}$H$_8$)]$^{1-}$ with Cp′, was less disordered and allowed a structural characterization of the naphthalenide dianion ligand (C$_{10}$H$_8$)$^{2-}$.

When **15-La** was treated with cyclooctatetraene, a new type of product, **18-La**, was generated in contrast to reactivity with the four-electron-reductant [K(2.2.2-cryptand)]$_2$[(Cp′$_2$La)$_2$(C$_6$H$_6$)], which gave the bis(cyclooctatetraenyl) product, [K(2.2.2-cryptand)][La(C$_8$H$_8$)$_2$],[13] **12-La**, a compound previously introduced in Chapter 3. Instead, **15-La** contains a [Cp″$_2$La(C$_8$H$_8$)]$^{1-}$ anion, resembling the [Cp′$_2$La(C$_8$H$_8$)]$^{1-}$ anion in **11-La**, also introduced in Chapter 3. Also observed in **18-La** was a new type of cation, [Cp″La(C$_8$H$_8$)K(18-crown-6)]$^{1+}$, with an inverse sandwich type structure.

CONCLUSION

The complex [K(18-crown-6)(THF)$_2$][(Cp″$_2$La)$_2$(μ-η^6:η^6-C$_6$H$_6$)], **15-La**, was for the first time definitively identified by X-ray crystallography since its initial synthesis by Lappert and coworkers. The structure of **15-La**, like its Cp^{tt} analogue, is disordered which precludes a detailed structural analysis. Magnetization studies of **15-La** are consistent with the La^{2+} $(C_6H_6)^{1-}$ La^{2+} assignment and demonstrate the first measurement of magnetic exchange coupling between two non-traditional 4f^{n}5d^1 Ln^{2+} ions bridged by a radical ligand. The structural characterization of the [K(18-crown-6)(THF)$_2$][Cp″$_2$La(C$_{10}$H$_8$)], **17-La**, and [K(18-crown-6)][(C$_8$H$_8$)LaCp″(C$_8$H$_8$)LaCp″$_2$], **18-La**, complexes demonstrate that the Cp″ ligand is similar to the Cp′ ligand in complexes of the $[Cp_2Ln(substrate)]^{1-}$ anion. The unusual thermal stability of this three-electron reductant is apparent in its reactivity in that **15-La** must be heated to react with substrates that have a reduction potential of −1.74 V vs SHE but not with those at −1.59 V vs SHE.

Table 4.1. Crystal data and structure refinement $Cp''_2La(C_{14}H_{10})K(18\text{-crown-6})$, **16-La**, $[K(18\text{-crown-6})(THF)_2][Cp''_2La(C_{10}H_8)]$, **17-La**, and $[K(18\text{-crown-6})][(C_8H_8)LaCp''(C_8H_8)LaCp''_2]$, **18-La**.

	16-La	**17-La**	**18-La**
Empirical formula	$C_{48}H_{76}KLaO_6Si_4$	$C_{52}H_{90}KLaO_8Si_4$	$C_{61}H_{103}KLa_2O_6Si_6$
Formula weight	1039.45	1133.60	1417.89
Temperature (K)	133(2)	88(2)	133(2)
Space group	$P2_1/n$	$Pbcn$	$Pna2_1$
a (Å)	10.7630(6)	28.8935(16)	22.913(3)
b (Å)	29.3538(16)	19.0830(10)	18.070(3)
c (Å)	17.5926(10)	22.3790(12)	21.549(3)
α (°)	90	90	90
β (°)	90.2020(9)	90	90
γ (°)	90	90	90
Volume ($Å^3$)	5558.1(5)	12339.2(12)	8922(2)
Z	4	8	4
ρ_{calcd} (g/cm^3)	1.242	1.220	1.056
μ (mm^{-1})	0.970	0.882	1.106
$R1^a$	0.1245	0.0455	0.0447
$wR2^b$	0.3201	0.1247	0.1050

Definitions: $^a R1 = \sum||Fo| - |Fc||/\sum|Fo|$; $^b wR2 = [\sum[w(Fo^2 - Fc^2)^2]/\sum[w(Fo^2)^2]\ ]^{1/2}$.

Table 4.2. Selected Bond Distances (Å) and Angles (deg) for [K(18-crown-6)(THF)$_2$][Cp″$_2$La(C$_{10}$H$_8$)], **17-La**, and [K(2.2.2-cryptand)][Cp′$_2$La(C$_{10}$H$_8$)].[28]

	17-La	[K(2.2.2-cryptand)][Cp′$_2$La(C$_{10}$H$_8$)][28]
Ln1–Cnt(Cp)	2.619	2.610
	2.646	2.592
Ln1–Mid1[a]	2.263	2.230
Ln1–C(Cp)$_{avg}$	2.89(2)	2.865(7)
Ln1–C(C$_{10}$H$_8$)	2.663(4)	2.570(5)
	2.694(4)	2.689(3)
	2.727(4)	2.732(5)
	2.743(4)	2.772(6)
	2.917(4)	3.068(3)
	2.924(4)	3.052(3)
Cnt(Cp)–Ln1–Cnt(Cp)	115.9	117.3
C23–C32	1.396(7)	*b*
C23–C28	1.432(8)	*b*
C23–C24	1.479(7)	*b*
C24–C25	1.430(7)	*b*
C25–C26	1.363(7)	*b*
C26–C27	1.467(6)	*b*
C27–C28	1.469(7)	*b*
C28–C29	1.413(6)	*b*
C29–C30	1.375(9)	*b*
C30–C31	1.37(1)	*b*
C31–C32	1.412(9)	*b*
Pln1–Pln2	152.6	155.5

[a] Mid1 is the midpoint of the vector between C24 and C27. [b] Not available due to disorder. [c] Pln1 and Pln2 are the planes of (C24-C27) and (C23-C24, C27-C28), respectively.

Table 4.3. Selected bond lengths (Å) and angles (°) of and [K(18-crown-6)][(C_8H_8)LaCp″(C_8H_8)LaCp″$_2$], **18-La**, and [K(2.2.2-cryptand)][Cp′$_2$La(C_8H_8)], **11-La**.

	18-La	**11-La**
Ln1–Cnt(Cp)	2.687	2.693
	2.704	2.687
Ln2–Cnt(Cp)	2.547	-
Ln1–Cnt(C_8H_8)	2.190	2.159
Ln2–Cnt(C_8H_8)	2.078	-
Ln1–C(Cp)$_{avg}$	2.95(5)	2.95(2)
Ln2–C(Cp)$_{avg}$	2.81(2)	-
Ln1–C(C_8H_8)$_{avg}$	2.86(4)	2.83(3)
Ln2–C(C_8H_8)$_{avg}$	*a*	-
Cnt(Cp)–Ln1–Cnt(Cp)	109.3	107.1
Cnt(Cp)–Ln1–Cnt(C_8H_8)	125.5	126.4
	125.2	126.4
Cnt(Cp)–Ln2–Cnt(C_8H_8)	117.7	-

[a] Not available due to disorder.

REFERENCES

(1) Cassani, M. C.; Gun'ko, Y. K.; Hitchcock, P. B.; Lappert, M. F. *Chem. Commun.* **1996**, *1996*, 1987-1988.

(2) Cassani, M. C.; Duncalf, D. J.; Lappert, M. F. *J. Am. Chem. Soc.* **1998**, *120*, 12958-12959.

(3) Gun'ko, Y. K.; Hitchcock, P. B.; Lappert, M. F. *Organometallics* **2000**, *19*, 2832-2834.

(4) Fryzuk, M. D.; Love, J. B.; Rettig, S. J. *J. Am. Chem. Soc.* **1997**, *119*, 9071-9072.

(5) Fryzuk, M. D.; Jafarpur, L.; Kerton, F. M.; Love, J. B.; Patrick, B. O.; Rettig, S. J. *Organometallics* **2001**, *20*, 1387-1396.

(6) Bochkarev, M. N. *Chem. Rev.* **2002**, *102*, 2089-2118.

(7) Huang, W.; Dulong, F.; Wu, T.; Khan, S. I.; Miller, J. T.; Cantat, T.; Diaconescu, P. L. *Nat. Commun.* **2013**, *4*, 1448–1455.

(8) Diaconescu, P. L.; Arnold, P. L.; Baker, T. A.; Mindiola, D. J.; Cummins, C. C. *J. Am. Chem. Soc.* **2000**, *122*, 6108-6109.

(9) Evans, W. J.; Kozimor, S. A.; Ziller, J. W.; Kaltsoyannis, N. *J. Am. Chem. Soc.* **2004**, *126*, 14533-14547.

(10) Arnold, P. L.; Mansell, S. M.; Maron, L.; McKay, D. *Nat. Chem.* **2012**, *4*, 668-674.

(11) Patel, D.; Tuna, F.; McInnes, E. J. L.; McMaster, J.; Lewis, W.; Blake, A. J.; Liddle, S. T. *Dalton Trans.* **2013**, *42*, 5224-5227.

(12) Camp, C.; Mougel, V.; Pécaut, J.; Maron, L.; Mazzanti, M. *Chem. Eur. J.* **2013**, *19*, 17528-17540.

(13) Kotyk, C. M.; Fieser, M. E.; Palumbo, C. T.; Ziller, J. W.; Darago, L. E.; Long, J. R.; Furche, F.; Evans, W. J. *Chem. Sci.* **2015**, *6*, 7267-7273.

(14) Xie, Z.; Chui, K.; Liu, Z.; Xue, F.; Zhang, Z.; W., M. T. C.; Sun, J. *J. Organomet. Chem.* **1997**, *549*, 239-244.

(15) Bain, G. A.; Berry, J. F. *J. Chem. Educ.* **2008**, *85*, 532-536.

(16) APEX2 Version 2014.9-0, Bruker AXS, Inc.; Madison, WI, 2014.

(17) SAINT Version 8.34a, Bruker AXS, Inc.; Madison, WI, 2013.

(18) Sheldrick, G. M.; SADABS, Version 2014/5, Bruker AXS, Inc.; Madison, WI, 2014.

(19) Sheldrick, G. M.; SHELXTL, Version 2014/7, Bruker AXS, Inc.; Madison, WI, 2014.

(20) International Tables for X-Ray Crystallography, 1992, Vol. C.; Dordrecht: Kluwer Academic Publishers.

(21) APEX2 Version 2014.11-0, Bruker AXS, Inc.; Madison, WI, 2014.

(22) Spek, A. L.; SQUEEZE, Acta Cryst. 2015, C71, 9-19.

(23) Spek, A. L.; PLATON, Acta. Crys. 2009, D65, 148-155.

(24) Evans, W. J.; Gonzales, S. L.; Ziller, J. W. *J. Am. Chem. Soc.* **1994**, *116*, 2600-2608.

(25) Huang, W.; Khan, S. I.; Diaconescu, P. L. *J. Am. Chem. Soc.* **2011**, *133*, 10410-10413.

(26) Huang, W.; Abukhalil, P. M.; Khan, S. I.; Diaconescu, P. L. *Chem. Commun.* **2014**, *50*, 5221-5223.

(27) Fryzuk, M. D.; Jafarpour, L.; Kerton, F. M.; Love, J. B.; Rettig, S. J. *Angew. Chem. Int. Ed.* **2000**, *39*, 767-770.

(28) Kotyk, C. M.; MacdDonald, M. R.; Ziller, J. W.; Evans, W. J. *Organometallics* **2015**, *34*, 2287-2295.

(29) Protchenko, A. V.; Zakharov, L. N.; Bochkarev, M. N.; Struchkov, Y. T. *J. Organomet. Chem.* **1993**, *447*, 209-212.

(30) Evans, W. J.; Allen, N. T.; Ziller, J. W. *J. Am. Chem. Soc.* **2000**, *122*, 11749-11750.

(31) Bochkarev, M. N.; Fedushkin, I. L.; Fagin, A. A.; Shumann, H.; Demtschuk, J. *Chem. Commun.* **1997**, 1783-1784.

(32) Hazin, P. N.; Bruno, J. W.; Schulte, G. K. *Organometallics* **1990**, *9*, 416-423.

(33) Evans, W. J.; Mueller, T. J.; Ziller, J. W. *J. Am. Chem. Soc.* **2009**, *131*, 2678.

(34) Hamaed, H.; Lo, A. Y. H.; Lee, D. S.; Evans, W. J.; Schurko, R. W. *J. Am. Chem. Soc.* **2006**, *128*, 12638-12639.

(35) Evans, W. J.; Fang, M.; Zucchi, G.; Furche, F.; Ziller, J. W.; Hoekstra, R. M.; Zink, J. I. *J. Am. Chem. Soc.* **2009**, *131*, 11195-11202.

(36) Fang, M.; Bates, J. E.; Lorenz, S. E.; Lee, D. S.; Rego, D. B.; Ziller, J. W.; Furche, F.; Evans, W. J. *Inorg. Chem.* **2011**, *50*, 1459-1469.

(37) Fang, M.; Lee, D. S.; Ziller, J. W.; Doedens, R. J.; Bates, J. E.; Furche, F.; Evans, W. J. *J. Am. Chem. Soc.* **2011**, *133*, 3784-3787.

(38) Rinehart, J. D.; Fang, M.; Evans, W. J.; Long, J. R. *J. Am. Chem. Soc.* **2011**, *133*, 14236-14239.

(39) Rinehart, J. D.; Fang, M.; Evans, W. J.; Long, J. R. *Nat. Chem.* **2011**, *3*, 538-542.

(40) Meihaus, M. R.; Fieser, M. E.; Corbey, J. F.; Evans, W. J.; Long, J. R. *J. Am. Chem. Soc.* **2015**, *137*, 9855-9860.

CHAPTER 5

Structural Variations in Reduced Arene Complexes of Lanthanum and Cerium

INTRODUCTION

As mentioned in Chapter 4, Lappert and co-workers reported a series of interesting $(C_5R_5)_3Ln/K$ reactions that gave products formulated to contain $(arene)^{1-}$ and $(arene)^{2-}$ anions on the basis of X-ray crystallography.[1-3] As in the seminal Lappert chemistry reported earlier,[2,3] obtaining definitive conclusions depends on accessing good crystal data. Reported here are variations of eq 4.1-4.5 that were successful with lanthanum, with the arenes benzene, toluene, and bis(trimethylsilyl)benzene, and with the ligands Cp′ and Cp″. Also reported is one reduced arene complex of cerium that crystallized.

EXPERIMENTAL

The syntheses and manipulations described below were conducted under argon with rigorous exclusion of air and water using glovebox, vacuum line, and Schlenk techniques. Solvents were sparged with UHP grade argon (Praxair) and passed through columns containing Q-5 and molecular sieves before use. NMR solvents (Cambridge Isotope Laboratories) were dried over NaK/benzophenone, degassed by three freeze−pump−thaw cycles, and vacuum transferred prior to use. Anhydrous Cp''_3Ln (Ln = La,[4] Ce[5]) were prepared according to the literature. 18-crown-6 (1,4,7,10,13,16-hexaoxacyclooctadecane, Aldrich) was sublimed before use. 2.2.2-Cryptand, (4,7,13,16,21,24-hexaoxa-1,10-diazabicyclo[8.8.8]hexacosane, VWR) was placed under vacuum (10^{-3} Torr) for 12 h before use. ^{1}H NMR (500 MHz) and ^{13}C NMR (125 MHz) were obtained on a Bruker GN500 or CRYO500 MHz spectrometer at 298 K. IR samples were

prepared as KBr pellets and the spectra were obtained on a Jasco FT/IR-4700 spectrometer. Elemental analyses were performed on a Perkin-Elmer 2400 Series II CHNS elemental analyzer. UV–vis spectra were collected in THF at 298 K using a Varian Cary 50 Scan UV–vis spectrophotometer.

[K(2.2.2-cryptand)][(Cp″$_2$La)$_2$(C$_6$H$_6$)], 19-La. In a glovebox free of coordinating solvents, Cp″$_3$La (100 mg, 0.130 mmol) and 2.2.2-cryptand (74 mg, 0.20 mmol) were dissolved in C$_6$H$_6$ (10 mL) and then transferred to a vial containing potassium (8 mg, 0.20 mmol) where an immediate color change to dark purple was observed. This color change was much quicker than that of **15-La** in Chapter 4. The mixture was stirred overnight at room temperature to yield an oily dark purple mixture. Toluene (1 mL) was added to the dark mixture and the volatiles were removed under reduced pressure to give a tacky purple solid. The tacky purple solid was washed with hexane (3 x 5 mL). The solids were then brought into a glovebox with coordinating solvents and dissolved in THF (4 mL) and the resultant blue solution was layered with hexane (15 mL). Storage of the mixture in the glovebox freezer (−35 °C) for 3 days to yielded dark crystals of **19-La** characterized by X-ray diffraction (49 mg, 47%). The UV-visible spectrum of **19-La** was identical to **15-La** reported in Chapter 4.

[(K(18-crown-6))$_2$(THF)$_3$][(Cp″$_2$Ce)$_2$(C$_6$H$_6$)], 20-Ce. Cp″$_3$Ce (100 mg, 0.130 mmol) and 18-crown-6 (52 mg, 0.20 mmol) were dissolved in C$_6$H$_6$ (10 mL) and then transferred to a vial containing potassium (8 mg, 0.20 mmol). The blue solution slowly began to turn dark purple. After 2 days, the resultant dark red slurry was centrifuged and the solids were collected and dried. They were then transferred to glovebox with coordinating solvents and subsequently dissolved in THF (5 mL). The resultant dark red solution was layered with hexane (15 mL) and stored at −35 °C in the glovebox freezer for 3 days to yield dark red single crystals characterized by X-ray

diffraction as **20-Ce** (66 mg, 67% based off of 4 equiv. of K). IR: 3054w, 2949s, 2894s 2826m, 1632br, 1472m, 1453m, 1434m, 1398w, 1385w, 1351m, 1315w, 1284w, 1247s, 1214m, 1108s, 1078s, 1063m, 962m, 924m, 829s, 722w, 751m, 681m, 636m, 625m cm^{-1}. Anal. Calcd for $C_{86}H_{162}Ce_2K_2O_{15}Si_8$: C, 51.15; H, 8.09. Found: C, 48.34; H, 7.53. Additional elemental analyses found C, 48.27; H, 7.67 and C, 45.49; H, 7.09. The found CH ratios of $C_{86}H_{159.6}$, $C_{86}H_{159.7}$, and $C_{86}H_{162.8}$ are consistent with the formula and suggest incomplete combustion.

[K(2.2.2-cryptand)]$_2$[(Cp′$_2$La)$_2$(C$_6$H$_4$(SiMe$_3$)$_2$)], 21-La. In an argon-filled glovebox, a scintillation vial was charged with Cp′$_3$La(THF) (50 mg, 0.08 mmol), 2.2.2-cryptand (61 mg, 0.16 mmol), and 1,4-bis(trimethylsilyl)benzene (9 mg, 0.04 mmol) and the mixture was dissolved in toluene (20 mL). KC_8 (22 mg, 0.16 mmol) was added to the resultant colorless solution which caused the mixture to turned dark purple immediately. The purple slurry was stirred for 3 h at room temperature and during this time a magenta colored oil precipitated from solution. The toluene supernatant was decanted from the oil and the oil was subsequently dissolved in THF (5 mL). The magenta colored mixture was centrifuged, filtered, and layered with hexane (15 mL). Storage in the glovebox freezer for 48 h at −35 °C yielded small red crystals characterized by X-ray crystallography as [K(2.2.2-cryptand)]$_2$[(Cp′$_2$La)$_2$(C$_6$H$_4$(SiMe$_3$)$_2$)], **21-La**. Only a few small crystals were obtained on the sides of the vial and the bulk of the reaction precipitated as a red intractable oil. Efforts to scale up the synthesis of **4** for characterization were unsuccessful. Crystal data for **21-La**: $C_{88}H_{162}K_2La_2N_4O_{14}Si_6$, triclinic, space group $P\bar{1}$, a = 13.2445(14) Å, b = 14.1700(15) Å, c = 15.5662(16) Å, α = 92.7974(13)°, β = 114.8535(12)°, γ = 98.4026(14)°, V = 2602.5(5) Å^3, Z = 1, D_c = 1.292 mg/m^3, T = 133(2) K, R1 = 0.0339 for 9624 reflections with $I > 2\sigma(I)$, wR2 = 0.0815.

[K(2.2.2-cryptand)][Cp′$_2$La(C$_7$H$_8$)], 22-La. In a reaction similar to that above except that the only arene present was the toluene solvent, KC_8 (22 mg, 0.16 mmol) was added to a toluene solution of Cp′$_3$La(THF) (50 mg, 0.08 mmol) and 2.2.2-cryptand (61 mg, 0.16 mmol) and the mixture turned dark purple immediately. The purple slurry was stirred for 3 h at room temperature and during this time a magenta colored oil precipitated out solution. The toluene supernatant was decanted away from the oil and the oil was subsequently dissolved in THF (5 mL). The magenta colored mixture was centrifuged, filtered, and layered with hexane (15 mL). Storage in the glovebox freezer for 48 h at −35 °C yielded small red crystals characterized by X-ray crystallography as [K(2.2.2-cryptand)][Cp′$_2$La(C$_7$H$_8$)], **22-La**. Similar to **21-La**, the reaction produced an intractable red oil and only a few very small crystals crystallized on the side walls of the scintillation vial. Crystal data for **22-La**: $C_{41}H_{70}KLaN_2O_6Si_2 \cdot C_4H_8O$, monoclinic, space group *C*2/*c*, a = 26.140(3) Å, b = 16.382(2) Å, c = 26.994(4) Å, β = 113.7890(19)°, V = 10577(2) Å^3, Z = 8, D_c = 1.247 mg/m^3, T = 88(2) K, R1 = 0.0515 for 8522 reflections with $I > 2\sigma(I)$, wR2 = 0.1156.

X-ray Data Collection, Structure Solution and Refinement for [K(2.2.2-cryptand)][(Cp″$_2$La)$_2$(C$_6$H$_6$)], 19-La. A grey crystal of approximate dimensions 0.130 x 0.160 x 0.500 mm was mounted in a cryoloop and transferred to a Bruker SMART APEX II diffractometer. The APEX2[6] program package was used to determine the unit-cell parameters and for data collection (25 sec/frame scan time for a sphere of diffraction data). The raw frame data was processed using SAINT[7] and SADABS[8] to yield the reflection data file. Subsequent calculations were carried out using the SHELXTL[9] program. The diffraction symmetry was 4/*m* and the systematic absences were consistent with the tetragonal space group $I4_1$ that was later determined to be correct. The structure was solved by dual space methods and refined on F^2 by full-matrix least-squares techniques. The analytical scattering factors[10] for neutral atoms were

used throughout the analysis. Hydrogen atoms were included using a riding model. Disordered atoms were included using multiple components with partial site-occupancy-factors. The molecule was a dimmer located about a two-fold rotation axis. The counter-ion was located on a two-fold rotation axis. Least-squares analysis yielded wR2 = 0.0985 and Goof = 1.058 for 389 variables refined against 10482 data (0.80 Å), R1 = 0.0380 for those 9790 data with I > 2.0σ(I). The absolute structure was assigned by refinement of the Flack parameter.[11] There were high residuals present in the final difference-Fourier map. It was not possible to determine the nature of the residuals although it was probable that benzene, hexane or tetrahydrofuran solvent(s) was/were present. The SQUEEZE[12] routine in the PLATON[13] program package was used to account for the electrons in the solvent accessible voids.

X-ray Data Collection, Structure Solution and Refinement for [(K(18-crown-6))$_2$(THF)$_3$][(Cp″$_2$Ce)$_2$(C$_6$H$_6$)], 20-Ce. A black crystal of approximate dimensions 0.110 x 0.123 x 0.284 mm was mounted in a cryoloop and transferred to a Bruker SMART APEX II diffractometer. The APEX2[6] program package was used to determine the unit-cell parameters and for data collection (60 sec/frame scan time for a sphere of diffraction data). The raw frame data was processed using SAINT[7] and SADABS[8] to yield the reflection data file. Subsequent calculations were carried out using the SHELXTL[9] program. There were no systematic absences nor any diffraction symmetry other than the Friedel condition. The centrosymmetric triclinic space group $P\bar{1}$ was assigned and later determined to be correct. The structure was solved by dual space methods and refined on F^2 by full-matrix least-squares techniques. The analytical scattering factors[10] for neutral atoms were used throughout the analysis. Hydrogen atoms were included using a riding model. The tetrahydrofuran ligand defined by atoms O(15), C(83), C(84), C(85), C(86), O(16), C(87), C(88), C(89), C(90) was disordered over two sites and was included using

partial-site-occupancy-factors and geometric constraints. Least-squares analysis yielded wR2 = 0.2059 and Goof = 1.026 for 1007 variables refined against 24465 data (0.83 Å), R1 = 0.0660 for those 14025 data with $I > 2.0\sigma(I)$. The complex was refined as a two-component twin. Pseudo-symmetry (possible orthorhombic crystal system) was investigated, however, refinement using space group *Pccn* did not converge. There were several high residuals present in the final difference-Fourier map. It was not possible to determine the nature of the residuals although it was probable that hexane solvent was present. The SQUEEZE[12] routine in the PLATON[13] program package was used to account for the electrons in the solvent accessible voids.

X-ray Data Collection, Structure Solution and Refinement for [K(2.2.2-cryptand)]$_2$[(Cp′$_2$La)$_2$(C$_6$H$_4$(SiMe$_3$)$_2$)], 21-La. A red crystal of approximate dimensions 0.044 x 0.107 x 0.216 mm was mounted in a cryoloop and transferred to a Bruker SMART APEX II diffractometer. The APEX2[6] program package was used to determine the unit-cell parameters and for data collection (60 sec/frame scan time for a sphere of diffraction data). The raw frame data was processed using SAINT[7] and SADABS[8] to yield the reflection data file. Subsequent calculations were carried out using the SHELXTL[9] program. There were no systematic absences nor any diffraction symmetry other than the Friedel condition. The centrosymmetric triclinic space group $P\bar{1}$ was assigned and later determined to be correct. The structure was solved by direct methods and refined on F^2 by full-matrix least-squares techniques. The analytical scattering factors[10] for neutral atoms were used throughout the analysis. Hydrogen atoms were included using a riding model. The molecule was located on an inversion center. There were two molecules of tetrahydrofuran solvent present per formula-unit. At convergence, wR2 = 0.0815 and Goof = 1.031 for 532 variables refined against 11392 data (0.78Å), R1 = 0.0339 for those 9624 data with $I > 2.0\sigma(I)$.

X-ray Data Collection, Structure Solution and Refinement for [K(2.2.2-cryptand)]$_2$[Cp′$_2$La(C$_7$H$_8$)], 22-La. A red crystal of approximate dimensions 0.109 x 0.116 x 0.175 mm was mounted in a cryoloop and transferred to a Bruker SMART APEX II diffractometer. The APEX2[6] program package and the CELL_NOW[14] were used to determine the unit-cell parameters. Data was collected using a 120 sec/frame scan time for a sphere of diffraction data. The raw frame data was processed using SAINT[7] and TWINABS[15] to yield the reflection data file (HKLF5 format).[15] Subsequent calculations were carried out using the SHELXTL[9] program. The diffraction symmetry was 2/*m* and the systematic absences were consistent with the monoclinic space groups *Cc*, and *C*2/*c*. It was later determined that space group *C*2/*c* was correct. The structure was solved by dual space methods and refined on F^2 by full-matrix least-squares techniques. The analytical scattering factors[10] for neutral atoms were used throughout the analysis. Hydrogen atoms were included using a riding model. There was one molecule of tetrahydrofuran solvent present. Least-squares analysis yielded wR2 = 0.1156 and Goof = 1.029 for 506 variables refined against 10373 data (0.80Å), R1 = 0.0515 for those 8522 data with $I > 2.0\sigma(I)$. The structure was refined as a two-component twin, BASF[9] = 0.1678. There were several high residuals present in the final difference-Fourier map. It was not possible to determine the nature of the residuals although it was probable that, hexane, diethylether, toluene or additional tetrahydrofuran solvent was present. The SQUEEZE[12] routine in the PLATON[13] program package was used to account for the electrons in the solvent accessible voids.

RESULTS

Synthesis and Crystallographic Characterization of [K(chelate)]$_n$[(Cp$_2$Ln)$_2$(arene)] Complexes. Variations of the reductions in Chapter 4 were performed using Cp″$_3$Ln (La, Ce) and

Cp'_3Ln precursors. The reduction of Cp''_3La with 1.5 equiv of K was performed but this time with 2.2.2-cryptand instead of 18-crown-6. Black crystals were obtained and characterized by X-ray crystallography as the bimetallic La^{2+} complex, $[K(2.2.2\text{-cryptand})][(Cp''_2La)_2(C_6H_6)]$, **19-La**, eq 5.1, Figure 5.1.

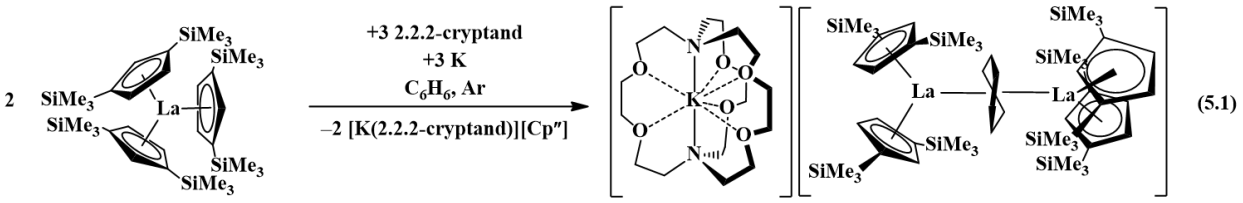

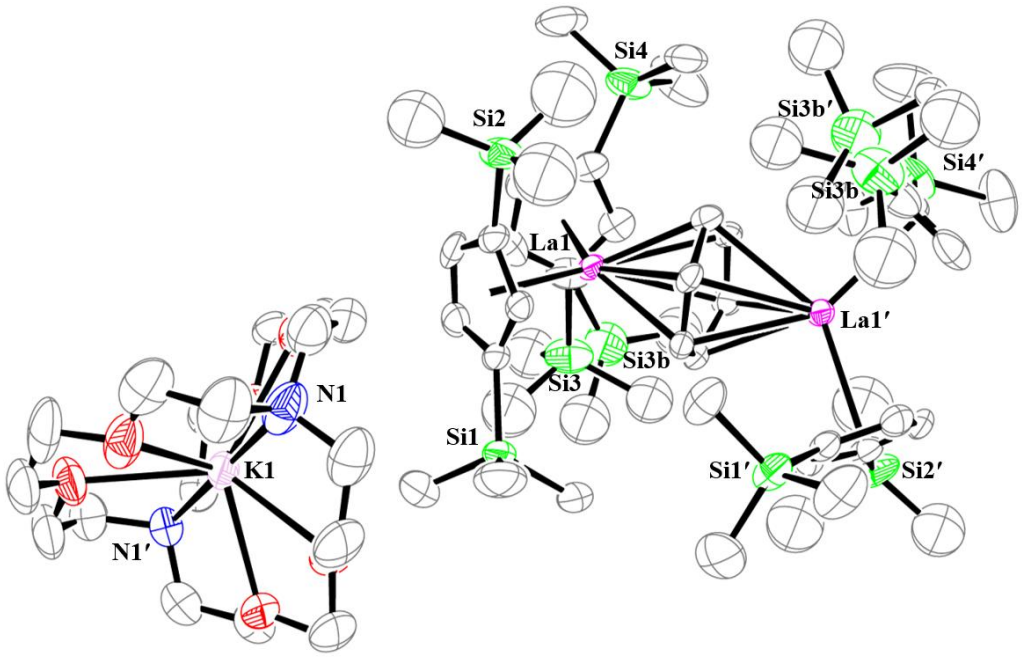

Figure 5.1. Molecular structure of $[K(2.2.2\text{-cryptand})][(Cp''_2La)_2(C_6H_6)]$, **19-La**, with thermal ellipsoids drawn at the 50% probability level. Hydrogen atoms are omitted for clarity.

19-La is the 2.2.2-cryptand analogue of **15-La** in Chapter 4. Compound **19-La** crystallizes in the $I4_1$ space group, and like **15-La**, can be described as two $Cp''_2La(II)$ metallocene units bridged by a benzenide monoanion ligand $(C_6H_6)^{1-}$. One difference between **15-La** and **19-La** is the

orientation of the cyclopentadienyl rings; in **19-La** they are tetrahedral and in **15-La** they are square planar. Another difference is that the $(C_6H_6)^{1-}$ ligand in **19-La** is non-planar. The use of 2.2.2-cryptand improved the refinement of the crystallographic data, but the quality of the data is still insufficient for a detailed structural analysis.

When Cp''_3Ce was treated with 1.5 equiv of K and equimolar 18-crown-6 in an analogous reaction, a bimetallic Ce^{2+} benzenide dianion complex, $[(K(18\text{-crown-}6))_2(THF)_3][(Cp''_2Ce)_2(C_6H_6)]$, **20-Ce**, was obtained and structurally characterized, eq 5.2, Figure 5.2. This complex is the Cp″ 18-crown-6 analog of the previously reported $[K(2.2.2\text{-cryptand})]_2[(Cp'_2Ce)_2(C_6H_6)]$.[16] **20-Ce** crystallizes in the $P2_1/c$ space group and this structure is also disordered. It is apparent, however, from this "connectivity only" structure that the Cp″ ligands are tetrahedral and the $(C_6H_6)^{2-}$ ring is nonplanar.

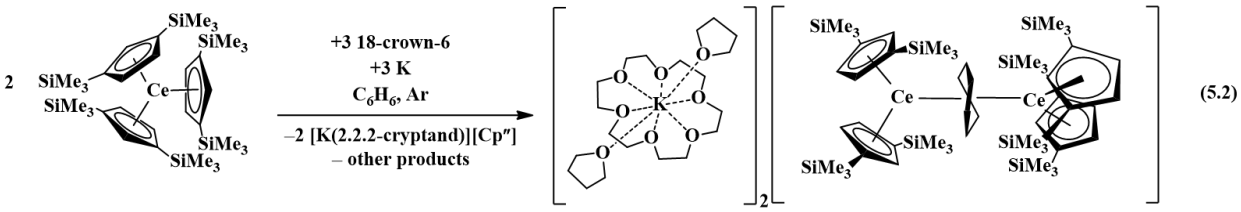

(5.2)

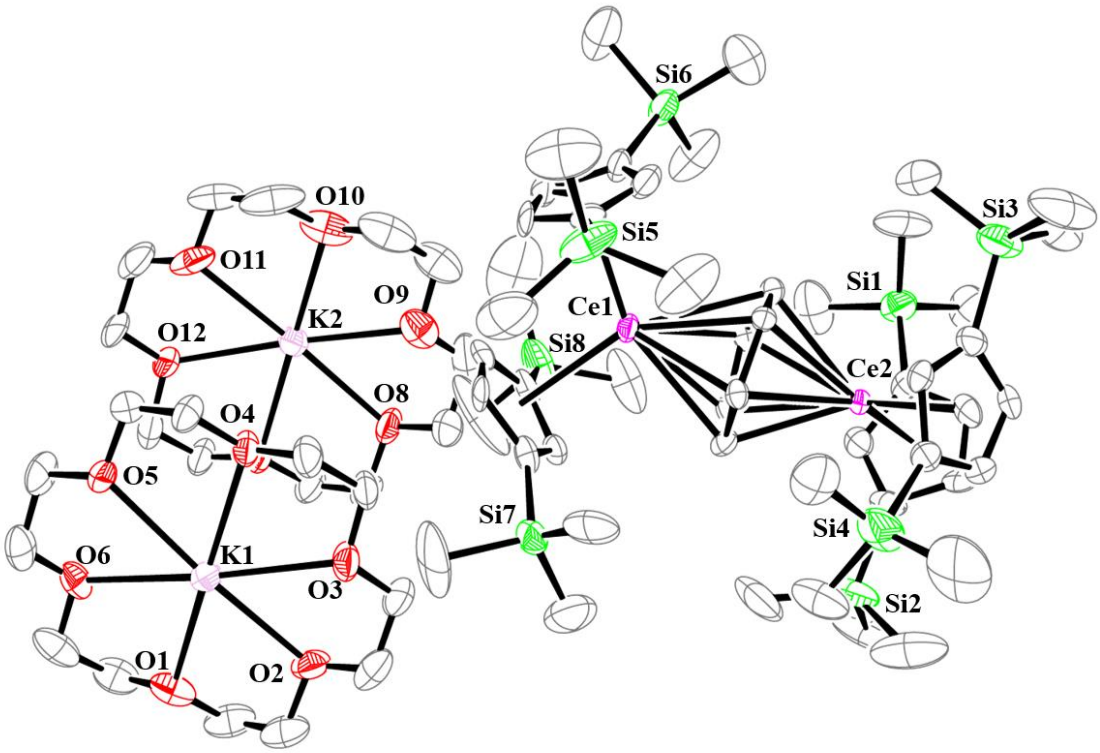

Figure 5.2. Molecular structure of $[(K(18\text{-crown-}6))_2(THF)_3][(Cp''_2Ce)_2(C_6H_6)]$, **20-Ce**, with thermal ellipsoids drawn at the 50% probability level. Hydrogen atoms are omitted for clarity.

Reductions were also performed with the Cp′ ligand to evaluate the effects of varying the cyclopentadienyl ligand on the structure of these reduced arene complexes. In reduction reactions analogous to those in eq 4.5[16] but with $C_6H_4(SiMe_3)_2$, the analogous disilyl-substituted arene complex was obtained, $[K(2.2.2\text{-cryptand})]_2[(Cp''_2La)_2(C_6H_4(SiMe_3)_2)]$, **21-La** eq 5.3, Figure 5.3. In the absence of $C_6H_4(SiMe_3)_2$, the La^{3+} complex forms with a toluenide dianion ligand, $[K(2.2.2\text{-cryptand})][Cp'_2La(C_7H_8)]$, **22-La**, eq 5.4, Figure 5.4. Complex **22-La** is the toluenide analogue of the benzenide complex $[K(18\text{-crown-}6)][Cp''_2La(C_6H_6)]$[1] previously reported by Lappert and coworkers in eq 5.1.

Unlike the previous structures, **21-La** and **22-La** gave X-ray data sufficient for a structural discussion. Below are structural comparisons between the **21-La** and **22-La** complexes with their benzenide $(C_6H_6)^{2-}$ analogues, $[K(2.2.2\text{-cryptand})]_2[(Cp'_2La)_2(C_6H_6)]$[16] and $[K(18\text{-crown-}6)][Cp''_2La(C_6H_6)]$,[1] respectively. Tables 5.1 compares the metrical parameters of **21-La** and $[K(2.2.2\text{-cryptand})]_2[(Cp'_2La)_2(C_6H_6)]$[16] and Table 5.2 compares **22-La** and $[K(18\text{-crown-}6)][Cp''_2La(C_6H_6)]$[1].

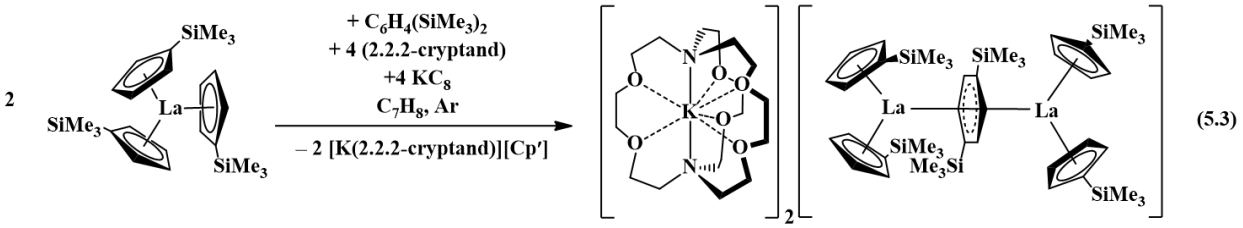

(5.3)

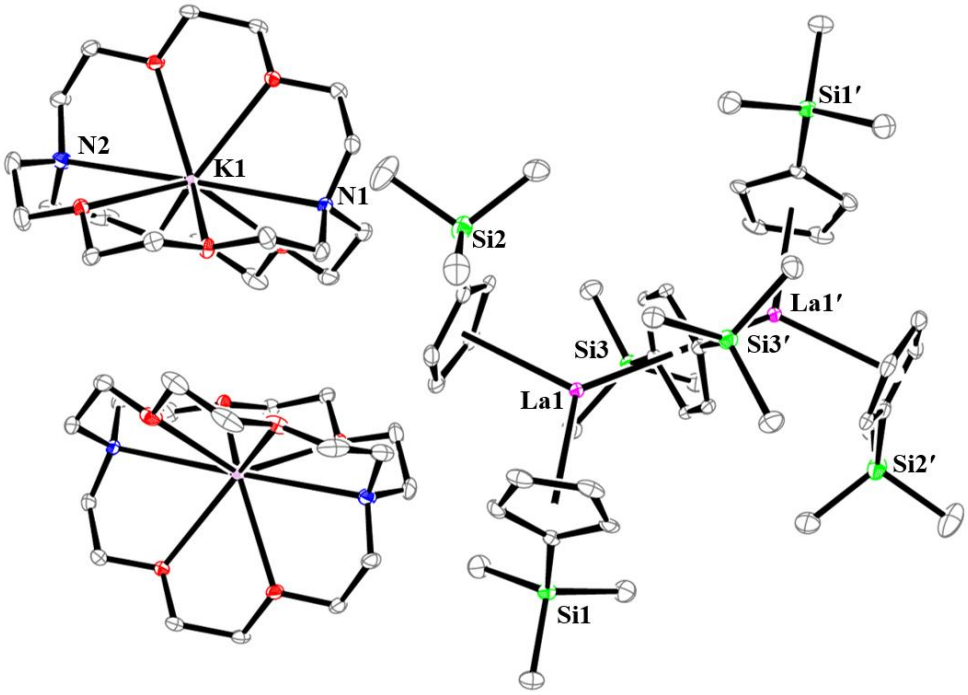

Figure 5.3. Molecular structure of $[K(2.2.2\text{-cryptand})]_2[(Cp''_2La)_2(C_6H_4(SiMe_3)_2)]$, **21-La**, with thermal ellipsoids drawn at the 50% probability level. Hydrogen atoms are omitted for clarity.

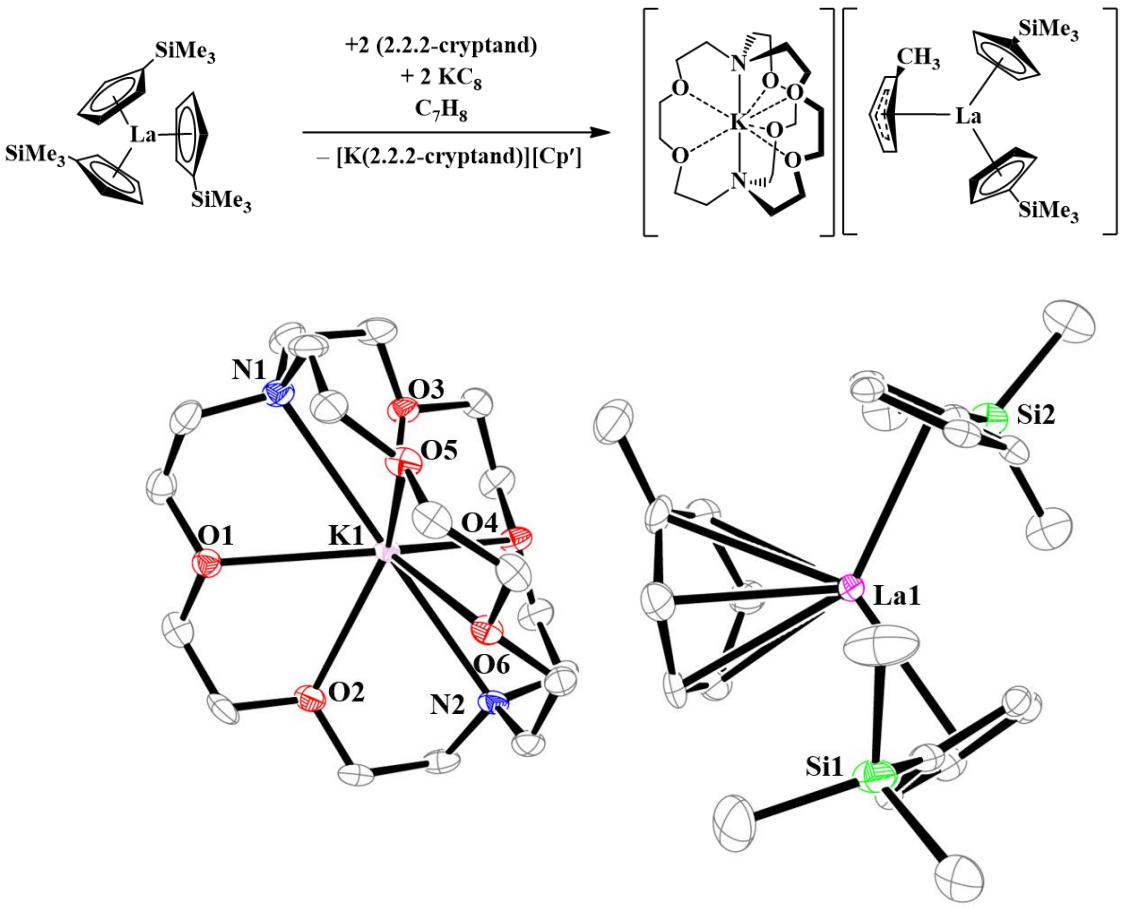

Figure 5.4. Molecular structure of [K(2.2.2-cryptand)][Cp′$_2$La(C$_7$H$_8$)], **22-La**, with thermal ellipsoids drawn at the 50% probability level. Hydrogen atoms are omitted for clarity.

Compound **21-La** crystallizes in the triclinic $P\bar{1}$ space group unlike [K(2.2.2-cryptand)]$_2$[(Cp′$_2$La)$_2$(C$_6$H$_6$)],[16] which crystallizes in the space group *Pccn*. **21-La** can be described as having two Cp′$_2$La(II) metallocene units that are bridged by a [C$_6$H$_4$(SiMe$_3$)$_2$]$^{2-}$ ligand. Interestingly, the metallocene moieties are eclipsed in **21-La**, Figure 5.5, whereas they are staggered in [K(2.2.2-cryptand)]$_2$[(Cp′$_2$La)$_2$(C$_6$H$_6$)]. The arene in **21-La** is planar like that in **15-La** and those reported by Lappert with the Cp^{tt} ligand.[2,3] In contrast, the arene in [K(2.2.2-cryptand)]$_2$[(Cp′$_2$La)$_2$(C$_6$H$_6$)] is bent with a dihedral angle of 11°. The 2.259 Å La–Cnt(arene) bond distance in **21-La** is slightly shorter than the analogous 2.273 and 2.278 Å distances in

$[K(2.2.2\text{-cryptand})]_2[(Cp'_2La)_2(C_6H_6)]$. The 1.455(5) Å average $(C–C)_{arene}$ distance in **21-La** is similar to the analogous 1.453(5) Å distance in $[K(2.2.2\text{-cryptand})]_2[(Cp'_2La)_2(C_6H_6)]$. Both are both longer than the 1.397(9) average $(C–C)_{arene}$ bond length in free benzene.[17] The 2.663(3)-2.716(3) Å range of M–C(arene) bond distances in **21-La** is consistent with the η^6 coordination of $[C_6H_4(SiMe_3)_2]^{2-}$ to La. The 2.737 Å La–Cnt$(Cp')_{avg}$ bond distance in **21-La** is longer than the analogous 2.690 Å distance in $[K(2.2.2\text{-cryptand})]_2[(Cp'_2La)_2(C_6H_6)]$, resulting in a 0.176 Å difference between **21-La a**nd its Cp'_3La La^{3+} precursor.

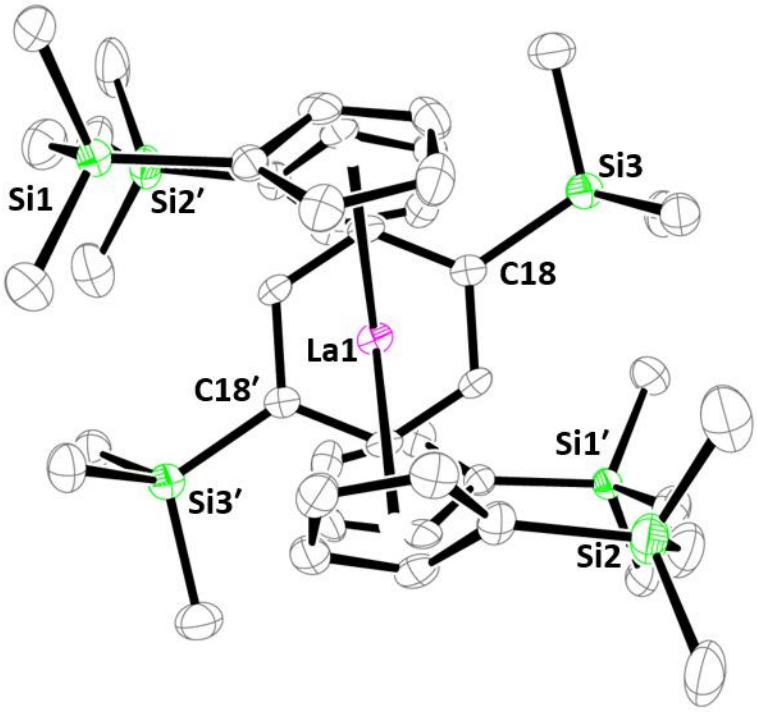

Figure 5.5. A thermal ellipsoid plot of the anion of $[K(2.2.2\text{-cryptand})][(Cp'_2La)_2(C_6H_4(SiMe_3)_2)]$, **21-La**, along the La1–(C_6 ring centroid)–La1′ axis with thermal ellipsoids drawn at the 50% probability level. Two $[K(2.2.2\text{-cryptand})]^{1+}$ cations and THF molecule have been removed for clarity.

22-La crystallizes in the *C*2/*c* space group and features a $Cp'_2La(III)$ metallocene unit bound to a terminal toluenide dianion ligand $(C_7H_8)^{2-}$. The structure of **22-La** is similar to [K(18-crown-6)][$Cp''_2La(C_6H_6)$], but [K(18-crown-6)][$Cp''_2La(C_6H_6)$] crystallizes in the space group $P2_1/n$. The 2.624 and 2.630 Å La–Cnt(Cp′) bond distances in **22-La** are similar to the 2.624(6) and 2.628(6) Å La–Cnt(Cp″) distances in [K(18-crown-6)][$Cp''_2La(C_6H_6)$], despite the bulkier Cp″ ligand in [K(18-crown-6)][$Cp''_2La(C_6H_6)$]. The 2.380 Å La–Cnt(arene) distance in **22-La** is shorter than the 2.427(6) Å distance in [K(18-crown-6)][$Cp''_2La(C_6H_6)$]. This may be attributed to the interaction between the $(C_6H_6)^{2-}$ ligand in [K(18-crown-6)][$Cp''_2La(C_6H_6)$] and the $[K(18\text{-crown-6})]^{1+}$ cation, which is not accessible in **22-La** due to the fully encapsulated K^+ ion in 2.2.2-cryptand. Interestingly, the $(C_7H_8)^{2-}$ ligand in **22-La** is bent towards the La^{3+} ion whereas in [K(18-crown-6)][$Cp''_2La(C_6H_6)$], the $(C_6H_6)^{2-}$ ligand is bent towards $[K(18\text{-crown-6})]^+$.

DISCUSSION

Variations of the reduction reactions previously reported were performed to correlate the structures of the products obtained from these reactions with the conditions used in their synthesis. The combinations of metal, cyclopentadienyl, chelate, and arene used in the reduction reactions to prepare [K(18-crown-6)$(THF)_2$][$(Cp''_2La)_2(\mu\text{-}\eta^6\text{:}\eta^6\text{-}C_6H_6)$], **15-La**, [K(2.2.2-cryptand)][$(Cp''_2La)_2(\mu\text{-}\eta^6\text{:}\eta^6\text{-}C_6H_6)$], **19-La**, [$(K(18\text{-crown-6}))_2(THF)_3$][$(Cp''_2Ce)_2(C_6H_6)$], **20-Ce**, and [K(2.2.2-cryptand)][$(Cp'_2La)_2(\mu\text{-}\eta^6\text{:}\eta^6\text{-}C_6H_4(SiMe_3)_2)$], **21-La**, along with those in Chapter 4, and those reported in the literature,[2,3,16] are shown in Table 5.3.

There are some correlations that can be drawn between the cyclopentadienyl ligand and the oxidation state of the arene. For example, the disubstituted Cp″ and Cp^{tt} ligands were successful for stabilizing Ln^{2+} complexes with the benzenide monoanion $(C_6H_6)^{1-}$ ligand, although one

example, **20-Ce**, was obtained with the benzenide dianion $(C_6H_6)^{2-}$ ligand. In contrast, all of the Ln^{2+} complexes isolated with the monosubsituted Cp′ ligand have dianionic $(arene)^{2-}$ ligands. This includes the planar $[C_5H_4(SiMe_3)_2]^{2-}$ in **21-La** along with the nonplanar $(C_6H_6)^{2-}$ found in the previously reported complexes $[K(2.2.2\text{-cryptand})]_2[(Cp'_2Ln)_2(C_6H_6)]$[16] (Ln = La, Ce).

The fact that Ln^{2+} complexes have been isolated with planar and nonplanar $(arene)^{n-}$ ligands suggests that the planarity of the $(arene)^{n-}$ ligand does not depend on *n*. It is more likely that the planarity of the ring is dependent on the overall orientation of the cyclopentadienyl rings; *i.e.* a tetrahedral orientation leads to non-planarity and square planar leads to planar rings. This is evident in the comparison of **21-La** and $[K(2.2.2\text{-cryptand})]_2[(Cp'_2Ln)_2(C_6H_6)]$ in Table 5.3. This is also evident when comparing **15-La** from Chapter 4 with its 2.2.2-cryptand analogue reported in this Chapter, **19-La**. Both have monoanionic $(C_6H_6)^{1-}$ ligands but **15-La** has a square planar arrangement of cyclopentadienyl ligands and a planar $(C_6H_6)^{1-}$ ligand. In contrast, **19-La** has a tetrahedral arrangement and a non-planar $(C_6H_6)^{1-}$ ligand. The fact that silyl substituents on the arene and the choice of chelate affect the planarity of the ring suggests the structures are determined by a confluence of steric and packing influences in the solid state rather than by the confinement of charges to metals or ligands.

CONCLUSION

A variety of reductions involving lanthanum and cerium precursors were performed in the presence of arenes to correlate structures with reaction conditions. The disubstituted Cp″ and Cp^{tt} ligands were successful in generating Ln^{2+} complexes with monoanionic arene ligands, $(arene)^{1-}$, as illustrated by $[K(18\text{-crown-6})(THF)_2][(Cp''_2La)_2(C_6H_6)]$, **15-La**, reported in Chapter 4, and its 2.2.2-cryptand analogue $[K(2.2.2\text{-cryptand})][(Cp''_2La)_2(C_6H_6)]$, **19-La**, along with reports by Lappert and coworkers on the complexes $[K(18\text{-crown-6})][(Cp^{tt}_2La)_2(C_6H_6)]$[2] and [K(18-crown-

6)][(Cp″$_2$Ln)$_2$(C$_7$H$_8$)] (Ln = La, Ce)[3]. The isolation of [(K(18-crown-6))$_2$(THF)$_3$][(Cp″$_2$Ce)$_2$(C$_6$H$_6$)], **20-Ce**, demonstrates that Cp″ and Cp^{tt} can also generate Ln^{2+} (arene)$^{2-}$ complexes. Reductions involving Cp′ precursors gave the La^{2+} (arene)$^{2-}$ complex, [K(2.2.2-cryptand)][(Cp′$_2$La)$_2$(C$_6$H$_4$(SiMe$_3$)$_2$)], **21-La**, and also a trivalent toluenide dianion complex, [K(2.2.2-cryptand)][Cp′$_2$La(C$_7$H$_8$)], **22-La**. There appears to be a correlation in the structures of the Ln^{2+} complexes between the planarity of the ring and the orientation of the cyclopentadienyl ligands in that when the cyclopentadienyl ligands are planar, the arene is planar. When the rings are tetrahedral, the arene is non-planar.

Table 5.1. Selected bond lengths (Å) and angles (°) of [K(2.2.2-cryptand)]$_2$[(Cp′$_2$La)$_2$(C$_6$H$_4$(SiMe$_3$)$_2$)], **21-La**, and [K(2.2.2-cryptand)]$_2$[(Cp′$_2$La)$_2$(C$_6$H$_6$)][16]

	21-La	[K(2.2.2-cryptand)]$_2$[(Cp′$_2$La)$_2$(μ-η^6:η^6-C$_6$H$_6$)][16]
Ln–Cnt(Cp)	2.735, 2.738	2.681, 2.687, 2.692, 2.709
Ln–Cnt(C$_6$H$_6$)	2.259	2.278, 2.273
Ln–C(Cp) range	2.944(3)-3.029(3)	2.929(5)- 2.996(4)
Ln–C(Cp) avg	2.99(3)	2.95(2)
Ln–C(C$_6$H$_6$)	2.663(3), 2.666(3), 2.678(3), 2.692(3), 2.706(3), 2.716(3)	2.635(5), 2.637(5), 2.639(4), 2.641(5), 2.676(4), 2.680(4), 2.683(4), 2.694(5), 2.766(4). 2.770(4), 2.776(5), 2.777(5),
Cnt(Cp)–Ln–Cnt(Cp)	108.6	111.5, 112.6
Cnt(Cp)–Ln–Cnt(C$_6$H$_6$)	125.4, 126.0	125.1,123.0, 123.4, 124.5
(C$_{arene}$–C$_{arene}$) range	1.434(4)-1.481(3)	1.446(6)-1.459(6)
(C$_{arene}$–C$_{arene}$) avg	1.455(6)	1.453(5)
Largest C$_6$ Torsion Angle[a]	0.04	11

[a] The largest dihedral angle between adjacent three-carbon planes in the benzenide ring.

Table 5.2. Selected bond distances (Å) and angles (°) for [K(2.2.2-cryptand)]$_2$[Cp′$_2$La(C$_7$H$_8$)], **22-La**, and [K(18-crown-6)] [Cp″$_2$La(C$_6$H$_6$)].

	22-La	[K(18-crown-6)] [Cp″$_2$La(C$_6$H$_6$)]
La–Cnt(Cp)	2.624	2.624(6)
	2.630	2.628(6)
La–Cnt(arene)	2.380	2.427(6)
La–C(Cp) range	2.866(4)-2.918(5)	2.853(6)-2.943(5)
La–C(Cp)$_{avg}$	2.89(2)	2.89(3)
La–C(arene) range	2.653(6)-2.853(5)	2.617(6)-2.811(6)
La–C(arene)$_{avg}$	2.77(8)	2.74(8)
Cnt(Cp)–La–Cnt(Cp)	117.3	116.7
Cnt(Cp)–La–Cnt(arene)	121.8, 120.8	120.5, 122.8
(C$_{arene}$–C$_{arene}$)$_{avg}$	1.42(5)	1.42(6)
Largest C$_6$ Torsion Angle[a]	21.5	21.2

[a] The largest dihedral angle between adjacent three-carbon planes in the benzenide ring.

Table 5.3. Summary of structural properties of rare earth complexes of La^{2+} and Ce^{2+} with reduced arene ligands.

Cp	Chelate	La, $(arene)^{n-}$	Planarity of Arene (Td or SP)[a]	Ce, $(arene)^{n-}$	Planarity of Arene (Td or SP)[a]
Cp′	crypt	**21-La**, $[C_6H_4(SiMe_3)_2]^{2-}$	Planar (SP)	K(2.2.2-cryptand)]$_2$ [(Cp′$_2$Ce)$_2$(μ-η^6:η^6-C_6H_6)][16], $(C_6H_6)^{2-}$	Bent (Td)
	crypt	[K(2.2.2-cryptand)]$_2$ [(Cp′$_2$La)$_2$(μ-η^6:η^6-C_6H_6)][16], $(C_6H_6)^{2-}$	Bent (Td)		
Cp″	crown	**15-La**, $(C_6H_6)^{1-}$	Planar (SP)	**20-Ce**, $(C_6H_6)^{2-}$	Bent (Td)
	crypt	**19-La**, $(C_6H_6)^{1-}$	Bent (Td)		
	crown	[K(18-crown-6)][(Cp″La)$_2$(C_7H_8)],[3] $(C_7H_8)^{1-}$	Planar (SP)	[K(18-crown-6)][(Cp″Ce)$_2$(C_7H_8),[3] $(C_7H_8)^{1-}$	Planar (SP)
Cp^{tt}	crown	[K(18-crown-6)][(Cp$^{tt}_2$La)$_2$(C_6H_6)], $(C_6H_6)^{1-}$	Planar (SP)		

[a] Td (tetrahedral) and SP (square planar) refers to the orientation of the cyclopentadienyl rings of the two Ln^{2+} metal ions.

REFERENCES

(1) Cassani, M. C.; Gun'ko, Y. K.; Hitchcock, P. B.; Lappert, M. F. *Chem. Commun.* **1996**, *1996*, 1987-1988.

(2) Cassani, M. C.; Duncalf, D. J.; Lappert, M. F. *J. Am. Chem. Soc.* **1998**, *120*, 12958-12959.

(3) Gun'ko, Y. K.; Hitchcock, P. B.; Lappert, M. F. *Organometallics* **2000**, *19*, 2832-2834.

(4) Xie, Z.; Chui, K.; Liu, Z.; Xue, F.; Zhang, Z.; W., M. T. C.; Sun, J. *J. Organomet. Chem.* **1997**, *549*, 239-244.

(5) Gun'ko, Y. K.; Hitchcock, P. B.; Lappert, M. F. *J. Organomet. Chem.* **1995**, *499*, 213-219.

(6) APEX2 Version 2014.11-0, Bruker AXS, Inc.; Madison, WI, 2014.

(7) SAINT Version 8.34a, Bruker AXS, Inc.; Madison, WI, 2013.

(8) Sheldrick, G. M.; SADABS, Version 2014/5, Bruker AXS, Inc.; Madison, WI, 2014.

(9) Sheldrick, G. M.; SHELXTL, Version 2014/7, Bruker AXS, Inc.; Madison, WI, 2014.

(10) International Tables for X-Ray Crystallography, 1992, Vol. C., Dordrecht: Kluwer Academic Publishers.

(11) Parsons, S.; Flack, H. D. *Acta Cryst.* **2013**, *B69*, 249-259.

(12) Spek, A. L.; SQUEEZE, Acta Cryst. 2015, C71, 9-19.

(13) Spek, A. L.; PLATON, Acta. Crys. 2009, D65, 148-155.

(14) Sheldrick, G. M.; Version 2008/4, Bruker AXS, Inc.: Madison, WI, 2008.

(15) Sheldrick, G. M.; Version 2012/1, Bruker AXS, Inc.: Madison, WI, 2012.

(16) Kotyk, C. M.; Fieser, M. E.; Palumbo, C. T.; Ziller, J. W.; Darago, L. E.; Long, J. R.; Furche, F.; Evans, W. J. *Chem. Sci.* **2015**, *6*, 7267-7273.

(17) Allen, F. H.; Kennard, O. K.; Watson, D. G.; Brammer, L.; Orpen, G. A.; Taylor, R. *J. Chem. Soc. Perkin Trans. II* **1987**, S1-S19.

CHAPTER 6

Comparisons of Lanthanide / Actinide +2 Ions in a Tris(aryloxide)arene Coordination Environment

INTRODUCTION†

As described in Chapters 1-5, the reduction of the tris(cyclopentadienyl) rare-earth metal complexes, Cp'_3Ln and Cp''_3Ln [$Cp' = C_5H_4SiMe_3$; $Cp'' = C_5H_3(SiMe_3)_2$], with KC_8 in the presence of a chelate such as 2.2.2-cryptand allowed the isolation of the first molecular Ln^{2+} complexes for nine new ions[1-5] (Ln = La, Ce, Pr, Gd, Tb, Y, Ho, Er, and Lu), eq 1.[1-10] These complexes differed from the

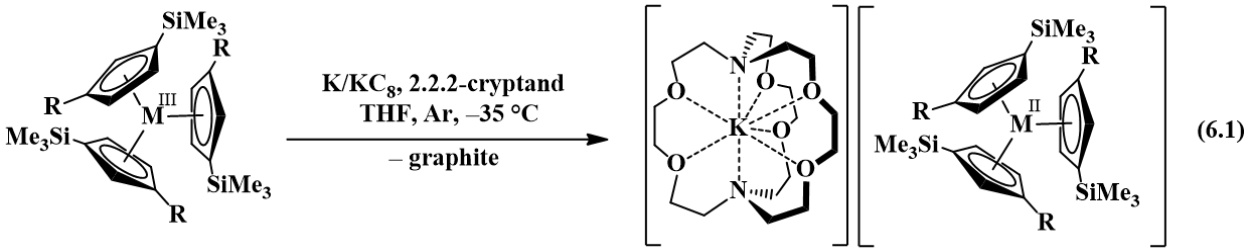

(6.1)

R = $SiMe_3$; M = La, Th, U, Pu
R = H; M = Y, La, Ce, Pr, Nd, Sm, Gd, Tb, Dy, Ho, Er, Tm, Lu, U

traditional six $4f^{n+1}$ Ln^{2+} ions (Ln = Eu, Yb, Sm, Tm, Nd, Dy) in that their complexes were much more intensely colored and the metal-(cyclopentadienyl ring centroid) distances in the Ln^{2+} complexes were only ca. 0.03 Å longer than the Ln^{3+} analogs. For complexes of traditional Ln^{2+} ions, metal-ligand bond distances are typically 0.12-0.20 Å longer than in +3 analogs. The properties of the new ions were consistent with reduction of the $4f^n$ Ln^{3+} precursors to form $4f^n5d^1$ ions rather than the traditional $4f^{n+1}$ ions, a result explained by density functional theory (DFT) calculations.[3-5]

† Portions of this chapter have been published: Fieser, M. E.; Palumbo, C. T.; La Pierre, H. S.; Halter, D. P.; Voora, V. K.; Ziller, J. W.; Furche, F.; Meyer, K.; Evans, W. J. *Chem. Sci.* **2017**, Advance Article.

To enable a direct comparison of the new $4f^n5d^1$ ions (La, Ce, Pr, Gd, Tb, Dy, Ho, Er, and Lu) with the traditional $4f^n5d^1$ ions (Eu, Yb, Sm, Tm, Nd, Dy) in a single coordination environment, [K(crypt)][Cp′$_3$Ln] complexes were synthesized for the entire lanthanide series (except Pm, which was not studied due to its radioactivity), eq 6.1. This revealed that in the $(Cp'_3)^{3-}$ coordination environment, Nd^{2+} and Dy^{2+} have properties consistent with $4f^n5d^1$ ground states, instead of the $4f^{n+1}$ ground state in previously identified Nd^{2+} and Dy^{2+} complexes. These ions therefore are not traditional $4f^{n+1}$ Ln^{2+} ions, but are configurational crossover ions that can have a variable electronic ground state depending on the ligand environment. This was an unusual result in molecular lanthanide chemistry, given that the limited radial extension of the 4*f* orbitals generally precludes ligand influences on the electronic configuration. The [K(crypt)][Cp′$_3$Ln] results suggest that there are now three classes of Ln^{2+} ions: traditional $4f^{n+1}$ ions, Ln = Eu, Yb, Sm, and Tm, the new $4f^n5d^1$ ions, Ln = La, Ce, Pr, Gd, Tb, Ho, Er, and Lu, and the configurational crossover ions, Ln =Nd and Dy, which can have either $4f^{n+1}$ or $4f^n5d^1$ configurations depending on the coordination environment. Since these groupings arise only from the $(Cp'_3)^{3-}$ ligand set, it was desirable to find other ligand environments for comparison.

The first crystallographically-characterized U^{2+} complex, [K(crypt)][Cp′$_3$U], was also obtained via eq 6.1.[6] Analyses of this complex by X-ray crystallography, UV-visible spectroscopy, and DFT were consistent with a quintet $5f^36d^1$ ground state for U^{2+} in this coordination environment and the complex displayed properties similar to those of the complexes with $4f^n5d^1$ Ln^{2+} ions. Shortly thereafter, a second U^{2+} complex was reported: the tris(aryloxide)arene U^{3+} complex, [((^{Ad,Me}ArO)$_3$mes)U], **23-U**, could be reduced to the U^{2+} complex, [K(crypt)][((^{Ad,Me}ArO)$_3$mes)U], **24-U**, eq 6.2.[11,12]

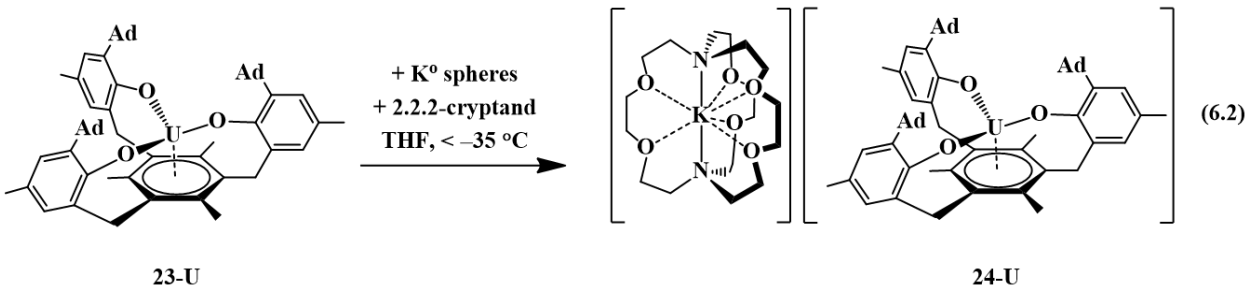

(6.2)

23-U **24-U**

Previous DFT studies on **23-U** revealed two SOMOs with δ backbonding interactions with *f* orbitals and one SOMO containing a non-bonding uranium 5*f* electron; **24-U** is similar except there are two non-bonding uranium 5*f* electrons. Hence, computational analysis of **24-U** was consistent with an $S = 2$, $5f^4$ ground state for U^{2+}. Experimental support for the predicted $5f^4$ electronic ground state was obtained by X-band EPR spectroscopy as well as solid-state and solution-phase magnetochemical studies.

The isolation of two U^{2+} complexes with different ground state configurations due to their respective coordination environments indicates that uranium should likewise fit into the configurational crossover class of +2 ions described above for the lanthanides. Since uranium is a congener of neodymium, the suggested classification has some periodic consistency. These results also suggested that in the case of Ln^{2+} ions, a comparative study with both ligand environments, $[(^{Ad,Me}ArO)_3mes]^{3-}$ and $[Cp']^{3-}$, may shed light on the nature of configurational crossover. To explore this possibility, the synthesis of complexes of new Ln^{2+} ions with the $[(^{Ad,Me}ArO)_3mes]^{3-}$ ligand was pursued. Numerous Ln^{3+} aryloxide complexes have been previously reported in the literature.[13-35] The synthesis and structural characterization of Ln^{3+} complexes of the $[(^{Ad,Me}ArO)_3mes]^{3-}$ ligand are reported here as well as their reduction chemistry. This has led to highly reactive Ln^{2+} complexes that often co-crystallize either with Ln^{3+} hydride or Ln^{3+} hydroxide byproducts. DFT analysis is used to evaluate the electronic structures and make comparisons with uranium.

EXPERIMENTAL

The syntheses and manipulations described below were conducted under an argon atmosphere with rigorous exclusion of air and water using glovebox, vacuum line, and Schlenk techniques. Solvents were sparged with ultrahigh purity (UHP) grade argon (Airgas) and passed through columns containing Q-5 and molecular sieves before use. NMR solvents (Cambridge Isotope Laboratories) were dried over NaK/benzophenone, degassed by three freeze−pump−thaw cycles, and vacuum-transferred before use. [Ln(N(SiMe$_3$)$_2$)$_3$] (Ln = Nd, Gd, Dy, Er),[36] KC$_8$,[37] and (^{Ad,Me}ArOH)$_3$mes,[11] were prepared according to literature. 2.2.2-Cryptand, 4,7,13,16,21,24-hexaoxa-1,10-diazabicyclo[8.8.8]hexacosane (Acros Organics), was placed under vacuum (10^{-3} Torr) for 12 h before use. 18-Crown-6 (Aldrich) was sublimed before use. ^{1}H NMR (500 MHz) spectra were obtained on a Bruker GN500 or CRYO500 MHz spectrometer at 298 K. IR samples were prepared as KBr pellets and the spectra were obtained on either a Varian 1000 or Jasco 4700 FT-IR spectrometer. Elemental analyses were performed on a PerkinElmer 2400 series II CHNS elemental analyzer. Electronic absorption spectra were obtained in THF or benzene at 298 K using a Varian Cary 50 Scan UV−vis or Jasco V-670 UV/Vis/NIR/MIR absorption spectrometer. EPR spectra were collected using X-band frequency (9.3-9.8 GHz) on a Bruker EMX spectrometer equipped with an ER041XG microwave bridge and the magnetic field was calibrated with DPPH (g = 2.0036).

[((^{Ad,Me}ArO)$_3$mes)Nd], 23-Nd. In an argon-filled glovebox, a sealable 100 mL side-arm Schlenk flask equipped with a greaseless stopcock was charged with a solution of (^{Ad,Me}ArOH)$_3$mes (256 mg, 0.290 mmol) in benzene (40 mL) and a magnetic stir bar. A solution of [Nd(N(SiMe$_3$)$_2$)$_3$] (251 mg, 0.305 mmol) in benzene (40 mL) was slowly added to the stirred solution. Higher concentrations resulted in gel-like precipitates and low yields. The flask was

attached to a Schlenk line and the mixture was stirred and heated at reflux for 18 h. The flask was brought back into the glovebox, the solution was filtered, and the solvent was removed from the colorless filtrate under vacuum. The resulting pale-blue solid was washed with hexanes then extracted into benzene (15 mL) and filtered. Toluene (5 mL) was added to the filtrate and removal of solvent under vacuum afforded **23-Nd** as a pale-blue powder (163 mg, 56%). Blue single crystals of **23-Nd**, suitable for X-ray diffraction, were grown from slow evaporation of a C_6D_6 solution. ^{1}H NMR (C_6D_6): δ 16.0 (s, 3H), 10.7 (s, 3H), 7.0 (s, 9H), 3.5 (br s, 18H), 1.1 (br s, 9H), 1.00 (br s, 6H), −6.2 (s, 9H), −7.2 (s, 9H), −16.3 (s, 9H). IR: 3074w, 2898s, 2845w, 2675w, 2652w, 1730w, 1601w, 1568w, 1492m, 1445s, 1380m, 1340m, 1305m, 1285s, 1245s, 1205m, 1184m, 1160m, 1113w, 1100m, 1066s, 1019m, 980m, 960m, 915m, 886m, 835s, 820s, 808s, 737m, 733s, 729m, 694m, 679w, 631w. Anal. Calcd for $C_{63}H_{75}NdO_3$: C, 73.86; H, 7.38. Found: C, 74.09; H, 7.35.

[((^{Ad,Me}ArO)$_3$mes)Gd], 23-Gd. As described for **23-Nd**, a solution of [Gd(N(SiMe$_3$)$_2$)$_3$] (73 mg, 0.12 mmol) in benzene (40 mL) was slowly added to a stirred solution of (^{Ad,Me}ArOH)$_3$mes (100 mg, 0.113 mmol) in benzene (30 mL) to afford **23-Gd** as an off-white solid (104 mg, 86%). Colorless single crystals of **23-Gd**, suitable for X-ray diffraction, were grown from an Et_2O/hexane solution at −35 °C. IR: 3067w, 3017w, 2960s, 2897s, 2849s, 2732w, 2672w, 2652w, 1739w, 1605w, 1568w, 1545w, 1494m 1453s, 1377m, 1366m, 1354m, 1341m, 1317s, 1308s, 1284s, 1252s, 1209s, 1184m, 1161m, 1116w, 1102m, 1068m, 1037w, 1017m, 983m, 960m, 937w, 911m, 915m, 888m, 881m, 858s, 835s, 820s, 809s, 765m, 748m, 729m, 694m, 683w, 668w, 653w, 646w, 643w, 607w. Anal. Calcd for $C_{63}H_{75}GdO_3$: C, 72.93; H, 7.29. Found: C, 73.04; H, 7.26.

[((^{Ad,Me}ArO)$_3$mes)Dy], 23-Dy. As described for **23-Nd**, a solution of [Dy(N(SiMe$_3$)$_2$)$_3$] (298 mg, 0.354 mmol) in benzene (20 mL) was slowly added to a stirred solution of

(^{Ad,Me}ArOH)$_3$mes (303 mg, 0.343 mmol) in benzene (30 mL) to afford **23-Dy** as an off-white solid (236 mg, 66%). Colorless single crystals of **23-Dy**, suitable for X-ray diffraction, were grown from an Et_2O/hexane solution at −35 °C. IR: 3068w, 2946s, 2899s, 2844s, 2725w, 2675w, 2653w, 1745w, 1605w, 1568w, 1545w, 1495w, 1447s, 1379m, 1366m, 1354m, 1341m, 1315m, 1306m, 1287s, 1250s, 1208m, 1186m, 1161m, 1114w, 1101m, 1068m, 1035m, 1020m, 980m, 963m, 937w, 923m, 917m, 878w, 880w, 845m, 835s, 822s, 809s, 767m, 748m, 728m, 693w, 674s, 666w, 650w, 631w, 606w. Anal. Calcd for $C_{63}H_{75}DyO_3$: C, 72.56; H, 7.25. Found: C, 72.28; H, 7.31.

[((^{Ad,Me}ArO)$_3$mes)Er], 23-Er. As described for **23-Nd**, a solution of [Er(N(SiMe$_3$)$_2$)$_3$] (78 mg, 0.120 mmol) in benzene (20 mL) was slowly added to a stirred solution of (^{Ad,Me}ArOH)$_3$mes (100 mg, 0.113 mmol) in benzene (20 mL) to afford **23-Er** as a pink solid (70 mg, 59%). Pale pink single crystals of **23-Er**, suitable for X-ray diffraction, were grown from an Et_2O/hexane solution at −35 °C. IR: 3075w, 2898s, 2845s, 2675w, 2653w, 1733w, 1601w, 1568w, 1542w, 1492m, 1447s, 1381m, 1341m, 1305m, 1286s, 1246s, 1207m, 1185m, 1161m, 1117w, 1100m, 1066s, 1019m, 980w, 961w, 915m, 878w, 856m, 836s, 821s, 809s, 766m, 748m, 735m, 695m, 680w, 652w, 631w. Anal. Calcd for $C_{63}H_{75}ErO_3$: C, 72.23; H, 7.22. Found: C, 72.88; H, 7.80.

[K(crypt)][((^{Ad,Me}ArO)$_3$mes)Nd], 24-Nd. In an argon-filled glovebox, [(^{Ad,Me}ArO)$_3$mes)Nd], **23-Nd** (60 mg, 0.059 mmol), was combined with 2.2.2-cryptand (22 mg, 0.058 mmol) in a vial containing a magnetic stir bar and dissolved in 1:1 THF/C_6H_6 (4 mL). KC_8 (15 mg, 0.11 mmol) was quickly added to the pale blue solution. The reaction immediately turned brown. After 2 min, the solution was filtered to remove the graphite. The resulting red-orange solution was layered with Et_2O (15 mL) and stored at −35 °C for 48 h to produce brown/orange crystals of **24-Nd** suitable for X-ray diffraction (16 mg, 23%). IR: 3065w, 2965m, 2897s, 2845s, 2812m, 2727w, 2676w, 2653w, 1730w, 1599w, 1560m, 1477m, 1444s, 1374w, 1360m, 1354s,

1341w, 1313m, 1284s, 1275s, 1256s, 1251s, 1210w, 1184w, 1163w, 1134m, 1106s, 1082m, 1059m, 1046w, 1000w, 980w, 950m, 935m, 911w, 903w, 895w, 876w, 856m, 831m, 818m, 804m, 767w, 748w, 727w, 720w, 715w, 707w, 693w, 684w, 680w, 677w, 670w, 667w, 663w, 657w, 651w, 647w, 639w, 631w, 625w, 618w, 612w, 609w, 603w. UV-vis (THF) λ_{max} nm (ε, $M^{-1}cm^{-1}$): 299 (19500), 387 (4000 shoulder), 416 (4200), 480 (2000 shoulder), 600 (300). Anal. Calcd for $C_{81}H_{111}KN_2NdO_9$: C, 67.56; H, 7.77; N, 1.95. Found: C, 66.23; H, 7.66; N, 1.71. The found CHN ratio of $C_{81}H_{111.6}N_{1.8}$ is consistent with the formula and suggests incomplete combustion.

[K(crypt)][((^{Ad,Me}ArO)$_3$mes)Gd] and [K(crypt)][((^{Ad,Me}ArO)$_3$mes)GdH], 24-Gd/25-Gd. As described for **24-Nd**, [((^{Ad,Me}ArO)$_3$mes)Gd], **23-Gd**, (60 mg, 0.06 mmol) and 2.2.2-cryptand (23 mg, 0.06 mmol) were dissolved in 1:1 THF/C_6H_6 (4 mL) to form an off-white solution, which was combined with KC_8 (20 mg, 0.15 mmol) to produce red crystals suitable for X-ray diffraction (51 mg). The crystals were characterized as a co-crystallized mixture of [K(crypt)][((^{Ad,Me}ArO)$_3$mes)Gd], **24-Gd**, and [K(crypt)][((^{Ad,Me}ArO)$_3$mes)GdH], **25-Gd**, of an approximate 65:35 ratio. UV-vis (THF) λ_{max} nm (ε, M^{-1} cm^{-1}): 305 (22000), 330 (6000 shoulder), 426 (4000), 520 (2000 shoulder), 580 (400).

[K(crypt)][((^{Ad,Me}ArO)$_3$mes)Er] and [K(crypt)][((^{Ad,Me}ArO)$_3$mes)ErH], 24-Er/25-Er. As described for **23-Nd**, [((^{Ad,Me}ArO)$_3$mes)Er], **23-Er**, (45 mg, 0.043 mmol) and 2.2.2-cryptand (16 mg, 0.04 mmol) were dissolved in 1:1 THF/C_6H_6 (2 mL) to form a pink solution, which was combined with KC_8 (18 mg, 0.13 mmol) to produce red crystals suitable for X-ray diffraction (22 mg). The crystals were characterized as a cocrystallized mixture of [K(crypt)][((^{Ad,Me}ArO)$_3$mes)Er], **23-Er**, and [K(crypt)][((^{Ad,Me}ArO)$_3$mes)ErH], **24-Er**, of an approximate 55:45 ratio. UV-vis (THF) λ_{max} nm (ε, M^{-1} cm^{-1}): 305 (21000), 330 (4800 shoulder), 430 (5600), 500 (2500 shoulder), 600 (300).

[K(crypt)][((^{Ad,Me}ArO)$_3$mes)Dy] and [K(crypt)][((^{Ad,Me}ArO)$_3$mes)DyH], 24-Dy/25-Dy. [((^{Ad,Me}ArO)$_3$mes)Dy], **23-Dy**, (20 mg, 0.019 mmol) and 2.2.2-cryptand (7 mg, 0.02 mmol) were dissolved in THF (1 mL) to form a colorless solution. The solution was transferred to scintillation vial with a potassium smear (excess) and stored overnight at −35 °C. The resultant dark red solution was layered with Et_2O (8 mL) and stored at −35 °C for 36 h to produce dark red crystals suitable for X-ray diffraction (10 mg). The crystals were characterized as a cocrystallized mixture of [K(crypt)][((^{Ad,Me}ArO)$_3$mes)Dy], **24-Dy**, and [K(crypt)][((^{Ad,Me}ArO)$_3$mes)DyH], **25-Dy**, of an approximate 63:37 ratio.

[K(crypt)][((^{Ad,Me}ArO)$_3$mes)Dy] and [K(crypt)][((^{Ad,Me}ArO)$_3$mes)Dy(OH)], 24-Dy/26-Dy. As described for **24-Nd**, [((^{Ad,Me}ArO)$_3$mes)Dy], **23-Dy**, (90 mg, 0.086 mmol) and 2.2.2-cryptand (32 mg, 0.085 mmol) were dissolved in 3:1 THF/C_6H_6 (3 mL) to form an off-white solution, which was combined with KC_8 (18 mg, 0.13 mmol) to produce red crystals suitable for X-ray diffraction. The crystals were characterized as a co-crystallized mixture of [K(crypt)][((^{Ad,Me}ArO)$_3$mes)Dy], **24-Dy**, and [K(crypt)][((^{Ad,Me}ArO)$_3$mes)Dy(OH)], **26-Dy**, of an approximate 2:3 ratio.

[K(18-crown-6)(THF)$_2$][((^{Ad,Me}ArO)$_3$mes)Dy] and [K(18-crown-6)(THF)$_2$][((^{Ad,Me}ArO)$_3$mes)DyH], 27-Dy/28-Dy. [((^{Ad,Me}ArO)$_3$mes)Dy], **23-Dy**, (50 mg, 0.048 mmol) and 18-crown-6 (13 mg, 0.048 mmol) were dissolved in THF (1 mL) to give a colorless solution. Excess potassium was added and the solution was stored overnight in the glovebox freezer. The resultant dark red solution was layered with Et_2O (4 mL) and stored at −35 °C for 48 h at −35 °C to produce red crystals suitable for X-ray diffraction (29 mg). The crystals were characterized as a co-crystallized mixture of [K(18-crown-6)(THF)$_2$][((^{Ad,Me}ArO)$_3$mes)Dy], **27-Dy**, and [K(18-crown-6)(THF)$_2$][((^{Ad,Me}ArO)$_3$mes)DyH], **28-Dy**, of an approximate 1:1 ratio with

two THF molecules in the lattice. UV-vis (THF) λ_{max} nm (ε, M^{-1} cm^{-1}): 300 (18000), 330 (3500 shoulder), 430 (4900), 480 (2600 shoulder), 550 (600 shoulder). Anal. Calcd for $C_{91}H_{131.5}DyKO_{13}$: C, 67.84; H, 8.20. Found: C, 65.15; H, 7.61. Additional elemental analyses experiments gave low carbon and hydrogen values. The found CH ratios of $C_{91}H_{131}$, $C_{91}H_{129.7}$ are consistent with the formula and suggest incomplete combustion.

X-ray Data Collection, Structure Solution and Refinement for [Nd(OAr^{Ad,Me})$_3$mes], 23-Nd. A blue crystal of approximate dimensions 0.301 x 0.088 x 0.071 mm was mounted on a glass fiber and transferred to a Bruker SMART APEX II diffractometer. The APEX2[38] program package was used to determine the unit-cell parameters and for data collection (120 sec/frame scan time for a sphere of diffraction data). The raw frame data was processed using SAINT[39] and SADABS[40] to yield the reflection data file. Subsequent calculations were carried out using the SHELXTL[41] program. The diffraction symmetry was 2/*m* and the systematic absences were consistent with the monoclinic space group $P2_1/c$ that was later determined to be correct. The structure was solved using the coordinates from mef30, the La analog. The analytical scattering factors[42] for neutral atoms were used throughout the analysis. Hydrogen atoms were included using a riding model. At convergence, wR2 = 0.0850 and Goof = 1.228 for 610 variables refined against 8875 data (0.83 Å), R1 = 0.0453 for those 7703 data with $I > 2.0\sigma(I)$. Details are given in Table 6.1.

X-ray Data Collection, Structure Solution and Refinement for [Gd(OAr^{Ad,Me})$_3$mes], 23-Gd. A colorless crystal of approximate dimensions 0.030 x 0.0.050 x 0.100 mm was mounted in a cryoloop and transferred to a Bruker SMART APEX II diffractometer. The APEX2[38] program package was used to determine the unit-cell parameters and for data collection (90 sec/frame scan time for a sphere of diffraction data). The raw frame data was processed using SAINT[39] and

SADABS[40] to yield the reflection data file. Subsequent calculations were carried out using the SHELXTL[41] program. The diffraction symmetry was 2/*m* and the systematic absences were consistent with the monoclinic space group $P2_1/c$ that was later determined to be correct. The structure was solved by direct methods and refined on F^2 by full-matrix least-squares techniques. The analytical scattering factors[42] for neutral atoms were used throughout the analysis. Hydrogen atoms were included using a riding model. At convergence, wR2 = 0.0943 and Goof = 0.958 for 610 variables refined against 12128 data (0.80Å), R1 = 0.0444 for those 8073 data with $I > 2.0\sigma(I)$. There were several high residuals present in the final difference-Fourier map. It was not possible to determine the nature of the residuals although it was probable that diethyether or hexane solvents were present. The SQUEEZE[43] routine in the PLATON[44] program package was used to account for the electrons in the solvent accessible voids. Details are given in Table 6.1.

X-ray Data Collection, Structure Solution and Refinement for [Dy(OAr^{Ad,Me})$_3$mes], 23-Dy. A colorless crystal of approximate dimensions 0.031 x 0.062 x 0.330 mm was mounted in a cryoloop and transferred to a Bruker SMART APEX II diffractometer. The APEX2[38] program package was used to determine the unit-cell parameters and for data collection (90 sec/frame scan time for a sphere of diffraction data). The raw frame data was processed using SAINT[39] and SADABS[40] to yield the reflection data file. Subsequent calculations were carried out using the SHELXTL[41] program. The diffraction symmetry was 2/*m* and the systematic absences were consistent with the monoclinic space group $P2_1/c$ that was later determined to be correct. The structure was solved by direct methods and refined on F^2 by full-matrix least-squares techniques. The analytical scattering factors[42] for neutral atoms were used throughout the analysis. Hydrogen atoms were included using a riding model. At convergence, wR2 = 0.0766 and Goof = 1.014 for 610 variables refined against 12284 data (0.80Å), R1 = 0.0339 for those 9267 data with $I > 2.0\sigma(I)$.

There were several high residuals present in the final difference-Fourier map. It was not possible to determine the nature of the residuals although it was probable that diethyether or hexane solvents were present. The SQUEEZE[43] routine in the PLATON[44] program package was used to account for the electrons in the solvent accessible voids. Details are given in Table 6.1.

X-ray Data Collection, Structure Solution and Refinement for [Er(OAr^{Ad,Me})$_3$mes], 23-Er. A pink crystal of approximate dimensions 0.030 x 0.035 x 0.224 mm was mounted in a cryoloop and transferred to a Bruker SMART APEX II diffractometer. The APEX2[38] program package was used to determine the unit-cell parameters and for data collection (90 sec/frame scan time for a sphere of diffraction data). The raw frame data was processed using SAINT[39] and SADABS[40] to yield the reflection data file. Subsequent calculations were carried out using the SHELXTL[41] program. The diffraction symmetry was 2/*m* and the systematic absences were consistent with the monoclinic space group $P2_1/c$ that was later determined to be correct. The structure was solved by direct methods and refined on F^2 by full-matrix least-squares techniques. The analytical scattering factors[42] for neutral atoms were used throughout the analysis. Hydrogen atoms were included using a riding model. At convergence, wR2 = 0.0741 and Goof = 0.985 for 610 variables refined against 12175 data (0.80Å), R1 = 0.0335 for those 9178 data with $I > 2.0\sigma(I)$. There were several high residuals present in the final difference-Fourier map. It was not possible to determine the nature of the residuals although it was probable that diethyether or hexane solvents were present. The SQUEEZE[43] routine in the PLATON[44] program package was used to account for the electrons in the solvent accessible voids. Details are given in Table 6.1.

X-ray Data Collection, Structure Solution and Refinement for [K(2.2.2-cryptand)][Nd(OAr^{Ad,Me})$_3$mes], 24-Nd. A red crystal of approximate dimensions 0.349 x 0.234 x 0.214 mm was mounted on a glass fiber and transferred to a Bruker SMART APEX II

diffractometer. The APEX2[45] program package was used to determine the unit-cell parameters and for data collection (20 sec/frame scan time for a sphere of diffraction data). The raw frame data was processed using SAINT[39] and SADABS[46] to yield the reflection data file. Subsequent calculations were carried out using the SHELXTL[47] program. The diffraction symmetry was $m\bar{3}$ and the systematic absences were consistent with the cubic space group $P2_13$ that was later determined to be correct. The structure was solved by direct methods and refined on F^2 by full-matrix least-squares techniques. The analytical scattering factors[42] for neutral atoms were used throughout the analysis. Hydrogen atoms were included using a riding model. The molecule was located on a three-fold rotation axis. At convergence, wR2 = 0.1279 and Goof = 1.174 for 285 variables refined against 6739 data (0.73 Å), R1 = 0.0482 for those 6400 data with $I > 2.0\sigma(I)$. The absolute structure was assigned by refinement of the Flack[48] parameter. There were several high residuals present in the final difference-Fourier map. It was not possible to determine the nature of the residuals although it was probable that toluene solvent was present. The SQUEEZE[43] routine in the PLATON[44] program package was used to account for the electrons in the solvent accessible voids. Details are given in Table 6.2.

X-ray Data Collection, Structure Solution and Refinement for [K(2.2.2-cryptand)][Gd(OAr^{Ad,Me})$_3$mes] / [K(2.2.2-cryptand)][GdH(OAr^{Ad,Me})$_3$mes], 24-Gd, 25-Gd. A red crystal of approximate dimensions 0.102 x 0.177 x 0.181 mm was mounted on a glass fiber and transferred to a Bruker SMART APEX II diffractometer. The APEX2[49] program package was used to determine the unit-cell parameters and for data collection (180 sec/frame scan time for a sphere of diffraction data). The raw frame data was processed using SAINT[39] and SADABS[46] to yield the reflection data file. Subsequent calculations were carried out using the SHELXTL[41] program. The systematic absences were consistent with the cubic space group $P2_13$ that was later

determined to be correct. The structure was solved by direct methods and refined on F^2 by full-matrix least-squares techniques. The analytical scattering factors[42] for neutral atoms were used throughout the analysis. Hydrogen atoms were included using a riding model. The molecule and counter-ion were located on three-fold rotation axes. The complex appeared to be a mixed composition of approximately Gd^{2+} (65%) / Gd^{3+}(35%). There was approximately 35% of a hydride ligand present bound to Gd(2). The position of the hydride was evident in the electron density map however it was necessary to fix the Gd-H distance and the hydride thermal parameter during refinement. An ether solvent molecule was disordered about a three-fold rotation axis and included with partial site-occupancy-factors. At convergence, wR2 = 0.0951 and Goof = 1.222 for 301 variables refined against 5062 data (0.81), R1 = 0.0372 for those 4861 data with $I > 2.0\sigma(I)$. The absolute structure was assigned by refinement of the Flack parameter.[48] Details are given in Table 6.2.

X-ray Data Collection, Structure Solution and Refinement for [K(2.2.2-cryptand)][Dy(OAr^{Ad,Me})$_3$mes] / [K(2.2.2-cryptand)][DyH(OAr^{Ad,Me})$_3$mes], 24-Dy, 25-Dy. A red crystal of approximate dimensions 0.371 x 0.438 x 0.566 mm was mounted in a cryoloop and transferred to a Bruker SMART APEX II diffractometer. The APEX2[38] program package was used to determine the unit-cell parameters and for data collection (10 sec/frame scan time for a sphere of diffraction data). The raw frame data was processed using SAINT[39] and SADABS[40] to yield the reflection data file. Subsequent calculations were carried out using the SHELXTL[41] program. The systematic absences were consistent with the cubic space group $P2_13$ that was later determined to be correct. The structure was solved by dual space methods and refined on F^2 by full-matrix least-squares techniques. The analytical scattering factors[42] for neutral atoms were used throughout the analysis. Hydrogen atoms were included using a riding model. The molecule

and counter-ion were located on three-fold rotation axes. The complex appeared to be a mixed composition of approximately Dy^{2+} (63%) / Dy^{3+}(37%). There was approximately 37% hydride ligand present bound to Dy(2). The position of the hydride was located from difference map however it was necessary to fix the Dy-H distance and the hydride thermal parameter during refinement. An ether solvent molecule was disordered about a three-fold rotation axis and included with partial site-occupancy-factors. At convergence, wR2 = 0.0970 and Goof = 1.218 for 307 variables refined against 6642 data (0.74), R1 = 0.0417 for those 6365 data with $I > 2.0\sigma(I)$. The absolute structure was assigned by refinement of the Flack parameter.[48] The structure was refined as a two-component twin. Details are given in Table 6.2.

X-ray Data Collection, Structure Solution and Refinement for [K(2.2.2-cryptand)][Er(OAr^{Ad,Me})$_3$mes] / [K(2.2.2-cryptand)][ErH(OAr^{Ad,Me})$_3$mes], 24-Er, 25-Er. A red crystal of approximate dimensions 0.200 x 0.240 x 0.280 mm was mounted on a glass fiber and transferred to a Bruker SMART APEX II diffractometer. The APEX2[49] program package was used to determine the unit-cell parameters and for data collection (3 sec/frame scan time for 99 frames of diffraction data). The raw frame data was processed using SAINT[39] and SADABS[40] to yield the reflection data file. Subsequent calculations were carried out using the SHELXTL[41] program. The systematic absences were consistent with the cubic space group $P2_13$ that was later determined to be correct. The structure was solved by direct methods and refined on F^2 by full-matrix least-squares techniques. The analytical scattering factors[42] for neutral atoms were used throughout the analysis. Hydrogen atoms were included using a riding model. The molecule and counter-ion were located on three-fold rotation axes. The complex appeared to be a mixed composition of approximately Er^{2+} (55%) / Er^{3+}(45%). There was approximately 45% of a hydride ligand present bound to Er(2). The position of the hydride was evident in the electron

density map however it was necessary to fix the Er-H distance and the hydride thermal parameter during refinement. An ether solvent molecule was disordered about a three-fold rotation axis and included with partial site-occupancy-factors. At convergence, wR2 = 0.0827 and Goof = 1.114 for 301 variables refined against 5953 data (0.73), R1 = 0.0413 for those 5352 data with I > 2.0σ(I). The absolute structure was assigned by refinement of the Flack parameter.[48] Details are given in Table 6.2.

X-ray Data Collection, Structure Solution and Refinement for [K(2.2.2-cryptand)][Dy(OAr^{Ad,Me})$_3$mes] / [K(2.2.2-cryptand)][DyOH(OAr^{Ad,Me})$_3$mes], 24-Dy, 26-Dy. A red crystal of approximate dimensions 0.200 x 0.230 x 0.260 mm was mounted on a glass fiber and transferred to a Bruker SMART APEX II diffractometer. The APEX2[49] program package was used to determine the unit-cell parameters and for data collection (10 sec/frame scan time for 112 frames of data). The raw frame data was processed using SAINT[39] and SADABS[40] to yield the reflection data file. Subsequent calculations were carried out using the SHELXTL[41] program. The systematic absences were consistent with the cubic space group $P2_13$ that was later determined to be correct. The structure was solved by direct methods and refined on F^2 by full-matrix least-squares techniques. The analytical scattering factors[42] for neutral atoms were used throughout the analysis. Hydrogen atoms were included using a riding model. The molecule was located on a three-fold rotation axis. The complex appeared to be a mixed composition of approximately Dy^{2+} (40%) / Dy^{3+}(60%). There was approximately 60% of a hydroxide ligand present. An ether solvent molecule was disordered about a three-fold rotation axis and included with partial site-occupancy-factors. At convergence, wR2 = 0.0956 and Goof = 1.043 for 303 variables refined against 4155 data (0.83Å), R1 = 0.0457 for those 3582 data with I > 2.0σ(I). The absolute structure was assigned by refinement of the Flack parameter.[48] Details are given in Table 6.3.

X-ray Data Collection, Structure Solution and Refinement for [K((18-crown-6)(THF)$_2$)][Dy(OAr^{Ad,Me})$_3$mes] / [K(18-crown-6)(THF)$_2$][DyH(OAr^{Ad,Me})$_3$mes], 27-Dy, 28-Dy. A brown crystal of approximate dimensions 0.128 x 0.194 x 0.231 mm was mounted in a cryoloop and transferred to a Bruker SMART APEX II diffractometer. The APEX2[38] program package was used to determine the unit-cell parameters and for data collection (90 sec/frame scan time for a sphere of diffraction data). The raw frame data was processed using SAINT[39] and SADABS[40] to yield the reflection data file. Subsequent calculations were carried out using the SHELXTL[41] program. The diffraction symmetry was *mmm* and the systematic absences were consistent with the orthorhombic space group *Pbcn* that was later determined to be correct. The structure was solved by direct methods and refined on F^2 by full-matrix least-squares techniques. The analytical scattering factors[42] for neutral atoms were used throughout the analysis. The complex appeared to be a mixed composition of approximately Dy^{2+} (50%) / Dy^{3+}(50%). There was approximately 50% of a hydride ligand present which was located from a difference-Fourier map and refined (x,y,z and U_{iso}). Hydrogen atoms were included using a riding model. There were two molecules of tetrahydrofuran solvent present. Least-squares analysis yielded wR2 = 0.1486 and Goof = 1.101 for 949 variables refined against 16156 data (0.82Å), R1 = 0.0583 for those 12496 data with $I > 2.0\sigma(I)$. There were several high residuals present in the final difference-Fourier map. It was not possible to determine the nature of the residuals although it was probable based on the observed geometry that diethylether solvent was present. The SQUEEZE[43] routine in the PLATON[44] program package was used to account for the electrons in the solvent accessible voids. Details are given in Table 6.3.

X-ray Data Collection, Structure Solution and Refinement for [(^{Ad,Me}ArOH)$_3$mes]. A colorless crystal of approximate dimensions 0.172 x 0.200 x 0.292 mm was mounted in a cryoloop

and transferred to a Bruker SMART APEX II diffractometer. The APEX2[38] program package was used to determine the unit-cell parameters and for data collection (90 sec/frame scan time for a sphere of diffraction data). The raw frame data was processed using SAINT[39] and SADABS[40] to yield the reflection data file. Subsequent calculations were carried out using the SHELXTL[41] program. There were no systematic absences nor any diffraction symmetry other than the Friedel condition. The centrosymmetric triclinic space group $P\bar{1}$ was assigned and later determined to be correct. The structure was solved by direct methods and refined on F^2 by full-matrix least-squares techniques. The analytical scattering factors[42] for neutral atoms were used throughout the analysis. Hydrogen atoms H(1), H(2) and H(3) were located from a difference-Fourier map and refined (x,y,z and U_{iso}). The remaining hydrogen atoms were included using a riding model. There were three molecules of diethylether present. Least-squares analysis yielded wR2 = 0.1517 and Goof = 0.96 for 754 variables refined against 11758 data (0.83 Å), R1 = 0.0570 for those 7122 data with $I > 2.0\sigma(I)$. Details are given in Table 6.4.

Computational Details. Density functional calculations on these compounds were done by Vamsee K. Voora in the group of Professor Filipp Furche. The initial geometries for complexes **23-Ln** and **24-Ln**, obtained from their respective crystal structures, were optimized using the Tao-Perdew-Staroverov-Scuseria (TPSS) functional.[50] Dispersion effects were incorporated using the semi-empirical D3 dispersion corrections.[51] In the case of **24-Ln**, the optimizations were carried out after removing the countercations. Small-core quasi-relativistic effective potentials[52] were used to model the innermost 28 core electrons of the Ln atoms. The solvation effects were modeled using the COSMO continuum solvation model.[53] A dielectric constant of 7.52, corresponding to tetrahydrofuran solvent, was used. All calculations were carried out in C1 symmetry using at least m3 fine grids. The ground state energies were converged to 10^{-6} a.u and the gradients were

converged to 10^{-3} a.u. Vibrational analyses were performed to confirm that all structures were minima on the molecular potential energy surface. All calculations were performed using the Turbomole quantum chemistry software.[54]

For **24-Nd**, the geometries were optimized using def2-TZVP[15] basis sets for the Ln and O atoms, and def2-SVP[16] basis sets for the C and H atoms. The quintet spin-state was established to be the ground state; the doublet configuration was found to be 13.4 kcal higher in energy than the quintet. The geometrical parameters of the optimized quintet structure were in good agreement with the experiments and matched better than the doublet further conforming that the ground state for **24-Nd** is a quintet. Vibrational analysis revealed three low-frequency vibrational modes for **24-Nd** to be imaginary but correspond to rotations of methyl groups located on the adamantyl groups.

In the case of **24-Gd,** we noticed that the spin-state ordering was sensitive to the choice of basis sets. We therefore carried out basis-set convergence studies. At the largest basis-set considered, we found that the nonet spin-state has the most stable electronic configuration which is in agreement with the EPR data. We used def2-QZVP basis on the Gd atom, def2-TZVP on the O atoms and the mesitylene carbon atoms, and def2-SV(P) basis on all other atoms. The septet state is 16.7 kcal/mol higher in energy at the present level of theory. The potential energy as a function of the Gd-centroid distance appears to have two minima. For both spin states, the minimum with longer Gd-centroid distance is preferred according to the calculations, and corresponds to a Gd^{2+} configuration, where the extra electron is in an orbital with mostly 6s and some 5d character. The LUMO is a mesitylene pi* orbital. For both spin states, the minimum with shorter Gd-centroid distance resembles an ionic configuration with a formal Gd^{3+} ion interacting with a negatively charged mesitylene ligand. The computed S^2 value for the nonet was 20.034,

indicating negligible spin contamination. Vibrational analysis confirmed that the structure corresponds to a minimum.

RESULTS AND DISCUSSION

Synthesis and Structure of the Ln^{3+} Complexes [((^{Ad,Me}ArO)$_3$mes)Ln], 23-Ln. The trivalent complexes, [((^{Ad,Me}ArO)$_3$mes)Ln], **23-Ln** (Ln = Nd, Gd, Dy, and Er), were synthesized by protonolysis of [Ln(N(SiMe$_3$)$_2$)$_3$] with the tris(phenol), (^{Ad,Me}ArOH)$_3$mes, eq 6.3, and identified by X-ray crystallography, Figure 6.1. The Gd, Dy, and Er complexes crystallize in the $P2_1/c$ space group and are isomorphous. **23-Nd** also crystallizes in $P2_1/c$ and is similar in structure, but is not isomorphous with the other **23-Ln** compounds (see Table 6.1). In comparison, **23-U** crystallizes in $P\bar{1}$.

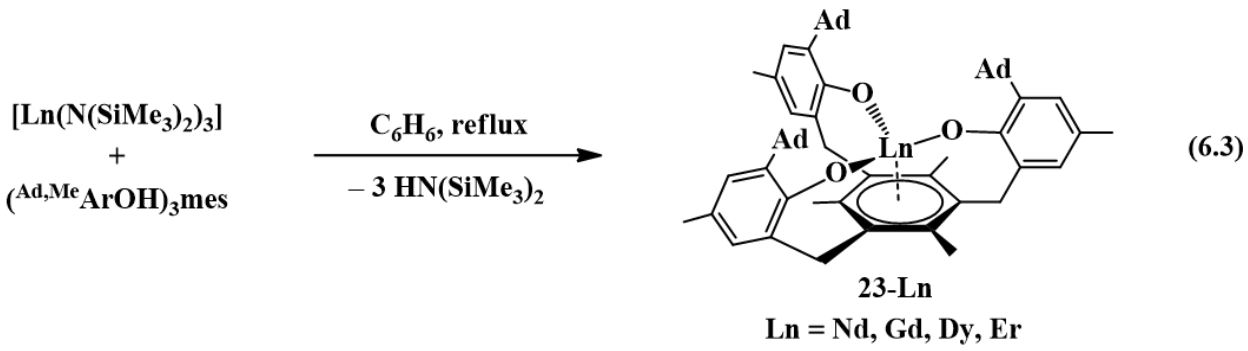

(6.3)

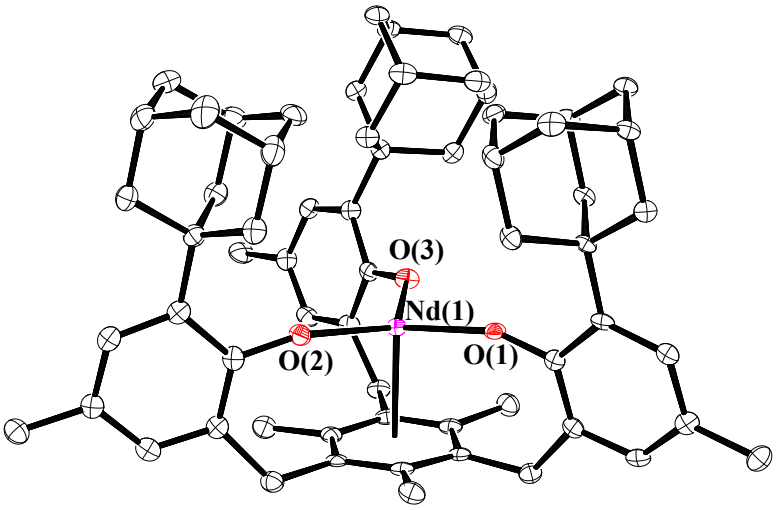

Figure 6.1. Molecular structure of [((^{Ad,Me}ArO)$_3$mes)Nd], **23-Nd**, with thermal ellipsoids drawn at the 50% probability level. Hydrogen atoms are omitted for clarity.

The structural parameters of **23-Ln** follow a regular trend based on the metal ionic radii, Table 6.1. Hence, the M–O distances and the M–(arene ring centroid) distances decrease regularly from Nd to Er as the size of the Ln^{3+} ion decreases. The Ln–O distances for **23-Ln** fall in the range of reported Ln–O(aryloxide) distances for complexes such as [Ln($OC_6H_3{}^tBu_2$-2,6)$_3$(THF)$_3$] (Ln = Nd,[55] Gd,[56] Er[57]), [Dy($OC_6H_3{}^iPr_2$-2,6)$_3$(DME)$_2$],[58] as well as other rare earth aryloxide complexes.[13-35] In contrast, the M–(arene centroid) distances of **23-Ln** are significantly shorter than those reported for Ln^{3+} arene complexes such as (arene)Ln[(μ-Cl)$_2$AlCl$_2$]$_3$.[59-70] For example, (η^6-1,3,5-$C_6H_3Me_3$)Nd[($AlCl_4$)$_3$][61] has a 2.566 Å Ln–(arene centroid) distance compared to 2.489 Å for **23-Nd**.

Table 6.1 also shows that the distances for **23-U** do not match those of **23-Ln** in terms of radial size and metal-ligand distance. Both the U–O and U–(arene centroid) distances of the U^{3+} complex are shorter than those of the lanthanides. This difference can be rationalized by greater

orbital overlap between the ligand orbitals and the 5*f* vs. the 4*f* metal orbitals. Regardless of these differences, the average C–C bond distances in the arene ring are within error of those of the free ligand, (^{Ad,Me}ArOH)$_3$mes, whose structure was determined as part of this study (see Table 6.4). Thus there is no evidence of reduction of the arene ring.

Reduction Reactions. Reduction of each **23-Ln** complex was carried out in a 1:1 THF/C_6H_6 with potassium graphite (KC_8) in the presence of 2.2.2-cryptand (crypt). In each case, highly absorbing red-colored solutions were obtained that were reminiscent of the intensely-colored solutions produced in the reductions of the Cp′$_3$Ln complexes in eq 6.1. The UV-visible electronic absorption spectra of these dark solutions, as shown in Figure 6.2, differ greatly from the line-like spectra typical of Ln^{3+} complexes (see **23-Nd**, Figure 6.3). Each complex has a strong broad absorption band in the visible region with the following maxima (λ_{max}, ε): Nd (416 nm, 4200 $M^{-1}\,cm^{-1}$), Gd (426 nm, 4000 $M^{-1}\,cm^{-1}$), Dy (431 nm, 4900 $M^{-1}\,cm^{-1}$), and Er (430 nm, 5600 $M^{-1}\,cm^{-1}$). The absorption energies and extinction coefficients of **24-Ln** are similar to those reported for the [K(crypt)][Cp′$_3$Ln] complexes (λ_{max}, ε): Nd (420 nm, 4700 $M^{-1}\,cm^{-1}$), Gd (430 nm, 4400 $M^{-1}\,cm^{-1}$), Dy (483 nm, 3400 $M^{-1}\,cm^{-1}$), and Er (502 nm, 4000 $M^{-1}\,cm^{-1}$). Although all of these absorption bands for **24-Ln** are broad, they appear to follow a trend in which the absorption energy decreases with increasing atomic number. Single crystals of the reduction products were obtained for Ln = Nd, Gd, Er, and Dy and are described below.

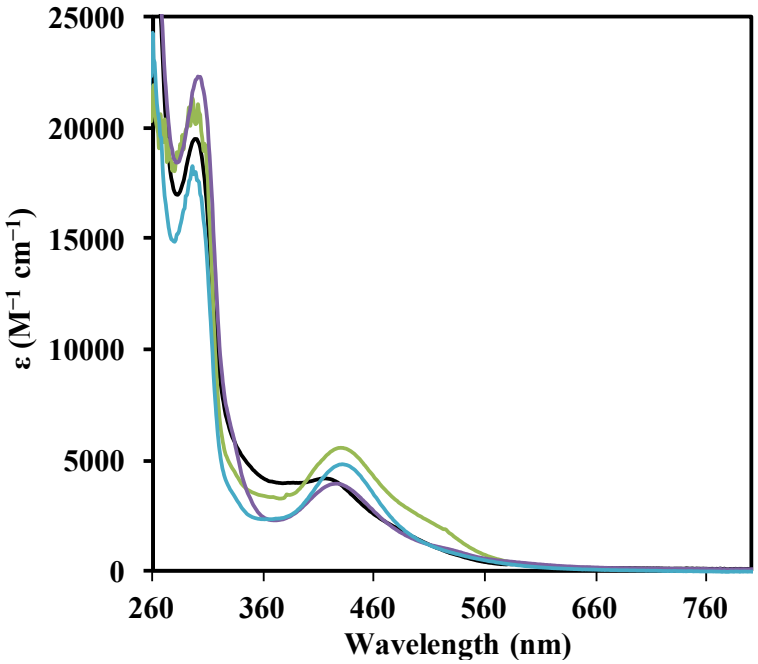

Figure 6.2. UV–visible spectra of [K(chelate)][((^{Ad,Me}ArO)$_3$mes)Ln] with Ln = Nd (black), Gd (purple), Er (green), and Dy (blue), recorded in THF at 298 K. The solutions were generated from crystals of **24-Nd**, **24-Ln/25-Ln** (Ln = Gd, Er), and **27-Dy/28-Dy**. Extinction coefficients, ε, for **24-Ln** (Nd, Gd, Er) and **27-Dy** were calculated using concentrations of Ln^{2+} estimated using Ln(1) occupancy from the crystallographic data.

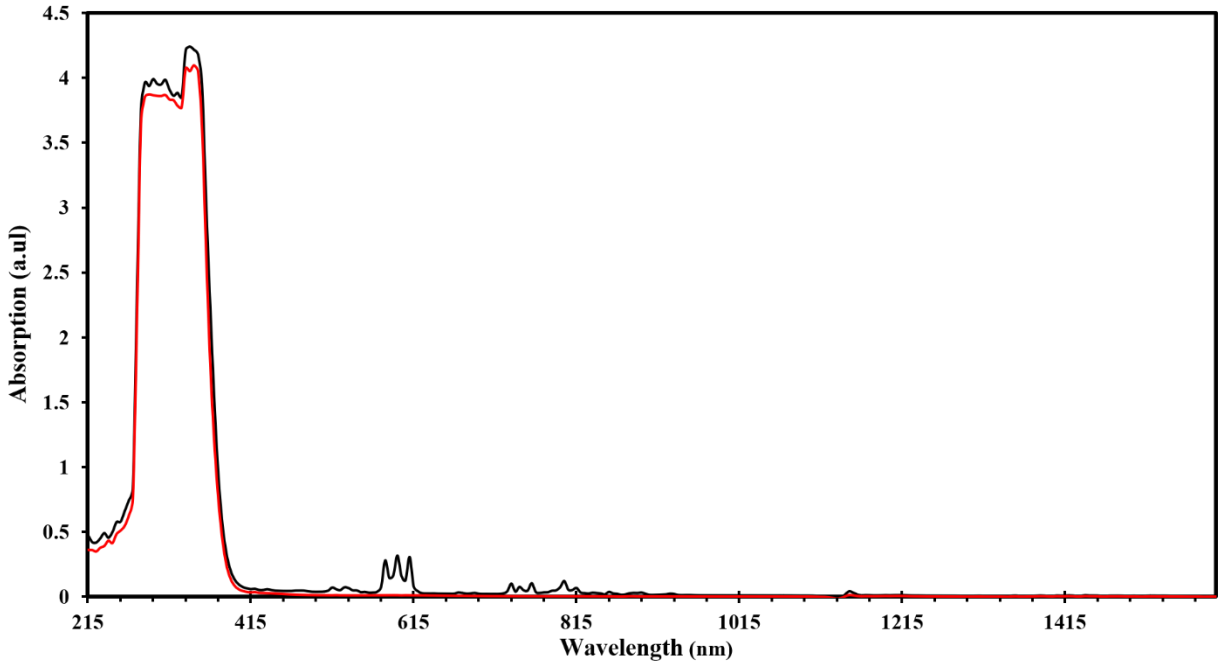

Figure 6.3. Electronic absorption spectra of [(^{Ad,Me}ArO)$_3$mes]Ln, **23-Ln** (Ln = Nd (black), Gd (red), as 10 mM solutions in benzene at room temperature.

Neodymium. Reduction of **23-Nd** produced a new example of a Nd^{2+} complex, [K(crypt)][((^{Ad,Me}ArO)$_3$mes)Nd], **24-Nd**, eq 6.4, which was confirmed by single-crystal X-ray diffraction, Figure 6.4. Crystals of **23-Nd** form in space group $P2_1/c$ and are isomorphous with crystals of the U^{2+} complex, [K(crypt)][((^{Ad,Me}ArO)$_3$mes)U], **24-U** (see Table 6.2).

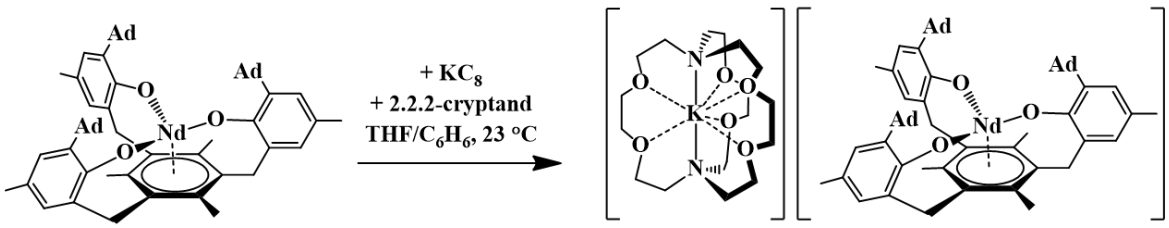

23-Nd **24-Nd** (6.4)

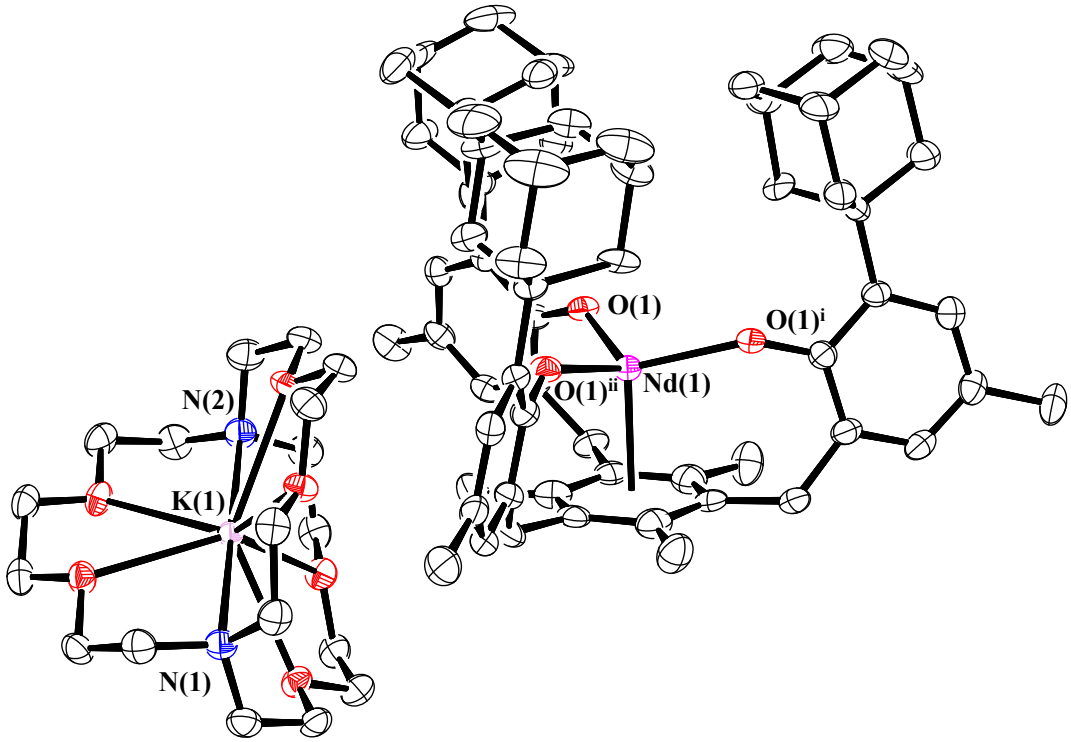

Figure 6.4. Molecular structure of [K(crypt)][((^{Ad,Me}ArO)$_3$mes)Nd], **24-Nd**, drawn at the 50% probability level. Hydrogen atoms are omitted for clarity.

Gadolinium and Erbium. Reductions of **23-Gd** and **23-Er**, performed in a manner analogous to that of eq 6.4, produced dark red single crystals suitable for X-ray diffraction that appeared to be isomorphous with **24-Nd** (see Table 6.2). However, the crystallographic data were best modeled by a mixture of two complexes: the divalent [K(crypt)][((^{Ad,Me}ArO)$_3$mes)Ln], **24-Ln**, and the trivalent hydride, [K(crypt)][((^{Ad,Me}ArO)$_3$mes)LnH], **25-Ln**, in a 65:35 ratio for Gd and 55:45 ratio for Er, eq 6.5, Figure 6.5. The metal centers in both **24-Ln** and **25-Ln** lie on a three-fold axis with the same ligand environment, in which Ln(1) represents the metal center for

24-Ln and Ln(2) represents the metal center for **25-Ln**. Consistent with the presence of a hydride ligand, the reaction of **24-Er/25-Er** with CCl_4 produced chloroform.[71]

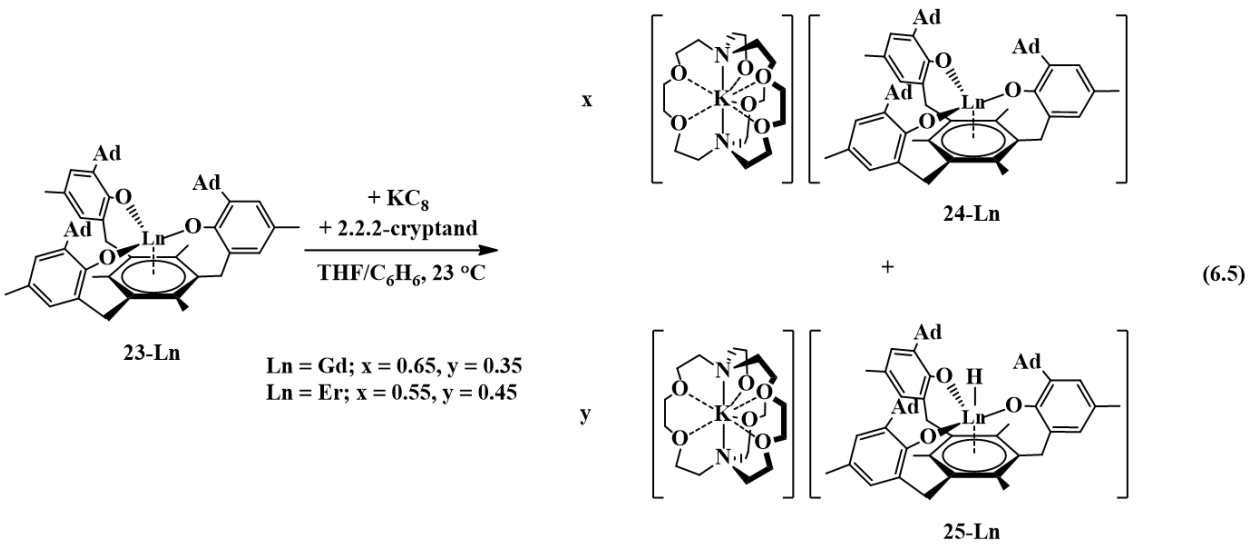

(6.5)

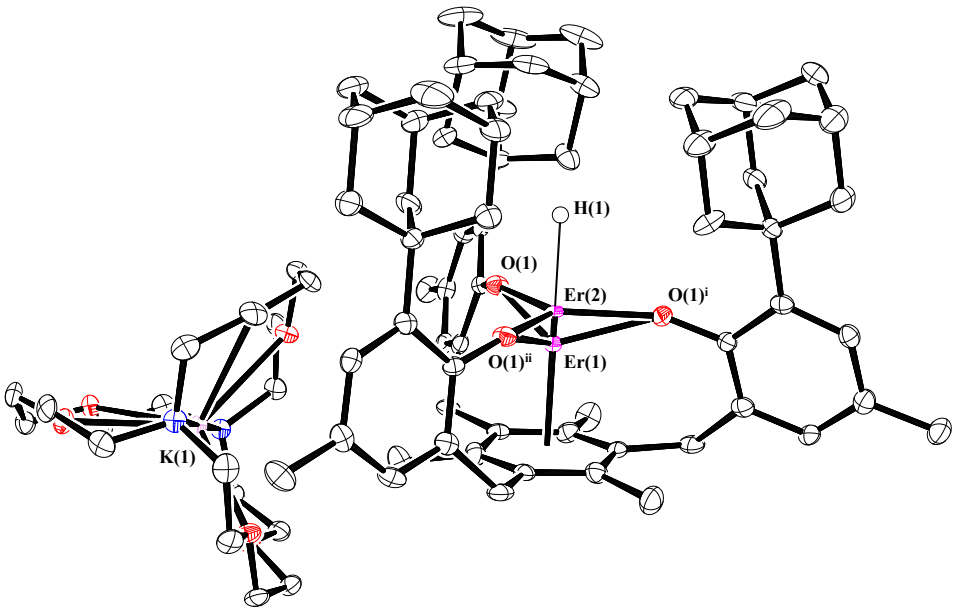

Figure 6.5. Molecular structure of [K(crypt)][((^{Ad,Me}ArO)$_3$mes)Er], **24-Er**, and [K(crypt)][((^{Ad,Me}ArO)$_3$mes)ErH], **25-Er**, which co-crystallize in an approximate 55:45 ratio. Thermal ellipsoids are drawn at the 50% probability level and hydrogen atoms, except H(1), are omitted for clarity. Er(1) is the metal position in **24-Er** and Er(2) is the metal position in **25-Er**.

Single crystals of **24-Gd/25-Gd** dissolved in THF display a single isotropic signal at g_{iso} = 1.990 in the room temperature X-band EPR spectrum, Figure 6.6a. This is similar to the X-band EPR spectra of the crystallographically-characterized Gd^{2+} complexes,[4,72] [K(crypt)][Cp′$_3$Gd] and [K(crypt)][Cp″$_2$CpGd] (Cp = C_5H_5), which also show isotropic signals at g_{iso} = 1.99. An S = 4, $4f^75d^1$ electron configuration has been proposed for those cyclopentadienyl complexes. Thus, the EPR spectrum of **24-Gd** is consistent with an S = 4, $4f^75d^1$ electron configuration for Gd^{2+} in the $(({}^{Ad,Me}ArO)_3mes)^{3-}$ ligand coordination, since it is unlikely that an EPR spectrum of a $4f^8$ Gd^{2+} complex would be observable under these conditions. Since an $4f^7/4f^8$ reduction eliminates a half-filled shell, whereas an $4f^7$ to a $4f^75d^1$ reduction does not, the latter process would be favored in this regard. Elimination of the half-filled shell is why the calculated redox potential for a $4f^7/4f^8$ process is so high, −3.9 V vs. SHE,[73] whereas the observed gadolinium reduction must occur at potentials less negative than −2.9 V vs SHE. The X-band EPR spectrum recorded in frozen THF solution at 10K, shown in Figure 6.6b, is further consistent with the presence of an S = 4 $4f^75d^1$ Gd^{2+} ion. Both the Gd^{3+} and Gd^{2+} species of the co-crystallized sample of **24-Gd** and **25-Gd** can be observed by EPR spectroscopy according to our simulations. The almost axial spectrum of **24-Gd** was simulated with g values at g_1 = 7.02, g_2 = 6.85, and g_3 = 3.97.

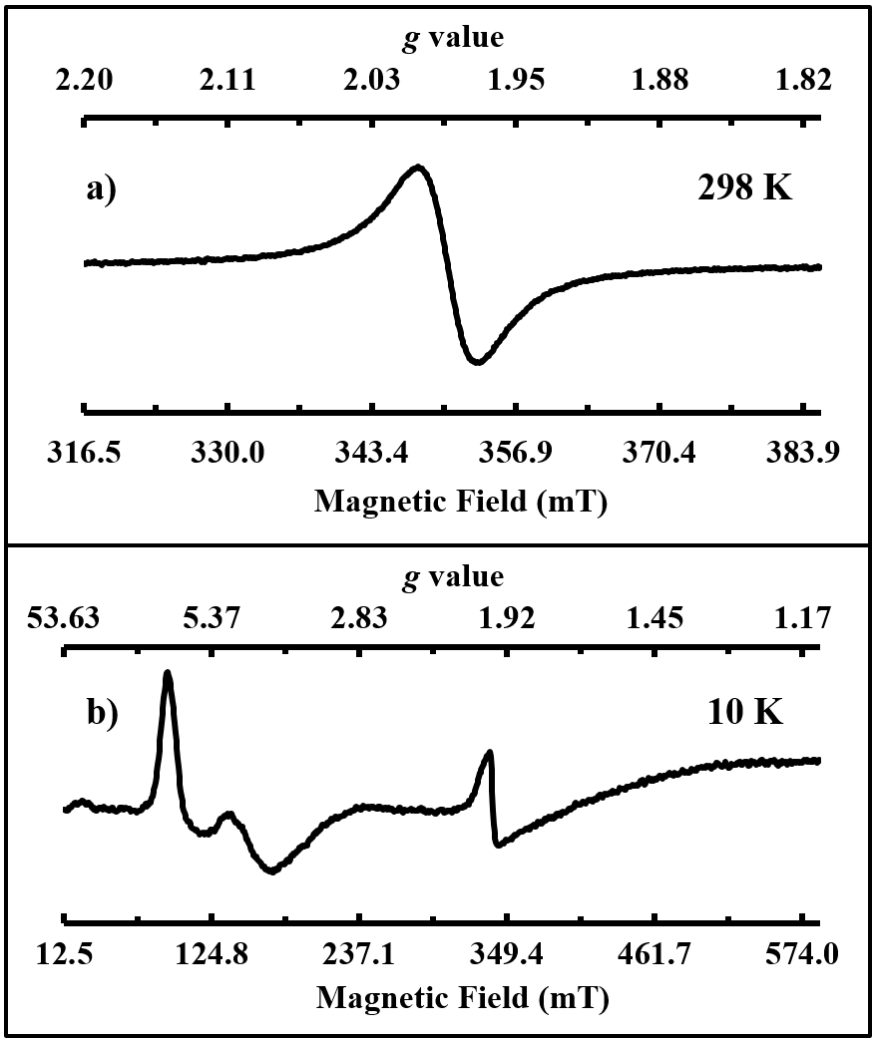

Figure 6.6. Experimental X-band EPR spectra of single crystals of **24-Gd/25-Gd** dissolved in THF (1 mM) at a) 298 K (Mode: perpendicular; g_{iso} = 1.990; ν = 9.762 GHz; P = 0.0203 mW; modulation amplitude = 0.902 mT) and b) 10 K (Mode: parallel; g_1 = 7.349, g_2 = 4.786, g_3 = 1.977; ν = 9.383 GHz; P = 2.026 mW; modulation amplitude = 1.002 mT).

Although co-crystallization of Ln^{3+} hydrides with the Ln^{2+} complexes complicates the structural analysis (see below), it does suggest that the $(({}^{Ad,Me}ArO)_3mes)^{3-}$ ligand set can enhance the bond activation reactivity of these Ln^{2+} ions. C–H bond activation previously has been observed with the Nd^{2+} complex, $[(C_5H_2{}^tBu_3)_2Nd(\mu\text{-}I)K(18\text{-crown-}6)]$, which forms

[$(C_5H_2{}^tBu_3)(C_5H_2{}^tBu_2CMe_2CH_2$-$\eta^5$:$\kappa^1$)Nd($\mu$-I)K(18-crown-6)].[74] This was also found in attempts to form indenyl Ln^{2+} complexes, which led to the indenyl dianion, $(C_9H_6)^{2-}$, in $[K(crypt)]_2[(C_9H_7)_2Dy(\mu$-$\eta^5$:$\eta^1$-$C_9H_6)]_2$.[72]

Dysprosium. Reduction of **23-Dy** produced dark red crystals suitable for X-ray diffraction that also appeared to be isomorphous with **24-Nd**. Instead, the crystallographic data were best modeled as a mixture of the divalent [K(crypt)][((^{Ad,Me}ArO)$_3$mes)Dy], **24-Dy**, and the trivalent hydroxide [K(crypt)][((^{Ad,Me}ArO)$_3$mes)Dy(OH)], **26-Dy**, in a 2:3 ratio. Like the **24-Ln/25-Ln** mixtures, **24-Dy** and **26-Dy** lie on a threefold axis with the same ligand environment, Figure 6.7, in which Dy(1) represents the metal center for **24-Dy** and Dy(2) represents the metal center for **26-Dy**. The origin of the hydroxide ligand in **26-Dy** is unknown. We include the data on this mixed crystal here, because it does contain a Dy^{2+} complex and shows that the Ln^{2+} complexes can co-crystallize with hydroxides as well as hydrides.

Given the unexpected hydroxide result above, the Dy reaction was examined further with 18-crown-6. Reduction of **23-Dy** with K in the presence of 18-crown-6 instead of 2.2.2-cryptand gave a dark colored solution similar to that observed to form the **24-Dy/26-Dy** mixture. Crystallization of this product gave single crystals that were modeled as a 1:1 mixture of [K(18-crown-6)(THF)$_2$]–[((^{Ad,Me}ArO)$_3$mes)Dy], **27-Dy**, and the trivalent hydride, [K(18-crown-6)(THF)$_2$)][((^{Ad,Me}ArO)$_3$mes)DyH], **28-Dy** (see Table 6.3). This **27-Dy/28-Dy** mixture is analogous to the **24-Ln/25-Ln** mixtures, except that the countercation is $[K(18\text{-crown-6})(THF)_2]^+$ rather than $[K(crypt)]^+$.

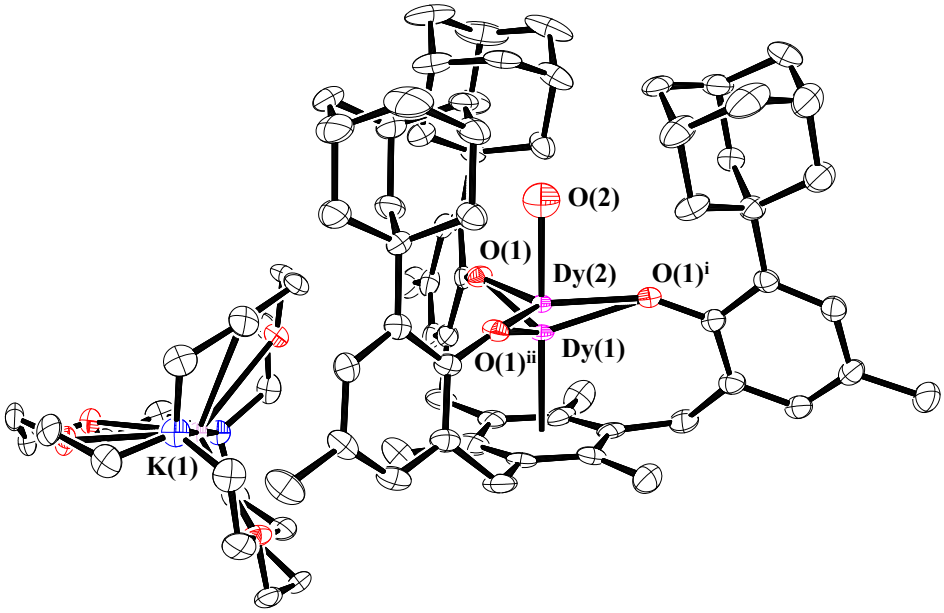

Figure 6.7. Molecular structure of [K(crypt)][((^{Ad,Me}ArO)$_3$mes)Dy]/[K(crypt)][((^{Ad,Me}ArO)$_3$mes)Dy(OH)], **24-Dy/26-Dy**, with thermal ellipsoids drawn at the 50% probability level. Hydrogen atoms and a disordered ether molecule are omitted for clarity. Dy(1) is the metal position in **24-Dy** and Dy(2) is the metal position in **26-Dy**.

Subsequently, the reduction of **23-Dy** was re-examined and single crystals containing a mixture of the Dy^{2+} complex and the Dy^{3+} hydride were obtained, *i.e.* **24-Dy/25-Dy**. In this case the ratio of Dy^{2+} to Dy^{3+} hydride was modeled by a 63:37 mixture, Table 6.3.

Structural Comparisons. Structural data on **24-Nd** and the co-crystallized **24-Gd/25-Gd**, **24-Dy/25-Dy**, **24-Er/25-Er**, **24-Dy/26-Dy**, and **27-Dy/28-Dy** mixtures are given in Table 6.6, along with the data for **24-U**. In contrast to the data on the Ln^{3+} **1-Ln** complexes shown in Table 6.5, the structural data on the mixtures presented in Table 6.6 do not follow the regular changes in distances with radial size for either the Ln^{2+} complexes, **24-Ln** and **27-Dy**, or for the Ln^{3+}

complexes, **25-Ln**, **26-Dy**, and **28-Dy**. The substantial differences in the metrical parameters of the $[K(crypt)]^+$ and $[K(18\text{-crown-6})(THF)_2]^+$ salts of the $[((^{Ad,Me}ArO)_3mes)Dy]^-$ anion, **24-Dy** and **27-Dy**, illustrate the complicated nature of these structural data. As a result, only the metrical data for **24-U** and **24-Nd** will be compared.

A comparison of the divalent complexes **24-Nd** and **24-U**, along with their trivalent analogs, is given in Table 6.7. The structural data on **24-Nd** show that the metal center is 0.123 Å closer to the arene centroid than in **23-Nd**. This change is not as large as the 0.17 Å difference between **23-U** and **24-U**, which is likely due to the limited radial extension of the 4*f* orbitals versus the 5*f* orbitals.[75] Just as in **24-U**, the arene carbon atoms are approximately planar in **24-Nd** and the C–C(arene) bond lengths only increase by approximately 0.01 Å. This is consistent with reduction of the metal and not the arene. As analyzed for uranium, the contraction of the M–(arene centroid) distance between **23-Nd** and **24-Nd** could suggest a greater interaction between the metal and arene due to a change in charge distribution.

Theoretical Insight. Density functional theory (DFT) calculations were carried out by Dr. Vamsee K. Voora of in collaboration with the group of Professor Filipp Furche. Calculations using the Tao-Perdew-Staroverov-Scuseria (TPSS) functional[50] and mixed basis sets were carried out on **23-Nd**, **24-Nd**, and **24-Gd** (see Computational Details).[76,77] For **23-Nd** and **24-Nd**, the calculated structural parameters match those observed within 0.04 Å (Table 6.8). The three valence electrons of **23-Nd** occupy predominantly 4*f*-type orbitals with little observable interaction with the mesitylene ring. This differs from **23-U** as expected for a 4*f* vs. 5*f* system. Calculations on **24-Nd** suggest a quartet ground state with two electrons in f orbitals and two electrons in f/π^* orbitals of δ symmetry (see Tables 6.9 and 6.10); the corresponding four SOMOs are shown in

Figure 6.8. This orbital picture resembles that of **24-U**.[12] The lowest unoccupied orbital with *d*-orbital character for **24-Nd** is about 2.9 eV above the HOMO and has d_z^2 character (see Figure 6.9). Hence, the DFT calculations suggest that the $((^{Ad,Me}ArO)_3mes)^{3-}$ ligand system favors a formal $4f^4$ electron configuration for Nd^{2+} rather than a $4f^35d^1$ configuration postulated for Nd^{2+} in the $(Cp'_3)^{3-}$ environment.[5] This assignment is consistent with Nd^{2+} being a configurational crossover ion and is further supported by the $5f^4$ configuration found for [K(crypt)][$(^{Ad,Me}ArO)_3mes$)U], **24-U**, vs. the $5f^36d^1$ configurations for [K(crypt)][Cp'_3U][6] and [K(crypt)][Cp''_3U], **7-U**.[7]

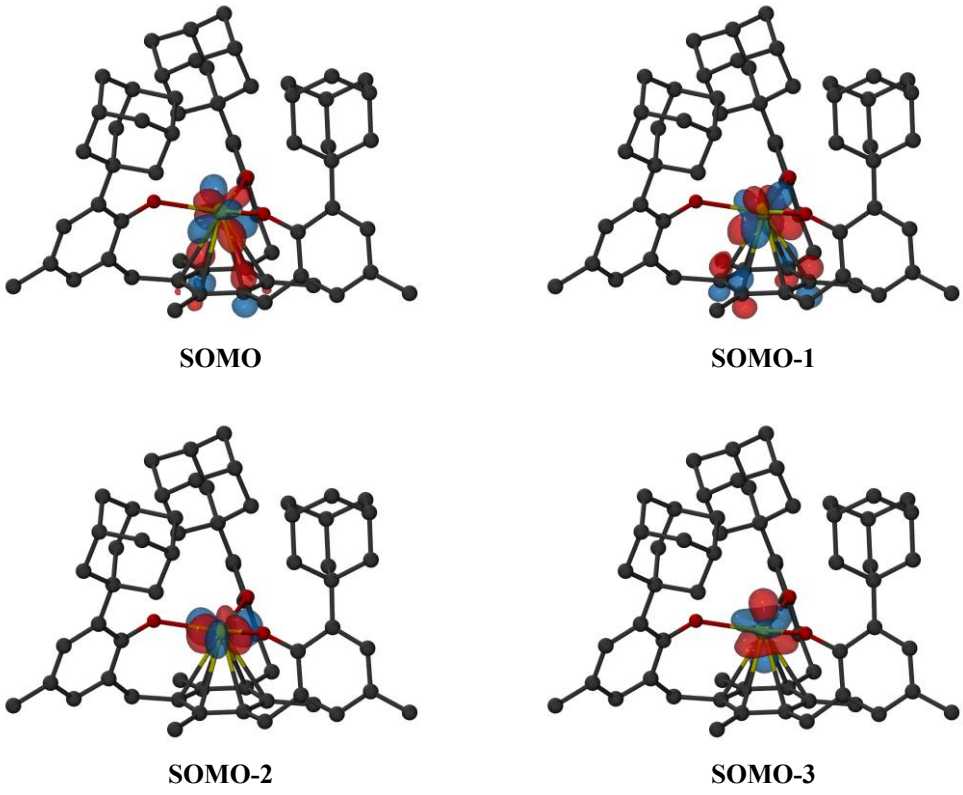

Figure 6.8. Isosurfaces for the four highest singly-occupied molecular orbitals of **24-Nd** corresponding to a contour value of 0.05. Hydrogen atoms are omitted for clarity.

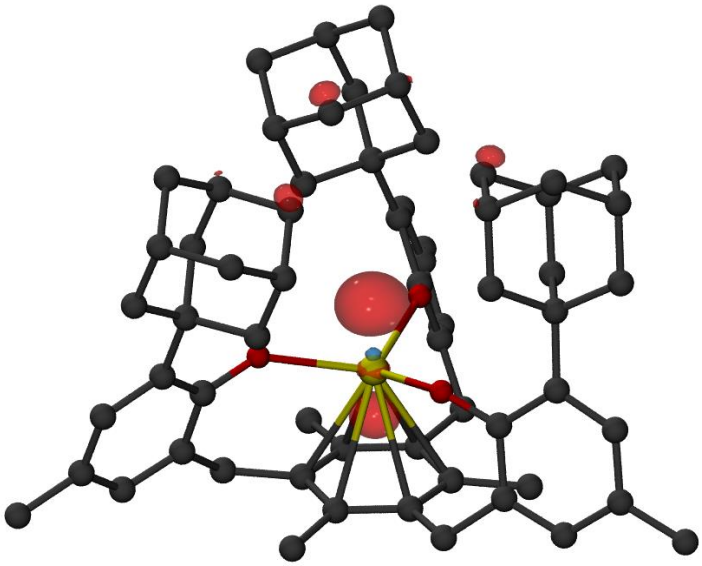

Figure 6.9. Isosurface for the lowest *d*-type unoccupied orbital **24-Nd** with a contour value of 0.05. Hydrogen atoms are omitted for clarity.

DFT calculations on **24-Gd** proved to be more challenging. The ground state of **24-Gd** is a nonet (8 unpaired electrons) with a $4f^7(5d/6s)^1$ configuration for the Gd atom (Figure 6.10). This result is similar to the $4f^75d^1$ configuration observed for [K(crypt)][Cp'_3Gd], except that the SOMO has 6*s* as well as 5*d* character. A nonet ground state is also supported by the observable EPR spectrum for **24-Gd** (Figure 6.6). However, the computed metal-arene bond-distance (3.17 Å) is larger than the experimentally observed bond-distance (2.29 Å) and the calculated metal out-of-plane distortion (−0.28 Å) is in a direction opposite to the experimental value (0.578 Å), see Table 6.8, indicating that the DFT results for **24-Gd** need to be interpreted with caution. The potential energy profile along the Gd out-of-plane distortion is fairly shallow and has several minima with different electronic character, and the DFT picture may not adequately capture the multi-configurational nature of the nonet ground state. In any case, it appears that the $((^{Ad,Me}ArO)_3mes)^{3-}$ ligand system can favor $4f^{n+1}$ over $4f^n5d^1$ with the configurational crossover ion, Nd^{2+}, but this

effect is not strong enough to overcome the stabilization derived from a $4f^7$ half-filled shell in Gd^{2+}.

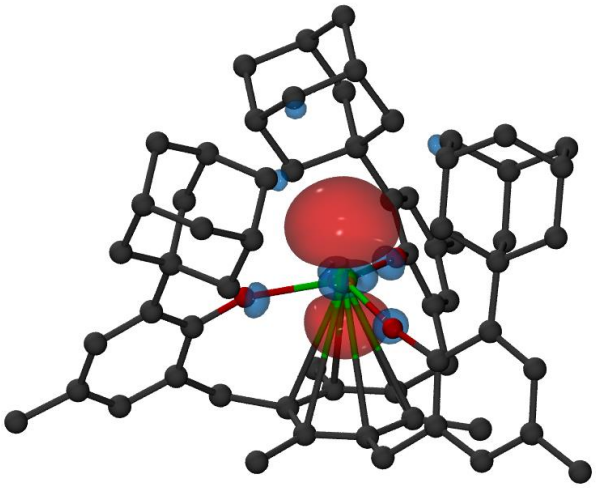

Figure 6.10. Isosurface of the highest SOMO of nonet **24-Gd** with a contour value of 0.05. Hydrogen atoms are omitted for clarity.

CONCLUSION

Tris(aryloxide) arene lanthanide(III) complexes, [((^{Ad,Me}ArO)$_3$mes)Ln], **23-Ln**, analogous to [((^{Ad,Me}ArO)$_3$mes)U], **23-U**,[11] have been synthesized and characterized by single-crystal X-ray diffraction for Ln = Nd, Gd, Dy, and Er. The four trivalent Ln complexes show structural regularity in metal ligand distances based on their decreasing radial size from Nd to Er. Complex **23-U** appears to have greater interaction with the tris(aryloxide)arene ligand consistent with greater radial extension of the 5*f* orbitals. Reduction of **23-Ln** generates four new Ln^{2+} complexes, [K(crypt)][((^{Ad,Me}ArO)$_3$mes)Ln], **24-Ln**, for Nd, Gd, Dy, and Er as well as the 18-crown-6 variant, [K(18-crown-6)(THF)$_2$][((^{Ad,Me}ArO)$_3$mes)Dy], **27-Dy**. **24-Gd**, **24-Dy**, **24-Er**, and **27-Dy** co-

crystallize with Ln^{3+} hydrides, [K(crypt)][((^{Ad,Me}ArO)$_3$mes)LnH], **25-Ln,** or [K(18-crown-6)(THF)$_2$)][((^{Ad,Me}ArO)$_3$mes)DyH], **28-Dy**. This suggests that the ((^{Ad,Me}ArO)$_3$mes)$^{3-}$ ligand environment is especially effective at promoting high reactivity.

DFT calculations indicate that the one Ln^{2+} complex isolated without Ln^{3+} co-crystallization, **2-Nd**, appears to have a $4f^4$ electron configuration with two electrons in 4f/π* orbitals and two electrons in other 4f orbitals. This contrasts with the $4f^35d^1$ configuration of [Cp′$_3$Nd]$^{1-}$ and is consistent with Nd^{2+} being a configurational crossover ion. Comparison of **24-Nd** with congeneric and isomorphous **24-U** shows closer interaction of the metal with the ligand in the case of the 5*f* vs. 4*f* metal, which is consistent with the relative radial extensions of these orbitals. EPR data and DFT calculations on [K(crypt)][((^{Ad,Me}ArO)$_3$mes)Gd]/[K(crypt)]-[((^{Ad,Me}ArO)$_3$mes)GdH], **24-Gd/25-Gd**, tentatively suggest a $4f^75d^1$ electron configuration that retains a half-filled 4*f* shell for Gd^{2+} in the [(^{Ad,Me}ArO)$_3$mes]$^{3-}$ coordination environment, although the poor agreement of the DFT metal-arene bond distance with the X-ray data merits further investigation Overall, the results suggest that the [(^{Ad,Me}ArO)$_3$mes]$^{3-}$ ligand has considerable flexibility in binding heavy metals.

Table 6.1. Crystal data and structure refinement for **23-Ln** (Ln = Nd, Gd, Dy, Er).

	23-Nd	**23-Gd**	**23-Dy**	**23-Er**
Empirical formula	$C_{63}H_{75}O_3Nd$	$C_{63}H_{75}O_3Gd$	$C_{63}H_{75}O_3Dy$	$C_{63}H_{75}O_3Er$
Formula weight	1024.47	1037.48	1042.73	1047.49
Temperature (K)	88(2)	88(2)	133(2)	133(2)
Space group	$P2_1/c$	$P2_1/c$	$P2_1/c$	$P2_1/c$
a (Å)	11.5124(10)	12.812(3)	12.7567(11)	12.7631(14)
b (Å)	36.810(3)	15.716(3)	15.6646(13)	15.6460(17)
c (Å)	11.9512(10)	29.962(6)	29.878(3)	29.910(3)
α (°)	90	90	90	90
β (°)	106.7298(9)	96.129(2)	96.2651(13)	96.4368(15)
γ (°)	90	90	90	90
Volume (Å^3)	4850.3(7)	5999(2)	5934.9(9)	5935.2(11)
Z	4	4	4	4
ρ_{calcd} (g/cm^3)	1.403	1.149	1.167	1.172
μ (mm^{-1})	1.119	1.145	1.299	1.454
$R1^a$	0.0453	0.0339	0.0444	0.0335
$wR2^b$	0.0850	0.0766	0.0943	0.0741

Definitions: $^a R1 = \sum||Fo| - |Fc||/\sum|Fo|$; $^b wR2 = [\sum[w(Fo^2 - Fc^2)^2]/ \sum[w(Fo^2)^2]]^{1/2}$.

Table 6.2. Crystal data and structure refinement for **24-Nd**, and **24-Ln/25-Ln** (Ln = Er, Dy Gd).

	24-Nd	**24-Gd/25-Gd**	**24-Dy/25-Dy**	**24-Er/25-Er**
Empirical formula	$C_{81}H_{111}KN_2NdO_9$	$C_{81}H_{111}GdKN_2O_9$ $(H)_{0.35}\bullet(C_4H_{10}O)$	$C_{81}H_{111}DyKN_2O_9$ $H_{0.37}\bullet(C_4H_{10}O)$	$C_{81}H_{111}ErKN_2O_9$ $(H)_{0.45}\bullet(C_4H_{10}O)$
Formula weight	1440.05	1527.53	1532.80	1537.64
Temperature (K)	88(2)	88(2)	133(2)	100(2)
Space group	$P2_13$	$P2_13$	$P2_13$	$P2_13$
a (Å)	19.7666(8)	19.7291(9)	19.798(3)	19.7501(6)
b (Å)	19.7666(8)	19.7291(9)	19.798(3)	19.7501(6)
c (Å)	19.7666(8)	19.7291(9)	19.798(3)	19.7501(6)
α (°)	90	90	90	90
β (°)	90	90	90	90
γ (°)	90	90	90	90
Volume (Å^3)	7723.2(9)	7679.3(11)	7760(3)	7703.9(7)
Z	4	4	4	4
ρ_{calcd} (g/cm^3)	1.238	1.321	1.312	1.326
μ (mm^{-1})	0.781	0.978	1.076	1.203
$R1^a$	0.0482	0.0372	0.0417	0.0413
$wR2^b$	0.1279	0.0951	0.0970	0.0827

Definitions: $^a R1 = \sum||Fo| - |Fc||/\sum|Fo|$; $^b wR2 = [\sum[w(Fo^2 - Fc^2)^2]/\sum[w(Fo^2)^2]\ ]^{1/2}$.

Table 6.3. Crystal data and structure refinement for **24-Dy/26-Dy** and **27-Dy/28-Dy**.

	24-Dy/26-Dy	**27-Dy/28-Dy**
Empirical formula	$C_{81}H_{111}DyKN_2O_{10}(OH)_{0.6}\bullet(C_4H_{10}O)$	$C_{83}H_{115.5}DyKO_{11}\bullet 2(C_4H_8O)$
Formula weight	1542.64	1635.05
Temperature (K)	100(2)	133(2)
Space group	$P2_13$	*Pbcn*
a (Å)	19.7730(7)	21.7362(14)
b (Å)	19.7730(7)	30.6130(19)
c (Å)	19.7730(7)	25.4472(16)
α (°)	90	90
β (°)	90	90
γ (°)	90	90
Volume (Å^3)	7730.7(8)	16932.8(19)
Z	4	8
ρ_{calcd} (g/cm^3)	1.325	1.283
μ (mm^{-1})	1.081	0.992
$R1^a$	0.0457	0.0583
$wR2^b$	0.0956	0.1486

Definitions: ^{a}R1 = $\sum||Fo| - |Fc||/\sum|Fo|$; ^{b}wR2 = $[\sum[w(Fo^2 - Fc^2)^2]/\sum[w(Fo^2)^2]\ ]^{1/2}$.

Table 6.4. Crystal data and structure refinement for (^{Ad,Me}ArOH)$_3$mes.

	(^{Ad,Me}ArOH)$_3$mes
Empirical formula	$C_{63}H_{78}O_3H_3$•3($C_4H_{10}O$)
Formula weight	1105.61
Temperature (K)	133(2)
Space group	$P\bar{1}$
a (Å)	13.904(3)
b (Å)	15.774(3)
c (Å)	16.856(3)
α (°)	99.238(3)
β (°)	109.444(2)
γ (°)	106.032(3)
Volume (Å^3)	3217.6(11)
Z	2
ρ_{calcd} (g/cm^3)	1.141
μ (mm^{-1})	0.070
$R1^a$	0.0570
$wR2^b$	0.1517

Definitions: ^{a}R1 = $\sum||Fo| - |Fc||/\sum|Fo|$; ^{b}wR2 = $[\sum[w(Fo^2 - Fc^2)^2]/\sum[w(Fo^2)^2]\ ]^{1/2}$.

Table 6.5. Selected bond lengths (Å) and angles (°) of **23-Ln** and **23-U** listed in order of decreasing ionic radius.

Metal	Six coordinate ionic radius[a]	M–O range	M–O avg	M–C_6 (ring centroid)	M out of plane[b]	C_6 Torsion Angle[c]
U	1.025	2.158(2)-2.178(2)	2.17(1)	2.35	0.475(2)	6.8
Nd	0.983	2.172(3)-2.200(2)	2.19(1)	2.489	0.268	5.6
Gd	0.938	2.132(2)-2.134(2)	2.133(1)	2.413	0.416	8.3
Dy	0.912	2.093(3)-2.095(3)	2.094(1)	2.368	0.443	8.1
Er	0.89	2.078(2)-2.081(2)	2.079(1)	2.336	0.477	7.9

[a]From Shannon.[31] [b]Distance of M from the plane defined by the three O atoms of the $((^{Ad,Me}ArO)_3mes)^{3-}$ ligand. [c]The largest dihedral angle between adjacent three-carbon planes in the mesitylene ring.

Table 6.6. Selected bond lengths (Å) and angles (°) of **24-U**, **24-Nd**, **24-Gd/25-Gd**, **24-Er/25-Er**, **24-Dy/26-Dy**, and **27-Dy/28-Dy**.

Metal	M–O	M–Cent	M–C(arene)	M–C(arene) avg	M out of plane[a]	O-M-O	Largest C_6 Torsion Angle (°)[b]
2-U	2.236(4)	2.18	2.597(5), 2.633(5)	2.615	0.668(2)	111.49(8)	5.9
2-Nd	2.237(4)	2.366	2.742(6), 2.788(7)	2.765	0.530	114.59(8)	6.2
2-Gd/ 3-Gd	2.203(3)/ 2.126(3)	2.286/ 2.863	2.672(5)/3.175 2.710(6)/3.216	2.691/ 3.196	0.578/ 0.001	113.37(8)/ 120.003(1)	8.8
2-Dy/ 4-Dy	2.222(3)/ 2.125(3)	2.177/ 2.683	2.586(5)/3.101, 2.605(6)/3.127	2.596/ 3.113	0.652/ 0.055	111.77(8)/ 119.93	6.3
5-Dy/ 6-Dy	2.16(3)/ 2.09(2)	2.232/ 2.789	2.592(4)/3.058 2.603(4)/3.068 2.613(4)/3.096 2.641(4)/3.128 2.665(4)/3.169 2.728(4)/3.234	2.64(5)/ 3.13(6)	0.556/ 0.001	114.39(12)/ 118.61 115.22(13)/ 121.78 111.28(12)/ 119.61	8.7
2-Er/ 3-Er	2.172(3)/ 2.077(3)	2.200/ 2.854	2.602(4)/3.170 2.634(4)/3.205	2.618/ 3.188	0.637/ 0.017	111.77(7)/ 119.993(2)	5.7

[a] Distance of M from the plane defined by the three O atoms of the $(({}^{Ad,Me}ArO)_3mes)^{3-}$ ligand.

[b] The largest dihedral angle between adjacent three-carbon planes in the mesitylene ring.

Table 6.7. Differences (Δ) in bond distances (Å) and angles (°) between **24-Nd** and **24-U** and their trivalent analogs, **23-Nd** and **23-U**, respectively.

Metal	**Δ(M–O)**	**Δ(M–Cent)**	**Δ(M out of plane)**[a]	**Δ(Largest C_6 Torsion Angle)**[b]
U	0.068	−0.170	0.193	−0.9
Nd	0.050	−0.123	0.262	0.6

[a] Distance of M from the plane defined by the three O atoms of the $((^{Ad,Me}ArO)_3mes)^{3-}$ ligand.

[b]The largest dihedral angle between adjacent three-carbon planes in the mesitylene ring.

Table 6.8. Comparison of selected bond lengths (Å) and angles (°) of **24-Nd**, **24-Gd**, and **23-Nd** obtained from experimental crystal structures with those from DFT calculations in solution phase. *Indicates averaged values.

Compound		**24-Nd**			**24-Gd**			**23-Nd**
	Expt.	Calc. (S=2)	Calc. (S=1)	Expt.	Calc. (S=4)	Calc. (S=3)	Expt.	Calc. (S=3/2)
M–O	2.237(4)	2.28	2.24*	2.203(3)	2.24	2.21*	2.19	2.19
M–Cent	2.366	2.37	2.32	2.286	2.29	2.99	2.489	2.48
M–C_{arene}	2.742(6),	2.74	2.75	2.672(5)	2.72	3.32		2.82
	2.788(7)	2.79	2.78	2.710(6)	2.71	3.30		2.85
		2.74	2.70		2.74	3.30		2.83
		2.79	2.79		2.59	3.27		2.88
		2.74	2.74		2.72	3.35		2.92
		2.79	2.74		2.72	3.30		2.86
M–C_{arene} avg	2.765	2.77	2.75	2.691	2.70	3.30		2.86
M_{oop}[a]	0.530	0.49	0.54	0.578	0.62	0.61	0.268	0.24
$\measuredangle$O-M-O	114.59(8)	115.6	115.3*	113.37(8)	112.5*	119.5*		118.9*
Largest C_6 Torsion Angle (°)[b]	6.2	6.9	12.3	8.8	15.5	6.18	5.6	6.1

[a] Distance of M from the plane defined by the three O atoms of the $(({}^{Ad,Me}ArO)_3mes)^{3-}$ ligand.

[b] The largest dihedral angle between adjacent three-carbon planes in the mesitylene ring.

Table 6.9. Mulliken population analysis of singly occupied orbitals of **24-Nd** and **24-Gd**.

		Total	s	p	d	f	g
				24-Nd			
SOMO-3	Nd	0.99130	0.01090	0.00089	-0.00003	0.97952	0.00001
SOMO-2	Nd	0.95718	0.01239	-0.00009	0.00671	0.93817	0.00001
SOMO-1	Nd	0.78501	0.00000	-0.00032	0.02173	0.76349	0.00011
	C^{mes}	0.18178	0.00306	0.17707	0.00164		
SOMO	Nd	0.78297	0.00000	-0.00032	0.02188	0.7613	0.00011
	C^{mes}	0.1875	0.00302	0.18029	0.00417		
				24-Gd			
SOMO	Gd	0.83585	0.62813	0.01506	0.18062	0.01201	0.00003

Table 6.10. Mulliken atomic spin density analysis of **24-Nd** and **24-Gd**.

	Total	s	p	d	f	g
			24-Nd			
Nd	3.63878	0.03172	0.01492	0.10303	3.48868	0.00042
O	-0.05041	-0.00744	-0.0444	0.00137	0.00006	
C^{mes}	0.39735	0.04741	0.34335	0.00661		
			24-Gd			
Gd	8.05374	0.7377	0.05963	0.3037	6.95281	-0.00009

REFERENCES

(1) Hitchcock, P. B.; Lappert, M. F.; Maron, L.; Protchenko, A. V. *Angew. Chem. Int. Ed.* **2008**, *47*, 1488-1491.

(2) MacDonald, M. R.; Ziller, J. W.; Evans, W. J. *J. Am. Chem. Soc.* **2011**, *133*, 15914-159147.

(3) MacDonald, M. R.; Bates, J. E.; Fieser, M. E.; Ziller, J. W.; Furche, F.; Evans, W. J. *J. Am. Chem. Soc.* **2012**, *134*, 8420-8423.

(4) MacDonald, M. R.; Bates, J. E.; Ziller, J. W.; Furche, F.; Evans, W. J. *J. Am. Chem. Soc.* **2013**, *135*, 9857-9868.

(5) Fieser, M. E.; MacDonald, M. R.; Krull, B. T.; Bates, J. E.; Ziller, J. W.; Furche, F.; Evans, W. J. *J. Am. Chem. Soc.* **2015**, *137*, 369-382.

(6) MacDonald, M. R.; Fieser, M. E.; Bates, J. E.; Ziller, J. W.; Furche, F.; Evans, W. J. *J. Am. Chem. Soc.* **2013**, *135*, 13310-13313.

(7) Windorff, C. J.; MacDonald, M. R.; Meihaus, M. R.; Ziller, J. W.; Long, J. R.; Evans, W. J. *Chem. Eur. J.* **2016**, *22*, 772-782.

(8) Windorff, C. J.; Chen, G. P.; Cross, J. N.; Evans, W. J.; Furche, F.; Gaunt, A. J.; Janicke, M. T.; Kozimor, S. A.; Scott, B. L. *J. Am. Chem. Soc.* **2017**, *139*, 3970-3973.

(9) Woen, D. H.; Evans, W. J. In *Handbook on the Physics and Chemistry of Rare Earths*; 1st ed.; Elsevier: Amsterdam, 2016; Vol. 50, p 337-394.

(10) Evans, W. J. *Organometallics* **2016**, *35*, 3088-3100.

(11) La Pierre, H. S.; Kameo, H.; Halter, D. P.; Heinemann, F. W.; Meyer, K. *Angew. Chem., Int. Ed.* **2014**, *53*, 7154-7157.

(12) La Pierre, H. S.; Scheurer, A.; Heinemann, F. W.; Hieringer, W.; Meyer, K. *Angew. Chem., Int. Ed.* **2014**, *53*, 7158-7162.

(13) Bradley, D. C.; Mehrotra, R. C.; Rothwell, I. P.; Singh, A. *Alkoxo and Aryloxo Derivatives of Metals*; Academic Press: London, 2001.

(14) Mehrotra, R. C.; Singh, A.; Tripathi, U. M. *Chem. Rev.* **1991**, *91*, 1287-1303.

(15) Boyle, T. J.; Ottley, L. A. M. *Chem. Rev.* **2008**, *108*, 1896-1917.

(16) Hitchcock, P. B.; Lappert, M. F.; Smith, R. G. *Inorg. Chim. Acta.* **1987**, *139*, 183-184.

(17) Stecher, H. A.; Sen, A.; Rheingold, A. L. *Inorg. Chem.* **1988**, *27*, 1130-1132.

(18) Lappert, M. F.; Singh, A.; Smith, R. G. *Inorg. Synth.* **1990**, *27*, 164-168.

(19) Boyle, T. J.; Bunge, S. D.; Clem, P. G.; Richardson, J.; Dawley, J. T.; Ottley, L. A. M.; Rodriguez, M. A.; Tuttle, B. A.; Avilucea, G.; Tissot, R. G. *Inorg. Chem.* **2005**, *44*, 1588-1600.

(20) van den Hende, J. R.; Hitchcock, P. B.; Holmes, S. A.; Lappert, M. F. *J. Chem. Soc., Dalton Trans.* **1995**, 1435-1459.

(21) Boyle, T. J.; Ottley, L. A. M.; Brewer, L. N.; Sigman, J.; Clem, P. G.; Richardson, J. J. *Eur. J. Inorg. Chem.* **2007**, 3805-3815.

(22) Butcher, R. J.; Clark, D. L.; Grumbine, S. K.; Vincent-Hollis, R. L.; Scott, B. L.; Watkin, J. G. *Inorg. Chem.* **1995**, *34*, 5468-5476.

(23) Deacon, G. B.; Fanwick, P. E.; Gitlits, A.; Rothwell, I. P.; Skelton, B. W.; White, A. H. *Eur. J. Inorg. Chem.* **2001**, 1505-1514.

(24) Deacon, G. B.; Feng, T.; Forsyth, C. M.; Gitlits, A.; Hockless, D. C. R.; Shen, Q.; Skelton, B. W.; White, A. H. *J. Chem. Soc., Dalton Trans.* **2000**, 961-966.

(25) Deacon, G. B.; Feng, T.; Skelton, B. W.; White, A. H. *Aust. J. Chem.* **1995**, *48*, 741-756.
(26) Deacon, G. B.; Nickel, S.; Mackinnon, P.; Tiekink, E. R. T. *Aust. J. Chem.* **1990**, *43*, 1245-1257.
(27) Deacon, G. B.; Forsyth, C. M.; Junk, P. C.; Skelton, B. W.; White, A. H. *Chem. -Eur. J.* **1999**, *5*, 1452-1459.
(28) Deacon, G. B.; Junk, P. C.; Moxey, G. J. *Chem. -Asian J.* **2009**, *4*, 1309-1317.
(29) Deacon, G. B.; Feng, T.; Junk, P. C.; Skelton, B. W.; White, A. H. *J. Chem. Soc., Dalton Trans.* **1997**, 1181-1186.
(30) Deacon, G. B.; Fallon, G. D.; Forsyth, C. M.; Harris, S. C.; Junk, P. C.; Skelton, B. W.; White, A. H. *J. Chem. Soc., Dalton Trans.* **2006**, 802-812.
(31) Deacon, G. B.; Gitlits, A.; Junk, P. C.; Skelton, B. W.; White, A. H. *Z. Anorg. Allg. Chem.* **2005**, *631*, 861-865.
(32) Deacon, G. B.; Junk, P. C.; Moxey, G. J.; Ruhlandt-Senge, K.; Prix, C. S.; Zuniga, M. F. *Chem. -Eur. J.* **2009**, *15*, 5503-5519.
(33) Deacon, G. B.; Junk, P. C.; Moxey, G. J. *Chem. -Asian J.* **2009**, *4*, 1717-1728.
(34) Clark, D. L.; Watkin, J. G.; Huffman, J. C. *Inorg. Chem.* **1992**, *31*, 1556-1558.
(35) Yang, L.-W.; Liu, S.; Wong, E.; Rettig, S. J.; Orvig, C. *Inorg. Chem.* **1995**, *34*, 2164-2178.
(36) Edelmann, F. T. *Synthetic Methods of Organometallic and Inorganic Chemistry*; George Thieme Verlag Struttgart: New York, 1997; Vol. 6.
(37) Bergbreiter, D. E.; Killough, J. M. *J. Am. Chem. Soc.* **1978**, *100*, 2126-2134.
(38) APEX2 Version 2014.11-0, Bruker AXS, Inc.; Madison, WI, 2014.
(39) SAINT Version 8.34a, Bruker AXS, Inc.; Madison, WI, 2013.
(40) Sheldrick, G. M.; SADABS, Version 2014/5, Bruker AXS, Inc.: Madison, WI, 2014.
(41) Sheldrick, G. M.; SHELXTL, Version 2014/7, Bruker AXS, Inc.; Madison, WI, 2014.
(42) International Tables for X-Ray Crystallography, 1992, Vol. C., Dordrecht: Kluwer Academic Publishers.
(43) Spek, A. L.; SQUEEZE, Acta Cryst. 2015, C71, 9-19.
(44) Spek, A. L.; PLATON, Acta. Crys. 2009, D65, 148-155.
(45) APEX2 Version 2014.1-1, Bruker AXS, Inc.; Madison, WI, 2014.
(46) Sheldrick, G. M.; SADABS, Version 2014/4, Bruker AXS, Inc.; Madison, WI, 2014.
(47) Sheldrick, G. M.; SHELXTL, Version 2014/6, Bruker AXS, Inc.; Madison, WI, 2014-.
(48) Parsons, S.; Flack, H. D. *Acta Cryst.* **2013**, *B69*, 249-259.
(49) APEX2 Version 2014.9-0, Bruker AXS, Inc.; Madison, WI, 2014.
(50) Tao, J.; Perdew, J. P.; Staroverov, V. N.; Scuseria, G. E. *Phys. Rev. Lett.* **2003**, *91*, 146401.
(51) Grimme, S.; Antony, J.; Ehrlich, S.; Krieg, S. *J. Chem. Phys.* **2010**, *132*, 154104.
(52) Andrae, D.; Hauessermann, U.; Dolg, M.; Stoll, H.; Preuss, H. *Theor. Chim. Acta.* **1990**, *77*, 123-141.
(53) Klamt, A.; Schüürmann, G. J. *J. Chem. Soc. Perkin Trans. 2* **1993**, 799-805.

(54) Furche, F.; Ahlrichs, R.; Hattig, C.; Klopper, W.; Sierka, M.; Weigend, F. *WIREs Comput. Mol. Sci.* **2014**, *4*, 91-100.
(55) Amberger, H.-D.; Reddmann, H.; Guttenberger, C.; Unrecht, B.; Zhang, L.; Apostolidis, C.; Walter, O.; Kanellakopulos, B. *Z. Anorg. Allg. Chem.* **2003**, *629*, 1522-1534.
(56) Skar, H.; Bienfait, A.; Schnitzlbaumer, M.; Törnroos, K. W.; Anwander, R. *Z. Anorg. Allg. Chem.* **2014**, *640*, 604-615.
(57) Steele, L. A. M.; Boyle, T. J.; Kemp, R. A.; Moore, C. *Polyhedron* **2012**, *42*, 258-264.
(58) Hamidi, S.; Deacon, G. B.; Junk, P. C.; Neumann, P. *Dalton Trans.* **2012**, *41*, 3541-3552.
(59) Cotton, F. A.; Schwotzer, W. *J. Am. Chem. Soc.* **1986**, *108*, 4657-4658.
(60) Cotton, F. A.; Schwotzer, W. *Organometallics* **1987**, *6*, 1275-1280.
(61) Fan, B.; Shen, Q.; Lin, Y. *J. Organomet. Chem.* **1989**, *376*, 61-66.
(62) Fan, B.; Shen, Q.; Lin, Y. *J. Organomet. Chem.* **1989**, *377*, 51-58.
(63) Fagina, A. A.; Bochkarev, M. N.; Kozimor, S. A.; Ziller, J. W.; Evans, W. J. *Z. Anorg. Allg. Chem.* **2005**, *631*, 2848-2853.
(64) Liang, H.; Shen, Q.; J., G.; Lin, Y. *J. Organomet. Chem.* **1994**, *474*, 113-116.
(65) Liu, S.; Ziller, J. W.; Zhang, Y. Q.; Wang, B. W.; Evans, W. J.; Gao, S. *Chem. Commun.* **2014**, *50*, 11418-11420.
(66) Liu, Q.; Lin, Y. H.; Shen, Q. *Acta Crystallogr., Sect. C: Cryst. Struct. Commun.* **1997**, *53*, 1579-1580.
(67) Filatov, A. S.; Gifford, S. N.; Kumara, D. K.; Petrukhina, M. A. *Acta Crystallogr., Sect. E: Cryst. Struct. Commun.* **2009**, *65*, m286-m287.
(68) Filatov, A. S.; Rogachev, A. Y.; Petrukhina, M. A. *J. Mol. Struct.* **2008**, *890*, 116-122.
(69) Liang, H.; Shen, Q.; Jin, S.; Lin, Y. *J. Chem. Soc., Chem. Commun.* **1992**, 480-481.
(70) Yao, Y.-M.; Zhang, Y.; Shen, Q.; Liu, Q.-C.; Meng, Q.-J.; Lin, Y.-H. *Chin. J. Chem.* **2001**, *19*, 588-592.
(71) Piper, T. S.; Wilkinson, G. *J. Inorg. Nucl. Chem.* **1956**, *3*, 104-124.
(72) Corbey, J. F.; Woen, D. H.; Palumbo, C. T.; Fieser, M. E.; Ziller, J. W.; Furche, F.; Evans, W. J. *Organometallics* **2015**, *34*, 3909-3921.
(73) Morss, L. R. *Chem. Rev.* **1976**, *76*, 827-841.
(74) Jaroschik, F.; Momin, A.; Nief, F.; Le Goff, X. F.; Deacon, G. B.; Junk, P. C. *Angew. Chem. Int. Ed.* **2009**, *48*, 1117-1121.
(75) Crosswhite, H. M.; Crosswhite, H.; Carnall, W. T.; Paszek, A. P. *J. Chem. Phys.* **1980**, *72*, 5103-5117.
(76) Weigend, F.; Ahlrichs, R. *Phys. Chem. Chem. Phys.* **2005**, *7*, 3297-3305.
(77) Schafer, A.; Horn, H.; Ahlrichs, R. *J. Chem. Phys.* **1992**, *97*, 2571-2577.

CHAPTER 7

Metal Versus Ligand Reduction in Ln^{3+} Complexes of a Mesitylene-Anchored Tris(Aryloxide) Ligand

INTRODUCTION†

As described in Chapters 1-6, studies of rare-earth metal reductive chemistry have revealed that +2 ions can be isolated for all the lanthanide elements except for promethium, which was not studied due to its radioactivity.[1-7] The number of Ln^{2+} ions known to form molecular complexes in solution in 2000, namely Ln = Eu, Yb, Sm, Tm, Nd, and Dy, was extended to nine new examples with Ln = La, Ce, Pr, Gd, Tb, Y, Ho, Er, and Lu,[1-5] *via* reduction of tris(cyclopentadienyl) rare-earth metal complexes, $[Cp'_3Ln]$ and $[Cp''_3Ln]$ (where $Cp' = C_5H_4SiMe_3$; $Cp'' = C_5H_3(SiMe_3)_2$), with KC_8 in the presence of a chelate such as 2.2.2-cryptand, eq 7.1.[1-10] This synthetic protocol provided

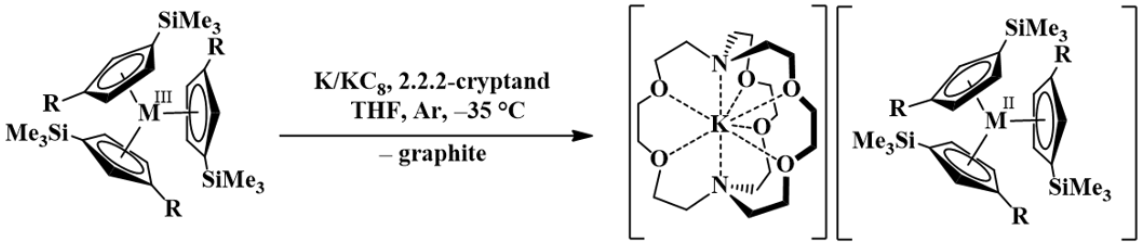

(7.1)

R = $SiMe_3$; M = La, Th, U, Pu
R = H; M = Y, La, Ce, Pr, Nd, Sm, Gd, Tb, Dy, Ho, Er, Tm, Lu, U

the complexes $(Cp'_3Ln)^{1-}$ and $(Cp''_3Ln)^{1-}$ that possess structural, spectroscopic, and magnetic properties consistent with reduction of the $4f^n$ Ln^{3+} precursors to form $4f^n5d^1$ Ln^{2+} ions rather than the traditional $4f^{n+1}$ Ln^{2+} electron configurations, previously found for Eu, Yb, Sm, Tm, Nd, and Dy. Density functional theory (DFT) calculations indicated that in these tris(cyclopentadienyl)

ligand environments, the energies of the $5d_z^2$ and 4*f* orbitals were such that the $4f^n5d^1$ electron configuration is the ground state for the complexes of La, Ce, Pr, Gd, Tb, Y, Ho, Er, and Lu.[1-4]

However, two of the traditional Ln^{2+} ions, namely Dy and Nd, were found to also adopt the $4f^n5d^1$ electron configuration, which showed that the ground state could vary depending on ligand environment.[5] Hence, three classes of divalent lanthanide complexes were identified in this tris(cyclopentadienyl) ligand environment: the traditional $4f^{n+1}$ ions of Eu, Yb, Sm, and Tm, the new $4f^n5d^1$ ions of La, Ce, Pr, Gd, Tb, Y, Ho, Er, and Lu, and the two configurational crossover ions of Dy and Nd, which could adopt either configuration depending on the ligand environment. These classes were consistent with the $4f^{n+1}$ to $4f^n5d^1$ promotion energies found in the gas phase for Ln^{2+}.[11] Eu, Yb, Sm, and Tm have the highest promotion energies and La, Ce, Gd, and Tb have the lowest. The configurational crossover ions, Dy and Nd, possess promotion energies in between those of the two groups. Pr, Ho, and Er have similar promotion energies to Dy and Nd, so it seems possible that they could also be crossover ions.[12,13]

Configuration crossover was also identified for U^{2+}, where the tris(aryloxide)arene U^{3+} complex, [((^{Ad,Me}ArO)$_3$mes)U], **23-U**, was reduced to the U^{2+} complex, [K(crypt)][((^{Ad,Me}ArO)$_3$mes)U], **24-U**, eq 7.2.[14,15] The physical properties and DFT analysis of **24-U**

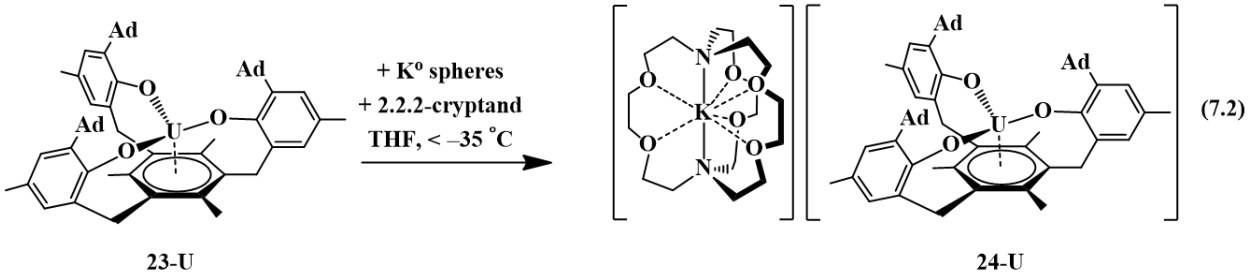

23-U **24-U**

were consistent with an S = 2, $5f^4$ ground state for U^{2+}. This is in contrast to U^{2+} in

[K(crypt)][Cp′$_3$U],[8] eq 7.1, and [K(crypt)][Cp″$_3$U],[9] for which the $5f^36d^1$ ground state was identified.

As described in Chapter 6, in order to investigate the generality of $((^{Ad,Me}ArO)_3mes)^{3-}$ vs. $(Cp')^{3-}$ in stabilizing f^{n+1} vs f^nd^1 configurations, the complexes [Ln($(^{Ad,Me}OAr)_3$mes)], **23-Ln**, with Ln = Nd, Gd, Dy, and Er, were synthesized and the electronic structure of their reduction products to [K(2.2.2-cryptand)]–[($(^{Ad,Me}ArO)_3$mes)Ln], **24-Ln**, was examined. Only in the case of Nd, was **24-Ln** obtained as a pure Ln^{2+} complex, eq 7.3. For the other

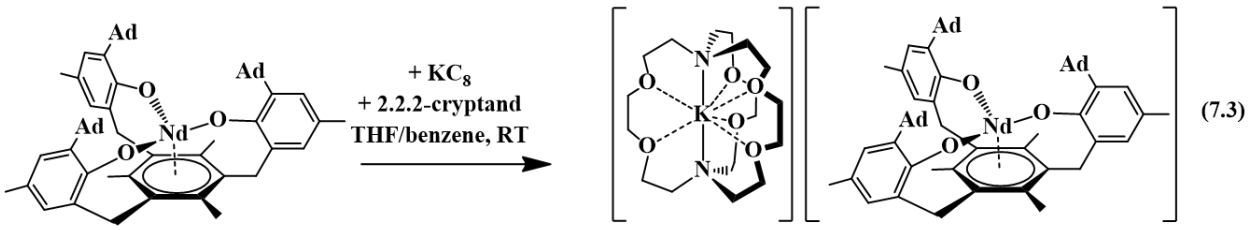

23-Nd **24-Nd**

Ln ions, the reduction products were obtained as co-crystallized mixtures of the Ln^{2+} complex, **24-Ln**, with a Ln^{3+} hydride, [K(2.2.2-cryptand)][($(^{Ad,Me}ArO)_3$mes)LnH], **25-Ln**, eq 7.4.

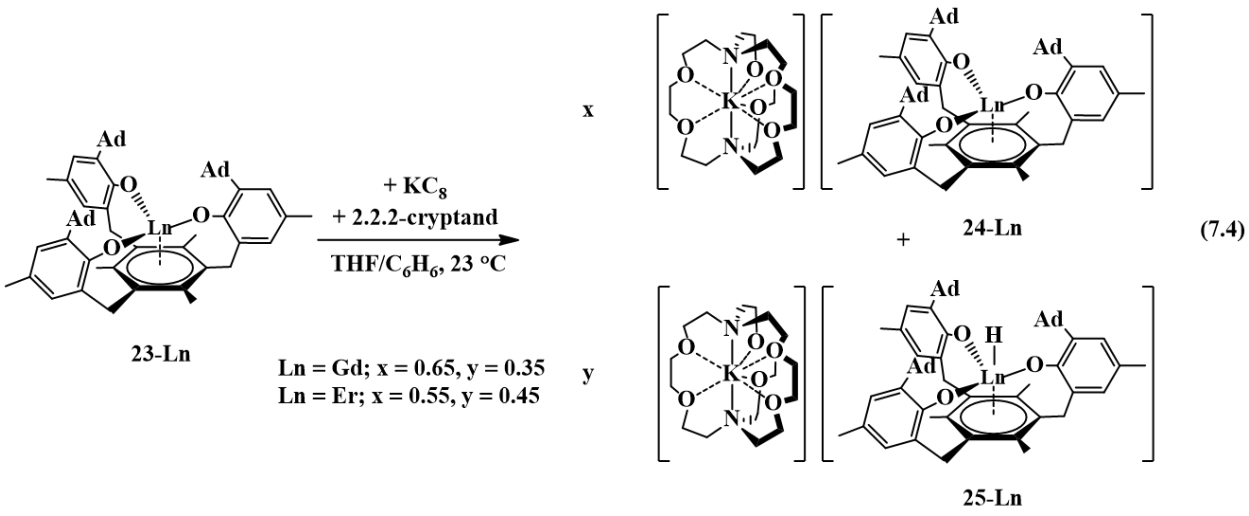

23-Ln

Ln = Gd; x = 0.65, y = 0.35
Ln = Er; x = 0.55, y = 0.45

24-Ln

25-Ln

This Chapter describes what could have been a routine expansion of equations 3 and 4 to the early lanthanides, La, Ce, and Pr, as well as to Sm and Yb, two ions known to form complexes with the traditional Ln^{2+} $4f^{n+1}$ electron configurations. However, this study has revealed significant differences from the complexes previously described in Chapter 6 and reveals an additional aspect of the redox-flexibility of the tris(aryloxide)mesitylene ligand. The synthesis, structure, and spectroscopy of the new complexes are reported here along with density functional theory calculations in collaboration with the Furche group.

EXPERIMENTAL

The syntheses and manipulations described below were conducted under argon with rigorous exclusion of air and water using glovebox, vacuum line, and Schlenk techniques. Solvents were sparged with ultrahigh purity (UHP) grade argon (Airgas) and passed through columns containing Q-5 and molecular sieves before use. NMR solvents (Cambridge Isotope Laboratories) were dried over NaK/benzophenone, degassed by three freeze−pump−thaw cycles, and vacuum-transferred before use. Anhydrous $[Ln(N(SiMe_3)_2)]_3$ (Ln = La, Ce, Pr, Sm, Yb),[16] KC_8,[17] and $((^{Ad,Me}ArOH)_3mes)$,[15] were prepared according to literature-reported procedures. 2.2.2-Cryptand, 4,7,13,16,21,24-hexaoxa-1,10- diazabicyclo[8.8.8]hexacosane (Acros Organics), was placed under vacuum (10^{-3} Torr) for 12 h before use. ^{1}H NMR (500 MHz) and ^{13}C NMR (125 MHz) spectra were obtained on a Bruker GN500 or CRYO500 MHz spectrometer at 298 K. IR samples were prepared as KBr pellets, and the spectra were obtained on a Varian 1000 FT-IR spectrometer. Elemental analyses were performed on a PerkinElmer 2400 series II CHNS elemental analyzer. Electronic absorption spectra were obtained in THF or benzene at 298 K using a Varian Cary 50 Scan UV−vis or Jasco V-670 UV/Vis/NIR/MIR absorption spectrometer. EPR spectra were collected using X-band frequency (9.3-9.8 GHz) on either (a) a Bruker EMX

spectrometer equipped with an ER041XG microwave bridge and the magnetic field was calibrated with DPPH (g = 2.0036) or (b) a JEOL CW spectrometer, JESFA200, equipped with an X-band Gunn diode oscillator bridge, a cylindrical mode cavity, as well as a nitrogen cryostat. Spectra were simulated with the program W95EPR.[18]

[(^{Ad,Me}ArO)$_3$mes)La], 23-La. In an argon-filled glovebox, a sealable 100 mL side arm Schlenk flask equipped with a greaseless stopcock was charged with a solution of (^{Ad,Me}ArOH)$_3$mes (100 mg, 0.113 mmol) in benzene (40 mL) and a magnetic stir bar. A solution of [La(N(SiMe$_3$)$_2$)]$_3$ (71 mg, 0.114 mmol) in benzene (40 mL) was slowly added to the stirred solution. Note: Higher concentrations results in precipitation of solids and low yields. The flask was attached to a Schlenk line and the mixture was stirred and heated to reflux for 18 h. The flask was brought back into the glovebox, the solution was filtered, and the solvent was removed from the colorless filtrate under vacuum. The resulting colorless solid was washed with hexane. The solids were extracted in benzene (15 mL). Hexane (5 mL) was added to the benzene solution and removal of solvent under vacuum afforded **23-La** as a colorless solid (59 mg, 51%). Colorless single crystals of **23-La**, suitable for X-ray diffraction, were grown from slow evaporation of a C_6D_6 solution. ^{1}H NMR (C_6D_6): δ 7.04 (br s, Ar*H*, 3H), 6.83 (br s, Ar*H*, 3H), 3.80 (s, benzylic C*H*$_2$, 6H), 2.41 (s, *Me*, 9H), 2.30 (br s, Ad C*H*$_2$, 18), 2.14 (br s, *Me*, 9H), 2.06 (br s, Ad C*H*, 9H), 1.82 (br m, Ad C*H*$_2$, 18H). ^{13}C NMR (C_6D_6): δ 158.5, 145.07, 137.4, 136.2, 129.5, 125.5, 41.9, 38.2, 37.4, 36.5, 29.7, 21.4, 21.4, 18.3, 15.6. IR: 3065w, 3019w, 3014w, 2911s, 2850s, 2734w, 2678w, 2654w, 1735w, 1601w, 1569w, 1495m, 1451s, 1375m, 1367m, 1342m, 1315m, 1283s, 1250s, 1200m, 1184m, 1162m, 1111w, 1100m, 1071m, 1036m, 1015m, 1006m, 980m, 960m, 930w, 915m, 878w, 852s, 820s, 808s, 762m, 750m, 728m, 694m, 667w, 661w, 604m cm^{-1}. Anal. Calcd for $C_{63}H_{75}LaO_3$: C, 74.24; H, 7.42. Found: C, 74.51; H, 7.59.

[(^{Ad,Me}ArO)$_3$mes)Ce], 23-Ce. As described for **23-La**, a solution of [Ce(N(SiMe$_3$)$_2$)]$_3$ (152 mg, 0.245 mmol) in benzene (40 mL) was slowly added to a stirred solution of (^{Ad,Me}ArOH)$_3$mes (200 mg, 0.226 mmol) in benzene (40 mL) to afford **23-Ce** as a pale green solid (199 mg, 80%). ^{1}H NMR (C_6D_6): δ 9.97 (br s, 3H), 7.72 (br s, 3H), 3.79 (br s, 9H), 3.00 (br s, 18H), 1.47 (br s, 6H), 0.63 (br s, 9H), −1.03 (br s, 9H), −1.56 (br s, 9H), −5.01 (br s, 9H). IR: 3069w, 3034w, 2905s, 2847s, 2731w, 2677w, 2654w, 1730w, 1601w, 1562w, 1493w, 1445s, 1375m, 1354m, 1342m, 1313m, 1283s, 1240s, 1202m, 1184m, 1161m, 1115w, 1101m, 1072w, 1034w, 1017m, 1005w, 980m, 961w, 924w, 914m, 880w, 853s, 833m, 821s, 808s, 787m, 762m, 750m, 729m, 694w, 677m, 662w, 604m, 577m, 517s cm^{-1}. Anal. Calcd for $C_{63}H_{75}CeO_3$: C, 74.16; H, 7.41. Found: C,74.03; H, 7.57.

[(^{Ad,Me}ArO)$_3$mes)Pr], 23-Pr. As described for **23-La**, a solution of [Pr(N(SiMe$_3$)$_2$)]$_3$ (148 mg, 0.238 mmol) in benzene (40 mL) was slowly added to a stirred solution of (^{Ad,Me}ArOH)$_3$mes (200 mg, 0.226 mmol) in benzene (40 mL) to afford **23-Pr** as a pale colorless solid (206 mg, 89%). Colorless single crystals of **23-Pr**, suitable for X-ray diffraction, were grown from an Et_2O/hexane solution at −35 °C. ^{1}H NMR (C_6D_6): δ 17.11 (br s, 3H), 10.80 (br s, 3H), 7.48 (br s, 9H), 4.26 (br s, 18H), −0.74 (br s, 9H), −1.30 (br s, 9H), −8.19 (br s, 9H), −9.37 (br s, 9H), −20.81 (br s, 6H). IR: 3069w, 3034w, 2905s, 2847s, 2731w, 2677w, 2654w, 1730w, 1601w, 1562w, 1493w, 1445s, 1375m, 1354m, 1342m, 1313m, 1283s, 1240s, 1202m, 1184m, 1161m, 1115w, 1101m, 1072w, 1034w, 1017m, 1005w, 980m, 961w, 924w, 914m, 880w, 853s, 833m, 821s, 808s, 787m, 762m, 750m, 729m, 694w, 677m, 662w, 604m, 577m, 517s cm^{-1}. Anal. Calcd for $C_{63}H_{75}O_3Pr$: C, 74.10; H, 7.40. Found: C, 74.11; H, 7.11.

[(^{Ad,Me}ArO)$_3$mes)Sm], 23-Sm. As described for **23-La**, a solution of [Sm(N(SiMe$_3$)$_2$)]$_3$ (150 mg, 0.238 mmol) in benzene (20 mL) was slowly added to a stirred solution of

(^{Ad,Me}ArOH)$_3$mes (200 mg, 0.226 mmol) in benzene (20 mL) to afford **23-Sm** as a pale yellow solid (156 mg, 67%). Pale yellow single crystals of **23-Sm**, suitable for X-ray diffraction, were grown from an Et_2O/hexane solution at −35 °C. ^{1}H NMR (C_6D_6): δ 8.06 (br s, 3H), 7.29 (br s, 3H), 2.84 (br s, 9H), 2.69 (br s, 6H), 2.56 (br s, 18H), 2.23 (br s, 9H), 0.78 (br s, 9H) 0.34 (br d, 9H), −1.23 (br d, 9H). IR: 3071w, 3034w, 2899s, 2847s, 2675s, 2652w, 1728w, 1603w, 1560w, 1447s, 1375m, 1354m, 1343m, 1306m, 1285s, 1246s, 1207m, 1184m, 1163m, 1101w, 1064w, 1034w, 1018w, 980w, 961w, 914w, 853w, 833m, 820m, 808s, 766w, 748w, 729m, 694w, 669m, 604w, 579w, 559w, 523s, 465w, 413m cm^{-1}. Anal. Calcd for $C_{63}H_{75}O_3Sm$: C,73.42; H, 7.33. Found: C, 73.69; H, 7.63.

[(^{Ad,Me}ArO)$_3$mes)Yb], 23-Yb. As described for **23-La**, a solution of [Yb(N(SiMe$_3$)$_2$)]$_3$ (156 mg, 0.238 mmol) in benzene (20 mL) was slowly added to a stirred solution of (^{Ad,Me}ArOH)$_3$mes (200 mg, 0.226 mmol) in benzene (20 mL afforded **23-Yb** as an orange solid (161 mg, 68%). Pale orange single crystals of **23-Yb**, suitable for X-ray diffraction, were grown from an Et_2O/hexane solution at −35 °C. IR: 3076w, 3023w, 2902s, 2846s, 2729w, 2677w, 2654w, 1736w, 1603w, 1566w, 1494w, 1447s, 1377m, 1366m, 1356m, 1343m, 1317m, 1307w, 1283s, 1240s, 1209w, 1202m, 1177m, 1163m, 1147m, 1102m, 1058w, 1036w, 1017m, 1006w, 976m, 961w, 924w, 916m, 880w, 856s, 834m, 819s, 810s, 786m, 765m, 748w, 728m, 694w, 679m, 652w, 642w, 619w, 611w, 605w cm^{-1}. Anal. Calcd for $C_{63}H_{75}O_3Yb$: C, 71.84; H, 7.18. Found: C, 71.77; H, 7.21.

[K(2.2.2-cryptand)][((^{Ad,Me}ArO)$_3$mes)La], 24-La. In an argon-filled glovebox, a scintillation vial was charged with a THF solution (2 mL) of [(^{Ad,Me}ArO)$_3$mes)La], **23-La** (20 mg, 20 μmol), and 2.2.2-cryptand (7 mg, 20 μmol) and the mixture was prechilled in the glovebox freezer (−35 °C). Potassium (excess) was added and the mixture was stored overnight in the

glovebox freezer. The resultant dark-red solution was filtered through a prechilled pipette packed with glass wool into a vial containing prechilled Et_2O (8 mL) so that upon exiting the pipette, the dark-red solution was under a layer of Et_2O. The mixture was then stored in the glovebox freezer and after 48 h, diffusion of Et_2O into the dark-red solution yielded dark red single crystals of **24-La** suitable for X-ray diffraction (12 mg, 43%). IR: 3067w, 2965m, 2897s, 2847s, 2814m, 2731w, 2675w, 2652w, 1730w, 1599w, 1560m, 1478m, 1445s, 1385m, 1358m, 1354s, 1343m, 1314m, 1281s, 1258s, 1256s, 1251s, 1210w, 1184w, 1175w, 1163w, 1134m, 1105s, 1076m, 1059m, 1047m, 1028w, 1000w, 980w, 951m, 934m, 918w, 903w, 871w, 856m, 831m, 822m, 802m, 783w, 770w, 758w, 748m, 708w, 700w, 691w, 679w, 677w, 665w, 661w cm^{-1}. UV-vis (THF) λ_{max} nm (ε, M^{-1} cm^{-1}): 340 (3500 shoulder), 325 (2600 shoulder), 416, (3200 shoulder), 460 (2100 shoulder). Anal. Calcd for $C_{81}H_{111}KLaN_2O_9$: C, 67.81; H, 7.80; N, 1.95. Found: C, 65.69; H, 7.65; N, 1.69. Incomplete combustion was observed in multiple samples.

[K(2.2.2-cryptand)][((^{Ad,Me}ArO)$_3$mes)Ce], 24-Ce. As described for **24-La**, [(^{Ad,Me}ArO)$_3$mes)Ce], **23-Ce**, (20 mg, 20 μmol) and 2.2.2-cryptand (7 mg, 20 μmol) were dissolved in THF (2 mL) and stored with potassium (excess) overnight in the glovebox freezer to produce dark-red crystals of **24-Ce** suitable for X-ray diffraction (4 mg, 14%). UV-vis (THF) λ_{max} nm (ε, M^{-1} cm^{-1}): 350 (1300 shoulder), 420 (3400), 490 (1000 shoulder). IR: 2960m, 2894s, 2842s, 2813m, 2725w, 2675w, 2652w, 1729w, 1598w, 1552m, 1475m, 1445s, 1397w, 1373w, 1360m, 1354m, 1341m, 1316m, 1291s, 1282s, 1258s, 1244m, 1213w, 1184w, 1178w, 1166w, 1133s, 1105s, 1076m, 1061m, 1049w, 1027w, 1009w, 980w, 950m, 932m, 912w, 901w, 874w, 854m, 830w, 818m, 801m, 782w, 774w, 769w, 762w, 750m, 734w, 70ww, 678w, 665w, 642w cm^{-1}. Anal. Calcd for $C_{81}H_{111}CeKN_2O_9$: C, 67.75; H, 7.79; N, 1.95. Found: C, 61.71; H, 7.09; N, 1.68. Incomplete combustion was observed in multiple samples.

[K(2.2.2-cryptand)][((^{Ad,Me}ArO)$_3$mes)Pr], 24-Pr. As described for **24-La**, [(^{Ad,Me}ArO)$_3$mes)Pr], **23-Pr**, (50 mg, 49 μmol) and 2.2.2-cryptand (18 mg, 49 μmol) were dissolved in THF (2 mL) and stored with potassium (excess) overnight in the glovebox freezer to produce dark-red crystals of **24-Pr** suitable for X-ray diffraction (11 mg, 16%). IR: 3067w, 2967m, 2901s, 2845s, 2814m, 2727w, 2677w, 2654w, 1730w, 1599w, 1560m, 1478m, 1445s, 1398w, 1375w, 1361m, 1354m, 1342m, 1314m, 1288s, 1277s, 1252s, 1207w, 1184w, 1175w, 1163w, 1134m, 1107s, 1078m, 1061m, 1045m, 1032w, 1001w, 980w, 951m, 934m, 914w, 901w, 874w, 856m, 831m, 820m, 802m, 783w, 768w, 750m, 700w, 689w, 665w cm^{-1}. UV-vis (THF) λ_{max} nm (ε, M^{-1} cm^{-1}): 347 (1300 shoulder), 430 (3300), 498 (1000 shoulder). Anal. Calcd for $C_{81}H_{111}KN_2O_9Pr$: C, 67.71; H, 7.79; N, 1.95. Found: C, 63.89; H, 7.59; N, 1.67. Incomplete combustion was observed in multiple samples.

[K(2.2.2-cryptand)][((^{Ad,Me}ArO)$_3$mes)Sm], 24-Sm. [(^{Ad,Me}ArO)$_3$mes)Sm], **23-Sm**, (30 mg, 29 μmol) and 2.2.2-cryptand (11 mg, 29 μmol) were dissolved in THF (2 mL) and stirred. To the yellow solution as added KC_8 (6 mg, 43 μmol) and the mixture immediately turned purple. The purple solution was filtered, layered with Et_2O (10 mL), and stored in the glovebox freezer to produce purple crystals of **24-Sm·Et$_2$O** suitable for X-ray diffraction (9 mg, 20%). IR: 3067w, 2965m, 2900s, 2846s, 2812m, 2727w, 2676w, 2652w, 1732w, 1601w, 1560m, 1475m, 1446s, 1398w, 1384m, 1374w, 1361m, 1354m, 1341m, 1315m, 1290s, 1277s, 1258s, 1246s, 1207w, 1183w, 1175w, 1163w, 1133m, 1106s, 1079m, 1061m, 1045m, 1034w, 1021w, 1001w, 981w, 950m, 938m, 915w, 901w, 889w, 883w, 879w, 873w, 867w, 857m, 838m, 831s, 826m, 820m, 816m 804m, 783w, 768w, 750m, 745w cm^{-1}. UV-vis(THF) λ_{max} nm (ε, M^{-1} cm^{-1}): 355 (900 shoulder), 390 (420). Anal. Calcd for $C_{85}H_{121}N_2O_{10}KSm$: C, 67.15; H, 8.02; N, 1.84. Found: 63.99; H, 7.78; N, 1.25. Incomplete combustion was observed in multiple samples.

[K(2.2.2-cryptand)][((^{Ad,Me}ArO)$_3$mes)Yb], 24-Yb. [(^{Ad,Me}ArO)$_3$mes)Yb], **23-Yb**, (30 mg, 28 μmol) and 2.2.2-cryptand (11 mg, 28 μmol) were dissolved in THF (2 mL) and stirred. To the orange solution was added KC_8 (6 mg, 43 μmol) and the mixture immediately turned green. The green solution was filtered, layered with Et_2O (10 mL), and stored in the glovebox freezer to produce purple crystals of **24-Yb·Et$_2$O** suitable for X-ray diffraction (10 mg, 23%). IR: 3067w, 2960m, 2900s, 2846s, 2814m, 2730w, 2676w, 2652w, 1730w, 1601w, 1555w, 1471m, 1447s, 1398w, 1384m, 1374w, 1361m, 1354m, 1342m, 1317m, 1292s, 1277s, 1258s, 1248s, 1207w, 1185w, 1162w, 1133m, 1106s, 1079m, 1060m, 1045m, 1030w, 1014w, 998w, 980w, 950m, 938m, 915w, 905w, 889w, 883w, 876w, 866w, 855m, 838m, 831s, 826m, 820m, 810m 802m, 783w, 768w, 750m cm^{-1}. UV-vis (THF) λ_{max} nm (ε, M^{-1} cm^{-1}): 345 (990 shoulder), 400 (700), 470 (320 shoulder), 700 (200). Anal. Calcd for $C_{85}H_{121}N_2O_{10}KYb$: C, 66.16; H, 7.90; N, 1.82. Found: 63.77; H, 8.09; N, 1.69. The low solubility of crystals of **24-Yb** precluded NMR analysis. Attempts to generate **24-Yb** *in situ* for analysis by NMR were unsuccessful due to the immediate crystallization of **24-Yb** in the NMR tube.

X-ray Data Collection, Structure Solution and Refinement for [(^{Ad,Me}ArO)$_3$mes)La], 23-La. A colorless crystal of approximate dimensions 0.175 x 0.162 x 0.060 mm was mounted on a glass fiber and transferred to a Bruker SMART APEX II diffractometer. The APEX2[19] program package was used to determine the unit-cell parameters and for data collection (90 sec/frame scan time for a sphere of diffraction data). The raw frame data was processed using SAINT[20] and SADABS[21] to yield the reflection data file. Subsequent calculations were carried out using the SHELXTL[22] program. The diffraction symmetry was 2/*m* and the systematic absences were consistent with the monoclinic space group $P2_1/c$ that was later determined to be correct. The structure was solved by direct methods and refined on F^2 by full-matrix least-squares

techniques. The analytical scattering factors[23] for neutral atoms were used throughout the analysis. Hydrogen atoms were included using a riding model. At convergence, wR2 = 0.0726 and Goof = 1.039 for 610 variables refined against 11962 data (0.75 Å), R1 = 0.0315 for those 10110 data with I > 2.0σ(I). Details are given in Table 7.1.

X-ray Data Collection, Structure Solution and Refinement for [(^{Ad,Me}ArO)$_3$mes)Pr], 23-Pr. A yellow crystal of approximate dimensions 0.100 x 0.137 x 0.337 mm was mounted in a cryoloop and transferred to a Bruker SMART APEX II diffractometer. The APEX2[24] program package was used to determine the unit-cell parameters and for data collection (90 sec/frame scan time for a hemisphere of diffraction data). The raw frame data was processed using SAINT[20] and SADABS[25] to yield the reflection data file. Subsequent calculations were carried out using the SHELXTL[26] program. The diffraction symmetry was 2/*m* and the systematic absences were consistent with the monoclinic space group $P2_1/c$ that was later determined to be correct. The structure was solved by direct methods and refined on F^2 by full-matrix least-squares techniques. The analytical scattering factors[23] for neutral atoms were used throughout the analysis. Hydrogen atoms were included using a riding model. Least-squares analysis yielded wR2 = 0.1265 and Goof = 1.015 for 610 variables refined against 10621 data (0.78Å), R1 = 0.0523 for those 7114 data with I > 2.0σ(I). Details are given in Table 7.1.

X-ray Data Collection, Structure Solution and Refinement for [(^{Ad,Me}ArO)$_3$mes)Sm], 23-Sm. A yellow crystal of approximate dimensions 0.097 x 0.143 x 0.276 mm was mounted in a cryoloop and transferred to a Bruker SMART APEX II diffractometer. The APEX2[24] program package was used to determine the unit-cell parameters and for data collection (20 sec/frame scan time for a sphere of diffraction data). The raw frame data was processed using SAINT[20] and SADABS[25] to yield the reflection data file. Subsequent calculations were carried out using the

SHELXTL[26] program. The diffraction symmetry was 2/*m* and the systematic absences were consistent with the monoclinic space group $P2_1/c$ that was later determined to be correct. The structure was solved by direct methods and refined on F^2 by full-matrix least-squares techniques. The analytical scattering factors[23] for neutral atoms were used throughout the analysis. Hydrogen atoms were included using a riding model. At convergence, wR2 = 0.0658 and Goof = 1.000 for 610 variables refined against 13192 data (0.78Å), R1 = 0.0286 for those 10480 data with I > 2.0σ(I). There were several high residuals present in the final difference-Fourier map. It was not possible to determine the nature of the residuals although it was probable that diethyether, tetrahydrofuran or hexane solvents were present. The SQUEEZE[27] routine in the PLATON[28] program package was used to account for the electrons in the solvent accessible voids. Details are given in Table 7.1.

X-ray Data Collection, Structure Solution and Refinement for [(^{Ad,Me}ArO)$_3$mes)Yb], 23-Yb. An orange crystal of approximate dimensions 0.118 x 0.200 x 0.254 mm was mounted in a cryoloop and transferred to a Bruker SMART APEX II diffractometer. The APEX2[24] program package was used to determine the unit-cell parameters and for data collection (60 sec/frame scan time for a sphere of diffraction data). The raw frame data was processed using SAINT[20] and SADABS[25] to yield the reflection data file. Subsequent calculations were carried out using the SHELXTL[26] program. There were no systematic absences nor any diffraction symmetry other than the Friedel condition. The centrosymmetric triclinic space group $P\bar{1}$ was assigned and later determined to be correct. The structure was solved by direct methods and refined on F^2 by full-matrix least-squares techniques. The analytical scattering factors[23] for neutral atoms were used throughout the analysis. Hydrogen atoms were included using a riding model. There were two molecules of the formula-unit present and one-half molecule of diethylether solvent and one-

quarter molecule of hexane solvent. The hexane molecule was located about an inversion center. At convergence, wR2 = 0.0986 and Goof = 1.021 for 1279 variables refined against 24713 data (0.80 Å), R1 = 0.0414 for those 17489 data with I > 2.0σ(I). There were several high residuals present in the final difference-Fourier map. It was not possible to determine the nature of the residuals although it was probable that diethylether, hexane, toluene and tetrahydrofuran solvents were present. The SQUEEZE[27] routine in the PLATON[28] program package was used to account for the electrons in the solvent accessible voids. Details are given in Table 7.1.

X-ray Data Collection, Structure Solution and Refinement for [K(2.2.2-cryptand)][(^{Ad,Me}ArO)$_3$mes)La], 24-La. A red crystal of approximate dimensions 0.093 x 0.112 x 0.202 mm was mounted in a cryoloop and transferred to a Bruker SMART APEX II diffractometer. The APEX2[19] program package was used to determine the unit-cell parameters and for data collection (90 sec/frame scan time for a hemisphere of diffraction data). The raw frame data was processed using SAINT[20] and SADABS[25] to yield the reflection data file. Subsequent calculations were carried out using the SHELXTL[26] program. The systematic absences were consistent with the cubic space group $P2_13$ that was later determined to be correct. The structure was solved by direct methods and refined on F^2 by full-matrix least-squares techniques. The analytical scattering factors[23] for neutral atoms were used throughout the analysis. Hydrogen atoms were included using a riding model. The molecule and counter-ion were located on three-fold rotation axes. Least-squares analysis yielded wR2 = 0.1686 and Goof = 1.063 for 285 variables refined against 4391 data (0.85), R1 = 0.0577 for those 3523 data with I > 2.0σ(I). The absolute structure was assigned by refinement of the Flack parameter.[29] Details are given in Table 7.2.

X-ray Data Collection, Structure Solution and Refinement for [K(2.2.2-cryptand)][(^{Ad,Me}ArO)$_3$mes)Ce], 24-Ce. A red crystal of approximate dimensions 0.158 x 0.272 x 0.330 mm was mounted in a cryoloop and transferred to a Bruker SMART APEX II diffractometer. The APEX2[24] program package was used to determine the unit-cell parameters and for data collection (60 sec/frame scan time for a sphere of diffraction data). The raw frame data was processed using SAINT[20] and SADABS[25] to yield the reflection data file. Subsequent calculations were carried out using the SHELXTL[26] program. The systematic absences were consistent with the cubic space group $P2_13$ that was later determined to be correct. The structure was solved by direct methods and refined on F^2 by full-matrix least-squares techniques. The analytical scattering factors[23] for neutral atoms were used throughout the analysis. Hydrogen atoms were included using a riding model. The molecule and counter-ion were located on three-fold rotation axes. The cerium atom was disordered approximately 0.95:0.05 and included with two components to account for the disorder. Ce(2) was assigned an isotropic thermal parameter. At convergence, wR2 = 0.0852 and Goof = 1.155 for 287 variables refined against 4923 data (0.82), R1 = 0.0378 for those 4709 data with $I > 2.0\sigma(I)$. The absolute structure was assigned by refinement of the Flack parameter.[29] There were several high residuals present in the final difference-Fourier map. It was not possible to determine the nature of the residuals although it was probable that diethylether or tertahydrofuran was present. The SQUEEZE[27] routine in the PLATON[28] program package was used to account for the electrons in the solvent accessible voids. Details are given in Table 7.2.

X-ray Data Collection, Structure Solution and Refinement for [K(2.2.2-cryptand)][(^{Ad,Me}ArO)$_3$mes)Pr], 24-Pr. A red crystal of approximate dimensions 0.185 x 0.244 x 0.352 mm was mounted in a cryoloop and transferred to a Bruker SMART APEX II diffractometer. The APEX2[24] program package was used to determine the unit-cell parameters and for data collection (60 sec/frame scan time for a sphere of diffraction data). The raw frame data was processed using SAINT[20] and SADABS[25] to yield the reflection data file. Subsequent calculations were carried out using the SHELXTL[26] program. The systematic absences were consistent with the cubic space group $P2_13$ that was later determined to be correct. The structure was solved by direct methods and refined on F^2 by full-matrix least-squares techniques. The analytical scattering factors[23] for neutral atoms were used throughout the analysis. Hydrogen atoms were included using a riding model. The molecule and counter-ion were located on three-fold rotation axes. The praseodymium atom was disordered approximately 0.96:0.04 and included with two components to account for the disorder. Pr(2) was assigned an isotropic thermal parameter. At convergence, wR2 = 0.0897 and Goof = 1.175 for 287 variables refined against 4872 data (0.82), R1 = 0.0367 for those 4729 data with $I > 2.0\sigma(I)$. The absolute structure was assigned by refinement of the Flack parameter.[28] There were several high residuals present in the final difference-Fourier map. It was not possible to determine the nature of the residuals although it was probable that diethylether or tertahydrofuran was present. The SQUEEZE[27] routine in the PLATON[28] program package was used to account for the electrons in the solvent accessible voids. Details are given in Table 7.2.

X-ray Data Collection, Structure Solution and Refinement for [K(2.2.2-cryptand)][(^{Ad,Me}ArO)$_3$mes)Sm], 24-Sm. A red crystal of approximate dimensions 0.280 x 0.305 x 0.318 mm was mounted in a cryoloop and transferred to a Bruker SMART APEX II

diffractometer. The APEX2[24] program package was used to determine the unit-cell parameters and for data collection (30 sec/frame scan time for a sphere of diffraction data). The raw frame data was processed using SAINT[20] and SADABS[25] to yield the reflection data file. Subsequent calculations were carried out using the SHELXTL[26] program. The systematic absences were consistent with the cubic space group $P2_13$ that was later determined to be correct. The structure was solved by dual space methods and refined on F^2 by full-matrix least-squares techniques. The analytical scattering factors[23] for neutral atoms were used throughout the analysis. Hydrogen atoms were included using a riding model. The molecule and counter-ion were located on three-fold rotation axes. An ether solvent molecule was disordered about a three-fold rotation axis and included with partial site-occupancy-factors. At convergence, wR2 = 0.0965 and Goof = 1.136 for 297 variables refined against 6196 data (0.76), R1 = 0.0374 for those 6012 data with $I > 2.0\sigma(I)$. The absolute structure was assigned by refinement of the Flack parameter.[29] Details are given in 7.2.

X-ray Data Collection, Structure Solution and Refinement for [K(2.2.2 cryptand)][(^{Ad,Me}ArO)$_3$mes)Yb], 24-Yb. A green crystal of approximate dimensions 0.093 x 0.138 x 0.152 mm was mounted on a glass fiber and transferred to a Bruker SMART APEX II diffractometer. The APEX2[24] program package was used to determine the unit-cell parameters and for data collection (90 sec/frame scan time for a sphere of diffraction data). The raw frame data was processed using SAINT[20] and SADABS[25] to yield the reflection data file. Subsequent calculations were carried out using the SHELXTL[26] program. The systematic absences were consistent with the cubic space group $P2_13$ that was later determined to be correct. The structure was solved by dual space methods and refined on F^2 by full-matrix least-squares techniques. The analytical scattering factors[23] for neutral atoms were used throughout the analysis. Hydrogen

atoms were included using a riding model. The molecule and counter-ion were located on three-fold rotation axes. An ether solvent molecule was disordered about a three-fold rotation axis and included with partial site-occupancy-factors. At convergence, wR2 = 0.0591and Goof = 1.100 for 297 variables refined against 5908 data (0.77), R1 = 0.0253 for those 5565 data with I > 2.0σ(I). The absolute structure was assigned by refinement of the Flack parameter.[29] Details are given in Table 7.2.

RESULTS

Synthesis and Structural Comparison of Ln^{3+} Precursors, [(^{Ad,Me}ArO)$_3$mes]Ln, 23-Ln. The protonolysis of [Ln(N(SiMe$_3$)$_2$)]$_3$ complexes with the tris(phenol), (^{Ad,Me}ArOH)$_3$mes, previously used to prepare [((^{Ad,Me}ArO)$_3$mes)Ln] complexes, **23-Ln** (Ln = Nd, Gd, Dy, Er), has been extended to Ln = La, Ce, Pr, Sm, and Yb, eq 7.5. Single crystals suitable for X-ray crystallography were obtained for all of the **23-Ln** complexes except **23-Ce,** which did not yield crystals suitable for X-ray crystallography in multiple attempts. The compounds were

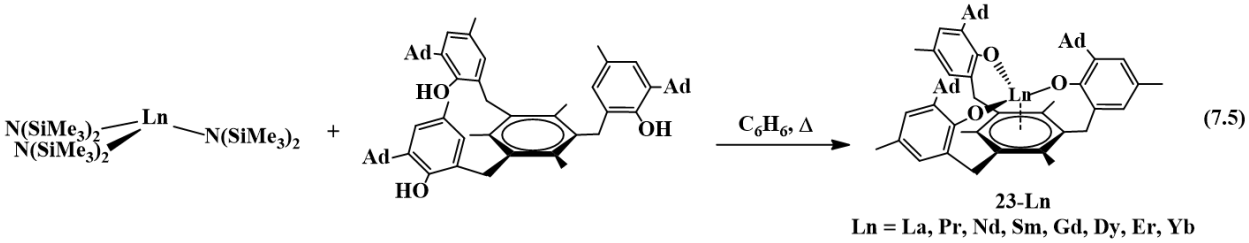

(7.5)

crystallographically characterized for definitive identification and for comparison with the reduction products described below.

All of the **23-Ln** complexes crystallize in space group $P2_1/c$, except for **23-Yb**, which crystallizes in the $P\bar{1}$ space group and has two molecules per asymmetric unit. The uranium analog, **23-U**, also crystallizes in the $P\bar{1}$ space group, but is not isomorphous with **23-Yb**. The compounds **23-La** and **23-Pr** are isomorphous with the previously reported **23-Nd**, whereas **23-**

Sm is isomorphous with **23-Gd**, **23-Dy**, and **23-Er**. These results are typical for classes of lanthanide complexes that can be synthesized across the entire series: the larger early metals often crystallize in a different space group than the smaller later lanthanides. Figure 7.1 shows a representative structure and the metrical parameters of the **23-Ln** complexes are compared in Table 7.3.

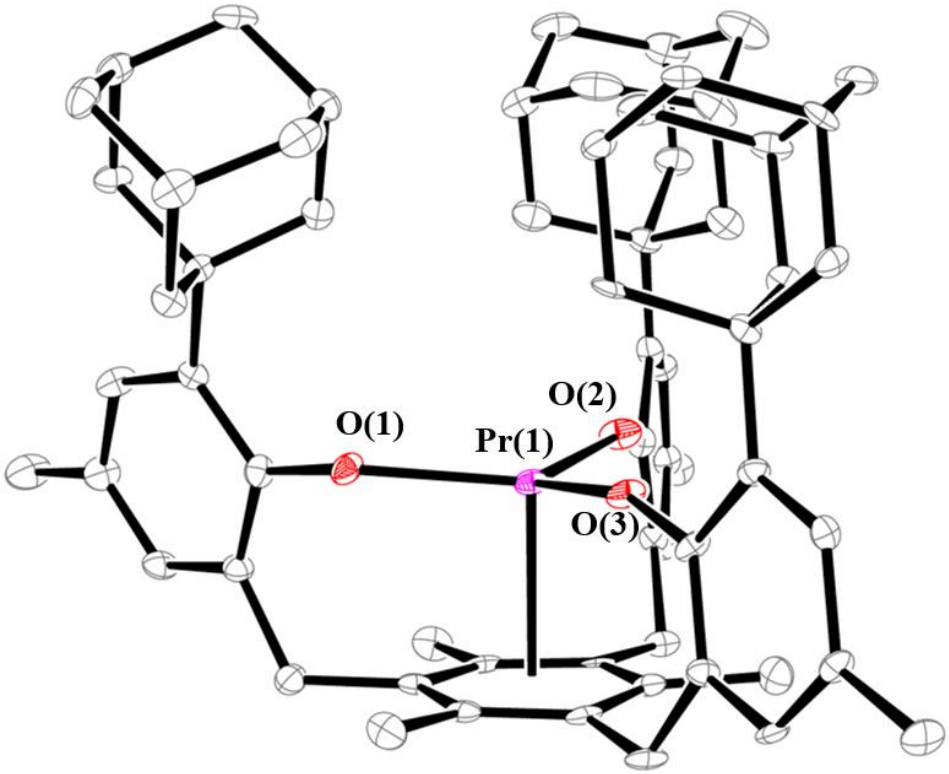

Figure 7.1. Molecular structure of [((^{Ad,Me}ArO)$_3$mes)Pr], **23-Pr**, with thermal ellipsoids drawn at the 50% probability level. Hydrogen atoms are omitted for clarity.

The M–O_{avg} and M–C_6 (ring centroid) bond distances of the **23-Ln** complexes decrease regularly across the series, which is consistent with the lanthanide contraction. The distances of **23-U** are not consistent with this trend, which is attributed to the greater orbital overlap of the 5*f*-orbitals compared to the 4*f*.[30] It should be noted that in all examples of **23-Ln**, as well as in **23-U**, the arene ring is not rigorously planar. The largest dihedral angle between adjacent three-carbon planes is between 5.3° and 9.3°. The smaller metals, Sm, Gd, Dy, Er, and Yb have the larger angles in this range, 8.7°-9.3°, but there is no monotonic change in angle with either the smaller or larger metals. It should be noted that there is a 3° torsional angle in the free triphenol, (^{Ad,Me}ArOH)$_3$mes.[30]

Reduction Reactions and Structural Characterization of [K(2.2.2-cryptand)][(^{Ad,Me}ArO)$_3$mes]Ln, 24-Ln. The new **23-Ln** complexes were treated with excess potassium metal in THF in the presence of 2.2.2-cryptand (crypt) at −35 °C, eq 7.6.

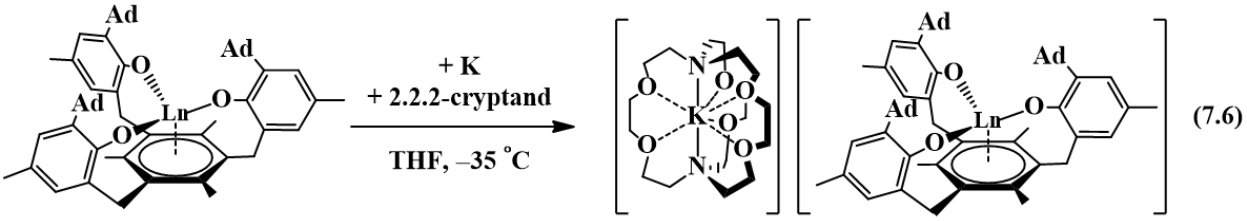

(7.6)

1-Ln **2-Ln**
Ln = La, Ce, Pr, Sm, Yb

The THF solutions generated from reductions of **23-Sm** and **23-Yb** were purple and green, respectively, Figure 7.2, with molar extinction coefficients ($\varepsilon < 1000$ $M^{1-}cm^{1-}$) in the visible region that are similar to those of the [K(2.2.2-cryptand)][Cp′$_3$Ln] complexes of the traditional 4f^{n+1} +2 ions of Eu, Yb, Sm, and Tm.[5] In contrast, for Ln = La, Ce, and Pr, intensely colored red solutions

were generated with extinction coefficients from 3200 to 3700 M^{-1} cm^{-1} that are larger than those of Sm and Yb, but not as large as those observed in the [K(2.2.2-cryptand)][Cp′$_3$Ln] complexes of the new 4f^{n}5d^1 +2 ions of La, Ce, Pr, Gd, Tb, Ho, Er, Lu; $\varepsilon \sim 5000$ $M^{1-}cm^{1-}$)[4,5] or in **24-Nd** ($\varepsilon = 4200$ $M^{-1}cm^{-1}$), **24-Gd** ($\varepsilon = 4000$ $M^{-1}cm^{-1}$), **24-Dy** ($\varepsilon = 4900$ $M^{-1}cm^{-1}$), and **24-Er** ($\varepsilon = 5600$ $M^{-1}cm^{-1}$).[30]

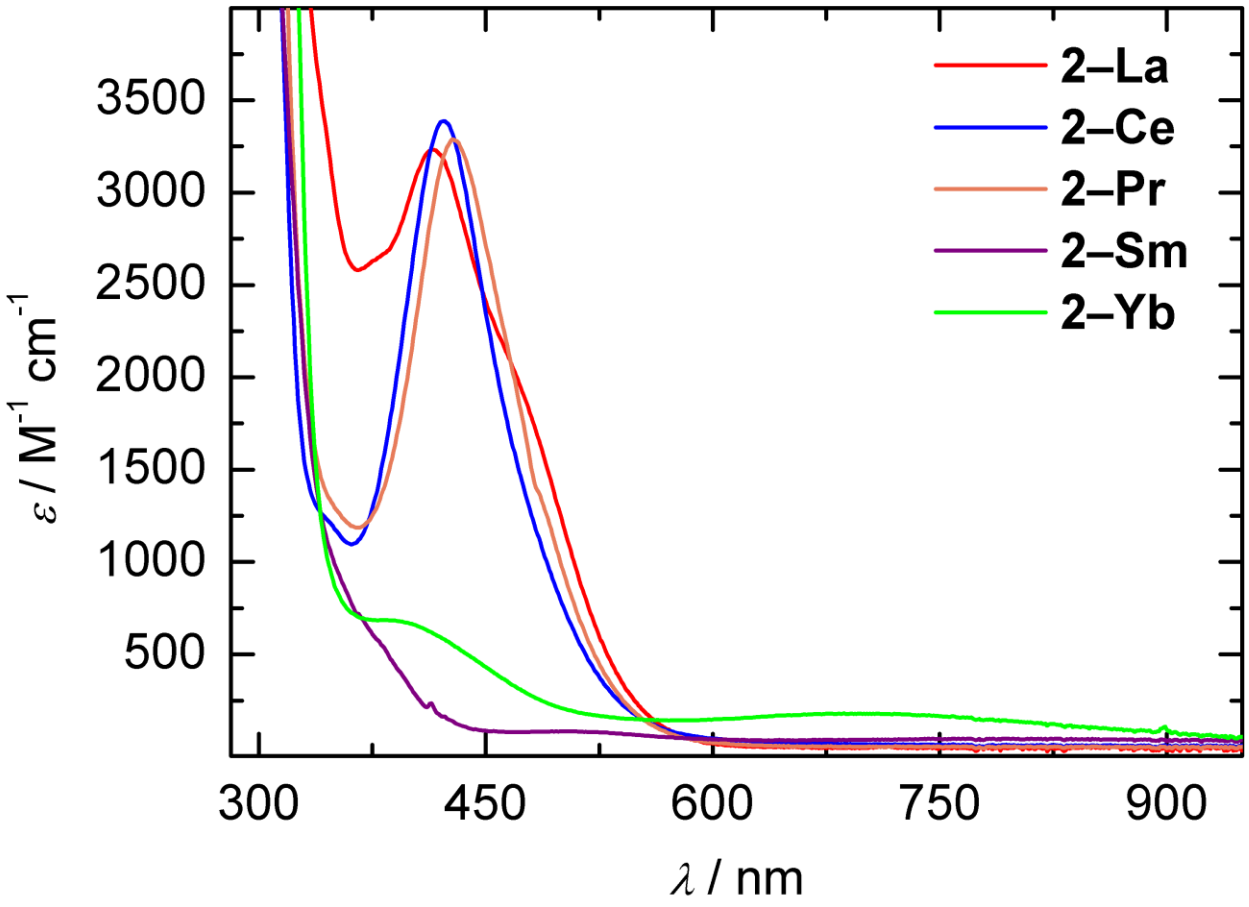

Figure 7.2. UV–visible spectra of [K(2.2.2-cryptand)][((Ad,MeArO)$_3$mes)Ln] (Ln = La (red), Ce (blue), Pr (orange), Sm (purple), Yb (green)), **24-Ln**, in THF at 298 K.

Diffusion of Et_2O into THF solutions of the **23-Ln** reduction product at −35 °C gave single crystals suitable for X-ray diffraction, Figure 7.3. The new complexes [K(2.2.2-

cryptand)][((^{Ad,Me}ArO)$_3$mes)Ln], **24-Ln** (Ln = La, Ce, Pr, Sm, Yb), crystallize in the *P2$_1$3* space group and are isomorphous with the previously reported **24-Ln** complexes of Nd, Gd, Dy, Er, and complex **2-U** (see Chapter 6, Table 6.2). In contrast to **24-Gd, 24-Dy, and 24-Er**, which co-crystallize as a mixture of a Ln^{2+} complex, [K(crypt)][((^{Ad,Me}ArO)$_3$mes)Ln], **24-Ln,** and a Ln^{3+} hydride complex, [K(crypt)][((^{Ad,Me}ArO)$_3$mes)LnH], **25-Ln**, eq 7.4,[30] complexes **24-La, 24-Sm**, and **24-Yb** crystallize as pure compounds, Figure 7.3. This was only observed previously for **24-Nd**, eq 7.3.[30]

Complexes **24-Ce** and **24-Pr** crystallize with disorder in the metal position, but it is not as severe as in the previously reported crystal data of **24-Gd**, **24-Dy**, and **24-Er**. Those three complexes were successfully modeled with 65:35, 63:37, and 55:45 mixtures, respectively, of [K(crypt)][((^{Ad,Me}ArO)$_3$mes)Ln], **24-Ln**, and [K(crypt)][((^{Ad,Me}ArO)$_3$mes)LnH], **25-Ln**.[30] The structures contained two different metal locations, the hydrides were located in the crystal structures, and the compounds react with CCl_4 to form $HCCl_3$. In **24-Ce** and **24-Pr**, there is one predominant component: the mixtures are 95:5 for Ce and 96:4 for Pr. No evidence for a hydride was found in the molecular structures of **24-Ce** and **24-Pr** and the 4% and 5% disordered metal positions differ from those of **25-Gd**, **25-Dy**, and **25-Er** in that the disordered ion is situated above the plane of the three oxygen atoms rather than in the plane as found for **25-Gd**, **25-Dy**, and **25-Er**. The origin of this disorder is unknown and in the following analysis, the data on the 95% and 96% components of **24-Ce** and **24-Pr**, respectively, are used. Metrical data on **24-Ln** are given in Table 7.2. In each of the **24-Ln** complexes, the metal is surrounded by three aryloxide oxygen donor atoms and the mesitylene ring.

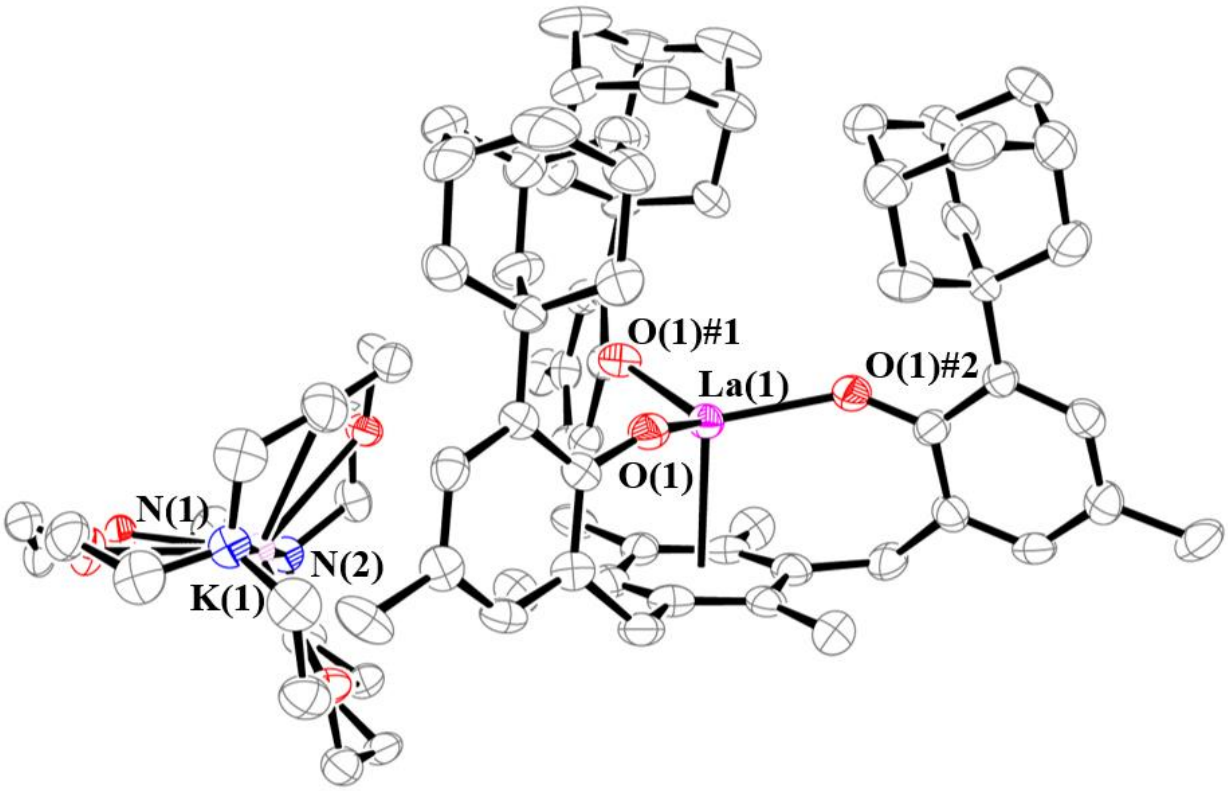

Figure 7.3. Molecular structure of [K(2.2.2-cryptand)][((^{Ad,Me}ArO)$_3$mes)La], **24-La**, with thermal ellipsoids drawn at the 50% probability level. Hydrogen atoms are omitted for clarity.

Structural Evaluation of the 24-Ln Complexes.

Previous studies of new +2 ions of the lanthanides and actinides have revealed that structural comparisons of the M^{3+} precursors and their reduced products can be useful in evaluating electron configurations.[1-10] For example, reduction of $4f^n$ Ln^{3+} complexes to $4f^{n+1}$ Ln^{2+} complexes of the metals that form traditional Ln^{2+} ions, i.e. Eu, Yb, Sm, and Tm, typically result in lengthening of bond distances by 0.1-0.2 Å. In contrast, reduction of $4f^n$ Ln^{3+} complexes to $4f^n5d^1$ Ln^{2+} complexes of the other lanthanides show only small increases in distances in the 0.02-0.04 Å range.[1-10] Table 7.5 presents the changes in Ln–O and Ln–arene ring centroid distances between **23-Ln** and **24-Ln.** The table also contains the differences in the distance of the metal out-of-plane

from the idealized plane of the three oxygen atoms. Also listed is the change in the planarity of the arene ring as measured by the change in the largest dihedral angle between adjacent three-carbon planes in the mesitylene ring. Scheme 7.1 shows these features. Data on **23-U** and **24-U** are also included for comparison.

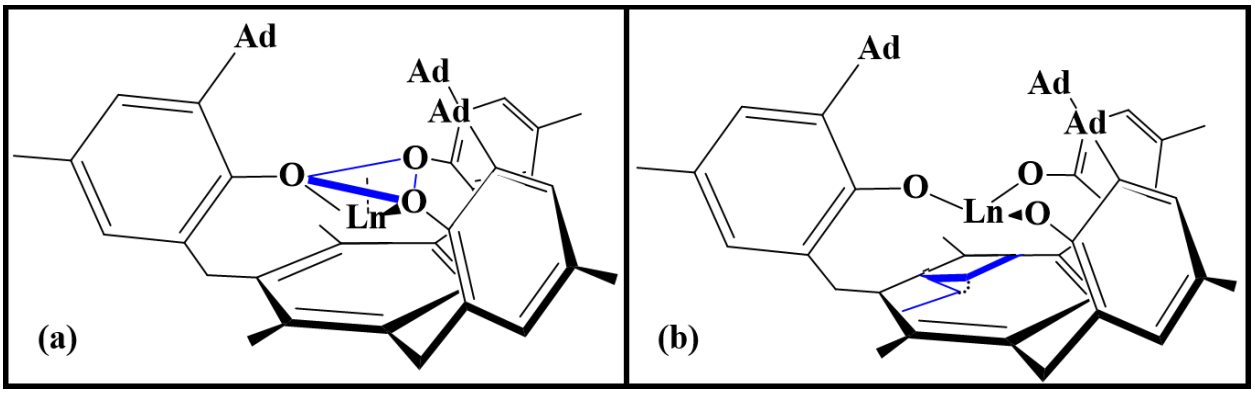

Figure 7.4. Graphical representation of the (a) metal out-of-plane distance and (b) the dihedral angle between adjacent three-carbon planes. The planes are shown in blue and the parameters are shown as dashed lines.

Sm and Yb. The data on **24-Sm** and **24-Yb** show distinctive features compared to all the other **24-Ln** complexes. **24-Sm** and **24-Yb** display the largest increase in Ln–O(aryloxide) distances of all the entries, 0.13 and 0.14 Å, respectively. These two complexes also have the only positive values for the change in the Ln–arene ring centroid distance, *i.e.* the metal moves further away from the arene ring upon reduction. As described above, lengthening of bond distances by 0.1-0.2 Å is a characteristic of reduction of $4f^n$ Ln^{3+} complexes to $4f^{n+1}$ Ln^{2+} complexes for the metals that form traditional Ln^{2+} ions, *i.e.* Eu, Yb, Sm, and Tm. Both **24-Sm** and **24-Yb** are also the only examples in the **24-Ln** series in which the change in the distance of the metal from the plane of the three aryloxide donor atoms is negative, *i.e.* the metals come closer to this plane. The

metals can come closer to the plane of the three oxygen donor atoms while the Ln–O distances lengthen due to the flexibility of the tris(aryloxide)mesitylene ligand system. Both **24-Sm** and **24-Yb** are also the only examples for which the arene ring becomes significantly more planar upon reduction, *i.e.* the numbers in the last column of Table 7.5 are negative.

La, Ce, and Pr. The structures of **24-La**, **24-Ce**, and **24-Pr** differ significantly from those of **24-Sm** and **24-Yb** in that the reduced complexes have only slightly lengthened Ln–O distances, 0.012 to 0.052 Å, and the metals get closer to the arene ring upon reduction. In addition, the arene becomes even more non-planar with *changes* of 4-6° in the dihedral angle between adjacent three carbon planes from the already non-planar rings in **23-Ln**.

Density Functional Theory Analysis

Density functional theory (DFT) calculations were carried out by Guo P. Chen, Alan K. Chan, Dr. Vamsee K. Voora in collaboration with the group of Professor Filipp Furche. Calculations were carried out on **24-Sm** and **24-Yb** and the calculated structural parameters match those observed within 0.15 Å. The highest occupied molecular orbitals for both **24-Yb** and **24-Sm**, Figure 7.5, were calculated to be 4*f*-type orbitals with no apparent interaction with the ligand. The calculations suggest that Yb^{2+} has a $4f^{14}$ ground state and Sm^{2+} has a $4f^{6}$ ground-state. In each case, the maximum ring distortion from planarity is only 3.4°. The longer observed Ln–arene distances and the fact that the arene ring becomes less distorted in **24-Yb** and **24-Sm** are consistent with little interaction of the Ln^{2+} ion with the arene ring.

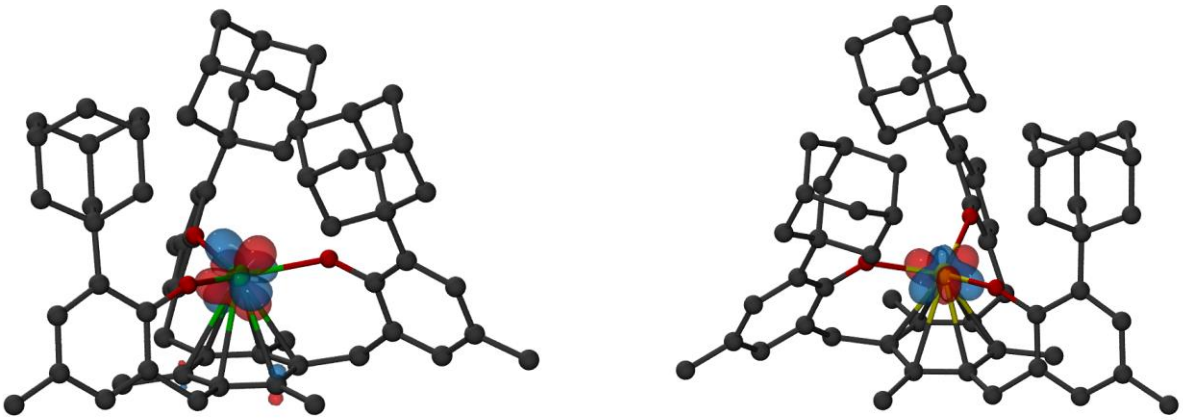

Figure 7.5. Isosurfaces for the highest singly-occupied molecular orbitals of (a) **24-Sm** and (b) **24-Yb** corresponding to a contour value of 0.05. Hydrogen atoms are omitted for clarity.

For the lanthanum complexes, **23-La** and **24-La**, the calculations reproduced the experimentally determined structures well, but a different picture of bonding emerges from the computational analysis. The LUMO of **23-La** and the HOMO of **24-La** possess predominantly mesitylene π* character, Figure 7.6. This indicates that reduction of

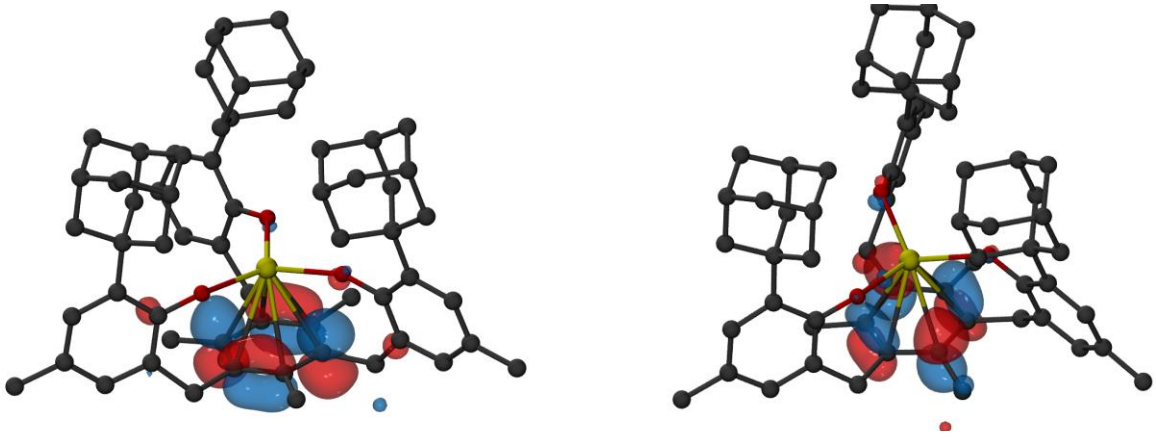

Figure 7.6. Isosurfaces for the lowest unoccupied molecular orbitals (LUMO+1) of **23-La** (left) and highest singly-occupied molecular orbitals of **24-La** (right) corresponding to a contour value of 0.05. Hydrogen atoms are omitted for clarity.

23-La formally adds an electron to the ligand, to generate a [((^{Ad,Me}ArO)$_3$mes)$^{4-}$] entity instead of reducing the metal from La^{3+} to La^{2+}. This is consistent with EPR spectra obtained for **24-La**, Figure 7.7. At 96 K, a solution of **24-La** in THF gave a spectrum with an irregular, slightly rhombic signal at g_1 = 2.0095, g_2 = 2.0020, g_3 = 1.9910, with no observable hyperfine coupling to lanthanum (^{139}La, I = 7/2, 99.9%), Figure 7.7a. Powdered samples of **24-La** at 90 K yielded an ill-defined signal at g = 2.000 with poorly resolved hyperfine coupling. At room temperature, powdered samples of **24-La** were simulated with a rhombic signal at g_1 = 2.0065, g_2 = 2.0008, g_3 = 1. 9967 with a hyperfine coupling constant of A = 7.9 G on all g values, Figure 7.7b. The very small coupling constant deviates significantly from the previously observed coupling constant of 154 G to the ^{139}La nucleus in the La^{2+} complex [K(2.2.2-cryptand)][Cp′$_3$La].[5] Hence, the EPR data strongly suggest that the additional electron in complex **24–La** resides at the ligand and not at the metal center.

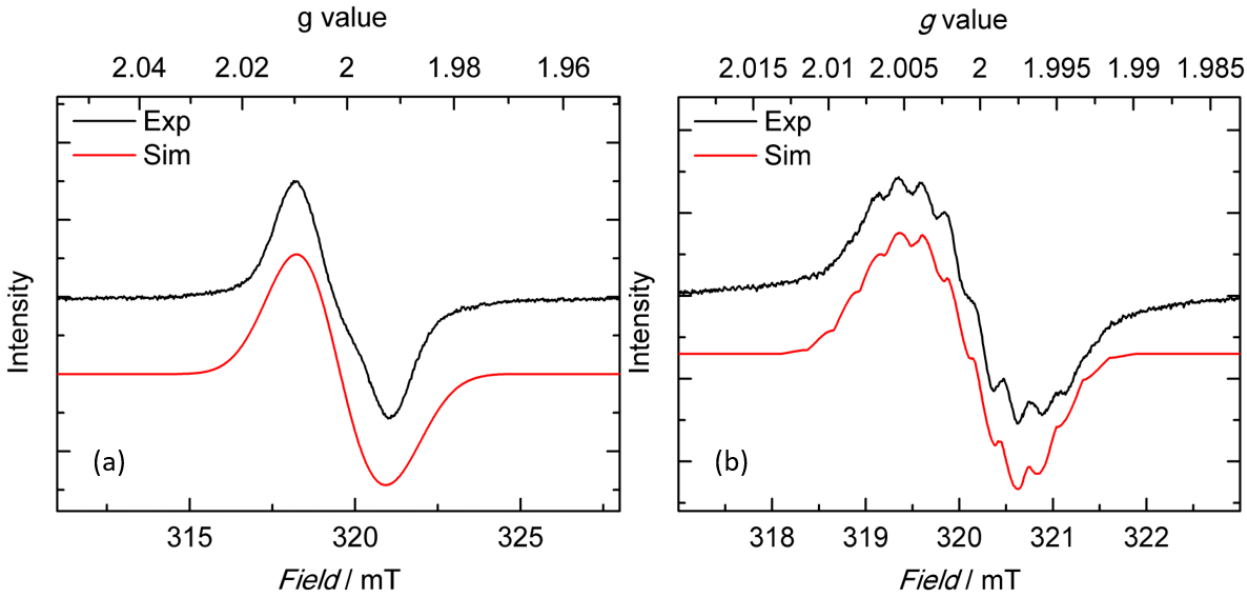

Figure 7.7. (a) X-Band EPR spectrum (ν = 8.961379 GHz, P = 1.0 mW, modulation width = 0.1 mT, T = 96 K) of complex [K(2.2.2-cryptand)][((^{Ad,Me}ArO)$_3$mes)La], **2-La**, recorded on a 10 mM sample in THF. The best fit was obtained for a rhombic spectrum with g_1 = 2.0095, g_2 = 2.0020,

g_3 = 1.9910 and line widths of W_1 = 1.2 mT, W_2 = 1.2 mT, and W_3 = 1.2 mT. (b) X-Band EPR spectrum (ν = 8.961379 GHz, P = 1.0 mW, modulation width = 0.05 mT, T = 298 K) of complex [K(2.2.2-cryptand)][((^{Ad,Me}ArO)$_3$mes)La], **2-La**, recorded on a powdered sample. The best fit was obtained for a rhombic spectrum with g_1 = 2.0065, g_2 = 2.0008, g_3 = 1. 9967 and line widths of W_1 = 0.2 mT, W_2 = 0.2 mT, and W_3 = 0.2 mT. The apparent hyperfine coupling was simulated with a coupling constant of A = 0.79 mT on all g values and a coupling to 6 identical I =1/2 nuclei. This is attributed to the benzylic hydrogens of the ligand.

consistent with further distortion of the arene ring away from planarity with a 9.8° dihedral angle between adjacent three-carbon planes.

The DFT picture of the structurally analogous **24-Ce** also suggests ligand reduction. The HOMO and HOMO−1 orbitals for **24-Ce** are singly occupied and are largely mesitylene π* orbitals, Figure 7.8. A population analysis of 1.3 electrons on Ce and 0.7 on the mesitylene ring is consistent with reduction of the mesitylene ligand in a complex of $4f^1$ Ce^{3+}. Although a solution of **24-Ce** in THF did not give an observable signal in its EPR spectrum, a signal was observed from **24-Ce** as a powder, Figure 7.9. The g values of g_1 = 2.0094, g_2 = 2.0012, g_3 = 1. 9926 and overall shape of the signal are similar to the solution **2-La** spectrum shown in Figure 7a.

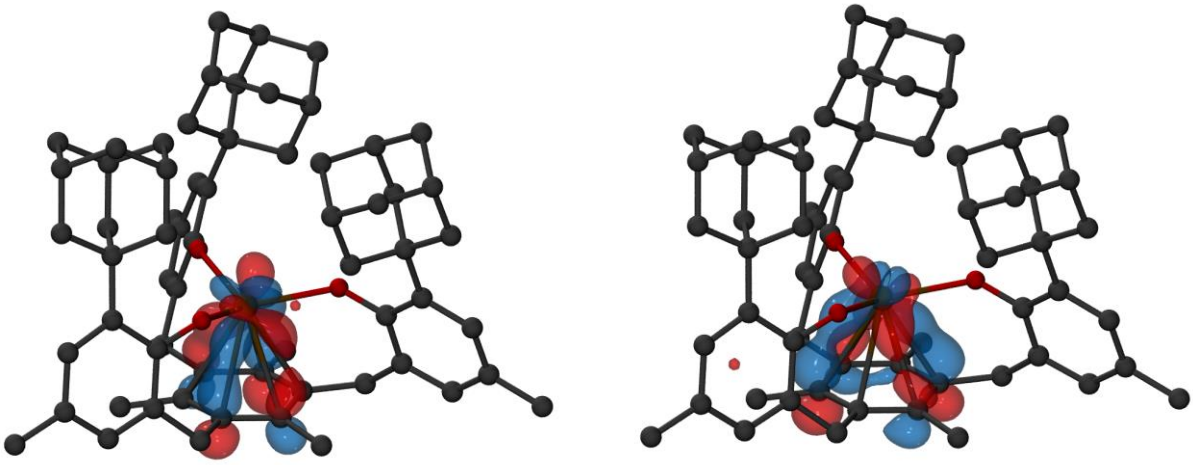

Figure 7.8. Isosurfaces for the SOMO (left) and SOMO−1 of **24-Ce** (right) corresponding to a contour value of 0.05. Hydrogen atoms are omitted for clarity.

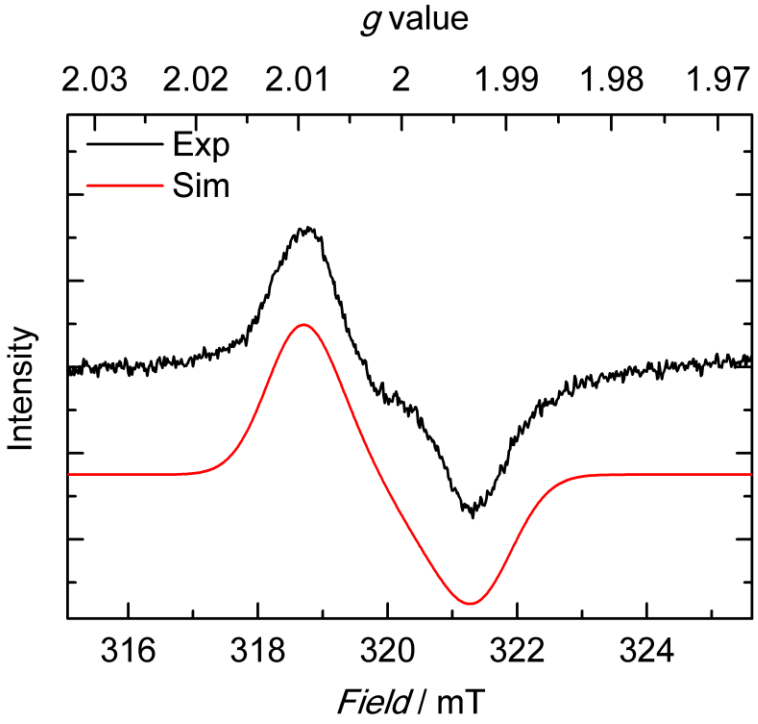

Figure 7.9. X-Band EPR spectrum (ν = 8.961379 GHz, P = 3.0 mW, modulation width = 0.1 mT, T = 96 K) of complex [K(2.2.2-cryptand)][((^{Ad,Me}ArO)$_3$mes)Ce], **2-Ce**, recorded on a powdered

sample. The best fit was obtained for a rhombic spectrum with g_1 = 2.0094, g_2 = 2.0012, g_3 = 1.9926 and line widths of W_1 = 6.1 mT, W_2 = 9.0 mT, and W_3 = 6.5 mT.

Complex **24-Pr** also shows significant ligand reduction. The population analysis of the spin density suggests 2.5 electrons on the Pr atom and 0.5 electrons on the mesitylene ring. For **24-Ce** and **24-Pr**, the calculated structural parameters match the experimental values within 0.1 and 0.02 Å, respectively. Overall, the population analysis of the various **24-Ln** complexes suggests that metal-based reduction is increasingly favored over ligand-based reduction as the series is traversed from La to Sm.

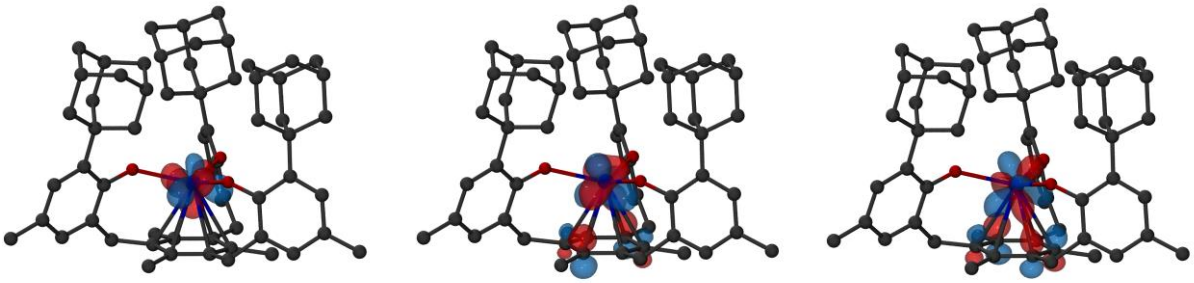

Figure 7.10. Isosurfaces for the SOMO (left) and SOMO−1 (center) and SOMO-2 (right) of **24-Pr** corresponding to a contour value of 0.05. Hydrogen atoms are omitted for clarity.

DISCUSSION

Reduction of the new tris(aryloxide)mesitylene complexes, [((^{Ad,Me}ArO)$_3$mes)Ln], **23-Ln**, to yield their respective reduction products, [K(2.2.2-cryptand)][((^{Ad,Me}ArO)$_3$mes)Ln], **24-Ln**, has revealed a new dimension of the tris(aryloxide)mesitylene ligand; namely, that it can be formally reduced to a ((^{Ad,Me}ArO)$_3$mes)$^{4-}$ tetraanion. Hence, reduction of the **23-Ln** complexes of the three largest metals in the series, La, Ce, and Pr, generates complexes formally regarded as Ln^{3+}

complexes of $((^{Ad,Me}ArO)_3mes)^{4-}$. DFT calculations support these assignments and match the structures of these complexes, which display even more non-planar arene rings than their **23-Ln** precursors and have shorter Ln-arene distances as might be expected for a tetraanionic ligand.

In contrast, reduction of **23-Yb** and **23-Sm** gives **23-Ln** complexes in which the arene rings become more planar and the metal ions move further away. DFT calculations suggest that these complexes contain traditional Ln^{2+} ions with $4f^{n+1}$ electron configurations.

The structure of **24-Nd**, the only other **24-Ln** complex that crystallizes without contamination of a Ln^{3+} hydride, differs from each type of complex above. Reduction of **23-Nd** to **24-Nd** causes little change in the non-planarity of the arene ring, while the metal moves closer to the arene. Previous DFT studies have generated a molecular orbital picture of Nd^{2+} that is similar to U^{2+}, *i.e.* two of the nf^4 M^{2+} ions' *f*-electrons are situated in non-bonding molecular orbitals and the other two are in singly occupied orbitals of proper symmetry for a delta bonding interaction with the π^* orbitals of the mesitylene ring.

The difference between the Yb and Sm reactions versus the La, Ce, and Pr reactions can be explained by their difference in reduction potentials. The calculated $4f^n + e^- \rightarrow 4f^{n+1}$ reduction potentials (vs SHE) of Yb (−1.15 V) and Sm (−1.55 V) are much less than those estimated for La (−3.1 V), Ce (−3.2 V), and Pr (−2.7 V).[31,32] Hence, it is much easier to reduce Yb^{3+} and Sm^{3+} to the Ln^{2+} ions. In the case of La, Ce, and Pr, metal reduction is more difficult and the reduction of the mesitylene ligand is the lowest energy pathway. However, reduction of the ring does not occur with **24-Nd**, which has a calculated $4f^n + e^- \rightarrow 4f^{n+1}$ reduction potential of −2.6 V. Since La, Ce, and Pr are the three largest metals in the series, it is possible that the reducibility of the ligand in these cases is also related to the size of these metals with respect to the size of the ligand cavity and concomitant ligand distortion.

CONCLUSION

Reduction of the $4f^n$ Ln^{3+} complexes, [((^{Ad,Me}ArO)$_3$mes)Ln], **23-Ln**, with La, Ce, and Pr with potassium reveals that the ((^{Ad,Me}ArO)$_3$mes)$^{3-}$ ligand can be formally reduced to ((^{Ad,Me}ArO)$_3$mes)$^{4-}$ with the largest metals in the series. Reductions of **23-Ln** with Yb and Sm show that this ligand will also support traditional Ln^{2+} ions with $4f^{n+1}$ electron configurations. These results demonstrate the redox-flexibility of the ((^{Ad,Me}ArO)$_3$mes)$^{3-}$ ligand system, which was previously used in the uranium-mediated catalytic generation of H_2 from H_2O,[33] and show that crystal structure data can be used in tandem with EPR spectroscopy to distinguish between metal- and ligand-based reduction products of metal complexes with this ligand.

Table 7.1. Crystal data and structure refinement for ((^{Ad,Me}ArO)$_3$mes)Ln (Ln = La, Pr, Sm, Yb), **23-Ln**.

	23-La	**23-Pr**	**23-Sm**	**23-Yb**
Empirical formula	$C_{63}H_{75}O_3La$	$C_{63}H_{75}O_3Pr$	$C_{63}H_{75}O_3Sm$	$C_{63}H_{75}O_3Yb$•½($C_4H_{10}O$)•¼(C_6H_{14})
Formula weight	1019.14	1021.14	1030.59	1111.87
Temperature (K)	133(2)	133(2)	133(2)	88(2)
Space group	$P2_1/c$	$P2_1/c$	$P2_1/c$	P-1
a (Å)	11.4819(4)	11.4697(17)	12.793(2)	15.585(2)
b (Å)	36.867(2)	36.682(6)	15.689(2)	15.766(2)
c (Å)	11.9433(5)	11.9101(18)	29.928(4)	28.332(4)
α (°)	90	90	90	105.3887(18)
β (°)	106.7174	106.757(2).	95.944(2)	105.3887(18)
γ (°)	90	90	90	113.4791(17)
Volume (Å^3)	4842.0(3)	4798.2(13)	5974.7(14)	6049.9(15)
Z	4	4	4	4
ρ_{calcd} (g/cm^3)	1.398	1.414	1.146	1.221
μ (mm^{-1})	0.931	1.064	1.022	1.589
$R1^a$	0.0315	0.0414	0.0286	0.0414
$wR2^b$	0.0726	0.0986	0.0658	0.0986

Definitions: ^{a}R1 = $\sum||Fo| - |Fc||/\sum|Fo|$; ^{b}wR2 = $[\sum[w(Fo^2 - Fc^2)^2]/\sum[w(Fo^2)^2]\ ]^{1/2}$.

Table 7.2. Crystal data and structure refinement for [K(2.2.2-cryptand)][((^{Ad,Me}ArO)$_3$mes)Ln] (Ln = La, Ce, Pr, Sm, Yb), **24-Ln**.

	24-La	**24-Ce**	**24-Pr**	**24-Sm**	**24-Yb**
Empirical formula	$C_{81}H_{111}LaKN_2O_9$	$C_{81}H_{111}CeKN_2O_9$	$C_{81}H_{111}KN_2O_9Pr$	$C_{81}H_{111}KN_2O_9Sm•C_4H_{10}O$	$C_{81}H_{111}KN_2O_9Yb•C_4H_{10}O$
Formula weight	1434.72	1435.93	1436.72	1520.28	1542.97
Temperature (K)	133(2)	88(2)	133(2)	88(2)	133(2)
Space group	$P2_13$	$P2_13$	$P2_13$	$P2_13$	$P2_13$
a (Å)	19.755(3)	19.7828(19)	19.7501(17)	19.79747(10)	19.755(3)
b (Å)	19.755(3)	19.7828(19)	19.7501(17)	19.79747(10)	19.755(3)
c (Å)	19.755(3)	19.7828(19)	19.7501(17)	19.79747(10)	19.755(3)
α (°)	90	90	90	90	90
β (°)	90	90	90	90	90
γ (°)	90	90	90	90	90
Volume (Å^3)	7710(3)	7742(2)	7704(2)	7756.2(12)	7710(4)
Z	4	4	4	4	4
ρ_{calcd} (g/cm^3)	1.236	1.232	1.239	1.302	1.329
μ (mm^{-1})	0.663	0.697	0.742	0.870	1.326
$R1^a$	0.0577	0.0378	0.0367	0.0374	0.0253
$wR2^b$	0.1686	0.0852	0.897	0.0965	0.0591

Definitions: ^{a}R1 = $\sum||Fo| - |Fc||/\sum|Fo|$; ^{b}wR2 = $[\sum[w(Fo^2 - Fc^2)^2]/\sum[w(Fo^2)^2]\ ]^{1/2}$.

Table 7.3. Selected bond lengths (Å) and angles (°) of **23-Ln** and **23-U** complexes listed in order of decreasing ionic radius.

Metal	Six coordinate ionic radius[a]	M–O Range	M–O avg	M–C_6 (ring centroid)	M out of plane[b]	C_6 Torsion Angle[c]
La	1.032	2.200(2)-2.249(2)	2.23(2)	2.575	0.157	5.5
U	1.025	2.158(2)-2.178(2)	2.17(1)	2.35	0.475(2)	6.8
Pr	0.99	2.175(3)-2.204(3)	2.19(1)	2.506	0.233	5.3
Nd	0.983	2.172(3)-2.200(2)	2.19(1)	2.489	0.268	5.6
Sm	0.958	2.138(2)-2.143(1)	2.140(2)	2.449	0.366	8.7
Gd	0.938	2.132(2)-2.134(2)	2.133(1)	2.413	0.416	8.3
Dy	0.912	2.093(3)-2.095(3)	2.094(1)	2.368	0.443	8.1
Er	0.89	2.078(2)-2.081(2)	2.079(1)	2.336	0.477	7.9
Yb[d]	0.868	2.053(3)-2.075(3)	2.063(9)	2.324(1)	0.486(5)	9.30/9.23

[a] From Shannon.[34] [b] Distance of M from the plane defined by the three O atoms of the $[(^{Ad,Me}ArO)_3mes]^{3-}$ ligand. [c] The largest dihedral angle between adjacent three carbon plane in the mesitylene ring. [d] Values taken as an average of the two molecules in the asymmetric unit.

Table 7.4. Selected bond lengths (Å) and angles (°) of **24-Ln** (Ln = La, Ce, Pr, Nd, Sm, Gd, Dy, Er, Yb) and **24-U**. Metrical parameters of **24-Ln** (Ln = Gd, Dy, Er) are obtained from the **24-Ln**/**25-Ln** co-crystals previously reported in Chapter 6.

Metal	M–O	M–C_6 (ring centroid)	M–C_{arene} avg	M out of plane[a]	O–M–O	C_6 Torsion Angle[b]
2-La	2.267(7)	2.459	2.846	0.429	116.50(11)	9.8
2-Ce	2.265(4)	2.413	2.804	0.505	115.12(7)	11.5
2-Pr	2.243(4)	2.403	2.797	0.505	115.10(7)	10.9
2-Nd	2.237(4)	2.366	2.765	0.530	114.59(8)	6.2
2-Sm	2.268(3)	2.573	2.934	0.276	118.54(3)	4.8
2-Gd	2.203(3)	2.286	2.691	0.578	113.37(8)	8.8
2-Dy	2.182(3)	2.238	2.651	0.608	112.55(8)	6.8
2-Er	2.172(3)	2.200	2.618	0.637	111.77(7)	5.7
2-Yb	2.207(3)	2.412	2.796	0.440	116.14(4)	4.8
2-U	2.236(4)	2.18	2.615	0.668(2)	111.49(8)	5.9

[a] Distance of M from the plane defined by the three O atoms of the $[(^{Ad,Me}ArO)_3mes]^{3-}$ ligand.

[b] The largest dihedral angle between adjacent three carbon planes in the mesitylene ring.

Table 7.5. Table comparing structural changes that occur upon reduction of the Ln^{3+} complexes **23-Ln** to give their respective reduction products, **24-Ln**. The changes between **23-U** and **24-U** have also been added for comparison.

Metal	ΔM–O (Å)	ΔM–C_6 (Ring Centroid) (Å)	ΔM out of plane [a] (Å)	ΔC_6 Torsion Angle (°)[b]
La	0.037	−0.116	0.272	4.3
Ce[b]	0.012	−0.124	0.298	-
Pr	0.052	−0.103	0.272	5.6
Nd	0.050	−0.123	0.262	0.6
Sm	0.130	0.124	−0.090	−3.9
Gd	0.070	−0.127	0.162	0.5
Dy[c]	0.088	−0.130	0.165	−1.3
Er	0.093	−0.136	0.160	−2.2
Yb	0.144	0.090	−0.045	−4.7
U	0.068	−0.170	0.193	−0.9

[a] Distance of M from the plane defined by the three O atoms of the $[(^{Ad,Me}ArO)_3mes]^{3-}$ ligand. [b]Obtained using interpolated metrical parameters for **23-Ce**.

REFERENCES

(1) Hitchcock, P. B.; Lappert, M. F.; Maron, L.; Protchenko, A. V. *Angew. Chem. Int. Ed.* **2008**, *47*, 1488-1491.

(2) MacDonald, M. R.; Ziller, J. W.; Evans, W. J. *J. Am. Chem. Soc.* **2011**, *133*, 15914-159147.

(3) MacDonald, M. R.; Bates, J. E.; Fieser, M. E.; Ziller, J. W.; Furche, F.; Evans, W. J. *J. Am. Chem. Soc.* **2012**, *134*, 8420-8423.

(4) MacDonald, M. R.; Bates, J. E.; Ziller, J. W.; Furche, F.; Evans, W. J. *J. Am. Chem. Soc.* **2013**, *135*, 9857-9868.

(5) Fieser, M. E.; MacDonald, M. R.; Krull, B. T.; Bates, J. E.; Ziller, J. W.; Furche, F.; Evans, W. J. *J. Am. Chem. Soc.* **2015**, *137*, 369-382.

(6) Woen, D. H.; Evans, W. J. In *Handbook on the Physics and Chemistry of Rare Earths*; 1st ed.; Elsevier: Amsterdam, 2016; Vol. 50, p 337-394.

(7) Evans, W. J. *Organometallics* **2016**, *35*, 3088-3100.

(8) MacDonald, M. R.; Fieser, M. E.; Bates, J. E.; Ziller, J. W.; Furche, F.; Evans, W. J. *J. Am. Chem. Soc.* **2013**, *135*, 13310-13313.

(9) Windorff, C. J.; MacDonald, M. R.; Meihaus, M. R.; Ziller, J. W.; Long, J. R.; Evans, W. J. *Chem. Eur. J.* **2016**, *22*, 772-782.

(10) Windorff, C. J.; Chen, G. P.; Cross, J. N.; Evans, W. J.; Furche, F.; Gaunt, A. J.; Janicke, M. T.; Kozimor, S. A.; Scott, B. L. *J. Am. Chem. Soc.* **2017**, *139*, 3970-3973.

(11) Dorenbos, P. *J. Phys.: Condens. Matter* **2003**, *15*, 575-594.

(12) Weakliem, H. A.; Kiss, Z. J. *Phys. Rev.* **1967**, *157*, 277-290.

(13) Sabisky, E. S. *Phys. Rev.* **1966**, *141*, 352-362.

(14) La Pierre, H. S.; Scheurer, A.; Heinemann, F. W.; Hieringer, W.; Meyer, K. *Angew. Chem., Int. Ed.* **2014**, *53*, 7158-7162.

(15) La Pierre, H. S.; Kameo, H.; Halter, D. P.; Heinemann, F. W.; Meyer, K. *Angew. Chem., Int. Ed.* **2014**, *53*, 7154-7157.

(16) Edelmann, F. T.; Poremba, P.; Hermann, W. A., Ed.; Thieme Verlag: Stuttgart, 1997; Vol. 6.

(17) Bergbreiter, D. E.; Killough, J. M. *J. Am. Chem. Soc.* **1978**, *100*, 2126-2134.

(18) Neese, F., University of Konstanz (78434-Konstanz/Germany), 1993.

(19) APEX2 Version 2014.9-0, Bruker AXS, Inc.; Madison, WI, 2014.

(20) SAINT Version 8.34a, Bruker AXS, Inc., Madison, WI, 2013.

(21) Sheldrick, G. M.; SADABS, Version 2014/4, Bruker AXS, Inc.; Madison, WI, 2014.

(22) Sheldrick, G. M.; SHELXTL, Version 2014/6, Bruker AXS, Inc.; Madison, WI, 2014.

(23) International Tables for X-Ray Crystallography, 1992, Vol. C. ed.; Dordrecht: Kluwer Academic Publishers.

(24) APEX2 Version 2014.11-0 ed.; Bruker AXS, Inc.: Madison, WI, 2014-.

(25) Sheldrick, G. M.; SADABS, Version 2014/5 Bruker AXS, Inc.; Madison, WI, 2014.

(26) Sheldrick, G. M.; SHELXTL, Version 2014/7, Bruker AXS, Inc.; Madison, WI, 2014.

(27) Spek, A. L.; SQUEEZE, Acta Cryst. 2015, C71, 9-19.

(28) Spek, A. L.; PLATON, Acta. Crys. 2009, D65, 148-155.

(29) Parsons, S.; Flack, H. D. *Acta Cryst.* **2013**, *B69*, 249-259.
(30) Fieser, M. E.; Palumbo, C. T.; La Pierre, H. S.; Halter, D. P.; Voora, V.; Ziller, J. W.; Furche, F.; Meyer, K.; Evans, W. J. *Chem. Sci.* **2017**, Advance Article.
(31) Morss, L. R. *Chem. Rev.* **1976**, *76*, 827-841.
(32) Morss, L. R. In *Handbook on the Physics and Chemistry of Rare Earths*; Gschneidner, K. A., Eyring, L., Choppin, G. R., Lander, G. H.; Elsevier: Amsterdam, 1994; Vol. 18, 239-291.
(33) Halter, D. P.; Heinemann, F. W.; Bachmann, J.; Meyer, K. *Nature* **2016**, *530*, 317-321.
(34) Shannon, R. D. *Acta Crystallogr A* **1976**, *32*, 751-767.

CHAPTER 8

Using Diamagnetic Yttrium and Lanthanum Complexes to Explore Ligand Reduction and C–H Bond Activation in the Tris(aryloxide)mesitylene Ligand System

INTRODUCTION

The studies mentioned in Chapters 6 and 7 involved comparisons of the tris(cyclopentadienyl) ligand sets, $(Cp'_3)^{3-}$ and $(Cp''_3)^{3-}$ ($Cp' = C_5H_4SiMe_3$; $Cp'' = C_5H_3(SiMe_3)_2$),[1-11] with the tris(aryloxide)mesitylene ligand $((^{Ad,Me}ArOH)_3mes)^{3-}$.[12-14] Reduction of the tris(cyclopentadienyl) complexes Cp'_3Ln and Cp''_3Ln has allowed the isolation of Ln^{2+} complexes for Y, all the lanthanides, Th, U, and Pu as shown in eq 8.1.[1-11]

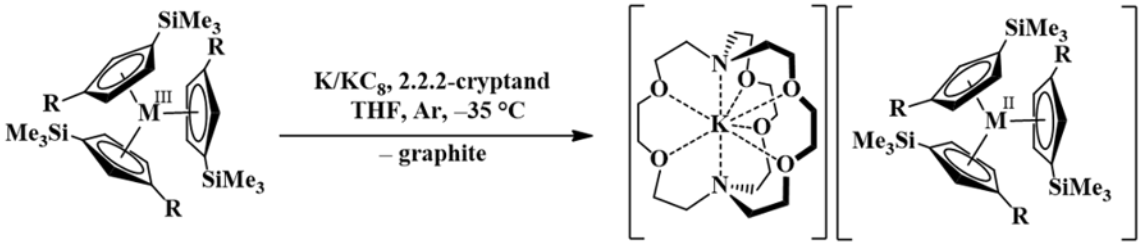

(8.1)

R = $SiMe_3$; M = La, Th, U, Pu
R = H; M = Y, La, Ce, Pr, Nd, Sm, Gd, Tb, Dy, Ho, Er, Tm, Lu, U

Reduction of the tris(aryloxide)mesitylene complexes, $((^{Ad,Me}ArO)_3mes)U$, **23-U**, and $((^{Ad,Me}ArO)_3mes)Ln$, **23-Ln**, has been used to generate M^{2+} complexes of U, Nd, Sm, and Yb, eq 8.2.

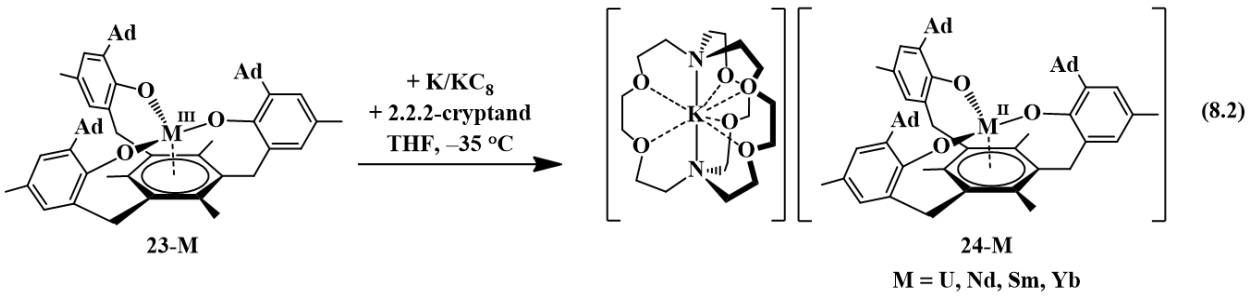

(8.2)

However, reduction of the **23-Ln** complexes of Gd, Dy, and Er was more complicated. In each case, a mixture of a Ln^{2+} complex, [K(2.2.2-cryptand)][((^{Ad,Me}ArO)$_3$mes)Ln], **24-Ln**, and a Ln^{3+} hydride product, [K(2.2.2-cryptand)][((^{Ad,Me}ArO)$_3$mes)LnH], **25-Ln**, co-crystallized, eq 8.3. The source of the hydride is unknown.

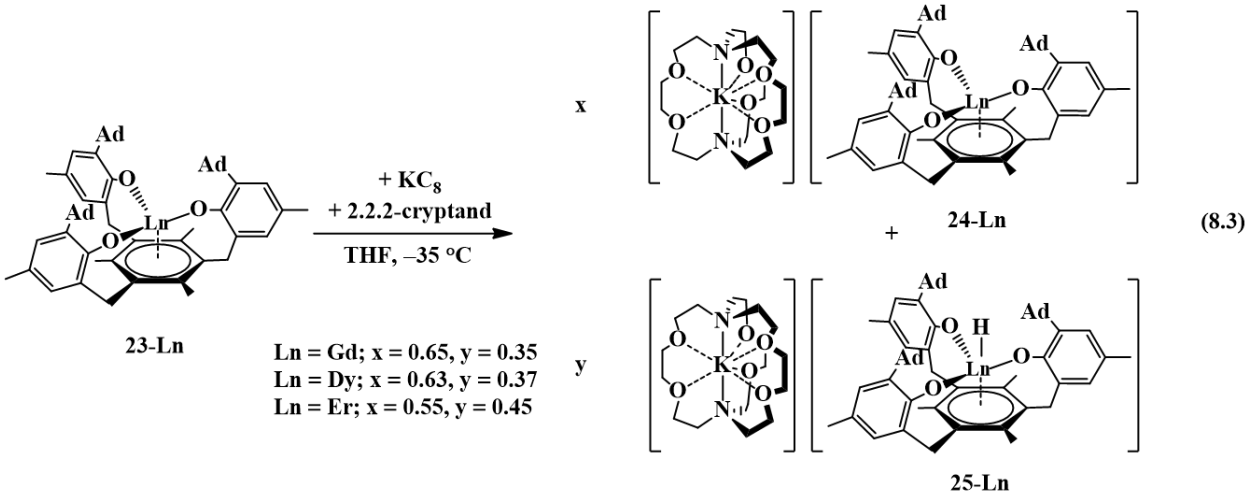

(8.3)

Reduction of **34-Ln** with Ln = La, Ce, or Pr, gave yet another result: the products are best described as Ln^{3+} complexes of a reduced [(^{Ad,Me}ArO)$_3$mes]$^{4-}$ ligand radical, eq 8.4.

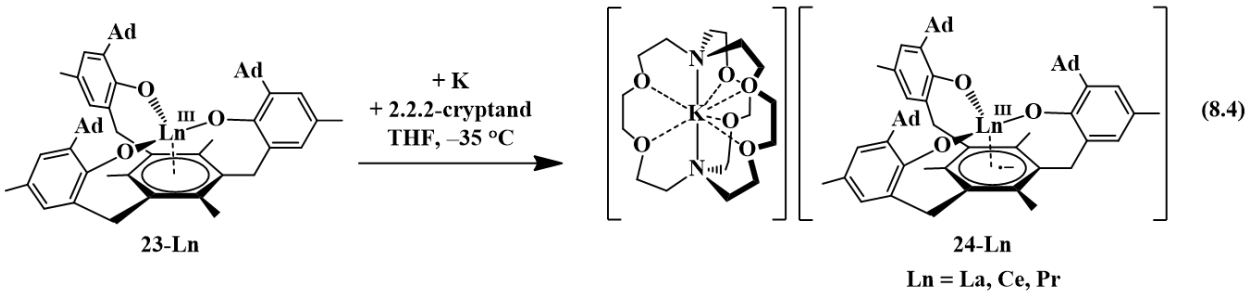

(8.4)

To obtain more information on the reductive chemistry of this flexible tris(aryloxide)mesitylene ligand system, studies have been extended to yttrium since the 100% natural abundance ^{89}Y isotope has a nuclear spin of ½ that can provide extra information via NMR and EPR spectroscopy for Y^{3+} and Y^{2+} complexes, respectively. Historically, Y^{3+} has been shown to display chemistry similar to the late lanthanides of similar size, Ho^{3+} and Er^{3+}. This has been very helpful in elucidating the chemistry of these highly paramagnetic ions that do not provide information by NMR spectroscopy. The reduction of the diamagnetic La^{3+} complex, $(({}^{Ad,Me}ArO)_3mes)La$, **23-La**, was also explored and a new product beyond **24-La** in eq 8.4 was found that could explain the source of the hydride ligands in eq 8.3.

EXPERIMENTAL

The syntheses and manipulations described below were conducted under an argon atmosphere with rigorous exclusion of air and water using glovebox, vacuum line, and Schlenk techniques. Solvents were sparged with ultrahigh purity (UHP) grade argon (Airgas) and passed through columns containing Q-5 and molecular sieves before use. NMR solvents (Cambridge Isotope Laboratories) were dried over NaK/benzophenone, degassed by three freeze−pump−thaw cycles, and vacuum-transferred before use. $Y(N(SiMe_3)_2)_3$,[15] $({}^{Ad,Me}ArOH)_3mes$,[13] and $(({}^{Ad,Me}ArO)_3mes)La$, **23-La**, were prepared according to their literature procedures. Potassium metal (Aldrich) was washed with hexane and scraped to provide fresh surfaces before use. 2.2.2-Cryptand, 4,7,13,16,21,24-hexaoxa-1,10-diazabicyclo[8.8.8]hexacosane (Acros Organics), was placed under vacuum (10^{-3} Torr) for 12 h before use. 18-Crown-6 (Aldrich) was sublimed before use. ^1H NMR (500 MHz) spectra were obtained on a Bruker GN500 or CRYO500 MHz spectrometer at 298 K. IR samples were prepared as KBr pellets and the spectra were obtained on either a Varian 1000 or Jasco 4700 FT-IR spectrometer. Elemental analyses were performed on a

PerkinElmer 2400 series II CHNS elemental analyzer. Electronic absorption spectra were obtained in THF or benzene at 298 K using a Varian Cary 50 Scan UV−vis or Jasco V-670 UV/Vis/NIR/MIR absorption spectrometer. EPR spectra were collected using X-band frequency (9.3-9.8 GHz) on a Bruker EMX spectrometer equipped with an ER041XG microwave bridge and the magnetic field was calibrated with DPPH (g = 2.0036).

[((^{Ad,Me}ArO)$_3$mes)Y], 23-Y. In an argon-filled glovebox, a sealable 100 mL side arm Schlenk flask equipped with a greaseless stopcock was charged with a solution of [(^{Ad,Me}ArOH)$_3$mes] (181 mg, 0.205 mmol) in benzene (40 mL) and a magnetic stir bar. A solution of Y(N(SiMe$_3$)$_2$)]$_3$ (123 mg, 0.216 mmol) in benzene (40 mL) was slowly added to the stirred solution. The flask was attached to a Schlenk line and the mixture was stirred and heated to reflux overnight. The solvent was then removed and the flask was brought back into the glovebox. The resultant colorless solids were washed twice with 10 mL of cold hexane (−35 °C), then dissolved in benzene, and filtered. Toluene (2 mL) was added to the colorless filtrate and the solvent was removed under vacuum. The resulting colorless gel was triturated once with hexane to afford **23-Y** as a colorless solid (155 mg, 78%). Colorless single crystals of **23-Y**, suitable for X-ray diffraction, were grown by cooling a concentrated hexane solution to −35 °. ^{1}H NMR (C_6D_6): δ 7.10 (d, J_{HH} = 2.0 Hz, Ar*H*, 3H), 6.77 (d, J_{HH} = 2.0 Hz, Ar*H*, 3H), 3.73 (s, benzylic C*H*$_2$, 6H), 2.41 (s, *Me*, 9H), 2.34 (br s, Ad C*H*$_2$, 18H), 2.17 (br s, *Me*, 9H), 1.91 (s, Ad C*H*, 9H), 1.85 (br m, Ad C*H*$_2$, 18H). ^{13}C NMR (C_6D_6): δ 158.2, 141.7, 137.7, 136.9, 129.4, 128.6, 126.6, 126.2, 125.8, 41.4, 37.9, 36.6, 29.6, 21.3, 18.9. IR: 3075w, 3033w, 2901s, 2845s, 2727w, 2673w, 2653w, 1604w, 1570w, 1449s, 1413m, 1377m, 1365w, 1355w, 1342m, 1317m, 1305m, 1286m, 1249s, 1208m, 1183m, 1162m, 1148w, 115w, 1101m, 1066w, 1036w, 1016m, 1003w, 980m, 961w, 938w, 923m, 916m, 881m, 858m, 837s, 821s, 810s, 765m, 748m, 741w, 727m, 715m, 702w,

694m, 688w, 677s, 666w, 659w, 653m, 649w, 644w, 640w, 635w, 632w, 627w, 623w, 618w, 614w, 607w, 601w cm^{-1}. Anal. Calcd for $C_{63}H_{75}YO_3$: C, 78.07; H, 7.80. Found: C, 68.41; H, 7.49 and C, 70.07; H, 8.27.

[K(2.2.2-cryptand)][((^{Ad,Me}ArO)$_3$mes)Y]/[K(2.2.2-cryptand)][((^{Ad,Me}ArO)$_3$mes)YH], 24-Y/25-Y. In an argon-filled glovebox, a scintillation vial was charged with a THF solution (2 mL) of [(^{Ad,Me}ArO)$_3$mes)Y], **23-Y** (24 mg, 25 μmol), and 2.2.2-cryptand (9 mg, 25 μmol) and the mixture was prechilled in the glovebox freezer (−35 °C). Potassium (excess) was added and the mixture was stored overnight in the glovebox freezer. The resultant dark-red solution was filtered through a prechilled pipette packed with glass wool into a vial containing prechilled Et_2O (8 mL) so that upon exiting the pipette, the dark-red solution was under a layer of Et_2O. The mixture was then stored in the glovebox freezer and after 48 h, diffusion of Et_2O into the dark-red solution yielded dark red single crystals of **24-Y/25-Y** suitable for X-ray diffraction (12 mg). Crystallographic modeling was consistent with a 47:53 ratio of **24-Y**/**25-Y**. ^{1}H NMR (THF-d_8): δ 7.81 (d, J_{YH} = 93 Hz, Y–*H*, 1H). ^{89}Y NMR (THF-d_8): −138.0. IR: 3070w, 2966s, 2899s, 2846s, 2812s, 2760m, 2726m, 2677m, 2653m, 1600w, 1566m, 1477m, 1444s, 1432s, 1418m, 1380m, 1361s, 1354s, 1341m, 1314m, 1307m, 1296s, 1284s, 1277s, 1256s, 1251s, 1210m, 1184m, 1164m, 1134s, 1106s, 1083s, 1071m, 1060m, 1047w, 1033w, 1022w, 1012w, 980m, 949s, 935m, 913m, 904m, 896w, 889w, 878m, 856m, 834m, 817m, 807m, 799m, 785w, 765m, 752m, 749m, 736w, 725w, 719w, 715w, 704w, 699w, 693w, 686w, 676w, 666w, 660w, 653w, 647w, 642w, 629w, 626w, 622w, 615w, 611w, 607w, 603w cm^{1-}. Anal. Calcd for $C_{81}H_{111.55}KN_2O_9Y$: C, 70.23; H, 8.12; N, 2.02. Found: C, 68.33; H, 8.60; N, 1.65 and C, 67.39; H, 8.63; N, 1.68 and C, 67.95; H, 8.24; N, 1.47.

[K(2.2.2-cryptand)][((^{Ad,Me}ArO)$_3$(C$_6$Me$_3$(CH$_2$)$_2$CH)La], 29-La. In an argon-filled glovebox, a scintillation vial was charged with **23-La** (48 mg, 47 μmol), 2.2.2-cryptand (18 mg, 47 μmol), and THF (4 mL). To the colorless solution was added excess potassium metal and the color slowly turned orange. After 16 h at −35 °C, the orange/red mixture was filtered, layered with Et_2O (15 mL), and stored at −35 °C for 48 h which yielded a mixture of crystals (presumably the previously characterized **24-La**) and bright orange powder. The powder was washed several times with Et_2O (3 x 10 mL). The residual solids were dissolved in THF (4 mL), filtered, and layered with hexane (15 mL). Storage at −35 °C for 48 h gave red/orange microcrystalline solids characterized as [K(2.2.2-cryptand)][((^{Ad,Me}ArO)$_3$(C$_6$Me$_3$(CH$_2$)$_2$CH)La(THF)], **27-La**, by X-ray crystallography (15 mg, 21%) (see SI for crystallographic details). ^{1}H NMR (THF-d_8): 6.60, 6.59, 6.56, 6.54, 6.51, 6.48, 3.96, 3.94, 3.79, 3.70, 3.50, 3.45, 3.18, 3.15, 2.47, 2.24, 2.21, 2.19, 2.17, 2.13 2.12, 2.10, 2.08, 2.03, 2.02, 1.93, 1.59, 1.57, 1.54. IR: 2898s, 2843s, 2725m, 2675m, 2652m, 1600w, 1551m, 1476m, 1444s, 1430m, 1369w, 1360s, 1353s, 1340m, 1314m, 1282s, 1257s, 1238s, 1209w, 1181w, 1173w, 1162w, 1133m, 1105s, 1077m, 1058m, 1027m, 989m, 949, 931m, 913w, 849m, 831m, 818m, 803m, 788w, 769w, 763w, 752m, 739w, 716w, 691w, 682w, 667w, 650w cm^{-1}. Anal. Calcd for $C_{85}H_{118}KLaN_2O_{10}$: C, 67.80; H, 7.90; N, 1.86. Found: C, 66.60; H, 7.73; 1.75.

X-ray Data Collection, Structure Solution and Refinement for [(^{Ad,Me}ArO)$_3$mes)Y], 23-Y. A colorless crystal of approximate dimensions 0.066 x 0.121 x 0.328 mm was mounted in a cryoloop and transferred to a Bruker SMART APEX II diffractometer. The APEX2[16] program package was used to determine the unit-cell parameters and for data collection (90 sec/frame scan time for a sphere of diffraction data). The raw frame data was processed using SAINT[17] and SADABS[18] to yield the reflection data file. Subsequent calculations were carried out using the

SHELXTL[19] program. The diffraction symmetry was 2/*m* and the systematic absences were consistent with the monoclinic space group $P2_1/c$ that was later determined to be correct. The structure was solved by dual space methods and refined on F^2 by full-matrix least-squares techniques. The analytical scattering factors[20] for neutral atoms were used throughout the analysis. Hydrogen atoms were included using a riding model. At convergence, wR2 = 0.1101 and Goof = 1.018 for 610 variables refined against 12179 data (0.80Å), R1 = 0.0455 for those 8673 data with $I > 2.0\sigma(I)$. There were several high residuals present in the final difference-Fourier map. It was not possible to determine the nature of the residuals although it was probable that hexane or benzene solvents were present. The SQUEEZE[21] routine in the PLATON[22] program package was used to account for the electrons in the solvent accessible voids. Details are given in Table 8.1.

X-ray Data Collection, Structure Solution and Refinement for [K(2.2.2-cryptand)][(^{Ad,Me}ArO)$_3$mes)Y] / [K(2.2.2-cryptand)][(^{Ad,Me}ArO)$_3$mes)YH], 24-Y/25-Y. A red crystal of approximate dimensions 0.0.547 x 0.582 x 0.836 mm was mounted in a cryoloop and transferred to a Bruker SMART APEX II diffractometer. The APEX2[16] program package was used to determine the unit-cell parameters and for data collection (15 sec/frame scan time for a sphere of diffraction data). The raw frame data was processed using SAINT[17] and SADABS[18] to yield the reflection data file. Subsequent calculations were carried out using the SHELXTL[19] program. The systematic absences were consistent with the cubic space group $P2_13$ that was later determined to be correct. The structure was solved by dual space methods and refined on F^2 by full-matrix least-squares techniques. The analytical scattering factors[20] for neutral atoms were used throughout the analysis. Hydrogen atoms were included using a riding model. The molecule and counter-ion were located on three-fold rotation axes. The complex appeared to be a mixed composition of approximately Y^{2+}(45%) / Y^{3+}(55%). There was approximately 55% of a hydride

ligand present bound to Y(2). The position of the hydride was evident in the electron density map and it was refined (x,y,z, and riding U_{iso}). At convergence, wR2 = 0.0892 and Goof = 1.182 for 289 variables refined against 5742 data (0.78), R1 = 0.0375 for those 5446 data with I > 2.0σ(I). The absolute structure was assigned by refinement of the Flack parameter.[23] There were residuals present in the final difference-Fourier map. It was not possible to determine the nature of the residuals although it was probable that diethylether solvent was present. The SQUEEZE[21] routine in the PLATON[22] program package was used to account for the electrons in the solvent accessible voids.

X-ray Data Collection, Structure Solution and Refinement for [K(2.2.2-cryptand)][(^{Ad,Me}ArO)$_3$mes)YH], 25-Y. A red crystal of approximate dimensions 0.108 x 0.144 x 0.211 mm was mounted in a cryoloop and transferred to a Bruker SMART APEX II diffractometer. The APEX2[16] program package was used to determine the unit-cell parameters and for data collection (90 sec/frame scan time for a hemisphere of diffraction data). The raw frame data was processed using SAINT[17] and SADABS[18] to yield the reflection data file. Subsequent calculations were carried out using the SHELXTL[19] program. The systematic absences were consistent with the cubic space group $P2_13$ that was later determined to be correct. The structure was solved by dual space methods and refined on F^2 by full-matrix least-squares techniques. The analytical scattering factors[20] for neutral atoms were used throughout the analysis. Hydrogen atoms were included using a riding model. The molecule and counter-ion were located on three-fold rotation axes. The hydride atom was refined (xyz) with riding U_{iso}. Least-squares analysis yielded wR2 = 0.1069 and Goof = 1.049 for 286 variables refined against 5290 data (0.80), R1 = 0.0459 for those 4218 data with I > 2.0σ(I). The absolute structure was assigned by refinement of the Flack parameter.[23] There were residuals present in the final difference-Fourier

map. The SQUEEZE[21] routine in the PLATON[22] program package was used to account for the electrons in the solvent accessible voids.

X-ray Data Collection, Structure Solution and Refinement for [K(2.2.2-cryptand)][((^{Ad,Me}ArO)$_3$(C$_6$Me$_3$(CH$_2$)$_2$CH)La], 29-La. The single crystal X-ray diffraction studies were carried out on a Bruker APEX II Ultra CCD diffractometer equipped with Mo K_a radiation (l = 0.71073). Crystals of the subject compound were used as received. (grown from THF, Et_2O) A 0.100 x 0.030 x 0.030 mm block was mounted on a Cryoloop with Paratone oil. Data were collected in a nitrogen gas stream at 100(2) K using f and v scans. Crystal-to-detector distance was 40 mm using exposure time 60s with a scan width of 1.0°. Data collection was 99.8% complete to 25.00° in *q*. A total of 67593 reflections were collected covering the indices,-17<=h<=17, -20<=k<=20, -20<=l<=20. 15356 reflections were found to be symmetry independent, with a R_{int} of 0.130. Indexing and unit cell refinement indicated a **Primitive**, **Triclinic** lattice. The space group was found to be ***P*-1**. The data were integrated using the Bruker SAINT[24] software program and scaled using the SADABS[18] software program. Solution by direct methods (SHELXT)[19] produced a complete phasing model consistent with the proposed structure. All nonhydrogen atoms were refined anisotropically by full-matrix least-squares (SHELXL-2014).[19] All hydrogen atoms were placed using a riding model. Their positions were constrained relative to their parent atom using the appropriate HFIX command in SHELXL-2014.[19] Notes: Diso solvent removed by Squeeze[21] procedure, 212 electrons per unit cell. Minor disorder on coordinated THF. H atoms removed from pics for clarity. Details are given in Table 8.1.

RESULTS

Protonolysis of the tris(amide) compound $Y(N(SiMe_3)_2)_3$ with the tris(phenol) $(^{Ad,Me}ArOH)_3mes$, gave colorless solids whose composition was determined to be $((^{Ad,Me}ArO)_3mes)Y$, **23-Y**, by X-ray crystallography, Figure 8.1. The structure was found to have metrical parameters that are intermediate between those of **23-Dy** and **23-Er**,[14] Table 8.2. This is consistent with the similar ionic radii of these three metals.

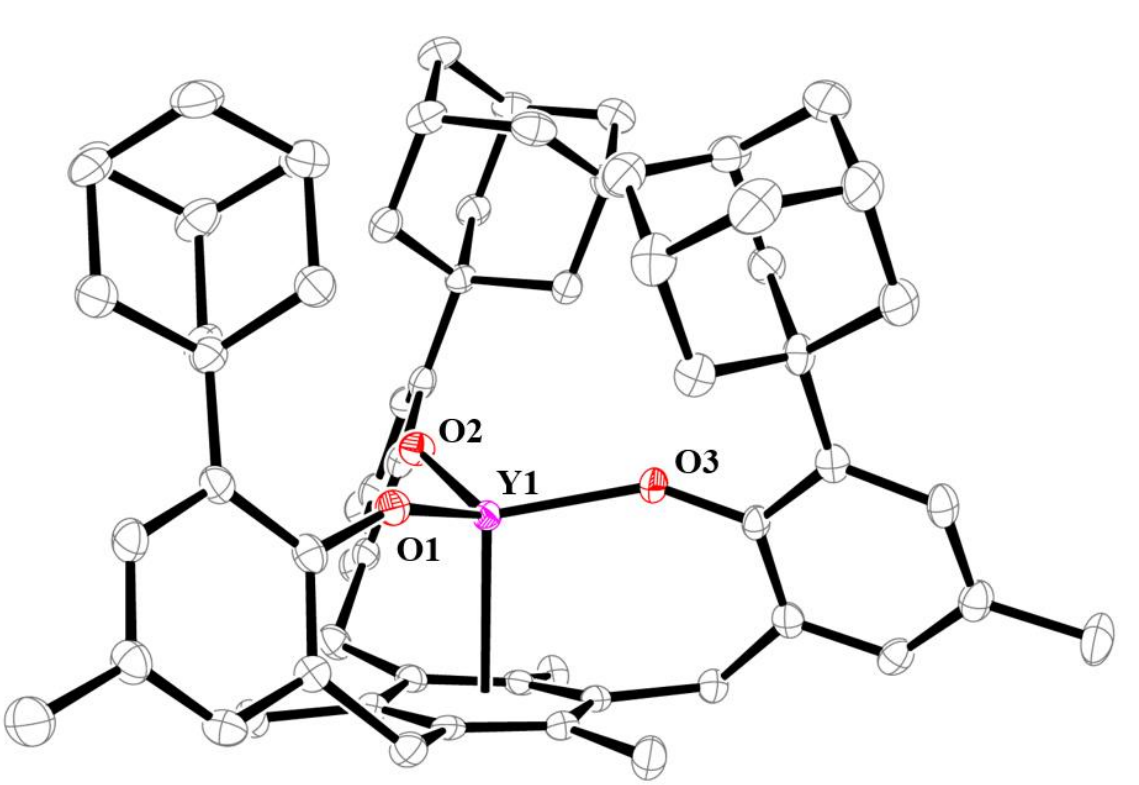

Figure 8.1. Molecular structure of $[((^{Ad,Me}ArO)_3mes)Y]$, **23-Y**, with thermal ellipsoids drawn at the 50% probability level. Hydrogen atoms are omitted for clarity.

Treatment of a colorless THF solution of **23-Y** with potassium metal in the presence of 2.2.2-cryptand generated a dark red solution reminiscent of the color of the **23-Ln** reductions, eq 8.2-8.4. Diffusion of Et_2O into the dark red THF solution similarly gave crystals, which were

identified as the co-crystallized mixture, [K(2.2.2-cryptand)][((^{Ad,Me}ArO)$_3$mes)Y] / [K(2.2.2-cryptand)][((^{Ad,Me}ArO)$_3$mes)YH], **24-Y/25-Y**, Figure 8.2, in a reaction analogous to eq 8.3. **24-Y**/**25-Y** crystallizes in the *P*2$_1$3 space group and is isomorphous with the previously reported **24-Ln**/**25-Ln** analogues of Gd, Dy, and Er that also co-crystallize as mixtures. The data were best refined as a 47:53 mixture of **24-Y**/**25-Y**. For comparison, the distributions for Gd, Er, and Dy were 65:35, 55:45, and 63:37, respectively.

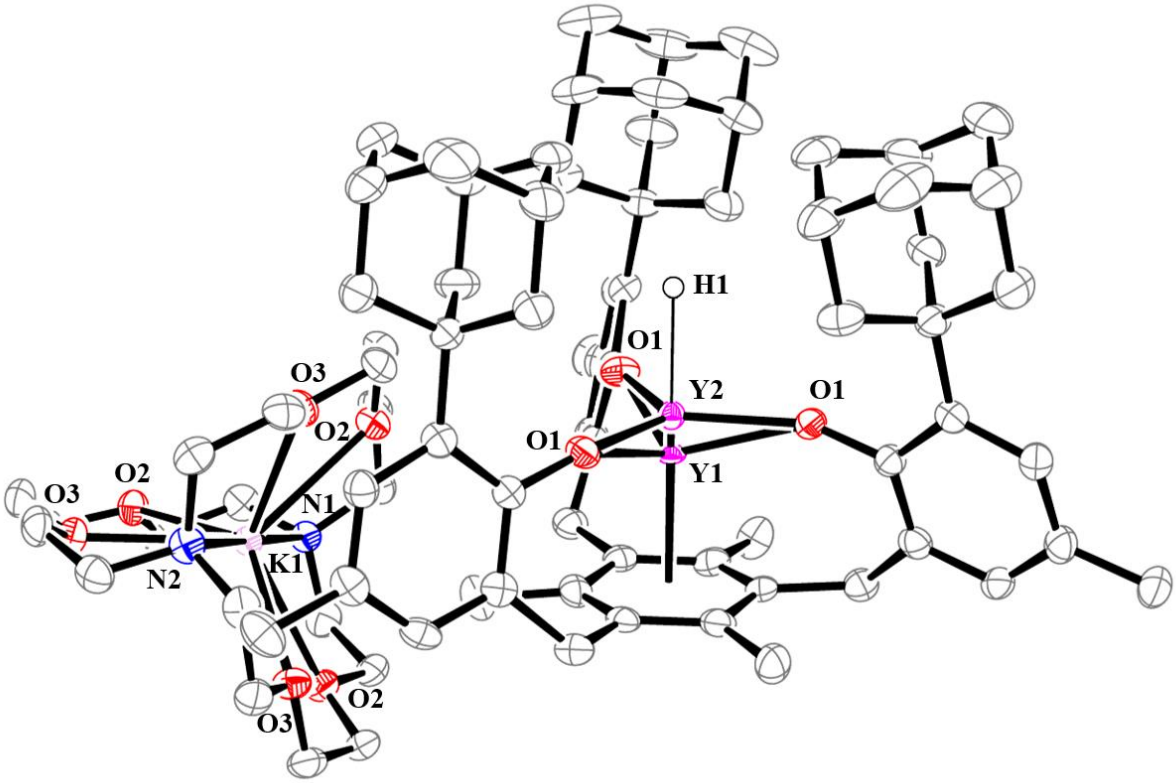

Figure 8.2. Molecular structure of [K(2.2.2-cryptand)][((^{Ad,Me}ArO)$_3$mes)Y] / [K(2.2.2-cryptand)][((^{Ad,Me}ArO)$_3$mes)YH], **24-Y/25-Y**, with thermal ellipsoids drawn at the 50% probability level. Hydrogen atoms except H1 are omitted for clarity.

In one reduction reaction, crystals of pure **25-Y** were obtained. This is the first pure tris(aryloxide)mesitylene rare-earth metal hydride complex isolated. Attempts to make this complex independently have not been successful, but the crystals of **25-Y** show the variation in metrical parameters that can occur between crystal data on the pure hydride, **25-Y**, and crystal data on **25-Y** in the **24-Y/25-Y** mixture. For this reason, the data on the co-crystallized mixtures has not been used to rationalize composition. The bond distances and angles for **24-Y/25-Y** and the differences between **24-Y** and **23-Y** are given in Tables 8.3 and 8.4. The other lanthanide examples and uranium have been added for comparison.

Although the ^{1}H NMR spectrum generated from the crystals of **24-Y**/**25-Y** in THF-d_8 is complicated, the resonance of the hydride ligand could be identified as a doublet centered at 7.81 ppm, Figure 8.3. The J_{YH} = 93 Hz coupling constant is larger than, but consistent with the J_{YH} = 74.8, 81.7, and 82.0 Hz coupling constants reported for the terminal hydride complexes, $[(C_5Me_4SiMe_3)_2YH(THF)]$,[25] $(C_5Me_5)_2YH(THF)$,[26] and $Ind(CH_3)_7]_2YH(THF)$,[27] respectively. An ^{89}Y–^{1}H HMQC experiment provided a correlation between the hydride resonance at 7.81 ppm with an yttrium resonance at −138.0 ppm in the ^{89}Y NMR spectrum of **24-Y**/**25-Y**. When CCl_4 is added to the NMR sample, the 7.81 ppm resonance disappears and chloroform grows in.

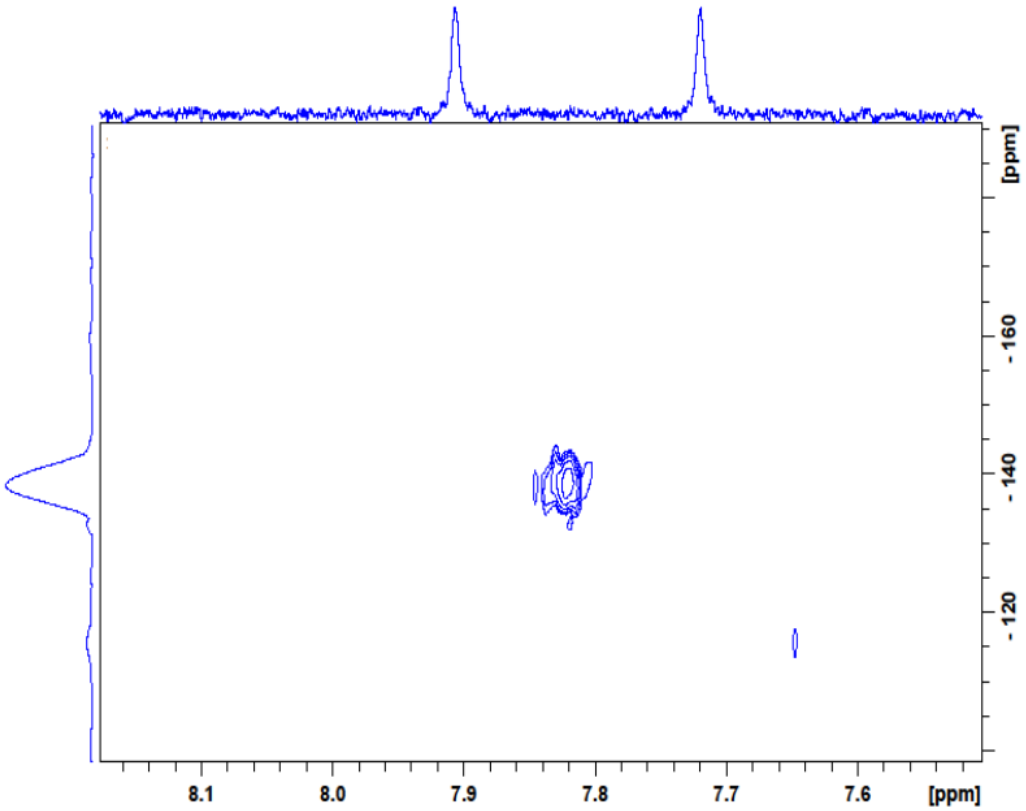

Figure 8.3. ^{89}Y-^{1}H HMQC NMR spectrum of crystals of **24-Y/25-Y** dissolved in THF-d_8 (10 mM) at 298 K.

EPR spectra were obtained with the assistance of Victoria Oswald in the lab of Andy Borovik. The EPR spectrum of a THF solution of crystals of the **24-Y/25-Y** mixture at 10 K showed an axial signal with g values at $g_1 = 2.036$ and $g_2 = 2.008$, Figure 8.4. At 77 K, the solution gives an isotropic singlet centered at $g_{iso} = 2.001$.

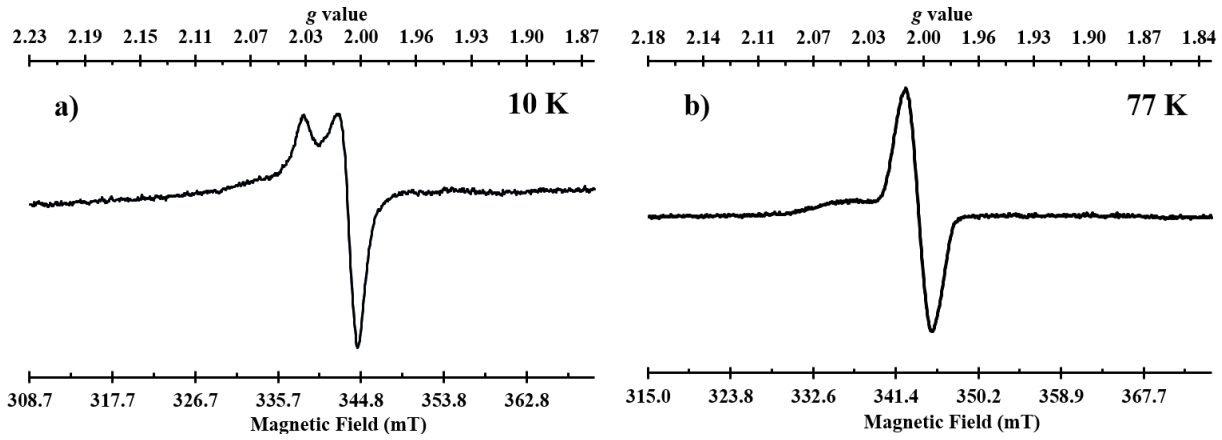

Figure 8.4. Experimental X-band EPR spectra of single crystals of **24-Y/25-Y** dissolved in THF (1 mM) at a) 10 K (Mode: perpendicular; g_1 = 2.036, g_2 = 2.008; ν = 9.643 GHz; P = 6.408 mW; modulation amplitude = 10.02 G) and b) 77 K (Mode: parallel; g_{iso} = 2.001; ν = 9.627 GHz; P = 6.408 mW; modulation amplitude = 10.02 G).

This is consistent with an organic radical rather than an Y^{2+} compound. Complexes of $4d^1$ Y^{2+} typically display doublets in their EPR spectra at g = 1.976-1.986 with hyperfine coupling constants of A = 34.6-46.9 G in tris(cyclopentadienyl) compounds[2,28] and A = 110 G in the tris(amide) $[Y(N(SiMe_3)_2]^{1-}$.[29] Hence, the **24-Y** component in the **24-Y**/**25-Y** crystal appears to contain Y^{3+} with a $[(^{Ad,Me}ArO)_3mes]^{4-}$ radical ligand. In this regard, **24-Y** is like **24-La**, **24-Ce**, and **24-Pr**, which were also characterized as Ln^{3+} complexes with a $[(^{Ad,Me}ArO)_3mes]^{4-}$ radical ligand. The EPR spectra of **24-La** under analogous conditions shown in Figure 8.5 appear similar to those of the **24-Y**/**25-Y** crystals. Solutions of **24-Y/25-Y** and **24-La** did not give observable EPR spectra at room temperature.

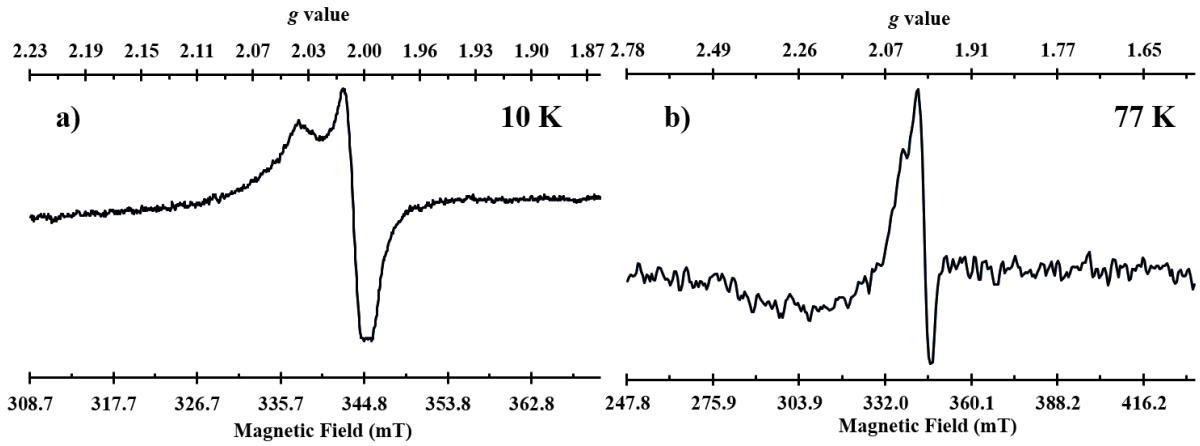

Figure 8.5. Experimental X-band EPR spectra of single crystals of **24-La** dissolved in THF (1 mM) at a) 10 K (Mode: perpendicular; g_1 = 2.036, g_2 = 2.008; ν = 9.643 GHz; P = 6.408 mW; modulation amplitude = 10.02 G) and b) 77 K (Mode: parallel; g_{iso} = 1.997; ν = 9.626 GHz; P = 2.021 mW; modulation amplitude = 10.02 G).

Density functional theory calculations were performed by Vamsee K. Voora in collaboration with the group of Filipp Furche. Computational studies on the anion in **24-Y**, $[(({}^{Ad,Me}ArO)_3mes)Y]^{1-}$, using the Tao-Perdew-Staroverov-Scuseria (TPSS) density functional approximation support the assignment made from the EPR data. The highest occupied orbital is predominantly localized on the mesitylene ring, Figure 8.6. The Mulliken population analysis using spin density difference indicates that about 0.8 excess negative charge is located on the ligand which indicates mesitylene-ring reduction. The calculations used def2-TZVPP* basis sets for the Y and O atoms, and def2-SVP* basis sets for other atoms.

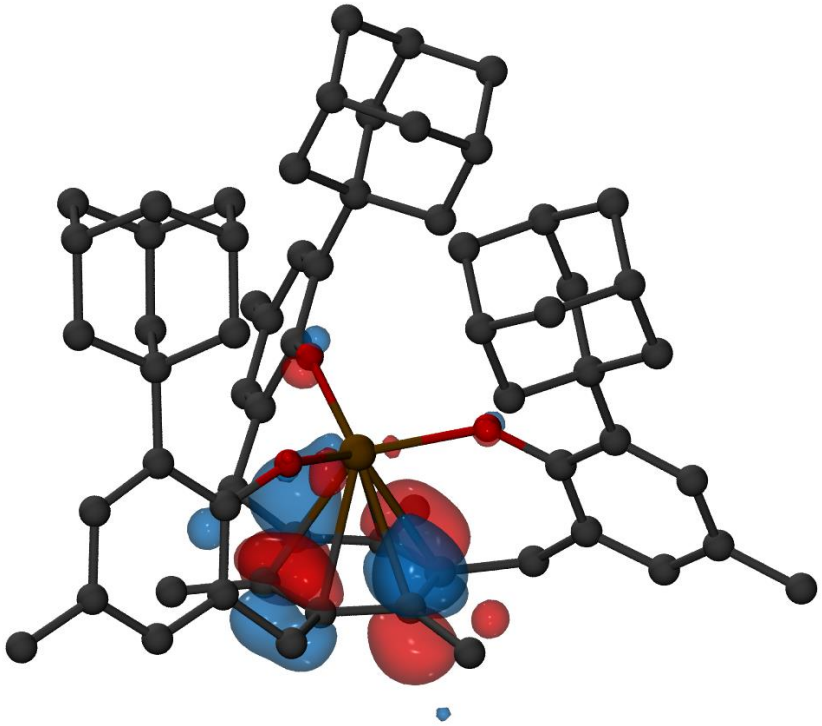

Figure 8.6. Isosurfaces for the highest singly occupied orbital of **24-Y** corresponding to a contour value of 0.05. Hydrogen atoms are omitted for clarity.

Given the useful results obtained by examining diamagnetic **23-Y**, further studies of the reduction of diamagnetic **23-La** were conducted. Instead of the red **24-La** product isolated in eq 8.4, large scale reactions were found to produce orange solids upon crystallization that upon workup could be recrystallized to give red microcrystals identified by X-ray crystallography as a complex that has lost hydrogen from a methylene group on the mesitylene component of the ligand: [K(2.2.2-cryptand)][((^{Ad,Me}ArO)$_3$($C_6Me_3(CH_2)_2CH$)La], **29-La**, Figure 8.7. Previously, a U^{4+} hydride complex of this ((^{Ad,Me}ArO)$_3$($C_6Me_3(CH_2)_2CH$))$^{4-}$ ligand, [((^{Ad,Me}ArO)$_3$($C_6Me_3(CH_2)_2CH$))U(μ-H)K(Et_2O)], had been isolated from the reaction of **23-U** with KC_8 or Na in benzene.[13] The two complexes are compared in Table 8.5. There are many similarities in the structures. Each complex has three rather different M–O(OAr) distances that

span 0.1 Å. The actual numbers differ because the ionic radius of seven coordinate La^{3+} is 0.15 Å larger than that of U^{4+}, but the differences for all three distances are close to this 0.15 Å value. The distance of the metal out of the plane of the three aryloxide oxygen atoms is similar in the two complexes as is the largest torsional angle of the arene ring which measures its non-planarity. In both complexes, the aryloxide arms of the ligand have undergone a T-shaped distortion in both complexes that gives three different O_{Ar}–La–O_{Ar} angles which are similar in **29-La** and [((^{Ad,Me}ArO)$_3$($C_6Me_3(CH_2)_2CH$))U(μ-H)K(Et_2O)]. Both complexes have one short C_{arene}-$C_{benzylic}$ bond distance consistent with a C=C bond. The complexes differ in that **29-La** has one short La–C bond, 2.668(6) Å, while all the others are over 2.816(6) Å. In contrast, [((^{Ad,Me}ArO)$_3$($C_6Me_3(CH_2)_2CH$))U(μ-H)K(Et_2O)] has all the U–C bonds in the narrow range of 2.729(3)-2.766(3) Å.

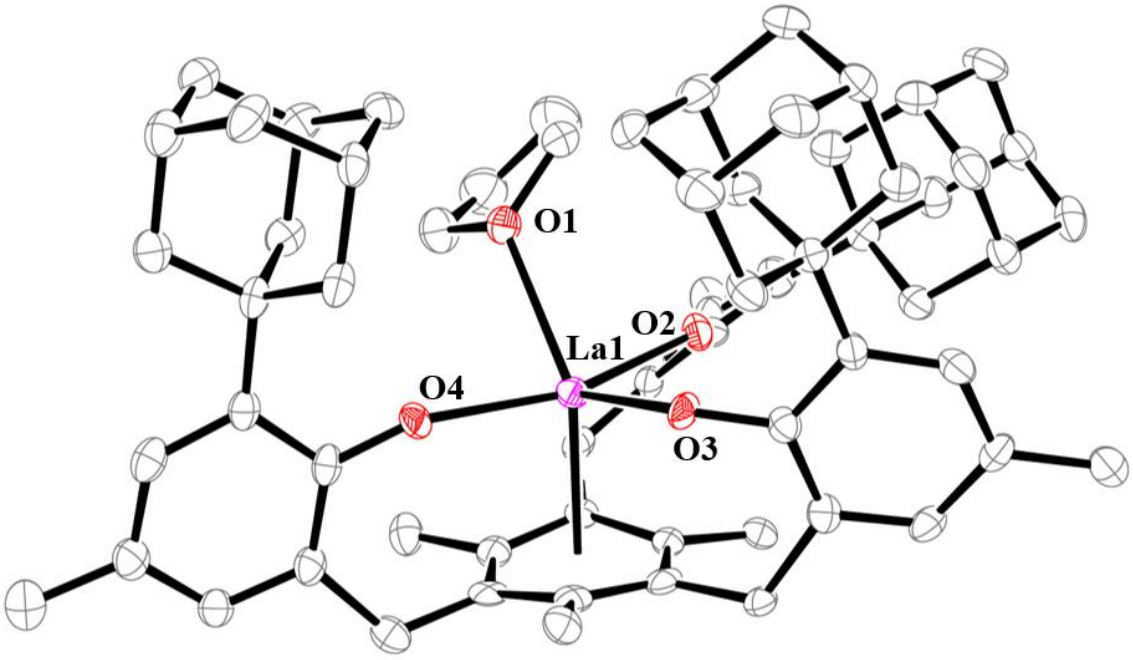

Figure 8.7. Molecular structure of the anion of [K(2.2.2-cryptand)][((^{Ad,Me}ArO)$_3$($C_6Me_3(CH_2)_2CH$))La], **29-La**, with thermal ellipsoids drawn at the 50% probability level. Hydrogen atoms and a $[K(2.2.2\text{-cryptand})]^+$ cation are omitted for clarity.

DFT calculations were done and are consistent with a $((^{Ad,Me}ArO)_3(C_6Me_3(CH_2)_2CH))^{4-}$ ligand where the charge is delocalized in the mesitylene and O2 aryloxide arm.

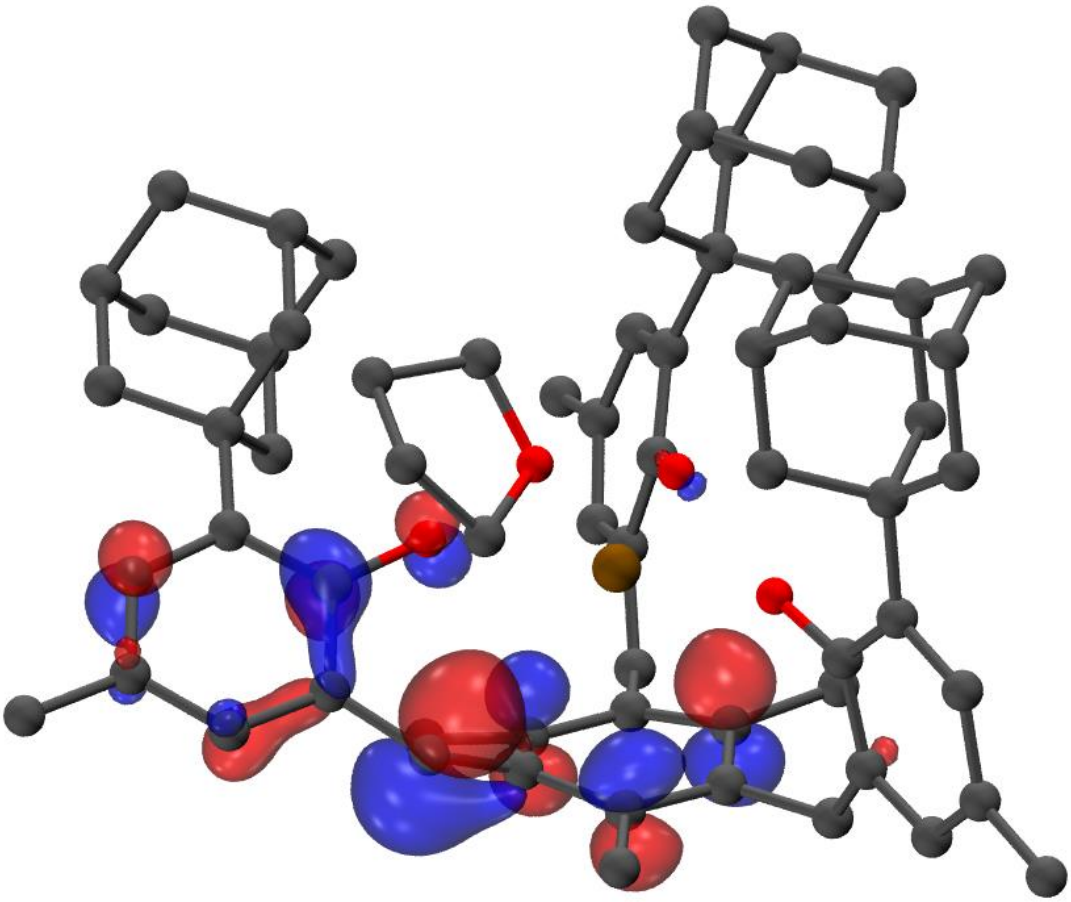

Figure 8.8. Isosurfaces for the HOMO of [K(2.2.2-cryptand)][$((^{Ad,Me}ArO)_3(C_6Me_3(CH_2)_2CH))$La], **29-La**, corresponding to a contour value of 0.05. Hydrogen atoms are omitted for clarity.

DISCUSSION

The extension of the $((^{Ad,Me}ArO)_3mes)^{3-}$ ligand system to yttrium has allowed the isolation and structural characterization of [$(^{Ad,Me}ArO)_3$mes)Y], **23-Y**, and its co-crystallized reduction products **24-Y**/**25-Y**, which are structurally analogous to those isolated for the late lanthanide

series Gd, Dy, and Er. The fact that Y^{3+} is diamagnetic has allowed the definitive identification of the hydride ligand by NMR spectroscopy. Evidence for the hydride ligand was also supported in the reactivity of the **24-Y**/**25-Y** crystal with CCl_4, which showed the disappearance of the hydride resonance and the appearance of the resonance for $CHCl_3$. The **24-Y** component of the **24-Y**/**25-Y** crystal is structurally similar to the **24-Ln** compounds previously reported in that the M–C_6(ring centroid) distance decreases upon reduction of **23-Ln** and the M–O_{Ar} distances increase slightly. However, EPR spectroscopy and our calculations suggest that **24-Y** is closer to its congener **24-La** and best described as a combination of Y^{3+} and a $[(^{Ad,Me}ArO)_3mes]^{4-}$ radical ligand.

The isolation of [K(2.2.2-cryptand)][$(^{Ad,Me}ArO)_3(C_6Me_3(CH_2)_2CH)$La], **29-La**, further demonstrates the flexibility of the $(^{Ad,Me}ArOH)_3mes)^{3-}$ ligand and provides another example of reactivity at the benzylic C–H position. Previously, the U^{4+} hydride complex [$(^{Ad,Me}ArO)_3(C_6Me_3(CH_2)_2CH)$U($\mu$-H)K($Et_2O$)] was isolated from reduction reactions involving **23-U** due to C–H bond activation at this position.[13] Subsequently, it was found that [$(^{Ad,Me}ArO)_3(C_6Me_3(CH_2)_2CH)$U($\mu$-H)K($Et_2O$)] could be generated from **24-U** upon exposure to additional reductant. In [$(^{Ad,Me}ArO)_3(C_6Me_3(CH_2)_2CH)$U($\mu$-H)K($Et_2O$)], one of the benzylic hydrogens is lost as a hydride ligand and binds to U^{4+}. Since lanthanum does not have access to a +4 oxidation state, a lanthanum product analogous to the [$(^{Ad,Me}ArO)_3(C_6Me_3(CH_2)_2CH)$U($\mu$-H)K($Et_2O$)] is not possible. Instead, **4-La** contains La^{3+} with a THF ligand in the newly opened coordination site analogous to the position of the hydride in [$(^{Ad,Me}ArO)_3(C_6Me_3(CH_2)_2CH)$U($\mu$-H)K($Et_2O$)]. Scheme 8.1 shows a route by which further reduction of **24-Ln** forms **29-Ln** and a hydride that can react with **23-Ln** to form the observed **25-Ln**.

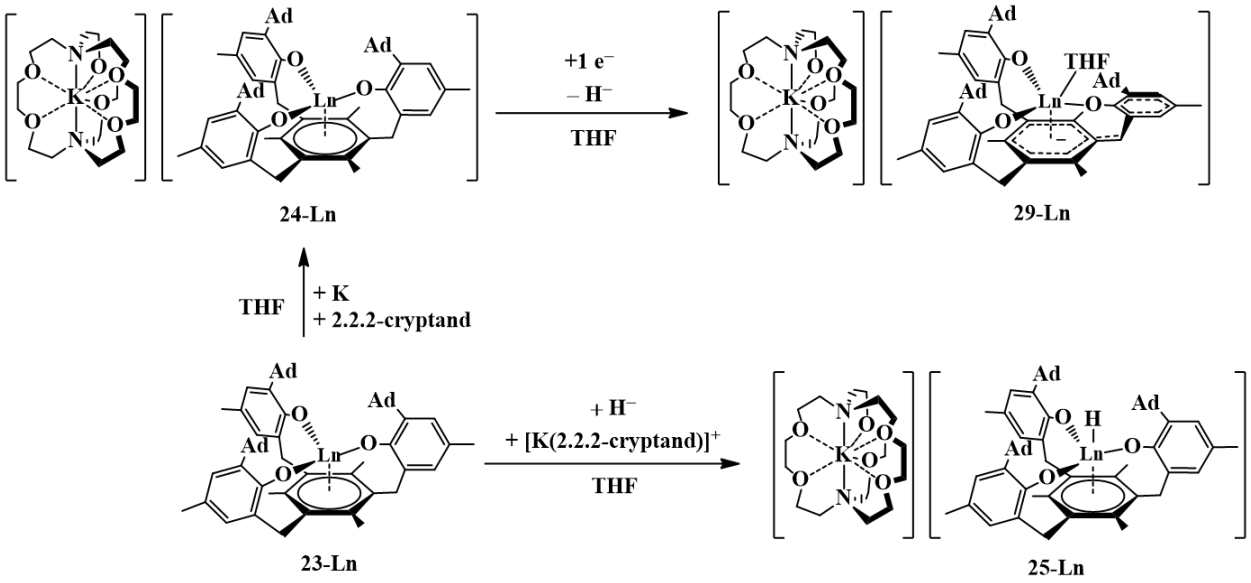

Scheme 8.1. Reaction scheme depicting a possible route to the Ln^{3+} hydride complexes [K(2.2.2-cryptand)][((^{Ad,Me}ArO)$_3$mes)LnH], **25-Ln**.

CONCLUSION

Reduction of the diamagnetic Y^{3+} complex, [((^{Ad,Me}ArO)$_3$mes)Y], **23-Y**, with potassium generates crystals consisting of two co-crystallized compounds [K(2.2.2-cryptand)][((^{Ad,Me}ArO)$_3$mes)Y] / [K(2.2.2-cryptand)][((^{Ad,Me}ArO)$_3$mes)YH], **24-Y/25-Y**. Complex **24-Y** provides EPR evidence that the ((^{Ad,Me}ArO)$_3$mes)$^{3-}$ ligand can be reduced to ((^{Ad,Me}ArO)$_3$mes)$^{4-}$. The hydride ligand in the **25-Y** component of **24-Y/25-Y** was definitively identified by NMR spectroscopy. The isolation of a pure crystal of **25-Y** further demonstrates that the metrical parameters of the co-crystalline mixtures of the **24-Ln**/**25-Ln** products should be evaluated with caution. The structural characterization of [K(2.2.2-cryptand)][((^{Ad,Me}ArO)$_3$(C$_6$Me$_3$(CH$_2$)$_2$CH))La], **29-La**, demonstrates that the ((^{Ad,Me}ArO)$_3$mes)$^{3-}$ ligand can exhibit C–H bond activation reactivity with rare-earth metals.

Table 8.1. Crystal data and structure refinement for **23-Y**, **24-Y/25-Y**, **25-Y**, and **29-La**.

	23-Y	**24-Y/25-Y**	**25-Y**	**29-La**
Empirical formula	$C_{63}H_{75}O_3Y$	$C_{81}H_{111}KN_2O_9YH_{0.55}$	$C_{81}H_{112}KN_2O_9Y$	$C_{85}H_{117}KLaN_2O_{10}$
Formula weight	969.14	1385.28	1385.73	1504.81
Temperature (K)	133(2)	133(2)	88(2)	100.0
Space group	$P2_1/c$	$P2_13$	$P2_13$	$P\bar{1}$
a (Å)	12.760(3)	19.8168(12)	19.7643(13)	15.0595(11)
b (Å)	15.661(3)	19.8168(12)	19.7643(13)	17.3788(13)
c (Å)	29.898(6)	19.8168(12)	19.7643(13)	17.4702(13)
α (°)	90	90	90	91.303(2)
β (°)	96.224(3)	90	90	107.463(2)
γ (°)	90	90	90	91.039(2)
Volume (Å^3)	5940(2)	7782.2(14)	7720.5(15)	4358.9(6)
Z	4	4	4	2
ρ_{calcd} (g/cm^3)	1.084	1.182	1.192	1.147
μ (mm^{-1})	1.022	0.857	0.864	0.590
$R1^a$	0.0455	0.0375	0.0459	0.0760
$wR2^b$	0.1101	0.0892	0.1069	0.1878

Definitions: ^{a}R1 = $\sum||Fo| - |Fc||/\sum|Fo|$; ^{b}wR2 = $[\sum[w(Fo^2 - Fc^2)^2]/\sum[w(Fo^2)^2]\ ]^{1/2}$.

Table 8.2. Selected bond lengths (Å) and angles (°) of **23-Y** and **23-Ln** (Ln = Gd, Dy, Er) complexes listed in order of decreasing ionic radius.

Metal	Six coordinate ionic radius[a]	M–O Range	M–O avg	M–C_6 (ring centroid)	M out of plane[b]	C_6 Torsion Angle[c]
Dy	0.912	2.093(3)-2.095(3)	2.094(1)	2.368	0.443	8.1
Y	0.90	2.085(2)-2.088(2)	2.087(1)	2.368	0.445	9.6
Er	0.89	2.078(2)-2.081(2)	2.079(1)	2.336	0.477	7.9

[a] From Shannon.[30] [b] Distance of M from the plane defined by the three O atoms of the $[(^{Ad,Me}ArO)_3mes]^{3-}$ ligand. [c] The largest dihedral angle between adjacent three carbon plane in the mesitylene ring.

Table 8.3. Selected bond lengths (Å) and angles (°) of the **25-Gd**, **25-Dy**, **25-Y**, and **25-Er** structures in in the **24-Ln/25-Ln** crystals listed in order of decreasing ionic radius. The pure **25-Y** was added for comparison.

Complex	M–O	M–Cnt	M–C(range)	M–H	M_{oop}	O–M–H	O–M–O
3-Gd	2.126(3)	2.864	3.176(6), 3.216(6)	1.94(7)	0.001	89.98(10)	120.003(1)
3-Dy	2.095(3)	2.838	3.154(4), 3.194(5)	1.92(7)	0.009	89.76(10)	119.997(1)
3-Y	2.095(2)	2.822	3.137(3), 3.177(3)	2.01(10)	0.002	89.94(6)	120.000(1)
3-Er	2.077(3)	2.854	3.170(4), 3.205(4)	1.91(7)	0.017	90.47(8)	119.993(2)
Pure 3-Y crystal	2.135(3)	2.775	3.103(4), 3.121(4)	2.00(8)	0.005	90.14(8)	120.000(1)

[a] From Shannon.[30] [b] Distance of M from the plane defined by the three O atoms of the $[(^{Ad,Me}ArO)_3mes]^{3-}$ ligand. [c] The largest dihedral angle between adjacent three carbon plane in the mesitylene ring.

Table 8.4. Table comparing structural changes that occur upon reduction of the Ln^{3+} complexes **23-Ln** to give their respective reduction products, **24-Ln**. The changes between **23-U** and **24-U** have also been added for comparison.

Metal	**ΔM–O (Å)**	**ΔM–C$_6$ (Ring Centroid) (Å)**	**ΔM out of plane [a] (Å)**	**ΔC$_6$ Torsion Angle (°)[b]**
La	0.037	−0.116	0.272	4.3
Ce[b]	0.012	−0.124	0.298	-
Pr	0.052	−0.103	0.272	5.6
Nd	0.050	−0.123	0.262	0.6
Sm	0.130	0.124	−0.090	−3.9
Gd	0.070	−0.127	0.162	0.5
Dy[c]	0.088	−0.130	0.165	−1.3
Y	0.097	−0.161	0.172	−2.7
Er	0.093	−0.136	0.160	−2.2
Yb	0.144	0.090	−0.045	−4.7
U	0.068	−0.170	0.193	−0.9

[a] Distance of M from the plane defined by the three O atoms of the $[(^{Ad,Me}ArO)_3mes]^{3-}$ ligand. [b]Obtained using interpolated metrical parameters for **23-Ce**.

Table 8.5. Selected bond lengths (Å) and angles (°) of [K(2.2.2-cryptand)][((^{Ad,Me}ArO)$_3$($C_6Me_3(CH_2)_2CH$)La], **29-La**, and [((^{Ad,Me}ArO)$_3$($C_6Me_3(CH_2)_2CH$))U(μ-H)K(Et_2O)].

	M–O	**M–C**	**M out of O_3 plane[a]**	**C_{arene}–$C_{benzylic}$**	**O–M–O**	**Largest C_6 Torsion Angle[b]**
29-La	2.349(4)	2.668(6)	0.18	1.410(9)	90.56(15)	18.4
	2.288(4)	2.816(6)		1.524(9)	103.64(15)	
	2.392(4)	2.841(6)		1.530(9)	162.75(14)	
		2.852(6)				
		2.914(6)				
		2.984(6)				
[((^{Ad,Me}ArO)$_3$-($C_6Me_3(CH_2)_2CH$))-U(μ-H)K(Et_2O)]	2.144(4)	2.729(3)	0.20	1.425(7)	83.20(13)	23.3
	2.181(3)	2.732(3)		1.508(7)	107.57(13)	
	2.232(3)	2.736(3)		1.523(8)	164.28(13)	
		2.754(3)				
		2.766(3)				
		2.774(3)				

[a] Distance of M from the plane defined by the three O atoms of the [(^{Ad,Me}ArO)$_3$mes]$^{3-}$ ligand. [b] The largest dihedral angle between adjacent three carbon plane in the mesitylene ring.

REFERENCES

(1) Hitchcock, P. B.; Lappert, M. F.; Maron, L.; Protchenko, A. V. *Angew. Chem.* **2008**, *47*, 1488-1491.

(2) MacDonald, M. R.; Ziller, J. W.; Evans, W. J. *J. Am. Chem. Soc.* **2011**, *133*, 15914-159147.

(3) MacDonald, M. R.; Bates, J. E.; Fieser, M. E.; Ziller, J. W.; Furche, F.; Evans, W. J. *J. Am. Chem. Soc.* **2012**, *134*, 8420-8423.

(4) MacDonald, M. R.; Bates, J. E.; Ziller, J. W.; Furche, F.; Evans, W. J. *J. Am. Chem. Soc.* **2013**, *135*, 9857-9868.

(5) Fieser, M. E.; MacDonald, M. R.; Krull, B. T.; Bates, J. E.; Ziller, J. W.; Furche, F.; Evans, W. J. *J. Am. Chem. Soc.* **2015**, *137*, 369-382.

(6) MacDonald, M. R.; Fieser, M. E.; Bates, J. E.; Ziller, J. W.; Furche, F.; Evans, W. J. *J. Am. Chem. Soc.* **2013**, *135*, 13310-13313.

(7) Langeslay, R. R.; Fieser, M. E.; Ziller, J. W.; Furche, F.; Evans, W. J. *Chem. Sci.* **2015**, *6*, 517-521.

(8) Windorff, C. J.; MacDonald, M. R.; Meihaus, M. R.; Ziller, J. W.; Long, J. R.; Evans, W. J. *Chem. Eur. J.* **2016**, *22*, 772-782.

(9) Windorff, C. J.; Chen, G. P.; Cross, J. N.; Evans, W. J.; Furche, F.; Gaunt, A. J.; Janicke, M. T.; Kozimor, S. A.; Scott, B. L. *J. Am. Chem. Soc.* **2017**, *139*, 3970-3973.

(10) Evans, W. J. *Organometallics* **2016**, *35*, 3088-3100.

(11) Woen, D. H.; Evans, W. J. In *Handbook on the Physics and Chemistry of Rare Earths*; 1st ed.; Elsevier: Amsterdam, 2016; Vol. 50, p 337-394.

(12) La Pierre, H. S.; Scheurer, A.; Heinemann, F. W.; Hieringer, W.; Meyer, K. *Angew. Chem. Int. Ed.* **2014**, *53*, 7158-7162.

(13) La Pierre, H. S.; Kameo, H.; Halter, D. P.; Heinemann, F. W.; Meyer, K. *Angew. Chem. Int. Ed.* **2014**, *53*, 7154-7157.

(14) Fieser, M. E.; Palumbo, C. T.; La Pierre, H. S.; Halter, D. P.; Voora, V.; Ziller, J. W.; Furche, F.; Meyer, K.; Evans, W. J. *Chem. Sci.* **2017**, Advance Article.

(15) Edelmann, F. T. *Synthetic Methods of Organometallic and Inorganic Chemistry*; George Thieme Verlag Struttgart: New York, 1997; Vol. 6.

(16) APEX2 Version 2014.11-0, Bruker AXS, Inc.; Madison, WI, 2014.

(17) SAINT Version 8.34a, Bruker AXS, Inc.; Madison, WI, 2013.

(18) Sheldrick, G. M.; SADABS, Version 2014/5, Bruker AXS, Inc.; Madison, WI, 2014.

(19) Sheldrick, G. M.; SHELXTL, Version 2014/7, Bruker AXS, Inc.; Madison, WI, 2014.

(20) International Tables for X-Ray Crystallography, 1992, Vol. C., Dordrecht: Kluwer Academic Publishers.

(21) Spek, A. L.; SQUEEZE, Acta Cryst. 2015, C71, 9-19.

(22) Spek, A. L.; PLATON, Acta. Crys. 2009, D65, 148-155.

(23) Parsons, S.; Flack, H. D. *Acta Cryst.* **2013**, *B69*, 249-259.

(24) SAINT Version 8.37a, Bruker AXS, Inc.: Madison, WI, 2015.

(25) Takenaka, Y.; Hou, Z. *Organometallics* **2009**, *28*, 5196-5203.

(26) Den Haan, K. H.; Wielstra, Y.; Teuben, J. H. *Organometallics* **1987**, *6*, 2053-2060.

(27) Gavenonis, J.; Tilley, T. D. *J. Organomet. Chem.* **2004**, *689*, 870-878.

(28) Corbey, J. F.; Woen, D. H.; Palumbo, C. T.; Fieser, M. E.; Ziller, J. W.; Furche, F.; Evans, W. J. *Organometallics* **2015**, *34*, 3909-3921.
(29) Fang, M.; Lee, D. S.; Ziller, J. W.; Doedens, R. J.; Bates, J. E.; Furche, F.; Evans, W. J. *J. Am. Chem. Soc.* **2011**, *133*, 3784-3787.
(30) Shannon, R. D. *Acta Crystallogr A* **1976**, *32*, 751-767.

CHAPTER 9

Structural Characterization of the Bent Metallocenes, $[C_5H_3(SiMe_3)_2]_2Sm$ and $[C_5H_3(CMe_3)_2]_2Ln$ (Ln = Eu, Sm), and the Mono(cyclopentadienyl) Tetraphenylborate Complex, $[C_5H_3(CMe_3)_2]Eu(\mu\text{-}\eta^6\text{:}\eta^1\text{-}Ph)_2BPh_2$

INTRODUCTION[†]

As mentioned in Chapters 1-8, studies of the reductive chemistry of the rare-earth metals have revealed that the +2 oxidation state is available in crystalline molecular complexes not only for Eu, Yb, Sm, Tm, Dy, and Nd, but also for all the metals in the series except radioactive Pm, eq 1.[1-6] Evidence for the new non-traditional ions was first shown with tris(cyclopentadienyl) La and Ce complexes of Cp″ = $C_5H_3(SiMe_3)_2$ and its all carbon analog, Cp^{tt} = $C_5H_3(CMe_3)_2$.[1,7-9] Subsequently, crystallographic evidence was obtained for +2 metal complexes of all the lanthanides with Cp′ = $C_5H_4SiMe_3$.[2,3,10,11] Eq 9.1 shows the reactions that led to the crystallographically-characterizable Ln^{2+} complexes.

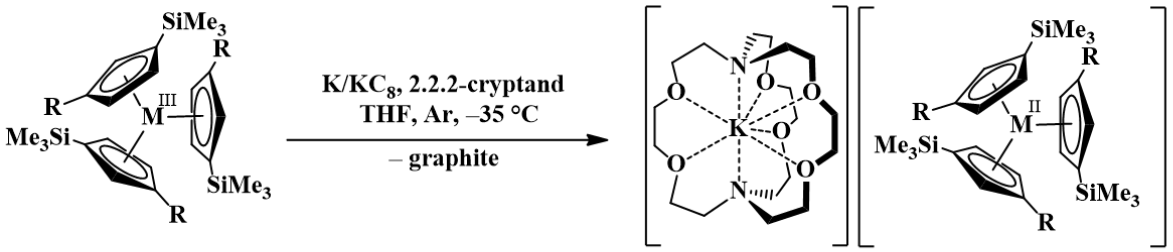

(9.1)

R = $SiMe_3$; M = La
R = H; M = Y, La, Ce, Pr, Nd, Sm, Gd, Tb, Dy, Ho, Er, Tm, Lu

The isolation of these new ions was attributed to the presence of a low lying d_z^2 orbital in the tris(cyclopentadienyl) coordination environment such that reduction of a $4f^n$ Ln^{3+} precursor

[†] Portions of this chapter have been published: Palumbo, C. T., Ziller, J. W., Evans, W. J. *J. Organomet. Chem.*, **2017**, In Press.

generated a $4f^n5d^1$ Ln^{2+} product. These products were preferred over the formation of the traditional $4f^{n+1}$ Ln^{2+} products.

It was later shown that La^{2+} and Ce^{2+} could also be isolated in a coordination environment of two cyclopentadienyl rings and a bridging benzene dianion, eq 9.2.[12] This result suggested the generalization that three anionic carbocyclic rings would stabilize new rare earth metal oxidation states.

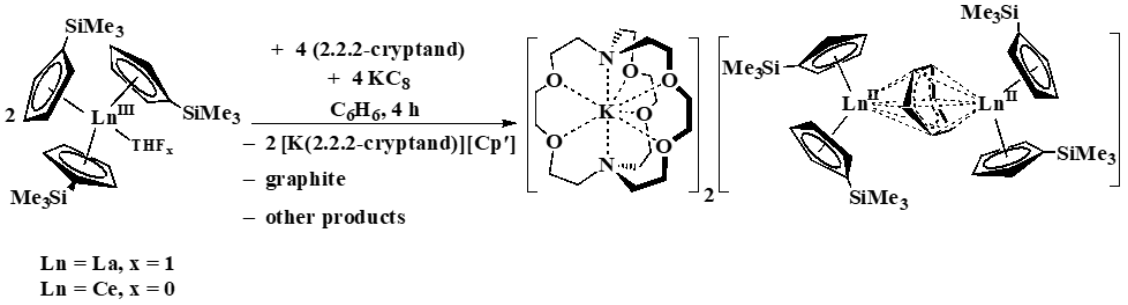

(9.2)

Once these new Ln^{2+} ions were identified, the synthesis of molecular complexes of Ln^{1+} became a target. All of the lanthanides form Ln^{1+} ions in the gas phase.[13] The +1 oxidation state has also been identified in molecular species in the case of scandium, the smallest rare-earth metal. Three examples have been characterized by X-ray crystallography: $[(\eta^5\text{-}P_3C_2{}^t\!Bu_2)Sc]_2(\mu\text{-}\eta^6\text{:}\eta^6\text{-}P_3C_3{}^t\!Bu_3)$,[14] $[Sc(\eta^5\text{-}P_3C_2{}^t\!Bu_2)(\mu\text{-}\eta^2\text{:}\eta^5\text{-}P_3C_2{}^t\!Bu_2)Sc(\eta^5\text{-}P_3C_2{}^t\!Bu_2)]$,[15] and $(LMgBr)_2ScBr$ (L = $Et_2NCH_2CH_2NC(Me)CHC(Me)NCH_2CH_2NEt_2$).[16] A spectrum of Sm^{1+} has been reported in a potassium chloride matrix doped with Sm^{2+} and exposed to γ radiation.[17] In addition, the isolation of Ln^{1+} complexes seems reasonable if one considers that Nd, Tb, Dy, Ho, Er, and Lu are known in the formally zero oxidation state in the bis(arene) complexes, $Ln[C_6H_3{}^t\!Bu_3\text{-}1,3,5]_2$.[18]

Reduction of $4f^7$ Eu^{2+} and $4f^6$ Sm^{2+} could form $4f^75d^1$ Eu^{1+} and $4f^7$ Sm^{1+} complexes. The former configuration matches that of Gd^{2+}, which has proven to be one of the more stable and characterizable Ln^{2+} ions,[2,19] and the latter configuration has the advantage of being a half-filled shell. Precursors containing three carbocyclic rings were sought as starting materials since this

was successful in eq 9.1 and 9.2. If tris(cyclopentadienyl) Ln^{2+} complexes, $[(C_5R_5)_3Ln]^{1-}$, were used as precursors to Ln^{1+} products, the target compounds would be dianions, $[(C_5R_5)_3Ln]^{2-}$. Since it could be less difficult to add an electron to a neutral precursor to make a monoanionic target, alternative neutral three ring starting materials were desirable. One class of such neutral complexes is the $(\eta^5\text{-}C_5Me_5)Ln(\mu\text{-}\eta^6\text{:}\eta^1\text{-}Ph)_2BPh_2$ series isolated from $(C_5Me_5)_2Ln$ and $[HNEt_3][BPh_4]$,[20,21] eq 9.3.

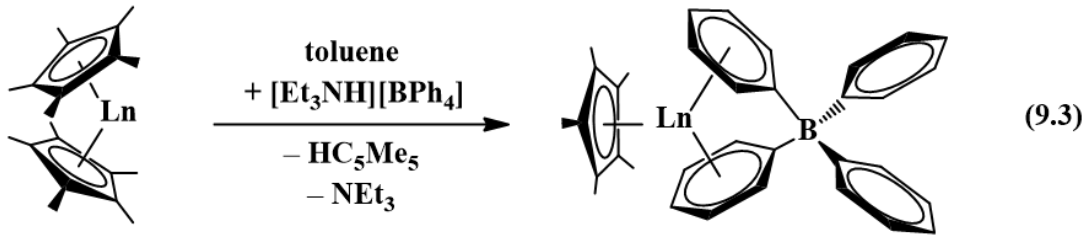

(9.3)

Ln = Sm, Eu, Yb

In this report, attempts to make precursors analogous to $(\eta^5\text{-}C_5Me_5)Ln(\mu\text{-}\eta^6\text{:}\eta^1\text{-}Ph)_2BPh_2$ are described with the Cp″ and Cp^{tt} ligands that had been used previously in the synthesis of Ln^{2+} ions.[1-6] This requires the synthesis of the unsolvated precursor metallocenes Cp''_2Ln, **30-Ln**, and Cp^{tt}_2Ln, **31-Ln**. **30-Eu** had previously been synthesized and structurally characterized, but the structure of the Sm analogue was not published when it was synthesized.[22] In the case of Cp^{tt}, the solvated complexes, $Cp^{tt}_2Ln(THF)$, Ln = Eu, Sm, are known.[23,24] The synthesis and structure of **30-Sm**, **31-Sm**, and **31-Eu**, are described here which allow a comparison of the Cp″ and Cp^{tt} ligands with +2 lanthanide ions. Attempts to convert these compounds to unsolvated monocyclopentadienyl tetraphenylborate complexes are also described.

EXPERIMENTAL

All manipulations and syntheses described below were conducted with rigorous exclusion of air and water using standard Schlenk line and glovebox techniques under an argon atmosphere. Solvents were sparged with UHP argon (Airgas) and dried by passage through columns containing Q-5 and molecular sieves prior to use. NMR solvents (Cambridge Isotope Laboratories) were dried over NaK alloy, degassed by three freeze-pump-thaw cycles, and vacuum transferred before use. Cp''_2Sm, **30-Sm**,[22] Cp''_2Eu, **1-Eu**,[25] $Cp^{tt}_2Sm(THF)$,[23] $Cp^{tt}_2Eu(THF)$,[24] and $[Et_3NH][BPh_4]$[26] were prepared as previously described. ^1H NMR spectra were recorded on Bruker GN500 or CRYO500 MHz spectrometers (^{13}C NMR at 125 MHz) at 298 K unless otherwise stated and referenced internally to residual protio-solvent resonances. IR samples were prepared as KBr pellets on a Jasco FT/IR-4700 system. Elemental analyses were conducted on a Perkin-Elmer 2400 Series II CHNS elemental analyzer.

Cp^{tt}_2Eu, 31-Eu. In a glovebox, a 20 mm x 320 mm tube attached to a high vacuum greaseless stopcock was charged with red solids of $Cp^{tt}_2Eu(THF)$ [24] (436 mg, 0.753 mmol). The apparatus was attached to a high vacuum line that can achieve pressures of 1 x 10^{-6} Torr and the sample was heated to 100 °C. After 6 h, orange solids had sublimed that still contained coordinated THF by IR spectroscopy. The material was re-sublimed two additional times under the same conditions and the apparatus was brought into a glovebox free of coordinating solvents. THF free **31-Eu** was collected as a bright orange solid (330 mg, 86%). Orange single crystals of **31-Eu** suitable for X-ray diffraction were grown during the sublimation. Anal. Calcd for $C_{26}H_{42}Eu$: C,

61.64; H, 8.36. Found: C, 61.44; H, 8.46. IR: 3065w, 2898m, 2860m, 1594w, 1460m, 1388w, 1355m, 1250s, 1200m, 1159w, 1050w, 1035w, 934w, 797s, 783s, 712m, 676w cm^{-1}.

Cp^{tt}_2Sm, 31-Sm. Following the procedure for **31-Eu**, dark green $Cp^{tt}_2Sm(THF)$[23] (355 mg, 615 mmol) was desolvated via sublimation by heating to 100 °C under high vacuum for 6 h. This was repeated two additional times until IR spectroscopy showed no evidence of THF. The apparatus was brought into a glovebox free of coordinating solvents and THF-free **31-Sm** was collected as dark green solid (199 mg, 64%). Anal. Calcd for $C_{26}H_{42}Sm$: C, 61.84; H, 8.38. Found: C, 61.49; H, 8.76. ^{1}H NMR (C_6H_6): δ 26.6 [2H, $C_5H_3(CMe_3)_2$], 8.72 [18H, $C_5H_3(CMe_3)_2$], −13.4 [1H, $C_5H_3(CMe_3)_2$]. ^{1}H NMR (C_7H_8): δ 26.1 [2H, $C_5H_3(CMe_3)_2$], 8.66 [18H, $C_5H_3(CMe_3)_2$], −12.3 [1H, $C_5H_3(CMe_3)_2$]. ^{13}C NMR (C_7H_8): δ 94.4 [$C_5H_3(CMe_3)_2$], 46.7 [$C_5H_3(CMe_3)_2$], −23.8 [$C_5H_3(C_5H_3)_2$], −96.8 [$C_5H_3(C_5H_3)_2$], −97.8 [$C_5H_3(C_5H_3)_2$]. IR: 3757w, 3633w, 3065w, 2962s, 2901s, 2858s, 1589w, 1459m 1387m, 1353m, 1250m, 1200m, 1159m, 1084w, 1051m, 1019w, 934m, 796s, 785s, 710s, 676m, 672m cm^{-1}. Solid **31-Sm** was dissolved in toluene and the solvent was subsequently removed to yield a dark residue. The residue was washed with hexane which left behind dark green single crystals of **31-Sm** characterizable by X-ray crystallography.

$Cp^{tt}Eu(\mu\text{-}\eta^6\text{:}\eta^1\text{-}Ph)_2BPh_2$, 32-Eu. In a glovebox free of coordinating solvents, $[Et_3NH][BPh_4]$ (39 mg, 0.09 mmol) was added to a stirring red-orange solution of **31-Eu** (47 mg, 0.09 mmol) in 5 mL of toluene. After the resultant red-orange slurry was stirred for 30 min, the volatiles were removed to give red solids. The solids were re-dissolved in toluene, filtered, and layered with hexane. The resultant mixture was stored at −35 °C for 2 d to yield **32-Eu** as red single crystals suitable for X-ray diffraction (22 mg, 37%). Anal. Calcd for $C_{37}H_{41}BEu$: C, 68.53; H, 6.37. Found: C, 68.50; H, 6.46. IR: 3060m, 2956s, 2934s, 2860m, 1564w, 1458m, 1428m,

1385w, 1361m, 1352m, 1307w, 1270w, 1251m, 1198w, 1181w, 1160m, 1150m, 1067w, 1032m, 930w, 857m, 805s, 781m, 748s, 736s, 711s, 685m, 626w cm^{-1}.

$Cp^{tt}Sm(\mu\text{-}\eta^6\text{:}\eta^1\text{-}Ph)_2BPh_2$, 32-Sm. In a glovebox free of coordinating solvents, $[Et_3NH][BPh_4]$ (88 mg, 0.208 mmol) was added to a stirred purple solution of **31-Sm** (100 mg, 0.198 mmol) in 5 mL of toluene at −35 °C. The resultant purple slurry slowly turned to dark blue as it was stirred. After 30 min, the mixture was centrifuged and filtered to remove insolubles and the volatiles and solvent were removed under reduced pressure to yield a blue-green solid. This solid was dissolved in toluene and filtered and the resultant solution was layered with hexane. Storing this mixture at −35 °C for 2 d gave **32-Sm** as dark blue-green microcrystalline clusters (55 mg, 43%). Anal. Calcd for $C_{37}H_{41}BSm$: C, 68.70; H, 6.39. Found: C, 68.90; H, 6.54. ^1H NMR (C_6H_6): δ 23.1 [18H, $C_5H_3(CMe_3)_2$], 9.13 [2H, $C_5H_3(CMe_3)_2$], −12.2 [1H, $C_5H_3(CMe_3)_2$].

X-ray Data Collection, Structure Solution and Refinement for Cp''_2Sm, 30-Sm. A black crystal of approximate dimensions 0.130 x 0.151 x 0.216 mm was mounted on a glass fiber and transferred to a Bruker SMART APEX II diffractometer. The APEX2[27] program package was used to determine the unit-cell parameters and for data collection (25 sec/frame scan time for a sphere of diffraction data). The raw frame data was processed using SAINT[28] and SADABS[29] to yield the reflection data file. Subsequent calculations were carried out using the SHELXTL[30] program. The diffraction symmetry was *mmm* and the systematic absences were consistent with the orthorhombic space group $P2_12_12_1$ that was later determined to be correct. The structure was solved using the coordinates of the europium analogue[25] and refined on F^2 by full-matrix least-squares techniques. The analytical scattering factors[31] for neutral atoms were used throughout the analysis. Hydrogen atoms were included using a riding model. Least-squares analysis yielded wR2 = 0.0664 and Goof = 1.021 for 511 variables refined against 12390 data (0.78Å), R1 = 0.0322

for those 11042 data with I > 2.0σ(I). The absolute structure was assigned by refinement of the Flack parameter.[32] Details are given in Table 9.1.

X-ray Data Collection, Structure Solution and Refinement for Cp^{tt}_2Sm, 31-Sm. A green crystal of approximate dimensions 0.181 x 0.294 x 0.444 mm was mounted on a glass fiber and transferred to a Bruker SMART APEX II diffractometer. The APEX2[27] program package and the CELL_NOW[33] were used to determine the unit-cell parameters. Data was collected using a 20_ sec/frame scan time for a sphere of diffraction data. The raw frame data was processed using SAINT[28] and TWINABS[34] to yield the reflection data file (HKLF5 format).[34] Subsequent calculations were carried out using the SHELXTL[30] program. There were no systematic absences nor any diffraction symmetry other than the Friedel condition. The centrosymmetric triclinic space group $P\bar{1}$ was assigned and later determined to be correct. The structure was solved by dual space methods and refined on F^2 by full-matrix least-squares techniques. The analytical scattering factors[31] for neutral atoms were used throughout the analysis. Hydrogen atoms were included using a riding model. There were two molecules of the formula-unit present. (Z = 4). At convergence, wR2 = 0.0914 and Goof = 1.081 for 513 variables refined against 9709 data (0.73 Å), R1 = 0.0342 for those 9015 with I > 2.0σ(I). The structure was refined as a three-component twin. Details are given in Table 9.1.

X-ray Data Collection, Structure Solution and Refinement for Cp^{tt}_2Eu, 31-Eu. A yellow crystal of approximate dimensions 0.124 x 0.263 x 0.271 mm was mounted on a glass fiber and transferred to a Bruker SMART APEX II diffractometer. The APEX2[27] program package was used to determine the unit-cell parameters and for data collection (15 sec/frame scan time for a sphere of diffraction data). The raw frame data was processed using SAINT[28] and SADABS[29] to yield the reflection data file. Subsequent calculations were carried out using the SHELXTL[30]

program. The diffraction symmetry was 2/*m* and the systematic absences were consistent with the monoclinic space group $P2_1/c$ that was later determined to be correct. The structure was solved by dual space methods and refined on F^2 by full-matrix least-squares techniques. The analytical scattering factors[31] for neutral atoms were used throughout the analysis. Hydrogen atoms were located from a difference-Fourier map and refined (x,y,z and U_{iso}). The europium atom was disordered (0.97:0.03) and included using two components with partial site-occupancy-factors. At convergence, wR2 = 0.0380 and Goof = 1.033 for 416 variables refined against 6244 data (0.73Å), R1 = 0.0168 for those 5682 data with I > 2.0σ(I). Details are given in Table 9.1.

X-ray Data Collection, Structure Solution and Refinement for $Cp^{tt}Eu(\mu\text{-}\eta^6\text{:}\eta^1\text{-}Ph)_2BPh_2$, 32-Eu. A red crystal of approximate dimensions 0.109 x 0.130 x 0.203 mm was mounted on a glass fiber and transferred to a Bruker SMART APEX II diffractometer. The APEX2[27] program package was used to determine the unit-cell parameters and for data collection (60 sec/frame scan time for a sphere of diffraction data). The raw frame data was processed using SAINT[28] and SADABS[29] to yield the reflection data file. Subsequent calculations were carried out using the SHELXTL[30] program. The diffraction symmetry was *mmm* and the systematic absences were consistent with the orthorhombic space groups *Pbcm* and $Pca2_1$. It was later determined that space group $Pca2_1$ was correct. The structure was solved by dual space methods and refined on F^2 by full-matrix least-squares techniques. The analytical scattering factors[31] for neutral atoms were used throughout the analysis. Hydrogen atoms were included using a riding model. There were two molecules of the formula-unit present (Z = 8). At convergence, wR2 = 0.0870 and Goof = 1.046 for 716 variables refined against 13471 data (0.78Å), R1 = 0.0396 for those 10641 data with I > 2.0σ(I). The structure was refined as a two-component inversion twin. Details are given in Table 9.1.

RESULTS AND DISCUSSION

Synthesis and Structural Characterization of Base-Free Metallocenes Cp_2Ln.

Cp''_2Sm, 30-Sm. The base free metallocene **30-Sm** was synthesized according to the previously reported procedure in which the ligated THF is removed from $Cp''_2Sm(THF)$ by repeated sublimation, eq 9.4. Dark green single crystals of **30-Sm** can be obtained from the residue that precipitates from a supersaturated toluene solution of the sublimate after washing with hexane, Figure 9.1. The complex crystallizes as an extended polymer and is isomorphous with Cp''_2Eu, **30-Eu**.[25]

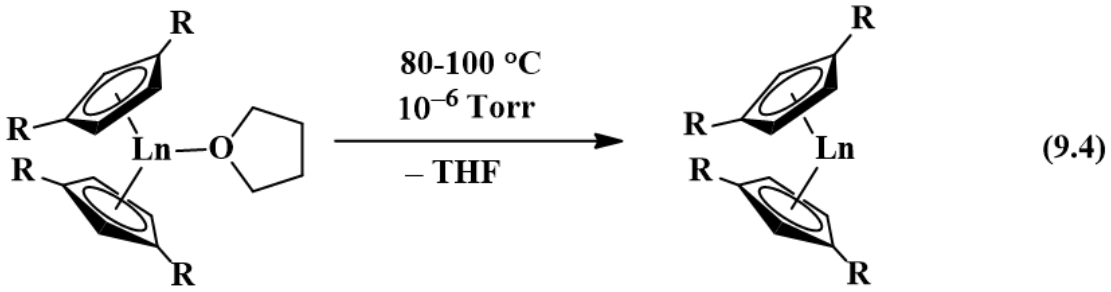

(9.4)

Although the structure of **30-Eu** has been published and the metrical parameters of **30-Sm** are very similar, the structure will be described briefly so a comparison can be made between both **30-Ln** complexes and both of the **31-Ln** structures described below. The metrical parameters of **30-Sm** are compared to those of **30-Eu** in Table 9.2. As expected, the distances for **30-Sm** are slightly smaller than those of **30-Eu**, which is consistent with the 0.02 Å smaller ionic radius of Sm^{2+} versus Eu^{2+}.[35]

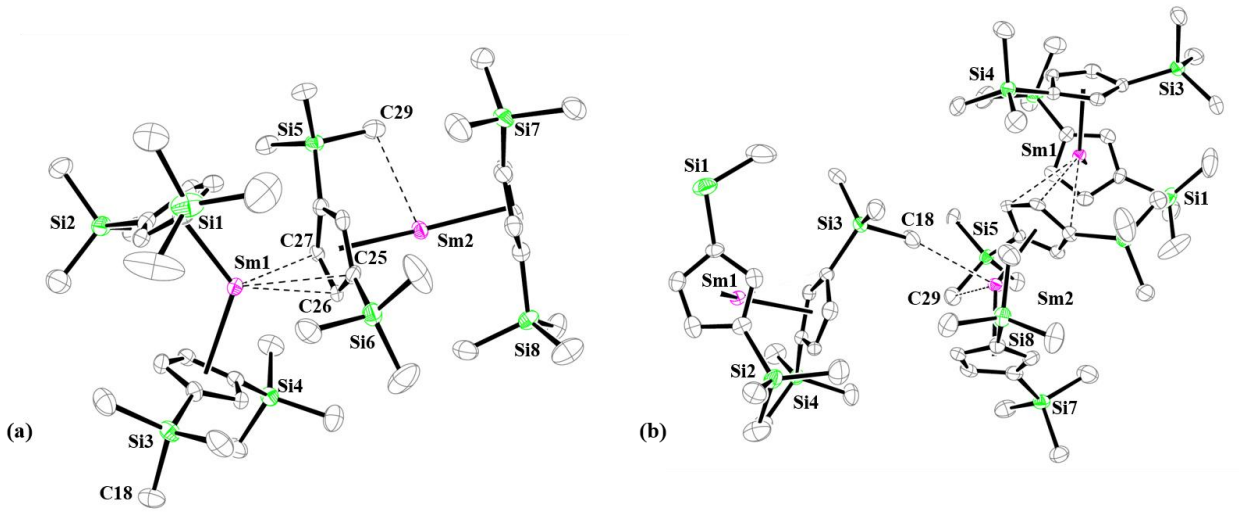

Figure 9.1. (a) Thermal ellipsoid plot of the bimetallic asymmetric unit of Cp″$_2$Sm, **30-Sm**, and (b) an image depicting the Sm2–C18 linkage forming the coordination polymer, drawn at the 50% probability level. Hydrogen atoms are omitted for clarity.

In the solid state, **30-Sm** features two crystallographically-independent Cp″$_2$Sm molecules per unit cell that are interconnected *via* a μ-η^3:η^5-Cp″ ligand that will be designated as Cp3. Sm1 is surrounded by two η^5-bound rings (Cp1 and Cp2) and one η^3-ring (Cp3). Sm2 interacts with Cp3 in an η^5-fashion and a terminally bound η^5-cyclopentadienyl ligand, Cp4. This bimetallic unit is arranged into a polymeric chain by a long range interaction between Sm2 and the C18 silylmethyl group of the Cp2 ligand bound to Sm1.

Sm1 has shorter metal–centroid distances to its terminal η^5-cyclopentadienyl ligands, 2.576 Å (Cp1) and 2.615 Å (Cp2), compared to the 2.857 Å length for the bridging η^3-Cp3, as is typical for terminal versus bridging ligands. The Sm1–Cp3 interaction is described as tri-hapto since three Sm–C bonds are between 2.891(5)-3.055(6) Å and two are much longer, 3.248(6) and 3.277(6) Å. The irregularity of the tris(cyclopentadienyl) coordination environment of Sm1 can be seen from three disparate (ring centroid)–Sm1–(ring centroid) angles, 125.6°, 121.3°, and 110.0°.

Sm2 also has a shorter distance to the ring centroid of the terminal Cp4 (2.510 Å) compared to the bridging Cp3 (2.569 Å), but the difference is not as great as with Sm1. The 147.9° (Cp3 ring centroid)–Sm2–(Cp4 ring centroid) angle of this metallocene fragment is quite large for a bent rare-earth metallocene. In fact it is 7.8° larger than the 140.1° (C_5Me_5 ring centroid)–Sm–(C_5Me_5 ring centroid) angle of $(C_5Me_5)_2Sm$.[36] Sm2 also has additional intramolecular and intermolecular interactions at long distances: an intramolecular Sm2–C29 contact at 3.137 Å and an intermolecular Sm2–C18 contact at 3.113 Å. The latter connection is the linkage that formally makes this complex into a coordination polymer. These long distances involving C29 and C18 can be compared to (a) the 2.81(5) Å average Sm2–C(Cp″ ring) bonds in **30-Sm**, (b) the 3.19(1) Å Sm–C(methyl) intermolecular distance in the solid state structure of $(C_5Me_5)_2Sm$,[36] and (c) the 2.880(7) and 2.889(6) Å Sm^{3+}–C(Me bridge) distances in $[(C_5Me_5)_2SmMe]_3$, which has shorter 2.454-2.460 Å Sm–(ring centroid) distances than in **30-Sm** since it is a Sm^{3+} complex.[37]

Cp^{tt}_2Ln, 31-Ln. The base-free Cp^{tt} metallocenes, **31-Sm** and **31-Eu**, were synthesized in a fashion similar to **30-Ln**, eq 9.4. The THF adducts, $Cp^{tt}_2Sm(THF)$[23] and $Cp^{tt}_2Eu(THF)$,[24] were repeatedly sublimed until complete removal of the THF was indicated by the disappearance of the THF stretches at 1028 and 874 cm^{-1} in the infrared spectra. Single crystals of **31-Sm** and **31-Eu** suitable for X-ray diffraction were grown by the slow evaporation of toluene and by sublimation, respectively, Figure 9.2.

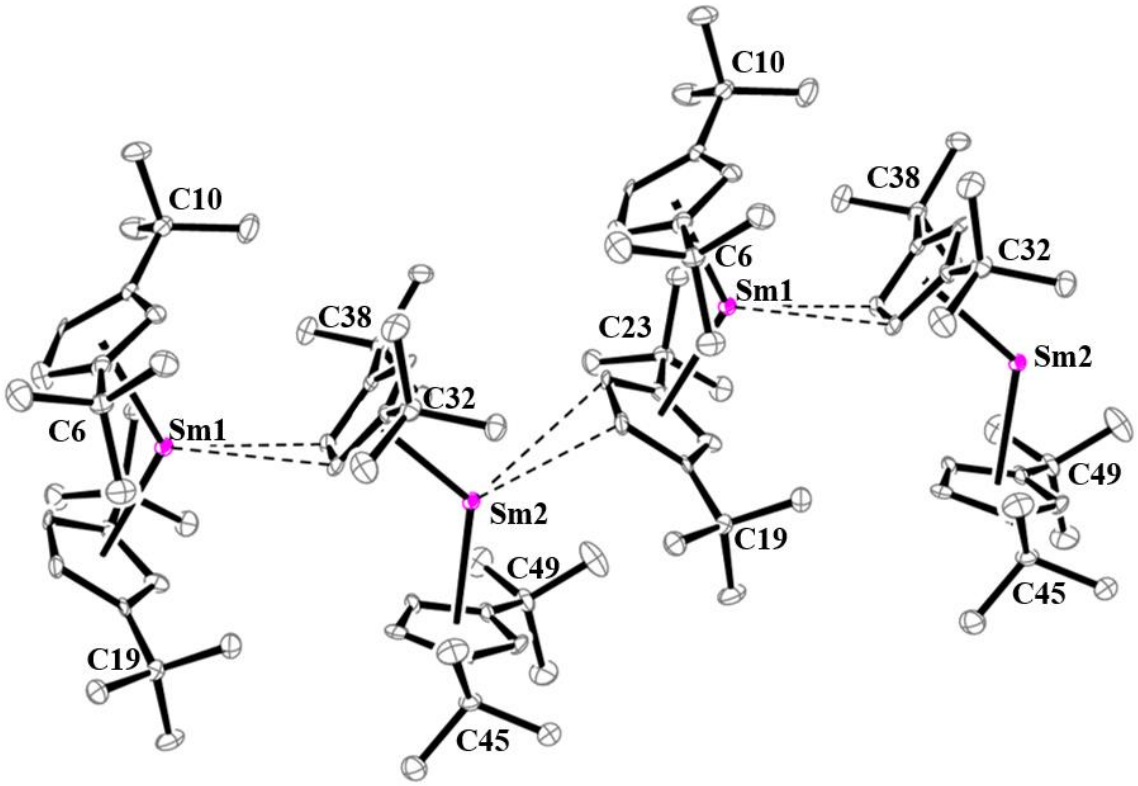

Figure 9.2. Thermal ellipsoid plot of Cp^{tt}_2Sm, **31-Sm**, drawn at the 50% probability level. Hydrogen atoms are omitted for clarity. Complex **31-Eu** is structurally similar, but not isomorphous.

Compounds **31-Sm** and **31-Eu** are structurally similar, but **31-Sm** crystallized in the $P\bar{1}$ space group with two independent Cp^{tt}_2Sm molecules per asymmetric unit cell, whereas **31-Eu** crystallized in $P2_1/c$ with one molecule per unit cell. In both structures, neighboring Cp^{tt}_2Ln units interact *via* intermolecular Ln–C(ring) interactions to make polymeric chains in the solid state. Hence, these complexes, like **30-Ln,** make coordination polymers, but **31-Ln** oligomerizes only

through bridging cyclopentadienyl groups and not through Si–Me–Ln linkages. This is an important difference in the Me_3Si-substituted complexes versus their Me_3C-substituted analogs.

In **31-Ln**, each Cp^{tt}_2Ln unit has one terminal ring containing the tert-butyl carbon atoms labeled C6 and C10 and one bridging Cp^{tt} ring containing C19 and C23. The Ln–(ring centroid) distances of the terminal rings are shorter than those of the bridging rings (2.552 versus 2.621 Å for **31-Sm**; 2.545 versus 2.627 Å for **31-Eu**), but the difference is not as great as that observed in **30-Ln**. In **31-Ln**, the bridging Cp^{tt} rings make the intermolecular connection only through two long and different distances to two of the ring carbons, 3.084 and 3.302 Å in one molecule of **31-Sm**, and 3.104 and 3.399 Å in the other. For **31-Eu**, the analogous distances are 3.158 and 3.415 Å. This is quite different from the μ-η^3:η^5-Cp″ bridging ligands in **30-Ln**. As a result, the 2.548-2.621 Å Sm–(Cp^{tt} ring centroid) distances of **31-Sm** and the 2.545-2.627 Å Eu1–(Cp^{tt} ring centroid) distances of **31-Eu** are both similar to the ranges of distances to the terminal Cp″ ligands of their **30-Ln** analogs. The 126.2 and 126.6° (Cp^{tt} ring centroid)–Sm–(Cp^{tt} ring centroid) angles in **31-Sm** and the 132.6° (Cp^{tt} ring centroid)–Eu1–(Cp^{tt} ring centroid) angle in **31-Eu** are both more bent than the analogous 140.1 and 140.3° angles for $(C_5Me_5)_2Sm$[36,38] and $(C_5Me_5)_2Eu$,[36] respectively. It is interesting to note that the difference between the (Cp^{tt} ring centroid)–Ln–(Cp^{tt} ring centroid) angles in **31-Sm** and **31-Eu** is 6° even though they have similar structures and the metals are similar in size. This can be attributed to the different crystal packing of the two structures and emphasizes the flexibility and variability of this angle.

Synthesis and Structural Characterization of $Cp^{tt}EuBPh_4$, 32-Eu. Synthesis of the targeted (η^5-Cp″)Ln(μ-η^6:η^1-Ph)$_2$BPh$_2$ and (η^5-Cp^{tt})Ln(μ-η^6:η^1-Ph)$_2$BPh$_2$, **32-Ln**, complexes was attempted by reacting **30-Ln** and **31-Ln**, respectively, with $[Et_3NH][BPh_4]$ in toluene following

the procedure used to synthesize [(Me$_3$Si)$_2$N](THF)Yb(μ-η^6:η^1-Ph)$_2$BPh$_2$[39] and (C$_5$Me$_5$)Ln(μ-η^6:η^1-Ph)$_2$BPh$_2$ (Ln = Sm, Eu, Yb),[20,21] eq 9.3. Although reactions occurred in all four cases, short reaction times were found to be necessary because the products slowly decompose in solution at room temperature. This contrasts to the stability of the (C$_5$Me$_5$)Ln(μ-η^6:η^1-Ph)$_2$BPh$_2$ complexes (Ln = Sm, Eu, Yb), which were crystallized at room temperature by slow evaporation of C$_6$D$_6$.[20,21] The samarium products were less stable than the europium products and only the Cp^{tt} complex of Eu, (η^5-Cp^{tt})Eu(μ-η^6:η^1-Ph)$_2$BPh$_2$, **32-Eu**, yielded crystals suitable for X-ray diffraction, eq 9.5. Recrystallization of the purple decomposition solids from a solution of the samarium analog, **32-Sm**, from THF gave crystals of the known [Sm(THF)$_7$][BPh$_4$]$_2$.[26] Attempts to reduce the products of the [Et$_3$NH][BPh$_4$] reactions to make Ln^{1+} complexes were unsuccessful.

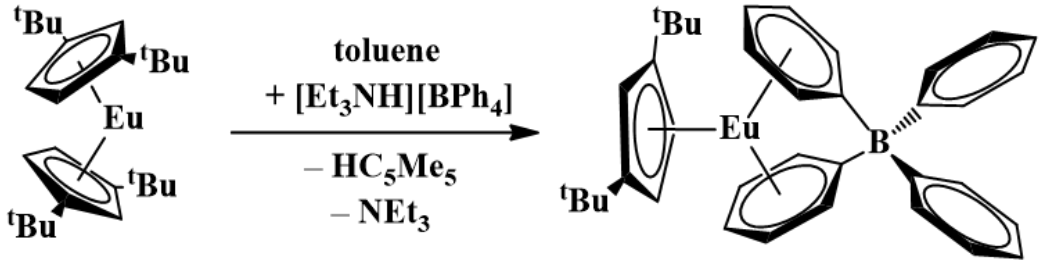

(9.5)

31-Eu **32-Eu**

X-ray analysis of a red rectangular block-like crystal of **32-Eu** showed two structurally independent molecules of **32-Eu** with nearly trigonal-planar arrangements around the europium atoms, Figure 9.3. The metrical parameters of **32-Eu** are shown in Table 9.3 and are compared against the related compound, (C$_5$Me$_5$)Eu(μ-η^6:η^1-Ph)$_2$BPh$_2$.[21] The 2.462-2.479 Å Eu–(Cp^{tt} ring centroid) distances are numerically only slightly shorter than the 2.505 Å Eu–(C$_5$Me$_5$ ring centroid) distance of (C$_5$Me$_5$)Eu(μ-η^6:η^1-Ph)$_2$BPh$_2$. The 2.652-2.688 Å Eu–(phenyl ring centroid) distances of **32-Eu** are all shorter than the 2.730 and 2.819 Å Eu–(phenyl ring centroid) distances in the (C$_5$Me$_5$)Eu(μ-η^6:η^1-Ph)$_2$BPh$_2$.

The biggest difference between **32-Eu** and $(C_5Me_5)Eu(\mu\text{-}\eta^6\text{:}\eta^1\text{-}Ph)_2BPh_2$ is that the three rings of **32-Eu** adopt the sterically-optimal trigonal arrangement with 176.2-176.7° (Cp^{tt} ring centroid)–Eu–B angles, whereas $(C_5Me_5)Eu(\mu\text{-}\eta^6\text{:}\eta^1\text{-}Ph)_2BPh_2$ has a pyramidal structure with a 146.2° (C_5Me_5 ring centroid)–Eu–B angle, Figure 9.4. Previous studies[20,21] have shown that $(C_5Me_5)Sm(\mu\text{-}\eta^6\text{:}\eta^1\text{-}Ph)_2BPh_2$ is also pyramidal, but the complex of the smaller metal, ytterbium, $(C_5Me_5)Yb(\mu\text{-}\eta^6\text{:}\eta^1\text{-}Ph)_2BPh_2$, has a 179.4° ($C_5Me_5$ ring centroid)–Yb–B angle like that in **32-Eu**. The earlier studies of the $(C_5Me_5)Ln(\mu\text{-}\eta^6\text{:}\eta^1\text{-}Ph)_2BPh_2$ complexes suggested that polarization and packing forces as well as metal size could lead to the trigonal structure for Yb versus the pyramidal structures for Eu and Sm. In the case of **32-Eu**, there is a 3.932 Å interplanar distance between two phenyl units of the neighboring molecules which is not observed in the packing structure of $(C_5Me_5)Eu(\mu\text{-}\eta^6\text{:}\eta^1\text{-}Ph)_2BPh_2$.

It is difficult to evaluate the effects of crystal packing, but the two different structures for **32-Eu** and $(C_5Me_5)Eu(\mu\text{-}\eta^6\text{:}\eta^1\text{-}Ph)_2BPh_2$ do conclusively show that the structure is not dictated by the $4f^7$ half-filled shell configuration of Eu^{2+}. One other difference in the two europium structures is that hydrogen on a phenyl ring in another molecule of $(C_5Me_5)Eu(\mu\text{-}\eta^6\text{:}\eta^1\text{-}Ph)_2BPh_2$ is oriented to the pyramidal metal center at a distance of 2.91 Å. This does not occur in **32-Eu**. It is interesting to note that the Eu…Me(CMe_3) distances in **32-Eu** are not equal. The closest methyl on C10, namely C12, is found at a distance of 3.488 Å from Eu, but the analogous methyl C9 on C6 is 3.783 Å away [for Eu2 these are Eu–C(C48), 3.469 Å; Eu–C(C46), 3.763 Å].

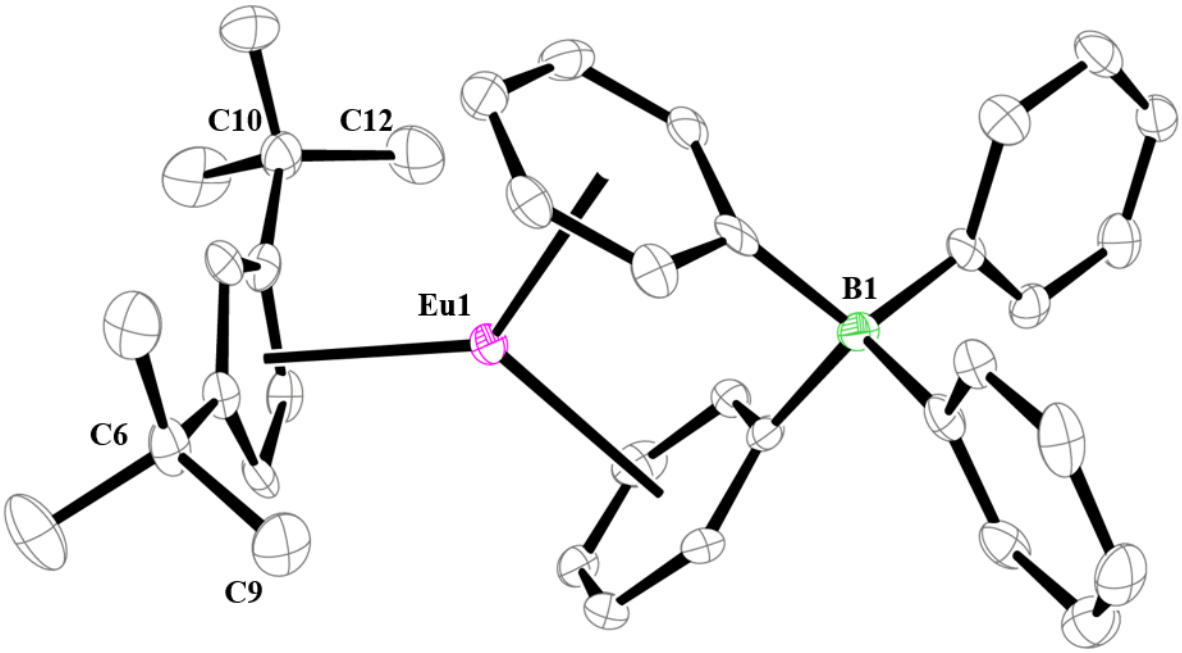

Figure 9.3. Thermal ellipsoid plot of $Cp^{tt}Eu(\mu\text{-}\eta^6\text{:}\eta^1\text{-}Ph)_2BPh_2$, **32-Eu**, drawn at the 50% probability level. Hydrogen atoms and one molecule of **32-Eu** are omitted for clarity.

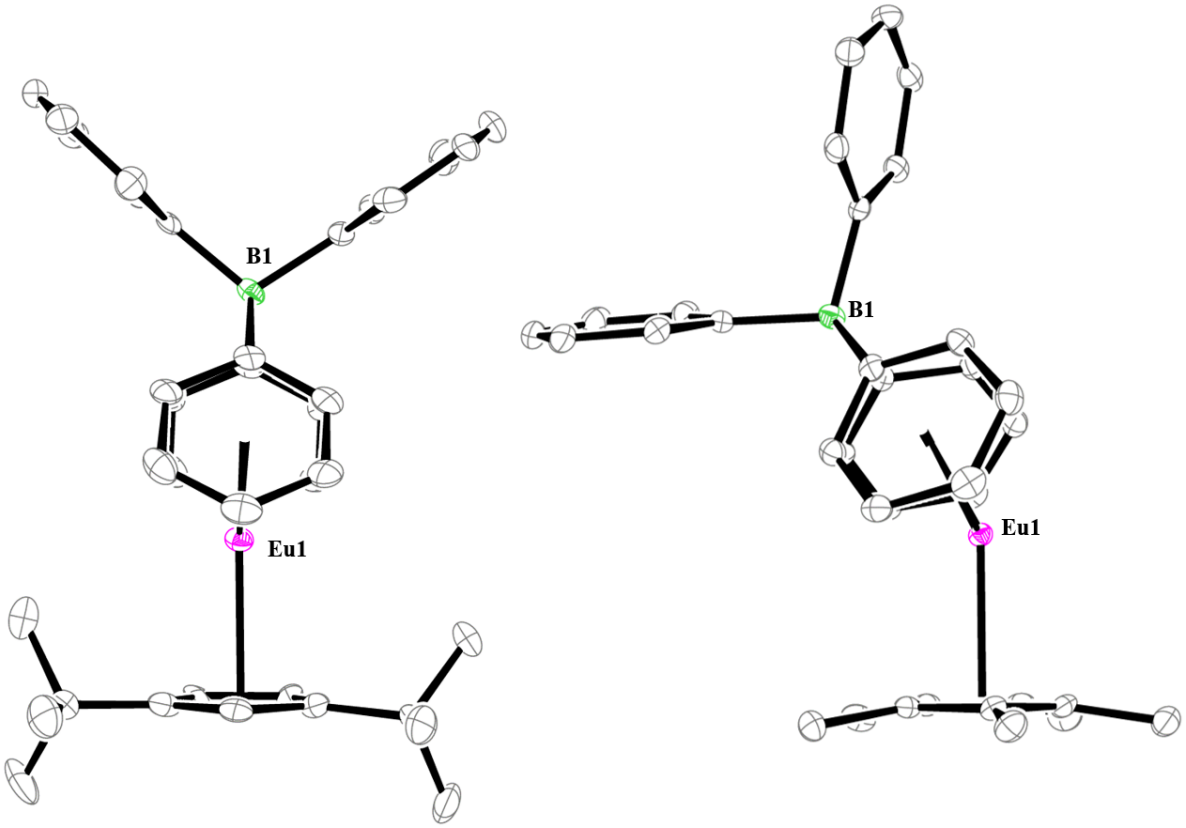

Figure 9.4. Side-on views of $Cp^{tt}Eu(\mu\text{-}\eta^6\text{:}\eta^1\text{-}Ph)_2BPh_2$, **32-Eu**, (left) and $(C_5Me_5)Eu(\mu\text{-}\eta^6\text{:}\eta^1\text{-}Ph)_2BPh_2$, (right) showing the trigonal-planar arrangement of three ring centroids in **32-Eu** and the pyramidal arrangement in $(C_5Me_5)Eu(\mu\text{-}\eta^6\text{:}\eta^1\text{-}Ph)_2BPh_2$. Thermal ellipsoids are drawn at the 50% probability level. Hydrogen atoms and one molecule in **32-Eu** have been emitted for clarity.

CONCLUSION

The bent metallocenes, Cp''_2Sm, **30-Sm**, Cp^{tt}_2Sm, **31-Sm**, and Cp^{tt}_2Eu, **31-Eu**, have been structurally characterized which allows comparisons of the Cp″ vs Cp^{tt} ligands with Ln^{2+} ions. The structures of **30-Ln** and **31-Ln** are significantly different due to the silylmethyl interactions found with **30-Ln** that are not present in **31-Ln**. Both Cp″ and Cp^{tt} are too small for two of these

ligands to sterically saturate the coordination sphere of the Ln^{2+} ions and hence additional interactions occur in the solid state to make coordination polymers. In contrast, C_5Me_5 generates bent metallocene structures with only long distance interactions to the side from methyl groups of neighboring molecules.[36,38] The Cp″ and Cp^{tt} ligands also differ from C_5Me_5 in terms of generating three-ring $(\eta^5\text{-}C_5R_5)Ln(\mu\text{-}\eta^6\text{:}\eta^1\text{-}Ph)_2BPh_2$ complexes. Although the C_5Me_5 compounds are thermally stable, the analogs with the smaller rings decompose in solution at room temperature. The structure of the one example isolated, $Cp^{tt}Eu(\mu\text{-}\eta^6\text{:}\eta^1\text{-}Ph)_2BPh_2$, **32-Eu,** differs from that of $(\eta^5\text{-}C_5Me_5)Eu(\mu\text{-}\eta^6\text{:}\eta^1\text{-}Ph)_2BPh_2$ in that the three rings are trigonal rather than pyramidal. These compounds are not ideal routes to Ln^{1+} compounds, but demonstrate the differences in structure and reactivity possible by varying cyclopentadienyl rings.

Table 9.1. Crystal data and structure refinement for Cp''_2Sm, **30-Sm**, Cp^{tt}_2Ln (Ln = Sm, Eu), **31-Ln**, and $Cp^{tt}Eu(\mu\text{-}\eta^6{:}\eta^1\text{-}Ph)_2BPh_2$, **32-Eu**.

	30-Sm	**31-Sm**	**31-Eu**	**32-Eu**
Empirical formula	$[C_{44}H_{84}Si_8Sm_2]_\infty$	$C_{26}H_{42}Sm$	$[C_{26}H_{42}Eu]_\infty$	$C_{37}H_{41}BEu$
Formula weight	1138.53	504.94	506.55	648.47
Temperature (K)	133(2)	88(2)	88(2)	133(2)
Space group	$P2_12_12_1$	$P\bar{1}$	$P2_1/c$	$Pca2_1$
a (Å)	14.8688(8)	10.5080(14)	10.8703(5)	31.6630(17)
b (Å)	17.4547(9)	11.5413(16)	21.4509(10)	9.9725(5)
c (Å)	21.6405(12)	20.578(3)	11.0734(5)	19.3490(10)
α (°)	90	104.8651(18)	90	90
β (°)	90	92.3621(18)	109.5762(5)	90
γ (°)	90	90.0591(16)	90	90
Volume ($Å^3$)	5616.4(5)	2409.8(6)	2432.82(19)	6109.6(5)
Z	4	4	4	8
ρ_{calcd} (g/cm^3)	1.346	1.392	1.383	1.410
μ (mm^{-1})	2.268	2.444	2.586	2.076
$R1^a$	0.0322	0.0342	0.0168	0.0396
$wR2^b$	0.0664	0.0381	0.0380	0.0870

Definitions: $^a R1 = \sum||Fo| - |Fc||/\sum|Fo|$; $^b wR2 = [\sum[w(Fo^2 - Fc^2)^2]/\sum[w(Fo^2)^2]\ ]^{1/2}$.

Table 9.2. Selected bond distances (Å) and angles (deg) for Cp''_2Sm, **30-Sm**, Cp^{tt}_2Sm, **31-Sm**, Cp^{tt}_2Eu, **31-Eu**, and Cp''_2Eu,[25] **30-Eu**.

	30-Sm	**31-Sm**	**31-Eu**	**30-Eu**[25 b]
Ln1–(Cnt1)	2.576	2.552	2.545	2.576
Ln1–(Cnt2)	2.615	2.621	2.627	2.610
Ln1–(Cnt3)	2.857	-	-	2.897
Ln2–(Cnt3)	2.569	2.618	-	2.558
Ln2–(Cnt4)	2.510	2.548	-	2.504
Ln1–C(Cnt1) range	2.811(6)-2.866(6)	2.768(5)-2.872(5)	2.755(2)-2.891(2)	2.795(6)-2.870(6)
Ln1–C(Cnt2) range	2.787(6)-2.952(6)	2.801(5)-2.974(5)	2.836(2)-2.953(2)	2.776(6)-2.956(6)
Ln1–C(Cnt3) range	2.891(6)-3.277(6)		-	2.897(6)-3.329[a]
Ln2–C(Cnt3) range	2.784(6)-2.898(6)	2.816(5)-2.943(5)	-	2.772(6)-2.903(5)
Ln2–C(Cnt4) range	2.747(5)-2.838(6)	2.754(5)-2.874(5)	-	2.724(6)-2.828(6)
Ln2–C29[a]	3.137	-	-	3.160
Ln2–C18	3.113(6)	-	-	3.091(6)
Ln1–C(Cp) Intermolecular contacts[a]	-	3.085, 3.302	3.158, 3.415	-
Ln2–C(Cp) Intermolecular contacts[a]	-	3.104, 3.399	-	-
(Cnt1) –Ln1–(Cnt2)	125.6	126.6	132.6	122
(Cnt1)–Ln1–(Cnt3)	110.0	-	-	113
(Cnt2)–Ln1–(Cnt3)	121.3	-	-	122
(Cnt3)–Ln2–(Cnt4)	147.9	126.2	-	147
Ln1 Twist angle[d]	25	31	45	24
Ln2 Twist angle	11	30	-	11

[a] Distance generated using Mercury software, no error reported.

[b]Numbering scheme different in citation. Numbers changed to match numbering in this report.

[c] Cnt1 is the ring centroid from Cp1 which contains C1-C5; Cnt2 is the ring centroid of Cp2 which contains C12-C6 (C14-C18 for **31-Ln**); Cnt3 is the ring centroid of Cp3 which contains C23-C26 (C27-C31 for **31-Sm**); Cnt4 is the ring centroid of Cp4 which contains C34-C38 (C40-C44 for **31-Sm**).

[d] The twist angle is defined as the average of the five smallest dihedral angles formed between the ten planes which consist of a ring carbon atom and the two ring centroids. An eclipsed structure has a 0° twist angle.

Table 9.3. Selected bond distances (Å) and angles (deg) of $Cp^{tt}Eu(\mu\text{-}\eta^6\text{:}\eta^1\text{-}Ph)_2BPh_2$, **32-Eu**, and $(C_5Me_5)Eu(\mu\text{-}\eta^6\text{:}\eta^1\text{-}Ph)_2BPh_2$.[21]

	3-Eu	$(C_5Me_5)Eu(\mu\text{-}\eta^6\text{:}\eta^1\text{-}Ph)_2BPh_2$[21]
Ln–Cnt(Cp)	2.479, 2.462	2.505
Ln–Cnt(C_6H_5)	2.688, 2.682	2.730
Ln–Cnt(C_6H_5)	2.652, 2.671	2.819
Ln–C(Cp) range	2.718(7)-2.783(7), 2.687(8)-2.786(8)	2.774(3)-2.786(3)
$Ln–C(Cp)_{avg}$	2.75(3), 2.74(3)	2.780(5)
Ln–C(C_6H_5) range	2.966(9)-3.065(9), 2.955(10)-3.094(12)	2.953(3)-3.298(3)
$Ln–C(C_6H_5)_{avg}$	3.03(3), 3.00(2) 3.02(4), 3.01(6)	3.1(1)
Cnt(Cp)–Ln–Cnt(C_6H_5)	126.2, 126.6	121.4
Cnt(Cp)–Ln–Cnt(C_6H_5)	126.5, 125.0	125.0
Cnt(C_6H_5)–Ln–Cnt(C_6H_5)	107.2, 108.2	103.3
Cnt(Cp)–Ln–B	176.7, 176.2	146.2

REFERENCES

(1) Hitchcock, P. B.; Lappert, M. F.; Maron, L.; Protchenko, A. V. *Angew. Chem. Int. ed.* **2008**, *47*, 1488-1491.

(2) MacDonald, M. R.; Bates, J. E.; Ziller, J. W.; Furche, F.; Evans, W. J. *J. Am. Chem. Soc.* **2013**, *135*, 9857-9868.

(3) Fieser, M. E.; MacDonald, M. R.; Krull, B. T.; Bates, J. E.; Ziller, J. W.; Furche, F.; Evans, W. J. *J. Am. Chem. Soc.* **2015**, *137*, 369-382.

(4) MacDonald, M. R.; Bates, J. E.; Fieser, M. E.; Ziller, J. W.; Furche, F.; Evans, W. J. *J. Am. Chem. Soc.* **2012**, *134*, 8420-8423.

(5) Woen, D. H.; Evans, W. J. In *Handbook on the Physics and Chemistry of Rare Earths*; 1st ed.; Elsevier: Amsterdam, 2016; Vol. 50, p 337-394.

(6) Evans, W. J. *Organometallics* **2016**, *35*, 3088-3100.

(7) Cassani, M. C.; Lappert, M. F.; Laschi, F. *Chem. Commun.* **1997**, 1563-1564.

(8) Cassani, M. C.; Duncalf, D. J.; Lappert, M. F. *J. Am. Chem. Soc.* **1998**, *120*, 12958-12959.

(9) Gun'ko, Y. K.; Hitchcock, P. B.; Lappert, M. F. *Organometallics* **2000**, *19*, 2832-2834.

(10) MacDonald, M. R.; Fieser, M. E.; Bates, J. E.; Ziller, J. W.; Furche, F.; Evans, W. J. *J. Am. Chem. Soc.* **2013**, *135*, 13310-13313.

(11) Langeslay, R. R.; Fieser, M. E.; Ziller, J. W.; Furche, F.; Evans, W. J. *Chem. Sci.* **2015**, *6*, 517-521.

(12) Kotyk, C. M.; Fieser, M. E.; Palumbo, C. T.; Ziller, J. W.; Darago, L. E.; Long, J. R.; Furche, F.; Evans, W. J. *Chem. Sci.* **2015**, *6*, 7267-7273.

(13) Dorenbos, P. *J. Phys.: Condens. Matter* **2003**, *15*, 575-594.

(14) Arnold, P. L.; Cloke, F. G. N.; Hitchcock, P. B.; Nixon, J. F. *J. Am. Chem. Soc.* **1996**, *118*, 7630-7631.

(15) Clentsmith, G. K.; Cloke, F. G.; Green, J. C.; Hanks, J.; Hitchcock, P. B.; Nixon, J. F. *Angew. Chem. Int. Ed.* **2003**, *42*, 1038-1041.

(16) Neculai, A. M.; Neculai, A. M.; Roesky, H. W.; Magull, J.; Baldus, M.; Andronesi, O.; Jansen, M. *Organometallics* **2002**, *21*, 2590-2592.

(17) Fong, F. K.; Cape, J. A.; Wong, E. Y. *Phys Rev* **1966**, *151*, 299-&.

(18) Anderson, D. M.; Cloke, F. G. N.; Cox, P. A.; Edelstein, N.; Green, J. C.; Pang, T.; Sameh, A. A.; Shalimoff, G. *J. Chem. Soc., Chem. Commun.* **1989**, 53-55.

(19) Corbey, J. F.; Woen, D. H.; Palumbo, C. T.; Fieser, M. E.; Ziller, J. W.; Furche, F.; Evans, W. J. *Organometallics* **2015**, *34*, 3909-3921.

(20) Evans, W. J.; Champagne, T. M.; Ziller, J. W. *Organometallics* **2007**, *26*, 1204-1211.

(21) Evans, W. J.; Walensky, J. R.; Furche, F.; DiPasquale, A. G.; Rheingold, A. L. *Organometallics* **2009**, *28*, 6073-6078.

(22) Evans, W. J.; Keyer, R. A.; Ziller, J. W. *J. Organomet. Chem.* **1990**, *394*, 87-97.

(23) Bel'sky, V. K.; Gunko, Y. K.; Bulychev, B. M.; Sizov, A. I.; Soloveichik, G. L. *J. Organomet. Chem.* **1990**, *390*, 35-44.

(24) Khvostov, A. V.; Bulychev, B. M.; Belsky, V. K.; Sizov, A. I. *Russ. Chem. Bull.* **1999**, *48*, 2162-2166.

(25) Hitchcock, P. B.; Howard, J. A. K.; Lappert, M. F.; Prashar, S. *J. Organomet. Chem.* **1992**, *437*, 177-189.

(26) Evans, W. J.; Johnston, M. A.; Greci, M. A.; Gummersheimer, T. S.; Ziller, J. W. *Polyhedron* **2003**, *22*, 119-126.
(27) APEX2 Version 2014.11-0, Bruker AXS, Inc.; Madison, WI, 2014.
(28) SAINT Version 8.34a, Bruker AXS, Inc.; Madison, WI, 2013.
(29) Sheldrick, G. M.; SADABS, Version 2014/5, Bruker AXS, Inc.; Madison, WI, 2014.
(30) Sheldrick, G. M.; SHELXTL, Version 2014/7, Bruker AXS, Inc.; Madison, WI, 2014.
(31) International Tables for X-Ray Crystallography, 1992, Vol. C., Dordrecht: Kluwer Academic Publishers.
(32) Parsons, S.; Flack, H. D. *Acta Cryst.* **2013**, *B69*, 249-259.
(33) Sheldrick, G. M.; Version 2008/4 ed.; Bruker AXS, Inc.: Madison, WI, 2008.
(34) Sheldrick, G. M.; Version 2012/1 ed.; Bruker AXS, Inc.: Madison, WI, 2012.
(35) Shannon, R. D. *Acta Crystallogr A* **1976**, *32*, 751-767.
(36) Evans, W. J.; Hughes, L. A.; Hanusa, T. P. *Organometallics* **1986**, *5*, 1285-1291.
(37) Evans, W. J.; Perotti, J. M.; Ziller, J. W. *J. Am. Chem. Soc.* **2005**, *127*, 3894-3909.
(38) Evans, W. J.; Hughes, L. A.; Hanusa, T. P. *J. Am. Chem. Soc.* **1984**, *106*, 4270-4272.
(39) Deacon, G. B.; Forsyth, C. M.; Junk, P. C. *Eur. J. Inorg. Chem.* **2005**, 817-821.

CHAPTER 10

Reductive Coupling of Diphenylacetylene to a Benzyldiphenylindenyl Anion Via La^{2+}

INTRODUCTION

Alkyne coupling is one general reaction effected by a variety of *f* element complexes. Both rare earth[1] and actinide complexes[2,3] have been used to manipulate alkynes and two representative reactions are shown below eq 10.1 and 10.2.

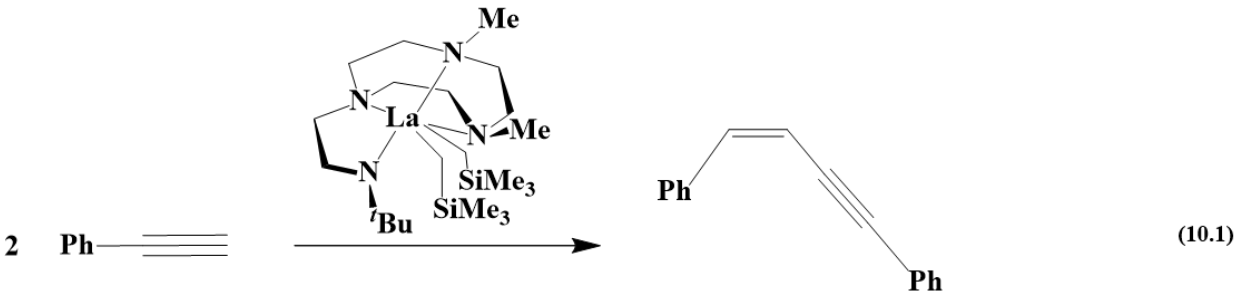

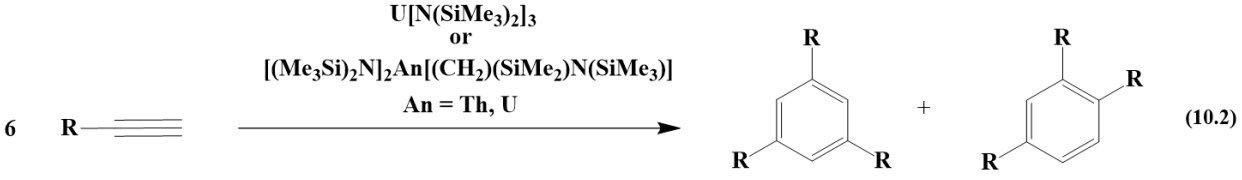

Previous chapters have described the fact that a new class of *f* element complexes was discovered in which the metal is in a +2 oxidation state and has an electron configuration with *d* orbital character. Reported in this Chapter is the unusual alkyne coupling chemistry obtained by treating the $5d^1$ La^{2+} complexes**,** [K(2.2.2-cryptand)][Cp′$_3$La] and [K(2.2.2-cyptand)]$_2$[(Cp′$_2$La)$_2$(C$_6$H$_6$)], with diphenylacetylene. Previously, the 4^6 Sm^{2+} metallocene (C$_5$Me$_5$)$_2$Sm(THF) has been found to react with diphenylacetylene to form the bimetallic Sm^{3+} complex [(C$_5$Me$_5$)$_2$Sm]$_2$(PhC=CPh).[4] This complex hydrolyzes to *trans*-stilbene. The $4f^9$ Dy^{2+} complex, DyI$_2$, also reacts with diphenylacetylene, but in this case the hydrolysis product is *cis*-

silbene. The uranium complexes, $(C_5Me_5)_3U$,[5] $[(C_5Me_5)_2U]_2(C_6H_6)$,[6] $(C_5Me_5)_2U(\mu\text{-}Ph)_2BPh_2$,[7] and $[(C_5Me_5)_2U(\mu\text{-}Cl)]_3$,[8] all react with diphenylacetylene to make the structurally characterized U^{4+} macrocycle, $(C_5Me_5)_2U(C_4Ph_4)$,[8] Scheme 1,[8,9]

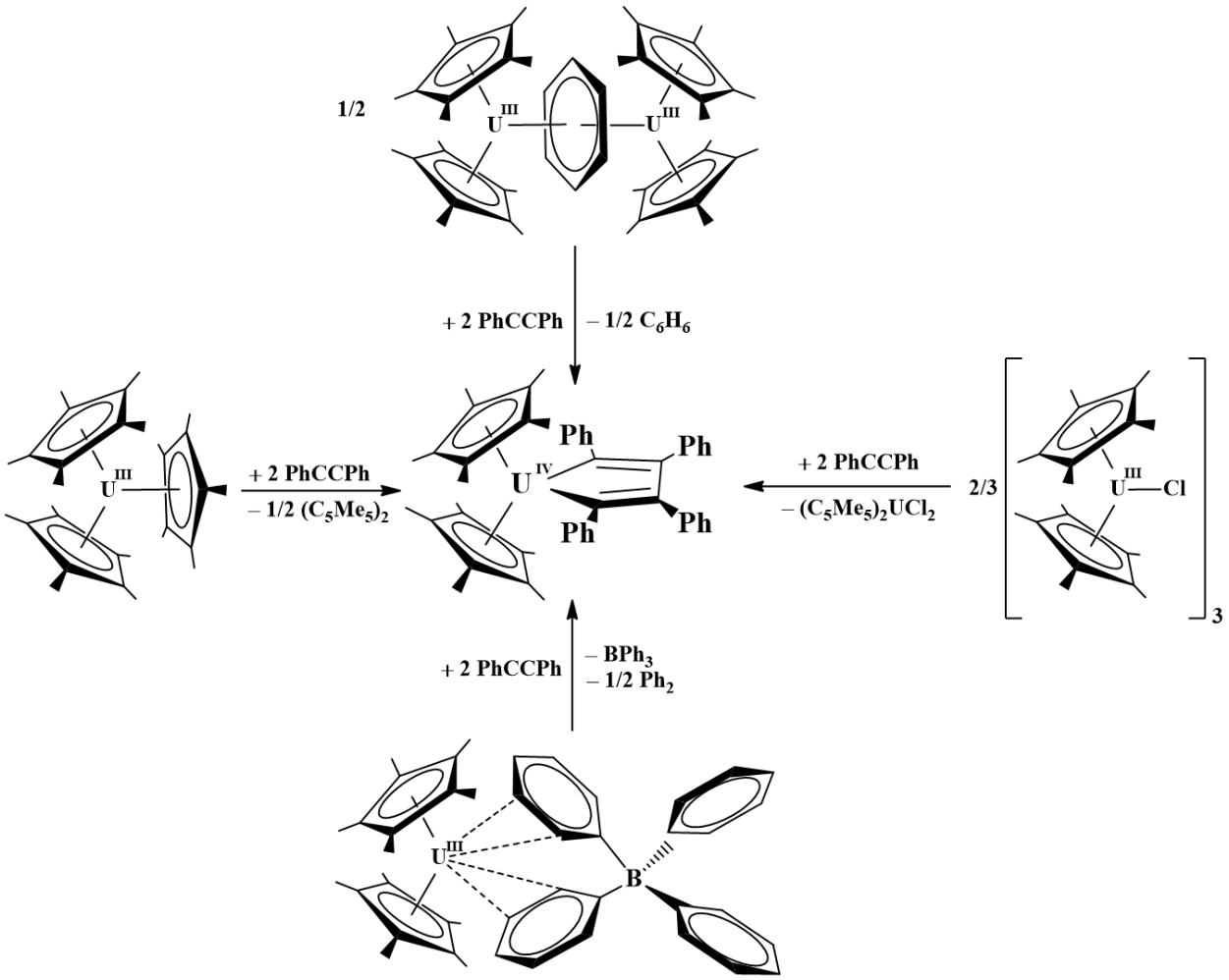

Scheme 1. Summary of reactions of uranium complexes with diphenylacetylene.[8,9]

but its hydrolysis products were not reported. The reduction of diphenylacetylene with $4d^1$ zirconocene, Cp_2Zr, has been observed by Takahashi and coworkers to generate the metallocycle $Cp_2Zr(C_4Ph_4)$, which reacts further to give indenes.[10] Reported in this Chapter is the reactivity of the $5d^1$ La^{2+} complexes, $[K(2.2.2\text{-cryptand})][Cp'_3La]$ and $[K(2.2.2\text{-cyptand})]_2[(Cp'_2La)_2(C_6H_6)]$,

with diphenylacetylene that led to a potassium salt of a 1-benzyl-2,3-diphenylindenyl anion, [K(2.2.2-cryptand)][($PhCH_2$)$Ph_2C_9H_4$], by reductive coupling.

EXPERIMENTAL

The syntheses and manipulations described below were conducted under argon with rigorous exclusion of air and water using glovebox, vacuum line, and Schlenk techniques. Solvents were sparged with ultrahigh purity (UHP) grade argon (Airgas) and passed through columns containing Q-5 and molecular sieves before use. NMR solvents (Cambridge Isotope Laboratories) were dried over NaK/benzophenone, degassed by three freeze−pump−thaw cycles, and vacuum-transferred before use. [K(2.2.2-cryptand)][Cp′$_3$La][11] and [K(2.2.2-cryptand)]$_2$[(Cp′$_2$La)$_2$(C_6H_6)][12] were prepared according to literature- procedures. 1,2-Dimethoxyethane (Aldrich) was dried with molecular sieves, degassed by three freeze–pump–thaw cycles, and vacuum-transferred before use. 2.2.2-Cryptand, 4,7,13,16,21,24-hexaoxa-1,10-diazabicyclo[8.8.8]hexacosane (Acros Organics), was placed under vacuum (10^{-3} Torr) for 12 h before use. Diphenylacetylene (Aldrich) was used as received. ^{1}H NMR (500 MHz) and ^{13}C NMR (125 MHz) spectra were obtained on a CRYO500 MHz spectrometer at 298 K. IR samples were prepared as KBr pellets, and the spectra were obtained on a Varian 1000 FT-IR spectrometer. Elemental analyses were performed on a PerkinElmer 2400 series II CHNS elemental analyzer. Kinetics experiments were performed on a CRYO500 MHz spectrometer and concentrations were monitored using 1,2-dimethoxyethane as an internal standard.

[K(2.2.2-cryptand)][($PhCH_2$)$Ph_2C_9H_4$]. In an argon-filled glovebox, diphenylacetylene (11 mg, 63 μmol,) in THF (3 mL) was added to a stirred dark purple solution of [K(2.2.2-cyptand)]$_2$[(Cp′$_2$La)$_2$(C_6H_6)] (29 mg, 16 μmol) in THF (5 mL) which caused an immediate color

change to orange. The orange mixture was stirred for 3 min and during this time the solution became noticeably darker. The volatiles were removed which left a dark orange/brown oil which was triturated several times with Et_2O. The dark oil was redissolved in THF (10 mL), filtered, and layered with hexane (10 mL). The layered mixture was then stored at room temperature for 48 h to yield yellow single-crystalline solids characterized by X-ray crystallography as the potassium indenyl salt, [K(2.2.2-cryptand)][($PhCH_2$)$Ph_2C_9H_4$].

Alternative Synthesis of [K(2.2.2-cryptand)][($PhCH_2$)$Ph_2C_9H_4$]. In an argon-filled glovebox, diphenylacetylene (29 mg, 0.16 mmol) in THF (5 mL) was added to a stirred dark purple solution of [K(2.2.2-cryptand)][Cp'_3La] (166 mg, 0.16 mmol) in THF (5 mL) and the reaction mixture immediately turned orange/yellow. The mixture was stirred for 2 min and during this time the solution became noticeably darker. The volatiles were removed under reduced pressure which yielded an orange-brown oil which was triturated several times with Et_2O. The dark oil was redissolved in THF (10 mL), filtered, and layered with hexane (10 mL). The mixture was then stored at room temperature for 36 h to yield yellow crystals characterized by X-ray crystallography as the potassium indenyl salt [K(2.2.2-cryptand)][($PhCH_2$)$Ph_2C_9H_4$].

Kinetic Data of "[K(2.2.2-cryptand)][$Cp'_2La(C_4Ph_4)$]", 33-La. In an argon-filled glovebox, diphenylacetylene (187 mM in THF-d_8, 300 μL, 54.1 μmol) was added to a scintillation vial charged with a dark purple solution of [K(2.2.2-cyptand)]$_2$[(Cp'_2La)$_2$(C_6H_6)] (45.0 mM in THF-d_8, 300 μL, 13.5 μmol). The mixture was stirred briefly to give an orange solution. The orange mixture was then transferred to a J-Young NMR tube, 1,2-dimethoxyethane (2.8 μL, 27 μmol) was added, and the sample was rushed to an NMR spectrometer. ^{1}H NMR of **33-La** in THF-d_8: δ 6.81 (t, C_4Ph_2, 4H), 6.71 (d, C_4Ph_4, 4H), 6.58 (t, C_4Ph_4, 4H), 6.54 (d, C_4Ph_4, 4H), 6.44 (t, C_4Ph_4, 2H), 6.38 (t, C_4Ph_4, 2H), 6.19 (t, $C_5H_4SiMe_3$, 4H), 6.13 (t, $C_5H_4SiMe_3$, 4H), 3.55 (s,

OC*H*$_2$C*H*$_2$O, 12H), 3.51 (t, NCH$_2$C*H*$_2$O, 12H), 2.53 (t, NC*H*$_2$CH$_2$O, 12H), 0.03 (s, C$_5$H$_4$Si*Me*$_3$, 18H).

Reaction with S$_8$. In an argon-filled glovebox, 1,2-diphenylacetylene (4 mg, 23 μmol) in THF (3 mL) was added to a stirred dark purple solution of [K(2.2.2-cyptand)]$_2$[(Cp′$_2$La)$_2$(C$_6$H$_6$)] (10 mg, 5.8 μmol) in THF (5 mL) and the mixture immediately turned orange. After 1 min, S$_8$ (3 mg, 12 μmol) was added and the mixture immediately turned bright yellow. After 2 min, the volatiles were removed which left a tacky yellow oil. Hexane was added to the oil and the mixture was stirred for 5 min, filtered, and then the volatiles were removed from the resultant yellow filtrate to leave a yellow oil. The resultant yellow oil was taken out of the glovebox, dissolved in chloroform (5 mL), and transferred to a 100 mL volumetric flask. Dilution to 100 mL with chloroform gave a mixture that was analyzed by GC-MS to contain 1,2-diphenylacetylene (presumably unreacted) and 1,2,3,4-tetraphenylthiophene M/Z = 388.16 (theoretical 388.13).

X-ray Data Collection, Structure Solution and Refinement for [K(2.2.2-cryptand)][(PhCH$_2$)Ph$_2$C$_9$H$_4$]. A yellow crystal of approximate dimensions 0.064 x 0.336 x 0.385 mm was mounted in a cryoloop and transferred to a Bruker SMART APEX II diffractometer. The APEX2[13] program package was used to determine the unit-cell parameters and for data collection (120 sec/frame scan time for a sphere of diffraction data). The raw frame data was processed using SAINT[14] and SADABS[15] to yield the reflection data file. Subsequent calculations were carried out using the SHELXTL[16] program. There were no systematic absences nor any diffraction symmetry other than the Friedel condition. The centrosymmetric triclinic space group $P\bar{1}$ was assigned and later determined to be correct. The structure was solved by dual space methods and refined on F^2 by full-matrix least-squares techniques. The analytical scattering

factors[17] for neutral atoms were used throughout the analysis. Hydrogen atoms were located from a difference-Fourier map and refined (x,y,z and U_{iso}). Least-squares analysis yielded wR2 = 0.0948 and Goof = 1.022 for 724 variables refined against 9166 data (0.78 Å), R1 = 0.0384 for those 7121 data with $I > 2.0\sigma(I)$.

RESULTS AND DISCUSSION

The treatment of the deep maroon solutions of either [K(2.2.2-cyptand)][Cp′$_3$La] or [K(2.2.2-cyptand)]$_2$[(Cp′$_2$La)$_2$(C_6H_6)] with diphenylacetylene in THF generates a transient orange solution that become very dark over the course of a few hours at room temperature. If the dark brown mixtures are layered with hexane and stored for 36 h, yellow single-crystalline solids of the potassium indenyl salt, [K(2.2.2-cryptand)][($PhCH_2$)$Ph_2C_9H_4$], can be obtained. Although the indene has been synthesized and characterized previously,[10,18-20] this is the first structural characterization of the [($PhCH_2$)$Ph_2C_9H_4$]$^{1-}$ anion. The structural details of the indenyl anion are not unusual.

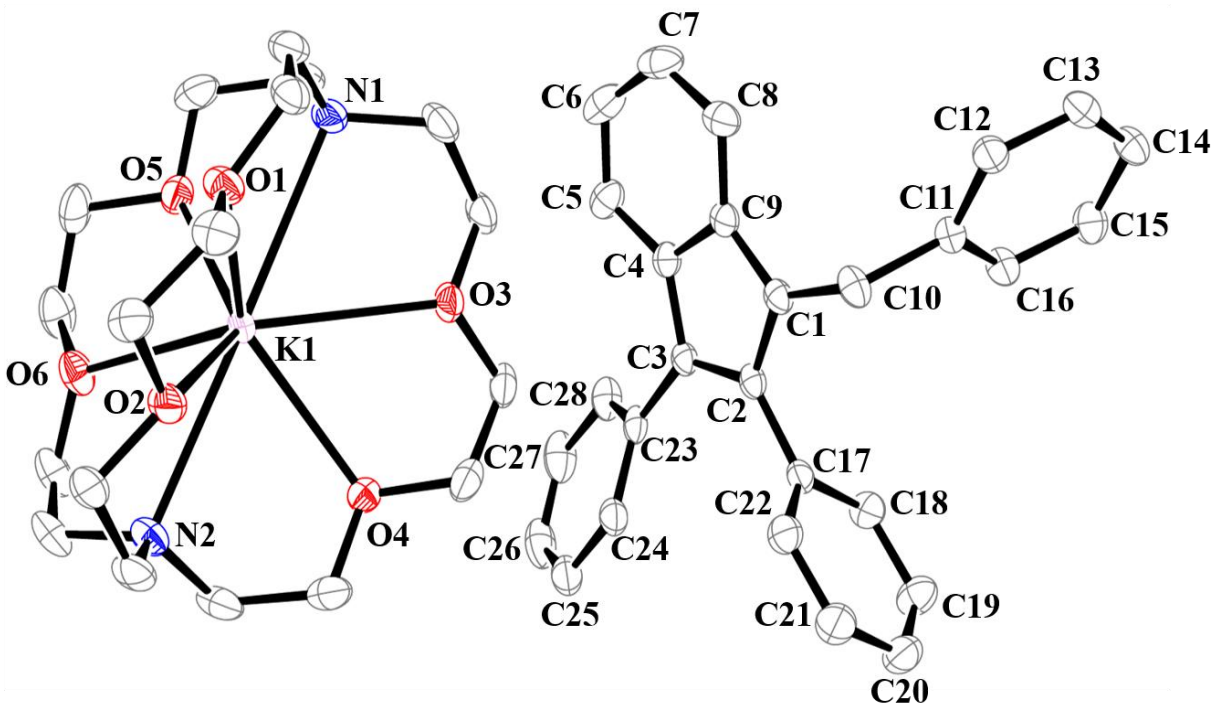

Figure 10.1. Thermal ellipsoid plot of [K(2.2.2-crytpand)][$(PhCH_2)Ph_2C_9H_4$] with thermal ellipsoids drawn at the 50% probability level. Hydrogen atoms are omitted for clarity.

To probe the mechanism of forming the indenide, the reactions were monitored by ^{1}H NMR spectroscopy. The NMR spectra of the orange solutions formed immediately after reductions of phenylacetylene by both [K(2.2.2-cyptand)][Cp'_3La] and [K(2.2.2-cyptand)]$_2$[$(Cp'_2La)_2(C_6H_6)$] showed a 4:4:4:4:2:2 integration pattern of the phenyl resonances that integrated to one equiv of

2.2.2-cryptand and two of Cp′, Figure 10.2.

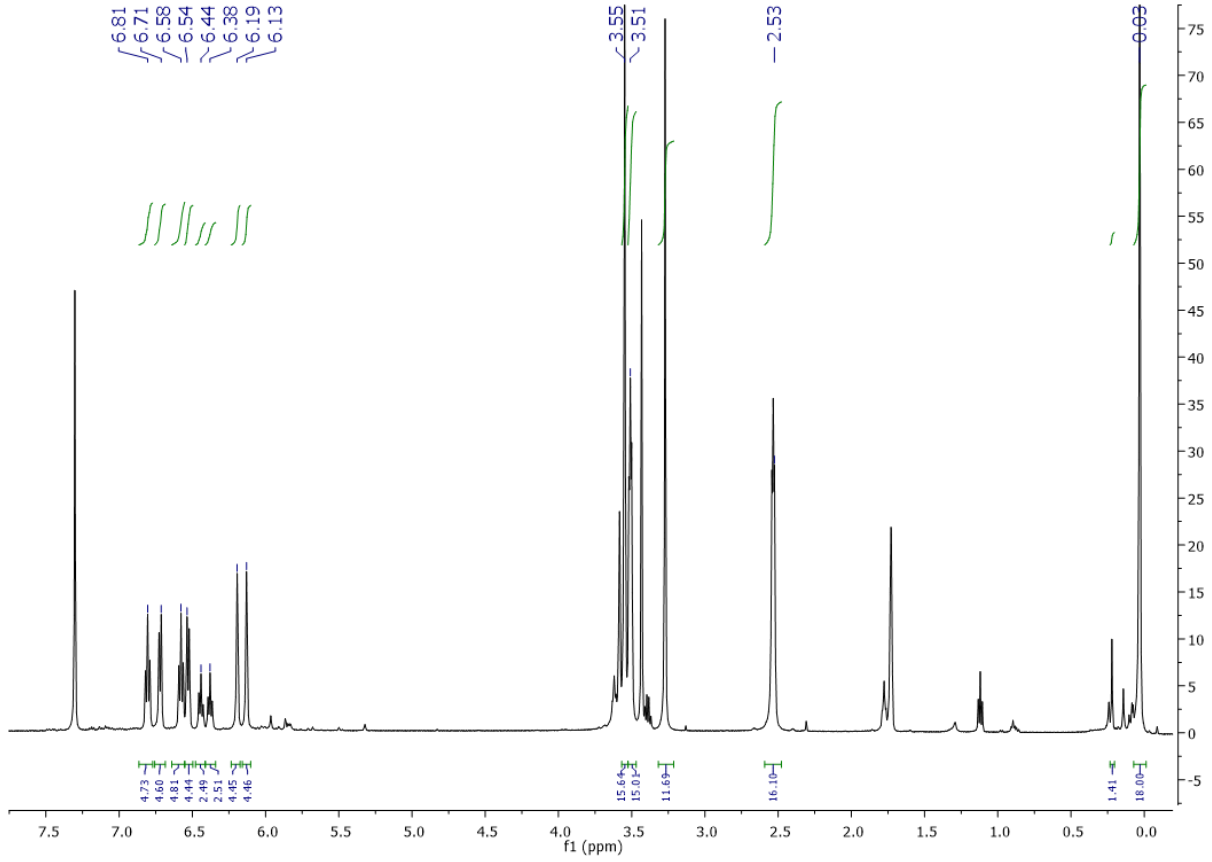

Figure 10.2. ^{1}H NMR spectrum of "[K(2.2.2-cryptand)][Cp′$_2$La(C$_4$Ph$_4$)]," **33-La**, in THF-d_8 at 298 K.

This is consistent with a metallocycle product of the formula "[K(2.2.2-cryptand)][Cp′$_2$La(C$_4$Ph$_4$)]," **33-La**. A similar pattern has been previously observed in the U^{4+} metallocycle, (C$_5$Me$_5$)$_2$U(C$_4$Ph$_4$).[21]

Further support for the presence of an intermediate like **33-La** is that the addition of S$_8$ to a solution of freshly generated **33-La** gave 1,2,3,4-tetraphenylthiophene, which was identified by mass spectroscopy. This insertion reactivity has been observed in an analogue of the thiophene

product in the reaction of $Cp_2Zr[C_4(C_6H_5)_2(C_6F_5)_2]$ with S_2Cl_2.[22] These reactions are summarized below in Scheme 2.

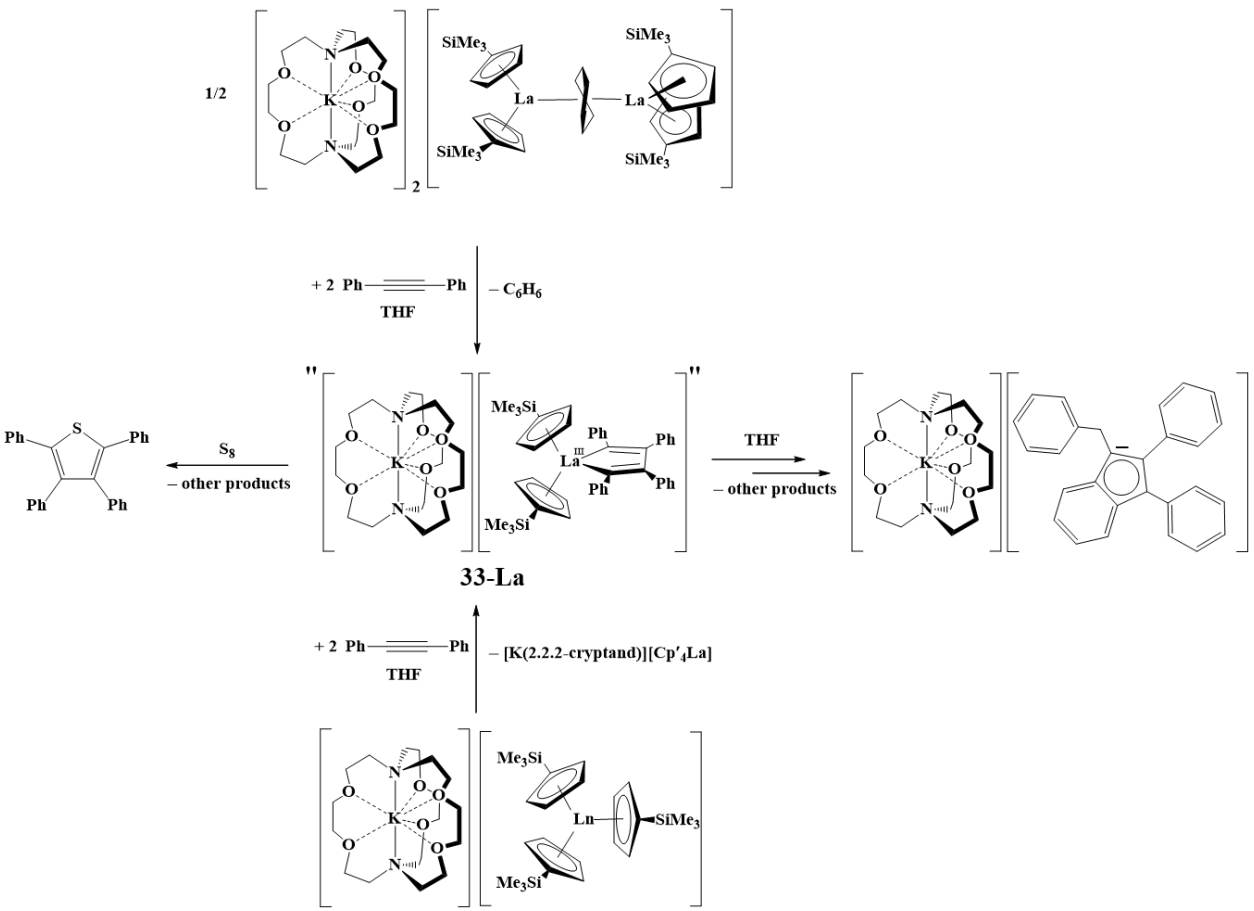

Scheme 2. Reactions of the reductive coupling of diphenylacetylene using [K(2.2.2-cyptand)][Cp′$_3$La] and [K(2.2.2-cyptand)]$_2$[(Cp′$_2$La)$_2$(C_6H_6)].

Kinetic studies of the decomposition of the orange intermediate were conducted in solvent with DME as an internal standard and an approximate 54% yield of the metallocycle **33-La** was determined by extrapolation of the experimental data. **33-La** is unstable in solution and decomposes according to first order kinetics with a rate constant k_{obs} = 8.621 x 10^{-5} s^{-1} ($t_{1/2}$ = 2.2

h), Figure 10.3. This contrasts to $(C_5Me_5)_2U(C_4Ph_4)$,[9,21] which is stable at room temperature, the lutetium metallocycles [M(chelate)][$Cp_2Lu(C_4Ph_2(SiMe_3)_2)$] (M= Li, K; chelate = 12-crown-4, 18-crown-6, 2.2.2-cryptand),[23] which can be heated to 90 °C without decomposition of the $(C_4R_4)^{2-}$ moiety, and the ferrocene diamide rare-earth metallocycles [$K(THF)_x$][$Fe(C_5H_4{}^{TBS}N)_2Ln(C_4Ph_4)$] (Ln = Sc, Y, and Lu),[24] which are stable at room temperature for at least 24 h. The analogous lanthanum ferrocene diamide complex [$K(THF)_x$][$Fe(C_5H_4{}^{TBS}N)_2La(C_4Ph_4)$] was not isolable and gave an intractable mixture.[24] Hydrolysis of the NMR sample used for the kinetic data and analysis of the mixture by mass spectrometry gave a major product with an M/Z = 358.22, consistent with the 358.17 expected for the indene $(PhCH_2)Ph_2C_9H_5$.

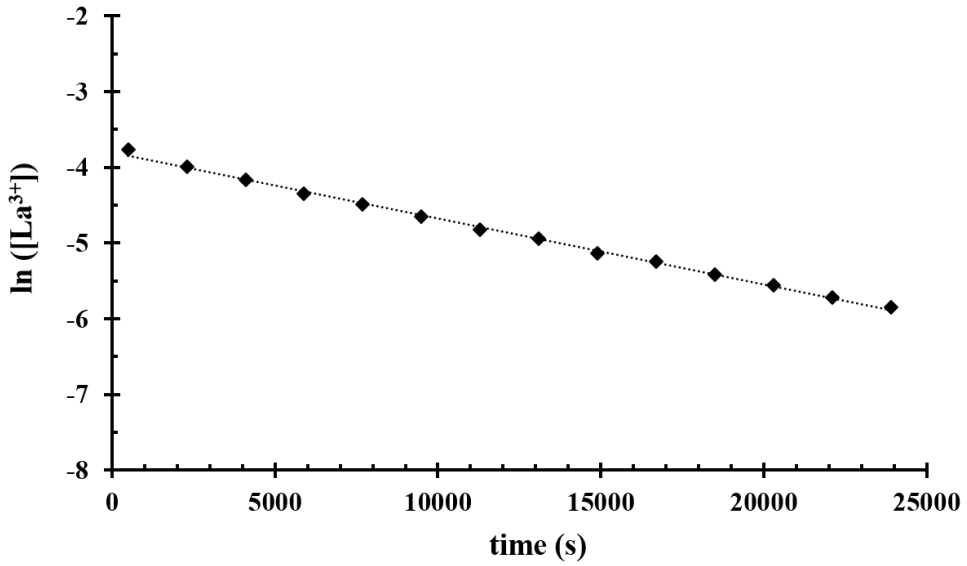

Figure 10.3. First order kinetic plot for the thermal decomposition of "[K(2.2.2-cryptand)][$Cp'_2La(C_4Ph_4)$]", **33-La**, in THF-d_8: T = 298 K, C_0 = 0.024 M (extrapolated), k_{obs} = 8.621 x 10^{-5} s^{-1} (R = 0.9999), $t_{1/2}$ = 2.2 h.

CONCLUSION

The reductive coupling of diphenylacetylene using $5d^1$ La^{2+} complexes [K(2.2.2-cryptand)][Cp′$_3$La] and [K(2.2.2-cryptand)][(Cp′$_2$La)$_2$(C_6H_6)] precursors generated solutions that were found to form the indenyl product, [K(2.2.2-cryptand)][($PhCH_2$)$Ph_2C_9H_4$]. The crystallographic characterization of [K(2.2.2-cryptand)][($PhCH_2$)$Ph_2C_9H_4$] demonstrates that the potassium salt of this known indene[10,18-20] in obtainable in single crystalline form. The ^{1}H NMR spectrum of the reaction mixture generated immediately after mixing [K(2.2.2-cryptand)][Cp′$_3$La] or [K(2.2.2-cryptand)][(Cp′$_2$La)$_2$(C_6H_6)] with diphenylacetylene suggests that a metallocycle "[K(2.2.2-cryptand)][Cp′$_2$La(C_4Ph_4)]", **33-La**, is generated. The **33-La** product is unstable in solution at room temperature and decomposes according to first order kinetics with a rate constant k_{obs} = 8.621 x 10^{-5} s^{-1}. Hydrolysis of the NMR sample gave a product whose mass spectrum was consistent with the indene ($PhCH_2$)$Ph_2C_9H_5$. These results indicate that compounds of $5d^1$ La^{2+} can do chemistry previously reported for $4d^1$ Cp_2Zr.[10] and may indicate that diphenylacetylene is a suitable substrate to differentiate the reactivity of $4f^n5d^1$ Ln^{2+} ions from the traditional $4f^{n+1}$ and configurational crossover Ln^{2+} ions.

REFERENCES

(1) Tazelaar, C. G. J.; Bambirra, S.; van Leusen, D.; Meetsma, A.; Hessen, B.; Teuben, J. H. *Organometallics* **2004**, *23*, 936-939.

(2) Batrice, R.; McKinven, J.; Arnold, P. L.; Eisen, M. S. *Organometallics* **2015**, *34*, 4039-4050.

(3) Liu, H.; Ghatak, T.; Eisen, M. S. *Chem. Commun.* **2017**, *Advance Article*.

(4) Evans, W. J.; Bloom, I.; Hunter, W. E.; Atwood, J. L. *J. Am. Chem. Soc.* **1983**, *105*, 1401-1403.

(5) Evans, W. J.; Forrestal, K. J.; Ziller, J. W. *Angew. Chem. Int. Ed.* **1997**, *36*, 774-776.

(6) Evans, W. J.; Kozimor, S. A.; Ziller, J. W.; Kaltsoyannis, N. *J. Am. Chem. Soc.* **2004**, *126*, 14533-14547.

(7) Evans, W. J.; Nyce, G. W.; Forrestal, K. J.; Ziller, J. W. *Organometallics* **2002**, *21*, 1050-1055.

(8) Fagan, P. J.; Manriquez, J. M.; Marks, T. J.; Day, C. S.; Vollmer, S. H.; Day, V. W. *Organometallics* **1982**, *1*, 170-180.

(9) Evans, W. J.; Kozimor, S. A.; Ziller, J. W. *Chem. Commun.* **2005**, 4681-4683.

(10) Xi, Z.; Guo, R.; Mito, S.; Yan, H.; Kanno, K.; Nakajima, K.; Takahashi, T. *J. Org. Chem.* **2003**, *68*, 1252-1257.

(11) Fieser, M. E.; MacDonald, M. R.; Krull, B. T.; Bates, J. E.; Ziller, J. W.; Furche, F.; Evans, W. J. *J. Am. Chem. Soc.* **2015**, *137*, 369-382.

(12) Kotyk, C. M.; Fieser, M. E.; Palumbo, C. T.; Ziller, J. W.; Darago, L. E.; Long, J. R.; Furche, F.; Evans, W. J. *Chem. Sci.* **2015**, *6*, 7267-7273.

(13) APEX2 Version 2014.11-0, Bruker AXS, Inc.; Madison, WI, 2014.

(14) SAINT Version 8.34a, Bruker AXS, Inc.; Madison, WI, 2013.

(15) Sheldrick, G. M.; SADABS, Version 2014/5, Bruker AXS, Inc.; Madison, WI, 2014.

(16) Sheldrick, G. M.; SHELXTL, Version 2014/7 ed.; Bruker AXS, Inc.: Madison, WI, 2014.

(17) International Tables for X-Ray Crystallography, 1992, Vol. C. ed.; Dordrecht: Kluwer Academic Publishers.

(18) Padwa, A.; Blacklock, T. J.; Loza, R. *J. Org. Chem.* **1982**, *47*, 3712-3721.

(19) Guesten, H.; Schulte-Frohlinde, D. *Liebigs Ann.* **1976**, 22-29.

(20) Eom, D.; Park, S.; Park, Y.; Ryu, T.; Lee, P. H. *Org. Lett.* **2012**, *14*, 5392-5395.

(21) Manriquez, J. M.; Fagan, P. J.; Marks, T. J. *J. Am. Chem. Soc.* **1978**, *100*, 3939-3941.

(22) Johnson, S. A.; Liu, F.-Q.; Suh, M. C.; Zürcher, S.; Haufe, M.; Mao, S. S. H.; Tilley, T. D. *J. Am. Chem. Soc.* **2003**, *125*, 4199-4211.

(23) Xu, L.; Wang, Y.; Wang, Y.-C.; Wang, Z.; Zhang, W.-X.; Xi, Z. *Organometallics* **2016**, *35*, 5-8.

(24) Brosmer, J. L.; Huang, W.; Diaconescu, P. L. *Organometallics* **2017**, *ASAP*.

APPENDIX A

INTRODUCTION

During the course of the studies in this dissertation, Professor Karsen Meyer and Dominik Halter discovered that the trivalent lanthanide complexes ((^{Ad,Me}ArO)$_3$mes)Ln, reported in Chapters 6-8, are active electrocatalysts for the reduction of H_2O to H_2. The purpose of this section is to describe the synthesis and characterization of complexes used to understand the mechanism of this transformation. Their reactivity was investigated to understand the mechanism shown in Scheme A.1 below.

EXPERIMENTAL

((^{Ad,Me}ArO)$_3$mes)Nd / ((^{Ad,Me}ArO)$_3$mes)Nd(H_2O). On a Schlenk line, H_2O (18 μL) was added to benzene (20 mL) and the resultant mixture was stirred for several hours with intermittent vigorous shaking. The H_2O/C_6H_6 mixture (0.98 mL) was added to pale blue ((^{Ad,Me}ArO)$_3$mes)Nd (50 mg, 0.005 mmol) in C_6H_6 (30 mL). The mixture was stirred overnight and the pale blue solution became lighter in color. The volatiles were removed *in vacuo* which left a benzene soluble blue/green oil. The ^{1}H NMR spectrum of the oil was consistent with a ca. 95:05 molar ratio of 23-Nd-H_2O / ((^{Ad,Me}ArO)$_3$mes)Nd and showed trace amounts of (^{Ad,Me}ArOH)$_3$mes. Single crystals of a co-crystallized mixture of ((^{Ad,Me}ArO)$_3$mes)Nd-H_2O / ((^{Ad,Me}ArO)$_3$mes)Nd in a 33.3:66.7 ratio were grown from C_6D_6 in an NMR tube. Attempts to prepare ((^{Ad,Me}ArO)$_3$mes)Nd-H_2O with stoichiometric H_2O gave insoluble blue solids and ((^{Ad,Me}ArOH)$_3$mes). ^{1}H NMR (C_6D_6, 500 MHz): δ 0.84 (s, 3H), 0.85 (br s, 6H), 0.87 (br s, 9H), 1.22 (br s, 18H), 1.26-1.43 (br m, 23H), 1.60 (m, 6H), 4.31 (m, 6H), 6.93 (m, 3H), 7.64 (m, 3H) ppm. IR: 3447w, 3066m, 2958s, 2927s, 2873s, 2859s, 2730w, 2677w, 1730s, 1600m, 1581m, 1489m, 1464s, 1449m, 1380m, 1354w,

1342m, 1280s, 1121s, 1073s, 1039s, 991w, 977w, 959m, 923w, 909w, 858w, 850w, 836w, 820w, 809w, 800m, 784m, 771m, 743s, 705m, 651m cm^{-1}.

X-ray Data Collection, Structure Solution and Refinement for ((^{Ad,Me}ArO)$_3$mes)Nd / ((^{Ad,Me}ArO)$_3$mes)Nd(H$_2$O). A colorless crystal of approximate dimensions 0.020 x 0.025 x 0.100 mm was mounted in a cryoloop. Data was collected on a Bruker Kappa four-circle micro-focus rotating anode diffractometer system equipped with an APEX II CCD detector. The APEX3[1] program package was used to determine the unit-cell parameters and for data collection (30 sec/frame scan time). The raw frame data was processed using SAINT[2] and SADABS[3] to yield the reflection data file. Subsequent calculations were carried out using the SHELXTL[4] program. The diffraction symmetry was 2/*m* and the systematic absences were consistent with the monoclinic space group $P2_1/c$ that was later determined to be correct. The structure was solved by dual space methods and refined on F^2 by full-matrix least-squares techniques. The analytical scattering factors[5] for neutral atoms were used throughout the analysis. Hydrogen atoms were included using a riding model. The water molecule bound to the neodymium atom was refined with site-occupancy-factors = 1/3. Several atoms were disordered and included using multiple components with partial site-occupancy factors. At convergence, wR2 = 0.0844 and Goof = 1.350 for 724 variables refined against 9182 data (0.82Å), R1 = 0.0461 for those 8410 data with $I > 2.0\sigma(I)$.

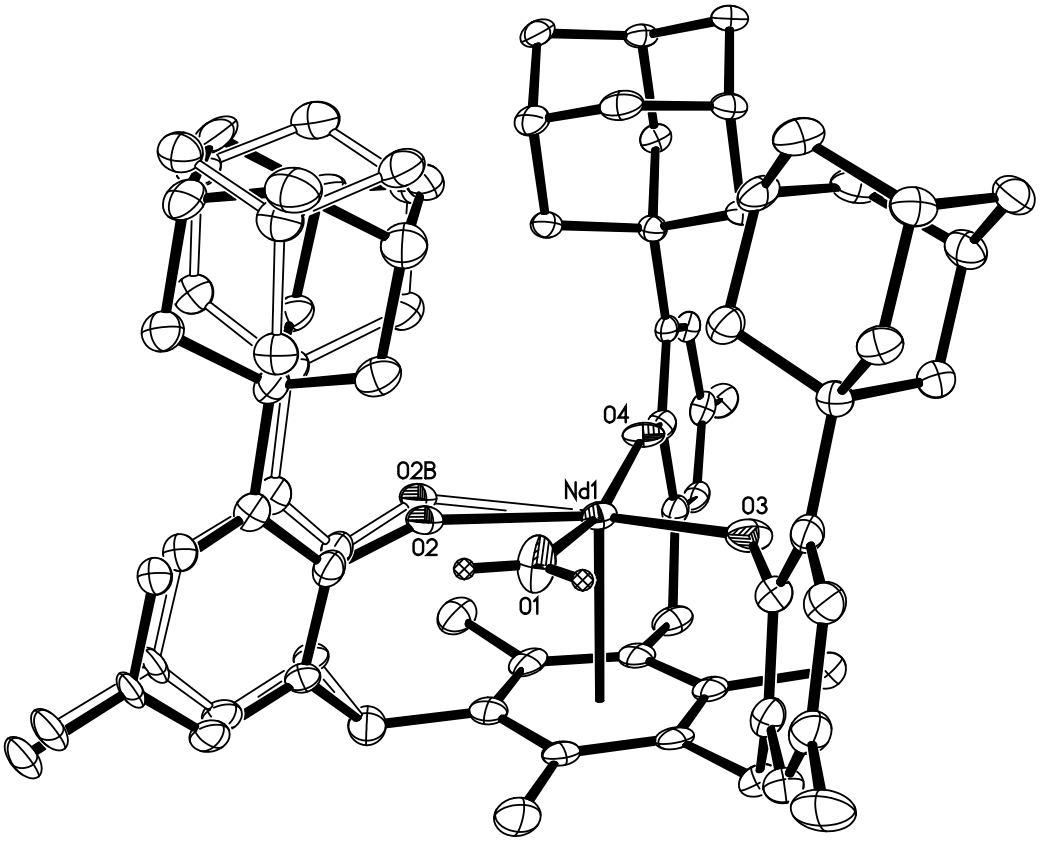

Figure A.1. Thermal ellipsoid plot of ((^{Ad,Me}ArO)$_3$mes)Nd / ((^{Ad,Me}ArO)$_3$mes)Nd(H_2O) drawn at the 50% probability level. Hydrogen atoms are omitted for clarity. The aquo ligand H_2O was refined with 33% occupancy.

[K(2.2.2-cryptand)][((^{Ad,Me}ArO)$_3$mes)Nd(OH)]. In a glovebox, H_2O (0.01 M in THF, 3.5 mL, 0.03 mmol) was added to a stirred scarlet red solution of [K(2.2.2-cryptand)][((^{Ad,Me}ArO)$_3$mes)Nd] (50 mg, 0.03 mmol) in THF (5 mL) and the solution immediately turned bright green and then pale blue. The pale blue solution was left to stir for 30 min and then the volatiles were removed *in vacuo* to yield [K(2.2.2-cryptand)][((^{Ad,Me}ArO)$_3$mes)Nd(OH)] as a pale blue powder (46 mg, 91%). Single-crystals suitable for X-ray crystallography were grown by vapor diffusion of Et_2O into a concentrated THF solution of [K(2.2.2-

cryptand)][((^{Ad,Me}ArO)$_3$mes)Nd(OH)] at −35 °C. ^{1}H NMR (500 MHz, THF-d_8, 298 K): δ 0.18 (br s, 18H), 1.00 (br s, 9H), 1.86 (s, 9H), 2.61 (br s, 12H), 2.78 (d, J_{HH} = 9.2 Hz, 9 H), 2.83 (s, 9H), 3.62 (br s, 12H), 3.70 (br s, 12H), 4.54 (d, J_{HH} = 9.8 Hz, 9H), 5.41 (s, 1H, *OH*), 5.93 (br s, 6H), 6.37 (s, 3H), 6.74 (s, 3H). IR: 3713m, 3073w, 2968s, 2899s, 2849s, 2816s, 2760w, 2729w, 2677w, 2652w, 1601w, 1557w, 1476m, 1146s, 1433m, 1375w, 1354m, 1341w, 1285s, 1260s, 1184w, 1163w, 1134m, 1105s, 1080m, 1030w, 980w, 951m, 934m, 914w, 881w, 858w, 831m, 818w, 804m, 768w, 750w, 677w, 621w, 605s cm^{-1}. Anal. calcd for $C_{81}H_{112}KN_2NdO_{10}$: C, 66.77; H, 7.75; N, 1.92. Found: C, 67.11; H, 7.88; N, 1.87.

[K(2.2.2-cryptand)][((^{Ad,Me}ArO)$_3$mes)Gd(OH)]. In a glovebox, H_2O (0.01 M in THF, 3.5 mL, 0.003 mmol) was added to a stirred scarlet red solution of **2-Gd** (50 mg, 0.03 mmol) in THF (5 mL) and the solution immediately turned bright green and then pale blue. The pale blue solution was left to stir for 30 min and then the volatiles were removed *in vacuo* to yield **3-Gd** as a pale blue powder. Single-crystals suitable for X-ray crystallography were grown by vapor diffusion of Et_2O into a concentrated THF solution of **3-Gd** at −35 °C. IR: 3379m, 3072w, 2954s, 2896s, 2844s, 2815s, 2757w, 2728w, 2675w, 2651w, 1600w, 1558w, 1477m, 1446s, 1432s, 1375w, 1361m, 1354m, 1340w, 1286s, 1260s, 1183w, 1163w, 1132m, 1104s, 1080m, 1030w, 1019w, 980w, 950m, 932m, 914w, 880w, 857m, 833m, 818m, 806m, 766w, 750m, 677w, 630w, 603w cm^{-1}.

X-ray Data Collection, Structure Solution and Refinement for [K(2.2.2-cryptand)][((^{Ad,Me}ArO)$_3$mes)Nd(OH)]. A green crystal of approximate dimensions 0.050 x 0.104 x 0.291 mm was mounted in a cryoloop and transferred to a Bruker SMART APEX II diffractometer. The APEX2[6] program package was used to determine the unit-cell parameters and for data collection (90 sec/frame scan time for a sphere of diffraction data). The raw frame data was processed using

SAINT[7] and SADABS[3] to yield the reflection data file. Subsequent calculations were carried out using the SHELXTL[4] program. The systematic absences were consistent with the cubic space group $P2_13$ that was later determined to be correct. The structure was solved by dual space methods and refined on F^2 by full-matrix least-squares techniques. The analytical scattering factors[5] for neutral atoms were used throughout the analysis. Hydrogen atoms were included using a riding model. The molecule and counter-ion were located on 3-fold rotation axes. The hydroxide hydrogen atom was disordered over three positions and included with a site-occupancy-factor = 1/3. Least-squares analysis yielded wR2 = 0.0709 and Goof = 1.049 for 288 variables refined against 4826 data (0.83 Å), R1 = 0.0329 for those 4270 data with $I > 2.0\sigma(I)$. The absolute structure was assigned by refinement of the Flack parameter.[8] There were residuals (probably unidentifiable solvent) present in the final difference-Fourier map. The SQUEEZE[9] routine in the PLATON[10] program package was used to account for the electrons in the solvent accessible voids.

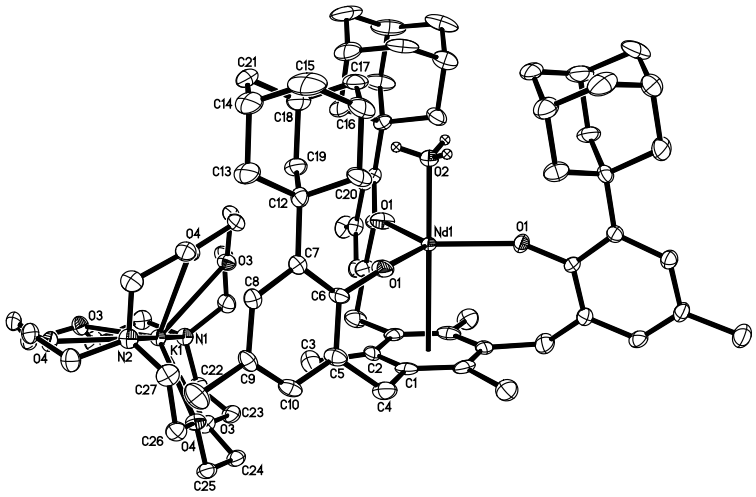

Figure A.2. Thermal ellipsoid plot of [K(2.2.2-cryptand)][((^{Ad,Me}ArO)$_3$mes)Nd(OH)] drawn at the 50% probability level. Hydrogen atoms are omitted for clarity. The hydroxo ligand is refined with 33% occupancy.

X-ray Data Collection, Structure Solution and Refinement for [K(2.2.2-cryptand)][((^{Ad,Me}ArO)$_3$mes)Gd(OH)]. A colorless crystal of approximate dimensions 0.202 x 0.212 x 0.274 mm was mounted in a cryoloop and transferred to a Bruker SMART APEX II diffractometer. The APEX2[11] program package was used to determine the unit-cell parameters and for data collection (30 sec/frame scan time for a sphere of diffraction data). The raw frame data was processed using SAINT[7] and SADABS[3] to yield the reflection data file. Subsequent calculations were carried out using the SHELXTL[4] program. The systematic absences were consistent with the cubic space group $P2_13$ that was later determined to be correct. The structure was solved by direct methods and refined on F^2 by full-matrix least-squares techniques. The analytical scattering factors[5] for neutral atoms were used throughout the analysis. Hydrogen atoms were included using a riding model. The molecule and counter-ion were located on three-fold rotation axes. The position of the hydroxide hydrogen atom was located from a difference-Fourier map and refined (x,y,z) with d(O-H) = 0.85Å and riding U_{iso}. H(2) was disordered about the three-fold axis and was included with site-occupancy-factor = 1/3. At convergence, wR2 = 0.0466 and Goof = 1.028 for 291 variables refined against 6646 data (0.74), R1 = 0.0205 for those 6295 data with $I > 2.0\sigma(I)$. The absolute structure was assigned by refinement of the Flack parameter.[8] There were residuals present in the final difference-Fourier map. The SQUEEZE[9] routine in the PLATON[10] program package was used to account for the electrons in the solvent accessible voids.

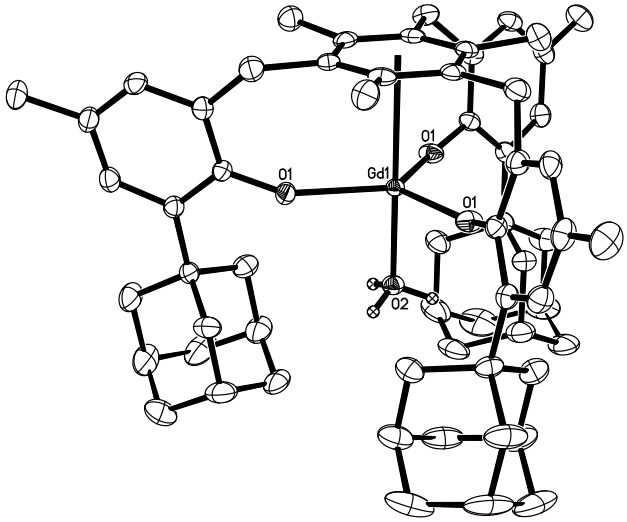

Figure A.3. Thermal ellipsoid plot of [K(2.2.2-cryptand)][((^{Ad,Me}ArO)$_3$mes)Gd(OH)] drawn at the 50% probability level. Hydrogen atoms are omitted for clarity. The hydroxo ligand is refined with 33% occupancy.

RESULTS AND DISCUSSION

Reactivity. The reactivity of the [K(2.2.2-cryptand)][((^{Ad,Me}ArO)$_3$mes)Ln(OH)] (Ln = Nd, Gd) complexes was explored to investigate the mechanism of catalysis of the ((^{Ad,Me}ArO)$_3$mes)Ln complexes. The reduction of [K(2.2.2-cryptand)][((^{Ad,Me}ArO)$_3$mes)Gd(OH)] with potassium graphite in the presence of 2.2.2-cryptand was performed to see whether the Gd^{2+} complex, [K(2.2.2-cryptand)][((^{Ad,Me}ArO)$_3$mes)Gd], reported in Chapter 6, would be generated. A similar reaction was proposed for a U^{4+} complex, ((^{Ad,Me}ArO)$_3$mes)U(OH).[12] For Gd, this would generate a scarlet red solution of [K(2.2.2-cryptand)][((^{Ad,Me}ArO)$_3$mes)Gd] and give a broad isotropic singlet at g = 1.990 in the EPR spectrum generated from the solution at 298 K (see Chapter 6). Instead, a pale colored solution was obtained that gave a sharp isotropic singlet at g = 2.001 in its

EPR spectrum, Figure A.4. This suggests that the regeneration of Gd^{2+} under these conditions is unlikely.

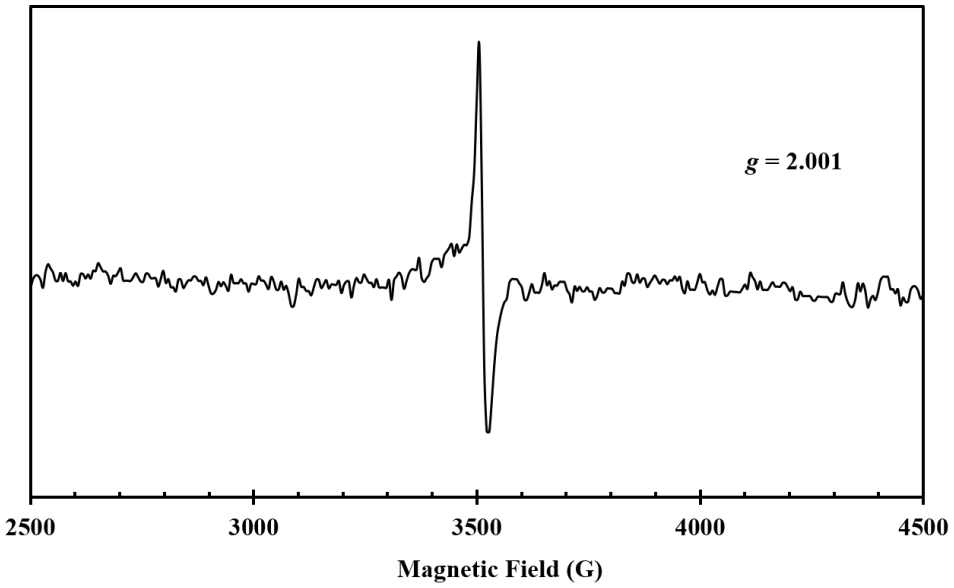

Figure A.4. Experimental X-band EPR spectrum after the addition of potassium graphite to a THF solution of [K(2.2.2-cryptand)][((^{Ad,Me}ArO)$_3$mes)Gd(OH)] and 2.2.2-cryptand at 298 K (Mode: perpendicular; g = 2.001; ν = 9.817 GHz; 2.026 mW; modulation amplitude = 10.02 G).

REFERENCE

(1) APEX3 Version 2016.1-0 ed.; Bruker AXS, Inc.: Madison, WI, 2016.

(2) SAINT Version 8.37a ed.; Bruker AXS, Inc.: Madison, WI, 2015.

(3) Sheldrick, G. M.; Bruker AXS, Inc.: Madison, WI, 2014; Vol. SADABS, Version 2014/5.

(4) Sheldrick, G. M.; SHELXTL, Version 2014/7 ed.; Bruker AXS, Inc.: Madison, WI, 2014.

(5) International Tables for X-Ray Crystallography, 1992, Vol. C. ed.; Dordrecht: Kluwer Academic Publishers.

(6) APEX2 Version 2014.11-0 ed.; Bruker AXS, Inc.: Madison, WI, 2014-.

(7) SAINT Version 8.34a ed.; Bruker AXS, Inc.: Madison, WI, 2013.

(8) Parsons, S.; Flack, H. D. *Acta Cryst.* **2013**, *B69*, 249-259.

(9) Spek, A. L.; Vol. SQUEEZE, Acta Cryst. 2015, C71, 9-19.

(10) Spek, A. L.; Vol. PLATON, Acta. Crys. 2009, D65, 148-155.

(11) APEX2 Version 2014.9-0 ed.; Bruker AXS, Inc.: Madison, WI, 2014--.

(12) Halter, D. P.; Heinemann, F. W.; Bachmann, J.; Meyer, K. *Nature* **2016**, *530*, 317-321.

APPENDIX B

INTRODUCTION

The purpose of this section is to provide documentation of additional complexes that were prepared and characterized but excluded from the main text. Most of these complexes were only structurally characterized.

EXPERIMENTAL

$Er(NPh_2)_3(THF)_2$. In a glovebox, $ErCl_3$ (243 mg, 0.887 mmol) and a stir-bar were added to scintillation vial and THF (10 mL) was added to give a pink slurry. $NaPh_2$ (500 mg, 2.62 mmol) was added to a separate vial and dissolved in THF (10 mL) to yield a green-yellow solution. Both vials were stored at −35 °C for 1 h before the solution of $NaPh_2$ was added dropwise to the stirring slurry of $ErCl_3$ over the course of 5 min. The resultant pink slurry was allowed to warm to room temperature and stirred overnight. The volatiles were removed under reduced pressure to yield a pink gel. The gel was triturated with hexane several times to yield pink solids which were then dissolved in Et_2O (17 mL) and stirred for several hours to ensure complete dissolution. Pink and colorless solids, presumably unreacted $ErCl_3$ and $NaNPh_2$, were centrifuged and the volatiles of the supernatant were evaporated until supersaturation. As the concentrated pink solution warmed to room temperature, large pink hexagonal crystals of $Er(NPh_2)_3(THF)_2$ suitable for X-ray diffraction grew over the course of a couple minutes (260 mg off first crop, 36%).

X-ray Data Collection, Structure Solution and Refinement for $Er(NPh_2)_3(THF)_2$. A pink crystal of approximate dimensions 0.332 x 0.389 x 0.482 mm was mounted on a glass fiber and transferred to a Bruker SMART APEX II diffractometer. The APEX2[1] program package was used to determine the unit-cell parameters and for data collection (15 sec/frame scan time for a

sphere of diffraction data). The raw frame data was processed using SAINT[2] and SADABS[3] to yield the reflection data file. Subsequent calculations were carried out using the SHELXTL[4] program. The diffraction symmetry was 2/*m* and the systematic absences were consistent with the monoclinic space group $P2_1/n$ that was later determined to be correct. The structure was solved by dual space methods and refined on F^2 by full-matrix least-squares techniques. The analytical scattering factors[5] for neutral atoms were used throughout the analysis. Hydrogen atoms were included using a riding model. One tetrahydrofuran ligand was disordered. The disordered atoms were included using multiple components with partial site-occupancy-factors. Least-squares analysis yielded wR2 = 0.0510 and Goof = 1.045 for 460 variables refined against 9687 data (0.73 Å), R1 = 0.0197 for those 8834 data with $I > 2.0\sigma(I)$.

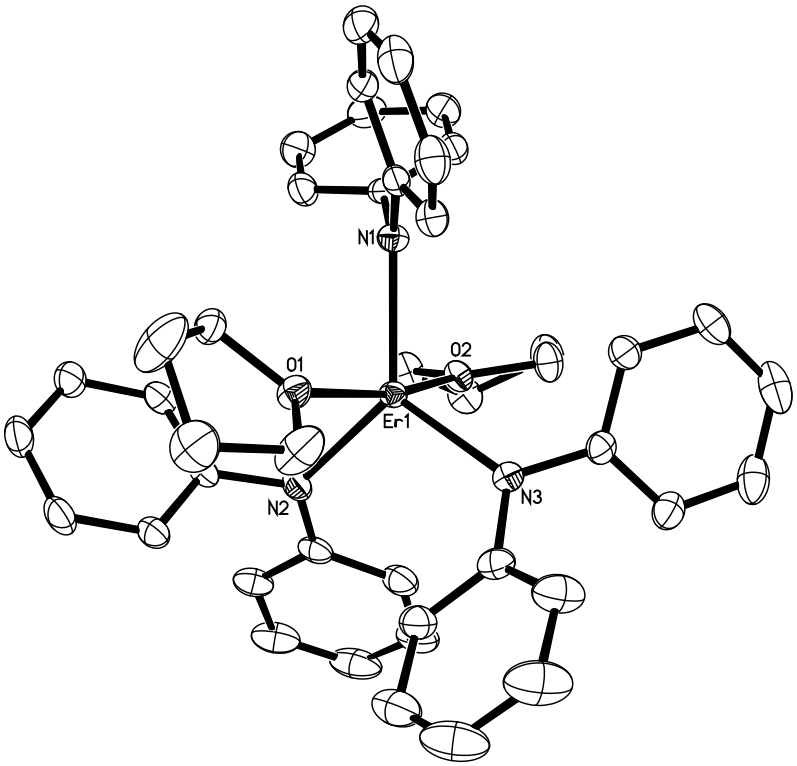

Figure B.1. Thermal ellipsoid plot of $Er(NPh_2)_3(THF)_2$ drawn at the 50% probability level. Hydrogen atoms and co-crystallized solvent molecules are omitted for clarity.

$[(NPh_2)_2Y(\mu\text{-}NPh_2)]_2$. In a glovebox, $Y[N(SiMe_3)_2]_3$ (300 mg, 0.526 mmol) was added to a scintillation vial and was dissolved in toluene (10 mL). A stir-bar was added and to the stirred solution, $HNPh_2$ (272 mg, 1.61 mmol) in toluene (10 mL) was slowly added. The resultant colorless solution was left to stir for 48 h and the transparent solution slowly turned to a yellow slurry. The volatiles were then removed and the resultant yellow solids were washed with hexane. The solids were then stirred in benzene for 48 h and the resultant yellow slurry was centrifuged to remove insolubles. Toluene (4 mL) was added to the supernatant and the solution was concentrated to 4 mL before it was layered with hexane (15 mL). After 48 h at room temperature, yellow rectangular blocks of $[(NPh_2)_2Y(\mu\text{-}NPh_2)]_2$ suitable for X-ray diffraction had.

X-ray Data Collection, Structure Solution and Refinement for $[(NPh_2)_2Y(\mu\text{-}NPh_2)]_2$. A colorless crystal of approximate dimensions 0.146 x 0.239 x 0.284 mm was mounted in a cryoloop and transferred to a Bruker SMART APEX II diffractometer. The APEX2[1] program package was used to determine the unit-cell parameters and for data collection (30 sec/frame scan time for a hemisphere of diffraction data). The raw frame data was processed using SAINT[2] and SADABS[3] to yield the reflection data file. Subsequent calculations were carried out using the SHELXTL[4] program. The diffraction symmetry was 2/*m* and the systematic absences were consistent with the monoclinic space group $P2_1/c$ that was later determined to be correct. The structure was solved using the coordinates of the dysprosium analogue and refined on F^2 by full-matrix least-squares techniques. The analytical scattering factors[5] for neutral atoms were used throughout the analysis. Hydrogen atoms were included using a riding model. The molecule was located about an inversion center. Least-squares analysis yielded wR2 = 0.0697 and Goof = 1.030 for 361 variables refined against 6851 data (0.73 Å), R1 = 0.0315 for those 5604 data with $I > 2.0\sigma(I)$.

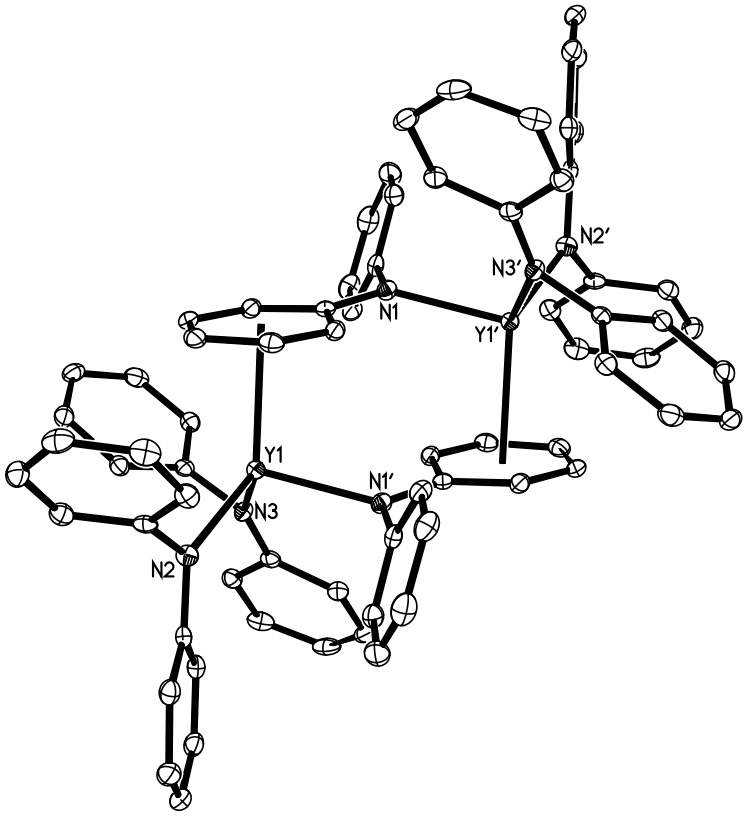

Figure B.2. Thermal ellipsoid plot of $[(NPh_2)_2Y(\mu\text{-}NPh_2)]_2$ drawn at the 50% probability level. Hydrogen atoms are omitted for clarity.

$[(NPh_2)_2Dy(\mu\text{-}NPh_2)]_2$. In a glovebox, $Dy[N(SiMe_3)_2]_3$ (300 mg, 0.466 mmol) was added to a scintillation vial and was dissolved in toluene (10 mL). A stir-bar was added and to the stirred solution, $HNPh_2$ (240 mg, 1.42 mmol) in toluene (10 mL) was slowly added. The resultant colorless solution was left to stir for 48 h and the transparent solution slowly turned to a yellow slurry. The volatiles were then removed and the resultant yellow solids were washed with hexane. The solids were then stirred in benzene for 48 h and the resultant yellow slurry was centrifuged to remove insolubles. Toluene (4 mL) was added to the supernatant and the solution was concentrated to 4 mL before it was layered with hexane (15 mL). After 48 h at room temperature, yellow rectangular blocks of $[(NPh_2)_2Dy(\mu\text{-}NPh_2)]_2$ suitable for X-ray diffraction had formed.

X-ray Data Collection, Structure Solution and Refinement for $[(NPh_2)_2Dy(\mu\text{-}NPh_2)]_2$.

A yellow crystal of approximate dimensions 0.111 x 0.116 x 0.201 mm was mounted in a cryoloop and transferred to a Bruker SMART APEX II diffractometer. The APEX2[1] program package was used to determine the unit-cell parameters and for data collection (20 sec/frame scan time for a sphere of diffraction data). The raw frame data was processed using SAINT[2] and SADABS[3] to yield the reflection data file. Subsequent calculations were carried out using the SHELXTL[4] program. The diffraction symmetry was 2/*m* and the systematic absences were consistent with the monoclinic space group $P2_1/c$ that was later determined to be correct. The structure was solved by dual space methods and refined on F^2 by full-matrix least-squares techniques. The analytical scattering factors[5] for neutral atoms were used throughout the analysis. Hydrogen atoms were included using a riding model. The molecule was located about an inversion center. Least-squares analysis yielded wR2 = 0.0652 and Goof = 1.046 for 361 variables refined against 7264 data (0.73 Å), R1 = 0.0255 for those 6207 data with $I > 2.0\sigma(I)$.

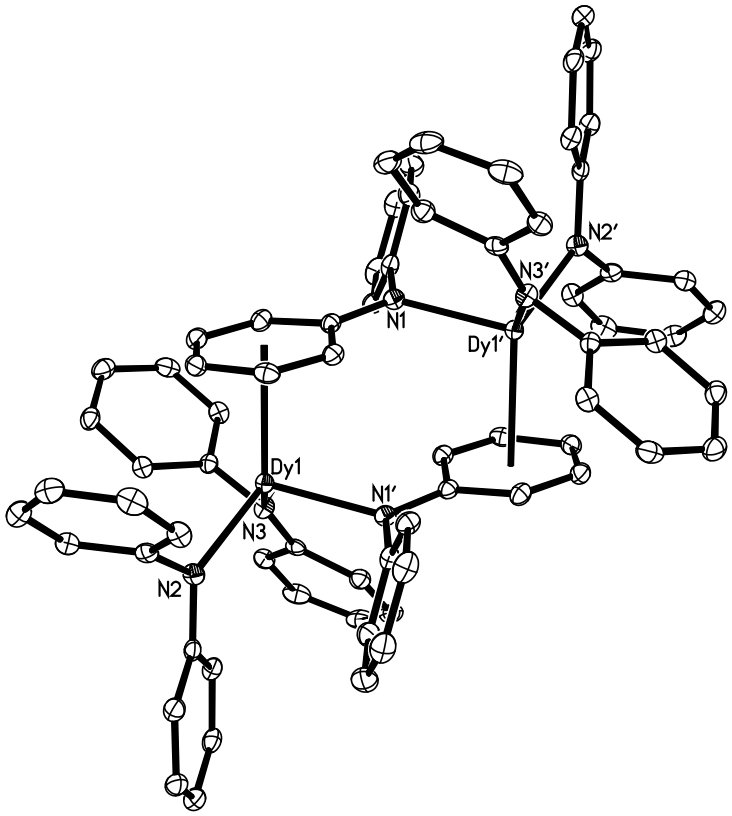

Figure B.3. Thermal ellipsoid plot of $[(NPh_2)_2Dy(\mu\text{-}NPh_2)]_2$ drawn at the 50% probability level. Hydrogen atoms are omitted for clarity.

$[(Ph_2N)_4Er_2(\mu\text{-}O)]_2$. In a glovebox, $Er[N(SiMe_3)_2]_3$ (300 mg, 0.463 mmol) was added to a scintillation vial and was dissolved in toluene (10 mL). A stir-bar was added and to the stirred solution, $HNPh_2$ (240 mg, 1.41 mmol) in toluene (10 mL) was slowly added. The resultant colorless solution was left to stir for 48 h and the transparent solution slowly turned to a yellow slurry. The volatiles were then removed and the resultant yellow solids were washed with hexane. The solids were then stirred in benzene for 48 h and the resultant yellow slurry was centrifuged to remove insolubles. Toluene (4 mL) was added to the supernatant and the solution was concentrated to 4 mL before it was layered with hexane (15 mL). After 48 h at room temperature,

yellow rectangular blocks of $[(Ph_2N)_4Er_2(\mu\text{-}O)]_2$ suitable for X-ray diffraction had formed. The oxo ligands are attributed to adventitious water.

X-ray Data Collection, Structure Solution and Refinement for $[(Ph_2N)_4Er_2(\mu\text{-}O)]_2$. A yellow crystal of approximate dimensions 0.106 x 0.278 x 0.347 mm was mounted on a glass fiber and transferred to a Bruker SMART APEX II diffractometer. The APEX2[1] program package and the CELL_NOW[2] were used to determine the unit-cell parameters. Data was collected using a 10 sec/frame scan time for a sphere of diffraction data. The raw frame data was processed using SAINT[3] and TWINABS[4] to yield the reflection data file (HKLF5 format)[4]. Subsequent calculations were carried out using the SHELXTL[5] program. There were no systematic absences nor any diffraction symmetry other than the Friedel condition. The centrosymmetric triclinic space group $P\bar{1}$ was assigned and later determined to be correct. The structure was solved by direct methods and refined on F^2 by full-matrix least-squares techniques. The analytical scattering factors[6] for neutral atoms were used throughout the analysis. Hydrogen atoms were included using a riding model. The molecule was located about an inversion center. There were two molecules of benzene solvent present per empirical formula-unit. At convergence, wR2 = 0.0624 and Goof = 0.96 for 552 variables refined against 10308 data (0.73Å), R1 = 0.0273 for those 9209 with $I > 2.0\sigma(I)$. The structure was refined as a three-component twin.

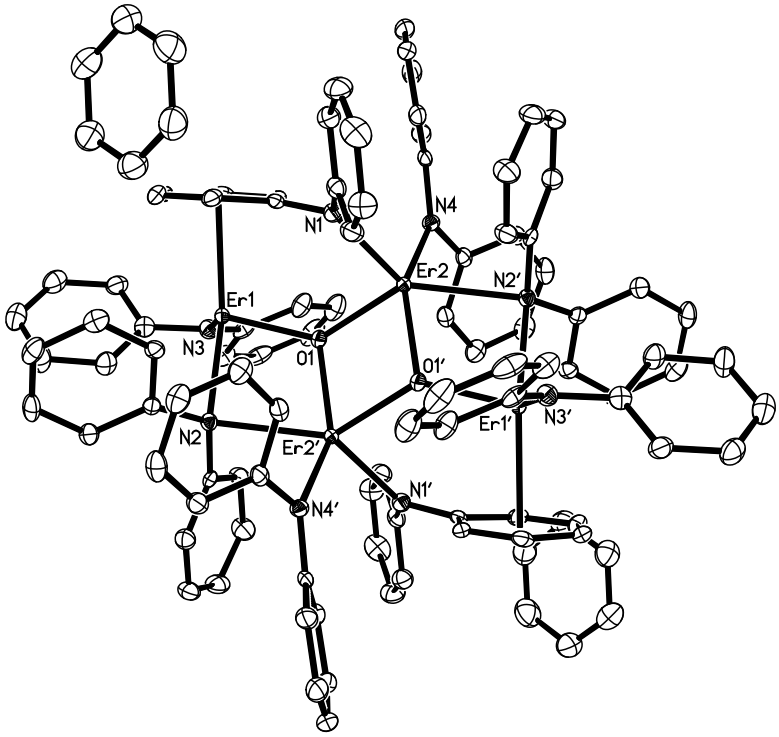

Figure B.4. Thermal ellipsoid plot of $[(Ph_2N)_4Er_2(\mu\text{-}O)]_2$ drawn at the 50% probability level. Hydrogen atoms are omitted for clarity.